OPTICAL INVESTIGATIONS OF THE ATMOSPHERE
USING ARTIFICIAL SATELLITES

M. S. Malkevich
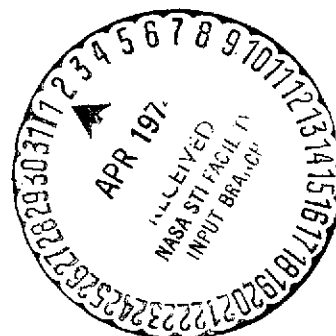
Translation of "Opticheskiye issledovaniya
atmosfery so sputnikov," Moscow, "Nauka"
Press, 1973, pp. 1 - 303.

NATIONAL AERONAUTICS AND SPACE ADMINISTRATION
WASHINGTON, D. C. 20546   MARCH 1974

1. Report No. NASA TT F-15,186	2. Government Accession No.	3. Recipient's Catalog No.
4. Title and Subtitle OPTICAL INVESTIGATIONS OF THE ATMOSPHERE USING ARTIFICIAL SATELLITES		5. Report Date March, 1974
		6. Performing Organization Code
7. Author(s) M.S. Malkevich		8. Performing Organization Report No.
		10. Work Unit No.
9. Performing Organization Name and Address SCITRAN Box 5456 Santa Barbara, CA 93108		11. Contract or Grant No. NASw-2483
		13. Type of Report and Period Covered Translation
12. Sponsoring Agency Name and Address National Aeronautics and Space Administration Washington, D.C. 20546		14. Sponsoring Agency Code

15. Supplementary Notes

Translation of "Opticheskiye issledovaniya atmosfery so sputnikov "Moscow", "Nauka" Press, 1973, pp. 1 - 303.

16. Abstract

This book describes methods of interpretation and results of measurements of the optical characteristics of the Earth, obtained by means of artificial satellites with the object of determining the physical parameters of the atmosphere, the clouds, and the Earth's surface. The methods are based on the use of a priori statistical characteristics of the structure of fields of the Earth's atmospheric parameters. Methods are presented for solving the problems of determining the temperature of the ground surface, and the temperature and characteristics of the three-dimensional structure of the cloud cover from measurements of radiation in the visible and infrared regions of the spectrum, taken from the satellites Kosmos 149, Kosmos 243 and Kosmos 320.

The book is intended for the use of scientists, graduate students and undergraduates specializing in atmospheric physics, meteorology and astrophysics.

17. Key Words (Selected by Author(s))	18. Distribution Statement Unclassified - Unlimited

19. Security Classif. (of this report) Unclassified	20. Security Classif. (of this page) Unclassified	21. No. of Pages 230	22. Price

ANNOTATION

This book describes methods of interpretation and results of measurements of the optical characteristics of the Earth, obtained by means of artificial satellites with the object of determining the physical parameters of the atmosphere, the clouds, and the Earth's surface. The methods are based on the use of a priori statistical characteristics of the structure of fields of the Earth's atmospheric parameters. Methods are presented for solving the problems of determining the temperature of the ground surface, and the temperature and characteristics of the three-dimensional structure of the cloud cover from measurements of radiation in the visible and infrared regions of the spectrum, taken from the satellites Kosmos 149, Kosmos 243 and Kosmos 320.

The book is intended for the use of scientists, graduate students and undergraduates specializing in atmospheric physics, meteorology and astrophysics.

PREFACE

The use of artificial Earth satellites (AES) to study the
Earth's atmosphere, which in recent years has engaged the
attention of a growing number of investigators in the fields of
atmospheric physics, meteorology, astrophysics, and neighboring
applied sciences, is one reason for the great expansion of
investigations of the Earth's radiation field and for a compre-
hensive study of the processes and factors responsible for the
formation and transformation of radiation on the Earth. At least
two factors have stimulated these investigations.

The first, and undoubtedly the most important, factor is
that practically all the information on the state of the atmosphere
and the Earth's surface, as well as processes in the troposphere and
the stratosphere which are important for problems in atmospheric
physics and meteorology, can be obtained from a satellite by
measuring the radiation reflected from the radiating Earth to
outer space in various ranges of the electromagnetic wave spectrum.

The second factor stems from the special features of satellite
measurements, which make up a complex of contemporary investiga-
tions of the physical mechanism of atmospheric processes on a world
scale. By means of satellites we can obtain, in a short space
of time (and even simultaneously, with appropriate launching of
several satellites) the field of emitted radiation for all regions
of the globe, and can track the spatial and timewise variation of
the radiation, and therefore can study the variability of the
meteorological phenomena and the physical parameters of the atmos-
phere responsible for the generation of the radiation fields.

---

* Numbers in the margin indicate pagination of original
foreign text.

Certain aspects of experiments to investigate the Earth's radiation field by means of satellites, including their great cost, require us to conduct theoretical investigations whose main purposes are:

1) To obtain a basic recommendation regarding the desirability of performing a certain experiment, to evaluate its feasibility, and to formulate requirements for the experiment, consistent with the task adopted;

2) To establish quantitative relations between the atmospheric parameters to be determined with an allowable accuracy, and the characteristics of the radiation field to be measured with an actually attainable accuracy;

3) A statement of the use of existing information on the physical parameters of the atmosphere in conducting measurements which are insufficiently complete at a given technical level;

4) To set up algorithms for processing the data from satellite measurements and to extract useful information regarding the physical mechanism of propagation of radiation and the random nature of the measured and desired parameters;

5) To develop methods for solving certain prospective problems in investigating the lower levels of the atmosphere and the underlying surface by means of satellite measurement of the Earth's radiation field.

The present monograph contains results of investigations in /8| this direction, which the author, and a group of co-workers at the Institute of Atmospheric Physics of the Academy of Sciences of the USSR (IFA), has carried out while developing methods of

optical probing of the Earth's atmosphere from satellites. These investigations were used, in particular, to design a scientific program of optical measurements on the AES's Kosmos 149, Kosmos 243, Kosmos 320, and to develop a group of onboard scientific equipment to accomplish these measurements, as well as processing and interpretation of the experimental data.

It should be mentioned that only part of the results presented can be considered as complete, in the sense that they have been confirmed, where possible, by experiment in similar or sufficiently close conditions. These other results of the work can be used in future development of methods of optical probing of the atmosphere by means of AES's and of corresponding experimental investigations which either have been already begun, or should be conducted in the future.

Naturally, the development of the rather wide range of topics considered in the book would be meaningless without the close scientific contact that the author has had with a number of his co-workers at the IFA and in related scientific establishments.

The author wishes to express his deep indebtedness to G. V. Rozenberg for a number of valuable ideas used in the present investigations, as well as to V. I. Dianov-Klokov, V. P. Kozlov, V. F. Turchin, and Ye. M. Feygel'son, with whom individual topics were discussed. The author also thanks V. G. Boldyrev, A. K. Gorodetskiy, I. A. Gorchakov, L. G. Ismotina, L. I. Koprova, A. P. Orlov, T. A. Sushkevich, V. I. Syachinov, G. P. Faraponova, L. U. Chagar, and L. M. Shukurov who took part in developing a number of topics and V. Ye. Vvedenskiy, K. S. Glazova, Z. N. Tarasenkov and N. S. Filippova for their help in calculations and in producing the figures.

Finally, the author feels obliged to comment that the investigations which have been made are based on principles developed in the work of the now deceased Ye. S. Kuznetsov, under whose guidance the author began his scientific activity.

TABLE OF CONTENTS

INTRODUCTION

The many experimental and theoretical investigations of the
transport of solar radiation in the Earth's atmosphere and on the
Earth's self radiation have allowed us to build up a definite theory
of the radiation field of our planet and in some cases to establish
quantitative relations between the radiation characteristics
and the physical parameters of the atmosphere which are responsible
for the Earth's radiation conditions. A comprehensive study has
also been made of the optical properties of atmospheric substances
which are active in the radiation sense, and of the underlying
surface, which plays an important part in forming the Earth's
radiation field. A special section of atmospheric optics deals
with investigations of the propagation of radiation in clouds,
or more generally, in optically dense media.

The quantitative relationship between characteristics of
the radiation field and parameters of the atmosphere or the under-
lying surface has been used to solve a number of problems in
atmospheric physics. An example is the problem of determining
the concentration and total mass of atmospheric gases absorbing
solar radiation and the Earth's self radiation (water vapor,
ozone, etc.), and also the problem of determining characteristics
of aerosols which scatter the solar radiation, or of artificial
sources of radiation.

Another important example of the use of results of radiation investigations is the problem of atmospheric energy balance, since the difference between the fluxes of solar radiation and the Earth's self radiation is the main source of energy for the processes taking place in the Earth's atmosphere.

A systematic account of the results of investigations in the area of atmospheric eptics has been given in monographs by K. Ya. Kondrat'yev [1-3], G. V. Rozenberg [4], K. S. Shifrin [5], V. V. Sobolev [6], Ye. M. Feygel'son [I.7], and Goode [8] as well as in the basic work of Ye. S. Kuznetsov on the theory of radiation transport in the Earth's atmosphere (see, e.g., [9]) and in a number of papers*. An analysis of the most important data on calculations and measurements of characteristics of the Earth's radiation field in the various spectral intervals is given in Chapters 1 and 2.

The present stage of development of atmospheric eptics is characterized by rising methods of studying radiation processes developed for idealized models to`study the real atmosphere.

The solution to the problem is associated with considerable difficulties, due mainly to the structural complexity and the great spatial and timewise variability of the atmosphere, as well as to the diversity of conditions under which propagation of radiant energy occurs in reality.

---

* In this book we adopt the following notations for literature references: when the ¡reference is to another chapter, the chapter number appears in front of the source number, while in other cases ordinary numbering is used.

The great magnitude of the problem is very clear. The advent of artificial Earth satellites has made its solution easier, in the sense that one can rapidly obtain information from the entire sphere of the Earth, since all regions can be uniformly accessible to satellites. The presence of a large number of satellites in orbits allows us to obtain worldwide information simultaneously. However, besides these indisputable advantages, investigations from satellites have an obvious shortcoming, viz., it is impossible to make direct measurements of the physical parameters of the underlying atmosphere, information concerning which is embodied in the characteristics of the radiation emitted to outer space from the upper boundary of the atmosphere.

At least three kinds of problems pertaining to atmospheric physics can be identified, which can be solved and already are being solved on the basis of radiation measurements obtained from satellites (some of the results of these investigations have been published in the books by Kondrat'yev [10,12], and in collections of articles [13, 15]).

1. The first type of problem is associated with investigations of the Earth's cloud cover derived from television pictures or photometric or radiometric data obtained from a satellite in the visible part of the spectrum on the illuminated part of the Earth, and in the infrared — on the non-illuminated side. The principle involved is as follows. From pictures of cloud systems of various scales, one can evaluate the type of cloud and also a number of meteorological processes in the atmosphere, since clouds serve as good indicators of the nature, position, and movement of pressure formations and frontal zones, and the character of vertical currents and distribution of precipitation zones.

The first results obtained from satellites of the series
Tiros (see [10, 12]) and Kosmos [16, 17], have shown that satellite
pictures of clouds allow us to determine the main features and even
some fine details of a meteorological formation (this is particu-
larly important for regions where cloud observations are rare or
totally absent). Also, analysis of the pictures enables us to
detect configurations of large-scale cloud systems, as well as a
number of properties of cloud formations and of associated atmos-
pheric conditions, which are in general inaccessible even for
a dense grid of ground meteorological stations.

However, the interpretation of the pictures obtained (nepho-
analysis) is limited mainly to determination of qualitative
relationships, which are unavoidably subjective in nature. In
addition, these methods are applicable only to cases of ordered
configurations of cloud systems and do not lend themselves to the
use of high-speed computers.

It is well established that the distribution of cloud elements,
particularly those having dimensions from several kilometers to
several tens of kilometers (meso-scale), is random. Therefore,
statistical methods of cloud picture processing are used at
present to determine quantitative characteristics of the structure
of cloud systems (the same thing is true of the interpretation
of data from absolute measurements of the characteristics of
the radiation field under cloudy conditions).

Questions on the determination of characteristics of the three-
dimensional structure of cloud systems are considered in detail
in this book during investigation of the structure of radiation
fields (see Chapter 5).

2. A second type of problem is associated with determining fluctuations in the Earth's radiation balance. The basic idea of an experiment required to solve this problem is quite simple, at first glance: a detector with a field of view of ~ 180°, carried on a satellite and pointed towards the Earth, is used to measure the flux of reflected solar radiation and of the Earth's self radiation (or the sum of these fluxes), integrated over all directions in the upper hemisphere, similar to what is done on an aircraft or on balloons. However, the performance of these measurements, which could be used for reliable determination of the variation of fluxes of radiant energy — required, for example, for weather prediction — encounters very serious difficulties associated with the angular or the three-dimensional structure of the radiation field. In fact, the solar radiation /11 reflected by various natural surfaces, clouds, or the atmosphere, depends to a varying degree on the direction of incidence of the direct solar radiation, and on the direction of reflection or scattering (the self radiation of objects also depends on the type of surface and the direction of observation).

With measurements of radiative fluxes on aircraft and balloons in the field of view of wide-angle receivers, there are comparatively limited sections of the Earth's surface and atmosphere for which one can assume that the angular distribution of radiation is uniform throughout the region of survey (only for cloudless conditions above a homogeneous surface of the Earth, or for continuous cloud cover). This allows us to replace integration of radiation over all directions in the upper (or lower) hemisphere by integration over the region of survey.

In the case of satellites, the field of view of a wide-angle detector can encompass huge sections of the Earth, including diverse objects with different angular distributions of emitted

radiation. Therefore, integration over space performed for these
measurements should not be considered as equivalent to integration
over directions for any part of a survey region, without appreciable
uncontrolled errors being introduced. In other words, these
measurements give quite a specific physical quantity, the flux of
radiant energy passing through a unit surface area of a sphere
with radius equal to the distance of the satellite from the
Earth's center. However, one cannot pinpoint a comparatively
limited region of the Earth to which this energy could be ascribed.

Hence one can conclude that the results of measurements of
radiative fluxes by wide-angle detectors have limited value, and
in any event, can give only the large-scale variations of the
radiative fluxes. In this sense the ideas of Suomi (see [18])
concerning the possibility of establishing a relationship between
radiative fluxes and pressure formations and cloud systems
have not been confirmed experimentally, as exemplified, in
particular, by the results of processing certain data on radia-
tive measurements on the satellite Explorer 7, as presented in
[19].

This was evidently the reason for using narrow angle de-
tectors (~ 50°) on satellites of the Tiros series. However,
this substitution does not correct the situation, since as
before there is an averaging over a large area, while the
measured quantity loses a simple physical meaning. And even if
the measurements are made by a detector with a sufficiently
narrow field of view, so that its survey region can be considered
uniform in the radiation sense, as was done on satellites of
the Kosmos [20] and the Nimbus [21] series, in fact what is
measured is the radiative intensity of this region in the
direction of the optical axis of the instrument, while the
radiation remains unknown in other directions. By using theoreti-
cal calculations of the angular distribution of reflected solar

radiation and of the self radiation for certain models of the
atmosphere, one can recover the flux of reflected radiation from
the measured radiative intensity in only one direction, as was
proposed in the work of Shifrin, et al. [22,20]. Since this kind
of conversion is based on calculations of the angular distribu-
tion of radiative intensity for certain models of the atmosphere
and the underlying surface, the reliability of the method des-
cribed in the work is in need of experimental verification. How-
ever, the idea itself, of determining the reflected radiative
flux from measurements of narrow-angle detectors, even if the
radiative intensity is measured only in one direction, is en-
couraging. Following the work of [22], we consider the possi-   /12
bility of obtaining the variations of fluxes both of reflected
solar radiation, and of the Earth's self radiation, by basing a
method on the dependence of the angular structure of the radiation
field on the vertical structure of the physical parameters of the
atmosphere (see Chapter 4).

3. A <u>third</u> <u>type</u> <u>of</u> <u>problem</u> embodies questions in optical
probing of the atmosphere and of the underlying surface. The con-
ventional ideas held that the problem is to determine the de-
pendence of certain atmospheric parameters $\varphi(y)$ from measurements
of a suitable characteristic of the radiation field $f(x)$, these
being interconnected by a relationship of the type

$$f(x) = A[x, y, \varphi(y)],$$ (1)

where A is an operator (in general, nonlinear) describing the
physical mechanism of the relationship. The corresponding
functional is also described by the structure of other atmospheric
parameters (optical or meteorological) which determine the
mechanism of radiative transfer in the atmosphere and can depend
on variables x or y. Some of these parameters require definition

as well as $\varphi(y)$, which presents considerable difficulties, for quite obvious reasons, in transforming the operator A.

Therefore, to determine all the desired parameters one must choose some group of measurements to obtain a closed system of the original data and appropriate equations of type (1), where the most informative characteristics of the radiation field must be measured, each of which should depend mainly on one of the atmospheric parameters being determined, while the dependence on the others should be weaker.

Another difficulty which arises in solving problems in optical probing is the following. In distinction from other planets, for which these problems were solved long ago in astrophysics, for the Earth one should not be limited to determining typical or average values of the physical parameters, since the majority of these can be considered as known for practically all regions of the globe. For problems in physics of the Earth's atmosphere and in meteorology, one needs information on the timewise and spatial variations of these parameters. Determination of these variations is connected firstly with rather strict requirements as to accuracy of measurements of the corresponding radiation characteristics. Secondly, it imposes additional requirements on the technique of interpretation of the measurements, which reduces in many cases to solving the inverse problems, which are incorrect from a mathematical point of view (incorrectness means that small errors in the measurements of the function $f(x)$ can lead to arbitrarily large errors in the quantities $\varphi(y)$ being determined, and sometimes even the physical meaning of the latter is distorted).

These difficulties are aggravated by the fact that the unknown and known atmospheric parameters responsible for the variations in the measured characteristics of the radiative field vary in a

random manner in actual conditions. Therefore, for a valid solution of problems of optical probing one needs tangible and quite reliable information as to the nature of these variations, particularly because one needs a priori information about the solution itself, in order to make incorrect problems tractable.

Fortunately, the Earth's atmosphere has been studied more thoroughly than the atmospheres of the other planets: there is a large number of measurements of various meteorological elements in different regions of the globe and over various time periods. The optical characteristics of the atmosphere and the underlying surface have also been measured. This information, represented in the form of statistical characteristics of the vertical and three-dimensional structure of the fields of meteorological elements and some optical parameters*, can be used as auxiliary data /13 in the solution of a number of problems in the optical probing of the atmosphere. The aggregate of statistical characteristics of the structure of atmospheric parameters determining the variations in the Earth's radiative field can be considered as an optical-meteorological model of the atmosphere. The basic principles in constructing a model, and examples of the structural characteristics of such elements for which there is a sufficient number of experimental data, will be described in detail in Chapter 3.

A proposed model of the atmosphere can be used not only to solve the inverse problems considered as problems of determining specific forms of the random function $\varphi(y)$ from measurements of values of another random function $f(x)$. This model also allows us to relate the structural characteristics of the atmospheric parameters

---

* Statistical characteristics of the spectral and angular structure can also be obtained for the optical parameters.

9

to the statistical characteristics of vertical, three-dimensional, angular, and spectral structure of the radiation model. The corresponding relationships, which form the content of Chapters 4 and 5, make it possible, on the one hand, to construct a model of the Earth's radiation field which is congruent with the optical model of the atmosphere, and, on the other hand, to expand our understanding of optical probing by including the problem of determining the structural characteristics of atmospheric parameters from the structural characteristics of the radiation models.

We note one further important property of the models constructed in this way: they allow us to obtain the best realization of the complete necessary system of atmospheric and radiation parameters of a particular situation from a finite number of reliably measured parameters of this system.

The theory of thermodynamic processes in the atmosphere and the long-term experience of ground-based, airborne and aerological observations indicate that the basic elements of global information which one must extract from radiation measurements, must be, as before, the temperature, pressure, humidity, cloudiness, wind speed and direction, composition of the underlying surface, and precipitation, as well as characteristics of energy flux in the atmosphere.

The need to obtain these parameters determines the choice of the characteristics of the Earth's radiation field to be measured by means of a satellite. Here one makes use of the numerous results of previously conducted experimental and theoretical investigations of the angular, spectral, vertical, and spatial distributions of solar radiation reflected from the Earth and of the planet's self radiation (some of the results are

considered in Chapters 1 and 2).

Of course, by no means all of the meteorological elements listed can be determined at present from satellite measurements of radiation characteristics. But radiation measurements are now being conducted to determine some of them, and methods have been developed to transfer from the directly measured quantities to the desired parameters. An example is the problem of determining the temperature of the underlying surface and of the clouds* from measurements of the Earth's self radiation in the "transparent windows" of the atmosphere at 8-12 or 10-12 μm. In these intervals the self radiation of the underlying surface must be distorted least by absorption and self radiation of the atmosphere. In actuality, the transformation of the Earth's radiation is appreciable even in the transparent windows and, which is very important, it is difficult to calculate, since it is determined mainly by the vertical distributions of atmospheric temperature and humidity, and also by the aerosol component, which all fluctuate strongly with time and place.

Methods of calculating the transformation of the self radiation of the underlying surface, using statistical characteristics of the vertical structure of the temperature and humidity fields, will be considered in detail in Chapter 8.

Clouds are responsible for appreciable transformation of radiation from the underlying surface. If an optically dense cloud lies in the field of view of an instrument, the radiation

---

* Allowing for the difference of natural surfaces from an absolutely black body, it is more correct to speak of the problem of determining the radiation temperature of the underlying surface and of the clouds.

temperature of its upper boundary, considered as an underlying surface, will in fact be measured. However, for clouds which are optically not dense enough, it is as yet difficult to resolve the problem of calculating distortions of self radiation of the underlying surface by this mechanism. Clearly in this case one needs a certain group of measurements to permit the absorption and the self radiation of these clouds to be evaluated.

Of the other problems in optical probing, the most advanced are problems in determining the vertical distribution of atmospheric temperature and humidity from measurements of the intensity of the Earth's self radiation, in particular intervals of the absorption bands of CO_2 at 15 μm and of water vapor at 6.3 μm (a similar problem can be set up also for the vertical profile of ozone from emission in the 9.6 μm band). The appreciable difficulties in solving these problems stem from the need for the high measurement accuracy necessary to determine the variations of the vertical profiles. The precision of measurements is also associated with the above-mentioned incorrectness of the inverse problem, to which the determination of these parameters reduces. In order to make the problem of determining the vertical profile of temperature and humidity regular, one makes use of a priori information in the form of statistical characteristics of the vertical structure of the fields of these elements. A detailed examination of the method of statistical regularization is given in Chapters 6 and 7. One of the most difficult problems in optical probing is to determine the atmospheric pressure very accurately. It seems possible, at first sight, to determine the partial pressure of the atmospheric gases whose concentration varies comparatively little under actual conditions, from measurements of reflected solar radiation in the regions of the absorption bands of these gases and in the

adjacent transparent windows, e.g., in the oxygen absorption band at 0.76 μm or for carbon dioxide at 2.1 μm.

However, preliminary calculations show that the atmospheric pressure cannot be determined with the necessary accuracy by this method (e.g., from the reflected radiation in the oxygen absorption band), since there are, in principle, a number of difficulties associated with calculation of aerosol scattering of radiation by the atmosphere or the clouds.

In the latter case, it is true that one can address the problem of determining the height of the upper boundary of the clouds as a function of the total mass of absorbing substance contained in the total column of the atmosphere between the reflecting surface and the absorbing one. If we assume that the concentration of the absorbing substance (e.g., O_2) is constant, the height of the reflecting surface will be a single-valued function of its mass. Chapter 9 deals with this matter.

We restrict ourselves in this book to the development of methods for determining only the above-mentioned physical parameters of the atmosphere, since the corresponding experimental work is presently being conducted, or is proposed, to allow the methods to be tested and their effectiveness to be evaluated. It should be noted that the methods of solving problems in <u>/15</u> optical probing, as is true for other problems of the radiation type, must be based on physically rigorous calculation of the selectivity of radiation absorption by atmospheric gases in a nonuniform and thermally layered medium, as well as on the use of reliable data on the reflectivity and emissivity of natural formations.

In recent times, extensive investigations (although as yet incomplete), both theoretical and experimental, of the absorption characteristics of atmospheric gases have been conducted, as well as of a number of other optical parameters of the atmosphere and underlying surface. Some results of this kind, required to solve the problems considered in this book, are presented in Chapters 1 and 2.

Besides accounting for the gaseous absorbing substance, to solve almost all of the above problems, one must also take account of the rapidly varying atmospheric aerosol component, which will produce uncontrolled distortion of the radiation characteristics used as original information. We cannot yet list any basic methods for calculating this component, because, as yet, there are no reliable results of measurements of aerosol absorption, scattering, and emission or radiation in the real atmosphere. However, it should be noted that it is a matter of independent interest to determine the characteristics of an aerosol, including the microstructure of aerosol and cloud formations from given angular and spectral distributions of solar radiation reflected and scattered by clouds and the atmosphere, and the subject is one of the important problems in optical probing. A first step in solving this problem is obviously to find the statistical characteristics of the structure of the distribution of particles according to size and height of the atmosphere and in clouds, and then to establish the relation between them and characteristics of the angular and spectral structure of the scattered radiation. Some suggestions of this kind will be given in Chapters 3 and 4.

This is the kind of problem considered in this monograph, the kind which can be solved from radiation measurements with satellites. The book by no means deals with all of the possibilities of using satellites for quantitative investigations of the

lower layers of the atmosphere. There are, for example, suggestions to determine the vertical distribution of air density from measurements of the phase and refraction angle of the radiation using a system of satellites [23]. The actual possibilities for solving this problem were considered by Tamarskiy [24].

Rozenberg and Mullamaa [25] proposed a method of determining the wind speed and direction above water surfaces from the measurements of reflected radiation from the "bright tracks" formed when there is sea swell (see also [26]). Methods are proposed in [27, 29] for determining the dynamic characteristics of the atmosphere, based on the use of radiation measurements and cloud pictures, obtained by means of satellites. All these topics are outside the limits of the above range of problems.

We note that the results of current works are definitely important also for the theory of radiative transfer in the atmosphere. As has already been mentioned, the space and time variations of the Earth's radiation field and the associated physical parameters of the atmosphere are obtained in solving the problems listed above. Since the final result is to establish a relation between the radiation characteristics of the atmospheric parameters, one needs to find a new approach to the investigation of radiant energy transfer in the real atmosphere. It must differ from the transfer mechanism usually considered in a medium in which the parameters describing absorption, scattering, and emission do not vary, or correspond to some specially chosen situation. To investigate the Earth's radiation field and to solve problems by means of radiation measurements on satellites, one should already extend consideration beyond /16 fixed models of the atmosphere, since in actual fact a rapid interchange of different atmospheric states is observed, and

each situation is described by some set of random functions which describe the corresponding atmospheric parameters.

The approach suggested in this book towards the theory of radiative transfer in the atmosphere is that the atmosphere is considered as a certain "dynamic" system with parameters either given or subject to definition by deterministic or statistically distributed parameters (the coefficients of absorption and scattering, the concentration of absorbing and scattering substances, the temperature, etc.). A certain deterministic or random signal with parameters given or with known statistical characteristics (flux of solar radiation, self emission of the underlying surface, flux of radiation reflected from clouds, etc.) comes as input to the system. The output signal, recorded by a measuring device, will be transformed in accordance with the distribution of parameters of the system itself and with operations on the input signal which describe the physical mechanism of radiative transfer.

In this approach the direct problem in the theory of radiative transfer in the atmosphere can be dealt with as follows: the characteristics are given for a deterministic or random function reaching the input of a system with given parameters (an optical and meteorological model of the atmosphere), which may also be deterministic or random functions, and one must determine the characteristics of the random function at the system output (model of the Earth's radiation field). The inverse problems of radiative transfer theory consist in determining the deterministic or random functions of the input signal or the characteristics of the system itself from the characteristics of deterministic or random functions given at the system output.

General methods for solution of problems of this kind are well developed in areas of science where one is concerned with transformations of random parameters of systems which permit

random perturbations of input signal. We shall use these methods to establish the relations between structural characteristics of the Earth's radiation field and the physical parameters of the atmosphere. The corresponding range of topics is the main content of Part I. The use of certain structural characteristics in solving the inverse problems will be considered in Part II.

Finally, we note that a number of theoretical relationships given in this book have been verified experimentally in measured data on the characteristics of the Earth's radiation field obtained by means of aircraft, balloons, rockets, and satellites, including the satellites Kosmos 149, Kosmos 243, and Kosmos 320 [30,31], and also the American Tiros and Nimbus series of satellites. Some results of these comparisons are included in appropriate sections of the book.

PART 1

STRUCTURE OF THE EARTH'S RADIATION FIELD

CHAPTER 1

FIELD OF REFLECTED SOLAR RADIATION

§ 1. Mechanism for Conversion of Solar Energy in the Atmosphere

1.1. Basic Conversion Processes

The conversion of solar radiation in the atmosphere, which
is practically all concentrated in the spectral interval 0.2 - 4 μm,
results from the following basic processes: scattering by air
molecules (molecular or Rayleigh scattering): scattering in
clouds and by aerosols: dust, water droplets, ice crystals
(aerosol scattering): absorption by molecules of atmospheric
gases: water vapor, carbon dioxide, ozone, etc. (selective
molecular absorption): absorption by water droplets, ice
particles or other aerosols, which can be regarded as diffuse
and molecular and atomic absorption of solar radiation, due to
dissociation of air molecules and emission of atmospheric
formations. In addition, solar radiation is absorbed, reflected,
and scattered by different kinds of natural underlying surfaces
(soil, water, snow, vegetation).

These processes lead to a change in the spectral composi-
tion of solar radiation in the atmosphere, namely that, as a
result of molecular and aerosol scattering, the absolute value
of the incident energy changes and there occurs a redistribution
in direction and in space. As a result of absorption, part of
the Sun's radiant energy is in general eliminated from some of

the spectral intervals (sometimes even completely) and is re-radiated in others. A general idea regarding the transformation of the spectral composition of solar radiation reaching the Earth's surface, and concerning the factors responsible for these changes, can be obtained from Figure 1.1. As a result of scattering in the atmosphere and in clouds, and also of reflection from the underlying surface, part of the solar radiation is returned to outer space, having in the meantime undergone transformation.

Thus, a "field of reflected solar radiation" is formed in the terrestial atmosphere (in meteorology, this radiation is called short-wave) in the sense that a parallel ray of solar energy of definite spectral composition, uniformly illuminating the top surface of a layer of the atmosphere (which we will still consider as flat, neglecting the Earth's curvature), is spectrally changed and scattered in all directions in accordance with the laws of absorption and scattering. Here, as a result of the vertical nonuniformity of the atmosphere, and also because of the variation in concentration of absorbing material along the path of propagation of the radiation, the spectral and angular distribution of the latter will depend on the height of the observer above the Earth's surface.

In addition, because of the horizontal nonuniformity of the atmosphere, the cloud cover, and the underlying surface, the spectral, angular, and vertical distribution of the transformed solar radiation will vary in space*. Finally, the regular

---

* The differentiation between the vertical and horizontal (three-dimensional) variations, adopted in atmospheric physics and meteorology, is connected with the difference in scales of the atmospheric processes in these directions.
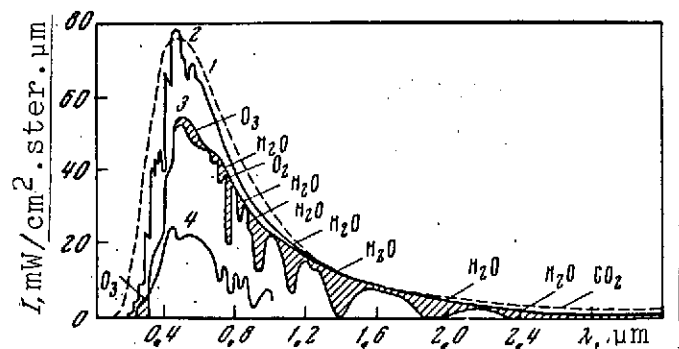
Figure 1.1. Spectral distribution of solar radiation: the absorption band of atmospheric gases are shaded 1- black body radiation at T = 6000° K; 2- solar radiation outside the atmosphere; 3- solar radiation at the Earth's surface at ζ = 60°; 4- solar radiation at ζ = 60°, reflected by the Earth to the zenith (θ = 0, A = 0.8)

and random variations of all these factors with time will result /18 in corresponding variations of the radiation characteristics. Therefore, the field of solar radiation in the Earth's atmosphere will have a complex spectral, angular, vertical, three-dimensional, and timewise structure. To describe it, one needs obvious relations between the characteristics of the radiation fields and the fields of the physical atmospheric parameters, clouds, and underlying surface, responsible for the conversion of solar radiation, and in these relations one must take into account, with sufficient economy, the multitude of conditions experienced in the atmosphere.

Proceeding to an investigation of the structure of the field of short-wave radiation reflected by the Earth to outer space, we consider first some results of calculations of radiation characteristics for particular models of the atmosphere and the underlying surface, as well as measured data on these character-istics under atmospheric conditions, as far as possible congruent with the conditions of the model calculations.

20

The object of this investigation is to obtain data on the range of variation of the characteristics examined under various conditions, which can then be used directly in investigating the structure of the radiation field, and also in solving a number of practical problems, e.g., in building measuring equipment.

One of the main tasks of the present chapter is to survey, compare, and to some extent systematize the presently available data on the field of reflected solar radiation, and also to recommend a method for determining the most representative of its characteristics.

Another task of this survey is to analyze existing measurements and calculations of the characteristics of reflected radiation, simultaneously with an analysis of the physical parameters. This will allow us to gather information on the field of reflected radiation in some of the spectral intervals, i.e., to make it possible to determine the physical parameters which play a basic role in the formation of the radiation field.

Finally, we will examine ways of departing from the traditional model of a plane-parallel atmosphere when taking into account the sphericity of the Earth and the horizontal nonuniformity of the underlying surface, and also methods will be suggested for accounting for the non-orthotropic features of the latter.

In the survey, we shall not deal with investigations of radiative transfer in clouds, since this question has been examined in sufficient detail in the monograph by Feydel'son [7]. However, contemporary data on the optical parameters of the atmosphere and clouds, which allow us to improve on the characteristics of the Earth's radiation field for particular spectral intervals in cloudy conditions, and to verify the theoretical /19

models assumed in the calculations, will be used in solving particular problems of optical probing.

1.2. Statement of the Problem and Basic Equations

For most of the problems considered in this book, the atmosphere can be regarded as a plane-parallel layer whose upper surface receives parallel rays of solar radiation, scattered and absorbed in the layer, while the lower boundary extends to the underlying surface, which reflects radiation according to a given law*. At each point z of the atmospheric layer, the radiation field can be described in terms of the radiative intensity $I_\nu(z,r)$, of frequency ν, propagating in the direction r, which is determined by the zenith and azimuthal angles θ and ψ (Figure 1.2). As is usual (see, e.g., [B.9]), we shall distinguish between the field of ascending or outgoing radiation, for which $0 \leqslant \theta \leqslant \pi/2$ (the intensity depends on positive values of r, generating directions in the upper hemisphere), and the field of descending or incoming radiation, for which $\pi/2 \leqslant \theta \leqslant \pi$ (the intensity depends on negative values of r, generating directions in the lower hemisphere).

For the atmospheric model considered, the radiation field will be described by the following system of integral-differential equations and boundary conditions:

---

* Other sources of short-wave emission can also exist in the atmosphere, for example, the self-luminosity of the atmosphere.
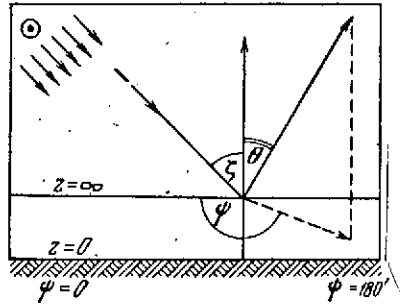
Figure 1.2. Diagram showing propagation of
solar radiation in a plane-parallel atmos-
pheric layer

for the ascending radiation

$$\cos\theta\,\frac{\partial I_\nu(z,\,r)}{\partial z} = -\,[\alpha_\nu(z)+\sigma_\nu(z)]\,I_\nu(z,\,r)+$$

$$+\frac{\sigma_\nu(z)}{4\pi}\Big[\int_+ I_\nu(z,\,r')\,\gamma_\nu(z;\,r,\,r')\,d\omega' + \int_- I_\nu(z,\,-r')\,\gamma_\nu(z;\,r,\,-r')\,d\omega'\Big]+ \qquad (1.1)$$

$$+f_\nu^{(1)}(z,\,r);$$

$$I_\nu(0,\,r) = \int_- I_\nu(0,\,-r')\,R_\nu(r,\,-r')\cos\theta'\,d\omega' + f_\nu^{(2)}(0,\,r); \qquad (1.2)$$

for the descending radiation

$$\cos\theta\,\frac{\partial I_\nu(z,\,-r)}{\partial z} = -\,[\alpha_\nu(z)+\sigma_\nu(z)]\,I_\nu(z,\,-r)+$$

$$+\frac{\sigma_\nu(z)}{4\pi}\Big[\int_+ I_\nu(z,\,r')\,\gamma_\nu(z;\,-r,\,r')\,d\omega' + \int_- I_\nu(z,\,-r')\,\gamma_\nu(z;\,-r,\,-r')\,d\omega'\Big]+ \qquad (1.3)$$

$$+f_\nu^{(1)}(z,\,-r);$$

$$I_\nu(\infty,\,-r) = \pi S_\nu \delta(\theta-\zeta_0)\,\delta(\psi-\psi_\odot). \qquad (1.4)$$

Here $\alpha_\nu(z)$ and $\sigma_\nu(z)$ are the volume coefficients for absorp-
tion and scattering of monochromatic radiation: $\gamma_\nu(z;\,r,\,r')$ is a
scattering index; $R_\nu(r,\,r')$ is the coefficient for reflection at the
underlying surface; $f_\nu^{(1)}(z,\,r)$, $f_\nu^{(2)}(0,\,r)$ are certain functions describ-
ing the distribution of radiation sources in the atmosphere and
at its lower boundary; S_ν is the solar constant; $\delta(\theta-\zeta_0)$ and
$\delta(\psi-\psi_\odot)$ is the delta function ($\zeta_0, \psi_\odot$ are the zenith distance and
the azimuth of the Sun); the integration in Equations (1.1)-(1.3)

is carried out over the top (+) and bottom (-) hemispheres; dw' is the element of solid angle. If we replace the angles θ corresponding to the lower hemisphere by $\pi - \theta$ in Equations (1.3)-(1.4), then all the rays will form acute angles with the vertical z-axis, and all directions will be positive in Equations (1.1) and (1.3).

Since we are mainly interested, in this book, in reflection of radiation from the Earth, we shall consider characteristics of ascending radiation. When confusion can arise, we shall denote intensity of the ascending radiation by $I_\nu^\uparrow$, and that of the descending radiation by $I_\nu^\downarrow$, omitting the minus sign for r.

The limitations which are imposed in using these equations to describe radiative transfer in the actual atmosphere are as follows:

a) The curvature of an atmospheric layer is not accounted for, which can lead to considerable errors in considering large angles θ and ζ_0 (in §8, Chapter 1 we described some methods of calculating reflected radiation, allowing for the sphericity of the Earth);

b) We neglect radiation sources located within the atmosphere; self radiation, which is in fact small in the shortwave spectral region, and self luminosity of the daytime atmosphere, which, generally speaking, can play an appreciable role, particularly in narrow spectral intervals;

c) No account is taken of horizontal nonuniformity, both of the medium itself, and of the underlying surface.

While limitations a) and b) do not play a large part for many problems in atmospheric physics, in which one is required to calculate solar radiation, limitation c) leads to a severe idealization of the atmospheric model, mainly because of the presence of clouds, nonuniformity in the underlying surface, and variability in the aerosol situation in the atmosphere. Below (§7, Chapter 1) we consider methods of computing the horizontal variations of optical characteristics of the underlying surface or of the clouds, and we point out the errors which then arise in solving Equations (1.1) - (1.4) in the horizontally uniform atmospheric model.

By assigning physical parameters of the problem $(\sigma_\nu, \alpha_\nu, \gamma_\nu, R_\nu,$ $S_\nu, f_\nu),$ and using the system of Equations (1.1) - (1.4), we can determine the intensity of short-wave radiation as a function of all the arguments considered. However, actual solution of this problem encounters great difficulty, due to the absence of reliable data for the majority of the parameters listed, and, what is more important, due to their large variability under actual conditions. In addition, the coefficients of absorption, scattering, and reflection are rather complex functions of ν, z, and r, and they are even unknown for a number of terrestial objects.

These circumstances generally cast doubt on the possibility and feasibility of solving a rather cumbersome system of Equations (1.1) - (1.4) for the diverse conditions encountered in the atmosphere. In addition the strong variation of the reflected radiation field under actual conditions requires a skillful approach to the choice of appropriate experimental investigations. One needs to conduct a group of photometric and spectrometric investigations of the solar radiation field in the atmosphere and of the optical characteristics of the medium which would permit determination of the optimal number of parameters describing the

variability of the radiation field and of the optical properties
of the atmosphere. In parallel with this, one must search for
optimal parameters, based on theoretical investigation of the
radiation field and similar experimental conditions.

As has been mentioned, these parameters can be determined
from the investigations of the statistical structure of radia-
tion fields and fields of the atmospheric and physical parameters
(see Chapters 3-5).

§ 2. Optical Parameters of the Atmosphere

Before going on to consider the radiation characteristics
obtained from various models of a scattering medium, we shall
make a short survey of the basic optical parameters of the
atmosphere which determine the field of solar radiation reflected
by the Earth. The survey includes contemporary data from measure-
ments and calculations of these parameters which will be used to
some extent in the problems listed in the Introduction.

2.1. Scattering Coefficients

The scattering coefficient of the atmosphere σ_λ which des-
cribes the attenuation of radiation due to scattering by air
molecules and impurity particles is the sum

$$\sigma_\lambda = a_\lambda + b_\lambda \tag{1.5}$$

of the molecular (a_λ) and the aerosol (b_λ) scattering coeffi-
cients. The molecular scattering coefficient is given, with
good accuracy, by the Rayleigh formula

$$a_\lambda = \frac{32\pi^3 (n-1)^2}{3 N_t \lambda^4} \ (\ cm^{-1}), \tag{1.6}$$

where n is the refractive index (for air n = 1.000278); N_0 =
2.687·10^{19} cm^{-3} is the Loshmidt number; $\lambda = 10^4/\nu$ is the wavelength,
μm (ν, cm^{-1}).

The spectral behavior of a_λ for the dry, absolutely pure atmosphere is shown in Figure 1.3a, from the calculations of Penndorf [1]. The dependence of a_λ on height for the isothermal atmosphere is given by the exponential function

$$a_\lambda(z) = a_\lambda(0) e^{-\alpha z} \quad (\alpha = 0.25 \text{ km}^{-1}) \qquad (1.7)$$

Allowance for vertical variations of atmospheric temperature leads to an increase of α_λ to a value which is no more than 8% greater than the isothermal scattering coefficient with a temperature gradient of 6°/km.

The variations of the scattering of solar radiation in the atmosphere are associated to a large degree with the variation in the aerosol scattering coefficient which, in contrast to the Rayleigh coefficient, depends in a rather complex manner on the wavelength and height, as well as on the nature of the particles and their size distribution. There are no reliable analytical methods to obtain these relations, apart from the case of spherical particles, for which the theory for scattering of radiation has been given in monographs by Shifrin [B.5] and Van de Hulms [2]*.

For this reason experimental investigations of aerosol scattering coefficients were undertaken under various meteorological conditions (see, e.g., [4-8]). Figure 1.3 shows typical kinds of spectral distributions of the coefficients b_λ obtained by Georgiyevskiy [8] by averaging over a sufficiently large number of measurements of transmission in the ground layer of the

---

* On the basis of this theory Shifrin, et al. [3] performed comprehensive calculations of the scattering coefficient and other optical parameters.
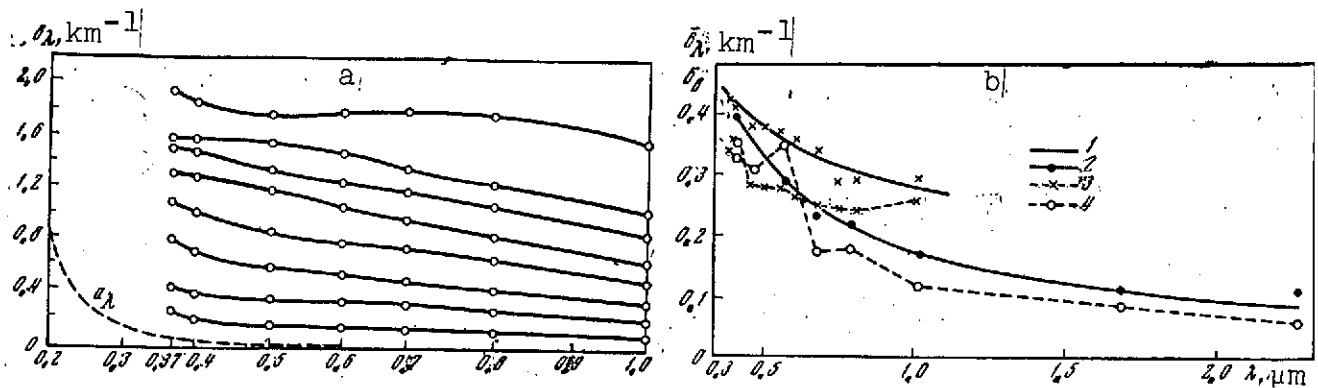
Figure 1.3. Spectral behavior of b_λ a- for different
conditions of turbidity of the ground layer of air,
according to [8]; b- approximation by formulas of
type (1.8); 1- in the ground layer [8]; 2- above a
water surface [7]; 3,4- corresponding mean-square
deviations of the scattering coefficients δ_b

atmosphere at the Zvenigodsk scientific base at the IFA (similar
curves of $\bar{b}_\lambda$ were calculated by Koprova [9] from the measurements
of Knestrik, et al. [7] above a water surface). The curves show
that there is no universal relationship of the type

$$\bar{b}_\lambda = b_0 \left(\frac{\lambda_0}{\lambda}\right)^n \quad (\lambda_0 = 0.55 \ \mu m) \tag{1.8}$$

in the atmosphere, such as normally describes the spectral
behavior of the aerosol scattering coefficient. While it is
possible to obtain this kind of approximation for the severely
averaged empirical curves of $\bar{b}_\lambda$, however, as can be seen from
Figure 1.3b, the parameters of Equation (1.8) depend on the
conditions of observation. For example, over dry land
$b_0 = 0.28$ km^{-1}, $n = 0.43$ from the data of [8], while over water
$b_0 = 0.18$ km^{-1}, $n = 0.9$, from the data of [7].

There are also serious difficulties in investigating the
radiation field of scattered solar radiation, associated with
the lack of reliable information on the vertical distribution

of the aerosol scattering coefficient. It has been shown, from
the results of airborne probing of the vertical transmittance
of the atmosphere in [6], that one can use an exponential varia-
tion of b_λ with height of the form

$$b_\lambda(z) = b_\lambda(0)\, e^{-\beta z},$$
(1.9)

where β varies in the range 0.5 - 1.5 km^{-1}. However, in actual
fact there are considerable irregular deviations from Equation
(1.9), and a layered structure for the scattering coefficients
$b_\lambda(z)$ is observed. As can be seen from Figure 1.4, which shows
curves of the vertical distribution of $b_\lambda(z)$ for $\lambda = 0.5$ and 0.7μ
obtained by Koprova [10] by averaging determinations of $b_\lambda(z)$ for
winter and summer [6], there is a sharply defined three-layer
structure (sometimes two-layer) for the aerosol scattering
coefficient, when one approximates it by three exponential
functions (or two when appropriate), e.g.:

$$\bar{b}_\lambda(z) = \begin{cases} b_\lambda(0)\, e^{-\beta_0 z}, & 0 \leqslant z \leqslant z_1 \approx 1.5\ km, \\ b_\lambda(z_1)\, e^{-\beta_1(z-z_1)}, & z_1 \leqslant z \leqslant z_2 \approx 3.5\ km, \\ b_\lambda(z_2)\, e^{-\beta_2(z-z_2)}, & z_2 \leqslant z \leqslant 10\ km. \end{cases}$$
(1.10)

The parameters of Equation (1.10) for the curves of Figure 1.4
are shown in Table 1.1.

TABLE 1.1 *

Parameters km^{-1}	$\lambda = 0.5\ \mu m$		$\lambda = 0.7\ \mu m$	
	Winter	Summer	Winter	Summer
$b_\lambda(0)$	0,22	0,17	0,22	0,105
$b_\lambda(z_1)$	0,038	0,053	0,022	0,037
$b_\lambda(z_2)$	0,017	0,022	0,007	0,012
β_0	1,18	0,87	1,60	0,71
β_1	0,40	0,44	0,58	0,54
β_2	0,22	0,24	0,23	0,27

* Translator's note: Commas in numbers represent decimal points.
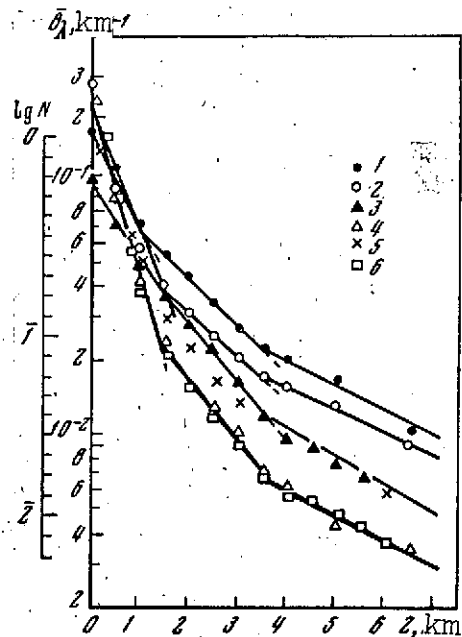
Figure 1.4. Approximation for b_λ by formulas of type (1.10) from data of [6]; $\lambda = 0.5$ m; 1- summer; 2- winter; $\lambda = 0.7$ µm; 3- summer; 4- winter; 5,6-distribution of relative aerosol concentration (in Leningrad) according to [11] for the hot and cold half-year periods, respectively

The layered structure of the scattering coefficient agrees with the nature of the vertical distributions of aerosol concentration N, presented by Selezneva [11].

Formula (1.10) is applicable for the troposphere. The scattering coefficients can be extrapolated to great heights by means of the aerosol scattering model proposed by Rozenberg, et al. [12]. As can be seen from Figure 1.5, the curves of $b_\lambda(z)$, /24 in the troposphere and stratosphere are in satisfactory mutual agreement, and also with the average curve of the Elterman model [13]. The presence of large variations in the vertical profiles $b_\lambda(z)$ of random nature points to the need to include physical and statistical methods describing the vertical structure of the aerosol scattering coefficients, as was done for the spectral relations.
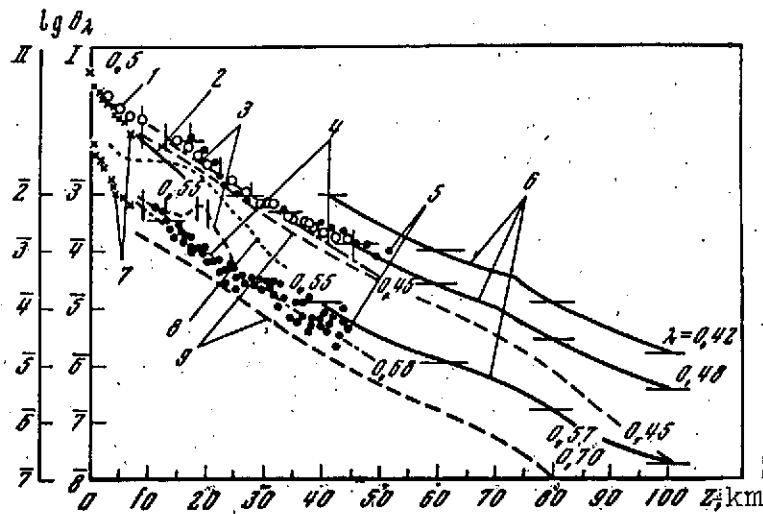
Figure 1.5. Vertical distribution of the aerosol scattering
coefficient   1,8- projected soundings [32,33]; 2,7- aircraft
measurement [32,6]; 3,5- observations from space vehicle [32];
4- calculation from aircraft data;   6- twilight soundings [32];
9- Rayleigh scattering. The figures on the curves indicate
the wavelengths in μm:
I - Scale 0.42; 0.45; 0.48; 0.5; 0.55;
II- Scale 0.57; 0.68; 0.7

2.2. Transmission Functions

The molecular absorption by atmospheric gases, which plays
a part in radiative transfer in the atmosphere, can be divided
into continuum (or diffuse) and selective.

The continuum absorption is connected either with practically
unresolved lines in certain regions, e.g., absorption by O_3 in
the Hartley-Huygens bands at 0.2-0.35 μm [14]), or with the
effect of wings of strong lines.

Recently Dianov-Klokov [15] observed diffuse absorption in
the atmosphere by the short-lived groups $[O_2]_2$ and $[O_2 — N_2]$,
which was comparable with the absorption by O_2 and O_3 molecules
(apart from the bands at 0.69 and 0.76 μm, in which absorption is
associated only with O_2 molecules).

31

The diffuse absorption in Equations (1.1) - (1.4) can be described, to a high degree of accuracy, by monochromatic absorption coefficients. To determine the transmission functions describing attenuation of radiation at a given frequency in the diffuse absorption region, one can use the Bouguet law

$$P_\nu(m) = e^{-k_\nu m}, \qquad (1.11)$$

where k_ν is the absorption coefficient and m is the mass of absorbing substance per unit length, reduced to normal pressure and temperature.

Calculation of selective gas absorption requires considerably more effort, since this absorption experiences strong variations in narrow spectral ranges, while the monochromatic absorption coefficient k_ν is determined by superposition of a large number of lines, whose shape, intensity, and half-width depend on the pressure and temperature of the absorbing medium. Selective absorption is also described by a transmission function, which has the form, for a homogeneous medium.

$$P_{\Delta\nu}(m) = \frac{1}{\Delta\nu} \int_{\Delta\nu} e^{-k_\nu m} d\nu. \qquad (1.12)$$

Here

$$k_\nu = \sum_{i=1}^{N} k_i(\nu)$$

is obtained by summation over N lines, for which the overlap for k_ν is allowed for at the given frequency ν; $\Delta\nu$ is the averaging frequency interval; and $k_i(\nu)$ is the absorption coefficient of the i-th line.

For a homogeneous medium

$$P_{\Delta\nu}(m) = \frac{1}{\Delta\nu} \int_{\Delta\nu} \exp\left[- \int_0^m k_\nu(u)\,du\right] d\nu, \qquad (1.13)$$

32

where k_{ν} depends on the medium pressure and temperature, and also on the concentration of absorbing material.

Until recently the calculation of selective absorption of atmospheric gases was done by constructing idealized models of the absorption bands, which allowed us to describe the spectral behavior of the transmission functions in terms of a comparatively small number of parameters. The most widely used is the Elsasser model, applicable for bands with sufficiently regular structure (see, e.g., [B.2]). According to this model, the transmission functions can be represented in the form of the integral

$$P(y) = 1 - \mathrm{sh}\,\beta \int_0^y \exp(-t\,\mathrm{ch}\,\beta)\,I_0(t)\,dt, \qquad (1.14)$$

where $\beta = 2\pi\gamma/d$; $y = Sm/d\,\mathrm{sh}\,\beta$; S and γ are the intensity and the half-width of a line whose profile is given by the Lorentz formula

$$k(v) = \frac{S}{\pi} \frac{\gamma}{(v - v_0)^2 + \gamma^2}; \qquad (1.15)$$

d is the distance between the lines; $I_0(t)$ is the Bessel function of imaginary argument; and v_0 is the line center.
If $\gamma \ll d$ (i.e., $\beta \ll 1$) , then

$$P(m) = 1 - \Phi\left(\sqrt{\frac{lm}{2}}\right), \qquad (1.16)$$

where $l = 2\pi S\gamma/d^2$ is a generalized absorption coefficient and

$$\Phi(x) = \frac{2}{\sqrt{\pi}} \int_0^x e^{-t^2}\,dt -$$

is the probability error integral.

Equation (1.16) is also applicable for a nonuniform atmosphere, if one replaces the true mass of absorbing material by the so-called effective (or reduced) mass

$$m_e = \int_0^z \rho_a(z_1) \left[\frac{p(z_1)}{p_0} \right]^x dz_1,$$ (1.17)

where $\rho_a(z)$ is the density of the absorbing material; $p(z)$, p_0 are the pressures at levels z and at the Earth's surface; $0 < x \leqslant 1$.

For absorption bands which have an irregular structure, it is desirable to use the Good statistical model [B.8], which is based on the assumption that the positions and intensities of absorption lines are random in nature, given by certain a priori distribution functions.

Extensive calculations of transmission functions for water vapor and carbon dioxide in the spectral range 500-100,000 cm^{-1} have been made by Plass, et al. [16,17], using a quasi-statistical model of molecular absorption bands (a random line distribution /26 is assumed only in a rather narrow spectral interval in comparison with the averaging interval). These calculations embraced quite a wide range of pressure (p = 0.01-1 atm), temperature (T = 200, 250, and 300 K) and mass of absorbing material (0.001-5 cm H_2O and 0.2-10,000 atm. cm of CO_2). The transmission functions were averaged over the different spectral intervals from 2.5 to 100 cm^{-1} (in [16,17] only data for $\Delta\nu$ = 50 and 100 cm^{-1} were used).

The results of the calculation (Figure 1.6, Curve 1) were compared with measured data for the transmission functions obtained in [18] (Curve 2) with a somewhat different spectral resolution. It can be seen that in specific cases (e.g., for the H_2O bands) the agreement of the curves cannot be considered satisfactory.
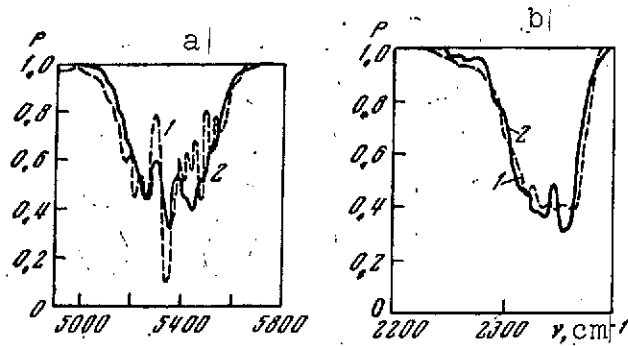
Figure 1.6. Examples of comparison of transmission functions
a- H_2O band at 1.8 μm (p = 765 mm Hg, m = 0.0483 cm in the experiment; p = 760 mm Hg, m = 0.05 cm in the calculation);
b- CO_2 band at 4.3 μm (p = 137 mm Hg, m = 0.195 amm cm); 1a, 1b-calculations of [20] and [21], respectively; 2- experiment [23]

Andreyev and Pokrovskiy [19], who made a similar comparison of the calculations [16,17] with data from laboratory experiments of [18] and [20], also observed substantial differences between the theoretical and experimental transmission functions.

The lack of reliability in calculating the selective absorption using band models has led investigators to seek empirical representations of spectrally averaged transmission functions for atmospheric gases.

If the averaging interval Δν spans the entire absorption band, as was done in the initial work of Howard, et al. [21], then the transmission functions can be described by a small number of parameters, which are obtained by approximating to the integral absorption

by the formulas:
$$A = \int_{\Delta v} (1 - e^{-k_v m}) \, dv$$

for weak absorption

$$A = cm^{1/s}(p + p_a)^k,$$

(1.18)

35

for strong absorption

$$A = C + D \log m + K \log (p + p_a).$$ (1.19)

Since formulas of type (1.19) can lead to absurd results for large m, another approximation was suggested in [22] for the integrated transmission functions $P = 1 - (A/\Delta v)$:

$$P(m, p) = \exp [- \alpha_0(p) m^{1-k_0(p)}].$$ (1.20)

The parameters α_0 and k_0 for the water vapor bands of m_{H_2O} (in cm), m_{CO_2} and m_{O_3} (in atm. cm) are shown in Table 1.2. We note that the parameter k_0 is practically independent of pressure and mass, and is close to the value 0.5 for small m and p (the "square root" law). However, for strong absorption bands k_0 varies when one goes to large mass. On the other hand, the parameter α_0 depends strongly on p, in fact

$$\alpha_0(p) = \bar{\alpha}_0 \left(\frac{p}{p_0}\right)^{\delta_0},$$ (1.21)

where $\bar{\alpha}_0$ is the value of α_0 at normal pressure p_0; and δ_0 is a constant whose values are given in the table for each band. For certain bands $\delta_0 \approx 1 - k_0$, so that Equation (1.20) can be rewritten in the form

$$P(m) = \exp\left[- \bar{\alpha}_0 \left(m \frac{p}{p_0}\right)^{1-k_0}\right],$$ (1.22)

i.e., the transmission function for these bands depends on the product of mass and pressure.

Recently new experimental and theoretical data have appeared on transmission functions for atmospheric gases. These functions, which are averaged over quite narrow spectral intervals Δv or measured with a specific spectral resolution, were obtained both

TABLE 1.2 *

Band centers λ, μm;	Parameters	P,mbar.									
		1	5	10	50	100	200	400	600	800	1000
0,94	α_0	0,03	0,04	0,05	0,08	0,10	0,12	0,14	0,16	0,18	0,19
($\delta_0 = 0,28$)	k_0	0,50	0,51	0,49	0,49	0,49	0,49	0,49	0,49	0,49	0,48
1,1	α_0	0,03	0,05	0,06	0,09	0,11	0,13	0,16	0,18	0,19	0,21
($\delta_0 = 0,27$)	k_0	0,49	0,50	0,49	0,48	0,50	0,49	0,50	0,5	0,48	0,47
1,38	α_0	0,12	0,19	0,24	0,39	0,48	0,64	0,74	0,89	0,96	1,18
($\delta_0 = 0,30$)	k_0	0,48	0,50	0,48	0,48	0,49	0,49	0,48	0,46	0,48	0,47
1,87	α_0	0,16	0,25	0,28	0,51	0,67	0,82	0,98	1,10	1,30	1,38
	$k_0 (m < 0,01)$	0,48	0,48	0,49	0,47	0,47	0,47	0,48	0,49	0,47	0,45
($\delta_0 = 0,29$)	$k_0 (m \geqslant 0,01)$	0,63	0,65	0,64	0,72	0,71	0,71	0,71	0,72	0,72	0,70
2,7 (H_2O)	α_0	0,38	0,54	0,61	0,82	0,92	1,03	1,16	1,24	1,30	1,35
($\delta_0 = 0,18$)	$k_0 (m < 0,01)$	0,48	0,47	0,49	0,47	0,46	0,46	0,49	0,49	0,47	0,50
	$k_0 (m \geqslant 0,01)$	0,68	0,47	0,70	0,70	0,70	0,70	0,70	0,70	0,70	0,70
6,3	α_0	0,41	0,61	0,71	1,00	1,15	1,34	1,56	1,72	1,84	1,92
($\delta_0 = 0,22$)	k_0	0,62	0,68	0,68	0,69	0,69	0,70	0,70	0,68	0,68	0,68
9,6 (O_3)	α_0	0,10	0,22	0,30	0,52	0,62	0,71	0,77	0,80	0,83	0,85
($\delta_0 = 0,31$)	k_0	0,48	0,47	0,47	0,58	0,60	0,63	0,66	0,68	0,69	0,69
15 (CO_2)	α_0	0,36	0,56	0,66	0,92	1,12	1,35	1,55	1,80	1,95	2,05
($\delta_0 = 0,23$)	k_0	0,66	0,71	0,71	0,74	0,77	0,78	0,78	0,75	0,73	0,70

* Translator's note: Commas in numbers represent decimal points.

for media with constant pressure and temperature along the
radiation path under laboratory or natural conditions (in the
ground layer of air), and also for a nonuniform atmosphere. The
results of extensive laboratory measurements, presented in [18,20],
have allowed empirical formulas of type (1.20) to be obtained
which are quite a good approximation to the transmission functions
for H_2O and CO_2 for a uniform medium in narrow spectral intervals.
The spectral behaviors of the parameters α_0 and k_0 so derived
from the data of [23] have been published in [22].

For a nonuniform medium one can use Equation (1.20) for the reduced mass of absorbing material (1.17), and the parameter $\varkappa$ which, in general, depends on $\Delta\nu$, is taken as constant in [20] for the whole of a given absorption band.

The data presented indicated that Equations (1.20) and (1.22) give quite a good description of the transmission of atmospheric gases in the entire range of change of mass of absorbing material and atmospheric pressure ordinarily used in practice. However, the use of these formulas with empirical parameters obtained from laboratory measurements to describe radiation absorption in the real atmosphere (both in the uniform ground layer, and in a nonuniform air column) requires experimental verification, especially for gases whose relative concentration varies along the light path. Such a verification was done from data on trans-
mission measurements in the ground layer of the atmosphere for the spectral region 0.3-1 μm in [8], and for the spectral region 1-5 μm, in [24,25].

Examples of comparison of natural (Figure 1.7, Curve 1), laboratory (Curve 2), and theoretical (Curve 3) transmission functions for the 4.3 μm CO_2 absorption band, for the two values of the ray path length L_0, are shown in Figure 1.7. (It is interesting to note that the considerable discrepancies in the long-wave wing of the 4.3 μm CO_2 band are due to absorption of radiation in the nitrous oxide band at 4.5 μm, which was not taken into account in the calculations, nor in the laboratory experiments.) Similar comparisons for the 0.76 μm O_2 bands are considered in Chapter 9.

A check of the empirical formulas for a nonuniform atmos-phere is complicated by the absence of reliable measurements both of the transmission functions, and of the concentration of absorbing material. In addition, when one goes to effective
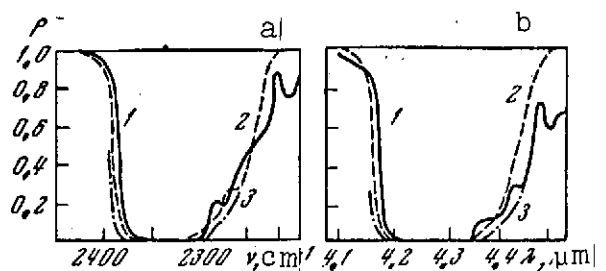
Figure 1.7. Comparison of the transmission functions in the CO_2 band of 4.3 μm 25:

a- L_0 = 777 m;   b- L_0 = 1909 m;   1,2- field and laboratory measurements, respectively;   3- calculations

masses or pressures in this case one has no assurance that additional empirical parameters are not required, dependent on the spectrally averaged interval and on the height of the observer, which greatly complicates the use of empirical formulas. Another difficulty in using empirical formulas obtained for some fixed spectral resolution is that different spectral resolutions are required in practice. In any case a number of contemporary problems of atmospheric physics, in particular, inverse problems (see Part II of this book), requires precise data on atmospheric transmission in narrow spectral ranges.

These circumstances have been one reason for using direct methods for calculating atmospheric gas transmission functions, based on molecular absorption band coefficients, describing the intensity and half-width of lines, as well as the shape of the lines. These calculations, which require the use of high-speed computers, are done for some practically achievable range of variation of mass of absorbing material and pressure in a uniform medium, or for different levels in a nonuniform atmosphere, while the relative concentration of the absorbing substance is constant. Such calculations of transmission functions in a

uniform medium at several values of mass and pressure of water vapor have been performed, for example, in [26] for the 2.7 μm H_2O band.

As can be seen from Figure 1.8, which shows a comparison of calculated and measured transmission functions taken from a balloon at a height of 13.7 km with a Sun zenith-distance of 71°, somewhat better agreement is obtained than in the model calculations, although there are noticeable differences, as before, in individual sections of a band. The authors of [26] were obliged to choose particular values of water vapor concentration and effective pressure to achieve satisfactory agreement. Therefore, on the basis of this comparison, one naturally cannot draw any conclusions as to the reliability of the parameters assumed in the calculations.

In order to increase the reliability of these calcula- tions, the system of molecular constants must produce good agreement between calculated and experimental transmission functions, for both a uniform and a nonuniform medium, in either laboratory or natural conditions. We used the above approach in calculating transmission functions for the 0.76 μm band of O_2 (see Chapter 9).

Thus, having computed transmission functions with rather small spectral averaging, one can use these in three cases, namely, when the required spectral resolution does not exceed that assumed in calculating the averaging interval; when the medium and the absorbing substance have constant pressures and temperatures; and when the relative concentration of absorbing substance is constant, although the medium can be nonuniform.

However, this becomes impossible, if the relative concentration of absorbing material varies along the ray path (e.g.,|
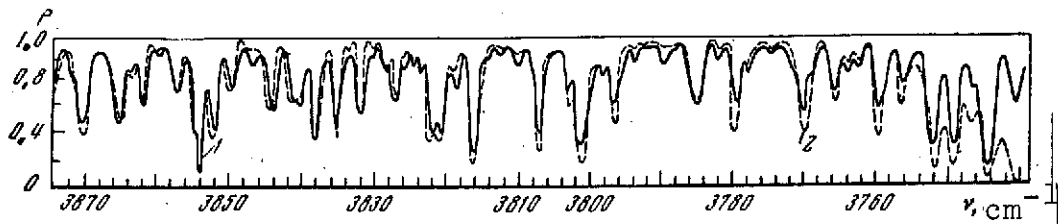
Figure 1.8. Comparison of transmission functions for H_2O in the 2.7 μm band, according to [19] p = 0.0691 atm; m = 0.0030 cm; T = 217° K; 1- theory; 2- experiment

for water vapor). In this case one must calculate transmission functions for average distributions of humidity and temperature, and express the variations in transmission in terms of the statistical characteristics of the vertical structure of the fields of these elements (see Chapter 3). We note, finally, that the question of aerosol absorption, for which some evaluations were made in [27-29], has not as yet received much study.

2.3._ Scattering_Index_

As can be seen from the radiative transfer Equations (1.1)-(1.4), the scattering index $\gamma(z, \varphi)$, which depends in quite a complex way on z and φ in the real atmosphere, plays an appreciable part in forming the radiation field. In addition, the index varies so strongly as a function of the aerosol particle size distribution, (and also of the shape), that it is practically impossible to calculate γ in every specific case by Equations (1.1) – (1.4). Considering that the scattering index meets the greatest difficulty when one solves the transfer equation, it is appropriate to evaluate its actual effect on the angular structure of the solar radiation field.

One important step in this direction is to clarify the dependence of the radiative intensity I on the model scattering indices assumed in calculations, which allows us to represent possible range of variations of I and to identify the ranges of

scattering angle or spectral interval for which the index has a substantial effect. These relations will be examined below (see § 3) for the scattering indices measured by Foitzik and Zschack [30], in the ground layer of the atmosphere for different visibility ranges L (Figure 1.9).

A determination of the connection between an index and the angular distribution of radiation should be accompanied, not only by quantitive characteristics (e.g., the authors of [31] classified indices according to the degree of their asymmetry), but also sufficiently detailed criteria on the physical state of the atmosphere for which the measurements are made.   /30

Thus, based on a classification of scattering indices, obtained for diverse conditions in the ground layer [32-34]*, qualitative physical characteristics of the turbidity of the atmosphere have been determined. Also, empirical relationships were used in these references, connecting the indices with the scattering coefficient and with the particle size distribution functions. In addition, knowledge of a number of statistical characteristics of the angular structure of the indices allows us to evaluate quantitatively the variation of the scattering index in the ground layer of the atmosphere (see Chapter 3).

It is quite a complex matter to determine the variation with height of a scattering index, since measurements like these require the measuring equipment to ascend (it is very clear that ground measurements [4, 35] give a scattering index which is averaged for the entire atmosphere).

---

* We recall that [33] obtained matrices for scattering of light in the ground layer, and [34] gave the halo part of the index.
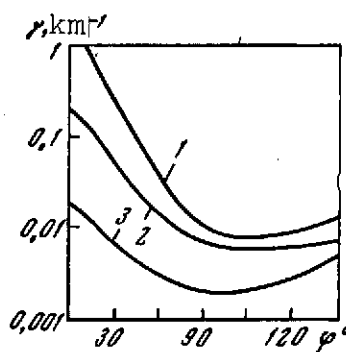
Figure 1.9. Scattering index, according to [33]
1- L = 5 km; 2- L = 20 km; 3- L = 100 km, φ is the scattering angle
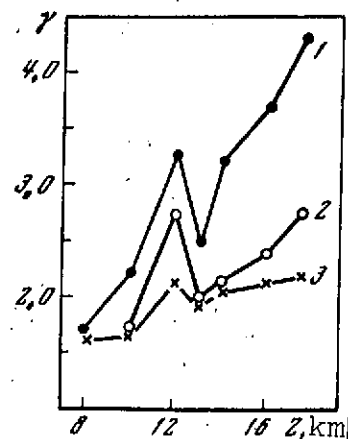
Figure 1.10. Vertical behavior of characteristics of the scattering index for the atmosphere according to [36] 1-3- λ = 0.635; 0.554 and 0.444 μm

The most reliable data on the vertical distribution of the scattering index up to a height of 17 km were obtained in [36] from airborne measurements of the brightness of the sky. An example of these measurements is given in Figure 1.10 (γ is in relative units; φ = 50°).

2.4. Reflectance of Natural Surfaces

The reflection of solar radiation plays a decisive role in the formation and the variation of the Earth's radiation field, since the reflectance of the ground surface and of cloud formations varies from 2-3 to 80-90%, both because of difference in the types of natural surfaces and type of clouds, and also because of the uncontrolled variation of the structure of these surfaces with time and place.

The spectral behavior of the reflectance in the visible and the IR ranges is also very variable, as was shown in [37-39]. An idea of the spectral dependence of the brightness coefficient of a number of natural surfaces can be obtained from Figures 1.11 and 1.12.
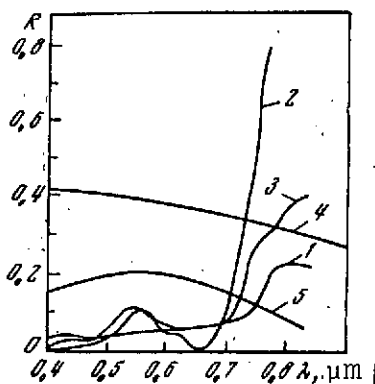
Figure 1.11. Spectral behavior of the brightness coefficient R in the visible and near IR, according to [37] 1- soil; 2- grass; 3- forest; 4- snow; 5- water
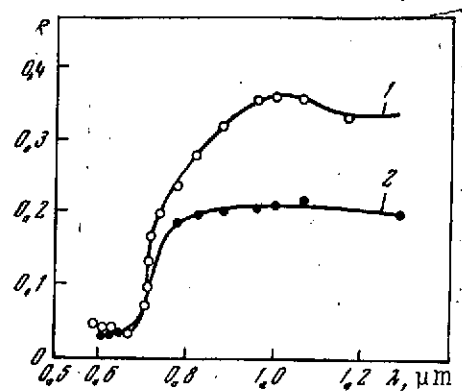
Figure 1.12. Spectral behavior of the brightness coefficient in the IR region of the spectrum, according to [38] 1- soil; 2- grass;

The reflection characteristics of surfaces depend in a complex manner on the direction of incidence of solar radiation and on the reflection angle. Experimental data show that the Lambert law does not hold for practically all real surfaces. Examples of brightness indices and certain surfaces illustrating the angular dependence are shown in Figure 1.13 [37-40]. The characteristics of reflection of solar radiation from clouds   /31 vary even more, as evidenced by the brightness indices and spectra for some types of clouds obtained in [41-44] (see Figure 1.29).

Since the optical parameters listed above for the atmosphere, clouds, and underlying surface, allow us, using the transfer Equations (1.1)- (1.4), to determine the spectral and angular distributions of the characteristics of the field of solar radiation reflected by the Earth, appropriate calculations for specific model atmospheres have been performed by a number of investigators. Analyzing these results and comparing them as far as possible with experiment, we can evaluate the role of each of the optical parameters considered, and from this kind of
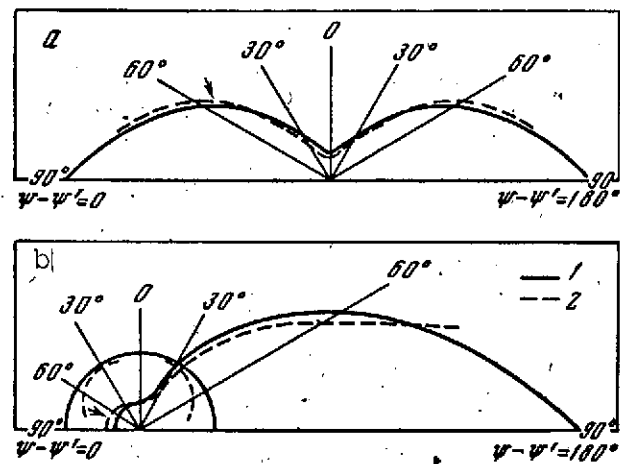
Figure 1.13. Brightness indices   a- fields of grain [37]; b- snow [40]:   1- measurements;   2- approximation by Equation (1.40).   Arrows show direction of incident radiation

analysis we can determine ways to seek the governing laws for the random fields of reflected solar radiation.

§ 3.   Reflected Radiation in the Visible (Pure Scattering)

The most detailed and numerous calculations of characteristics of the solar radiation field scattered in the Earth's atmosphere, as well as the majority of measurements, have been performed for the visible part of the spectrum. This is due, first, to the possibility of visual observations, associated with practical problems of determining the range of visibility of objects in the atmosphere and conditions in conducting astronomical investigations. Secondly, for this spectral region there are attractive possibilities for experimental investigations by photographic methods (this has been widely applied, for example, in aerophotography from different heights), and also photometric and spectrophotometric methods, thanks to the availability of high-sensitivity detectors (photomultipliers).

Thirdly, an important point has been the possibility of neglecting the comparatively weak absorption of solar radiation by ozone in the Chappieu (0.45-0.6 μm), oxygen (0.69 μm), and water vapor (0.72 μm) bands, i.e., to regard the atmosphere as a medium in which radiant energy of the spectral range 0.35-0.75 μm is scattered only by air molecules and by particles. Appreciable errors from neglect of absorption in weak bands can arise only for directions of propagation of the radiation close to horizontal (where the plane-parallel model of the atmosphere should never be used), or at high spectral resolution.

The neglect of weak absorption allows an appreciable simplification in the solution of Equations (1.1) - (1.4), since we can then put $\alpha_\nu \equiv 0$, and the basic dependence of I_ν on frequency can be expressed in terms of the optical thickness

$$\tau_\nu(z) = \int_0^z \sigma_\nu(t)\, dt. \tag{1.23}$$

If in addition we neglect the dependence of the scattering index and the brightness coefficient of the ground surface on ν, then the spectral composition of scattered radiation will be completely determined by the behavior of the optical thickness. This relation eliminates the need to solve the transfer equation for each frequency ν. It is enough to obtain a solution as a function of the optical thickness τ (with the other parameters given). Then the dependence of τ on ν, together with the spectral dependence of the direct solar radiation, determines the spectral behavior of I_ν.

This is the principle used to construct all solutions of the transfer equation in a purely scattering medium. Here we examine papers where these solutions were obtained for quite a wide (and comparable) range of variation of the optical parameters

46

of the atmosphere and the illumination conditions, reflection from the underlying surface, and observational directions.

3.1.　Models of the Scattering Medium

For a molecular atmosphere, described by a Rayleigh scattering coefficient (1.6) and a Rayleigh scattering index

$$\gamma_P(\varphi) = 1 + \frac{1}{2} P_2(\cos\varphi),$$

(1.24)

where $P_2(x) = (^1/_2)(1 - 3\,x^2)$ is a Legendre polynomial of second order, solutions were obtained in [45] for the transfer equations (1.1) – (1.4). An electronic computer was used, together with Chandrasekar functions [46] to make highly accurate calculations of $I^\uparrow$ and $I^\downarrow$, as well as the polarization characteristics of scattered radiation for various values of τ, ζ_0, θ and ψ. It was assumed that the   /33 underlying surface is orthotropic, i.e., it reflects according to the Lambert law (independently of the reflection direction), and the reflection is described by various values of the albedo A:

$$I^\uparrow(0) = \frac{A}{\pi} \int_{-1}^{\cdot} \, I^\downarrow(0, r') \cos\theta' \, d\omega'.$$

(1.25)

In the real atmosphere one does not find conditions which are similar in the visible part of the spectrum to a molecular model of a purely scattering medium. Nevertheless, this solution is of great interest, since it is something of a standard, with which one can compare both the results of measurements, and solutions of the transfer equations, obtained for conditions which, although not for very strictly defined optical parameters of the medium, are however closer to the actual conditions. Such solutions were obtained in [47-50], and later by Fraser [51].

The aerosol scattering was calculated in [47-48] by introducing empirical scattering indices [30] for different ranges of visibility and optical thickness varying from 0.1 to 0.8. The scattering indices were represented in the form of an expansion in Legendre polynomials

$$\Upsilon(z, \varphi) = \sum_{k=1}^{n} C_k(z) P_k(\cos \varphi),$$ (1.26)

where the dependence of C_k on z was assumed to be as follows: for the lower layer of the atmosphere, which makes up 75% of the total atmosphere in optical thickness, the coefficients C_k corresponded to strongly asymmetrical indices (L_0 = 1 -| 100 km). For the upper layer, comprising 25% of the optical thickness, C_k corresponded to a slightly extended index, typical for a very pure atmosphere (L = 200 km).

The underlying surface was assumed orthotropic, and its reflective properties were described by values of albedo A = 0.0.1; 0.2; 0.4; 0.6; 0.8.

Calculations of the radiative intensity from (1.1) - (1.4), obtained for four positions of the Sun (ζ_0 = 30, 45, 60, 75°), were used in the spectral region 0.35-0.7 μm. The radiative transfer equation was solved by the method of successive approximations, with an error which did not exceed 10-15%, even in cases of severe turbidity.

It is difficult to make practical use of the results obtained in [47-48], because they lack objective criteria which would allow one to determine the initial optical parameters for specific atmospheric conditions.

This defect was avoided to some extent in [49, 50]. They examined a closed model of the atmosphere, for which the optical characteristics were introduced in such a way that they could be determined using simple measurable parameters. For example, the authors of [49] proposed to take the optical thickness of the atmosphere $\tau^*(\lambda_0) = \tau(\infty, \lambda_0)$ and the horizontal visibility at the Earth's surface $L(\lambda_0)$ for wavelength $\lambda_0 = 0.55$ μm, as the parameters. The first of these can easily be expressed in terms of the transmittance of the atmosphere $e^{-\tau(\lambda_0)}$ while the second is very close to the integral range of visibility. The atmospheric scattering coefficient is represented as the sum of Rayleigh and aerosol coefficients

$$\sigma_\lambda(z) = a_0\left(\frac{\lambda_1}{\lambda}\right)^4 e^{-\alpha z} + b_0\frac{\lambda_0}{\lambda}e^{-\beta z}, \qquad (1.27)$$

where $a_0 = 0.0119$ km^{-1}, $\alpha = 0.125$ km^{-1} are the Rayleigh scattering parameters described above in an isothermal atmosphere (1.7): and b_0 and β are aerosol scattering parameters connected with $\tau^*(\lambda_0)$ and $L(\lambda_0)$ by the following relations:

$$b_0 = \frac{3.91}{L(\lambda_2)} - a_0; \qquad \beta = \frac{b_0}{\tau^*(\lambda_2) - a_0/\alpha} . \qquad (1.28)$$

It is easy to show that the optical thickness $\tau^*(\lambda_0)$ of this optical model of the atmosphere does not depend on $L(\lambda_0)$.

The atmospheric scattering index in [49] was accounted for in the form of a superposition of a Rayleigh index γ_p and an aerosol index γ_a.

$$\gamma_\lambda(\varphi) = \frac{1}{\tau^*(\lambda_2)}\left[\frac{a_0}{\alpha}\left(\frac{\lambda_0}{\lambda}\right)^4 \gamma_p(\varphi) + \frac{b_0}{\beta}\frac{\lambda_0}{\lambda}\gamma_a(\varphi)\right]. \qquad (1.29)$$

The aerosol indices in (1.29) were taken from [30] for several atmospheric conditions described by the parameter $L(\lambda_0)$.

TABLE 1.3*

Type of atmosphere		0,4	0,45	0,50	0,55	0,60	0,65	0,70	0,75	0,80
Molecular		0 376	0,217	0,151	0,104	0,071	0,055	0,039	0,029	0,021
Slightly turbid	measured	0,49		0,38	0,25	0,14		0,13		0,07
	calculated	0,55	0,40	0,31	0,25	0,21	0,18	0,16	0,14	0,13
Average turbidity	measured	0,66		0,43	0,30	0,21		0,13		
	calculated	0,62	0,46	0,36	0,30	0,25	0,22	0,20	0,18	0,16
Severely turbid	measured	0,95		0,59	0,5	0,44		0,46		0,25
	calculated	0,90	0,71	0,58	0,5	0,44	0,39	0,35	0,32	0,30

Column header above: λ, μm

* Translator's note: Commas in numbers represent decimal points.

The radiative transfer Equation (1.1) - (1.4) was solved by the Sobolev method [52], in which one can account for first order scattering quite exactly, and approximately for higher order scattering.

As was shown in [48], this method introduces considerable errors in determining the intensity of multiple scattered radiation, particularly at large optical thicknesses or for strongly asymmetrical indices, i.e., for large atmospheric turbidity. In addition, in spite of the well-known simplicity of the method, the calculations are quite laborious, in that one performs the calculation for each wavelength. Therefore the authors of [49] calculated the scattered radiation intensity only for $\lambda_0 = 0{,}55$, μm.

We have given a detailed description of the method of [49, 50], since, because of its closed form and the possibility of introducing optical parameters comparatively simply, corresponding to individual values of atmospheric conditions, it is

considered to be a method which makes it possible to calculate characteristics of a radiation field which are quite close to the real values. From this point of view we perform some analysis, both of the optical parameters themselves, and of the results of solution of the radiative transfer equation, obtained on the basis of the model [49, 50]. Airborne and ground measurements of radiative attenuation coefficients in the atmosphere (1.5) - (1.8) allow one to verify the assumptions of linear decay of $b_\lambda(z)$ with λ [n = 1 in Equation (1.8)], and the exponential law of its behavior with z, Equation (1.9).

An experimental check of these assumptions was performed in [6], in which it was shown that Equation (1.8) was fulfilled satisfactorily with n = 1 only in the lower layer of the atmosphere, 0-0.5 km, while an irregular spectral behavior of b_λ was observed at large altitudes. We note, however, that, according to the data of [8], n differs from unity even in the ground layer (see also [9]), while for a layer over water [7], the average scattering coefficient $\bar{b}_\lambda$ is approximated by Equation (1.8) with n $\approx$ 1.

As far as the vertical distribution of $b_\lambda(z)$ is concerned, according to the investigations of [6], the exponent in Equation (1.9) is satisfied with an error less than 50% in 78.5% of cases. A more reliable approximation is obtained using two or three exponential functions in (1.10), and even then only for the average profile of $\bar{b}_\lambda(z)$.

Nevertheless, the total optical thickness $\tau^*(\lambda)$, obtained by integrating the average values of $\bar{b}_\lambda(z)$ with respect to z, is described satisfactorily by the model [49,50]. By way of illustration, Table 1.3 shows a comparison of experimental values of $\tau^*(\lambda)$, taken from [6], with the results of calculations

of $\tau^*(\lambda)$ using the formula

$$\tau^*(\lambda) = \frac{a_0}{\alpha}\left(\frac{\lambda_0}{\lambda}\right)^4 + \left[\tau^*(\lambda_0) - \frac{a_0}{\alpha}\right]\frac{\lambda_0}{\lambda}, \qquad (1.30)$$

which is obtained by integrating (1.27) with respect to z from 0 to ∞.

The spectral composition of the reflected radiation depends mainly on $\tau^*(\lambda)$, and probably to a lesser extent on the spectral behavior of the scattering index (we shall omit discussion for the moment of the role of the spectral dependence of the brightness coefficient of the underlying surface).

However, since all the calculations in [49,50] were performed only for $\lambda_0 = 0.55$ μm and the result was then multiplied by the solar constant S_λ, the spectral distribution of the scattered solar radiation I_λ (without counting the radiation reflected directly from the ground surface) is exactly the spectral distribution of the solar radiation outside the atmosphere. The absolute values of I_λ for each wavelength depend only on the vertical distribution of optical thickness and on the index for $\lambda_0 = 0.55$ μm, i.e., the entire specific atmospheric situation is determined by the physical characteristics of the atmosphere only at that wavelength. This means that the postulates examined above regarding the spectral dependences of the optical parameters were not used, in fact, in the calculations in [49, 50]. Therefore, one might expect large differences between the calculated and actual distributions of the scattered radiation as regards the spectrum, particularly when there is weak reflection from the underlying surface.

A general defect of the work in [47-50] is neglect of polarization of scattered radiation in the aerosol atmosphere. Therefore, it is interesting to examine the data of Fraser [51], who calculated the intensity and the degree of polarization of

TABLE 1.4 *

Model	Optical thickness	Ratio of forward and back scatter- ing	Visibility range, km
Index V	0,2	1,8	100
Index VI	0,2	2,5	50
C₅	0,25	6,4	27
C₆	0,15	7,4	35
D₆	0,25	11,6	19

* Translator's note: Commas in numbers represent decimal points.

reflected solar radiation for two models of the aerosol
atmosphere and compared them with the results of [47].

In [51] the first model (C), which corresponds to continental
conditions, is characterized by a Yung type size distribution
(finely dispersed fraction), and the second model (D)- by a distri-
bution of coarser particles, mainly larger than 0.5 µm (ocean
conditions or industrial regions). The radiative transfer
equation for the Stokes parameters is solved by the Sekera
method [53] for the sum of the Rayleigh and aerosol scattering
matrices.   <u>/36</u>

The latter is computed using Mie theory for both models,
assuming spherical particles. A solution of the transfer equa-
tion is found in the form of a sum of Stokes parameters, calcu-
lated for Rayleigh scattering, and single scattering by the
aerosol atmosphere.

Neglect of multiple aerosol scattering in [51] does not

Page intentionally left blank

invalidate a comparison with the results of calculations [47], nor does it make it impossible to evaluate the effect of polarization on the intensity of reflected polar radiation. In addition, the atmosphere models assumed in both references are very different as regards the scattering index, although they are close as regards optical thickness (the optical characteristics of the models are given in Table 1.4, where V and VI are the numbers of the indices in [47], and the symbols C_5, C_6, and D_6 of the model of the atmosphere [51] correspond to wavelengths 0.503 and 0.625 μm).

In spite of these differences in the atmospheric models considered in [47-51], it is nevertheless profitable to compare the above methods of calculation, evaluate their validity and shortcomings, and to try to formulate methods of improving computational methods on the basis of existing methods. Here one should bear in mind simplifications which would allow results of calculations to be used in practical examples.

A clear idea of the comparative characteristics of the methods considered can be obtained from Table 1.5. It is easy to see that each method has definite advantages and shortcomings both from the viewpoint of introducing real optical parameters into the calculation, and also from the viewpoint of validity of the quantities being determined. A general shortcoming of these methods, as yet difficult to eliminate, is that the tables of data represent intangible material, even in cloudless atmospheric conditions (for which conditions alone the data are applicable)*.

* They are also applicable for dense layered clouds, considered as an underlying surface.

The application of these data in practice is complicated, not only by the fact that the input parameters of the tables are very complex for measurement, but also because these parameters vary strongly throughout the atmosphere. However, by comparing results of calculations for the atmospheric models considered, one can obtain some criteria for validity of the basic laws of the spectral and angular structures of characteristics of reflected radiation fields, and also their range of variation.

3.2. Spectral Composition of Reflected Radiation

As has been noted above, the spectral distribution of solar radiation scattered in the atmosphere, assuming neutral reflection from the underlying surface, is determined by the spectral composition of the solar radiation (see Figure 1.1) and by the dependence of the optical parameters (optical depth and index) on wavelength. If the dependence of the index on λ is neglected, then I_λ can be represented in the form of the product of S_λ and some function which depends only on τ_λ.

We shall compare the results of [47] and [49] for the optical parameters obtained as follows. In order to use [47] we take $\tau^*(\lambda)$ from the data of Rabinovich [6] for an atmosphere of average turbidity (see Table 1.3). Thus we can determine I_λ for any wavelength, if we properly choose scattering indices which are also input parameters of the tables [47]. The starting point for such a choice is closeness of the corresponding spectral indices given in [30] to the integral indices used in the calculations of [47].

After determining $\tau^*(\lambda_0)$ for $\lambda_0 = 0.55 \, \mu m$ with the help of Table 1.3, it is not difficult to use the tables of [49, 50] to

construct the function $I_\lambda^\uparrow$ for suitable values of the visibility $L(\lambda_0)$, typical for average turbidity (L = 20 and 10 km), although, as the calculations of [49,50] have shown, the radiation leaving the upper boundary of the atmosphere is practically independent of $L(\lambda_0)$.* As far as the scattering index is concerned, it is evaluated by the same method of calculation in [49] for $\lambda_0 = 0.55$ µm. But, since the scattering indices calculated in [47] and [49] were borrowed from the same source [30], they turn out to be very close for this wavelength.

Figure 1.14 shows the spectral intensities of reflected solar radiation, calculated by the three methods for $\zeta_0 = 60°$; $A = 0$ and 0.8; $\theta = 0$ and 75°. As one might expect, the spectral distributions of reflected radiation obtained in [47, 49] for A = 0 are different: while, according to the data of [49], $I_\lambda^\uparrow$ is an exact replica of the spectral distribution of solar radiation outside the atmosphere, in the other models the spectral distribution of reflected radiation differs substantially for different positions of the Sun and different angles of observation. It is interesting to comment on a number of details in this spectral behavior of $I_\lambda^\uparrow$ for the different models. For A = 0, $\theta = 0$ and $\lambda = 0.35$ µm, the value of $I_p^\uparrow$ (molecular atmosphere) is larger by a factor of two than the values of $I_a^\uparrow$ obtained in [47], and by a factor of four than the values of $\widetilde{I}_a^\uparrow$ of [49]. For $\lambda = 0.45 - 0.5$ µm $I_p^\uparrow \approx I_a^\uparrow$, and for $\lambda > 0.5$ µm $I_p^\uparrow$ is several times smaller than $I_a^\uparrow$. Similar relations between $I_p^\uparrow$ and $\widetilde{I}_a^\uparrow$ are encountered at somewhat larger values of λ.

---

* We note that in [49, 50] the maximum height for which $I_\lambda^\uparrow$ was calculated was 10 km, while in [47, 48] $I_\lambda^\uparrow$ was obtained for the upper boundary of the atmosphere. However, the atmospheric layers above 10 km do not significantly change the intensity of reflected radiation.

For A = 0.8 the results of calculations with all of the models converge, since the main contribution to $I^\uparrow_\lambda|$ is from reflection of direct solar radiation (we note that in the method of calculation in [49] the spectral behavior of attenuation of radiation directly reflected from the ground surface was accounted for).

These relationships can be explained by comparing values of $\tau^*(\lambda)$ assumed in the different models, for the same values of λ. For example, the results obtained in [49, 50] with $\tau^*(\lambda)/$ were underestimated for $\lambda < 0.55$ µm and somewhat overestimated for $\lambda > 0.55$ µm (see Table 1.3 for average turbidity). In comparing the intensities of reflected radiation in the molecular and aerosol atmospheres, one should bear in mind the difference in the scattering indices. Since Rayleigh back-scatter exceeds the corresponding aerosol scatter, $I^\uparrow_p|$ is larger than $I^\uparrow_a|$ in the shortwave region, where the optical thicknesses (λ) and $\tau_{a|}(\lambda)$ are comparable.   /39

The data obtained give an idea as to the possible variability of the spectral composition of solar radiation reflected from the Earth in the visible region of the spectrum. It is very obvious that reflection from the underlying surface plays the main part in the variations of $I^\uparrow_\lambda|$; the actual variations in the albedo can lead to changes in absolute magnitudes of $I^\uparrow_\lambda|$ of almost one and a half orders. The nature of the spectral distribution of $I^\uparrow_\lambda|$ also depends strongly on the value of the albedo. For a small albedo the intensity of reflected radiation in the aerosol atmosphere case varies only a little with λ. This is due to the complex interactions of spectral distributions of direct solar radiation with the optical thickness of the real atmosphere. For an increase in A the spectrum of reflected radiation becomes
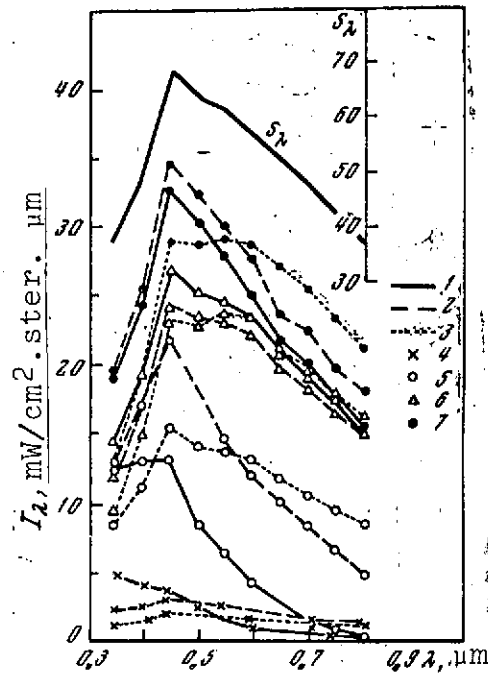
Figure 1.14. Spectral behavior of the intensity I_λ^* for molecular and aerosol models of the atmosphere with $\zeta_0 = 60°$, $\psi = 0°$
1- according to [45]; 2- according to [47]; 3- according to [49]; 4- $A = 0, \theta = 0; 5 - A = 0, \theta = 75°; 6 - A = 0.8, \theta = 0; 7 - A = 0, \theta = 75°$
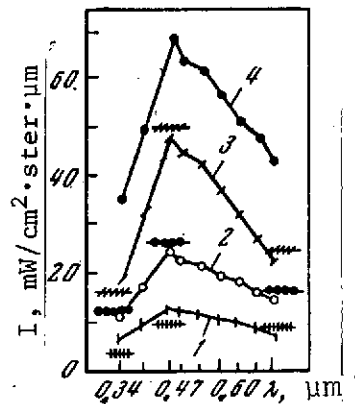
Figure 1.15. Comparison of theoretical and experimental distributions (sections of straight lines) of the spectral brightness of the Earth: 1- A = 0.25; 2- A = 0.4; 3- A = 0.8; 4- solar spectrum $\zeta_0 = 50°$

increasingly similar to the solar spectrum, because of the
increase in the contribution to $I_\lambda|$ of direct solar radiation
immediately reflected from the underlying surface, whose albedo,
under our assumption, is independent of λ.

However, the reflection of the majority of actual surfaces
has a pronounced spectral dependence, which varies strongly with
the condition of the surface. For this reason the spectrum
can vary so capriciously (see Figure 1.11 for a herbaceous|
covering), that the effects of radiation scattering in the atmo-
sphere are not important in forming the spectral behavior of
the reflected radiation.

The spectral distribution of reflected radiation depends
also on the position of the Sun and the angle of the observation.
These dependences can be explained by superposition of the
spectral nature of the immediately reflected direct solar radia-
tion (which increases with wavelength, if the reflection is
neutral), and the radiation scattered in the atmosphere, which,
generally speaking, decreases with wavelength.

The data presented on the spectral structure of the field
of solar radiation reflected by the Earth can be used to evaluate
the range of variation of the energy characteristics of the field.
These data have been used, in particular, to investigate and
calibrate two narrow-angle telephotometers (view angle $\sim 3°$),
mounted on the AES Kosmos 149 [B.29]. Each of the telephotometers
measured the absolute intensity of the solar radiation reflected
by the Earth in three spectral intervals of width 50 $\overset{o}{A}$: the
first in the range 0.34 ($\Delta\lambda = 100$ $\overset{o}{A}$): 0.47 and 0.74 μm, with
scanning in a plane perpendicular to the satellite velocity vector,
and the second in the H_2O 0.72 μm and the O_2 0.76 μm absorption
bands and in the range 0.74 μm, with scanning along the flight

(a detailed description of the experiment of Kosmos 149 is given in [B.30, B.31]). A comparison of the results of measurements with theoretical spectra of reflected solar radiation under comparable conditions of atmospheric illumination and reflection of the underlying surface is illustrated in Figure 1.15 (the reflection characteristics taken were the brightness coefficient of a test surface at the nadir $R_\lambda(0) = I_{meas}/S_\lambda \cos \zeta_0$). <u>/40</u>

The calculated values of the absolute brightness of the Earth in the corresponding sections of the spectrum agreed satisfactorily with the experimental data. The scatter in the latter for the same conditions of illumination and reflection fell within the measurement error and the possible variations in the turbidity of the atmosphere (in particular, the measured brightnesses I_{meas} for $\lambda = 0.34$ μm proved to be low in comparison with theory, which can be due to systematic error of the instrument). The analysis made justifies the conclusion that the model atmospheres adopted in [47-50] and the methods of computation give quite a valid determination of the spectral distribution of solar radiation reflected by the Earth in the visible part of the spectrum.

3.3. Angular Variation of Reflected Radiation

The angular distribution of solar radiation reflected by the Earth, i.e., the dependence of the intensity I_λ on the angle of incidence of the direct solar radiation and of the direction of observation, is determined by the following physical parameters: the scattering index, which is connected with the particle size distribution at different atmospheric levels; the optical thickness in the directions of incidence of solar radiation and observation of the scattered radiation; and the brightness coefficient of the reflecting surface.

The latter factor greatly complicates analysis of the angular distribution of reflected radiation. Therefore, we first consider reflection of an orthotropic surface with different albedo values,

and this is very reasonable, since the calculations in the papers analyzed [45, 47-51], were performed for precisely this kind of surface. It is natural to begin by considering the special case of an absolutely black surface with A = 0 (the ocean can be considered to approximate to such a surface if the height of the Sun is not too low), when the angular behavior of the reflected radiation is determined only by scattering in the atmosphere.

A comparison was made in [54] of the angular behavior for a molecular atmosphere [45] with $\tau^* =$ 0.2 and 0.6 and for models of a slightly and a highly turbid atmosphere [47], described by the same values of τ^*, and with aerosol scattering indices appropriate for slight and high turbidity in [47] these were denoted by subscripts VI and VIII). The dependences of I, expressed in relative units *, on the angle θ in the plane of the solar vertical (ψ = 0 is the azimuth of the Sun) are shown in Figure 1.16. For both small and large values of τ^*, the differences in the angular behavior of $I(\theta)$ for these atmospheric models turn out to be considerable, which is confirmed also by the comparisons made by Arking [55] between the theory of [45, 47] and the experimental results on the Tiros IV satellite (Figure 1.17). Figure 1.16 shows that the angular distribution of the Earth's brightness varies with the atmospheric turbidity, the position of the Sun, and especially with variation of the albedo of the underlying surface. This explains some of the laws governing the angular behavior of reflected radiation.

For A = 0 the intensity of radiation increases with increase of the angle θ, especially in the half-plane ψ = 0, although for the molecular atmosphere the Earth is brighter (at $\zeta_0 = 30°$) and still brighter (at $\zeta_0 = 75°$) in the opposite azimuth. The minimum of brightness for $\zeta_0 = 75°$ is obtained at the nadir, and for $\zeta_0 = 30°$ it differs from the nadir by 15-30° on the ψ = 0 side. /42

---

* To obtain I_λ in absolute units one must multiply I by the solar constant S_λ for wavelengths corresponding to the given τ^*, and γ.
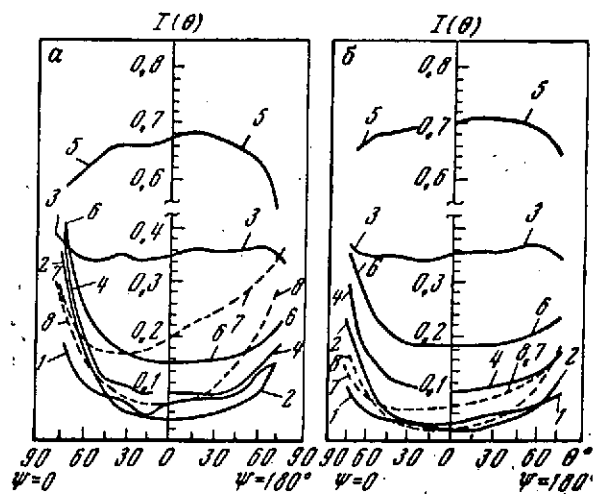
Figure 1.16. Angular behavior of relative intensity of reflected solar radiation for the molecular (broken lines) and aerosol (solid lines) models of the atmosphere

$a - \tau^* = 0.8$; $\delta - \tau^* = 0.2$. $\zeta_0 =$
$= 30$ and $75°$. $1,2 - A = 0$; $3,4 -$
$A = 0.4$; $5,6 - A = 0.8$; $7,8 -$
$A = 0$
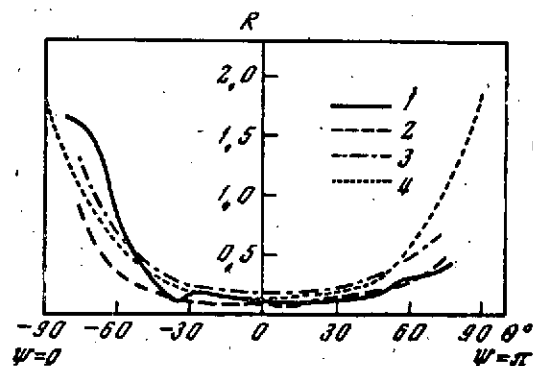
Figure 1.17. Integral brightness coefficients over the ocean
1- measurements [55]; 2- calculations [47] with $\tau = 0.2$; 3- calculations [47] with $\tau = 0.8$; 4- calculations [45] with $A = 0$
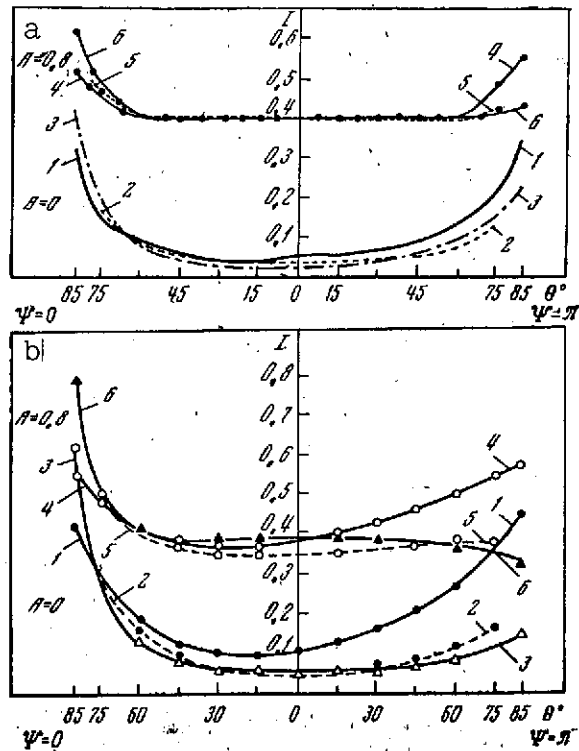
Figure 1.18.   Angular distributions of relative Earth brightness
   a- $\tau^* = 0.2$;   b- $\tau^* = 0.5$. $\zeta = 60°$; 1,4- model of molecular
   atmosphere [45];   2,5 and 3,6- models of the aerosol atmosphere
   from [47] and [49], respectively

All these laws stem mainly from the nature of the scattering
index assumed in a particular model atmosphere, and are easy to
explain when one considers the scattering angles which are obtained
for given values of θ and ζ_0 .   When the observer's plane differs
from that of the solar vertical, the angular distributions of
$I(\theta)$ presented in Figure 1.16 are smoothed out, but their
character does not change.

The parameter $I(\theta)$ undergoes a much greater transformation
with increase of A.   It follows from Figure 1.16 that, with
increase of A for small ζ_0 , we go from an increase of brightness
towards the horizontal ("limb brightening") to a practically
complete independence of the reflected radiation on θ (for A = 0.4)
or even to "darkening" of the horizontal (for A = 0.8).   For large
values of ζ_0 the nature of $I(\theta)$ does not vary for any values of A.

64

It is noteworthy that there is some convergence of the angular distribution of the Earth brightness for the different atmospheric models, as ζ_{0j} increases and τ^* decreases, especially for large A. This process is illustrated in Figure 1.18, which shows curves of the angular behavior of the relative intensity of reflected solar radiation for the molecular [45] and the aerosol atmospheric models considered above [47, 49]. Practically complete agreement for $I(\theta)$ is obtained with the values calculated from tables in [47, 49]. This is evidence of the validity of the general nature of the angular structure of the field of reflected solar radiation, which is determined by the atmospheric models adopted in [47, 49], and by the calculation methods. The description of the variation of the angular behavior is confirmed by the results of measurements of Earth brightness, obtained using a telephotometer mounted on the AES Kosmos 149 [B.29, B.30], which scanned along the flight trajectory and measured the intensity of reflected solar radiation in the 0.74 μm spectral region. The stabilization of the satellite was good enough to allow determination of the measurements of the same section of the Earth viewed by the telephotometer at different angles during successive scans. A comparison of the experimental and theoretical angular distributions of the intensity of reflected solar radiation, obtained using Kosmos 149, in the spectral region 0.74 μm, is shown in Figure 1.19. Within the natural scatter of the empirical quantities, the measurements confirm the transformation of $I(\theta)$ with variation of A. Here it should be borne in mind that the experimental data were obtained for the azimuthal plane, which is almost perpendicular to the plane of the solar vertical. This is probably the reason why the empirical curves $I(\theta)$ in Figure 1.19 are close to the theoretical data corresponding to an orthotropic model of the reflecting surface. Similar results of comparing calculated and averaged results of measurements of cloud brightness from the satellite Tiros IV in the spectral ranges 0.55-0.75 and 0.2-6 μm [56] are shown in Figure 1.20.
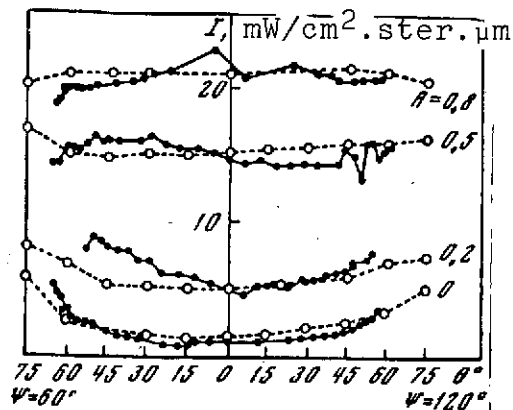
Figure 1.19. Comparison of theoretical (broken lines) and experimental (solid lines) angular distributions of the intensity of reflected solar radiation
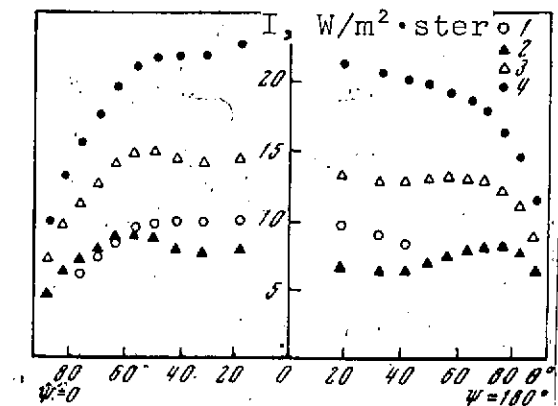
Figure 1.20. Angular distributions of the solar radiation reflected by clouds from [56] 1- measurements 2-4- calculations with $\tau^* = 4,19; 8,89$ and $16,8. \zeta_0 = 0 \div 25,8°$

The variations in the angular dependence of reflected solar radiation, illustrated in Figures 1.18 and 1.19, can be explained by the different relationships of the two components of the Earth's brightness: the direct solar radiation, immediately reflected from the ground surface and attenuated by the atmosphere, and radiation which is multiply scattered in the atmosphere.

For small A the contribution of the first component is small; the increase in the Earth brightness towards the horizon is associated with increase in the layer of haze and therefore of the second component.

For average values of A and small ζ_0, the contribution of the first component increases so much that the multiple scattering scarcely compensates for its attenuation in the atmosphere in the backward path towards the observer. As a result practically neutral behavior of $I(\theta)$ is obtained.

For large A and small ζ_0 the contribution of radiation immediately reflected from the underlying surface increases so much that attenuation of this energy along the path to the observer for large θ is no longer compensated for by multiple scattering of the radiation by the atmosphere and a decrease of brightness towards the horizon is obtained. But if ζ_0 is large, then, because of decrease of the incident flux of the direct solar radiation by the factor ζ_0, the contribution of the directly reflected solar radiation will not be so large, and the nature of the angular dependence of $I(\theta)$ will be the same as before (I increases with θ).

The role of the scattering index has already been noted above when we compared the brightness of the molecular and aerosol models of the atmosphere. Since the calculations in [47] were carried out for different indices, but with the other parameters fixed, we can also evaluate the effect of variation of the aerosol scattering indices. The angular distributions of reflected radiation for scattering indices with different degrees of asymmetry are shown in Figure 1.21. The differences associated with the index are small: the relative differences reach 30% for $A = 0, \zeta_0 = 30°$ for indices VII and VIII $(\tau^* = 0.6)$. An increase in the turbidity of the atmosphere or of the albedo leads, as one would expect, to smoothing out of the effects of the indices.

One can obtain an idea as to the role of the scattering index and polarization of light in the angular structure of the field of reflected solar radiation from the work of Fraser [51], who performed calculations for scattering matrices corresponding to some specific particle size distribution functions, and compared these calculations with the data of [47] (Figure 1.22). It can be seen that polarization does not affect the basic laws of the angular behavior. As far as more detailed differences are concerned, they cannot be explained by polarization effects
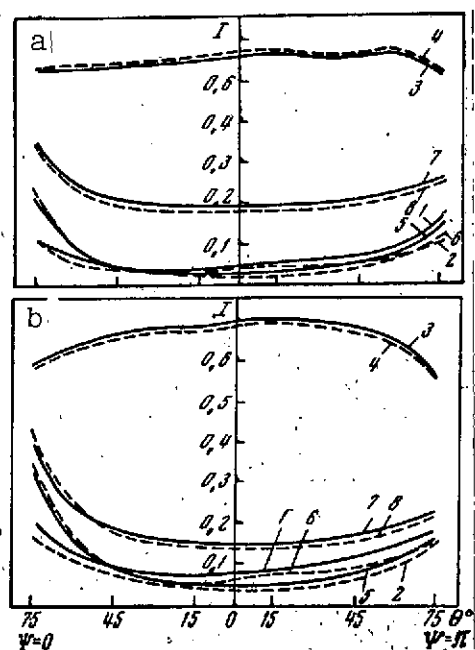
Figure 1.21. Angular behavior of intensity of reflected radiation for different scattering indices (denoted by Roman numerals), from [47] a- $\tau^* = 0.2$ (V, VI); b- $\tau^* = 0.6$ (VII, VIII) The solid curves V, VII: the broken curves VI, VIII, 1,2- A = 0, $\zeta_0 = 30°$; 3,4- A = 0.8, $\zeta = 30°$; 5,6- A = 0, $\zeta_0 = 75°$; 7,8- A = 0.8, $\zeta_0 = 75°$
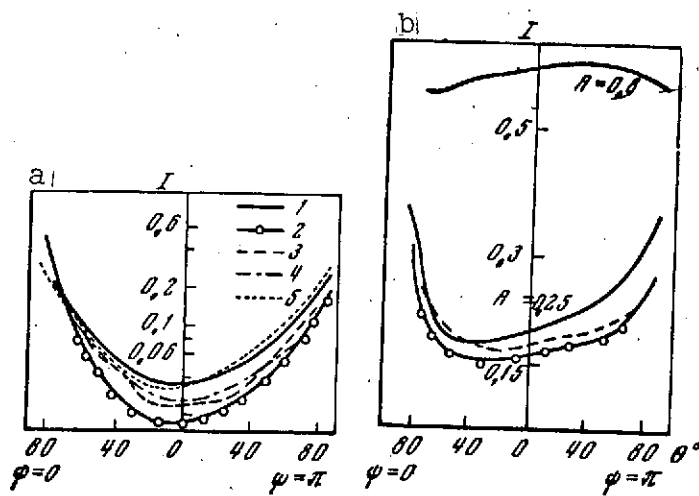
Figure 1.22. Comparison of the angular behavior of the reflected solar radiation a- $\tau^* = 0.2$, $\zeta = 75°$, A = 0; b- $\tau^* = 0.15 - 0.25$, $\zeta_0 = 36.9$, A = 0.25 and 0.8.

1,2- calculations of [51] for $\lambda = 0.5$ and 0.625 μm, respectively; 3,4- calculations of [47] for indices VI and V, respectively; 5- Rayleigh index

68

alone, since the atmospheric models used in [47,51] are not the same. The differences decrease as the albedo of the underlying surfaces increases, and for A = 0.8 the curves of $I(\theta)$ practically coincide, which is in complete agreement with the dependence considered for the angular behavior on the index albedo.

All the conclusions presented above refer to the case when the Lambert law holds. However, the tables calculated in [47-50] allow us to introduce a brightness coefficient and to calculate the immediate reflection of direct solar radiation from a nonorthotropic surface exactly, and the reflection of multiply scattered radiation approximately (in § 6 we consider this question in more detail).

The angular distribution of reflected Earth radiation is also affected by horizontal nonuniformity of the underlying surface, atmosphere, or clouds. To allow for horizontal nonuniformities one must solve a three-dimensional radiation transfer equation (see § 7).

Finally, for large values of θ and ζ_0 one cannot use the /45 plane model of the atmosphere, since the sphericity of the atmosphere begins to play a part under these conditions. We shall discuss this question in § 8.

In conclusion, we recall some of the results of measurements of solar radiation reflected by the Earth. In spite of the comparative simplicity of measurement, for the visible part of the spectrum, there are very few reliable absolute values of Earth brightness, particularly of spectral brightness. We know only of the results of airborne measurements of I_λ in the visible and the near IR spectral regions, obtained by Chapurskiy, et al. above different kinds of underlying surface and cloud [57]. The comparison made in [57] between experimental and theoretical

data showed satisfactory agreement.

Numerous experimental data on the field of absolute Earth brightness in several spectral regions of the visible and UV were obtained using Kosmos 149 (some of these data have been already mentioned above). These data have confirmed the validity of the basic characteristics of the field of reflected solar radiation, which is evidence of the similarity to actual conditions of the atmospheric models adopted in the calculations.

§ 4. Reflected Radiation in the UV, 0.20-0.35 μm (Absorption by Ozone)

4.1. Survey of Present Data

The solar radiation in the UV spectrum from 0.20-0.30 μm is strongly absorbed by ozone, present in the atmospheric layer from 10-50 km, and practically none reaches the Earth's surface. In addition, this radiation is strongly scattered by air molecules and aerosols, even in the rarified atmosphere lying above the ozone layer. Therefore, some fraction of solar energy in this spectral range is reflected by the atmosphere to outer space, and does not reach levels where the concentration of ozone is high.

However, until recently, the question of the spectral, angular, vertical, and spatial distributions of this energy had not been considered in geophysics. The reason was the absence of radiation measurements at large heights. For this reason, and also because of the difficulties in calculation, no computations were made of scattered UV radiation in the ozone absorption region.

The use of rockets and satellites to probe the atmosphere above the ozone layer has allowed experimental investigations

to be performed, and has also stimulated calculations of the Earth's brightness in this spectral range. Spectral measurements have been made of the absolute intensity of solar radiation reflected by the Earth, in the spectral range 0.22 to 0.33 μm with a resolution of 14 $\overset{\circ}{A}$, on the satellites Kosmos 45 and Kosmos 65 [58-60], and photographic data were also obtained in the spectral regions 0.255 μm (resolution of 140 $\overset{\circ}{A}$) and 0.284 μm (resolution 70 $\overset{\circ}{A}$) on the USA satellites [61, 62]. The spectral brightness of the Earth in the range 0.15 - 0.32 μm was obtained with a resolution of 4 $\overset{\circ}{A}$ at various heights, from 28 to 124 km, using rockets [63]. The literature also has results of rocket measurements of brightness in the spectral ranges 0.22 and 0.26 μm [64], and measurements on the X-15 aircraft at a height of about 60 km for λ = 0.24, 0.26, and 0.28 μm [65]. These measurements, and the results of calculations of reflected intensity of UV radiation I_λ [66-68], are evidence as to the considerable variation of the intensity of reflected radiation, due mainly to the variations in the vertical distribution of ozone *. To explain the variation of I_λ we draw mainly on the results of calculation, using experimental data to estimate the validity of the atmospheric model adopted in the theoretical investigations.

/46

Detailed calculations of the intensity of radiation in the interval 0.20 - 0.32 μm, scattered by the Rayleigh atmosphere to outer space, for various positions of the Sun and directions of observations, and several vertical distributions of ozone concentration, have been made by Green [66]. He restricted consideration to single scattering, and all the physical parameters

---

* However, this does not exclude the possibility that these differences are associated with the special features of the methods of specific calculations or experiments. Unfortunately, the matter of method is not discussed in sufficient detail in the papers cited.

(vertical distribution of ozone concentration and air density, and the dependence of absorption[*] and scattering coefficients, and of solar radiation on wavelength) were approximated by analytical expressions. This allowed him to express the intensity of outgoing radiation in analytical form.

It should be noted that one must account for high-order scattering in the wings of the ozone absorption band and for large optical path lengths of UV radiation. In addition, for these conditions an appreciable part is played by scattering of radiation by aerosols in the high layers of the atmosphere (meteor trails, cosmic dust, and noctilucent clouds). Probably one should not ignore also the phenomenon of luminescence in these calculations, which is responsible for reradiation of solar energy absorbed in the Schumann-Runge bands (1750-2000 Å), in the form of emission of the daytime sky in the region 1750-4500 Å (it was shown in [69] that this emission is greater than the Rayleigh scattering above 80 km).

An important special feature of radiative transfer in the atmosphere for the spectral regions examined, and one which complicates calculations, is the quite complex dependence of the ozone absorption coefficient on the wavelength λ and the height z, which manifests itself in the complex vertical structure of the optical depth of the atmospheric layer

$$\tau_\lambda(z) = \int_0^z [\jmath_\lambda(t) + a_\lambda(t)] \, dt \qquad (1.31)$$

---

[*] Later on (see [63]) Green also took absorption of radiation by molecular oxygen into account in the calculations.
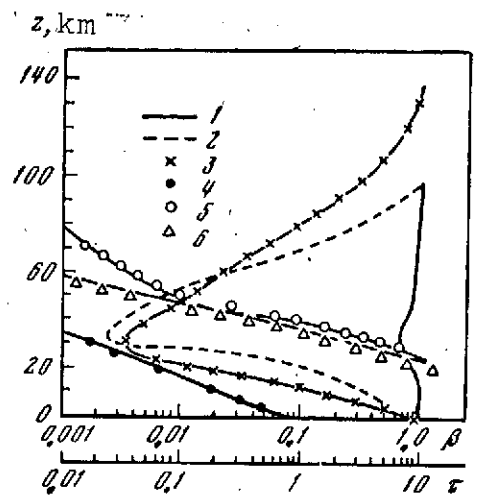
Figure 1.23. Vertical distribution of β (1-3) and τ (4-6); 1,4- for λ = 0.34 μm and m(z) after Johnson [71]; 2,5- for λ = 0.28 μm and m(z) after Johnson [71]; 3,6- for λ = 0.28 μm and m(z) after Green [66] for the standard O_3 profile.

and of the parameter

$$\beta_\lambda(z) = \frac{\sigma_\lambda(z)}{\sigma_\lambda(z) + \alpha_\lambda(z)}. \qquad (1.32)$$

As can be seen from Figure 1.23, in the strong absorption region (large τ_λ, which can reach 150) the effective reflecting layer of the atmosphere is optically thin, since the parameter β_λ differs from zero only in a narrow layer. When the absorption decreases this layer expands, and in the wings of the band (in the pure scattering region) the radiation field is formed by the entire atmosphere.

Some results of calculations of characteristics of the field of reflected radiation in the spectral range 0.20 - 0.35 μm for various positions of the Sun and directions of the observer, allowing for multiple scattering, have been given in [67, 68]. These calculations are based on a numerical method of solving the radiative transfer equation, developed by Germogenova [70]. The atmospheric model adopted in the calculations was determined

by the following parameters: air density varied exponentially
with height

$$\rho(z) = \rho_0 e^{-\alpha z} \mid \quad (\alpha = 0.125 \text{ km}^{-1}); \quad (1.33)$$

only Rayleigh scattering of radiation by air molecules and
absorption by ozone molecules was considered; the vertical
distribution of the ozone concentration $m(z)$ up to 70 km was
taken from data from the rocket measurements of Johnson [71],
and extrapolated to 100 km. It was also assumed that the under-
lying surface does not reflect in the spectral range considered,
and that there were no internal radiative sources in the atmo-
sphere*.

References [67, 68] have calculated the intensity of the
ascending $I_\lambda^\uparrow \mid$ and descending $I_\lambda^\downarrow \mid$ radiation at the nodal points τ
for directions θ = 10, 23, 36, 48, 60, 70, 80,85, 89, 90°, ψ =
0 to 180°; ζ_0 = 0, 30, 60, 80° at chosen wavelengths in the
region 0.20-0.35 µm, with a pitch of $\Delta\lambda = 0.01$ µm.

4.2. Spectral Distribution of Outgoing Radiation

An example of the spectral distribution of the intensity
of outgoing radiation in the spectral range 0.2 - 0.35 µm, for
the case $\zeta_0 = 0$; $\theta = 10°$ obtained in [67], is shown in Figure 1.24.
The figure shows similar calculations of Chapman, Green, and
other authors, as well as experimental data on $I_\lambda^\uparrow \mid$, obtained
by means of rockets and satellites, which allow the variation
of $I_\lambda^\uparrow \mid$ to be evaluated. The overestimate of Curves 1 and 2 in

---

* In fact, in the long-wave part of the O_3 band (λ > 0.3 µm),
reflection from the underlying surface cannot be neglected.

comparison with Curve 3 of Figure 1.24 arises from the fact that the distributions assumed in Chapman's calculations and in [67] diminish more rapidly at large heights, than the standard distribution m(z) used by Green [66]. This entails an opposite behavior for the parameter $\beta_\lambda(z)$ with height, which is responsible for an increase in the effective thickness of the atmospheric layer which scatters the solar UV radiation backwards, and therefore, for a growth in the intensity $I_\lambda^\uparrow$. We note that because $I_\lambda^\uparrow$ is so sensitive to variations of m(z) in the O_3 bands, the measurements of $I_\lambda^\uparrow$ are used to determine the ozone concentration at large heights (see, for example, [60, 62, 63]).

Another probable cause for the reduced values of $I_\lambda^\uparrow$ in [66] may be the neglect of multiple scattering. However, a special calculation of $I_\lambda^\uparrow$ for the Green model has shown that multiple scattering makes a negligible contribution for λ = 0.25 µm, although this contribution is appreciable even for λ = 0.28 µm, and it reaches 70% of the single scattering for λ = 0.32 µm (see the points on Figure 1.24).

By comparing the theoretical curves we see that the intensities of the reflected radiation at their minimum values differ by a factor of 3 or 4, and taking account of all Green's results [66], by an order of magnitude 0.001 - 0.01 mW/cm^2.ster.µm. /48 The data of measurements of brightness, obtained from satellites and rockets in the above sections of the UV spectrum, also differ by a factor of 2 or 3. It turns out that each of these values is close to $I_\lambda^\uparrow$ in an appropriate section of the spectrum of one of the calculated curves present in the figure. The spectral measurements of brightness of [59] do not exhibit such large variations in brightness, expecially in the strong absorption region.
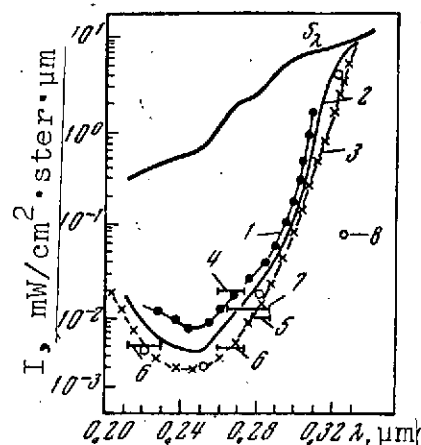
Figure 1.24. Distribution of intensity of reflected solar radiation 1- calculation of Chapman [61]; 2- calculation of Germogenova [67]; 3- calculation of Green [66]; 4,5- satellite measurements of Friedman [61] and of Rawcliffe [62]; 6,7- rocket measurements of Mazefield, et al. [63]; 8- allowing for multiple scattering in the Green model [66]. S_λ is the smoothed curve of solar radiation outside the atmosphere

Thus, the available measurements in the literature are not sufficient for a comprehensive evaluation of the limits and causes for changes in the spectral brightness of the atmosphere in the UV region. However, in comparing the results of satellite, rocket, and aircraft measurements (see Table 1.6), one cannot ignore the fact that the rocket and aircraft data in the central part of the ozone band (0.24-0.26 μm) are somewhat low in comparison with the satellite measurements. For example, for the region $\lambda = 0.24$ μm $I_\lambda = 0.1 \cdot 10^{-3}$ from the aircraft data of [65]; /49 $5 \cdot 10^{-3}$ from rocket measurements of [63], $10 \cdot 10^{-3}$ mW/cm^2·ster·| μm from the satellite measurements of [59]; and for the region $\lambda = 0.26$ μm, respectively $I_\lambda = 1 \cdot 10^{-3}$ from [65], $5 \cdot 10^{-3}$ from [59], and even $20 \cdot 10^{-3}$ mW/cm^2 ster·|μm from the satellite measurements of [61]. The most plausible explanation of these ratios is that, in the strong ozone absorption region, the UV radiation reflected by the Earth results from scattering at quite large heights, not reached by the X-15 aircraft [65] and the lower altitude rockets [68]. This fact is clearly illustrated by the transformation of the spectral brightness curves obtained in the rocket ascent of

[63], and is confirmed by calculations of the vertical behavior of the brightness in the different ozone sections [68].

A possible cause of the above discrepancies is also additional radiation from fluorescence [69]. It is true that, according to an estimate in [69], the fluorescent energy averaged over the spectral range 0.2-0.3 µm does not exceed 10^{-3} mW/cm^2·|ster·| µm, which is several times less than the above differences. However, there is as yet no information on its spectral distribution, apart from the information which one gets by considering the spectra obtained in [59].

4.3. Calculation of Aerosol Scattering

Since very little is known of the distribution of aerosols with height and particle size, and also their optical properties, particularly in the upper layer of the atmosphere, we can make only nominal evaluations of aerosol scattering of UV radiation. It is interesting to examine scattering by such objects as noctilucent clouds or meteor trails, which have an optical thickness considerably greater than that of a corresponding molecular layer. Taking into account that the aerosol scattering index is considerably elongated in the small scattering angle region, we can expect that, for specific relative locations of the Sun and the observer, the intensity of UV radiation scattered by the aerosol layer to outer space will be appreciably greater than the intensity of the molecular scattering. In other words, against the very weak background which is determined by scattering of atmospheric molecules in the central part of the band, for example, at λ = 0.25 µm, in daylight conditions, one can observe luminous aerosol layers of the type of noctilucent clouds or meteor trails, if one carried out appropriate measurements of outgoing radiation.

TABLE 1.6. INTENSITY OF REFLECTED SOLAR RADIATION $I_\lambda^\uparrow$

(mW/cm^2.ster. μm) AND BRIGHTNESS COEFFICIENT r_λ (in %) **

Calculations			Measurements					
References	$I_\lambda^\uparrow \cdot 10^3$	r_λ	Method of measurement	λ, μm	Δλ	ζ_0, deg.	θ, deg.	$I_\lambda^\uparrow \cdot 10^3$
[65]	2	0.3	Satellite [61]	0,255	140	49	0	20
			" [62]	0,284	70	0	0	9
			" [59]	0,24	14	8—69	7	6—11
			The same	0,25	14	8—69	7	5
[60]	7.5	1.1	"	0,26	14	8—69	7	5—10
[60]	3	0.4	"	0,27	14	8—69	7	4—17
[65]	3	0.4	"	0,28	14	8—69	7	2—10
			Rocket at height 40 km [63]	0,24	4	60	60	1,0
[66]	4.5	0.6	Rocket at height 70 km [63]	0,24	4	60	60	1,5
[59]	3	0.4	Rocket at height 100 km [63]	0,24	4	60	60	6
			Rocket [66]	0,26	100	22	0	5
			The same	0,27	200	—	—	10
			Aircraft [65]	0,24	—	48	30	0,1
			The same	0,26	—	48	30	1
			"	0,28	—	48	30	10

*Notes: The calculations are for $\lambda = 0.25$ μm; $\zeta_0 = 0$; $\theta = 0$ ($S_\lambda = 0{,}71\,\text{mW/cm}^2 \cdot \text{ster} \cdot$ μm). The measurements are $I_\lambda^\uparrow$ for various λ, Δλ, ζ_0 and θ obtained in the experiments.

** Translator's note: Commas in numbers represent decimal points.

Calculations of $I_\lambda^!$ have been made to verify this hypothesis for the case when there is an aerosol layer (noctilucent clouds) between 75 and 80 km. The particle sizes a of the noctilucent clouds were taken from data of direct rocket soundings of noctilucent clouds [72]: $a \approx 0.1$ µm, and $N = (4-30) \cdot 10^{-4}$ cm^{-3}, which corresponds to a total optical thickness of 0.005, which was also assumed in the calculation (the molecular optical thickness turned out to be an order less). The parameter β_λ in this layer was taken to be unity. The scattering index, corresponding to the value $2\pi a/\lambda = 2.5 \ (\lambda = 0.25$ µm), was assumed in the form of an expansion (1.26) of ten Legendre polynomials (the series coefficients were taken from the tables in [73]).

A comparison of the angular behavior of $I_\lambda(\theta)$ for Rayleigh and aerosol scattering, for two values of λ shown in Figure 1.25, shows that for small ζ_0, and also in the wing of the band ($\lambda = 0.34$ µm), the Earth's brightness with noctilucent clouds present is even several times less than that for the purely molecular atmosphere.

The apparent reason for this is that at the scattering angles encountered in the conditions considered, the values of the aerosol scattering index are so much less than the values of the Rayleigh index that they are not compensated for by an increase /50 in intensity of scattered radiation due to the increased optical thickness of the scattering layer. However, at large ζ_0 and θ when the scattering angles are small and the aerosol index becomes considerable, the intensity of reflected radiation in the aerosol layer increases notably (by approximately a factor of 4 for $\zeta_0 = 80°, \theta = 80°$, and $\lambda = 0.25$ µm). Thus, from these calculations we can identify relative positions of the Sun and the observer's direction for which there will be quite a sharp contrast between the "dark" background in the region of strong UV radiation absorption by ozone and the "bright" noctilucent cloud,

which reflects the radiation strongly.

The effect of aerosol scattering in the lower layers of the atmosphere on the outgoing UV radiation in different parts of the ozone band can be seen from Figure 1.26, which shows curves at I_λ at several levels [68]. It is not difficult to appreciate that the aerosol scattering in the layer z < 40 km can be calculated satisfactorily only for λ > 0.30 μm(the same applies to calculation of the albedo of the underlying surface). The laws for the vertical behavior of UV radiation are considered in detail in [68].
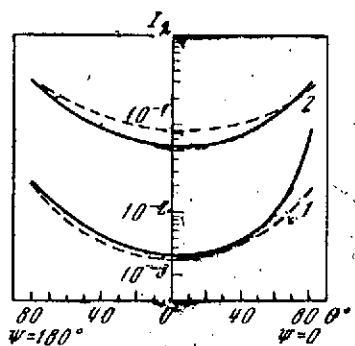
Figure 1.25. Comparison of the angular behavior of the relative intensity for the molecular atmosphere (broken line) and for the aerosol layer at 75-80 km (solid lines)

1- λ = 0.25 μm; 2- λ = 0.34 μm, ζ_0 = 80°
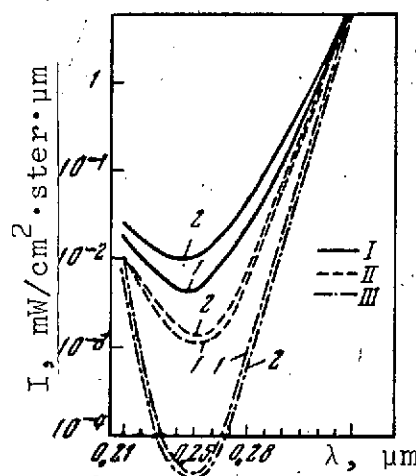
Figure 1.26. Formation of spectral dependence of reflected radiation with height $(\zeta_0 = 0°)$ I-III= z = 100, 60 and 40 km, respectively; 1.2- θ = 10 and 80°, respectively

4.4. Angular Distribution of Reflected UV Radiation

The angular distribution of reflected UV radiation is determined by the vertical distribution of ozone and the ratio between the scattering and the absorption of the atmosphere for radiation propagating in different directions, i.e., it depends appreciably on λ. An example considered in [68] of the dependence of $I_\lambda(\theta)$ for various λ and ζ_0 in the plane of the Sun's vertical is shown in Figure 1.27. In the strong absorption region ($\lambda = 0.25$ μm) $I'(\theta)$ doe not vary much in the range $0 \leqslant \theta \leqslant 60°$ and increases sharply for $\theta \to 90°$. However, as ζ_0 increases, this growth begins even for small θ, even in the weak absorption region ($\lambda = 0.34$ μm). A similar behavior of $I'(\theta)$ occurs even for pure scattering, as indicated by the dot-dash curve in the figure. We note that for $\zeta_0 = 10°$ $I'(\theta)$ even decreases somewhat with increase of θ.

The increase of I' for large θ is determined by the increase in the geometric thickness of the atmospheric layer in which the flux of backward-reflected radiation is mainly generated. In the strong absorption region this layer is optically thin and begins to play an appreciable role only for very large θ. For weak absorption, on the other hand, the whole atmosphere scatters. This gives an appreciable contribution from multiple scattering, which compensates for the limb "darkening", although not for all values of ζ_0.

We note that the results of similar calculations in [66], in contrast with [68], indicate the absence of dependence of the angular behavior of $I'(\theta)$ on λ and ζ_0. The reason is that [65] used approximations for singly-scattered radiation which are certainly not applicable to the wings of the ozone absorption band. This statement is confirmed by the experimental data obtained in [59] on the angular relationships.
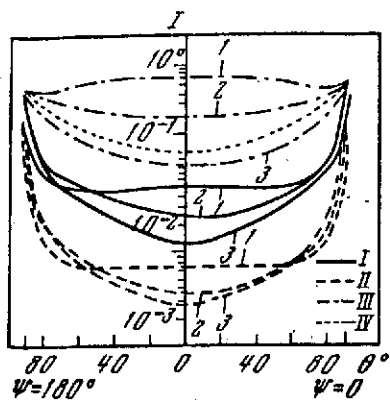
Figure 1.27. Angular behavior of intensity of reflected UV radiation (relative units)

I- λ = 0.21 µm; II- λ = 0.25 µm; -III- λ = 0.34 µm; IV) Pure Rayleigh scattering for τ^* = 0.8, λ = 0.34 µm; 1- ζ_0 = 10°; 2- ζ_0 = 60°; 3- ζ_0 = 80°
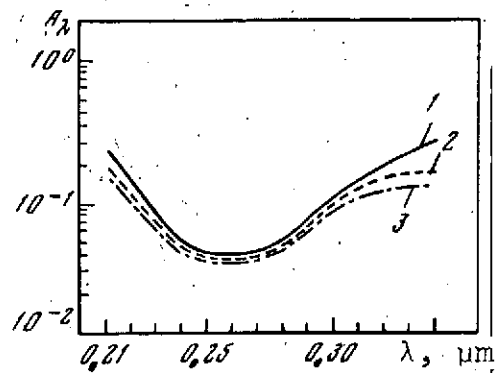
Figure 1.28. Spectral behavior of A_λ in the ozone absorption band.

1-3- ζ_0 = 0, 60 and 80°, respectively

Reference [68] investigated the dependence of $I_\lambda^\dagger$ on ζ_0 for different parts of the ozone band and fixed θ. It was shown that for small θ the value of I decreases with increase of ζ_0 faster, the less is the absorption. Conversely, at large θ an increase of I along with ζ_0 was observed in the center of the band and a weak variation in the wings. This relationship allows us to extrapolate the measurements obtained for fixed values of the angle ζ_0 to other zenith distances of the Sun, and the extrapolated curves are different for different sections of the ozone absorption band. Therefore none of these should be used to extrapolate $I_\lambda^\dagger$ with respect to ζ_0 for all the other wavelengths, as was proposed in [61], based on results of Green's calculations [66].

These peculiarities of the angular dependence of I on θ and ζ_0 for different λ are also apparent in the spectral distribution of the albedo for a plane atmospheric layer in the UV region, as can be seen in Figure 1.28 (the albedo of the underlying surface was taken as zero).

Reference [68] also examined the variation of $I(\theta)$ with height, which allows us to investigate the role of absorption and scattering in determining the angular structure of the UV radiation at different heights.

§ 5. Reflected Radiation in the Near Infrared

(0.75 -5 μm)

The radiation field of the Earth in the near IR has two peculiarities, which determine the degree and nature of investigations of its characteristics: this region has many absorption bands of water vapor, carbon dioxide, oxygen, and other atmospheric constituents; in the long-wave half of the IR range ($\lambda > 3\mu m$), /52 the radiation leaving the Earth is a superposition of comparable fluxes of reflected solar radiation and self-radiation of the planet (the amount of the latter increases with wavelength).

Because of the first peculiarity, considerable attention is usually paid to the integral characteristics of the absorption in the bands associated with atmospheric energy calculations. Recently, because of the use of the absorption bands and the "transparent windows" in the IR range to investigate the atmosphere and the underlying surface from satellites, a number of experimental data have been obtained on the spectral transmission of the atmosphere (some of these data were referred to in § 2), as well as on the spectra of reflected solar radiation and self radiation in this region [42-44, 72, 74, 75]. Calculations of the characteristics of the field of reflected solar radiation were obtained in [42, 76-79]. We shall make some analysis of these data from the viewpoint of questions related to optical probing of the atmosphere.
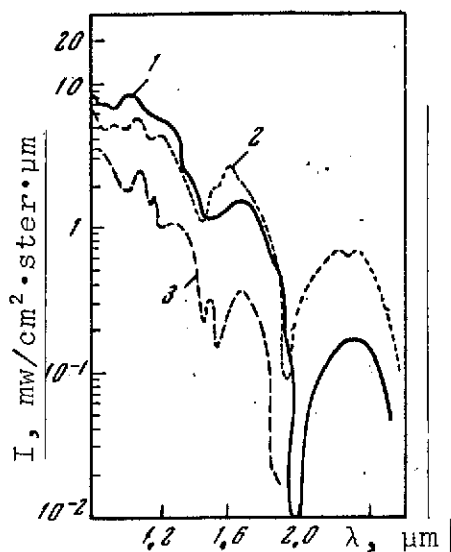
Figure 1.29. Spectral behavior
of brightness of clouds and
ice, after [57]

1- noctilucent clouds;
2- cumulus clouds; 3- ice
and snow

The main peculiarity of
spectra of IR radiation measured
from aircraft [42-44, 57] and
rocket [74, 75] soundings is the
variation of the absorption bands
as a function of the kind of under-
lying surface or cloud, and also,
probably, of the moisture content
of the atmosphere. For example,
in the spectra obtained by
Chapurskiy, et al. [57] for solar
radiation reflected from cumulus
and noctilucent clouds (Figure
1.29), it is observed that the
centers of absorption bands
corresponding to water vapor
absorption (1.38 and 1.86 μm)
are shifted in the long-wave
direction (1.45 and 1.94 μm for the liquid drop phase in the case of
cumulus clouds, and 1.50 and 2.0 μm, respectively, for the solid
phase in the case of noctilucent clouds). Minima near 1.5 and
2.0 μm are recorded also in the curves of spectral brightness
for ice and snow (Figure 1.29),which supports the validity
of the interpretation of these minima as absorption bands from
ice particles.

Similar results were obtained in [43] for the spectral
region 1.2-3.6 μm. The spectra of noctilucent clouds also show
only solid phase absorption bands (near 1.48, 1.97 and 2.85 μm).

Thus, from the well-resolved spectra of reflected solar
radiation in the IR, measured from a satellite, one can determine
the phase content and type of clouds. There is particular interest
in measurements in the "transparent window" at 3-4 μm, because of

84

interpretation of television pictures of the Earth, obtained
currently from satellites (Nimbus series) in this spectral range
[B. 21].

Since, on the one hand, television is based on contrasts
of temperatures expressed via contrasts of self-radiation, of
natural surfaces and clouds, and on the other hand self-radiation
of the latter is comparable in this spectral range with the
reflected solar radiation, appreciable errors can arise under
daytime conditions in the analysis of a picture, even for weakly
reflecting surfaces. For this reason measurements of the emission
spectra of terrestrial objects in the long-wave section of the
IR [44, 57] were undertaken. These measurements show that   <u>/53</u>
there will be interference from solar radiation for cumulus
clouds or strongly reflecting vegetation.

Reflected solar radiation will create serious difficulties
also when we try to solve the problem of determining the vertical
profile of atmospheric temperature from the self-radiation of
the Earth in the CO_2 band at 4.3 µm. Therefore, we must find a
relation between these components of the Earth's IR radiation and
determine conditions under which either the scattering and
reflection of solar radiation, or the self-radiation, can be
neglected in Equations (1.1) - (1.4), and in the intermediate
case we can evaluate the contribution of each component at the
various wavelengths.

Another problem of method, important in determining the mass
of water vapor or other absorbing substance from the reflection of
solar radiation in the IR, is the development of a method for
reliable calculation of the intensity of absorption in clouds.
This effect can result in the appearance of weak absorption bands
of water and ice, located in the IR sections of the spectrum,

(e.g., for $\lambda = 0.74$ and 1.03 μm in the measurements of reflected solar radiation on the satellites Kosmos 149 and Kosmos 320).

§ 6. Calculation of Non-orthotropic Underlying Surfaces

In the above survey we noted the need to evaluate the effect of a non-orthotropic surface on the characteristics of the reflected radiation field. However, it is difficult to solve the radiative transfer equation (1.1) - (1.4), allowing for the brightness coefficient of the underlying surface with anisotropic scattering in the atmosphere, and it is not a very attractive problem because of the complex dependence of the brightness coefficient on many factors which are not amenable to calculation. Therefore, a method was proposed in [76, 80] for calculating the brightness coefficient R only for radiation directly reflected from the underlying surface; and multiple scattering must be expressed in terms of the albedo of this surface. Estimates were made in [80] of the errors from this computation of a non-orthotropic surface, and methods were proposed to determine the albedo used for calculating the multiple scattering.

These estimates were obtained from the relations of Kuznetsov [81] for the intensity of scattered solar radiation in the case of a spherical scattering index ($\gamma = 1$):

$$I_R(\tau, r) = \left[\pi R(r, r_\odot) \exp(-\tau^* \sec \zeta_0) \cos \zeta_0 + \int_0^{\tau^*} K_R(t)\, dt \int \exp(-t \sec \theta) \times \right. $$
$$\left. \times R(r, r')\, d\omega' \right] \exp(-\tau \sec \theta) + \sec \theta \int_0^{\tau} K_R(t) \exp[-(\tau - t) \sec \theta]\, dt.$$

(1.34)

The source function $K_R(\tau)$ is determined from the integral equation:

$$K_R(t) = \frac{1}{4} \exp[-(\tau^* - \tau)\sec\zeta_0] + \frac{1}{4}\exp(-\tau^*\sec\zeta_0) \times$$
$$\times \cos\zeta_0 \int_- \exp(-t\sec\theta) R(r, r_\odot)\, d\omega + \frac{1}{2}\int_0^{\tau^*} K_R(t) \times \qquad (1.35)$$
$$\times \left\{ E_1(|\tau - t|) + \frac{1}{2\pi}\int_+\int_+ \exp[-(\tau\sec\theta + t\sec\theta')]R(r, r')\, d\omega\, d\omega' \right\} dt.$$

Here

$$E_k(x) = \int_1^\infty e^{-xs} s^{-k}\, ds \qquad (1.36)$$

is an integral index function; and $r_\odot$ is the direction of incidence of the solar radiation.

Equations (1.34) and (1.35) are a generalization of the well-studied equations to determine the source function $K_A(\tau)$ and the intensity $I_A(\tau, r)$, in the case of an orthotropic surface, whose reflecting properties are described by an albedo A (see, e.g., [82]).

In the methods formulated above for approximate calculation of the non-orthotropic surface, the error in determining I_R will be decided by the difference between the functions $K_R(\tau)$ and $K_A(\tau)$. It was shown in [80] that when the conditions

$$\frac{1}{2}\int_- R(r, r_\odot)\exp(-\tau\sec\theta)\, d\omega = AE_2(\tau) + \delta_1(\tau, r_\odot);$$
$$\frac{1}{2\pi}\int_+ A(r')\exp(-\tau\sec\theta')\, d\omega' = AE_2(\tau) + \delta_2(\tau, r_\odot), \qquad (1.37)$$

where

$$A = A(r_\odot) = \int_+ R(r, r_\odot)\cos\theta\, d\omega, \qquad (1.38)$$

are fulfilled, and δ_1 and δ_2 are restricted in amplitude to a quite small and constant δ , the difference

$$|K_R(\tau) - K_A(\tau)|$$ (1.39)

will be small.

If the brightness coefficient is represented in the form of the sum

$$R(r, r') = \frac{1}{\pi} \sum_{k=0}^{K} \sum_{n=0}^{N} \sum_{m=0}^{M} a_{kn}^{(m)} \cos k\theta \cos n\theta' \cos m(\psi - \psi'),$$ (1.40)

then $K_R(t)$ can be expressed as the sum

$$K_R(\tau) = \sum_i b_i \varphi_i(\tau),$$ (1.41)

where $\varphi_i(\tau)$ are universal functions determined from the integral equations

$$\varphi_i(\tau) = f_i(\tau) + \frac{1}{2} \int_0^{\tau^*} \varphi_i(t) E_1(|\tau - t|) dt \qquad (i = 1, 2, \ldots),$$ (1.42)

and the coefficients b_i are expressed as a linear combination of $a_{kn}^{(0)}$ and quadratures of $\varphi_i(\tau)$. The free terms in Equation (1.42) have the form:

$$f_0(\tau) = \frac{1}{4} \exp[-(\tau^* - \tau) \sec \zeta_0]; \qquad f_i(\tau) = E_{i+1}(\tau) \qquad (i = 1, 2, \ldots).$$ (1.43)

Effective solutions of Equation (1.41) were obtained in [80] for two types of non-orthotropic surface:

vegetation cover, from which the reflection is described by the symmetric function (1.40) with coefficients

$$a_{00}^{(0)} = a_{11}^{(0)} = 1{,}8; \quad a_{10}^{(0)} = -1{,}8; a_{01}^{(0)} = -1{,}7; a_{kn}^{(m)} = 0, \text{ for } m > 0, k > 1, n > 1;$$

snow with frozen crust, for which

$$a_{00}^{(0)} = -a_{00}^{(1)} = -a_{11}^{(1)} = 2{,}4; \quad a_{10}^{(0)} = -a_{10}^{(1)} = -2{,}4; a_{01}^{(0)} = -3; a_{01}^{(1)} = 2{,}4;$$
$$a_{11}^{(0)} = 2{,}34; a_{kn}^{(m)} = 0 \text{ for } m > 1, n > 1, k > 1.$$

Curves illustrating the true brightness coefficients and their approximate values were given earlier in Figure 1.14.

In spite of the great asymmetry in the brightness coefficients with respect to θ and ψ (e.g., for snow in the direction $\theta = 0$ the reflection is less by a factor of 26 than for $\theta = 90°$), the differences between $K_R(\tau)$ and $K_A(\tau)$ are not greater than 12% for $\tau = 0$ and decrease as $\tau \to \tau*$ (see Figure 1.30, for $\zeta_0 = 30$ and $60°$, $\tau* = 0.6$). It was shown in [80] that the albedo A required to calculate $K_A(\tau)$ is given by the expression

$$A = A(r_\odot) + \tilde{A}(\zeta, \tau*),$$ (1.44)

where

$$A(r_\odot) = \int_+ R(r, r_\odot) \cos\theta\, d\omega,$$ (1.45)

$$\tilde{A}(\zeta, \tau*) = \frac{\int_0^{\tau*} K_R(t) \int_+ \left[\frac{1}{2\pi} \int_+ R(r, r') \exp(-t \sec\theta')\, d\omega' - R(r, r_\odot) E_2(t) \right] \cos\theta\, d\omega\, dt}{0{,}5 \exp(-\tau* \sec\zeta_0) \cos\zeta_0 + \int_0^{\tau*} K_R(t) E_2(t)\, dt}.$$ (1.46)

The errors in $I_R(\tau, r)$ obtained by replacing $K_R(\tau)$ by $K_A(\tau)$ in Equation (1.34), are also small (Figure 1.31).

Thus, for spherical scattering the brightness coefficient can be calculated only for radiation directly reflected from the underlying surface, and one must use a surface albedo to calculate multiple scattering of the radiation. This conclusion allows us to make complete use of the calculations of scattered radiation obtained earlier for orthotropic surfaces, and when the reflection is given $R(r, r')$ (one needs only to determine A for the given surface, in addition to R). It is clear that calculation of A from Equations (1.44) – (1.46) requires Equation (1.35) to be

89
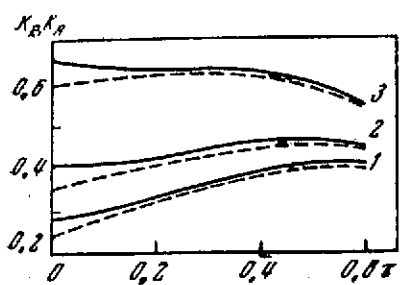
Figure 1.30. Comparison of K_R (solid lines) and K_A (broken lines) for the brightness coefficients shown in Figure 1.13

Curves 1 correspond to Figure 1.13, a, $\zeta_0 = 60°$; curves 2 and 3 correspond to Figure 1.13, b, $\zeta_0 = 60°$ and $30°$, respectively.
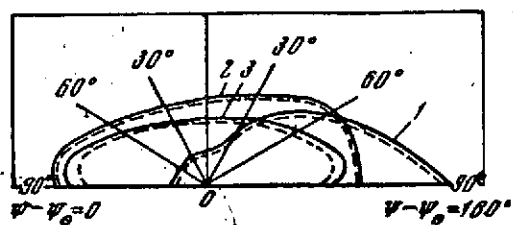
Figure 1.31. Comparison of the intensity of reflected and incident radiation, I_R (solid lines) and I_A (broken lines) for R of snow (see Figure 1.13, b)

1- $I\uparrow$ at the ground surface; 2- $I\uparrow$ at the upper boundary of the atmosphere; 3- $I\downarrow$ at the ground surface

solved and $R(r, r')$ to be calculated. However, one can determine A approximately, by taking a first approximation as $A_1 = A(r_\odot)$. By calculating the function $K_A(\tau)$ for $A(r_\odot)$ and substituting it into Equation (1.46) instead of $K_R(\tau)$, one finds the next approximation A_1, and so on. This calculation gives the following values for snow, for example:

ζ_0	$A_1 = A(r_\odot)$	A_2	A_{act}
30	0.592	0.618	0.620
60	0.68	0.663	0.663

The correction to A_1 means the actual dependence of the albedo of the surface-atmosphere system on the optical properties of the surface for a given position of the Sun. From the data presented it can be seen, in particular, that for small ζ_0 of the atmosphere, the albedo increases, while for large values, it decreases.

90

It was noted in [80] that the hypothesis concerning the
anisotropy of atmospheric scattering cannot seriously alter
the results obtained, at least for only slightly asymmetric
scattering indices. As an example, the index

$$\gamma(\varphi) = 1 + \varkappa_1 \cos \varphi \qquad (1.47)$$

was examined in [80] with $\varkappa_1 = 1, \tau^* = 0.3$ and $\zeta_0 = 60°$. In this case
$K_R(\tau, r)$ is expressed, as before, in terms of universal functions,
which are solutions of equations of type (1.49).

As can be seen from the data presented above, K_R and K_A do
not differ very much, apart from small τ)i.e., close to the
levels near the surface), where the differences can reach 20%.
We note, that for anisotropic scattering, K_R and K_A depend on
the direction (the source functions are given for ascending
radiation), and the largest differences relate to the directions
for which the index takes minimum values:

τ	0	0.04	0.08	0.12	0.16	0.20	0.24	0.28	0.30
K_R	0.190	0.182	0.181	0.174	0.169	0.162	0.154	0.141	0.134
K_A	0.152	0.155	0.158	0.157	0.156	0.153	0.147	0.137	0.131

Near the top, K_R and K_A practically coincide, and therefore
the differences between I_R and I_A will be small, as before.

We note, finally, that from Figure 1.31 we can conclude
that the non-orthotropic surface is smoothed by the atmosphere,
because of multiple scattering of the radiation in a turbid
medium. Allowance for the anisotropy of scattering in the
real atmosphere will not alter this conclusion substantially for
reflected radiation, since for it the scattering angles take
values for which actual scattering indices are comparatively
symmetrical.

§ 7. Calculation of Nonuniformity of the Underlying Surface

7.1. Basic Relations

The results considered in § 3-6 of the present chapter for calculations of reflected solar radiation, like the great majority of investigations of the Earth's radiation field, are based on the assumption that the medium and the underlying surface are homogeneous in the horizontal direction. This assumption, which makes it possible to greatly simplify solutions of many problems in transfer theory, is a great idealization of the actual conditions because of the horizontal variations of the characteristics of the atmosphere, clouds, and underlying surface.

To determine the characteristics of the radiation field of a horizontally nonuniform medium one must use a three-dimensional radiative transfer equation. Approximate solutions of this equation were obtained by Jefferies and Giovannelli [83, 84], using the Eddington method. However, in one important case, when only horizontal variations of the albedo of a Lambert-type under-lying surface are considered, and the atmosphere is a plane-parallel anisotropically scattering medium, the solution of the three-dimensional transfer equation is obtained in the form of a comparatively simple generalization of the corresponding solutions with constant albedo [85-87]. In fact, while the albedo of the underlying surface A = A (x,y) is a function of the horizontal coordinates x and y, the intensity of solar radiation I (x,y,z;θ,ψ) in this case can be determined from the equation

$$\cos\theta\,\frac{\partial I}{\partial z} + \sin\theta\sin\psi\,\frac{\partial I}{\partial x} + \sin\theta\cos\psi\,\frac{\partial I}{\partial y} = \sigma(z)\,[G(x, y, z) - I(x, y, z; \theta, \psi)]; \qquad (1.48)$$

$$G(x, y, z) = \frac{1}{4\pi}\int I(x, y, z; \theta, \psi)\,d\omega \qquad (1.49)$$

and the boundary conditions

$$I^{\uparrow}(0, x, y; \theta, \psi) = \frac{A(x, y)}{\pi} \int I^{\downarrow}(0, x, y; \theta, \psi) \cos\theta \, d\omega; \quad (1.50$$

$$I^{\downarrow}(\infty, x, y; \theta, \psi) = \pi S \delta(\theta - \zeta_0) \delta(\psi - \psi_\odot). \quad (1.51)$$

Introducing scales for nonuniformities of the underlying surface for the axes x and y (L_x, L_y), and the new variables $\xi = x/L_x$, $\eta = y/L_y$, $\tau(z) = \int_0^z \sigma(t)\,dt$, $\tau^* = \tau(\infty)$, we obtain, instead of Equations (1.48) – (1.51):

$$\cos\theta \frac{\partial I}{\partial \tau} + \frac{\sin\theta \sin\psi}{a(\tau)} \frac{\partial I}{\partial \xi} + \frac{\sin\theta \cos\psi}{b(\tau)} \frac{\partial I}{\partial \eta} = G(\tau, \xi, \eta) - I(\tau, \xi, \eta; \theta, \psi); \quad (1.52)$$

$$G(\tau, \xi, \eta) = \frac{S}{4} \exp\left[-(\tau^* - \tau)\sec\zeta_0\right] + \frac{1}{4\pi} \int I(\tau, \xi, \eta; \theta, \psi)\,d\omega; \quad (1.53)$$

$$I^{\uparrow}(0, \xi, \eta; \theta, \psi) = \frac{A(\xi, \eta)}{\pi}\left[\pi S e^{-\tau^* \sec\zeta_0} \cos\zeta_0 + \int I^{\downarrow}(0, \xi, \eta; \theta, \psi)\cos\theta\,d\omega\right]; \quad (1.54)$$

$$I^{\downarrow}(\tau^*, \xi, \eta; \theta, \psi) = 0. \quad (1.55)$$

Here $a(\tau) = L_x \sigma[z(\tau)]$; $b(\tau) = L_y \sigma[z(\tau)]$ are dimensionless functions describing the relations between the scales of nonuniformities and the vertical turbidity of the atmosphere. In particular, if we use an exponential law for the scattering coefficient $\sigma(z) = \sigma_0 e^{-kz}$, $\tau = (\sigma_0/k)(1 - e^{-kz}) = \tau^*(1 - e^{-kz})$, then

$$a(\tau) = a_0(\tau^* - \tau); \qquad b(\tau) = b_0(\tau^* - \tau); \qquad a_0 = L_x k; \qquad b_0 = L_y k. \quad (1.56)$$

To avoid laborious calculations, we consider the case when the albedo is a function of only one coordinate, e.g., $A = A(\xi)$, and the underlying surface is homogeneous along η (then the term with $\partial I/\partial \eta$ drops out in Equation (1.52))[*]. We

---

[*] A generalization of the results then obtained in the three-dimensional case does not present difficulties in principle.

assume further that the albedo A (ξ) can be expanded in a Fourier series

$$A(\xi) = \sum_{n=0}^{\infty} (p_n \sin n\xi + q_n \cos n\xi).$$ (1.57)

We represent the intensity of the ascending $I^\uparrow$ and descending $I^\downarrow$ radiations, and also the function G (τ, ξ) in the form of Fourier series:

$$I^\uparrow = \sum_{n=0}^{\infty} [A_n^{(1)} \cos n\xi + B_n^{(1)} \sin n\xi]; \qquad I^\downarrow = \sum_{n=0}^{\infty} [A_n^{(2)} \cos n\xi + B_n^{(2)} \sin n\xi];$$

$$G = \sum_{n=0}^{\infty} [G_n^{(1)} \cos n\xi + G_n^{(2)} \sin n\xi].$$

Following numerous but quite simple operations (see [85]), we obtain /58 a system of differential equations:

$$\varphi_0(\tau) = \frac{S}{4} \exp[-(\tau^* - \tau)\sec\zeta_0] + \frac{1}{2}\int_0^{\tau^*} \varphi_0(t) E_1(|\tau - t|) dt;$$ (1.58)

$$G_0(\tau) = E_2(\tau) + \frac{1}{2}\int_0^{\tau^*} G_0(t) E_1(|\tau - t|) dt;$$ (1.59)

$$G_n(\tau) = \Psi_2\left[\tau, \frac{n}{a_0}\ln\left(1 - \frac{\tau}{\tau^*}\right)\right] + \frac{1}{2}\int_0^{\tau^*} G_n(t)\,\Psi_1\left[|\tau - t|, \frac{n}{a_0}\ln\frac{\tau^* - \tau}{\tau^* - t}\right] dt,$$ (1.60)

where

$$\Psi_k(x, y) = \int_1^{\infty} e^{-sx} J_0(xy\sqrt{s^2 - 1}) s^{-k} ds \qquad (k = 1, 2, \ldots; n = 1, 2, \ldots)$$ (1.61)

are transcendental functions which it is convenient to regard as a function of the two variables x and y, although in the final analysis they are functions only of the variable τ and the basic parameters.

All the intermediate functions of the problem and the final solution of Equation (1.52) can be expressed in terms of solutions of the integral Equations (1.58) — (1.60), φ_0, G_0, G_n , e.g.,

$G_0(\tau) = \varphi_0(\tau) + H_0 G_0(\tau);\ G_n^{(1)}(\tau) = H_n^{(1)}\ G_n \cdot (\tau);\ G_n^{(2)}(\tau) = H_n^{(2)} G_n(\tau)$. The constants H_0, $H_n^{(1)}$, $H_n^{(2)}$ are determined from a system of algebraic equations (generally speaking, of infinite order), whose coefficients are expressed in terms of quadratures of the universal functions φ_0, G_0, G_n (see [85]).

It is easy to see that the universal functions $\varphi_0(\tau)$ and $G_0(\tau)$ coincide in accuracy with the corresponding functions for the one-dimensional case (see, e.g., Equation (1.42)). As far as the new functions $G_n(\tau)$ are concerned, they are solutions of the integral equations whose free terms and kernel are generalizations of the exponential integral functions used in one-dimensional theory of radiative transfer [82]. The final solution of Equation (1.52) for $I^\dagger$ is in the form of the series

$$
\begin{aligned}
I^\dagger(\tau, \xi;\theta, \psi) = {}& 2e^{-\tau \sec\theta} \sum_{n=0}^{\infty} \left\{ H_n^{(1)} \cos n\left[\xi + \frac{\operatorname{tg}\theta \sin\psi}{a_0} \ln\left(1 - \frac{\tau}{\tau^*}\right)\right] + \right. \\
& + H_n^{(2)} \sin n\left[\xi + \frac{\operatorname{tg}\theta \sin\psi}{a_0} \ln\left(1 - \frac{\tau}{\tau^*}\right)\right]\biggr\} + \\
& + \sec\theta \int_0^\tau \exp\left[-(\tau - t)\sec\theta\right]\left\{\varphi_0(t) + \right. \\
& + \sum_{n=0}^{\infty}\left[H_n^{(1)} \cos n\left(\xi + \frac{\operatorname{tg}\theta \sin\psi}{a_0} \ln\frac{\tau^* - \tau}{\tau^* - t}\right) + \right. \\
& + H_n^{(2)} \sin n\left(\xi + \frac{\operatorname{tg} 0 \sin\psi}{a_0} \ln\frac{\tau^* - \tau}{\tau^* - t}\right)\biggr] G_n(t)\biggr\} dt.
\end{aligned}
\tag{1.62}
$$

The flux of ascending radiation

$$
F^\dagger(\tau, \xi) = \int_+ I^\dagger(\tau, \xi;\theta, \psi)\cos\theta\, d\omega
$$

has the form

$$
F^\dagger(\tau, \xi) = 2\pi \sum_{n=0}^{\infty} [H_n^{(1)} \cos n\xi + H_n^{(2)} \sin n\xi]\left\{2\Psi_3\left[\tau, \frac{n}{a_0}\ln\left(1 - \frac{\tau}{\tau^*}\right)\right] + \int_0^\tau \Psi_2\left(\tau - t, \frac{n}{a_0}\ln\frac{\tau^* - \tau}{\tau^* - t}\right) G_n(t)\, dt\right\}.
\tag{1.63}
$$

Since the functions $\Psi_k (x, y)$ will be used later in other problems, we describe their properties, which are considered in [85].

We consider the transcendental functions

$$\Psi_n (x, y; \beta) = \int_0^\infty \exp\left(- x \sqrt{u^2 + \beta^2}\right) J_0 (yu) \frac{u\, du}{(u^2 + \beta^2)^{\frac{n+1}{2}}} \quad (x > 0,\; n = 1, 2, \ldots), \quad (1.64)$$

which are converted to the functions (1.61) for β = 1 and with replacement of the variable of integration $\sqrt{u^2 + 1}$ = s; udu = sds. It is easy to see that these functions are a generalization of the exponential integral functions (1.37) used in one-dimensional theory of radiative transfer. In fact, for y = 0,

$$\Psi_n (x, 0; \beta) = \frac{E_n (\beta x)}{\beta^{n-1}}. \quad (1.65)$$

For x = 0, the functions Ψ_n (x, y, β) take the form

$$\Psi_n (0, y; \beta) = \frac{(y/2\beta)^{(n-1)/2}}{\Gamma\,[(n + 1)/2]} K_{(n-1)/2} (\beta y), \quad (1.66)$$

where K_m (βy) is a McDonald function; and Γ [(n + 1)/2] is the gamma function (see [88]).

It can be seen from Equations (1.65) and (1.66) that

$$\Psi_0 (0, 0; \beta) = \infty; \qquad \Psi_1 (0, 0; \beta) = \infty; \qquad \Psi_n (0, 0; \beta) = \frac{1}{n-1} \cdot \frac{1}{\beta^{n-1}}; \quad (1.67)$$

$$\Psi_n (\infty, y; \beta) = \Psi_n (x, \infty; \beta) = 0 \qquad (n > 1).$$

The functions Ψ_n (x, y; β) are bounded above:

$$\Psi_n (x, y; \beta) \leqslant \frac{E_n (\beta x)}{\beta^{n-1}}; \qquad \Psi_n (x, y; \beta) \leqslant \frac{(y/2\beta)^{(n-1)/2}}{\Gamma\,[(n + 1)/2]} K_{(n-1)/2} (\beta y). \quad (1.68)$$

The functions $\Psi_n(x, y; \beta)$ are given by recurrent relations, which it is easy to obtain from consideration of the following identity (see [88]):

$$\int_0^\infty J_0(yu) \frac{K_{n+1}(x\sqrt{u^2+\beta^2})}{\sqrt{(u^2+\beta^2)^{n+\frac{1}{2}}}} du = \frac{1}{x^{n+1/2}} \left(\frac{\sqrt{x^2+y^2}}{\beta} \right)^{n-1/2} K_{n-1/2}(\beta\sqrt{x^2+y^2}) \qquad (1.69)$$

and from expanding $K_{n\pm\frac{1}{2}}$ in the series

$$K_{n+1/2}(z) = \sqrt{\frac{\pi}{2z}} e^{-z} \sum_{k=0}^n \frac{(n+k)!}{k!(n-k)!} \cdot \frac{1}{(2z)^k} \cdot \qquad (1.70)$$

For example,

$$\Psi_0(x, y; \beta) = \frac{\exp(-\beta\sqrt{x^2+y^2})}{\sqrt{x^2+y^2}}; \qquad (1.71)$$

$$\Psi_1(x, y; \beta) + \frac{\Psi_2(x, y; \beta)}{x} = \frac{\exp(-\beta\sqrt{x^2+y^2})}{\beta x}; \qquad (1.72)$$

$$\Psi_2(x, y; \beta) + \frac{3}{x}\Psi_3(x, y; \beta) + \frac{3}{x^2}\Psi_4(x, y; \beta) =$$
$$= \frac{\sqrt{x^2+y^2}}{(\beta x)^2} \exp(-\beta\sqrt{x^2+y^2}) \left[1 + \frac{1}{\beta\sqrt{x^2+y^2}} \right] \qquad (1.73)$$

and so on. To separate adjacent functions Ψ_3 and Ψ_4, in formulas of type (1.73), we differentiate the integral (1.64) with respect to β:

$$\frac{\partial \Psi_n(x, y; \beta)}{\partial \beta} = -\beta [x\Psi_{n+1}(x, y; \beta) + (n+1)\Psi_{n+2}(x, y; \beta)]. \qquad (1.74)$$

Hence for n = 0, we obtain the expression

$$\Psi_2(x, y; \beta) = -\left[\frac{1}{\beta} \frac{\partial \Psi_0}{\partial \beta} + x\Psi_1 \right], \qquad (1.75)$$

which exactly coincides with (1.73). For n = 1,

$$\Psi_3(x, y; \beta) = -\frac{1}{2}\left[\frac{1}{\beta} \frac{\partial \Psi_1}{\partial \beta} + x\Psi_2 \right]. \qquad (1.76)$$

It is easy to find Ψ_4, and so on, from combining Equations (1.73) and (1.76).

Thus, to determine any function Ψ_n (x, y; β) one needs the form of the function Ψ_1 (x, y; β). For this purpose, from the obvious identity

$$\frac{\partial \Psi_n}{\partial x} = - \Psi_{n-1}$$

(1.77)

we obtain, for n = 1,

$$\Psi_1(x, y; \beta) = \int_x^\infty \frac{\exp[-\beta \sqrt{t^2+y^2}]}{\sqrt{t^2+y^2}} \, dt = K_0(\beta y) - \int_0^x \frac{\exp[-\beta \sqrt{t^2+y^2}]}{\sqrt{t^2+y^2}} \, dt.$$

(1.78)

By replacing the variables

$$t^2 + y^2 = u^2, \qquad t\,dt = u\,du$$

we bring the integral (1.78) to the form

$$\Psi_1(x, y; \beta) = \int_{\sqrt{x^2+\beta^2}}^\infty \frac{e^{-\beta u}}{u} \left(1 - \frac{y^2}{u^2}\right)^{-1/2} du,$$

(1.79)

whence, by expanding the integrand in Equation (1.79) in a binomial series and then integrating, we obtain

$$\Psi_1(x, y; \beta) = \sum_{n=0}^\infty \frac{(2n-1)!!}{2^n n!} \left(\frac{y}{x^2+y^2}\right)^n E_{2n+1}(\beta \sqrt{x^2+y^2}), \quad (-1)!! = 1.$$

(1.80)

A similar series can be obtained also for $\partial \Psi_1 / \partial \beta$. In particular, for x = 0, from Equation (1.80) we obtain an expansion of the McDonald function in a series of exponential integral functions

$$K_0(y) = \sum_{n=0}^\infty \frac{(2n-1)!!}{2^n n!} E_{2n+1}(y).$$

(1.81)

From Equation (1.80) we can also find a lower estimate for the function Ψ_1:

$$\Psi_1(x, y; \beta) \geqslant E_1(\beta \sqrt{x^2+y^2}).$$

(1.82)

98

Since the series (1.80) converges slowly for large y or small x, it is more convenient to use another expression, obtained from Equation (1.78) to determine Ψ_1 (x, y; β) in such cases:

$$\Psi_1(x, y; \beta) = K_0(\beta y) - \sum_{n=0}^{\infty} \frac{(2n-1)!!}{2^n n!} \times$$
$$\times \left[E_{2n+1}(\beta y) - \left(\frac{y^2}{x^2+y^2} \right)^n E_{2n+1}(\beta \sqrt{x^2+y^2}) \right]. \qquad (1.83)$$

We note finally a symmetry property of the function

$$\Psi_n(x, y; \beta) = \Psi_n(x, -y; \beta).$$

Later on we will consider only the special case of the functions Ψ_n (x, y; β) for $\beta = 1$, retaining the previous notation Ψ_n (x, y).

Formulas (1.80), (1.83) for Ψ_1 (x, y) and the recurrent relations (1.75) enable us to tabulate Ψ_n for any n.

7.3. Some Results of Calculations

From the above properties of the function Ψ_n, we can make some qualitative investigations of solutions of the radiative transfer equation above a nonuniform surface. Since $\Psi_n = 0$ for all n $\neq$ 0 for $\tau = \tau^*$ in Equation (1.63), then F↑ at the upper boundary of the atmosphere $\tau = \tau^*$ will be close to some average flux. As regards the intensity of radiation I↑, to determine its value as $\tau \to \tau^*$ we need to sum the series (1.62), each term of which becomes infinitely oscillatory at the top boundary of the atmosphere, for all $\theta \neq 0$ or $\psi \neq 0$.

To illustrate numerical evaluations of the effect of nonuniformity of the underlying surface, the characteristics were calculated for a radiation field of an atmosphere uniform in height [86]. In this case $a(\tau) = a_0$, $b(\tau) = b_0$, and we replace the

99

argument of the type $(1/a_0) \ln (1 - \tau/\tau^*)$ in all the above formulas by linear expressions of the type $(\tau^* - \tau)/a_0$. The variations of the albedo of the underlying surface are described in [86] by the expression

$$A (\xi) = q_0 + q_1 \sin \xi, \qquad (1.84)$$

where q_0 and q_1 are constants; $q_0 + q_1 \leq 1$; $q_0 = q_1 \geq 0$. The calculations were performed for $a_0 = 0.1$; 1 and 10, which corresponds, for the usually assumed order of magnitude of the scattering coefficient $\sigma = 0.1$ km^{-1}, to uniformity scales $L = 1.10$ and 11 km. Examples of solutions of the integral equations (1.60) for $n = 1$ and 2 and $a_0 = 0.1$ and 10, given in [86] for $\tau^* = 0.3$, are evidence that the scale L plays a substantial role in smoothing out horizontal nonuniformities. For example, the functions $G_1 (\tau)$ and $G_2 (\tau)$ which describe the decrease with τ of the first and second harmonics in series of type (1.62) and (1.63), are reduced in the interval $0 \leq \tau \leq 0.3$ by a factor of 20 for $L = 1$ km, and by less than a factor of 2 for $L = 100$ km.

A very clear illustration of smoothing of the features of the underlying surface is the behavior of the albedo of the surface-atmosphere system with height (Figure 1.32) for the case $q_0 = 0.5$, $q_1 = 0.3$ (this corresponds to variation of the surface albedo from 0.2 to 0.8 with a mean value $\overline{A} = 0.5$).

Similar results are obtained also for other integral characteristics of the radiation field (direction integrals). The intensity of the ascending radiation will be determined mainly by the value of the albedo of the section of underlying surface intersected by the line of sight of an observer located at the given height τ in the direction (θ, ψ). The contribution to $I^{\dagger}$ of radiation reflected by adjoining sections of the surface and scattered by the comparatively transparent atmosphere considered in [86] is as high as 15%.
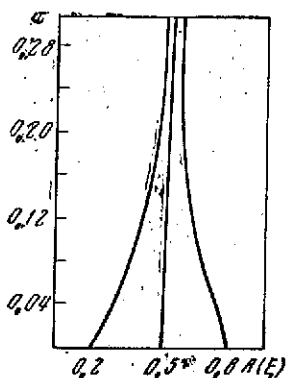
Figure 1.32. Variations of A (ξ, τ) with height for $\tau^* = 0.3$, $a_0 = 0.1$, $\zeta_0 = 60°$

Similar estimates for $I^{\downarrow}$ show that this contribution does not exceed 3-4%. Therefore, in calculations of the characteristics of the Earth's radiation field above a nonuniform underlying sur- /62 face, we can neglect deviations of the surface albedo from its mean value in evaluating $I^{\downarrow}$. This conclusion is very important in simplifying methods of allowing for irregularities of the underlying surface in radiative transfer problems.

7.4. Approximate Method of Calculation

If we assume that we know the intensity of incident radiation for an average value of albedo A of a nonuniform underlying surface, we can use a Fourier transformation* to solve Equations (1.52) — (1.55)

$$\widetilde{I}(\tau, \omega; \theta, \psi) = \int_{-\infty}^{+\infty} I(\tau, \xi; \theta, \psi) e^{i\omega\xi} d\xi; \tag{1.85}$$

$$\widetilde{G}(\tau, \omega) = \int_{-\infty}^{+\infty} G(\tau, \xi) e^{i\omega\xi} d\xi. \tag{1.86}$$

Here it is assumed that the functions A (ξ) allow the Fourier transformation

$$\widetilde{A}(\omega) = \int_{-\infty}^{+\infty} A(\xi) e^{i\omega\xi} d\xi. \tag{1.87}$$

---

* We recall that we considered the two-dimensional forms of the equations for reason of simplicity.

In this case, as was shown in [87], the solution of the trasnfer Equation (1.52) reduces to solutions of Equations (1.58), (1.59), and the integral equations

$$\varphi_k(\tau, \omega) = f_k(\tau, \omega) + \frac{1}{2} \int_0^\tau \Psi_1\left[\tau - t, \frac{\omega}{a}(\tau - t)\right] \varphi_k(t, \omega)\, dt \qquad (1.88)$$

for the Fourier forms $\varphi_k(\tau, \omega)$ of several universal functions.

Reference [87] obtained an effective solution for this problem for the frequently encountered case of a step function $A(\xi)$, when two uniform underlying surfaces with different reflectances have a sharp line of demarcation (e.g., land and sea). We assume that

$$A(\xi) = \begin{cases} A_1 e^{\varepsilon\xi}, & -\infty < \xi < 0, \\ A_2 e^{-\varepsilon\xi}, & 0 < \xi < \infty, \end{cases} \qquad (1.89)$$

and that the intensity of the incident radiation is given as follows:

$$I^\downarrow(\tau, \xi; \theta) = \begin{cases} I_1^\downarrow(\tau, \theta) e^{\varepsilon\xi}, & -\infty < \xi < 0, \\ I_2^\downarrow(\tau, \theta) e^{-\varepsilon\xi}, & 0 < \xi < \infty, \end{cases} \qquad (1.90)$$

where $I_1^\downarrow$, $I_2^\downarrow$ are the intensities of incident radiation obtained in each hemisphere for the corresponding values of the albedo A_1 and A_2*. Then

$$\tilde{A}(\omega, \varepsilon) = \frac{\varepsilon(A_1 + A_2)}{\omega^2 + \varepsilon^2} + i\omega \frac{A_2 - A_1}{\omega^2 + \varepsilon^2}. \qquad (1.91)$$

An approximate solution of the transfer equation (1.52) for the case considered $A(\xi)$, obtained in [87], allows us to express the source function $G(\tau, \xi)$ in terms of solutions of the one-dimensional transfer equation in each semi-plane K_{A_1} and K_{A_2}:

---

* We note that the method considered does not require $A(\xi)$ to be given, nor $I^\downarrow(\tau, \xi; \theta)$ at the point $\xi = 0$ where these parameters have a discontinuity. A small enough positive value of ε is introduced to allow the Fourier transformation to be performed.
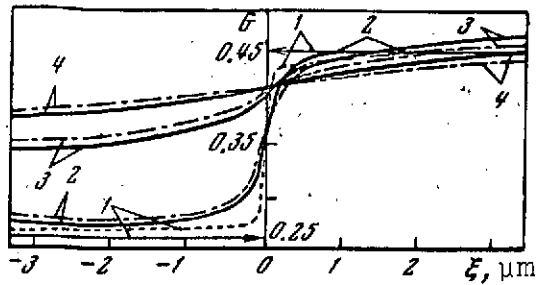
Figure 1.33. Comparison of the functions G (τ, ξ) for $g_1 = 0.2$, $q_2 = 0.8$, $a_0 = 1$, $\tau^* = 0.3$, $\zeta_0 = 60°$

1-4- $\tau = 0$; 0.02; 0,16 and 0.30, respectively

$$\hat{G}(\tau, \xi) = K_{A_1}(\tau) - \frac{K_{A_1}(\tau) - K_{A_1}(\tau)}{\pi} \operatorname{arcctg} \frac{\xi}{\tau} \qquad \left(0 \leqslant \operatorname{arcctg} \frac{\xi}{\tau} \leqslant \pi\right). \qquad (1.92)$$

Figure 1.33 shows results of calculation of G (τ, ξ), based on exact solutions of Equation (1.88) (broken lines) and according to Equation (1.92) (solid lines) at various heights τ. It is easy to see that only at the level of the underlying surface ($\tau = 0$) do the exact and approximate solutions differ appreciably, and that $\hat{G}$ (τ, ξ) has a discontinuity at $\xi = 0$. With increase of τ the variations of the function $\hat{G}$ (τ, ξ) are smoothed out, and it becomes close to G (τ, ξ).

Using the Fourier form of the function $\hat{G}$:

$$G(\tau, \omega) = K_{A_1}(\tau) \delta(\omega) - i \frac{K_{A_1}(\tau) - K_{A_1}(\tau)}{\pi} [1 - e^{-\tau|\omega|}]$$

as a first approximation, we can determine the following approximations for G (τ, ξ) and other characteristics of the radiation field. In particular, we can evaluate the brightness of the sky near the boundary of the underlying surfaces and approach this strip from both sides of $\xi = 0$, within which one cannot neglect the jump in the albedo (in [87] the dependence of this kind of strip on the angle θ was given). Outside this strip the characteristics of the radiation field follow an asymptotic approach to the limiting values, equal to the respective characteristics of the uniform radiation field for A_1 or A_2.

Finally, we point out that this method can be extended without difficulty in principle to the three-dimensional case, when A = A (ξ, η). Using a double Fourier transformation of the form

$$\widetilde{I}^{\dagger}(\tau, \omega_{\xi}, \omega_{\eta}; \theta, \psi) = \int\limits_{-\infty}^{+\infty}\int\limits_{-\infty}^{+\infty} I^{\dagger}(\tau, \xi, \eta; \theta; \psi) \exp\left[-i\left(\xi\omega_{\xi} + \eta\omega_{\eta}\right)\right] d\xi\, d\eta;$$

$$\widetilde{G}(\tau, \omega_{\xi}, \omega_{\eta}) = \int\limits_{-\infty}^{+\infty}\int\limits_{-\infty}^{+\infty} G_{.}(\tau, \xi, \eta) \exp\left[-i\left(\xi\omega_{\xi} + \eta\omega_{\eta}\right)\right] d\xi\, d\eta,$$

we obtain equations for determining $\widetilde{I}^{\dagger}$ and $\widetilde{G}$. For example, for an atmosphere uniform with height

$$\widetilde{G}(\tau, \omega_{\xi}, \omega_{\eta}) = \widetilde{A}(\omega_{\xi}, \omega_{\eta}) \Psi_2\left(\tau, \frac{\tau}{a_0}\rho\right) + f(\tau)\delta(\omega_{\xi}, \omega_{\eta}) +$$
$$+ \frac{1}{2}\int\limits_{0}^{\tau} G(t, \omega_{\xi_0}, \omega_{\eta}) \Psi_1\left[\tau - t, \frac{\tau - t}{a_0}\rho\right] dt, \tag{1.93}$$

where

$$\rho = \sqrt{\omega_{\xi}^2 + \omega_{\eta}^2.} \tag{1.94}$$

The solution of Equation (1.93) can be represented, as before, in <u>/64</u> the form of a superposition of universal functions, dependent on the two wave numbers ω_{ζ} and ω_{η}.

§ 8. Allowance for Sphericity of the Earth

To investigate the field of solar radiation reflected by the Earth as a planet to outer space for large angles ζ_0 and θ, we need to consider a spherical model of the atmosphere.

The intensity of radiation I (r, φ, λ; θ, ψ) scattered by a spherical medium at each point P (τ, φ, λ) with coordinates r (distance from the sphere center), φ, λ (latitude and longitude) in a direction described by angles θ and ψ, is given by the following transfer equation:

$$[\cos\theta\cos\varphi + \sin\theta\sin\varphi\cos(\lambda - \psi)]\frac{\partial I}{\partial r} +$$
$$+ \frac{1}{r}[\cos\theta\cos\varphi - \sin\theta\sin\varphi\cos(\lambda - \psi)]\frac{\partial I}{\partial\varphi} -$$
$$- \frac{\sin\theta\sin(\lambda - \psi)}{r\sin\varphi}\frac{\partial I}{\partial\lambda} = -[\sigma(r, \varphi, \lambda) + \alpha(r, \varphi, \lambda)]I(r, \varphi, \lambda; \theta, \psi) +$$
$$+ \frac{\sigma(r, \varphi, \lambda)}{4\pi}\int I(r, \varphi, \lambda; \theta'\psi')\gamma(r, \varphi, \lambda; \theta, \psi; \theta', \psi')d\omega'. \tag{1.95}$$

104

Here it is assumed that the scattering coefficient G and the absorption coefficient α depend on all three coordinates and that the self-radiation of the medium can be neglected. The boundary conditions remain the same as for the plane problem (see § 1). If we assume that σ and α depend only on r and that the underlying surface is uniform, then Equation (1.95) can be made symmetrical with respect to the radius vector joining the center of the Earth to the Sun. In this coordinate system Equation (1.95) takes the form

$$\cos\theta\,\frac{\partial I}{\partial r} - \frac{\sin\theta}{r}\,\frac{\partial I}{\partial\theta} + \frac{\sin\theta\sin\varphi}{r}\,\frac{\partial I}{\partial\varphi} - \frac{\operatorname{ctg}\varphi\sin\theta\sin\psi}{r}\,\frac{\partial I}{\partial\psi} =$$
$$= -\,[\alpha(r) + \sigma(r)]\,I + \frac{\sigma(r)}{4\pi}\int I(r,\varphi;\theta,\psi)\,\gamma(r,\varphi;\theta,\psi;\theta',\psi')d\omega'. \qquad (1.96)$$

We retain the previous notation for coordinates of the point P and the ray direction, since we can then consider any section of the sphere.

References [89-91] described approximate methods for solving Equation (1.96), in which the intensity of radiation I was replaced by the value J averaged over all directions, and they considered special cases of solving this equation for constant and exponentially diminishing absorption coefficients.

Reference [92] considered a method of solving Equation (1.95) by successive approximations, where the zero order approximation was the solution of the transfer equation for a plane-parallel model of the atmosphere. In this approach the coordinate system is transformed so that the radius passing through the center of the Earth and the point P coincides with the local zenith. Then the position of P will be determined, as in the plane model, by the height above the surface of the Earth, while the displacement of P can be expressed in terms of the zenith distance ζ_0 and the solar azimuth $\psi_\odot$. The direction of the rays will also be determined by the zenith azimuthal angles ϑ and δ. It is easy to show that

Equation (1.95) takes the form

$$\cos\vartheta\,\frac{\partial I}{\partial r}-\frac{\sin\vartheta}{r}\,\frac{\partial I}{\partial\vartheta}+\frac{\sin\vartheta\sin\zeta_0}{r}\times$$

$$\times\left[-\frac{\cos(\psi_\odot-\delta)}{\sin\zeta_0}\,\frac{\partial I}{\partial\zeta_0}+\frac{\cos\zeta_0\sin(\psi_\odot-\delta)}{\sin^2\zeta_0}\,\frac{\partial I}{\partial(\psi_\odot-\delta)}\right]=$$

$$=-[\mathfrak{s}(r)+\alpha(r)]\,I(r,\vartheta,\delta;\zeta_0,\psi_\odot)+\frac{\sigma(r)}{4\pi}\int I(r,\vartheta',\delta')\times$$

$$\times\gamma(r,\vartheta,\delta;\vartheta',\delta')\,d\omega'+\frac{\pi S}{4}\,[\sigma(r)+\alpha(r)]\,\gamma(r,\vartheta,\delta;\zeta_0,\psi_\odot)\times \qquad (1.97)$$

$$\times\exp\left\{-\int\limits_r^\infty[\mathfrak{s}(h)+\alpha(h)]\,dh\right\}.$$

Further simplification of Equation (1.97) is achieved by considering <u>/65</u> the molecular scattering atmosphere ($\alpha\equiv0$, $\sigma=$ const), for which the air mass $m(z,\zeta_0)=\int\limits_z^\infty\rho(h)\sec\zeta_0(h)\,dh$ and the optical thickness $\tau=\sigma m\cdot$ (z,ζ_0) can be expressed in terms of the so-called Chapman function Ch (r/H, ζ_0) and the height of the homogeneous atmosphere H. In this case Equation (1.97) takes the form

$$-\cos\vartheta\,\frac{\partial I}{\partial\tau}+\frac{H}{r\tau}\left\{-\sin\vartheta\,\frac{\partial I}{\partial\vartheta}+\sin\vartheta\sin\zeta_0\times\right.$$

$$\times\left[-\frac{\cos(\psi_\odot-\delta)}{\sin\zeta_0}\,\frac{\partial I}{\partial\zeta}+\frac{\cos\zeta_0\sin(\psi_\odot-\delta)}{\sin^2\zeta_0}\,\frac{\partial I}{\partial(\psi_\odot-\delta)}\right]\right\}= \qquad (1.98)$$

$$=-I+\frac{1}{4\pi}\int I\gamma\,d\omega'+\frac{\pi S}{4}\,\gamma(\theta,\delta;\zeta_0,\psi_\odot)\exp\left[-\tau\,\mathrm{Ch}\left(\frac{r}{H},\zeta_0\right)\right].$$

We can use Equation (1.98) to obtain qualitative estimates of the curvature of the atmosphere, described by the term in curved brackets*. Quantitatively, the effect of the curvature is determined by the parameter H/r, in terms of which the solution of Equation (1.98) was given in [92]:

$$I(\tau,\vartheta,\delta;\zeta_0,\psi_\odot)=\sum_{n=0}^\infty\left(\frac{H}{r}\right)^n I_n(\tau,\vartheta,\delta;\zeta_0,\psi_\odot). \qquad (1.99)$$

The functions I_n are successive approximations to the solution, and I_0 is a solution of the transfer equation in the plane-parallel atmosphere.

---

* The effect of temperature increases with decrease of τ and with increase of ζ_0 or ϑ. When ϑ and $\zeta_0\to0$ the effect of curvature is vanishingly small.

The convergence of the series (1.99) and the behavior of the solutions under different conditions, especially for large ϑ and ζ_0, and also in the terminator region, was not examined in [92]. Also, no effective solution of the spherical problem was given, although, as was shown in the monograph [B.12], some calculations and evaluations of the brightness distribution over the Earth's disk were obtained later in [93]. The approximate methods considered in [90-92] were not accompanied by an estimate of the error, which can be small even in conditions where the curvature of the atmosphere is important. In addition, these simplified methods require quite laborious calculations, even for relatively simple atmospheric models. Therefore, rigorous solutions are needed for the transfer equation for radiation in a spherical atmosphere whose optical parameters correspond to the actual conditions.

Solutions like these were obtained recently by Marchuk et al. [94, 95] using a Monte Carlo method, which allows the process of photon transport in a turbid medium to be modeled with quite low statistical error (the calculations were done on a BESM-6 computer).

To illustrate the possibilities of the method, reference [95] obtained angular distributions of the brightness of the twilight light above the Earth's surface for the model atmosphere constructed by Rozenberg et al. [96] from observations of space twilight on the /66 space vehicle Vostok 6.

Comprehensive computer calculations of the brightness of the spherical Earth were performed in [79, 97] from numerical solutions of the radiative transfer function in a scattering, absorbing, and radiating atmosphere with quite broad assumptions as to the spatial distribution of optical and physical parameters of the atmosphere and of the clouds, governing the brightness field. These calculations used a finite-difference method for integrating the

transfer equation, embodying characteristics of the equation to insure stability of the computational algorithms, permitting investigation of the local structure of the solution of the transfer equation, and given high accuracy, in spite of the complexity of the atmospheric model.

CHAPTER 2

THE EARTH'S SELF RADIATION

§ 1.   Generation of Self-Radiation in the Atmosphere

1.1.   Basic Processes in Formation of Thermal Radiation

The solar radiation absorbed by the Earth's surface and
atmosphere is an energy source which feeds thermal and dynamic
processes on the Earth. The distributions of temperature,
humidity, and clouds resulting from these processes mainly deter-
mine the self-emission of the Earth and its variation.

The underlying surface, and every volume element of the
atmosphere, having a given temperature, are sources of thermal
radiation, which, for ground temperatures of 200 - 320° K, is
concentrated in the spectral range 3 - 5 μm, with a maximum
energy in the range 8 - 15 μm.

The emission of the underlying surface is determined not
only by its temperature T_0, but also by the emittance δ, which
depends on the type of structure, the moisture content, and other
characteristics of the underlying surface, as well as on frequency.
This emission is entirely or partially absorbed (depending on ν)
in the atmosphere by water vapor, carbon dioxide, ozone, and
other substances, while the part not absorbed goes to outer space.

The thermal radiation absorbed in the atmospheric layer up
to 70 km is reradiated in accordance with the conditions of local
thermodynamic equilibrium, following Kirchhoff's law: the ratio
of the emission coefficient η_ν to the absorption coefficient α_ν

depends only on the temperature of a radiating gas T(z) at level z:

$$\frac{\eta_\nu}{\alpha_\nu} = B_\nu [T(z)],$$

where $B_\nu[T(z)] = 2hc\nu^3/(e^{h\nu/kT} - 1)$ is the Planck function, c = $3 \cdot 10^{10}$ cm/sec is the speed of light; h = $6.62 \cdot 10^{-27}$ erg/sec is the Planck constant; and k = $1.38 \cdot 10^{-16}$ erg/deg is the Boltzmann constant. Therefore, each volume element of the atmosphere emits radiation of a certain frequency in all directions, depending on the temperature of the element, the concentration of absorbing substances, the total and partial pressure, and also on parameters describing the fine structure of absorption bands.

The radiation from the atmosphere and the underlying surface is absorbed by lower-lying layers of the atmosphere or clouds. Here rather dense clouds, which practically completely absorb the thermal radiation, can be considered as an underlying surface interposed above the ground surface and radiating independently of the radiation conditions in the sub-cloud atmospheric layer. Only in particular parts of the spectrum, where absorption is not as great, need one take into account scattering of thermal radiation by cloud particles (see [B.7]). However, the Earth loses only part of the atmospheric emission. The other part is radiated backwards to the underlying surface, which may partially reflect it back. The reflected radiation undergoes the same changes on its way to the upper boundary as the self-emission from the surface does.

The result of these phenomenological processes generating thermal radiation is a field of Earth self-emission (in meteoro- /68 logy this radiation is called "long-wave," to distinguish it from the "short-wave" solar radiation reflected by the Earth, and considered in Chapter 1).

The presently existing data from experimental and theoretical investigations of the field of self-radiation indicate that it has a rather complex vertical, spatial, and angular structure, due mainly to the spatial variations of fields of temperature, humidity, and clouds. The spectral structure of the field, which is due to selective absorption of radiation by atmospheric gases, is also complex.

The present chapter gives a brief survey and analysis of some of the results of investigations of the Earth's self-radiation field, which investigations are important for aspects of optical probing aimed at exploring possibilities of gleaning data from appropriate measurements on the physical parameters of the atmosphere which play an important part in forming the radiation field. We also consider questions of transformations of radiant energy in the atmosphere, accounting for horizontal nonuniformities in the fields of underlying surface temperature or cloud, and present some results from investigations of the long-wave radiation field for the spherically symmetrical atmospheric model.

1.2. The Radiative Transfer Equation

In accordance with the above mechanism for forming thermal radiation, we can put $\sigma_v \equiv 0$; $f_v^{(1)} = a_v B_v [T(z)]$; $f_v^{(2)} = \delta_v B_v(T_0)$; $R_v = 1 - \delta_v$; $\pi S_v = 0$ in Equations (1.1) - (1.4). Then, using the relation $dp = -\rho g dz$, we obtain the following equations for determining the intensity of ascending $I_\lambda^\uparrow(p, \theta)$ and descending $I_\lambda^\downarrow(p, \theta)$ radiation at the level p:

$$\cos\theta \frac{\partial I_v^\uparrow}{\partial p} = c_v(p)\{I_v^\uparrow(p, \theta) - B_v[T(p)]\};$$

(2.1)

$$-\cos\theta \frac{\partial I_v^\downarrow}{\partial p} = c_v(p)\{I_v^\downarrow(p, \theta) - B_v[T(p)]\}.$$

(2.2)

111

Here the boundary conditions will have the form

$$I_\nu^\downarrow (p_0, \theta) = \delta_\nu B_\nu (T_0) + (1 - \delta) \int I_\nu^\downarrow (p_0, \theta) \cos \theta \, d\omega; \qquad (2.3)$$

$$I_\nu^\downarrow (0, \theta) = 0. \qquad (2.4)$$

If we assume that at frequency ν the radiation is absorbed by n substances of relative concentration $q_i(p)$ and mass absorption coefficient $k_\nu^{(i)}(p)$,* then the volume absorption coefficient can be represented in the form

$$\alpha_\nu (p) = \frac{1}{g} \sum_{i=1}^{n} k_\nu^{(i)} (p) \, q_i (p). \qquad (2.5)$$

Introducing the variable $\zeta = p/p_0$ (p_0 is standard pressure) and the characteristic scales for concentration of absorbing substances $q_0^{(i)} = q_i (p_0)$, we obtain a solution for Equations (2.1) - (2.4): /69

$$I_\nu^\downarrow (\zeta, \theta) = \delta_\nu B_\nu (T_0) \exp \left[- \sec \theta \sum_{i=1}^{n} w_0^{(i)} \int_\zeta^1 k_\nu^{(i)} (t) \, q_i (t) \, dt \right] -$$

$$- \int_\zeta^1 B_\nu [T(t)] \frac{\partial}{\partial t} \left\{ \exp \left[- \sec \theta \sum_{i=1}^{n} w_0^{(i)} \int_\zeta^t k_\nu^{(i)} (u) \, q_i (u) \, du \right] \right\} dt - \qquad (2.6)$$

$$- 2 (1 - \delta_\nu) \exp \left[- \sec \theta \sum_{i=1}^{n} w_0^{(i)} \int_\zeta^1 k_\nu^{(i)} (t) \, q_i (t) \, dt \right] \times$$

$$\times \int_0^1 B_\nu [T(t)] \frac{\partial}{\partial t} \left\{ E_3 \left[\sum_{i=1}^{n} w_0^{(i)} \int_t^1 k_\nu^{(i)} (u) \, q (u) \, du \right] \right\} dt,$$

$$I_\nu^\downarrow (\zeta, \theta) = \int_0^\zeta B_\nu [T(t)] \frac{\partial}{\partial t} \left\{ \exp \left[- \sec \theta \sum_{i=1}^{n} w_0^{(i)} \int_t^\zeta k_\nu^{(i)} (u) \, q_i (u) \, du \right] \right\} dt. \qquad (2.7)$$

Here $w_0^{(i)} = p_0 q_0^{(i)}/g$ is the mass of the $i^{\underline{th}}$ absorbing substance in a uniform atmosphere at standard pressure and temperature.

Because of the complex spectral behavior of $k_\nu^{(i)}$, we usually consider the average intensity over a range $\Delta \nu$

* In fact, the coefficients $k_\nu^{(i)}$ depend not only on the pressure p, but also on the air temperature T(p), and on the concentration of material, although this dependence can be neglected for the problems considered in this book.

112

$$\widetilde{I}_{\Delta \nu} = \frac{1}{\Delta \nu} \int_{\Delta \nu} I_\nu d\nu, \qquad (2.8)$$

for which we introduce the transmission function

$$P_\nu(\zeta, t, \theta) = \frac{1}{\Delta \nu} \int_{\Delta \nu} \exp\left[-\sec\theta \sum_{i=1}^{n} w_0^{(i)} \int_{\zeta}^{t} k_\nu^{(i)}(u)\, q_i(u)\, du\right] d\nu. \qquad (2.9)$$

Assuming that δ_ν is independent of ν within the range $\Delta\nu$, we obtain, from Equations (2.6) and (2.7):

$$\widetilde{I}_\nu^{\uparrow}(\zeta, \theta) = \delta_\nu \bar{B}_\nu(T_0)\, P_\nu(1, \zeta, \theta) - \int_{\zeta}^{1} \bar{B}_\nu[T(t)] \frac{\partial P_\nu(\zeta, t, \theta)}{\partial t}\, dt - \qquad (2.10)$$

$$- 2(1 - \delta_\nu)\, P_\nu(1, \zeta, \theta) \int_{0}^{1} \bar{B}_\nu[T(t)] \frac{\partial \widehat{P}_\nu(t, \zeta, \theta)}{\partial t}\, dt;$$

$$\widetilde{I}_\nu^{\downarrow}(\zeta, \theta) = \int_{1}^{\zeta} \bar{B}_\nu[T(t)] \frac{\partial P_\nu(t, \zeta, \theta)}{\partial t}\, dt. \qquad (2.11)$$

Here

$$\bar{B}_\nu = \frac{1}{\Delta \nu} \int_{\Delta \nu} B_\nu d\nu;$$

$$\widehat{P}_\nu(t, \zeta, \theta) = \frac{1}{\Delta \nu} \int_{\Delta \nu} \exp\left[-\sec\theta \sum_{i=1}^{n} w_0^{(i)} \int_{\zeta}^{1} k_\nu^{(i)}(u)\, q_i(u)\, du\right] \times \qquad (2.12)$$

$$\times E_3\left[\sum_{i=1}^{n} w_0^{(i)} \int_{t}^{1} k_\nu^{(i)}(u)\, q_i(u)\, du\right] d\nu.$$

We shall keep the subscript ν for the average values, corresponding, for example, to the center of the interval $\Delta\nu$ (we shall omit the subscript in what follows). Thus, the basic question in calculating characteristics of the Earth's self-radiation is how reliable is our description of the selective emission of atmospheric gases.

§ 2.   Transmission Functions for the Atmosphere

As was true for the short-wave region of the spectrum (see
§ 2 of Chapter 1), in describing the selective absorption of
thermal radiation by triatomic gases (water vapor, carbon dioxide,
and ozone), whose absorption bands consist of a large number of
overlapping lines, we use transmission functions obtained by
experiment or calculation from idealized band models (the Elsasser
model, which represents the transmission function analytically by
Equation (1.14) or (1.16), the Good [B.8] statistical band
model, or the quasi-statistical model of Planck, Equations (1.16),
(1.17).   We also use a number of empirical expressions for the
transmission functions, e.g., Equations (1.18) - (1.21).   All the
arguments put forward in § 2, Chapter 1 with respect to the
applicability of the empirical or theoretical formulas for P_ν in
the real atmospheric conditions apply equally to the thermal
region of the spectrum.   However, since the spectra of the
atmospheric self-radiation will be used to solve some inverse
problems which require maximum possible similarity between the
atmospheric transmission characteristics used and the real values,
we will consider in more detail the existing data on transmission
functions of atmospheric gases in the chosen spectral ranges.

2.1.   Transmission Function for Water Vapor in the 6.3 μm Band

In the region 3 - 50 μm water vapor has a strong rotation-
vibration band at 6.3 μm, and a series of rotational bands in the
long-wave region beyond 25 μm.   In this range, there are so-called
transparent windows in the ranges 8 - 12 and 16 - 24 μm, in which,
however, there are a number of weak bands, and appreciable diffuse
absorption of radiation by the atmosphere is observed.   The nature
of this absorption has not finally been explained: it is suggested
that absorption in the windows is due either to aerosols, or to
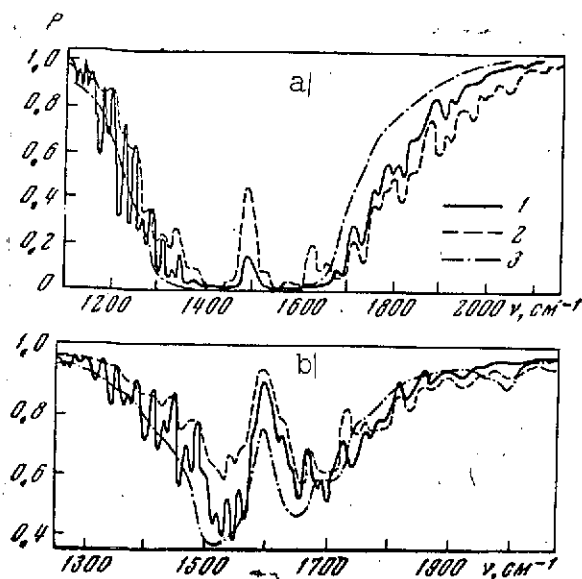
Figure 2.1. Comparison of experimental and calculated transmission functions in the 6.3 μm H_2O band

1- experiment [18]; 2- calculation [16]; 3- calculation using Equation (1.16); a-p = 805 mm Hg, w = 0.077 cm (experiment); p = 760 mm Hg, w| = 0.1 cm (calculation; b-p = 773 mm Hg, w = 0.0018 cm (experiment); p = 760 mm Hg, w = 0.002 cm (calculation)

the effect of the wings of the strong absorption bands of water vapor and carbon dioxide (the latter hypothesis is preferred).

Detailed laboratory measurements of | the absorption spectra for the thermal radiation spectra of water vapor for rather wide range of variation of the total and partial pressures were performed in [1.20 - 1.23]. Examples of these measurements are given in Figures 2.1 and 2.2 for the H_2O absorption band at 6.3 μm.

A comparison of experimental /71 transmission functions in [1.22] with the calculations of Plass, et al. [1.16], and also with the calculations of P_ν using Equation (1.16) with the generalized absorption coefficients l_ν, obtained by Yamamoto [1], shows (Figure 2.1) that the Plass and Elsasser 6.3 μm band models do not satisfactorily approximate the trans-| mission functions. One reason for this divergence may be the different spectral averaging (in the experimental curves the spectral resolution is 6 cm^{-1}, and in the calculations of [1.16] it is 20 cm^{-1}, while the coefficients l_ν are obtained with an averaging interval of $\Delta\nu = 25$ cm^{-1}). We note that Equation (1.16) gives roughly the same approximation to the experimental data, as the more "exact" Plass quasi-statistical model [1.16].

Figure 2.2. Approximations for the experimental transmission function in the 6.3 μm H_2O band [18] (solid curves), and Equation (1.20) (broken lines)

1- p = 34 mm Hg, w = 0.004 cm;   2- p = 810 mm Hg, w = 0.01 cm.

A substantially better approximation for the spectral behavior of the transmission functions at 6.3 μm, as can be seen from Figure 2.2, is obtained by the empirical formulas of type (1.20), whose parameters were obtained in [1.20, 1.23] (for some bands these parameters are given in Table 1.2).

However, to use these formulas under actual conditions requires detailed comparison of refined laboratory measurements with measurements of radiative absorption in a multi-component and homogeneous medium like the atmosphere. No detailed comparisons have been made as yet. Calculation of the vertical behavior of pressure, temperature and humidity in the atmosphere, using the effective values of pressure and water vapor mass proposed in [1.20, 1.23] for transmission functions of the type (1.20), is not well-founded, as yet. An exception is the rotational bands of water vapor in the region 20 - 50 μm, for which Kondrat'yev, et al. [2] made a series of calculations of transmission functions, and showed that an approximate allowance for atmospheric non-uniformity, using an effective mass or an effective pressure, gives quite acceptable accuracy for some atmospheric radiative transfer problems.

116

The spectral measurements made up till now of transmission functions for thermal radiation through water vapor in natural ground layer paths (see, e.g., [1.24, 3]), and also in balloon probing of transmission of solar radiation by the atmosphere in the 6.3 µm band [4] are haphazard in nature. And since no comparisons have been made between laboratory and natural transmission spectra, the latter have only an illustrative significance as regards their use in transfer theory.

At present transmission functions are being calculated directly with the help of fast computers (these calculations are based on some idealized structures of bands, e.g., an assumption of line shape). Besides the H_2O 2.7 µm bands [1.26] mentioned in § 2 of Chapter 1, we should mention the results of computer calculations of transmission functions in particular ranges of the H_2O rotational bands (18 - 25 µm), which were obtained in [5]. However, there are no such calculations of transmission /72 functions for the very complicated water vapor band at 6.3 µm, mainly because the structure of this band has not yet been studied and all the required molecular constants have not been determined. Taking into account the quite satisfactory approximations to transmission functions by formulas of type (1.20), we will use these in a number of calculations below, including solution of the inverse problem of determining the vertical humidity profile from satellite measurements of the Earth's self-radiation in the 6.3 µm H_2O band (see Chapter 7). To explain the method of solution of the direct and inverse problems, we will also use transmission functions of the form (1.16) with generalized Yamamoto l_{Ya} coefficients [1.6] (Table 2.1). For comparison, the table also shows l_E, calculated by Elsasser [7] with somewhat larger frequency averaging ($\Delta \nu$ = 40 cm^{-1}). The appreciable discrepancies between l_E and l_{Ya} are probably due to the different initial transmission functions (or the masses of absorbing material) for which

TABLE 2.1*

v, см⁻¹	l_E, см⁻¹	v, см⁻¹	l_{Ya}, см⁻¹	v, см⁻¹	l_E, см⁻¹	v, см⁻¹	l_{Ya}, см⁻¹
2080	0,110	2087,5	0,024	760	0,004	764	0,140
2040	0,257	2062,5	0,050	720	0,012	735,5	0,185
		2037,5	0,085			712,5	0,225
2000	0,617	2012,5	0,17	680	0,037	687,5	0,305
1260	1,38	1987,5	0,26	640	0,107	662,5	0,40
		1962,5	0,43			637,5	0,54
1920	3,16	1937,5	0,70	600	0,282	612,5	0,74
		1912,5	1,12	560	0,702	587,5	1,15
1880	8,13	1862,5	2,8			562,5	1,60
		1887,5	1,8	520	1,70	537,5	2,25
1840	24,0	1837,5	5,0			512,5	3,3
1800	72,4	1812,5	9,3	480	3,98	487,5	5,0
1760	147,9	1787,5	18,0	440	8,91	462,5	7,5
		1762,5	36,0			437,5	12
1720	195,0	1737,5	70	400	19,95	422,5	18
		1712,5	155	360	40,7	387,5	30
1680	120,2	1687,5	245			362,5	52
1640	36,3	1662,5	270	320	91,2	337,5	96
		1637,5	245			312,5	170
1600	30,90	1612,5	145	280	169,8	287,5	260
1560	102,3	1597,5	55	240	281,8	262,5	400
		1562,5	160			237,5	600
1520	288,4	1537,5	410	200	407,4	212,5	700
		1512,5	450			187,5	1100
1480	112,2	1487,5	270	160	489,8	162,5	1230
1440	43,6	1462,5	130	120	467,7	137,5	1250
		1437,5	78			112,5	1200
1400	18,6	1412,5	48,	80	295,1	87,5	970
		1387,5	13	40	109,6	62,5	650
1360	7,08	1362,5	10			37,5	330
1320	2,24	1334,5	4,4	40	12,6	12,5	12
		1312,5	1,9				
1280	0,550	1287,5	0,95				

* Translator's note: Commas in numbers represent decimal points.

l_γ were calculated. We prefer to use Yamamoto's data [1, 6], since they were improved | by the authors of [1] using measurements of transmission functions in the 6.3 μm band, and have proved to agree well with the data of Palmer [3] for the H_2O rotational band.

Finally, we note the universal calculations of monochromatic /73 water vapor absorption coefficients performed by Zhevakin, et al. [8] for the spectral range 8 μm - 2 cm, which includes a transmission window at 8 - 12 μm and a CO_2 band at 15 μm.

2.2. The 8 - 12 μm Transmission Window

Spectral measurements of transmission in the 8 - 12 μm window show that the atmosphere absorbs appreciably and emits radiation in this region of the spectrum. In fact, it can be seen from Figure 2.3 that there are a number of relatively weak lines (mainly H_2O and CO_2), and also the strong 9.6 μm ozone band. As regards the true transmission windows quite devoid of lines, they occupy rather narrow spectral ranges (they are denoted by the numbers 1 - 13 in the figure).
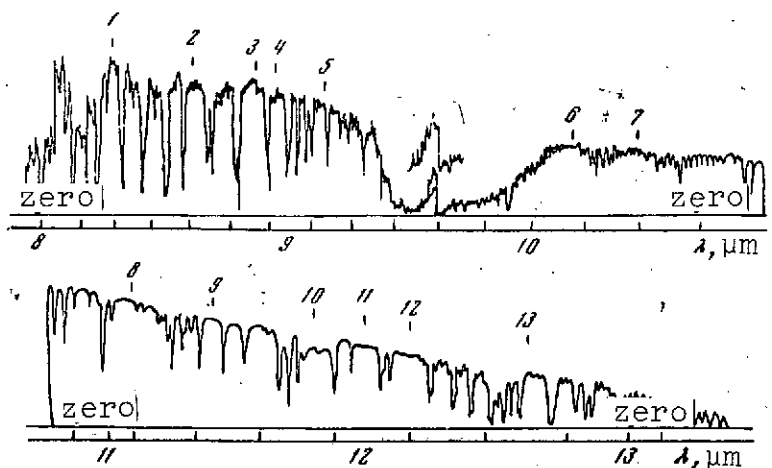
Figure 2.3. Spectral distribution of solar radiation in the transparent "windows", after [11]

References [9 - 15] obtained experimental data on the transmission of solar radiation by the atmosphere in the 8 - 12 μm region, which is evidence that appreciable and variable attenuation of radiation is observed in the windows. From these measurements, the selective absorption and continuum attenuation

of the radiation could be separated, which is not difficult when the spectral resolution is high enough.

A more complex problem is that of determining the contribution of substances responsible for continuum attenuation in the windows. It is well known (see, e.g., [9]), that there are two hypotheses regarding this matter: according to one hypothesis, the continuum attenuation in the windows is determined mainly by absorption of radiation in the wings of the strong water vapor bands located in the far IR; according to the other hypothesis, it is due to the aerosol component.

References [10 - 14] adopted the following procedure in separating the contributions of H_2O vapor and aerosols. From direct measurements of the intensity of solar radiation I_ν (m), for different air masses m in clear and stable weather throughout the entire measurement, "Bouguer" lines were constructed

$$\ln I_\nu = \ln I_\nu^0 - \tau m,$$

where I_ν^0 is a constant obtained by extrapolating measured values of $\ln I_\nu$ to m = 0; τ is the optical depth of the vertical atmospheric layer (for absolute measurements I_ν^0 is the solar radiation outside the atmosphere, and for relative measurements it also /74 describes the constancy of the parameters of the measuring equipment and allows us to evaluate the measurement errors under stable weather conditions).

Experimental values of τ, determined for stable daytime conditions, together with the masses of water vapor in the vertical column of the atmosphere w, which are constant during the day, are approximated by linear functions

$$\tau (w) = k_0 w + \tau_0,$$

(2.13)

where k_0 is the coefficient of absorption of radiation by water vapor, τ_0 is the optical depth of the dry atmosphere, including aerosols or other gaseous substances not associated with water vapor.

If we make no stiuplations regarding the nature and origin of aerosols, it automatically follows from this approximation, because of [11 - 14], that the continuum attenuation in the 8 - 12 μm windows is determined mainly by absorption in the wings of strong water vapor bands, since w in these papers is the total mass of H_2O vapor in the vertical atmospheric column, measured by radiosonde | or optical hygrometers. The values of k_0 then measured differ by approximately a factor of two.*

The characteristics of the residual absorption τ_0 in [11 - 14] turned out negative for several transparent windows in the range λ > 11 μm (Figure 2.4 a), which the authors in question think can be explained by the nonlinear dependence of τ on w. /75 As was pointed out in [14], a confirmation of this hypothesis is the nonlinear dependence of τ on w obtained in laboratory measurements [16] at large partial pressures of water vapor in a flask. | The authors of [12, 13] who obtained τ_0 > 0 with the linear approximation of type (2.13) for their measurements in all the windows, believe that negative values of τ_0 in [11] arise from errors of measurement.**

---

* In some references (e.g., [11]), the effective masses of water vapor w_e, defined by Equation (1.17) with $\kappa = 1$ are used in lieu of w in Equation (2.13). This leads to an increase of k_0 in Equation (2.13) of 20 - 30%, which one should bear in mind when comparing data of [11] with that of [12 - 14], where no exact mention was made of what w was used in approximations of the type (2.13).

** It should be noted that in [13], besides the graphical approximations of type [2.13), which are also reproduced in [12] for the same windows, a table is given showing scatter in values of τ, observed in [13] for the different ranges of w. However, this scatter is not taken into account in [12, 13] in constructing the straight lines [13], which makes it difficult to compare the appropriate results of [12, 13] with data from other references.
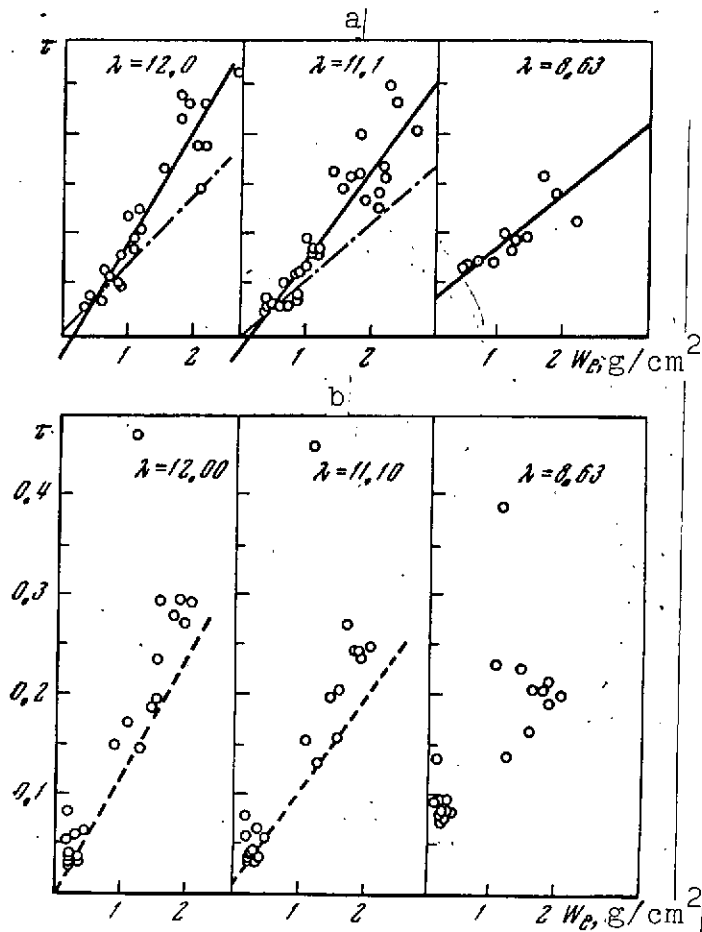
Figure 2.4. Approximations of Equation (2.13) for the experimental values of τ

a- in [11]; b- in [15]; the broken lines show approximations for the minimum value of τ; the wavelength λ is in μm

Without going into a detailed discussion of the correctness of the linear approximation in (2.13), we note that if it were valid, then the values of τ_0 obtained correspond in essence to a dry aerosol atmosphere, for which the attenuation in nondusty atmospheric conditions can be considered quite small, or corres-| pond| to substances not associated with water vapor. But in humid atmospheric conditions, a substantial contributor to the attenuation can be liquid or solid water particles whose concentration

and size can be closely correlated with the water vapor. There is no basis for considering that the tendency for τ to decrease with increase of w, as observed experimentally [11, 14], is evidence of the dominant role of water vapor in the continuum attenuation. In addition, the existence of situations where water vapor is found to be highly correlated with drops or crystalline moisture can fully explain the above large differences in the values of k_0 and the negative values of τ_0, if these parameters were obtained by the approximation of (2.13) to the experimental data.

In fact, the observed scatter in [11, 14] goes beyond the limits of measurement and reflects actual variations in the optical depths. In particular, as can be seen from Figure 2.4, the values of τ can differ by a factor of 2 - 3 for the same values of w, and consequently, in the framework of a monotonic dependence of τ on w, which in fact was looked for in [11 - 14], this scatter is due to other factors (very likely it corresponds to conditions for which a different law holds between the mass of water vapor and the concentrations for the size range of particles of aqueous origin). The formal approximation to the experimental data by Expression (2.13), performed, for example, by the method of least squares, can lead (and in fact does) also to negative τ_0 and to overestimated values of k_0, especially for large scatter of τ in a comparatively narrow range of variation of w, in particular in the absence of measurements for low w. Therefore, the negative values of τ_0 obtained in [11, 14] do not constitute, in our opinion, sufficient basis for a conclusion that the dependence of τ on w is linear, nor for any other physical conclusions. Also, the reasons for an overestimate of k_0 in the straight-line approximation are fully understood in the case of large scatter in τ: the presence of large values of τ, which are not directly connected with the mass of water vapor, always leads to an increase in the slope of the straight lines in [2.13]. In
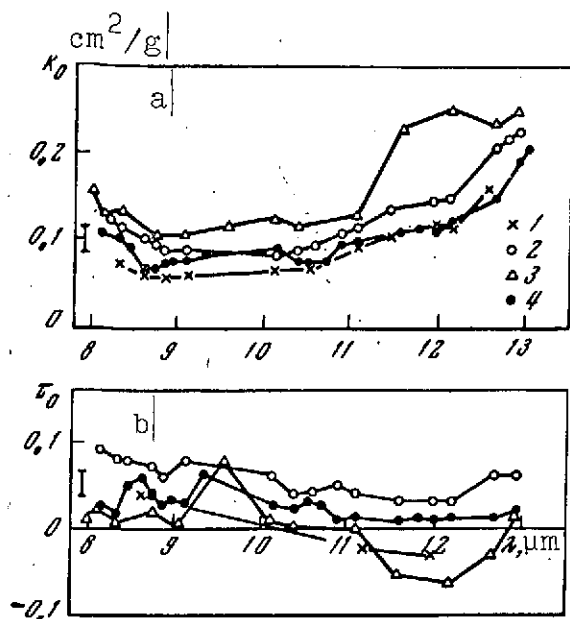
Figure 2.5. Comparison of coefficients k_0 (a) and τ_0 (b) of Equation (2.13), obtained in [11] (1), [12] (2), [14] (3), and [15] (4)

fact, as can be seen from Figure 2.4, it is enough to exclude large τ for fixed w in the range $1 < w < 2$ cm, as the value of τ_0 becomes positive, and the values of k_0 decrease (broken line in Figure 2.4 a). Hence, we deduce, among other things, criteria for choosing the points τ, which we must approximate by the straight lines of (2.13) to determine the parameters k_0 which are closest to the actual coefficients for absorption of radiation by water vapor. The straight lines of (2.13) are drawn for minimum values of τ for different (and necessarily small) values of w, within the range of scatter of the points, due to the actual errors in the experiment. This approach was used in [15] in treating measurements of transmission of IR solar radiation by the atmosphere, and of emission of an artificial source in the ground layer of air. It can be seen from Figures 2.4 b and 2.5 b that the residual attenuation remains positive in all the windows, while from Figure 2.5 a, it is seen that the coefficients k_0 have a minimum value and are close to the values of k_0 obtained in [11] for an entirely transparent atmosphere (the effective masses of water vapor w_e were used in Equation (2.13) in comparing these data). Here, one must bear in mind that the realization of small values of τ for large w is a rare event, since under these conditions there is very probably the closest relationship between the mass of water vapor and the aerosol characteristics. Therefore, the coefficients k_0

obtained with this kind of approximation can turn out to be only an upper limit on the actual values of coefficients for absorption of IR radiation in the wings of the water vapor bands.

Conclusive proof that a close relation between vapor and water particles can lead to an apparent dependence of radiation attenuation on water vapor mass is given by results of measurements of transmission in the ground layer of the atmosphere (path lengths 1.4 km) for different windows in the UV, visible, and IR spectral regions. As can be seen from Figure 2.6, the maximum dependence of the attenuation coefficient σ on w appears in the ranges λ = 0.37 and 0.50 µm, where water vapor absorption bands are totally absent. This effect is apparently connected with the increase in aerosol scattering with increase in w. There is an appreciable dependence of σ on w also for λ = 3.16 µm, due to the presence in this region of the strongest water vapor absorption band. In the window at 3.9 µm, where both the aerosol scattering and the water vapor absorption are low, σ is practically independent of w (the scatter in the points is also a minimum here). But in the windows at 2.7 and 10 µm the dependence of σ on w is more distinct from the background scatter, since aerosol scattering is still noticeable in the first window, and absorption in the second window.

We shall briefly discuss the nonlinear relation $\tau(w)$ examined in [11] as a basic cause of negative values of τ_0. The nonlinearity was attributed in [11] to self-broadening of the water vapor lines and to a positive temperature dependence of the continuum absorption coefficients in the wings. However, recent measurements of radiation transmission in the windows [17], obtained by one of the authors of [11] under laboratory conditions, showed a negative temperature gradient of absorption. For this reason, doubt was expressed in [17] about the correctness of the previous nonlinear behavior of $\tau(w)$, given in [11], and it was
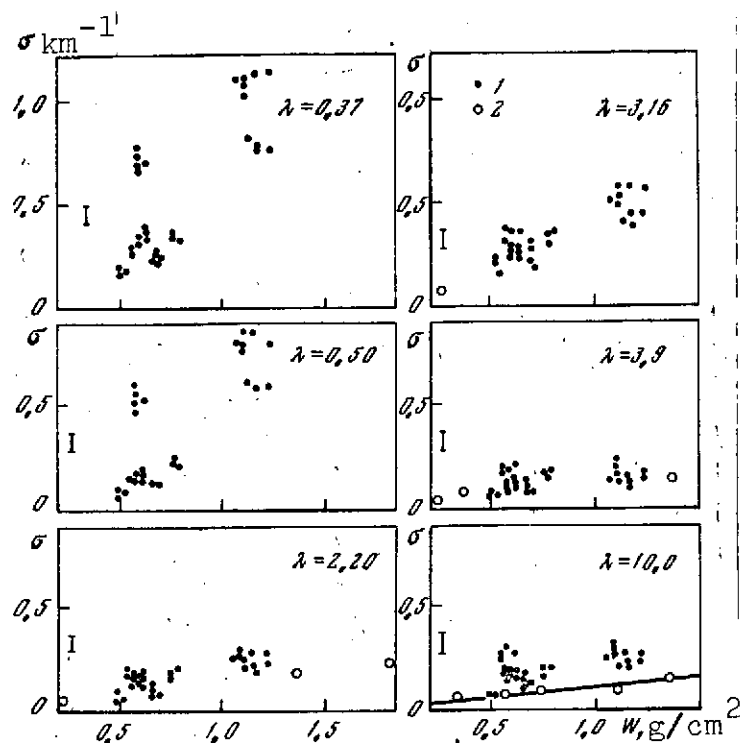
Figure 2.6. Dependence of the atmospheric attenuation coefficient
in the different UV, visible, and IR spectral regions (λ is in
μm)

1- in the ground layer; 2- in a vertical column of the atmosphere,
reduced to a uniform atmosphere using the average humidity pro-
file. The vertical sections show the errors in measurement of
λ (in μm)

proposed to investigate the effect of dimer molecules of water
vapor. The example given in [17] of nonlinear behavior of the
optical thickness in the window at 11.1 μm with increase of the
partial pressure of water vapor in a vessel from 10 to 35 mbar,
is evidence that, for high humidity, the nonlinear effects can
play an important part in the variations of the continuum
absorption. However, the nature of these nonlinear effects is
not clear. In particular, one cannot exclude the possibility
that they are associated with the formation of aqueous aerosols
in the vessel, as was shown in [18, 19].

We note that the existence of nonlinear dependences of τ on the humidity characteristics by no means contradicts the above linear approximation (2.13) for minimum values of τ, as long as we are looking for an empirical relation dependence on only one humidity parameter, w. But if we attempt to explain the dependence of τ on other humidity characteristics, we must then have a more general group of measurements of the variation of atmospheric attenuation, before determining numerical characteristics of an aerosol responsible for these variations.

Thus, the interpretation of the above results of measurements of attenuation of IR radiation in the transparent windows of the atmosphere at 8 - 12 μm allows|conclusions to be drawn regarding the predominant contribution to this attenuation of aerosols of aqueous origin, even under pure and, presumably, dust-free atmospheric conditions.

2.3. CO_2 Transmission Function /78

Since the 15 μm CO_2 band is important for the problem considered in Chapter 6, i.e., determining the vertical distribution of the atmospheric temperature from satellite measurements of Earth's radiation, we present rather detailed data on the structure of this band and on the transmission in its various sections, obtained in [20 - 26]. As is known (see, e.g., [24]), the 15 μm CO_2 band is made up of vibrational-rotational bands, corresponding to vibrational transitions of the different isotopes of CO_2 in the atmosphere. Each of these bands includes two systems of P and R branch lines, lying on both sides of the vibrational transition ν_0, and a system of Q branch lines, concentrated near ν_0. The intervals between the P and R branch lines are 1.45 - 1.70 cm^{-1}, while the Q branch occupies a range of the order of 1 cm^{-1}, and so the distance between its lines is a hundred times less

(half of the intensity of the entire 15 μm band falls in the Q branch).

The intensities at the line centers were calculated by Yamamoto, et al. [21], and also by Dreison, et al. [22]. The latter reference determined these parameters for 7,000 lines, including the Q branch lines, and for six values of temperature in the range 175 - 300°K, and the range of variations of intensity was 7 orders of magnitude. The centers and the intensities of the strongest lines obtained in [21, 22] turned out to be rather close, with certain exceptions. This encourages us to hope that the transmission functions determined from calculated characteristics of the band fine structure, which must be supplemented by data on the shape and half-width of the lines, are representative. Usually atmospheric transmission functions are calculated using a Lorentz line shape (1.15). But for the 15 μm CO_2 band, even at pressures less than 100 mbar, one must take account of Doppler broadening of the lines and calculate the absorption coefficient using a mixed line shape (Voigt profile):

$$k(\omega) = \frac{k_0 a}{\pi} \int\limits_{-\infty}^{+\infty} \frac{e^{-x^2}\, dx}{a^2 + (\omega - x)^2} \cdot \qquad (2.14)$$

Here

$$k_0 = (S/\gamma_D)\sqrt{\ln 2/\pi}; \quad a = (\gamma_L/\gamma_D)\sqrt{\ln 2}; \quad \omega = [(\nu - \nu_0)/\gamma_D]\sqrt{\ln 2},$$

$\gamma_D = 5.6 \cdot 10^{-4}$ cm^{-1} (at T = 240°K) is the Doppler half-width of the lines; γ_L is the Lorentz half-width, equal to 0.064 cm^{-1} at standard pressure, and T = 298° K, according to Kaplan, et al. [26]. The integrals in (2.14) were calculated in [24, 27] for a wide range of change of the basic parameters.

In more recent experimental investigations of the 15 μm band (see, e.g., [20]) and other CO_2 bands, it was observed that γ_L depends on the quantum number J, and varies in the range

$0.06 - 0.126$ cm^{-1}. By analyzing the results of these investigations, the authors of [25] suggested the use of the constant value $\gamma_L = 0.08$ cm^{-1} for the entire band, which gives an approximation to the experimental transmission functions obtained in [28] for a wide range of pressure and CO_2 mass, with practically the same accuracy as for the variable value of γ_L (Figure 2.7). The exception is the high pressure case, in which $\gamma_L = 0.06$ cm^{-1} is a better approximation. The authors of [25] did not give a satisfactory explanation for this discrepancy, but assumed that it is associated with experimental errors.*

We now consider some results of determining the transmission /79 functions in the 15 µm CO_2 band. Yamamoto, et al. [21], using a somewhat improved Elsasser model, calculated the 15 µm band transmission function with a spectral average equal to the distance d = 1.7 cm^{-1} between the strongest lines. For this series, the transmission function was determined using Equation (1.14). Reference [21] also calculated correlations for a second series /80 of weaker lines, for which it was assumed that their centers were located at the same distance d apart, as the centers of lines of the first series, and at the same distance δ from the latter.

As regards the transmission function in the Q branch, for which the overlap with the P and R branches is calculated by multiplying by the appropriate transmission functions, the calculation is performed by the formula proposed by Kaplan, et al. [26]:

$$P_Q(\nu) = e^{-k_Q(\nu)},\tag{2.15}$$

where

$$k_Q(\nu) = \frac{S_Q \zeta^2}{2\pi\gamma} \int_0^\infty \frac{e^{-x^2}\,dx}{(x - \xi)^2 + \zeta^2}\tag{2.16}$$

---

* We note that Drayson, one of the authors of [25], always used the value $\gamma_L = 0.064$ cm^{-1} [23] in his calculations of transmission functions.
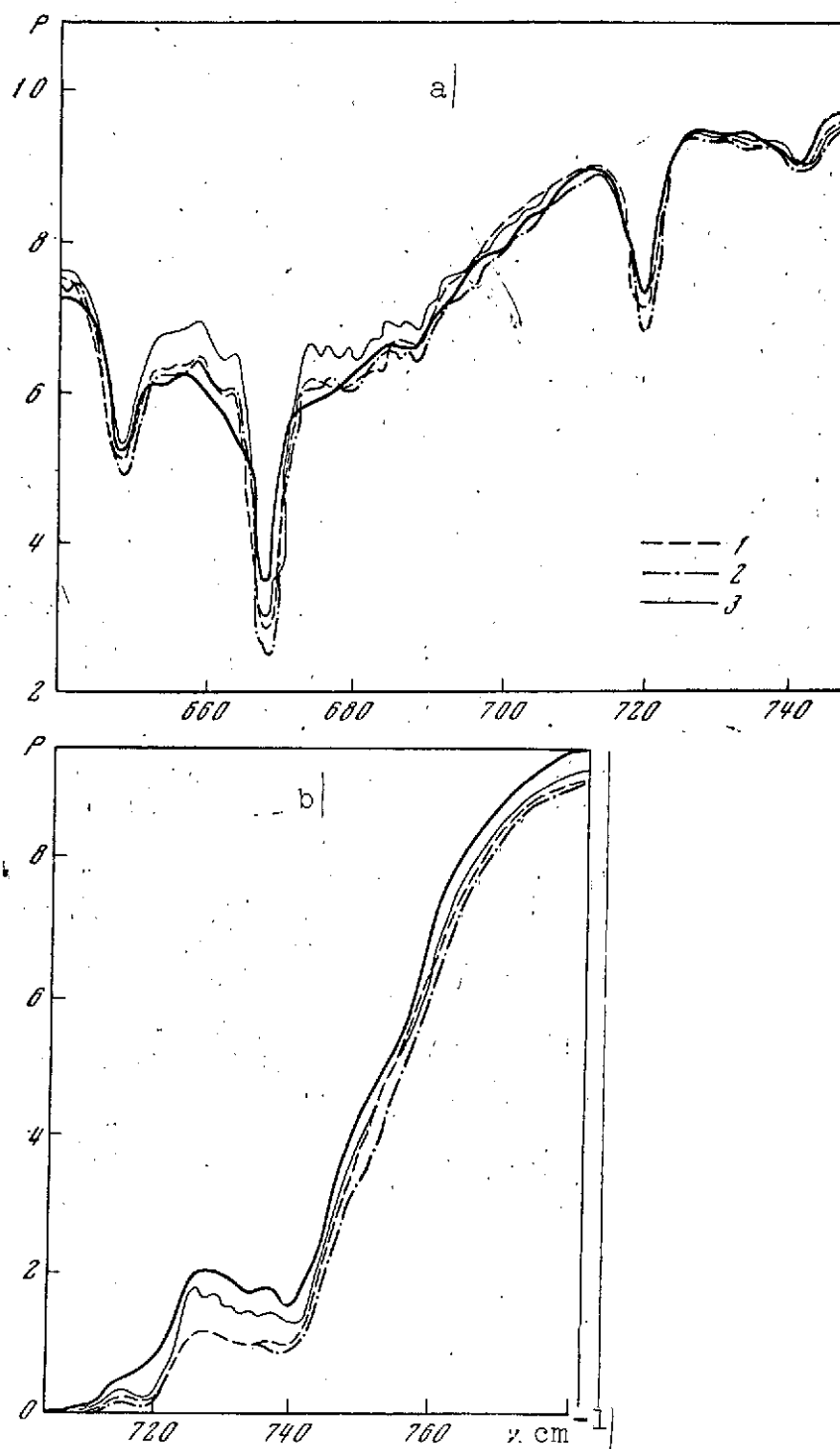
Figure 2.7. Comparison of experimental transmission functions in the 15 μm CO_2 band [28] (boldface curves) with the calculations of [25]

a- p = 0.0205 atm, u = 6.3 atm cm; b- p = 1 atm, u = 106.2 atm cm; 1- γ_L is variable; 2- γ_L = 0.08 cm^{-1}; 3- γ_L = 0.06 cm^{-1}

is the absorption coefficient in the Q branch; S_Q is the intensity of absorption in the whole Q branch; $\zeta = a\gamma/(B' - B'')$; $\xi = a(v - v_0)/(B' - B'')$; $a = hcB''/kT$; B' and B" are the lower and upper positions of the rotational constants.

Nonuniformity of the atmosphere with height was accounted for in [21] by introducing an effective mass which, because the relative concentration of CO_2 was constant, is directly related to the pressure by the following relationship:

$$u_e = u_0\left(1 - \frac{p^2}{p_0^2}\right),$$

(2.17)

where $u_0 = c_0 p_0/g\rho_0$ is the total mass of CO_2 in a vertical column of the atmosphere at constant pressure p_0 and volume concentration c_0 (u_0 is in atm·cm).

A better method of calculating the transmission function in the 15 μm CO_2 band was used in [1.17]. Using molecular constants of the 15 μm CO_2 band calculated for actual isotopic constituents of the CO_2 molecule, the authors of [1.17] determined the transmission functions, using a quasi-statistical model of the absorption band, as was done for water vapor (see section 2.2 of Chapter 1). They assumed that the line shape was given by the Lorentz formula for the central part and the Benedict formula in the line wings, i.e.,

$$k(v) = \begin{cases} \dfrac{S}{\pi}\dfrac{\gamma_L}{(v - v_0)^2 + \gamma_L^2}, & |v - v_0| \leqslant d, \\ \dfrac{SA}{\pi}\dfrac{\gamma_L}{(v - v_0)^2 + \gamma_L^2}\exp(-a|v - v_0|^b), & |v - v_0| \geqslant d, \end{cases}$$

(2.18)

where the constant A is chosen so that the profile is continuous for $|v - v_0| = d$, = 2.5 cm^{-1}; the constants a = 0.0675 $cm^{0.7}$, b = 0.7; γ_L = 0.06 cm^{-1} at T = 300° K and standard pressure. The more rapid decrease in line intensity given by (2.18) at the
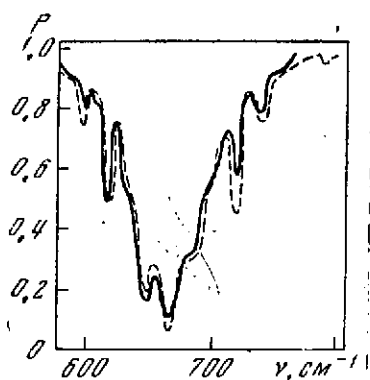
Figure 2.8. Comparison of experimental transmission functions in the 15 μm CO_2 band [28] (solid lines) with calculations of [17] (broken lines) for p = 15.6 mm Hg, u = 46.4 atm cm

wings, in comparison with the Lorentz line shape, gives better agreement with experimental data. The calculations of transmission in [1.17] were done for values of temperature, pressure, mass of carbon dioxide and spectral averaging intervals given in section 2.2 of Chapter 1. To illustrate the quality of the data obtained, the authors of [1.17] compared calculations of transmission functions with the experimental data of Birch, et al. [28] (Figure 2.8). It can be seen that the agreement between the two curves is quite satisfactory, apart from the region of the extremes (according to the assumption in [1.17], the discrepancy arises from differences in the spectral averages used in the calculation and in the experiment).

However, in comparing the results of [1.17] with direct calculations of transmission functions in a nonuniform atmosphere, performed by Drayson [23] (Figure 2.9), appreciable discrepancies were observed (particularly in the Q branch region), which the author of [23] attributed to defects in the quasi-statistical band model, and also to differences between the intensities of the lines accounted for in the calculations. The overestimate of abdorption in [1.17] can also be due to the Curtiss-Godson approximation used to adjust the transmission function to the conditions of a nonuniform atmosphere.

/81
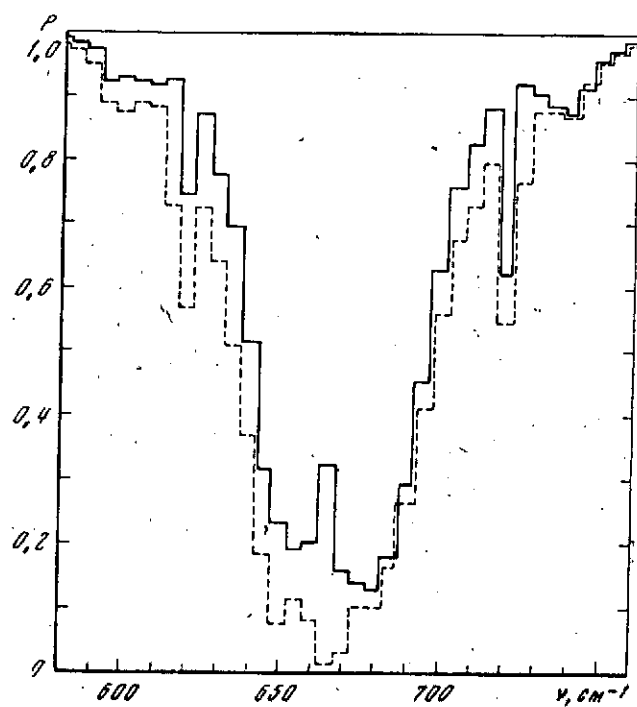
Figure 2.9. Comparison of the 15 μm CO_2 transmission functions calculated in [17] (broken line) and [23] (solid line)

Since we will use the Drayson transmission functions [23] later, we give a more detailed description of the method of calculation used in [23], which is based on molecular constants for the position and intensity of 2,000 lines of the 15 μm CO_2 band [22]. It was established by a calculation in [23] that the lines whose intensity is less than 10^{-4} cm^{-1} (atm cm)$^{-1}$ at T = 275° K have a negligibly small effect on absorption inside the interval of 0.1 cm^{-1} containing these lines. This allows us to separate the 982 strong and about 1,000 weak lines taken into account differently in [23].

The transmission function was calculated in a column of the atmosphere from the upper boundary down to each of 34 levels between 0.3 and 1013.25 mbar at six zenith angles: θ = 0.15, 30, 45, 60, and 75° (data were given in [23] only for θ = 0). The

133

volume concentration of CO_2 was calculated to be 0.0314%, and the vertical temperature profile was calculated from the standard model atmosphere US 1962. Down to the level of 1,000 mbar in [23] the Lorentz line shape was taken and the line halfwidth $\gamma_L(p_0)$ at p_0 = 1 atm and T = 298° K was considered to be the same for all lines and equal to 0.064 cm^{-1}. Above 100 mbar, the mixed Lorentz-Doppler line shape of Equation (2.14) was taken, where γ_D was calculated from the equation

$$\gamma_D = 3.58 \cdot 10^{-7} \nu_0 \sqrt{\frac{T}{M}} \quad (cm^{-1}),\qquad (2.19)$$

where M is the molecular weight. At a low enough pressure $\gamma_L \ll \gamma_D$ and then it follows from Equation (2.14) that

$$k(\nu) = k_0 e^{-\omega^2},\qquad (2.20)$$

i.e., one can use a purely Doppler absorption coefficient.

Very great computational complications arise from frequency averaging of the transmission functions. In [23] averaging was performed over intervals of 0.1 cm^{-1}, which made it possible to perform further averaging over wider intervals, allowing for the instrument function, for practically all existing spectral instruments. Certain approximate relations were used to simplify calculation of monochromatic transmission functions in the line wings. The Gauss quadrature formula was used in the central parts of the strong lines.

Reference [23] presented tables of transmission functions averaged over intervals of 5 cm^{-1}, with a shift of 1 cm^{-1} (Figure 2.10). For the Q branch (667.4 cm^{-1}), which consists of a large number of strong lines, more detailed transmission functions were given with a resolution of 0.1 cm^{-1} in the range 665.5 - 670.5 cm^{-1}.
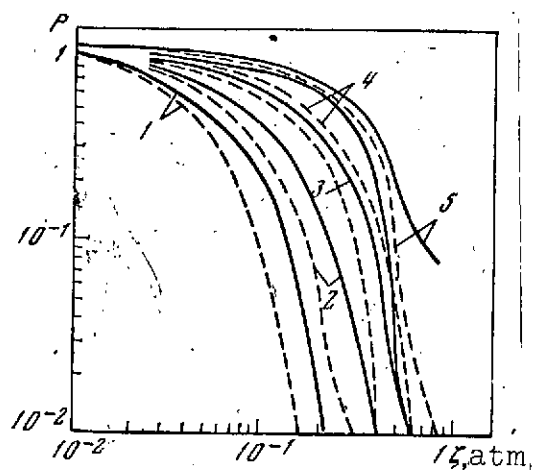
Figure 2.10. Comparison of the
vertical distributions of
transmission functions in six
ranges of the 15 µm CO_2 band,
obtained in [23] (solid
curves) and in [30] (broken
curves)

1- ν = 677.5; 2- 691; 3-
697; 4- 703; 5- 709 cm^{-1}

As has been mentioned, the
results of Drayson [23] disagree
with the calculated transmission
functions of Plass [1.17], and
yet there is no reason to consider
that [23], in spite of the validity
of the direct calculations, gives
a better approximation to the
true transmission functions. The
author of [23] does not give quan-
titative estimates of errors
associated with the uncertainty
in the band parameters assumed in
the calculation and associated
with the simplifying assumptions
(constant half-width, error in
determining the intensity and
position of lines, deviation of
air temperature from standard and

variations in CO_2 concentration), mentioning only that there is
presently no need for more exact calculations. Some estimates
of this kind were given by Kondrat'yev, et al. [29], who showed
that use of approximate methods for accounting for nonuniformity
and thermal stratification of the atmosphere (e.g., the Curtiss-
Godson method) in determining transmission functions in six
spectral intervals of the 15 µm band (see below) did not go out-
side the range of the actual accuracy of the direct calculations
of Drayson [23]. However, a comparison of the latter with trans-
mission functions in the same six spectral intervals 669; 677.5;
691; 697; 703; 709 cm^{-1}, calculated in [25] by the Curtiss-Godson
method (these data of York, et al. [30] were used to determine
the temperature profile from the emission I_ν of the atmosphere in
these regions of the spectrum) have shown that the transmission

functions of [23] exceed the data of [30] (Figure 2.10). This may be due both to the above-mentioned effect of the Curtiss-Godson method, and also to the possible calculation in [30] of selective and continuum absorption of water vapor in the spectral sections considered. One probable cause for the divergence of P in Figure 2.10 may be the differences in the band molecular constants or in the spectral averages adopted in the calculations [23, 30], as /83 well as differences in the atmospheric models used (for [30] we do not know the data*).

The results presented show that the 15 μm CO_2 band can be considered as well understood from the viewpoint of its fine structure and the behavior of the transmission functions, averaged over different spectral intervals, but one cannot yet state which of the above band models is the most valid. We note, further, that in the real atmosphere one must take into account overlap of absorption bands in CO_2, H_2O, and O_3. This is performed at present by multiplying the transmission functions of each gas component. Since the structure and the molecular constants of the H_2O and O_3 bands are not well enough known as yet, and the contribution of these components is rather small (in comparison with that of CO_2), it is allowable to use generalized Elsasser coefficients. As regards the continuum absorption in the windows of the 15 μm band, some data were given in section 2.2.

---

* We note that the results of the calculations of transmission functions which D. York kindly sent to the author privately, turned out, however, to be quite representative, as evidenced by the agreement of the measured values of I_ν with calculations employing these functions (see Chapter 6).

§ 3. Spectral Distribution of the Earth's Self-Radiation

3.1. Basic Properties of the Radiation Spectra

It follows from Equations (2.6) and (2.7), that the spectral distribution of the Earth's self-emission at an arbitrary level in the atmosphere ζ is a combination of the following radiation components:

1) Emission from the underlying surface, governed by its temperature T_0, the emittance δ_ν and the spectral absorbance of the atmospheric gases (the first term in Equation (2.6);

2) Emission from the atmosphere, which is a superposition of emissions from the constituent layers, and therefore, is completely determined by the vertical distribution of temperature and concentration of absorbing materials, and also by the absorption and emission spectra of the latter (the second term in Equation (2.6));

3) The descending atmospheric radiation, reflected by the underlying surface attenuated by the column of atmosphere lying above it (described by the third term in Equation (2.6), and determined by all the above parameters of the atmosphere and the underlying surface). Since the basic ground objects radiate in the thermal part of the spectrum, almost like black bodies (δ is /84 close to unity), the contribution of this component to the Earth's radiation is negligibly small (an exception is surfaces such as dry sand or clouds).

The characteristic special features and the variations in the spectral distribution of the Earth's self-radiation can be evaluated from the spectral measurements performed in recent years
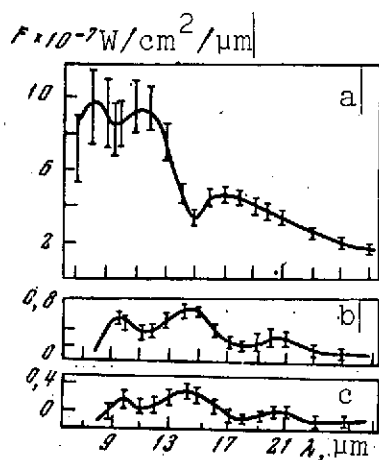
Figure 2.11. Examples of spectral measurements of the Earth's self-radiation according to Equation (2.23) a- at the nadir; b- at 0.5 - 1 degree above the horizon; c- at 1 - 1.5 degrees above the horizon

on Soviet satellites of the Kosmos series [31 - 33], the American VVS satellite [34], and on balloons [35] in conjunction with calculations of I_ν from formulas of the type (2.6) and (2.7) for certain model atmospheres [1, 36 - 38]. In spite of the comparatively coarse resolution of the spectral equipment used in the measurement of [31 - 33] (this was 1.2 - 1.4 μm in the spectral range 7 - 15 μm, and 2.4 - 2.7 μm in the range 16 - 27 μm), the results obtained give quite a satisfactory idea of the spectral behavior and the absolute intensity values of the Earth's radiation.

The use of equipment with higher resolution, (on the order of 0.4 μm in the range 6 - 15 μm, in the measurements of [34]) does not yield appreciable detail in a spectral picture of the radiation. As can be seen from Figures 2.11, a - 2.12, during observations within the terrestrial disc, the spectra showed minima of intensity, corresponding to the strong absorption bands of H_2O at 6.3 μm, of O_3 at 9.6 μm (Figure 2.12, a), of CO_2 at 15 μm, and of H_2O at 20 μm, and maxima at the transparent windows in the regions 8 - 12 and 17 - 18 μm (Figure 2.12, b). This basic property of the spectral curves means that the radiation temperature in the absorption bands will be less than the radiation temperature in the transparent windows. This follows from the relations between the emission of the underlying surface,
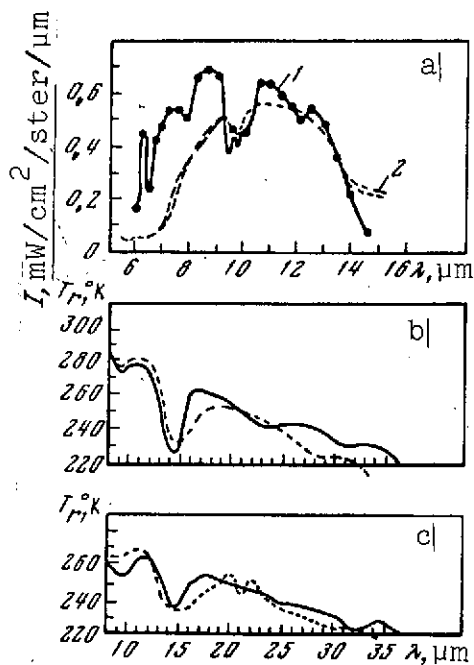
Figure 2.12. Comparison of experimental (solid curves) and calculated (broken curves) spectra of Earth radiation

a- from the data of [34]; b, c- from [32]

attenuated by the atmosphere (strongly in the absorption band, weakly in the windows), and the self-radiation of the atmosphere (mainly of the troposphere) which has a lower temperature. The result of this superposition is that the atmosphere radiates appreciably less in the absorption bands than in the adjoining transparent windows.

However, in measurements /85 outside the Earth's disc, when only the atmosphere falls in the field of view (Figure 2.11 b, c), the intensity of the emission, conversely becomes a maximum in the absorption bands (it will be shown below that a similar "inversion" can be observed also above high altitude cold clouds).

This inversion arises from emission of the warm layer of the mesosphere (30 - 50 km) which contains an appreciable amount of water vapor, carbon dioxide, and ozone, and, in accordance with Kirchhoff's law, causes an increase of the emitted energy in the bands relative to the transparent windows.

These peculiarities, which were also obtained theoretically from solution of the transfer equation for a plane [1, 36 - 38] and a spherical atmospheric model [39 - 45], should be regarded as a very simple criterion of the validity of the satellite measurements of the Earth's self-radiation in the various spectral

regions. In particular, the radiation temperature in the window at 8 - 12 μm should always increase the radiation temperature corresponding to the integrated emission (3 - 30 μm) (apart, possibly, from cases of measurements above high altitude cold clouds).

However, even within the framework of these very general laws, satisfactory agreement between measurements and calculations is not always obtained. This can be seen, for example, from Figure 2.13, which illustrates substantial differences between measured and calculated spectra, even of a qualitative nature.
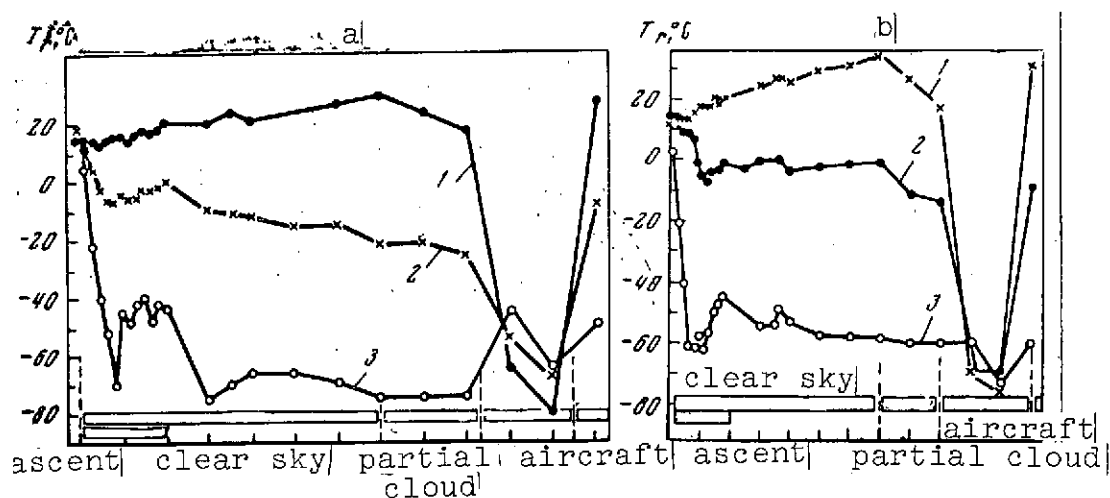
Figure 2.13. Distribution of radiation temperature above the ground and above clouds, from balloon measurements of [35] a- 1 - 3- λ = 8.5, 7.6, and 6.4 μm; b- 1 - 3- λ = 10.3, 9.63, and 14.5 μm

For example, in averaging the calculations over the spectral range 1.2 - 1.5 μm (in accordance with the experimental conditions of [31]), the comparatively narrow ozone band at 9.6 μm vanishes, although it remains quite strong in the experimental data. The lack of reliable control of the operation of the radiometric and spectral equipment on satellites makes it impossible

140

to determine the cause of these discrepancies. However, as shown by the results of many experiments on satellites of the Tiros and Kosmos series, the sensitivity of this equipment varies appreciably under space conditions. This, together with a number of other shortcomings of the measuring equipment (e.g., the large spatial displacement during spectral scanning in the interval 7 - 15 μm [31] which took 20 seconds) limits the possibilities of using the data obtained for the optical probing questions considered in the present book.

One such application might be to verify the method of calculating the spectrum of the Earth's thermal radiation and to validate the physical parameters of the atmosphere used in the calculations. For this purpose, one could also use balloon spectral measurements of [35], obtained using a Fourier spectrometer of quite high resolution (about 5 cm^{-1} in the 15 μm CO_2 band) and high accuracy (0.5% of the minimum flux of 1 $mW/cm^2 \cdot ster \cdot \mu m$). We shall perform this check for the specified spectral ranges used in the solution of the inverse problems.

The data on the Earth's emission spectrum also find another application associated with correcting the absorption and self-emission of the atmosphere when determining the temperature of the underlying surface from measurements of the latter's radiation in the transparent window at 8 - 12 μm (see Chapter 8). For example, York, et al. [1] used calculations of the Earth's radiation spectrum for a large number of atmospheric models determined by the actual profiles of temperature and humidity.

Calculations or measurements of the spectral composition of the Earth's radiation are very important for developing methods of solving the inverse problems, i.e., determination of the vertical profiles of temperature, humidity (see Chapters 6, 7) or the other atmospheric parameters. Such calculations allow us to

model the spectra of the expected Earth's radiation for given distributions of temperature, humidity, CO_2 concentrations, and other absorbing substances, and also for variations of the models adopted in the calculations for the absorption bands of these substances, the levels of the emitting surfaces and values of their emittances. In this way, we can investigate limits of /86 variation of the Earth's self-radiation in spectral regions of interest as a function of the actual variations of the physical parameters governing the spectral distribution of the radiation. At the same time, we gain information on the different spectral ranges as regards the atmospheric parameters of interest and their regions of influence in forming the radiation spectra under actual conditions, which is important for a statement of the inverse problems.

Calculations of the Earth's radiation spectra can also be used to derive the instrument function of a spectrometer or a radiometer filter for absolute calibrations of instruments using a blackbody, |whose emission spectra differ from those of terrestrial objects. This was done in [1] in relating values of the radiation I, directly measured by the radiometer of the Tiros satellite in the wide spectral range 7 - 30 μm, to the quantities $\int_{\Delta\nu} I_\nu d\nu$, in which the effect of the filter was eliminated; the process reduced to determining the effective boundaries of the spectral intervals, allowing for transmission of the filters used in these radiometers.

3.2. The Role of Temperature and Humidity Profiles

It follows from Equations (2.6) and (2.7) that the variations in the vertical profiles of atmospheric temperature and humidity play an appreciable part in the variations of the spectral distribution of the Earth's self-radiation. This is confirmed by

numerous measurements on the Kosmos satellites [31 - 33], and also by the calculations of York, et al. [1] for more than 100 profiles of temperature and humidity, corresponding to different climatic zones and meteorological conditions.

Direct examination of the results of measurements or calculations of the functional

$$I_\nu = I_\nu \left[T\left(P\right), q\left(p\right)\right]$$ (2,21)

does not allow us to establish any kind of tangible laws for the dependence of this functional on $T(p)$ or $q(p)$.

The reason is that the values of I_ν in different spectral regions are determined by the temperature and humidity at different levels: in regions of strong H_2O absorption, I_ν depends on the temperature and humidity in the upper layer of the troposphere and in the stratosphere: in regions of less strong absorption, the temperature and humidity of the lower and middle troposphere play an important part; and in weak absorption regions, the role of $T(p)$ and $q(p)$ is small, while the temperatures of the under-lying surface and of the clouds are of primary importance. In the regions of strong absorption bands of other gases, e.g., CO_2 (or O_3), the humidity generally plays a small part, and the radiation is determined by the profiles of temperature and concentration of these gases.

Here the emission of each elementary layer of the atmosphere contributes to the total radiation with a weight depending on the wavelength and the vertical distribution of concentration of absorbing gases. Therefore, to establish the thermal equivalent of monochromatic emission or the emission, averaged over a certain spectral range, a rather simple and obvious characteristic is used, viz., the radiation temperature, i.e., the temperature of

a perfect blackbody |whose emission is equal to the given Earth
emission. Since the radiation temperature will lie between the
maximum and minimum temperatures of the atmospheric layer, one
can find a level, of course, for which the true temperature
coincides with the radiation temperature.

This is sometimes used in meteorology to determine some
certain "constant" levels obtained empirically. An example is
the 400 mbar level, which, according to the calculations of
Kolosov [46], corresponds to the radiation temperature of the
integrated Earth radiation (we note, however, that direct measure-
ments of fluxes of integrated radiation conducted by Kostyanoy|
[47] using an actinometric radiosonde have shown that this level
varies, in fact).

As has been mentioned, the decrease with height of the tropo-
sphere temperature at which the main mass of absorbing material
is concentrated is the reason why the radiation temperature in
cloud-free conditions decreases with increase of absorption.
The presence of temperature inversions in the boundary layer of
the troposphere and in the mesosphere (20 - 50 km) smooths out
this effect somewhat. In addition, if the emitting surface is a
dense high-altitude cloud with a cold top surface, an inversion
can be observed: the radiation temperature in the strong absorp-
tion region is larger than in the transparent window of the
atmosphere. This effect was obtained both in the calculations
of [37], and experimentally on the Tiros III satellite [B.14]
and on balloons [35]. Radiation exhibiting this inversion is
shown in Figures 2.13 and 2.14. The depth of this inversion,
which reached 40 degrees for 6.4 μm (Figure 2.13 a), for
example, is easily explained from analysis of the two main com-
ponents of Earth radiation: emission of the hot underlying
surface attenuated by the atmosphere, and self-emission of the
latter. If the temperature of the underlying surface is high
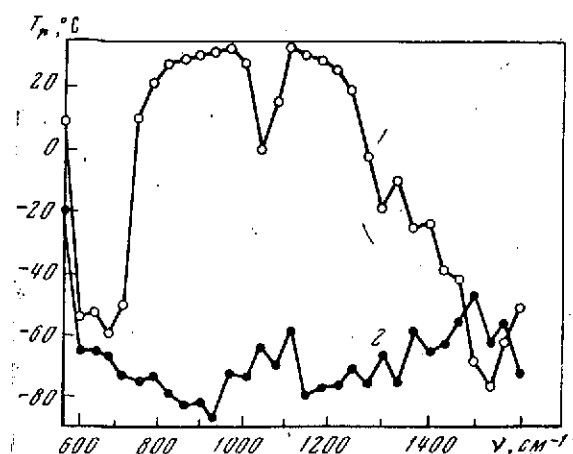
Figure 2.14. Spectral behavior of radiation temperature from balloon measurements of [35]

1- in cloud-free conditions;
2- above high-altitude dense cloud

enough, then, in spite of a certain amount of attenuation in the region of relative transparency of the atmosphere, there is more outgoing radiation than in the strong absorption region where the emission comes from higher layers of the troposphere. And /88 if the underlying surface has a low temperature, then the outgoing radiation in the strong absorption regions is determined to a significant extent by the warm layer of the mesosphere (in spite of the low concentration of absorbing material in this layer), while the cold underlying surface radiates in the transparent windows, and the contribution of the mesosphere will be negligibly small. As a result, the radiation temperature in strong absorption regions can be higher than in the transparent regions. These contradictions in the radiation temperature can be used to detect high-altitude cold clouds (in particular, thunder clouds) from satellite measurements of radiation in the transparent windows and the absorption bands of H_2O or CO_2 gases.

3.3. The Role of the Underlying Surface and of Clouds

A significant part in the variation of the Earth radiation spectrum is played by the underlying surface and the clouds, considered as a radiating surface. This is due to variations of temperature and emittance of ground formations and particularly of clouds (see Figure 2.14). It is quite clear that the most noteworthy effect of these factors appears in the transparent

windows, while in the strong absorption regions the effect is comparatively small. This is illustrated in Figure 2.13, which shows both the three-dimensional behavior of the gradient of radiation temperature in different spectral regions. The smoothing out of the gradient of radiation temperatures of ground surfaces in clouds as the absorption of the atmosphere increases can be used to solve one qualitative problem of satellite meteorology, i.e., the identification of clouds against an underlying surface background which has the same reflecting properties or emits the same kind of radiation in the transparent windows as the cloud does (e.g., against a background of snow).

The method considered in detail in [37] is based on the difference in absorption of radiation by clouds and background in the atmospheric layer above it. This difference arises from the fact that almost always the upper boundary of clouds lies above the level of the Earth's surface, but the concentration of absorbing material falls off rapidly with height. Therefore, the masses of substances contained between the cloud and the observer will be less than the mass between the observer and the ground surface, and as a result the self-emission of a cloud will be absorbed less on the path to the observer than the emission from the ground surface. Therefore, the contrasts between the radiation temperatures of the window and of a band large enough for a background will diminish with increase of height of the cloud.

In this problem, as in quantitative investigations of the atmosphere and the underlying surface, one needs data on the spectral emittance of the latter. From measurements of the emission spectra of a number of natural surfaces [48 - 52], one can conclude that the majority of these (snow, water, vegetation, and certain types of soil) emit almost like blackbodies. | However, some of the surfaces (dry quartz sand, spruce forests, and even water) have an appreciable reflectance, which increases with

increase of the angle of incidence and reflection of the radiation. This circumstance should lead, at first sight, to a large deviation of Earth radiation from that of a blackbody | at the surface temperature. In actual fact, there is a partial or even complete compensation (depending on the air temperature gradient) of the surface radiation by the atmosphere radiation reflected from this surface. This is illustrated by the radiation spectra obtained in [52] for dry sand and grass cover under daytime and night-time conditions (Figure 2.15). It is easy to see that the spectra over sand with a cloudly sky and over grass are Planckian, while the minimum in the sand spectrum for night-time conditions is somewhat smoothed out in comparison with that for the daytime case.

A similar situation will probably be observed also above clouds whose albedo, according to calculations of [7], in the transparent window for stratified clouds can exceed 20%, regardless of their water content and geometric thickness. Recent calculations by Yamamoto, et al. [53] in the 8 - 12 μm spectral regions have shown that the emittance depends on the cloud characteristics, and that δ = 0.9 for dense clouds.

Appreciable variations in the field of Earth self-radiation are associated with cirrus clouds whose transparency can vary over wide limits. Assuming that cirrus clouds are made up of spherical ice particles and considering their different concentrations in [1.29], the attenuation of the intensity of ascending radiation was calculated for the 8 - 12 μm transparent window, the 6 - 6.5 μm H_2O band, and the entire thermal region of the spectrum. The calculations were performed for several types of atmospheric stratification, corresponding to different latitudes, and in each of the models account was taken of the transformation of radiation by cirrus clouds with different concentration of
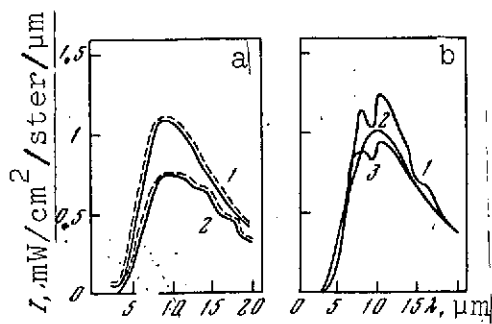
Figure 2.15. Spectra of natural radiation of surfaces, from [52]

The broken lines show black-body radiation at the temperature of the surface. a- grass cover: 1- daytime radiation (T = 305° K); 2- night-time radiation (T = 283° K); b- dry sand: 1, 3- daytime and night-time radiation in cloud-free conditions; 2- daytime radiation with dense cloud

absorbing and scattering particles N = 0; $5 \cdot 10^{-4}$; $3 \cdot 10^{-3}$; $1 \cdot 10^{-2}$ and $1 \cdot 10^{-1}$ cm^{-3} (for N < 10^{-2} cm^{-3} cirrus clouds are no longer seen). As can be seen from Figure 2.16, even for N = 10^{-2} cm^{-3}, the emission is reduced by 5 - 15% and for N = 10^{-1} cm^{-3}, this decrease reaches 70% for tropical regions. The attenuation of radiation by cirrus clouds is the most probable reason why the radiation temperature of the underlying surface, including the ocean, obtained from measurements of Earth radiation in the transparent windows at 8 - 12 μm from satellites, differs appreciably from the true temperature (see Chapter 8).
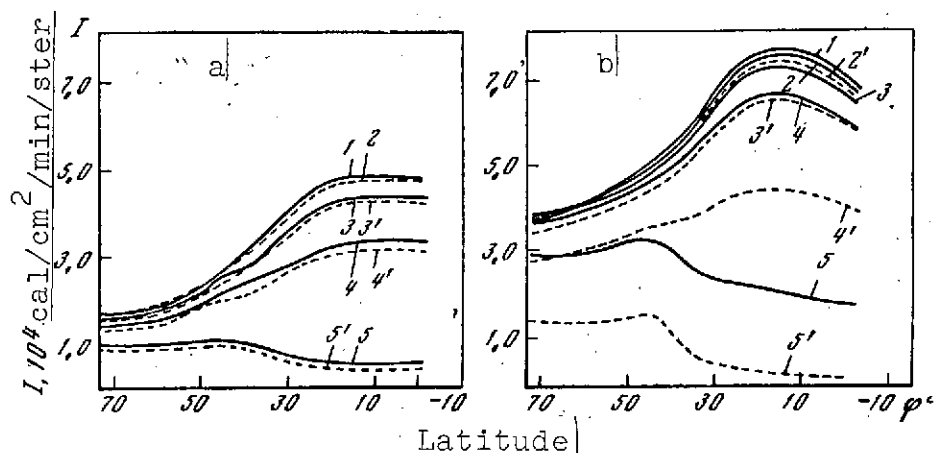
Figure 2.16. Latitude dependence of intensity of outgoing radiation (θ = 0)

The solid curves show absorption; the dotted curves show scattering. a- λ = 6 - 6.5 μm; b- λ = 8 - 12 μm; 1 - 5- N = 0; $5 \cdot 10^{-4}$; $3 \cdot 10^{-3}$; 10^{-2} and 10^{-1} cm^{-3}

148

The angular distribution of self-radiation of a plane-
parallel atmosphere I(θ) is determined mainly by the vertical
profiles of temperature and air humidity. Therefore, the
function I(θ) should vary noticeably over the globe and with time,
and depend strongly on the spectral region. There is evidence
of this, for example, in the calculations of intensity of outgoing
radiation obtained in [1] for a large range of variation of ver-
tical distributions of temperature, humidity, and ozone concentra-
tion.

In [1], the angular behavior of the intensity of outgoing
radiation in the spectral range 7 - 30 μm was determined from
calculations of I(θ) for 106 atmospheric models at the angles
θ = 0; 20; 45; 60 and 78.5°. The ratios I(θ)/I(0) shown in
Figure 2.17 for some of these models, including some of the
extreme cases, indicate that the function I(θ) varies from strong
darkening of the Earth's limb in cloud-free conditions at high
humidity (this type of behavior is typical for the Earth's
atmosphere) to practically complete independence of θ in condi-
tions of dense cloud at the level 400 mbar above which the
humidity is small. When there is a severe temperature inversion
near the ground, there is even some brightening of the horizon.

Reference [1] determined the curve of $\bar{I}(\theta)$, averaged for
all 106 cases (see Figure 2.17) and approximated by the poly-
nomial

$$I(\theta) = I(0)(1 + a\theta + b\theta^2 + c\theta^3),$$ (2.22)

where $a = -1.989 \cdot 10^{-4}$, $b = 5.876 \cdot 10^{-6}$; $c = -1.928 \cdot 10^{-7}$ (θ is in
degrees).
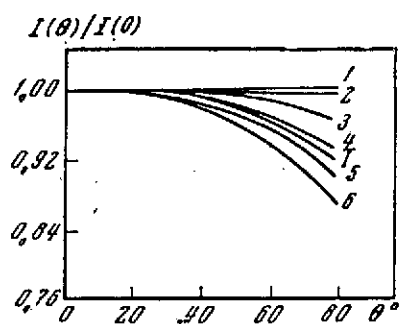
Figure 2.17. Calculation of the angular behavior of $I(\theta)/I(0)$ for typical atmospheric stratification, according to Equation (2.1)

1- clear sky, large inversion near the ground; 2- dense cloud, 400 mbar; 3- clear sky, weak inversion near the ground; 4- dense cloud, 700 mbar; 5- dense cloud, 930 mbar; 6- clear sky, high humidity; $\bar{I}(\theta)$ averaged over 106 models
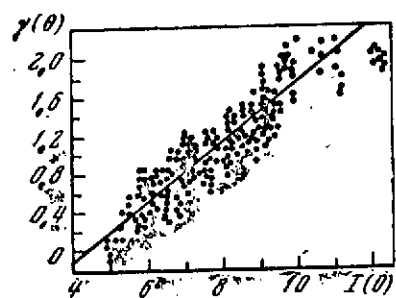
Figure 2.18. Dependence of $\gamma(\theta)$ on $I(\theta)$

In order to calculate the variation of darkening in the best manner, the authors of [1] determined the ratio

$$\gamma(\theta) = \frac{I(0)/I(0) - 1}{a0 + b\theta^2 + c\theta^3},$$ (2.23)

which goes to unity in the case $I = \bar{I}(\theta)$.

Values of $\gamma(\theta)$ are shown in Figure 2.18 as a function of the absolute intensity at the nadir $I(0)$, calculated for each given case. It can be seen that these deviations have a systematic character, described by the $\alpha + \beta I(0)$. The increase of darkening with increase of $I(0)$ corresponds to a systematic variation in the vertical gradient of temperature and humidity in going from warm cloud-free regions to cold regions, or to conditions with dense clouds. In addition, a random scatter in $\gamma(\theta)$ was observed, due to random variations in the vertical profiles of atmospheric temperature and humidity.

It was shown in [1] that these variations are not very important in calculating the fluxes of outgoing radiation

150
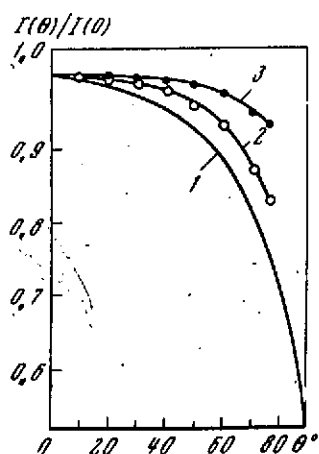
Figure 2.19. Comparison of measured angular profile of $I(\theta)$ in the 8 - 12 µm transparent window [39] (1), with the theoretical values obtained in [54] by averaging calculated curves for July (2) and January (3)

$$F = 2\pi \int_0^{\pi/2} I(\theta) \cos\theta \sin\theta \, d\theta. \qquad (2.24)$$

In using the empirical formula /91 proposed in [1]

$$I(\theta) = I(0)\{1 + [\alpha + \beta I(0)]$$
$$(a\theta + b\theta^2 + c\theta^3)\}, \qquad (2.25)$$

where $I(0) = 7.6$ mW/cm$^2 \cdot$ster; $\alpha = -1.375$; $\beta = 0.313$, the error in F does not exceed 2%.

From similar calculations in [54], approximate expressions of type (2.23) were constructed for $I(\theta)$ in the 8 - 12 µm transparent window of the atmosphere (Figure 2.19). These calculations, which are important for the problem of determining the temperature of the underlying surface, are evidence of a more variable behavior of $I(\theta)$ in comparison with the integrated case of [1]. This result can probably be explained by the fact that in actually posing the problem, the calculations of [54] were not done for the clouds considered as an underlying surface. We note, however, that this conclusion follows from investigation of the angular behavior in the 8 - 12 µm window according to experimental data obtained on satellites of the Tiros series [39].

The method of measurement of radiation on the Tiros satellites does not allow determination of $I(\theta)$ for a single atmospheric situation simultaneously over a wide enough range of angles θ (as was obtained, for example, from the data of the scanning telephotometer on Kosmos 149 for the visible part of the spectrum [55]). Therefore, [39] constructed distribution functions for

measured values of I(θ) for all ranges of θ. Then they determined average angular profiles for different time intervals and latitude belts. From these results, the authors of [39] suggested an empirical curve for the angular behavior of Earth radiation in the 8 - 12 μm window, which is well approximated by the formula

$$I(\theta) = I(0) [1 + a\theta + b\theta^2 + c\theta^3 + d\theta^4] \frac{\delta(t, \varphi)}{\delta_0},$$ (2.26)

where $a = -1.116 \cdot 10^{-4}$; $b = -5.873 \cdot 10^{-5}$, $c = 1.387 \cdot 10^{-6}$; $d = -1.523 \cdot 10^{-8}$. The function in $\delta(t, \varphi)/\delta_0$ in Equation (2.26) describes the timewise and latitude variations of the angular profiles. The behavior of the polynomial in θ, which the authors of [39] called a statistically invariant form of the disc darkening, is shown in Figure 2.19. The function $\delta(t, \varphi)$, given in [39] in the form of a two-dimensional table of order 10 (the average of 100 values is $\delta_0 = 0.0427$) is approximated by the sum of products of trigonometric functions (in t) and Legendre polynomials (in φ). It can be seen from the figure that the empirical function I(θ)/I(0) is underestimated for all θ in comparison with the theoretical angular profiles of [54], and the difference /92 between corresponding values remains the same for all θ > 30. One possible cause for this systematic underestimate is the fact that the calculations in [54] did not account for the tropical zone of increased humidity, while the experimental curve in [39] was obtained from measurements at all latitudes, $-75° \leq \varphi \leq 75°$. Another cause may be the above-mentioned absorption of radiation by cirrus clouds located at large altitudes and therefore capable of producing a more rapid behavior of disc darkening. In any case, this comparison, like the other results of [39] (e.g., the differences in the latitude and timewise behavior of I(θ) from the data of Tiros IV and VII) shows that the laws of the angular behavior of Earth radiation require additional investigations with allowance for sphericity.

Examining the question of the use of the angular radiation profiles obtained to determine radiative fluxes F from the measurement of I(0) in the case of partial cloud cover, the authors of [1] reached the conclusion that errors in the corresponding averages will depend on the range of observation angles, and also on the ratio of scales of nonuniformities and angles of view of the radiometer. However, in order to investigate the three-dimensional structure of the radiation field, we need methods for allowing for horizontal nonuniformities in the fields of temperature, humidity, and cloud cover in the theory of thermal radiation transfer. On the other hand, we should also account for random variations in the vertical profiles of temperature and humidity, which, as follows from Figure 2.18, are the cause of corresponding variations in I(θ). These problems will be considered in detail below.

As regards the role of the sphericity of the Earth in determining I(θ), we restrict ourselves to a brief listing of the results obtained, since they will not find immediate application in what follows.

§ 5. Calculation of Horizontal Nonuniformities

5.1. Basic Relations

The plane-parallel atmospheric model can be used only to examine homogeneous or very limited sections of the underlying surface, atmosphere, and clouds. In the real conditions, there are spatial variations of the vertical profiles of atmospheric temperature and humidity, as well as of the temperature of the underlying surface and the clouds, which entail corresponding variations in the characteristics of the field of Earth self-radiation.

We assume that the temperature and specific humidity of the air depend on the horizontal coordinates x and y, i.e., T = T(p, x, y) and q = q(p, x, y). Then the three-dimensional equation to determine the radiative intensity I_ν(p, x, y; θ, ψ) will have the form:

$$\cos\theta\frac{\partial I_\nu}{\partial p} - \frac{\sin\theta\sin\psi}{\rho g}\frac{\partial I_\nu}{\partial x} - \frac{\sin\theta\cos\psi}{\rho g}\frac{\partial I_\nu}{\partial y} = \qquad (2.27)$$
$$= -\frac{k_\nu(p)\,q\,(p,\,x,\,y)}{g}\{I_\nu(p,\,x,\,y;\,\theta,\,\psi) - B_\nu[T\,(p,\,x,\,y)]\}.$$

For simplicity, we consider the two-dimensional case, where the given and the unknown function depend only on a single horizontal coordinate, e.g., x, i.e., the fields of T(p, x) and q(p, x) are uniform along y and $\partial I_\nu/\partial y \equiv 0$ (it is not difficult to generalize the results obtained to the three-dimensional case).

Going over to dimensionless coordinates ξ = x/L, ζ = p/p_0 (L is the average scale of horizontal nonuniformities), we write Equation (2.27) in the following form:

a)   for the intensity of the ascending radiation $I_\nu^\uparrow$:

$$\cos\theta\frac{\partial I_\nu^\uparrow}{\partial\zeta} - \frac{a}{\zeta}\sin\theta\sin\psi\frac{\partial I_\nu^\uparrow}{\partial\xi} = k_\nu(\zeta)\,w_0 q\,(\zeta,\,\xi)\,[I_\nu^\uparrow - B_\nu]; \qquad (2.28)$$

b)   for the intensity of the descending radiation $I_\nu^\downarrow$:

$$-\cos\theta\frac{\partial I_\nu^\downarrow}{\partial\zeta} - \frac{a}{\zeta}\sin\theta\sin\psi\frac{\partial I_\nu^\downarrow}{\partial\xi} = k_\nu(\zeta)\,w_0 q\,(\zeta,\,\xi)\,[I_\nu^\downarrow - B_\nu]. \qquad (2.29)$$

Here a = $p_0/\rho_0 gL$ = H/L is a dimensionless parameter (ρ_0 is the surface air density; H is the height of the uniform atmosphere); and w_0 = $p_0 q_0/g$ is the mass of water vapor in a column of the atmosphere reduced to standard pressure at q_0 = q(p_0). It was assumed in deriving Equations (2.28) and (2.29) that the air

density varies with height according to the same law as the pressure does.

The boundary conditions for determining $I_\nu^\downarrow$ and $I_\nu^\downarrow$ are:

$$I_\nu^\downarrow(1, \xi; \theta, \psi) = B_\nu[T_0(\xi)];\qquad(2.30)$$

$$I_\nu^\downarrow(0, \xi; \theta, \psi) = 0.\qquad(2.31)$$

Further, let

$$T(\zeta, \xi) = \bar{T}(\zeta) + T'(\zeta, \xi);\qquad \overline{T'(\zeta, \xi)} = 0;\qquad(2.32)$$

$$q(\zeta, \xi) = \bar{q}(\zeta) + q'(\zeta, \xi);\qquad \overline{q'(\zeta, \xi)} = 0,\qquad(2.33)$$

where $\bar{T}(\zeta)$ and $\bar{q}(\zeta)$ are the average profiles of temperature and humidity (the bar denotes averaging over the entire interval of ξ considered); and T'(ζ, ξ) and q'(ζ, ξ) are deviations from the mean profiles, with T' $\ll \bar{T}$, so that, to a high degree of accuracy, we have

$$B_\nu[T(\zeta, \xi)] = B_\nu[\bar{T}(\zeta)] + \frac{\partial B_\nu[\bar{T}(\zeta)]}{\partial T}\, T'(\zeta, \xi).\qquad(2.34)$$

We represent the desired function in the form of the sum

$$I_\nu(\zeta, \xi; \theta, \psi) = \bar{I}_\nu(\zeta, \theta, \psi) + I_1'(\zeta, \xi; \theta, \psi),\qquad(2.35)$$

where $\bar{I}_\nu$ is the average value of I_ν over the range of ξ; and I'$_\nu$ is the deviation from this average, which is quite small compared with I_ν.

Substituting Expressions (2.32) - (2.34) into Equations (2.28) and (2.29), we obtain equations for determining $\bar{I}_\nu$ and I'$_\nu$:[*]

---

[*] We shall perform calculations for the ascending radiation; the results are similar for the descending radiation.

$$\cos\theta\,\frac{\partial \bar{I}_\nu}{\partial\zeta} = w_0 k_\nu(\zeta)\,\bar{q}\,(\zeta)\,\{I_\nu(\zeta,\,\theta,\,\psi) - B_\nu[\bar{T}\,(\zeta)]\} +$$
$$+ w_0 k_\nu(\zeta)\left\{\overline{q'\,(\zeta,\,\xi)\,I_\nu(\zeta,\,\xi;\,\theta,\,\psi)} - \frac{\partial B_\nu\,[\bar{T}\,(\zeta)]}{\partial T}\,\overline{q'\,(\zeta,\,\xi)\,T'(\zeta,\,\xi)}\right\};\qquad (2.36)$$

$$I_\nu(1,\,\theta,\,\psi) = B_\nu(\bar{T}_0);\qquad\qquad 2.37)$$

$$-\cos\theta\,\frac{\partial I'_\nu}{\partial\zeta} - \frac{a}{\zeta}\sin\theta\sin\psi\,\frac{\partial I'_\nu}{\partial\xi} =$$
$$= w_0 k_\nu(\zeta)\,\bar{q}\,(\zeta)\left\{I'_\nu(\zeta,\,\xi;\,\theta,\,\psi) - \frac{\partial B_\nu\,[\bar{T}\,(\zeta)]}{\partial T}\,T'(\zeta,\,\xi)\right\} +$$
$$+ \omega_0 k_\nu(\zeta)\,q'(\zeta)\,\{I_\nu(\zeta,\,\theta,\,\psi) - B_\nu[\bar{T}\,(\zeta)]\};\qquad (2.38)$$

$$I'_\nu(1,\,\xi;\,\theta,\,\psi) = \frac{\partial B_\nu\,(\bar{T}_0)}{\partial T}\,T'_0(\xi).\qquad\qquad (2.39)$$

The formal solution of Equation (2.36) with boundary condi- /94
tions (2.37) has the form

$$I_\nu(\zeta,\,0,\,\psi) = B_\nu(\bar{T}_0)\exp\left[-\tau\,(\zeta,\,1,\,\theta)\right] - \int_\zeta^1\left\{\frac{\partial B_\nu\,[\bar{T}\,(t)]}{\partial T} - \right.$$
$$-\frac{1}{q\,(t)}\left[\overline{q'\,(t,\,\xi)\,I'_\nu(t,\,\xi;\,\theta,\,\psi)} - \frac{\partial B_\nu\,[\bar{T}\,(t)]}{\partial T}\times\right.$$
$$\left.\left.\times\,\overline{q'(t,\,\xi)\,T'(t,\,\xi)}\right]\right\}\frac{\partial\exp\left[-\tau\,(\zeta,\,t,\,\theta)\right]}{\partial t}\,dt,\qquad (2.40)$$

where

$$\tau\,(\zeta,\,t,\,\theta) = \omega_0\sec\theta\int_\zeta^t k_\nu(t_1)\,\bar{q}\,(t_1)\,dt_1.$$

It contains the unknowns $\overline{q'I'_\nu}$ and $\overline{q'T'}$, to determine which
we need additional equations. However, if these quantities in
Equation (2.40) are small, they may be omitted, i.e., we consider
the value $I_\nu(\zeta,\,\theta)$ thus obtained as a first approximation, which
allows us to determine I'_ν from Equations (2.38) and (2.39),
and therefore, also $\overline{q'I'_\nu}$ (we need to know $\overline{q'T'}$ from empirical
data).

Applying a Fourier transformation to Equations (2.38) and
(2.39)

156

$$J_\nu(\zeta, \omega; \theta, \psi) = \frac{1}{2\pi} \int_{-\infty}^{+\infty} I_\nu'(\zeta, \xi; \theta, \psi) e^{i\omega\xi} d\xi \quad (2.41)$$

(ω is the wave number), and assuming that $I_\nu'(\zeta, \xi; \theta, \psi) \to 0$ for $\xi \to \pm \infty$, we obtain an equation for J_ν:

$$\cos\theta \frac{\partial J_\nu}{\partial \zeta} + \frac{i\omega a}{\zeta} \sin\theta \sin\psi J_\nu =$$
$$= w_0 k_\nu(\zeta) \bar{q}(\zeta) \left\{ J_\nu(\zeta, \omega; \theta, \psi) - \frac{\partial B_\nu[\bar{T}(\zeta)]}{\partial T} \rho(\zeta, \omega) \right\} + \quad (2.42)$$
$$+ w_0 k_\nu(\zeta) \sigma(\zeta, \omega) \{\bar{J}_\nu(\zeta, \theta) - B_\nu[\bar{T}(\zeta)]\};$$

$$J_\nu(1, \omega; \theta, \psi) = \frac{\partial B_\nu(\bar{T}_0)}{\partial T} \rho_0(\omega). \quad (2.43)$$

Here,

$$\rho(\zeta, \omega) = \frac{1}{2\pi} \int_{-\infty}^{+\infty} T'(\zeta, \xi) e^{i\omega\xi} d\xi; \qquad \rho_0(\omega) = \frac{1}{2\pi} \int_{-\infty}^{+\infty} T_0'(\xi) e^{i\omega\xi} d\xi; \quad (2.44)$$

$$\sigma(\zeta, \omega) = \frac{1}{2\pi} \int_{-\infty}^{+\infty} q'(\zeta, \xi) e^{i\omega\xi} d\xi, \quad (2.45)$$

where we assume that the functions T' and q' admit of Fourier transformation, i.e., they tend to zero in the required manner as $\xi \to \pm \infty$.

The solution of Equation (2.4) with boundary condition (2.34) has the form

$$J_\nu(\zeta, \omega; \theta, \psi) = \frac{\partial B_\nu(\bar{T}_0)}{\partial T} \rho_0(\omega) \zeta^{-i\omega a \, \text{tg} \, \theta \sin\psi} \exp[-\tau(\zeta, 1, \theta)] -$$
$$- \int_{\zeta}^{1} \left\{ \frac{\partial B_\nu[\bar{T}_1(t)]}{\partial T} \rho(t, \omega) - \frac{\sigma(t, \omega)}{\bar{q}(t)} [\bar{I}_\nu(t, \theta) - B_\nu(\bar{T}(t))] \right\} \times \quad (2.46)$$
$$\times \left(\frac{t}{\zeta}\right)^{i\omega a \, \text{tg} \, \theta \sin\psi} \frac{\partial \exp[-\tau(\zeta, t, \theta)]}{\partial t} dt.$$

If we carry out the inverse Fourier transformation for Equation (2.46),

$$I'_\nu(\zeta, \xi; \theta, \psi) = \int_{-\infty}^{+\infty} J_\nu(\zeta, \omega; \theta, \psi)\, e^{i\omega\xi} d\omega,$$

then, taking into account that

$$T'(\zeta, \xi) = \int_{-\infty}^{+\infty} \rho(\zeta, \omega)\, e^{i\omega\xi} d\omega; \quad q'(\zeta, \xi) = \int_{-\infty}^{+\infty} \sigma(\zeta, \omega)\, e^{i\omega\xi} d\nu,$$

we obtain the final solution of Equation (2.38):

$$
\begin{aligned}
I'_\nu(\zeta, \xi; \theta, \psi) = {} & \frac{\partial B_\nu(\bar{T}_0)}{\partial T}\, T'_0\,[\mu(\zeta, \xi, 1; \theta, \psi)]\exp[-\tau(\zeta, 1, \theta)] - \\
& - \int_\zeta^1 \left\{ \frac{\partial B_\nu[\bar{T}(t)]}{\partial T}\, T'[t, \mu(\zeta, \xi, t; \theta, \psi)] - \right. \\
& \left. - \frac{\bar{I}_\nu(t; \theta) - B_\nu[\bar{T}(t)]}{\bar{q}(t)}\, q'[t, \mu(\zeta, \xi, t; \theta, \psi)] \right\} \frac{\partial \exp[-\tau(\zeta, t, \theta)]}{\partial t}\, dt.
\end{aligned}
$$

(2.47)

Here

$$\mu(\zeta, \xi, t; \theta, \psi) = \xi - a\,\mathrm{tg}\,\theta \sin\psi \ln\frac{t}{\zeta}.$$

The function $\tilde{I}'_\nu = (1/\Delta\nu)\int_{\Delta\nu} I'_\nu d\nu$ (or $\tilde{J}_\nu$), averaged over the spectral interval $\Delta\nu$, can be represented in terms of the transmission function $P_\nu(\zeta, t, \theta)$ (we drop the ~ sign):

$$
\begin{aligned}
I'_\nu(\zeta, \xi; \theta, \psi) = {} & \frac{\partial B_\nu(\bar{T}_0)}{\partial T}\, T'_0\,[\mu(\zeta, \xi, 1; \theta, \psi)]\, P_\nu(\zeta, 1, \theta) - \\
& - \int_\zeta^1 \left\{ \frac{\partial B_\nu[\bar{T}(t)]}{\partial t}\, T'[t, \mu(\zeta, \xi, t; \theta, \psi)] - \right. \\
& \left. - \frac{\bar{I}_\nu(t, \theta) - B_\nu[\bar{T}(t)]}{\bar{q}(t)}\, q'[t, \mu(\zeta, \xi, t; \theta, \psi)] \right\} \frac{\partial P_\nu(\zeta, t, \theta)}{\partial t}\, dt.
\end{aligned}
$$

(2.48)

Expressions (2.47) and (2.48) show that the horizontal nonuniformities in the radiation field described by the function I'$_\nu$ are determined mainly by the functions T'(ζ, ξ) and q'(ζ, ξ), and also by the parameters of the problem, i.e., the transmission P$_\nu$ of the atmosphere, the nonuniformity scale L, etc. In the actual conditions, T' and q' are random functions, and therefore

I'$_\nu$ will also be a random function of its coordinates. Therefore, large-scale calculations of I'$_\nu$ using the quite cumbersome formulas (2.47) or (2.48) will not be sensible. It is clearly desirable to determine the statistical characteristics of horizontal nonuniformities, which will be done in Chapters 4 and 5.

However, we can obtain some idea of the behavior of the function I'$_\nu$ with change of its arguments without making detailed calculations.

5.2. Behavior of the Function I'$_\nu$

The functions T' and q', used to express I'$_\nu$, depend on a difference of the type $\xi - a\,\mathrm{tg}\,\theta\,\sin\psi\,\ln(t/\zeta)$, which is a characteristic of Equation (2.38). Therefore, radiation I'$_\nu$, determined by temperature variations T' and humidity variations q' at points with coordinates t and $\mu = \xi - a\,\mathrm{tg}\,\theta\,\sin\psi\,\ln(t/\zeta)$, comes to the point (t, ξ) in the direction (θ, ψ).

When $\zeta \to 0$ and ξ is a finite quantity, the functions T'(t, η) and q'(t, η) go to zero for all $\theta \neq 0$ and $\varphi \neq \pi/2$. Then the function I'$_\nu$ also goes to zero. This means that, at an infinite distance from a plane layer of the atmosphere, there is complete smoothing out of features of the radiation field, due to smoothing of the fields of temperature and humidity as $\xi \to \pm\infty$ (from the definition of the validity of the Fourier transformation).

We consider the behavior of I'$_\nu$ as a function of changes in the other parameters. It is easy to see that for $\theta = 0$ (the direction of observation is to the nadir) the dependence of I'$_\nu$ on ξ is completely governed by the variations in the profiles of T' and q' above the point ξ, while the variations T' and q' along

the horizontal coordinates play a part in an inclined direction ($\theta \neq 0$). In particular, when $\xi = 0$ and $\theta = 0$, the smoothing of I'_ν will be determined only by absorption and self-radiation of the vertical column of the atmosphere.

A similar effect is obtained also for $\psi = \pi/2$, i.e., for a direction of observation along the y axis. In this case, the radiation reaches the observer from a horizontal uniform layer of the atmosphere corresponding to the coordinate ξ. If $\theta \to \pi/2$, i.e., the direction of observation is close to horizontal, then I'_ν is determined by the values of T' at the point (ζ, ξ), and

$$\lim_{\theta \to \pi/2} I'_\nu(\zeta, \xi; \theta, \psi) = \frac{\partial B_\nu [\bar{T}_\cdot(\zeta)]}{\partial T} T'(\zeta, \xi).$$

Such a simple relation arises from the fact that the plane layer of the atmosphere which we are considering radiates in the horizontal direction like a blackbody with a temperature equal to that at the point of observation.

The behavior of I'_ν depends to a considerable extent also on the parameter a, which depends mainly on the scale of nonuniformities L. With decrease of L (increase of a), the smoothing out of details of the radiation field occurs at lower levels of ζ. Conversely, if the nonuniformity scales are large (a is small), the horizontal nonuniformity of the radiation field will appear up to very great heights. Finally, the effect of variations of T' and q' on the variation of the intensity of radiation depends on the nature of atmospheric absorption in the given spectral range, and also on the mass of absorbing material in the path of propagation of the radiation.

5.3. Variations of Radiative Fluxes

We note one further important consequence of Equations (2.47) or (2.48). Practically all instruments measuring Earth radiation have a finite aperture, and sum the radiation which arrives from a certain solid angle, defined by the angular sensitivity of the instrument $\kappa(\theta)$. Therefore, the variations in the radiative fluxes

$$F_\nu'(\zeta, \xi) = \int\limits_0^{2\pi} \int\limits_0^{\pi/2} I_\nu'(\zeta, \xi; \theta, \psi)\, \varkappa(\theta) \sin\theta\, d\theta\, d\psi \qquad (2.49)$$

will describe the actually measured horizontal nonuniformities of the radiation field, averaged over the instrumental field of view, whose optical axis is directed towards the nadir.

We represent the angle of sensitivity of the instrument in the form

$$\varkappa(\theta) = \cos^n\theta \qquad \left(0 \leqslant \theta \leqslant \frac{\pi}{2};\quad n = 0, 1, 2, \ldots\right) \qquad (2.50)$$

(the special cases $n = 0$ and $n = 1$ correspond to instruments with spherical and plane detecting surfaces, with an angle of view of 2π).

We assume, further, that the dependence of $\bar{I}(\theta)$ on θ can be neglected (the results of § 4 of the present chapter show that this is valid). Then it is not difficult to determine the Fourier transform for the flux $F_n'(\zeta, \xi)$

$$\Phi_n(\zeta, \omega) = \frac{1}{2\pi} \int\limits_{-\infty}^{+\infty} F_n'(\zeta, \xi)\, e^{i\omega\xi} d\xi \qquad (2.51)$$

(the subscript ν has been dropped).

In fact, by substituting Equation (2.51) into Equation (2.49), and taking into account Equation (2.46) for $J_\nu(\zeta, \omega; \theta, \psi)$, and carrying out integration with respect to θ and ψ, we obtain:

$$\Phi_n(\zeta, \omega) = \frac{\partial B_\nu(T_0)}{\partial T}\rho_0(\omega)\,\Psi_{n+1}\left[w_0\int_\zeta^1 k_\nu(t)\,\bar{q}(t)\,dt,\;\omega a\ln\frac{1}{\zeta}\right] -$$
$$- \int_\zeta^1\left\{\frac{\partial B_\nu[\bar{T}(t)]}{\partial T}\rho(t, \omega) - \frac{\bar{I}_\nu(t) - B_\nu[\bar{T}(t)]}{\bar{q}(t)}\sigma(t, \omega)\right\}\times$$
$$\times\frac{\partial}{\partial\tau}\Psi_{n+2}\left[w_0\int_\zeta^t k_\nu(u)\,\bar{q}(u)\,du,\;\omega a\ln\frac{t}{\zeta}\right]dt.$$

(2.52)

Here

$$\Psi_k(\tau, v) = \int_1^\infty e^{-s\tau}J_0\left(v\sqrt{s^2 - 1}\,\frac{d\rho}{s^k}\right) \qquad (k = 1, 2, \ldots) -$$

are generalized exponential integral functions of the two variables τ, v, obtained above from solution of the analogous problem of reflected solar radiation (see § 7, Chapter 1); and $\partial/\partial\tau$ denotes the partial derivative with respect to

$$\tau = w_0\int_\zeta^t k_\nu(u)\,\bar{q}(u)\,du.$$

Taking into account the properties of the function Ψ_k, we can investigate the asymptotic behavior of $\Phi_n(\zeta, \omega)$, e.g., the rate of damping of radiative flux variations with change of the absorption k_ν, the mass of absorbing material w_0, the scale of nonuniformities a, or the position of the observer ζ. In particular, for $\zeta \to 0$ (the top boundary of the atmosphere going to infinity), the flux variations go to zero. The properties of the function $\Phi_n(\zeta, \omega)$ will be considered in greater detail in Chapter 5, when we investigate the relation between random variations of the radiation field and random variations in the fields of meteorological elements, since the physical meaning of this function will then become clearer.

§ 6.   Allowance for Sphericity of the Earth

Because of three-dimensional nonuniformity of the fields of
atmospheric temperature and humidity, and also the temperature of
the underlying surface and of the clouds, allowance for sphericity
reduces to solving the three-dimensional radiative transfer
equation, similar to Equation (1.96); the Planck function is the
source function in this kind of equation.

However, since the clouds and the underlying surface create
the main effects of the spatial nonuniformities of the radiation
field, one can restrict attention to a spherically symmetric
model of the Earth, when calculating the basic laws for the
intensity of radiation to be used in most applications. A
characteristic of this model is that the temperature of the
atmosphere and the underlying surface, the concentration of absorb-
ing material and the absorption coefficient depend only on the
distance r from the Earth's center. In this case, the intensity
of the radiation $I_v(r, \theta)$, which depends on r and the angle θ
between the direction of propagation of the radiation and the
angle to the nadir, is given by the transfer equation

$$\cos\theta \frac{\partial I_v}{\partial r} - \frac{\sin\theta}{r} \frac{\partial I_v}{\partial \theta} = \alpha_v(r)\{I_v(r, \theta) - B_v[T(r)]\}. \qquad (2.53)$$

The first problem formulated in this way was considered
by Kuznetsov [40] whose object was to determine the vertical
temperature profile in a spherical atmosphere. In recent years,
from solution of Equation (2.53) for quite a large number of
atmospheric models, numerous data have been obtained on the angular
distribution of the Earth self-radiation in various regions of the
spectrum [B.12, 41 – 45, 56]. Some experimental data have also
been obtained from radiometric investigations of the angular
structure of the radiative field, using balloons, rockets, and

satellites [16, 33, 57 - 59]. Naturally, the angular behavior
of the Earth radiation near the horizon is of very great interest.

From calculations of the intensity of outgoing radiation for
three mean-season and mean-latitude stratifications of the atmos-
phere: ϕ = 0 (equator, summer) and ϕ = 65 degrees (summer, winter)
under cloudless conditions, and for dense clouds at 3 and 9 km,
Kondrat'yev, et al. [B.12, 41] investigated the basic laws for
the angular behavior of Earth radiation, in 13 spectral ranges,
including the absorption bands of H_2O, CO_2, and O_3, the trans-
parent windows, and the whole range of thermal radiation. Simi-
lar investigations for typical atmospheric models, corresponding
to mean latitudes, and for the tropics, the arctic, and deserts,
under cloudy and cloud-free conditions were performed by Hanel,
et al. [43], and also in [45]. For specific synoptic situations,
including partial cloud conditions, the angular behavior of the
self-radiation was calculated by Kondrat'yev, et al. [42]. The
refraction of the atmosphere in the thermal spectral region was
calculated by Wark, et al. [44] for four model atmospheres,
embodying a wide range of variations of meteorological conditions.
Yakushevskaya [56] compared the angular behavior of radiation
from the spherical Earth with and without allowance for
refraction.

The results of these calculations show that the angular
profiles of Earth radiation near the horizon depend strongly on
both the spectral range and on the meteorological conditions.
The main features of the angular behavior of the radiation in
different spectral regions are repeated with certain variations
in all the theoretical calculations. For cloud-free conditions,
the following general laws apply for the angular profiles near
the horizon:

1. In weak atmospheric absorption regions, the radiation rapidly falls to zero as the perigee of the rays increases. For example, for the transparent window in the range 10 - 11 μm, it goes to zero even for rays with a perigee of 10 - 15 km.

2. In the CO_2 and H_2O absorption bands, the radiation near the horizon can even increase and then slowly decrease, going to zero for rays with a perigee of 50 - 60 km.

3. As regards the 9.6 μm O_3 absorption band, quite strong darkening of the edge of the disc towards the horizon is obtained, and then there is quite a sharp fall-off in radiation in the outer layer at the fringes of the 10 km atmospheric layer, and a slow decline for rays with large perigee.

These laws have a comparatively simple explanation when one considers the vertical profiles of temperature and concentration of absorbing material in the atmosphere, and also the cloud cover, which can introduce appreciable changes in the nature of the angular profiles. A detailed account of these topics has been given in a book [B.12].

CHAPTER 3
THE STRUCTURE OF FIELDS OF ATMOSPHERIC PARAMETERS

§ 1. Method of Construction of an Optical Meteorological Model of the Atmosphere

Taking into account the results presented in Chapters 1 and 2 and the special methods used for the problems solved in this book concerning optical probing of the atmosphere from satellites, we can suggest a rational method for constructing an optical-meteorological model of the atmosphere. This model includes a system of statistical characteristics for the vertical and three-dimensional structure of the fields of meteorological elements and optical parameters responsible for generating the Earth's radiation field, as well as statistical characteristics for the spectral or angular structure of the latter. A determination of these characteristics must be based on statistical treatment of a sufficient quantity of measurements of the atmospheric parameters considered as random functions of their arguments.

Let all realizations of a random function $f_i(x)$ ($i = 1$, 2, ..., N) be given in the interval $a \leq x \leq b$ or at discrete points x_k ($k = 1, 2, ..., n$) of the interval $[a, b]$ (in this case, $f_i(x_k)$ are considered as a set N of random n-dimensional vectors). We will describe the structure of this ensemble by the functional characteristics (or their vector and matrix analogs in the discrete case), enumerated below.

1.   The mean function or the norm

$$\bar{f}(x) = \frac{1}{N} \sum_{i=1}^{N} f_i(x),$$

(3.1)

describing the mean profiles of a given random function.

2.   The dispersion of the random function

$$D_f(x) = \frac{1}{N} \sum_{i=1}^{N} [f_i'(x)]^2$$

(3.2)

or the mean square deviation

$$\sigma_f(x) = \sqrt{D_f(x)},$$

(3.3)

which describe the behavior with respect to x of the deviation $f_i'(x) = f_i(x) - \bar{f}(x)$.

3.   The autocorrelation function

$$B_{ff}(x, y) = \frac{1}{N} \sum_{i=1}^{N} f_i'(x) f_i'(y) \qquad (a \leqslant y \leqslant b).$$

(3.4)

describes the correlation between the deviations f'$_i$ at two arbitrary levels x and y. For random vectors, the analog of the autocorrelation function is the autocorrelation matrix

$$B_{ff}(x_k, x_l) = \frac{1}{N} \sum_{i=1}^{N} f_i'(x_k) f_i'(x_l).$$

(3.5)

In practice, we often use also the normalized correlation function <u>/100</u>

$$r_{ff}(x, y) = \frac{B_{ff}(x, y)}{\sigma_f(x) \sigma_f(y)}$$

(3.6)

or the normalized correlation matrix

$$r_{ff}(x_k, x_l) = \frac{B_{ff}(x_k, x_l)}{\sigma_f(x_k)\sigma_f(x_l)} \cdot$$

(3.7)

The values of the function (3.6) or the elements of the matrix (3.7) are coefficients of correlation between the deviations f'_i at the different points x and y (or x_k and x_l).

4. The system of empirical orthogonal functions, which are eigenfunctions of the autocorrelation function (3.4), considered as a symmetric kernel of the Fredholm integral equation

$$\mu\varphi(x) = \int_a^b B_{ff}(x, y)\varphi(y)\,dy,$$

(3.8)

where μ are eigenvalues of the kernel B_{ff}. In the discrete case, the analog of the eigenfunctions are the eigenvectors of the autocorrelation matrix (3.5).

As has been shown by Obukhov [1] and Bagrov [2], the empirical orthogonal functions can be used to approximate any random function $f'_i(x)$ with a given error by means of a minimum number (for all orthogonal systems) of basic functions. Here the ratio of the sum of the corresponding eigenvalues to the trace of the matrix describes the accuracy of this approximation.

5. The statistical relationship between the variations $f'_i(x)$ and the variations of a random function $g'_i(y)$ defined in the interval $c \leqslant y \leqslant d$, generally speaking, of another argument y (and therefore, describing another simultaneously recorded random atmospheric parameter), are described by the joint correlation functions

$$B_{fg}(x, y) = \frac{1}{N}\sum_{i=1}^{N} f'_i(x)g'_i(y)$$

(3.9)

or, in the discrete case, by the joint correlation matrices

$$B_{fg}(x_k, y_l) = \frac{1}{N} \sum_{i=1}^{N} f_i'(x_k) g_i'(y_l).$$ (3.10)

The values of the normalized function

$$r_{fg}(x, y) = \frac{B_{fg}(x, y)}{\sigma_f(x) \sigma_g(y)}$$ (3.11)

and the elements of the matrix

$$r_{fg}(x_k, y_l) = \frac{B_{fg}(x_k, y_l)}{\sigma_f(x_k) \sigma_g(y_l)}$$ (3.12)

are coefficients for the correlation between f'_i and g'_i for different values of the arguments x and y. Determination of the statistical characteristics enumerated requires only very general postulates regarding random functions, i.e., stochastic continuity and existence of finite moments of first and second order. If the values $f_i(x)$ are distributed according to the normal law, then these characteristics contain complete information on the /101 structure of the random function. For an arbitrary distribution, the moments of higher order must be determined.

Similarly, one can describe the structure of two-dimensional random functions $f_i(x, y)$, but in general the moments will be functions of four variables. But if one constructs an ensemble of one-dimensional functions which are sections $f_i(x, y)$ in fixed directions in the (x, y) plane, then one can obtain the statistical characteristics (3.1) - (3.12), which depend para-metrically on the direction. If there is no such dependence, it will mean that the random field is isotropic.

Two-dimensional statistical characteristics are also obtained in the case of non-isotropic but homogeneous random fields, when the moments of the function f(x, y) depend only on the displace-ments ξ and η along the x and y axes. For example, the correlation

function will have the form

$$B_{ff}(\xi, \eta) = \int\limits_{-\infty}^{+\infty} \int\limits_{-\infty}^{+\infty} f'(x+\xi, y+\eta) f'(x, y) \, dx \, dy. \qquad (3.13)$$

For a homogeneous and isotropic field, the correlation moments of second and higher orders will be functions of a single variable, the distance e between the points (x, y) and (x', y'), e.g.,

$$B_{ff}(\rho) = \int\limits_{-\infty}^{+\infty} f'(\rho+r) f'(r) \, dr. \qquad (3.14)$$

6. An important statistical characteristic is the spectral density, defined for a homogeneous field as the Fourier transformation

$$S_{ff}(\omega_x, \omega_y) = \frac{1}{4\pi^2} \int\limits_{-\infty}^{+\infty} \int\limits_{-\infty}^{+\infty} B_{ff}(\xi, \eta) \exp\left[i(\xi\omega_x + \eta\omega_y)\right] d\xi \, d\eta,$$

where ω_x, ω_y are components of the two-dimensional wave number vector.

In the case of an isotropic and homogeneous field, the spectral density will be the one-dimensional function

$$S_{ff}(\omega) = \frac{1}{2\pi} \int\limits_{-\infty}^{\infty} B_{ff}(\rho) e^{i\omega\rho} d\rho. \qquad (3.15)$$

The spectral density describes the distribution of dispersion of a random function with respect to frequency ω.

In the case of locally homogeneous and locally isotropic fields, the spatial structure can also be described by the structure function

170

$$D_{ff}(\rho) = \int\limits_{-\infty}^{+\infty} [f(r+\rho) - f(r)]^2 \, dr, \qquad (3.16)$$

which is related to the correlation function by the relation

$$D_{ff}(\rho) = 2 [B(0) - B(\rho)]. \qquad (3.17)$$

These statistical characteristics used to describe the vertical
and spatial structure of the fields of temperature, humidity,
cloud, and other meteorological elements, as well as the vertical
and spectral structure of the scattering coefficients, the
absorption functions, and other optical parameters, constitute
the optical-meteorological model of the atmosphere.* Here one
should bear in mind that the statistical characteristics will be /102
determined from a finite choice of empirical random vectors.
Therefore, estimates of the closeness of these parameters to
the correlation moments determined vigorously with the help of
multi-dimensional distribution functions (see [3]) can be based
on comparison of the results of statistical processing of differ-
ent samples. The same thing holds for application of the theory
of homogeneous random fields to fields of the atmospheric
parameters.

The proposed model, whose specific elements will be presented
below, gives a representation in tangible form of the laws of
the distribution of meteorological and optical parameters, which
are stored, as it were, by the atmosphere from amongst the very
many random variations. However, this model allows us the best
determination of the required information to describe a given
sample of the optical and meteorological state of the atmosphere
in terms of some minimum number of measurements of the specific
parameters at the chosen points. For this purpose, we use well-
known methods of statistical linear approximation, interpolation,

* To this model one must also add the statistical characteristics
of the optical parameters of the underlying surface.

and extrapolation, used by Gandini [4] for other problems.

In fact, if we know $\bar{f}(x_k)$ at all the points x_k and we have specific samples $f_i(x_k)$ at certain points x_k ($k = 1, 2, \ldots$; $m < n$), and must determine the value f_i of this sample at the other points $x_l \neq x_k$, then, using the representation

$$f_i'(x_l) = \sum_{k=1}^{m} c_k^{(l)} f_i'(x_k) \qquad (m < l \leqslant n) \tag{3.18}$$

and the condition for the functional to be a minimum

$$F[c_k^{(l)}] = \frac{1}{N} \sum_{i=1}^{N} \left[f_i'(x_l) - \sum_{k=1}^{m} c_k^{(l)} f_i'(x_k) \right]^2, \tag{3.19}$$

we obtain a system of equations for determining $c_k^{(l)}$:

$$\sum_{j=1}^{m} c_j^{(l)} B_{ff}(x_k, x_j) = B_{ff}(x_k, x_l). \tag{3.20}$$

The coefficients of this system are the elements of the auto-correlation matrix (3.5). Solving the system (3.20) and substituting the $c_k^{(l)}$ into (3.19), we can obtain an estimate of the error in the optimum interpolation of (3.18):

$$F[c_k^{(l)}] = B_{ff}(x_l, x_l) - \sum_{k=1}^{m} c_k^{(l)} B_{ff}(x_k, x_l).$$

Similarly, from measurements of $f_i(x_k)$ we can establish a function $g_i(y_k)$ correlated with $f_i(x_k)$, by using the approximation

$$q_i'(y_k) = \sum_{j=1}^{n} d_j^{(k)} f_i'(x_j) \tag{3.21}$$

and determining the minimum of the functional

$$G[d_j^{(k)}] = \frac{1}{N} \sum_{i=1}^{N} \left[q_i'(y_k) - \sum_{j=1}^{n} d_j^{(k)} f_i'(x_j) \right]^2. \tag{3.22}$$

To determine the $d_j^{(k)}$ we obtain the system of equations

$$\sum_{j=1}^{n} d_j^{(k)} B_{ff}(x_j, x_k) = B_{fg}(x_k, y_k).$$ (3.23)

The errors in this approximation can also be expressed in terms of the correlation coefficients r_{jg}:

$$G[d_j^{(k)}] = B_{gg}(y_k, y_k) - \sum_{j=1}^{n} d_j^{(k)} B_{fg}(x_j, y_k).$$ (3.24)

The optimum approximation (or interpolation and extrapolation) can be obtained using the correlation moments of higher orders. We illustrate this via an example where the random vector $g_i(y_k)$ at the point y_k is represented in the form of a power series in another random vector $f_i(x_k)$:

$$g_i(y_k) = \sum_{m=1}^{M} c_m^{(k)} [f_i(x_k)]^m.$$

From the condition for a minimum of the functional

$$G[c_m^{(k)}] = \frac{1}{N} \sum_{i=1}^{N} \left\{ g_i(y_k) - \sum_{m=1}^{M} c_m^{(k)} [f_i(x_k)]^m \right\}^2$$

we obtain a system of equations for determining $c_m^{(k)}$:

$$\sum_{l=1}^{M} c_l^{(k)} B_{ff}^{(l, m)}(x_k, x_k) = B_{gf}^{(1, m)}(y_k, x_k) \qquad (m = 1, 2, \ldots, M),$$ (3.25)

where

$$B_{gf}^{(l, m)}(y_k, x_k) = \frac{1}{N} \sum_{i=1}^{N} [g_i(y_k)]^l [f_i(x_k)]^m; \qquad B_{ff}^{(l, m)}(x_k, x_k) = \frac{1}{N} \sum_{i=1}^{N} [f_i(x_k)]^{l+m}.$$ (3.26)

If, in the optimum interpolation, we take account of uncorrelated errors of measurement due to dispersion, then, as was shown in [5], additional terms appear in equations of the type (3.20) or (3.23).

The use of statistical characteristics to achieve optimum closures of the system of optical-meteorological parameters used in investigating the Earth radiation field can be regarded as a generalization of the method for construction of a closed optical model proposed by Shifrin [49]. At present, examples have already been obtained of statistical characteristics of the vertical structure of the fields of temperature and humidity [6 - 13], the boundaries of layer-type cloud [15], and a number of other meteorological elements [16 - 19]. In addition, characteristics have been computed for the vertical and spectral structure of the aerosol scattering coefficient [1.8, 1.10], and the angular structure of the scattering index [1.33, 1.34, 20]. There are also data on the spatial structure of the fields of temperature and cloud [5.21 - 25]. The suitably ordered set of these characteristics can be considered as a first approximation for the optical-meteorological atmospheric model.

As experimental data accumulates, the model must be added to and refined. For these refinements, one can also use a model of the Earth radiation field whose structural characteristics are associated with those of the optical-meteorological model (see Chapters 4 and 5). Specific possibilities for improving the model are being identified by solution of the inverse problems (see Chapters 6 - 9), which results in determination of specific realizations of the atmospheric parameters. Here the statistical characteristics are used as a priori information on the solution.

§ 2. Vertical Structure of the Temperature Field

To study the statistical characteristics of the vertical /104 structure of the temperature field of the Earth atmosphere, we use data from radiosonde probing of the atmosphere in various regions of the globe and in different seasons.

Because of the limited number of regular soundings during a 24-hour period and the nonuniformity in the distribution of points where regular soundings are made on the globe, and also because satisfactory and sufficiently complete results of soundings up to the heights of 20 - 30 km which interest us have appeared only in recent years, the reliable data available constitute a comparatively small group of samples of vertical profiles of the temperature $T_i(p)$. To eliminate daily variations, the soundings of T_i should be taken during the same period, and to eliminate latitude or longitude effects, the vertical structure is investigated for fixed points. Therefore, the empirical material is classified on the basis of intuitive ideas as to the homogeneity of a sample of temperature profiles. For example, in [6], the samples of $T_i(p)$ were combined into eight groups with the following designations: continental (Bismark 46° 50' N, 100° 35' W), /105 and oceanic (vessel "C," 52° 45' N, 35° 30' W), stations for July and January at 00 and 12 hours, Greenwich time.

The statistical characteristics of $T_i(P_k)$ were determined from a set of more than 100 temperature profiles in each group at standard levels p_k = 1000, 850, 700, 500, 400, 300, 250, 150, 100, and 50 mbar (we note that the level 1000 mbar usually means the height of the Stevenson screen in which the ground temperature is measured).* This kind of breakdown gives an idea of the fluctuations in the statistical characteristics due to seasonal and geographic conditions and to time of day.

The average vertical profiles $\bar{T}(p)$ and the mean square deviations $\sigma_T(p)$ for all eight groups given in [6] show the following well-known peculiarities of the vertical behavior of $\bar{T}(p)$ and $\sigma_T(p)$, which it is important to take into account for

---

* To increase the number of samples of $T_i(p_k)$, Boltenkov [7] used data from soundings at 60 stations. With this choice of data, naturally, he obtained smoother characteristics for the vertical structure.

our work: the presence of surface inversions in January or at night in July above a continental area (there are no inversions above the ocean); a considerable daily variation of $\bar{T}(p)$ at the surface and a very slight variation above the sea; maxima of $\sigma_T(p)$ at the ground surface in summer, and at levels 500 - 700 mbar in winter (the latter correspond to the cloud layer height) and at the level of the tropopause, i.e., at the ground-atmosphere, cloud-atmosphere, or troposphere-stratosphere interfaces.

Conclusions were also drawn in [6] regarding the vertical structure of temperature fluctuations $T'_i(p) = T_i(p) - \bar{T}(p)$, described by the autocorrelation matrices $B_{TT}(p_k, p_l)$ or the correlation coefficients $r_{TT}(p_k, p_l)$ (Figure 3.1). For each level above the tropopause, the values of r_{TT} diminish with height (apart from certain values of p_k), go through zero at almost the same level near the tropopause, reach large negative values above the tropopause, and then become close to zero again near p = 50 mbar. If the level p_k lies above the tropopause, then r_{TT} diminishes without taking negative values. This /106 type of behavior of r_{TT} corresponds to the typical behavior of temperature fluctuations with height: positive values of $T'(p)$ in the troposphere are usually accompanied by negative values of $T'(p)$ above the tropopause, and conversely. The physical nature of this phenomenon is not clear. It can be supposed (see [6]), that, for example, heating of the lower atmospheric layers due to radiation, advection of heat, or other factors, creating expansion of the entire atmospheric layer, leads to cooling of high atmospheric layers, since at these levels the above factors may not act, and expansion occurs due to decrease in internal energy and therefore, to decrease in temperature (similar reasoning can also be applied to the case of cooling of the lower layers). The above properties of the correlation matrix B_{TT} were confirmed by calculations in [7], which used averaging over many radiosonde stations, and investigated the latitude behavior of B_{TT} for two meridian sections above the continent and the

176
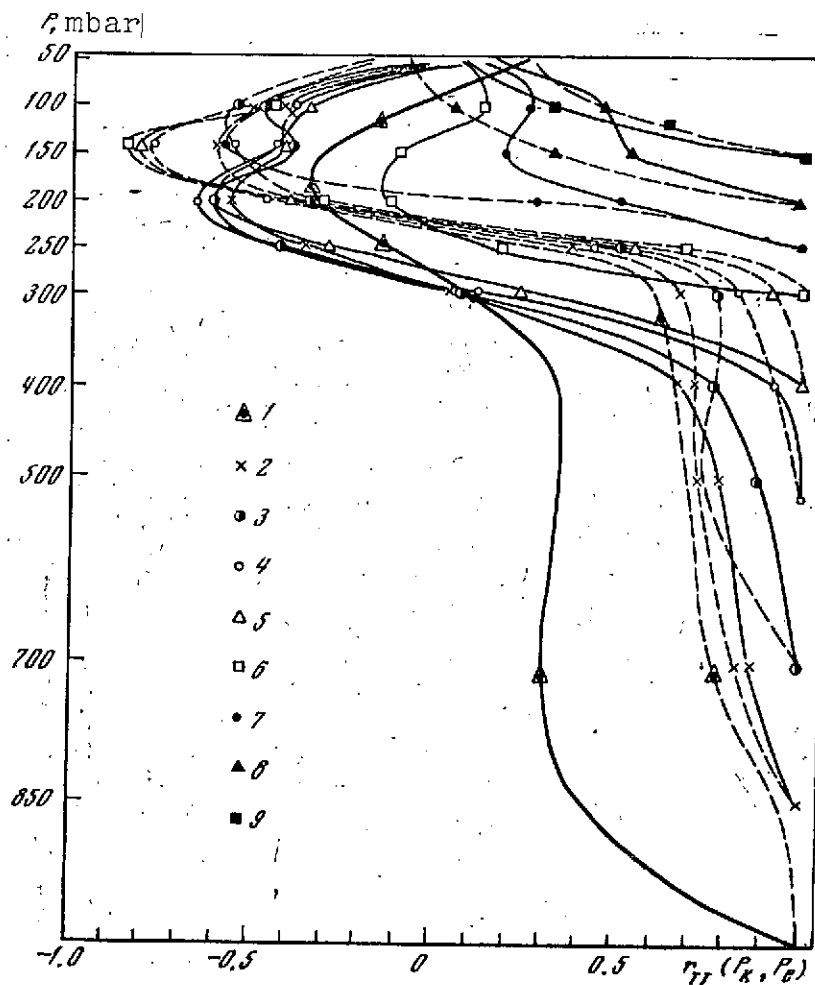
Figure 3.1. Vertical behavior of the correlation coefficient r_{TT} [6] for the Bismark station in January (solid lines) and July (broken lines). The levels p_k (in mbar) are: 1- 1000; 2- 850; 3- 700; 4- 500; 5- 400; 6- 400; 7- 250; 8- 200; 9- 150

ocean [8]. In addition, as can be seen from Figure 3.2, there is a tendency for a reduced correlation at lower latitudes. Reduced values of $r_{TT}(p_0, p_k)$ are observed particularly at the interfaces, above the underlying surface p_0 at the level of the tropopause, and also above layered clouds (see § 4).
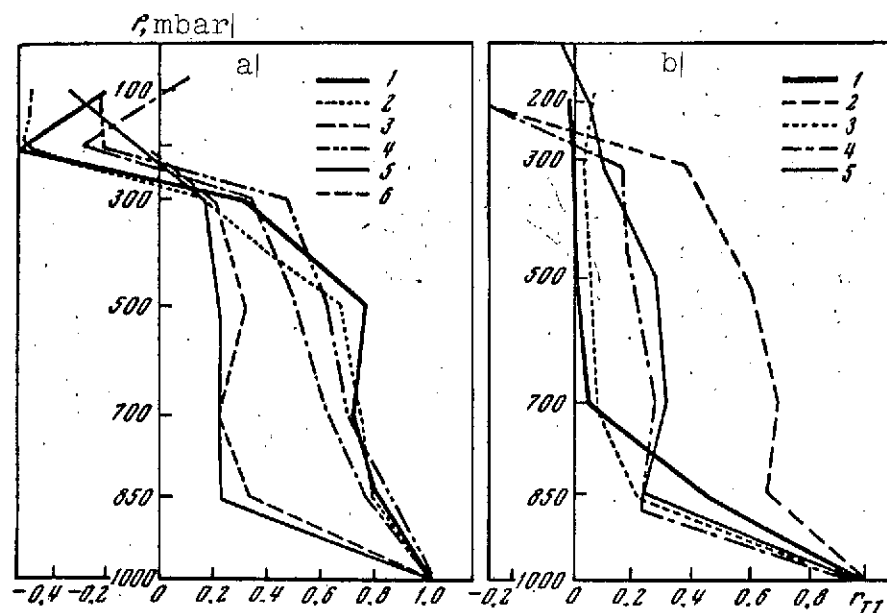
Figure 3.2. Latitude dependence of the correlation coefficients $r_{TT}(p_0, p_k)$

a- continental section: 1- Arkhangelsk (64°); 2- Vologda (59°); 3- Kursk (51°); 4- Rostov (47°); 5- Tuapse (44°); 6- Ash-khabad (36°); b- ocean section: 1- vessel 1 (44°); 2- vessel 2 (52°); 3- vessel 3 (35°); 4- vessel 4 (62°); 5- Cape Zhelaniya (73°). The latitude of the points is given in brackets

The increase in the ceiling for radiosonde work and the increased number of rocket soundings have permitted investigation of the vertical structure T(p) at large heights. Examples of r_{TT}, obtained in [26] from radiosonde data up to the 2 mbar level [39], show that the variations of T in the 20 - 30 km atmospheric layer may again be positively correlated with T' at the surface and in the lower troposphere. We note, finally, that all the laws mentioned above for the vertical structure of the fields of T(p) were also obtained in [10, 11].

§ 3. Vertical Structure of the Humidity Field

Because of difficulties in making reliable measurements of atmospheric humidity (particularly at great heights), the vertical structure of the relative concentration of water vapor q(p), treated as a random function, has not generally been investigated until recently. The first statistical characteristics of the structure of q(p) were obtained by Popov [6] from the same radiosonde data considered in § 2 of this chapter for the temperature field, at six standard levels below 300 mbar.

Examples of average profiles $\bar{q}(p)$ and mean square deviations $\sigma_0(p)$ are given in Table 3.1.

To allow extrapolation to large heights, the curves were approximated in [6] by the formula

$$\bar{q}(p) = \bar{q}_0 \left(\frac{p}{p_0} \right)^{\varkappa}$$
(3.27)

or by the exponential law

$$q(z) = \bar{q}_0 e^{-\varkappa z}.$$
(3.28)

Here $\bar{q}_0, p_0$ are the mean specific humidity and the air pressure at the ground surface; and $\varkappa, \alpha$ are empirical parameters.

Table 3.1 shows that the parameters κ and α vary slightly in the conditions considered. However, Equations (3.27) or (3.28) provide a good approximation only in the free atmosphere. However, in the atmospheric boundary layer, especially over the continents, the actual profiles of $q_i(p)$, like those of $\bar{q}(p)$, depart seriously from the distributions of (3.27) or (3.28).

TABLE 3.1. EXAMPLES OF THE VERTICAL PROFILES OF $\bar{q}(p)$ AND $\sigma_q(p)$ AND VALUES OF THE PARAMETERS $\bar{q}_0$, α AND κ IN EQUATIONS (3.27) AND (3.28)*

p, mbar	Bismark, January $\bar{q}_0=3.3$, g/kg, $\alpha=0.391$, km^{-1}, $\kappa=3.00$		Bismark, July $\bar{q}_0=12$, g/kg, $\alpha=0.447$, km^{-1}, $\kappa=3.54$	
	$\bar{q}$	σ_q	$\bar{q}$	σ_q
1000	1,92	1,05	7,73	2,01
850	1,76	0,98	6,82	1,72
700	1,08	0,70	3,92	1,56
500	0,40	0,23	0,96	0,66
400	0,18	0,17	0,52	0,30
300	—	—	0,10	0,10

p, mbar	Vessel "C", January $\bar{q}_0=9.4$, g/kg, $\alpha=0.440$, km^{-1}, $\kappa=3.54$		Vessel "C", July $\bar{q}_0=9.4$, g/kg, $\alpha=0.440$, km^{-1}, $\kappa=3.53$	
	$\bar{q}$	σ_q	$\bar{q}$	σ_q
1000	4,00	1,42	7,28	1,57
850	2,32	1,52	5,18	5,40
700	1,17	1,04	3,05	2,85
500	0,36	0,11	0,90	0,41
400	0,17	0,013	0,38	0,07
300	—	—	0,13	0,003

* Translator's note: Commas in numbers represent decimal points.

There is an interesting decrease in the correlation moments of the matrices $B^i_{qq}(p_k, p_l)$ and $r_{qq}(p_k, p_l)$ (Figure 3.3) between the levels 700 and 500 mbar, due, probably, to the formation of clouds at that layer. Therefore, the fluctuations of humidity here are determined not only by mixing, but also by condensation processes. Thus, as was true for the temperature field, the vertical structure of the humidity exhibits "interfaces," at which the fluctuations of specific humidity are slightly correlated with q' at the other levels. Similar results were also obtained in [8, 12, 26] from more complete radiosonde data.

/107

180
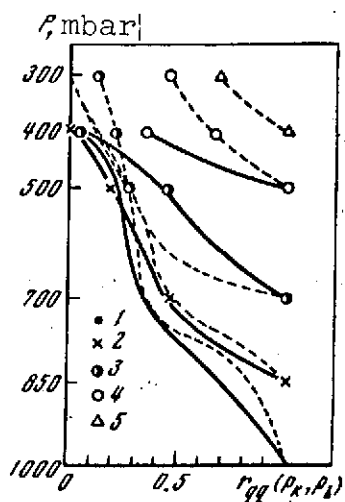
Figure 3.3. Vertical behavior of the correlation coefficients $r_{qq}(p_k, p_l)$ in January (solid lines) and July (broken lines). The levels p_k (in mbar) are:

1- 1000; 2- 850; 3- 700; 4- 500; 5- 400
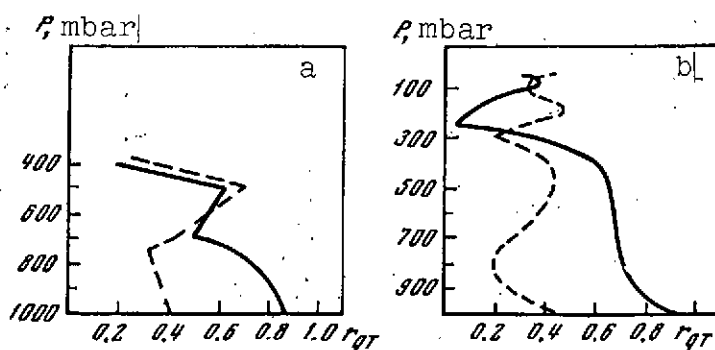
Figure 3.4. Correlation coefficients $r_{qT}(p_k, p_k)$ for January (solid lines) and July (broken lines)

a- calculations of [3.6] for the Bismark station; b- calculations of [26] from the data of [9]

The relationship of the fluctuations q' and T' at the different levels is described by the joint correlation matrices $Bq_T(p_k, p_l)$ and $r_{qT}(p_k, p_l)$. The results of calculations of B_{qT} and r_{qT}, given in Figure 3.4 for summer and winter months at continental and oceanic stations from the data of [6], indicate considerable differences between $r_{qT}(p_k, p_l)$ for the winter (0.8 - 0.9) and for summer (0.3 - 0.4) above continents (roughly the same ratio r_{qT} was obtained for land and water). The causes of these differences are probably processes occurring during temperature fluctuations in summer conditions above dry land, and causing humidity fluctuations of opposite sign.

In particular, the increased temperatures in summer in the surface layer implies, on the one hand, an increase in specific humidity due to increase of evaporation, and, on the other hand, a decrease of $q(p_0)$ because of convective fluxes which reduce the humidity at the ground surface. The effect of this kind of opposing factors is illustrated in the curves of r_{qT} in Figure

181
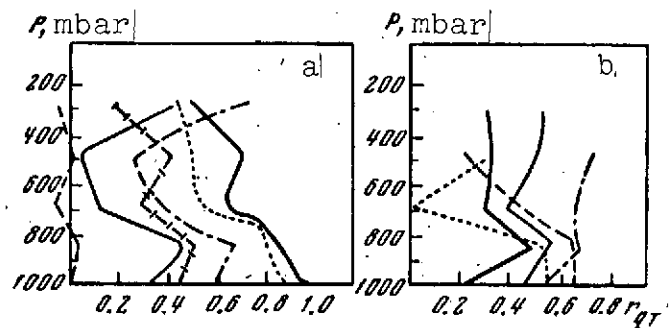
Figure 3.5. Latitude behavior of $r_{qT}(p_k p_k)$ for the same
sections as Figure 3.2
a- continental section; b- ocean section

3.5, obtained by Boldyrev, et al. [8] for the above-mentioned
meridian sections. It can be seen from Figure 3.5 that there
is a large latitude variation of r_{qT}, where r_{qT} decreases
toward the south. For example, in desert conditions (Ashkhabad),
this kind of correlation between q' and T' is practically absent
at all levels. In [8] the decrease of r_{qT} toward the south is
due to an increased moisture deficit, the result of which is
that even considerable temperature fluctuations do not imply a
variation in the specific moisture content. This hypothesis
receives some support from the more uniform latitude behavior
of r_{qT} above the ocean.

The latitude behavior r_{qT} is probably associated with other
processes, in the first place with condensation and cloud
formation. This is precisely why almost all the curves of r_{qT}
have minima, corresponding to the condensation levels (see
Figures 3.4 and 3.5). However, for more reliable conclusions and
reliable use of the characteristics examined, one must carry out
calculations for different seasons, regions of the globe, time
of day, cloud conditions, and certain specific conditions (e.g.,
temperature inversions). It is also interesting to determine

B_{qq} and B_{qT} at great heights. The results of processing the radiosonde data of [9] confirm the basic peculiarities of the vertical behavior of r_{qT} and r_{qq} in the lower troposphere, obtained in [6].

§ 4. Vertical Structure of Boundaries of Stratified Clouds /109

To take account of the effect of random cloud fluctuations on the variation of the Earth radiation field is an extremely complex matter, even if we consider clouds as a radiating or reflecting surface, i.e., ignoring the fluctuations of micro-structure, geometric thickness, water content, radiative transfer process in the cloud and a configuration of its boundaries. For reflected solar radiation, the effect of this simplified model of a cloud could be accounted for using fluctuations in the brightness coefficient or the albedo, by relating these optical parameters to some cloud parameters capable of comparatively simple measurement (e.g., the height of the top boundary, thickness, and moisture content). However, the absence of data on simultaneous measurements of the characteristics of the reflectance and any other cloud parameters does not allow us at present to establish such relationships experimentally. In addition, because of very strong scattering and comparatively weak absorption of short-wave radiation in a cloud (outside regions of absorption bands of water vapor and other atmospheric gases), the formation of reflected radiation takes place in quite a thick layer of cloud and therefore its fluctuations depend on many parameters of the latter.

The question of fluctuations in the self-radiation is some-what simpler. Since the thermal emission is very strongly absorbed by water droplets, the formation of the emission of a sufficiently dense cloud takes place in a comparatively narrow surface layer

and is determined in practice by the temperature of the top
boundary of the cloud.* Since we have already numerous data
from aircraft measurements of the positions of cloud boundaries,
and vertical profiles of temperature and humidity in a sounding
layer, including cloud boundaries (see e.g., [27]), we can obtain
statistical characteristics of the vertical structure of cloud
boundaries and the corresponding meteorological elements. It is
natural to begin to determine these characteristics for stratified
clouds as being the simplest cloud formation, and this has been
done in [5] from data of aircraft soundings, obtained by Polovina
[27] in the daytime with a ten-point, single-layer, massive
stratus and stratocumulus cloud during the cool and warm half-
year periods.**

The homogeneity of the experimental data was determined from
the qualitative characteristics of the cloud type, which entailed
the inclusion of several "extraneous" cases in the samples being
considered (as will be shown below, these cases can be detected
by means of objective statistical characteristics of the cloud
field).

The experimental data for each half-year period included two
groups of independent data, each containing more than 100 values
of the temperature $T(z_k)$ and the specific humidity $q(z_k)$ at
ten fixed levels z_k from $z_1 = 0.15$ to 5 km (this included the
850 and 700 mbar isobars) and at levels varying from case to
case: at the lower and upper cloud boundaries h_1 and h_2, and
also at the top boundary of the inversion layer h_3. The heights
of the h_m boundaries were also treated statistically with $T(z_k)$
and $q(z_k)$.

---

* An exception is the transparent windows in which radiation from
the clouds can be distinguished from blackbody │radiation at the
temperature of the upper boundary.

** The cool season includes cases of soundings from November to
March, and the warm season includes the remaining months; there-
fore, within each half-year period, the distribution of sounding
cases was quite nonuniform.

We can immediately calculate $\bar{I}(z_k)$ and $\bar{q}(z_k)$, the mean heights of the interfaces $\bar{h}_m$, the correlation matrices $B_{TT}(z_k, z_l)$, $B_{qq}(z_k, z_l)$, $B_{qT}(z_k z_l)$, $B_{Th}(z_k, h_m)$, $B_{qh}(z_k, h_m)$, $B_{hh}(h_m, h_s)$, as well as the appropriate correlation coefficients relating the variations $T'(z_k)$, $q'(z_l)$ and h'_m ($k, l = 1, 2, \ldots, 10$; $m, s = 1, 2, 3$).

Tables 3.2 and 3.3 show the mean heights of the cloud /110 boundaries and of the inversion layer $\bar{h}_m$, the mean square deviations σ_h, the mean temperatures $\bar{T}(z_k)$ and humidities $\bar{q}(z_k)$, together with their mean square deviations σ_T and σ_q at these boundaries, and the correlation coefficients r_{hT} and r_{hq}.

An interesting feature is the almost exact coincidence between the mean heights of the cloud boundaries and the inversion, and also their dispersions in the warm and cool periods of the year; here the mean cloud thickness $\Delta h = h_2 - h_1 \approx 0.4$ km proves to be comparable with the mean square deviations of the boundary heights. This result may be due in part to the above-mentioned qualitative approach in the distribution of clouds with season, although the main cause is apparently the physical mechanism of the formation of stratified clouds (which, as follows from [28], is as yet unclear).

It is interesting to note several peculiarities of the temperature at the upper cloud boundary: the mean values $\bar{T}$ here differ markedly from the analogous values at the same level in the atmosphere (the figures in brackets), in comparison with the corresponding differences for the lower boundary of the clouds or the inversion boundary. This is due to the special situation of the upper boundary of the clouds as being a surface whose radiation is not compensated by counter-radiation of the atmosphere.

TABLE 3.2.   STATISTICAL CHARACTERISTICS OF BOUNDARIES
OF CLOUDS AND AN INVERSION*

m	$\bar{h}_m$, km	σ_h, km	$\bar{T}(h_m)$, °C	$\bar{q}(h_m)$, g/gk	σ_T, °C	σ_q, g/gk	r_{hT}	r_{hq}
			warm half-year period					
1	0,61	0,38	5,4(6,2)	5,9(5,8)	3,9	1,8	—0,22	0,29
2	0,99	0,39	3,6(5,3)	5,6(5,5)	3,9	2,5	—0,23	0,04
3	1,2	0,40	5,2(4,9)	5,3(5)	4,5	1,7	—0,15	—0,21
			cool half-year period					
1	0,60	0,35	—6,7(—6)	2,2(2,3)	3,4	0,71	—0,20	—0,16
2	0,97	0,37	—8,9(—5,6)	2,1(2,3)	3,5	0,66	—0,19	—0,12
3	1,29	0,39	—3,9(—5,3)	2,1(2,1)	4,2	0,9	0,31	—0,20

* Translator's note: Commas in numbers represent decimal points.

TABLE 3.3.   CORRELATION MATRICES $B_{hh}(h_m, h_s)$ AND CORRELATION
COEFFICIENTS $r_{hh}(h_m, h_s)$*

m	warm half-year period			cool half-year period		
1	0,147	0,132	0,120	0,119	0,114	0,099
2	0,89	0,154	0,140	0,88	0,139	0,127
3	0,79	0,90	0,158	0,73	0,88	0,151

* Translator's note: Commas in numbers represent decimal points.

Note: The elements B_{hh} (in km^2), are located on and above the main diagonal; the r_{hh} elements are located below the main diagonal; $r_{hh}(h_m, h_m) = 1$.

The correlation coefficients r_{hT} between fluctuations in the cloud boundaries and the temperature fluctuations at these boundaries (of the order of -0.2) are unexpectedly low (although they are also negative). The variations in the boundary levels
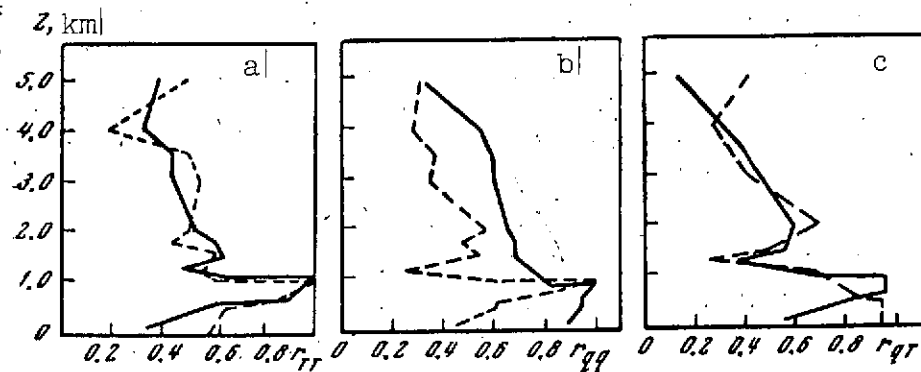
Figure 3.6. Vertical distributions of the correlation coefficients of [15] for the warm (solid lines) and cool (broken lines) half-year periods

a- $r_{TT}(h_2, z_k)$;   b- $r_{qq}(h_2, z_k)$;   c- $r_{qT}(z_k, z_l)$

are very weakly correlated with the atmospheric temperature and humidity at other levels (see [15]). The other moments, e.g., of the correlation between the temperature or humidity at the level h_2 and at all the higher levels z_k, are quite high (see Figure 3.6 a, b). The same result can be seen in Figure 3.6 c, which shows the correlation coefficients r_{qT} at the same levels. An interesting feature is the rather large value of r_{qT} = 0.96 at the cloud boundaries for the warm period (r_{qT} = 0.56 at the Earth surface for this period, which confirms the comment above regarding the effect of clouds on reducing the value of r_{qT} in the surface layer during summer). In the cool period, the opposite situation is observed: r_{qT} = 0.93 at the ground and the lower cloud boundary, and 0.68 at the upper boundary. An interesting point is the high coefficient obtained in the calculations of [15] for the correlation between fluctuations of the levels of the upper and lower cloud boundaries, and also between the latter and the inversion level (see Table 3.3). A close correlation of the boundaries like this allows us to resolve the interesting practical question of optimal distribution of the height of the upper cloud boundary from measurements of the lower boundary from the ground, and, conversely, to determine

the height of the lower boundary from satellite measurements of the upper boundary. Taking into account the rather high correlation between the temperature and the humidity at the two boundaries, this question can be resolved for T and q.

Regarding the other meteorological elements, the characteristics of whose vertical structure are required for investigating the fluctuations in the radiation field, we should mention the ozone concentration $m(p)$, the pressure p (or the geopotential H) and the air density ρ. Examples of constructing autocorrelation matrices B_{pp} or B_{HH} have been given by Obukhov [1], Rukhovets [16], and Mertsalova, et al. [17]. Numerous calculations of the statistical characteristics of the structure of the vertical distribution of the atmospheric density have been performed by Cole and Court [18]. The structure of the $m(p)$ profiles were investigated in detail by Shafrin [19]. However, these characteristics will not be used directly in this book, and we therefore restrict ourselves simply to these references.

§ 5. Structure of the Aerosol Scattering

The main fluctuations of solar radiation scattered by the atmosphere are due, as was shown in Chapter 1, to the spectral and vertical fluctuations of the coefficient $b(\lambda, z)$ and of the aerosol scattering index $\gamma_\lambda(z, \varphi)$, as well as to variations in the angular behavior of the latter. For an optimum description of these fluctuations, one must construct the system of statistical characteristics listed in § 1 of Chapter 3 of the parameters $b(\lambda, z)$ and $\gamma_\lambda(z, \varphi)$, regarded as random functions of their arguments.

In § 2 of Chapter 1 we presented the average dependences of $\bar{b}(\lambda)$ on λ in the surface air layer ($z = 0$) and the vertical profiles of $\bar{b}(\lambda_i, z)$ for some wavelengths λ_i. The measured data

188
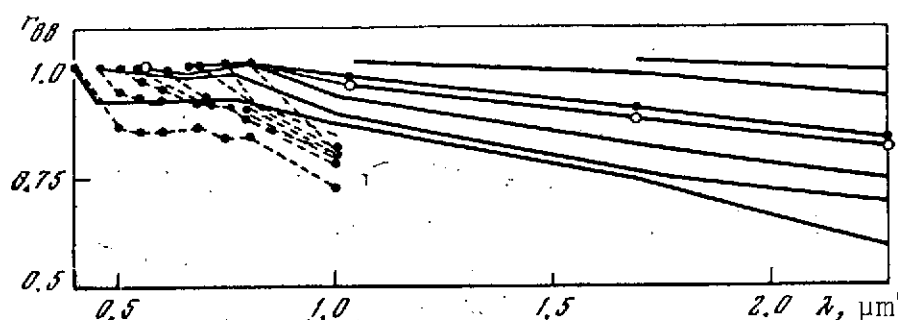
Figure 3.7. Correlations coefficients r_{bb}, calculated from the measurements of b_λ in the surface layer [1.8] (broken lines) and the ocean layer (solid lines) [1.7] of the atmosphere

allows determination for these cases of the autocorrelation matrices $B_{bb}(\lambda_i, \lambda_j)$ and $B_{bb}(z_k, z_l)$, and also the joint correlation matrices $B_{bq}(z_k, z_l)$, $B_{bu}(z_k, z_l)$, and $B_{bT}(z_k, z_l)$ (u is the relative humidity). As regards the scattering index $\gamma_\lambda(z, \varphi)$, the available measurements are only adequate to determine the characteristics of its angular structure in the surface air layer and at certain heights (examples of these characteristics for the halo part of the index have been given in [1.34], and for large angles φ, in [1.33, 20]).

5.1. Spectral Structure of the Scattering Coefficient

The correlation matrices $B_{bb}(\lambda_i, \lambda_j)$ were obtained by Georgiyevskiy [1.8] from extensive measurements of $b(\lambda)$ in the surface air layer for the spectral range 0.35 - 1 μm. It can be seen from Figure 3.7 that there is quite a close correlation between $b'(\lambda_i)$ for different λ_i (r_{bb} is greater than 0.75 throughout the whole range). Similar characteristics were determined by Koprova [1.10] from the measurements of Knestrik, et al. [1.7] in the surface air layer over water for the spectral range 0.45 - 2.5 μm; the value of r_{bb} turned out to be substantially larger than for the ground layer in the region $\lambda < 1$ μm.

189
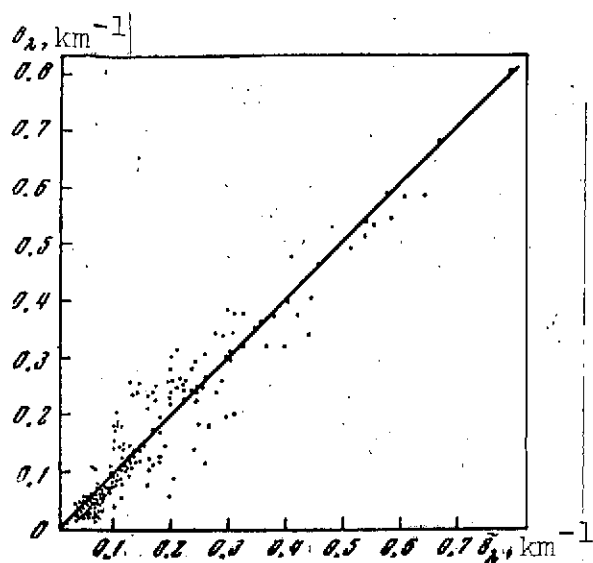
Figure 3.8. Regression between the measured [1.8] and calculated [1.9] aerosol attenuation coefficients b_λ, from Equation (3.29)

This high correlation of $b'(\lambda)$ enables us to carry out very good extrapolation over the spectrum with an acceptable accuracy and thereby to determine the spectral behavior of the scattering coefficient in a specific situation from measurements of $b(\lambda)$ for one or several wavelengths. We illustrate this with the example /113 of measurement of $b(\lambda_0)$ at some fixed wavelength λ_0. Directly from the value of $b(\lambda_0)$ and the set of average scattering coefficients shown in Figure 1.3, we find the norm $\bar{b}(\lambda)$, which it is convenient to use in the extrapolation. Then, determining $b'(\lambda_0) = b(\lambda_0) - \bar{b}(\lambda_0)$ and using Equation (3.19) with m = 1, we obtain the result that for all λ:

$$\bar{b}(\lambda) = \bar{b}(\lambda) + \frac{B_{bb}(\lambda_0, \lambda)}{B_{bb}(\lambda_0, \lambda_0)} b'(\lambda_0).$$
(3.29)

The mean square error in determining $\bar{b}'(\lambda)$ from Equation (3.29) is given by

$$\delta_b(\lambda) = \sigma_b(\lambda) \sqrt{1 - r_{bb}^2(\lambda_0, \lambda)}$$
(3.30)

As was shown in [1.8] and [1.9], the error for $\bar{b}(\lambda)$ does not exceed 30%. The true errors are shown in Figure 3.8 by the regression between $b(\lambda)$ and $\bar{b}(\lambda)$.

190

5.2. Vertical Structure of the Scattering Coefficient

The statistical characteristics of the vertical structure of $b_\lambda(z)$ were calculated by Koprova [1.10] from aircraft measurements of aerosol attenuation in the troposphere (6 - 7 km) [1.6] and the data of projectile soundings [1.13] up to 35 km, and also by Faraponov from the measurements of [1.5]. The vertical behavior of $\bar{b}_\lambda(z)$ and $\sigma_b(z)$ for $\lambda = 0.5$ and 0.65 μm, resulting from these calculations, is shown in Table 3.4.

TABLE 3.4. VERTICAL BEHAVIOR OF $\bar{b}_\lambda(z)$ AND $\sigma_b(z)$ (IN km^{-1})*

	literature source	z, km										
		0	0,5	1	1,5	2	2,5	3	3,5	4	5	6,5
$\bar{b}_{0,5}$	[16]	0,175	0,099	0,072	0,053	0,043	0,035	0,027	0,022	0,020	0,017	0,010
σ_b		0,135	0,040	0,030	0,028	0,026	0,021	0,016	0,011	0,012	0,012	0,009
$\bar{b}_{0,65}$	[1.13]	—	—	—	—	—	—	$0,0^2 82$	$0,0^2 76$	$0,0^2 84$	$0,0^2 48$	$0,0^2 30$
σ_b		—	—	—	—	—	—	$0,0^2 51$	$0,0^2 50$	$0,013$	$0,0^2 39$	$0,0^2 25$

		z, km										
		8	10	12	14	16	18	20	25	30	33	35
$\bar{b}_{0,65}$	[1.13]	$0,0^2 29$	$0,0^2 28$	$0,0^2 28$	$0,0^2 26$	$0,0^2 24$	$0,0^2 24$	$0,0^2 16$	$0,0^3 43$	$0,0^3 14$	—	$0,0^4 51$
σ_b	•	$0,0^2 22$	$0,0^2 18$	$0,0^2 16$	$0,0^2 12$	$0,0^2 10$	$0,0^2 11$	$0,0^3 78$	$0,0^3 34$	$0,0^3 15$	—	$0,0^4 59$
$\bar{b}_{0,65}$	[29]	—	—	—	—	—	$0,0^2 30$	$0,0^2 21$	$0,0^3 57$	$0,0^3 19$	$0,0^3 13$	—
σ_b		—	—	—	—	—	$0,0^2 15$	$0,0^3 90$	$0,0^3 27$	$0,0^4 94$	$0,0^3 10$	—

* Translator's note: Commas in numbers represent decimal points.

The correlation coefficients $r_{bb}(z_k, z_l)$ obtained from the measured data of [1.5] and [1.6], are shown in Figure 3.9. From comparison of the corresponding curves we can see that the typical features of the vertical behavior of $r_{bb}(z_k, z_l)$ are identical, which is evidence of the correctness of the statistical characteristics. The most important property of these
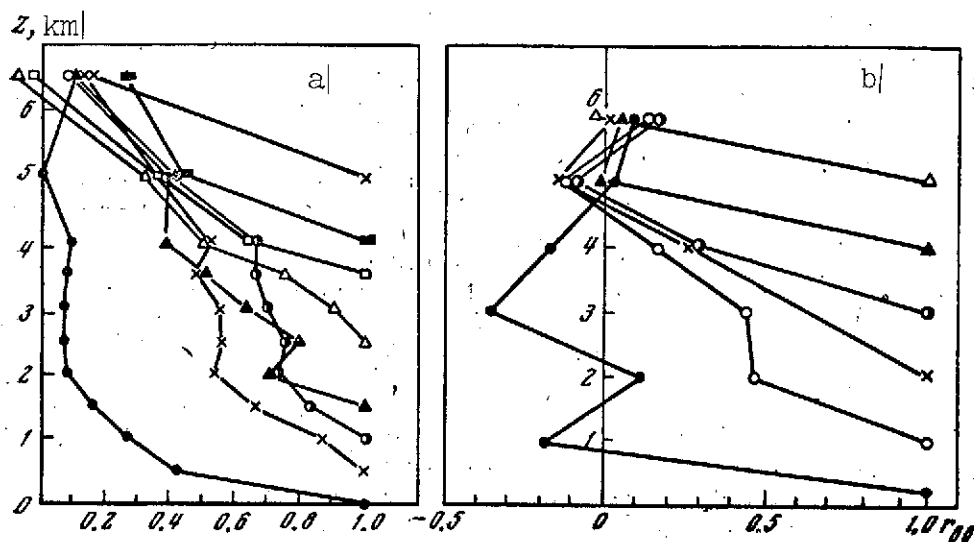
Figure 3.9.   Calculations of correlation coefficients r_{bb}
a- from measurements of $b_\lambda(z)$ [1.6], $\lambda = 0.5$ μm;   b- from
 measurements of [1.5], $\lambda = 0.45$ μm

characteristics is the rather weak correlation between $b'_\lambda(z)$
in the atmospheric boundary layer and at the other levels z.
The probable cause is difference in the processes accompanying   /114
the formation of aerosols at different heights in the atmosphere
and leading to the formation of aerosol layers. As was true for
the meteorological parameters, the aerosol attenuation coefficient
within a given layer or at the interfaces is slightly correlated
with $b'_\lambda(z)$ in another layer.

In order to explain the causes of these peculiarities of the
vertical structure of $b'_\lambda(z)$, we must examine the joint corre-
lation coefficients $r_{bq}(z_k,\ z_l)$, $r_{bT}(z_k,\ z_l)$ and $r_{bu}(z_k,\ z_l)$
(Figure 3.10) where u is the relative humidity. The figure shows
that $r_{bu} \approx 0$ under summer conditions at the ground surface, while
$r_{bu} \approx 0.5$ in the 1 - 3 km layer. But in winter conditions $r_{bu} \approx$ /
0.3 - 0.5 near the ground, while outside the boundary layer
these coefficients are close to zero (or even negative). The
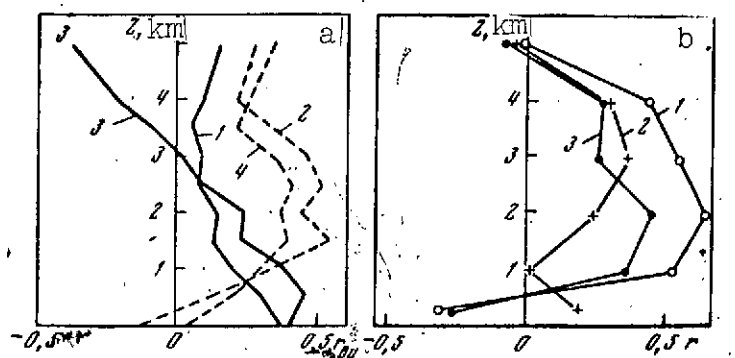
Figure 3.10. Calculations of the joint correlation coefficients
a- $r_{bu}(z_k, z_k)$ from measurements [1.6]; solid lines are for
winter, broken lines are for summer; 1, 2- $\lambda = 0.7$ μm; 3, 4-
$\lambda = 0.5$ μm; b- from measurements of [1.5]; 1- r_{bq}; 2- r_{bu};
3- r_{bT}

absence of correlation in summer at the ground surface is
probably due to the same causes as the weak correlation between
q' and T' (see Figure 3.4). In fact, the fluctuations in $b_\lambda(z)$
are determined by the fluctuations in u, which are large in the
summer at the ground and depend both on the absolute humidity and
on the temperature variations. In most cases an increase in
humidity, which leads to an increase in b_λ, is accompanied by the
development of convection and turbulence, the result being that
there is a transport of ground aerosols to higher layers of the
atmosphere, i.e., a decrease of $b_\lambda(0)$ and an increase of $b_\lambda(z)$
at the other heights. The combination of these processes also
leads to the formation of the vertical structure of $b'_\lambda(z)$
obtained in summer. As was shown by Rozenberg [30], the type of
air mass must play an important part here, i.e., the nature of
the condensation nuclei. However, the quantitative characteris-
tics of this parameter have not as yet been determined with a
completeness sufficient for our purposes.
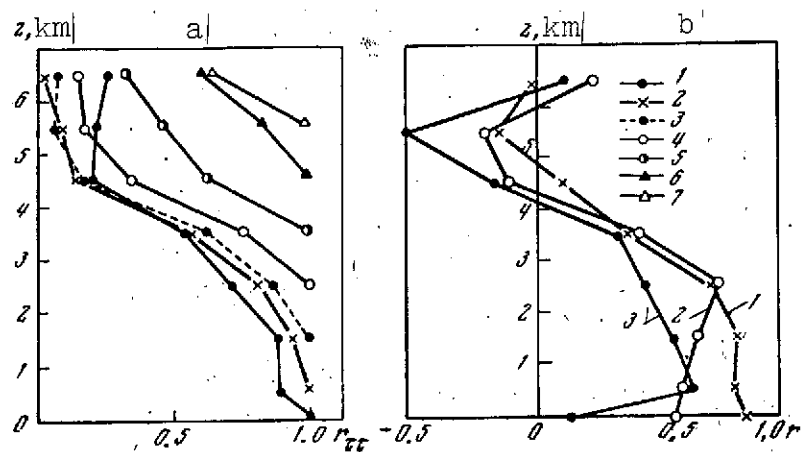
Figure 3.11. Calculations of correlation coefficients from measurements of [1.5]·

a- $r_{\tau\tau}(z_k, z_l)$: 1- $z_k = 0$; 2- 0.5; 3- 1.5; 4- 2.5; 5- 3.5; 6- 4.5; 7- 5.5 km; b: 1- $r_{\tau w}(z_k, z_k)$; 2- $r_{\tau q}(z_k, z_k)$; 3- $r_{\tau T}(z_k, z_k)$

When we consider the values of r_{bb} and r_{bu} obtained, we must not exclude the effect of errors in determining $b_\lambda(z)$, resulting from differentiating the directly measured values of atmospheric transmission. Therefore, for practical applications it is expedient to use correlations for integral characteristics of aerosol attenuation and humidity as well, i.e., the optical depth

$$\tau_\lambda(z) = \int_z^\infty b_\lambda(t)\, dt$$

and the water vapor mass

$$w(z) = \int_z^\infty \rho_w(t)\, dt$$

Naturally, here the above errors are reduced, but the dependent random quantities are functionally correlated, and so the correlation coefficients $r_{\tau\tau}(z_k, z_l)$ increase noticeably. The joint

194
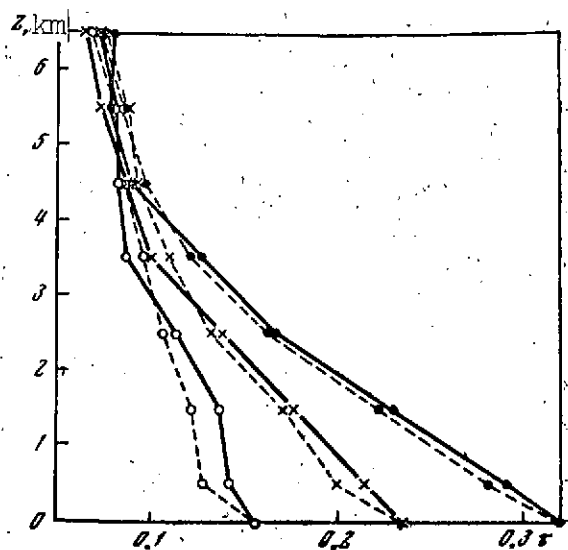
Figure 3.12. Comparison of profiles of $\tau(z)$

The solid lines are measurements of [1.5]; the broken lines are calculated by the optimum approximation method

correlation $r_{\tau W}(z_k, z_l)$ also becomes tighter (Figure 3.11). However, even these characteristics reveal the layered nature of the aerosol atmosphere ($r_{\tau\tau}$ decreases sharply above 3 to 4 km).

Using the statistical characteristics obtained, it is not difficult to find the vertical behavior of $b_\lambda(z)$ or $\tau_\lambda(z)$ in the optimum fashion from measurements of these quantities at some point z. Examples of determining the optical depths at various levels z from measurement of $\tau(0)$ at the ground surface are given in Figure 3.12.

The examples given should be regarded only as an illustration of the empirical approach to the determination of complex relationships between meteorological and optical characteristics. In spite of the weak joint correlation, the results obtained contain some information on the possible processes which contribute to the vertical structure of aerosol attenuation.

5.3. Angular Structure of the Scattering Index

From the numerous measurements of the scattering index in the surface air layer for the range of scattering angles φ = 12 - 168° [1.33], and for the halo part of the index φ = 0.3 - 6° [1.34], statistical characteristics have been constructed for the angular structure of the coefficient of directional aerosol

195
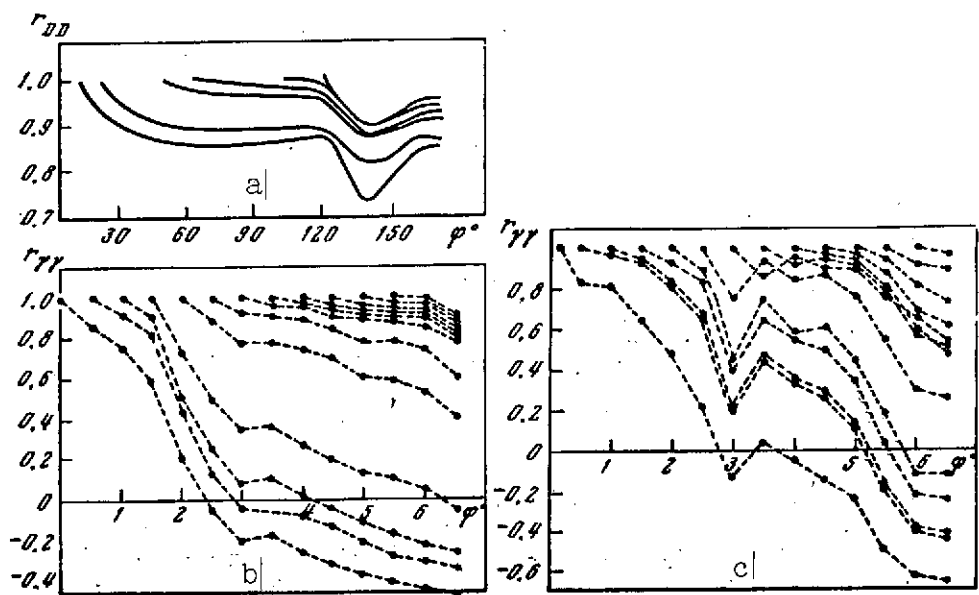
Figure 3.13.   Correlation coefficients $r_{\gamma\gamma}$ and r_{DD}
a- from measurements of [1.33], λ = 0.5 μm;   b- from measurements of [1.34], λ = 0.47 μm;   c- from measurements of [1.34], λ = 0.888 μm

scattering $\gamma(\varphi)$ in the visible part of the spectrum. Unfortunately, the experimental conditions did not allow the authors [1.33, 1.34] to determine these characteristics for comparable types of optical conditions: in [1.33], the measurements were performed for atmospheric mist with a typical effective particle radius of 0.1 - 0.2 μm, while in [1.34], they were done for foggy mist and fog with typically coarser particles of 1 - 30 μm. This makes it impossible to obtain the angular structure throughout the whole range of angles φ for the diverse atmospheric conditions. We note also that, owing to large variations in the scattering index (by several orders in the above range of angles φ), the statistical characteristics were determined for $D(\varphi)$ = lg $\gamma(\varphi)$.

The examples of the normalized correlation matrices $r_{DD}(\varphi_h, \varphi_l)$ shown in Figure 3.13, a show that, in the scattering angle range 10 - 170°, there is a close correlation of the fluctuations in the coefficients of directional scattering. A noteworthy feature is the minimum r_{DD} = 0.74, corresponding to $\varphi = 135°$, i.e., the rainbow region. In the halo part of the scattering index (Figure 3.13 b, c), the fluctuations of $\gamma'(\varphi)$ in the small angle region ($\varphi < 2°$) are negatively correlated with the fluctuations of γ' in the region $\varphi > 2°$, while with increase of the wavelengths at which the measurements were taken in [1.34], the transition of the correlation coefficient through zero shifts to the region of larger angles. We note that in the region of large φ, the correlation increases. Similar differences in the correlation $r_{\gamma\gamma}$ for large and small φ were obtained in [20] for the brightness index at height 17 km.

An explanation of the statistical laws of the angular spectral and vertical structures of aerosol scattering can be given from study of the nature of the formation mechanism and the structure of particle size distribution under actual conditions. Some of these problems, which make up a special section of atmospheric optics, fall outside the scope of the present section. The only exception is the matter of certain formal connections between the statistical characteristics of the spectral and angular structure of the scattering coefficient and scattering index and the statistical characteristics of particle size distribution.

5.4. Relationship with the Particle Size Distribution Structure Function

As is known (see e.g., [B.5]), the aerosol scattering coefficient $b(\lambda)$ and the scattering index $\gamma(\varphi)$ are connected with the particle size distribution function $f(\rho)$ by the following

relations:

$$b(\lambda) = \int_0^\infty k_1(\lambda, \rho) f(\rho) \, d\rho; \quad (3.31)$$

$$\gamma(\varphi) = \int_0^\infty k_2(\varphi, \rho) f(\rho) \, d\rho. \quad (3.32)$$

In Equations (3.21) and (3.32), $k_1(\lambda, \rho)$ and $k_2(\varphi, \rho)$ are known functions and describe the scattering coefficient and scattering index of a single spherical particle of radius ρ. These relations, considered as integral equations, are customarily used to determine $f(\rho)$, and in fact the integration in (3.31) and (3.32) is carried out in a finite range of the dimensions (a, b).

It is not difficult to obtain, from Equations (3.31) and (3.32), a relation between the statistical characteristics of the scattering coefficient (or index) and the distribution function for the mean values

$$\bar{b}(\lambda) = \int_a^b k_1(\lambda, \rho) \bar{f}(\rho) \, d\rho; \quad (3.33)$$

$$\bar{\gamma}(\varphi) = \int_a^b k_2(\varphi, \rho) \bar{f}(\rho) \, d\rho \quad (3.34)$$

and the correlation functions

$$B_{bb}(\lambda, \lambda') = \int_a^b \int_a^b k_1(\lambda, \rho) k_1(\lambda', \rho') B_{ff}(\rho, \rho') \, d\rho \, d\rho'; \quad (3.35)$$

$$B_{\gamma\gamma}(\varphi, \varphi') = \int_a^b \int_a^b k_2(\varphi, \rho) k_2(\varphi', \rho') B_{ff}(\rho, \rho') \, d\rho \, d\rho'. \quad (3.36)$$

198

Similar relations can be obtained for the joint correlation
functions

$$B_{b\gamma}(\lambda, \varphi) = \int_a^b \int_a^b k_1(\lambda, \rho) k_2(\varphi, \rho') B_{ff}(\rho, \rho') d\rho \, d\rho'; \qquad (3.37)$$

$$B_{bf}(\lambda, \rho') = \int_a^b k_1(\lambda, \rho) B_{ff}(\rho, \rho') d\rho; \qquad (3.38)$$

$$B_{\gamma f}(\varphi, \rho') = \int_a^b k_2(\varphi, \rho) B_{ff}(\rho, \rho') d\rho. \qquad (3.39)$$

Thus, the correlation functions for the optical aerosol
parameters can be expressed in terms of the correlation function
B_{ff} for the size spectrum of the particles. Therefore, the value
of the correlation between the random fluctuations in the attenu-
ation coefficient $B_{bb}(\lambda, \lambda')$ at different wavelengths λ and λ' (or
of the scattering index $B_{\gamma\gamma}(\varphi, \varphi')$ at different scattering angles
φ and φ') is determined within the framework of the universal
relations (3.31) and (3.32), the only uncertainty being the
weights to be taken in Equations (3.35) - (3.39) for the correla-
tion $B_{ff}(\rho, \rho')$ for the different radii ρ and ρ'.

Investigations of the statistical characteristics of the
structure of aerosol particle size distribution functions were
done in [1.8] and [1.34] from the results of measurements of
aerosol particle spectra obtained using filters. Figure 3.14
shows normalized correlation matrices $r_{ff}(\rho_k, \rho_l)$ describing the
relation between random variations in the number of particles of
various sizes in mist and fog conditions. There is quite a close
correlation between the number of particles of adjacent sizes,
and it rapidly diminishes with increase in the difference of the
particle sizes.
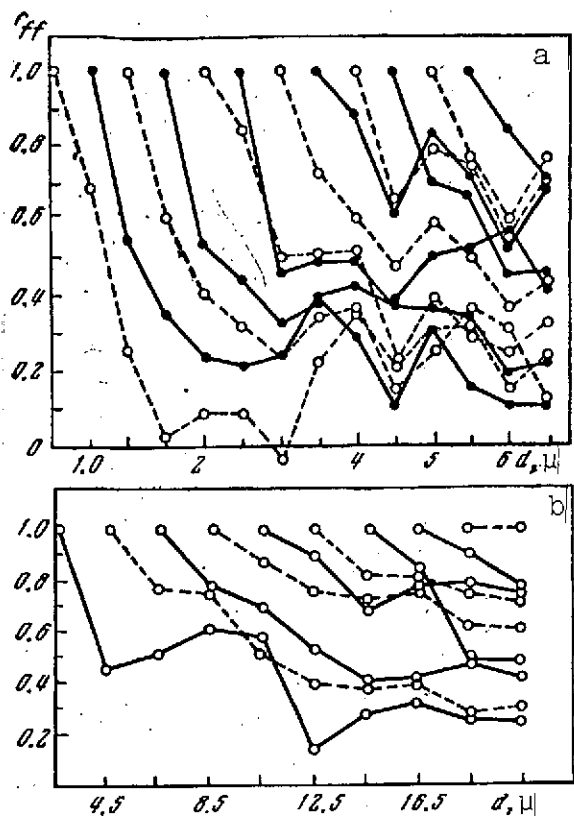
Figure 3.14. Normalized correlation matrices $r_{ff}(p_k, p_l)$ for fluctuations in the aerosol particle size distribution functions

a- atmospheric mist [1.8]; b- fog [1.34]

An interesting feature is the rather pronounced minimum of r_{ff} in the medium radius region for the particle size range considered (for particles whose radii lie in the range $2 \leqslant \rho \leqslant 6$ µm, a rather definite minimum of r_{ff} corresponds to $d = 2\rho \approx 3$ µm; for the range $2 \leqslant \rho \leqslant 20$ µm, the minimum is strongly smeared, and corresponds to $d = 2\rho = 12 - 14$ µm).

The presence of these minima of correlation is evidence as to the existence of some statistical law for the formation and disintegration of particles of fine, medium, and large size. Without considering specific mechanisms for the process of aerosol formation (see [30], we note that a decline of correlation in the medium size region can indicate either a difference in these mechanisms for different sizes, or the existence of a mechanism where the formation of particles of various sizes proceeds from disintegration of particles of other sizes (some confirmation of this process comes from the results of measurements of concentration of droplets of different sizes, obtained in [31]).

The second alternative should lead to negative correlation for certain values of ρ. The absence of this feature in the curves of Figure 3.14 could be due to the existence of a process leading to fluctuations of opposite signs in the number of

particles of corresponding sizes, and also to the large errors
of measurement of particle spectrum by means of filters. The
results obtained and the hypothesis concerning anticorrelation
of the variations in the number of particles of different sizes
allows us to explain the special features of the spectral and
angular structure of aerosol scattering parameters.

It is known (see e.g., [B.5]), that the scattering coeffi-
cient $b(\lambda)$ is determined mainly by small particles whose number
is an order of magnitude greater than that of large particles.
The close correlation between variations and sizes of these
particles is the cause of the large positive correlation between
$b'(\lambda)$ for different values of λ. For larger λ, the variations
in $b'(\lambda)$ are determined by larger particles which are less
intercorrelated, which also causes attenuation of the correlations /119
of $b'(\lambda)$ for small and large wavelengths. We can similarly
explain the high correlation of the index variations in the
angular range $\varphi = 10 - 170°.$|

However, in the range of small φ, the variations in the
scattering index are determined by variations in the number of
large particles, and with increase of φ, by variations in the
small particles. Therefore, the structure of the correlation
functions $B_{\gamma\gamma}(\varphi, \varphi')$| can be fully explained. The anticorrelation
for large and small angles φ can arise only when the variation
in the number of small particles is anticorrelated with variations
in the number of large particles, as would follow from the above
hypothesis concerning the mechanism of formation and disintegra-
tion of particles of different sizes.* A close positive

---

* Statistical reduction of direct measurements of the spectra of
particles in fog confirms this| conclusion as to the existence of
anticorrelation of the number of large and small particles [3.14].

correlation between variations of the index at large scattering angles reflects a positive correlation between the variations and the number of small particles governing the index in this region of φ.

Incidentally, the shift towards the large φ region of the zeros of the correlation coefficients $r_{\gamma\gamma}(\varphi, \varphi')$ for $\lambda = 0.888$ μm (see Figure 3.13 c) is evidence of the increasing role of the medium and large particles in scattering of this wavelength of radiation in a wider interval of small angles φ.

The above conclusions can also be obtained from analysis of Equations (3.35) and (3.36), if we assume that the correlation function $B_{ff}(\rho, \rho')$ for fixed ρ changes its sign when ρ' takes certain sufficiently large values. In fact, the kernel $k_1(\lambda, \rho)$ in Equation (3.35) is an attenuation coefficient for radiation of wavelength λ' by a single particle of radius ρ, and is given for spherical particles, by the Stratton-Hayton function [I.5], which approaches a constant value asymptotically, even for small ρ. Thus, the weight accompanying the values of the correlation function $B_{ff}(\rho, \rho')$ for fixed λ, but for different ρ, is roughly /120 constant (apart from at very small ρ). But, since the number and the dispersion of small particles are large, the main contribution to the correlation function $B_{bb}(\lambda, \lambda')$ comes from the correlation moments $B_{ff}(\rho, \rho')$ for small particles. The role of the correlation moments between small and large particles for which there is an anticorrelation is small, because of the low values of these moments. Therefore, the presence of negative values of $B_{ff}(\rho, \rho')$ in the region of transition from small to medium and large particles cannot seriously diminish the correlation of the attenuation coefficient with respect to λ.

As regards Equation (3.36), the situation is somewhat more complicated. The kernel $k_2(\varphi, \rho)$ for small angles φ is given, as is known, by the formula

$$k_2(\varphi, \rho) = \frac{J_1^2(\varphi \tilde{\rho})}{\varphi^2} \tilde{\rho}^2,$$ (3.40)

where $J(\varphi, \tilde{\rho})$ is a Bessel function; $\tilde{\rho} = 2\pi\rho/\lambda$, so that k_2 depends also on λ.

It follows from Equation (3.40) that at small φ the kernel $k_2 \sim \tilde{\rho}^4$, i.e., it is large only for large particles, while with increase of φ the kernel k_2 rapidly decreases and becomes uniform. Therefore, in determining $B_{\gamma\gamma}(\varphi, \varphi')$ for small φ from Equation (3.36), the negative correlation moments $B_{ff}(\rho, \rho')$, which must exist, according to our postulates, between the variations of small and large particles, enter into the integral (3.36) with large weight. The result is that we obtain a negative correlation between variations of the index at small and large φ. Looking now at the large φ region, we equalize the weight of the positive correlation moments B_{ff} which are large in absolute value, between the variations of small particles and the comparatively low negative moments between small and large particles. As a result, we must obtain a positive correlation between the variations of the index at large values of φ.

This superposition of the correlation relationships between variations in the number of large and small particles manifests itself, very probably, also in the rather marked separation of $r_{\gamma\gamma}$ for large and small angles.

In concluding this section, we note that to investigate the structure of radiation fields, and for problems of optical probing, it is important to have data on variations of atmosphere transmission functions which are associated with variations in atmospheric humidity and temperature.

Because experimental data required to determine these relationships in a statistical sense is not yet inadequate, we shall put aside discussion of this question for the present. We note also that some evaluations of the statistical characteristics of transmission and humidity functions were obtained in [32, 33].

§ 6. Empirical Orothogonal Functions

6.1. Basic Property of the Empirical Functions

The important characteristics of the statistical structure of fields of meteorological elements, widely used in this book, are the systems of the so-called statistically orthogonal functions, for which a rigorous theory was constructed | by Obukhov [1] (see, also, [2, 3]).

It was shown in [1] that for an arbitrary stochastically continuous random function f(x), defined in the interval [a, b] and having finite moments of first and second order, one can determine an orthonormal|system of basic functions $\varphi_k(x)$| which will yield an optimum approximation for any sample of a random function f(x):

$$f_n(x) = \sum_{k=1}^{n} c_k \varphi_k(x); \qquad c_k = \int_a^b f(x) \varphi_k(x)\, dx.$$ (3.41)

This means that with a given error of approximation the   /121
statistically orthogonal functions $\varphi_k(x)$| give this approximation (on the average) with the minimum number of terms n of the sum (3.41) or, conversely, for a given number n the system φ_k gives minimum error for the approximation (3.41), on the average.

The optimum system of basic functions is the system of eigenfunctions of the correlation function $B_{ff}(x, y)$, regarded as the kernel of the integral equation (3.8). As a symmetric positive-definite function B_{ff} has a denumerable multitude of eigenfunctions $\varphi_k(x)$ and positive eigenvalues μ_k.

With this definition of the functions $\varphi_k(x)$, the error in the approximation

$$\sigma_n^2 = \overline{\int_a^b [f(x) - f_n(x)]^2 \, dx}$$

(3.42)

will be a minimum and equal to the residual sum of the eigenvalues μ_k, corresponding to the $\varphi_k(x)$ rejected in (3.41), i.e.,

$$\sigma_n^2 = \sum_{k=n+1}^{\infty} \mu_k$$

(3.43)

From the definition of the expansion coefficients c_k, we get the derivation, important for applications, that the eigenvalues μ_k have the meaning of dispersions of the expansion coefficients of the random functions $f(x)$ in terms of the optimum basis $\varphi_k(x)$, i.e.,

$$\overline{c_k^2} = \overline{\left[\int_a^b f(x)\, \varphi_k(x)\, dx \right]^2} = \mu_k$$

(3.44)

The identity (3.44) is easily proved by carrying out all the operations and taking into account Equation (3.8) and the fact that the system $\varphi_k(x)$ is orthonormal.

When the values of the random functions are given at discrete points x_j, i.e., there is a multitude of samples of the random vectors $f_i(x_j)$, the analog of the orthogonal functions is the

eigenvectors $\varphi_k(x_j)$ of the autocorrelation matrix $B_{ff}(x_j, x_l)$, which has the properties of optimum systems of functions mentioned above.

6.2. Optimal Systems for the Temperature and Humidity Profiles

For the autocorrelation matrices $B_{TT}(p_k, p_l)$ and $B_{qq}(p_k, p_l)$ constructed by Popov [6] from several ensembles of vertical temperature and specific humidity profiles (see § 2 and §3 of the present chapter), eigenvectors and eigenvalues of these matrices were determined in [34]. The fact that reference [6] considered a multitude of samples of temperature and humidity for diametrically opposite conditions of atmospheric sounding (dry land and sea, summer and winter, day and night), enables the statistical stability to be evaluated for the optimal systems of orthonormal vectors in these conditions.

Examples of eigenvectors $\varphi_k(p_l)$, eigenvalues μ_k of the matrices $B_{TT}(p_k, p_l)$, and of the residual dispersions

$$\delta_k = \sum_{i=k+1}^{n} \mu_i \Big/ \sum_{i=1}^{n} \mu_i$$

are given in Figure 3.15 and Table 3.5. We note several special features of the systems of orthonormal vectors obtained. In all cases, the first eigenvectors φ_1 have zero value near the tropopause level, i.e., where the coefficients go to zero for the correlation between the temperature deviations at the tropopause level and at the lower levels (see Figures 3.1 and 3.2).

From the physical viewpoint, this kind of behavior of $\varphi_1(p_j)$ means that the first eigenfactor describes the most typical vertical distribution of the temperature deviations $T'(p_j)$ from
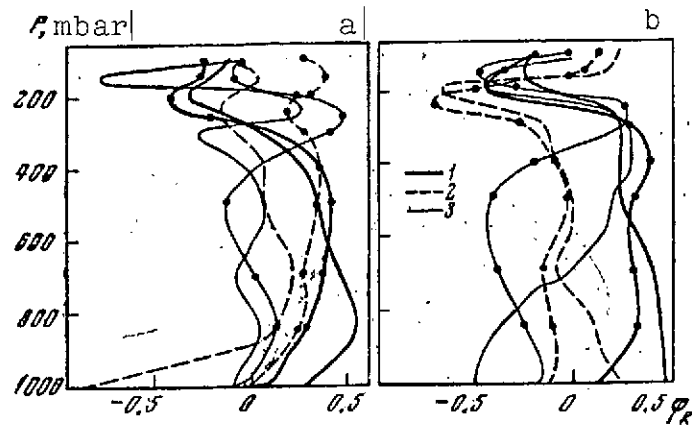
Figure 3.15. Vectors φ_k of the matrix B_{TT} for the continent and the ocean (curves with points)

a- July; b- January; 1- φ_1; 2- φ_2; 3- φ_3

TABLE 3.5. EIGENVALUES μ_k (IN DEGREES C) OF THE MATRICES $B_{TT}(p_k, p_l)$ AND $B_{qq}(p_k, p_l)$ AND VALUES OF THE DISPERSIONS $\varepsilon_k(1 - \delta_k) \cdot 100\%$*

k	Bismark, July				Bismark, January				Vessel "C", July				Vessel "C", January			
	μ_k^T	μ_k^q	ε_k^T	ε_k^q	μ_k^T	μ_k^q	ε_k^T	ε_k^q	μ_k^T	μ_k^q	ε_k^T	ε_k^q	μ_k^T	μ_k^q	ε_k^T	ε_k^q
1	95,3	7,0	67	71	201	1,9	54	74	81,2	8,1	62	79	137,5	3,2	45	78
2	20,1	1,9	79	90	52,1	0,4	68	82	18,5	1,2	77	90	65,2	0,5	67	86
3	12,6	0,5	88	95	30,1	0,2	76	98	9,1	0,7	83	97	34,6	0,3	78	99
4	6,1	0,4	92	100	28,8	0,04	83	99	6,2	0,3	88	100	21,0	0,05	85	100
5	4,5	0,05	95	—	19,8	0,02	89	100	5,4	0,03	92	—	11,1	—	89	—
6	2,6	—	97	—	14,2	—	93	—	2,9	—	95	—	9,8	—	92	—

* Translator's note: Commas in numbers represent decimal points,

the mean profile $\bar{T}(p_j)$. It is precisely this "guess" by the first eigenvector as to the basic behavior of $T'(p_j)$ which makes possible the optimum approximation to $T'(p_j)$.

The universal nature of the first eigenvectors $\varphi_1(p_j)$ in all the cases examined, which span the temperature distribution with height for typical conditions, is evidence of the statistical

stability of the basic harmonic. As regards the second and
third eigenvectors, which take account of details of the vari-
ations in $T'(p_j)$ of higher order, although their reproducibility
is deficient at individual levels, the vertical behavior in the
main is quite similar in the different cases.

Successive eigenvectors differ noticeably even in such
stable cases as the day and night profiles of $T'(p_j)$ over the
ocean, although their contribution stays less than 20% of the
total dispersion of the coefficients for the expansion of $T'(p_j)$
in a series with respect to $\varphi_k(p_j)$. An interesting point is the
difference in the number of zeros for the second and third
eigenvectors above dry land and the ocean: φ_2 and φ_3 over the
ocean have one and two zeros, respectively, while over dry
land φ_2 has two or three zeros, and φ_3 has two or four zeros.
This means that the basic behavior of $T'(p_j)$ with height over
dry land and the ocean is the same, but details of the vertical
profile above dry land are much more complex, because a more
complex structure of high order harmonics is required. The same
is true of eigenvectors in the different seasons (January to
July). While previously the first eigenvector for January has
the same behavior with height as for July, now the second and
third eigenvectors differ from the July values. There are also
noticeable differences between φ_2 and φ_3 for the two daily
periods (00 and 12 hours), and the number of zeros of φ_2 and φ_3
increases in the daytime conditions. One should also note the
increase in the eigenvalues μ_k^T in winter conditions, which reflects
an increase in the variations of T' in winter, in comparison
with summer.

A similar system of orthogonal normalized functions has been
obtained also to describe the vertical structure of the field of
specific humidity in terms of the correlation matrices $B_{qq}(p_k, p_l)$

208
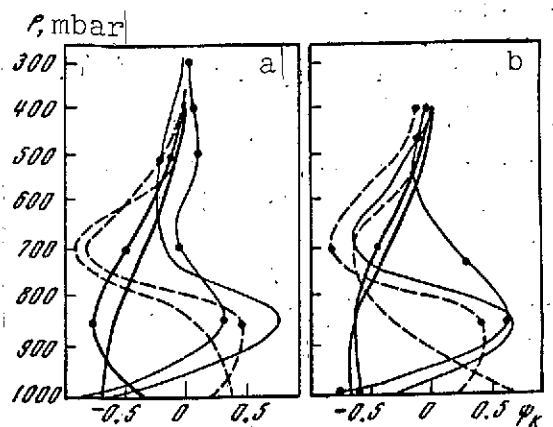
Figure 3.16. Vectors ψ_k of the matrix B_{qq}. Symbols are the same as in Figure 3.15

obtained in [6] for the same daytime cases as $B_{TT}(p_k, p_l)$. Examples of eigenvectors and eigenvalues are given in Figure 3.16 and Table 3.5.

An interesting point is the universal nature of the eigenvectors $\psi_k(p_j)$ for dry land and the ocean, which is considerably more marked than for the vectors φ_k for the temperature field. Amongst typical features of the vertical behavior of the ψ_k vectors, we should note the absence of zeros in ψ_1, as well as the sharp fall of ψ_k with height. The vectors ψ_k can describe details of the vertical structure of the humidity field, as evidenced by the example of vessel C (January): for this case, the vector ψ_1 reaches a maximum at the same level (850 mbar) for which a maximum is observed in the mean square deviation $\sigma_q(p_j)$. It follows from Table 3.5 that even the first three eigenvectors yield an approximation with a residual dispersion of 2 to 5%. As regards the eigenvalues μ_k^q, they increase for summer conditions, which is typical of the large range of fluctuations of q'(p_j) in summer in comparison with winter.

Based on what has been said, we can conclude that the differences in the first eigenvectors φ_k and ψ_k for the diametrically opposite cases considered above (dry land and ocean, winter and summer) are not very major and reflect details of the random fluctuations T'(p_j) and q'(p_j). Therefore, we can consider the eigenvectors as statistically universal and use any of these systems as a basis for expansion of the random vectors $T'_i(P_j)$ or $q'_i(p_j)$ from any ensemble.

The empirical orthogonal functions considered, which most economically describe the vertical structure of the temperature field, can be used to solve a number of problems in atmospheric physics. One such problem, that of determining the vertical profiles of atmospheric temperature and humidity from the outgoing Earth radiation in the absorption bands of carbon dioxide and water vapor, will be considered in Chapters 6 and 7.

6.3. Theoretical Considerations

The empirical orthonormal systems of functions or vectors are also used for the optimum parametric representation of the fields of meteorological elements in the solution of problems in dynamic meteorology, including that of weather forecasting [16, 35 - 39]. Taking into account that random fluctuations of meteorological elements are due to atmospheric disturbances of different scales, we can find the connection between the eigenfunctions and the scales of such disturbances. Investigations of this kind, based on solution of the corresponding equations of the dynamics of atmospheric flow of heat and moisture, were proposed by Marchuk [35, 36], Gavrilin [37], and Holmström [39]. The basic principle for solution of this problem, formulated in general form in [36], is to examine the spectral problem for the given operator and conjugate operators. The eigenfunctions of the appropriate operators proved to be biorthogonal, while the eigenvalues are conjugate. These investigations yield the physical parameters of the atmosphere responsible for the same characteristics of the vertical structure of the fields of meteorological elements which remain stable during random variations of the latter. By way of example of theoretical determination of eigenfunctions, we consider the results obtained by Gavrilin [37] for the vertical structure of the specific humidity. Simplifying the moisture flow equation, in accordance with the requirements of the problem,

$$\frac{\partial q}{\partial t} + \frac{u}{a \sin \theta} \frac{\partial q}{\partial \lambda} + \frac{v}{a} \frac{\partial q}{\partial \theta} + w^* \frac{\partial q}{\partial p} = k_h \Delta q + \frac{\partial}{\partial p} w_v p^2 \frac{\partial q}{\partial p} - g \frac{\partial}{\partial p} p q_b \frac{v}{RT} \, \cdot$$

where qb is the concentration of moisture drops; $\tilde{v}$ is the weighted mean speed of descent of the drops; u, v are the horizontal components of the wind speed; w* is the "vertical component" of the velocity; a is the radius of the Earth; θ, λ, p are coordinates of the point in space; $\omega_v = k_z (q/RT)^2 = k_z/H^2$; k_z, k_h are the vertical and horizontal turbulent diffusion coefficients; and H is the height of the uniform atmosphere, the author of [37] derived the following system of equations and boundary conditions

$$\frac{d}{dp} \left[p^2 \frac{dq(p)}{dp} \right] - \alpha_1 \frac{d}{dp} [pq(p)] = \lambda q(p); \tag{3.45}$$

$$\alpha_2 \Delta q (x, y) = - \lambda q (x, y); \tag{3.46}$$

$$p \frac{dq}{dp} - \alpha_3 q = 0 \quad \text{for} \quad p = p_0 \text{ and } p_1. \tag{3.47}$$

Here $\alpha_1 = c/\bar{v}H/k_z$; $\alpha_2 = k_h/k_z H^2$; $\alpha_3 = 1/e (\partial e/\partial T) p (\partial T/\partial p) - 1$ ($\alpha_3 \approx 2.6$ for the troposphere); and p_0 and p_1 are the lower and upper boundaries of the atmosphere.

The eigenvalues and the eigenfunctions of the problem (3.45), (3.47) have the form

$$\lambda_0 = - (\alpha_3 + 1) (\alpha_1 - \alpha_3); \qquad \lambda_n = - \left[\left(\frac{\pi n}{\zeta_1} \right)^2 + \left(\frac{\alpha_1 + 1}{2} \right)^2 \right] \quad (n = 1, 2, \ldots); \tag{3.48}$$

$$q_0(\zeta) = c_0(\zeta)^{\alpha_1};$$

$$q_n(\zeta) = c_0(\zeta)^{\frac{\alpha_1-1}{2}}\left[\frac{\pi n}{\ln\frac{1}{\zeta_1}}\cos\pi n\left(\frac{\ln\zeta}{\ln\zeta_1}\right) - \frac{2\alpha_3-\alpha_1+1}{2}\sin\pi n\left(\frac{\ln\zeta}{\ln\zeta_1}\right)\right];$$

$$\zeta = \frac{p}{p_0}, \quad \zeta_1 = \frac{p_1}{p_0}.$$

(3.49)

The eigenvalues λ_n^* of the operator conjugate with (3.45) and (3.47) coincide with λ_n, and the eigenfunctions have the form:

$$q_0^*(\zeta) = c_0(\zeta)^{-\frac{\alpha_1+1}{2}};$$

$$q_n^*(\zeta) = c_0(\zeta)^{-\frac{\alpha_1+1}{2}}\left[\frac{\pi n}{\ln\frac{1}{\zeta_1}}\cos\pi n\left(\frac{\ln\zeta}{\ln\zeta_1}\right) - \frac{2\alpha_3-\alpha_1+1}{2}\sin\pi n\left(\frac{\ln\zeta}{\ln\zeta_1}\right)\right].$$

(3.50)

The functions $q_n(\zeta)$ and $q_n^*(\zeta)$ are orthogonal, and the functions $q_n(p)$ are orthogonal with weight in the interval $[\zeta_1, 1]$; /125

$$\int_{p_1}^{p_0} p^{-\alpha_1} q_n(p) q_m(p)\, dp = \delta_{nm} N_n^2,$$

(3.51)

where

$$\delta_{nm}\begin{cases}1, & n=m,\\ 0, & n\neq m;\end{cases}$$

$$N_0^2 = \frac{1-(\zeta_1)^{2\alpha_3-\alpha_1+1}}{2\alpha_3-\alpha_1+1}; \qquad N_n^2 = 2\ln\frac{1}{\zeta_1}\left[\left(\frac{\pi n}{n\frac{1}{\zeta_1}}\right)^2 + \left(\frac{2\alpha_3+\alpha_1+1}{2}\right)^2\right].$$

(3.52)

Comparison of the eigenfunctions (3.50) with the empirical eigenfunctions $\psi_k(p)$ considered above shows that the theory proposed in [37] gives quite a good description of the basic features of the vertical structure of the humidity field (3.17). The results obtained allow determination of the scales of the disturbances associated with each harmonic. In fact, Equation (3.46) in an infinite plane has the form:

$$q_n(y) = e^{-\frac{y}{L_n}}; \qquad L_n = H\sqrt{-\frac{k_h}{k_z\lambda_n}}.$$

(3.53)

212
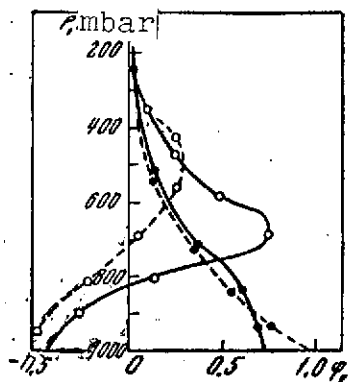
Figure 3.17. Comparison of the empirical (solid lines) and theoretical (broken lines) eigenfunctions for the vertical profiles of specific humidity. The points show ψ_0, and the circles show ψ_1

Putting $\alpha_1 \approx 3$ (for a drop radius of ~5 μm), $\alpha_3 = 2.6$; $\alpha_2 = 7.2 \cdot 10^{12}$ m^2 (for $k_h = 10^6$ m^2/sec; $k_z = 10$ m^2/sec; H = 8 km), $\ln (p_0/p_1) = 1.6$ (p_1 = 200 mbar) the author of [37] obtained the values $L_n = 2700/\sqrt{-\lambda_n}$; $\lambda_0 = -1.41$; $\lambda_n = |-[3.8 n^2 + 1.05]|$; $L_0 = 2270$ km; $L_n = 1380/\sqrt{n^2 + 1.05}$. Hence it follows that the zero order eigenfunction corresponds to a wave of ~2500 km (planetary scale), and the others to 960, 610, 430, 340 km, and so on.

§ 7. Horizontal Structure of the Atmospheric Parameters

An investigation of the horizontal structure of the fields of the atmospheric parameters is a much more complicated problem than investigation of the vertical structure, mainly because of the two-dimensional nature of the random functions. Another complexity arises from the absence of experimental data on horizontal fluctuations for practically all the optical atmospheric parameters. For these reasons, investigations of the horizontal structure have been made only for meteorological elements (pressure, temperature, clouds, etc.), and in most cases, the fields in question are assumed to be homogeneous and isotropic. This assumption enables one to construct one-dimensional correlation functions which depend only on the distance ρ between meteorological stations whose data are used in the statistical analysis.
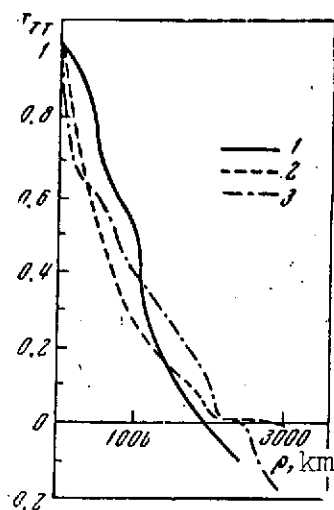
Figure 3.18. Comparison of the correlation coefficients $r_{TT}(\rho)$ from the calculations (21] (1), [5] (2), and [23] (3)

For the surface temperature field, the correlation functions $B_{TT}(\rho)$ were obtained in [5, 21 - 23].

Comparison of the normalized autocorrelation functions $r_{TT}(\rho)$ calculated in [5, 21, 23] is shown in Figure 3.18.

It is easy to see that the general behavior of r_{TT} of the ratio between values of the correlation coefficients at the same distances, and also the radius of correlation ρ_0, determined from the condition $r_{TT}(\rho_0) = 0$, prove to be quite close in all cases. This is evidence of the reliability of the smoothed correlations of the surface temperature field within the hypothesis made. However, these results have limited use in practice, since the actual temperature fields can be appreciably inhomogeneous and anisotropic, e.g., because of the latitude behavior, the effect of orography, and, for the surface temperature case, also the effect of the microclimate.

A more reliable matter is the direct calculation of autocorrelation matrices describing the correlation between simultaneous fluctuations of temperature or humidity at a given level and different stations. In this case, there is no need to postulate that the random fields are homogeneous and istropic, and therefore these calculations allow the above hypotheses to be checked. Some steps in this direction have been taken in [23]. By correlating the surface temperature fluctuations $T'(p_0)$ at

Figure 3.19. Map of lines of equal value for the correlation coefficient $r_{TT}(\rho)$, in %, from [23]

1- Moscow; 2- Paris

fixed stations (in [23], the stations near Moscow and Paris were taken) with fluctuations $T'(p_0)$ at other stations, the authors of [23] constructed lines of equal correlation coefficients, describing|the degree of isotropy of the $T'(p_0)$ field. /127 As can be seen from Figure 3.19, under continental conditions, this field can be regarded as isotropic, to a certain approximation, although on the periphery of the region one sees noticeable anisotropy, connected, to a considerable extent, with the effect of the oceans. This influence on the anisotropy of the $T'(p_0)$ field shows up rather clearly in coastal regions and is illustrated in the figure by the example of the calculation of r_{TT} near Paris.

As regards the degree of homogeneity of the field $T'(p_0)$, to evaluate it we must construct the correlation matrix $B_{TT}(\rho_k, \rho_l)$

215

e.g., for the fluctuations $T'(p_0)$ at stations chosen in a given direction, as was done in [23] for the same cases of continental and coastal regions. For a homogeneous field, the elements of the matrix $B_{TT}(\rho_k, \rho_l)$, which satisfy the condition $|k - l| = \text{const}$ should be identical.

A convenient estimate of the homogeneity of random fields is afforded by the eigenvectors of the autocorrelation matrices, which coincide with trigonometric functions in the case of homogeneous fields [14].

The question of the homogeneity of two-dimensional random fields will be considered in more detail in Chapter 5.

CHAPTER 4
VERTICAL, ANGULAR, AND SPECTRAL STRUCTURE
OF THE RADIATION FIELD

§ 1. Statement of the Problem

The results presented in the previous chapters indicate the
directions in which it is profitable to seek the laws for fluctu-
ations in the Earth's radiation field. The relationship of the
intensity or radiative flux with the physical parameters of the
atmosphere, cloud and underlying surface, the random nature of
whose variations implies random fluctuations in the radiation
field characteristics, can be established using the radiative
transfer equation for the atmosphere. Therefore, the statistical
characteristics of the structure of random radiation fields
forming the atmospheric radiation model must also depend in a
specific way on the statistical characteristics of the fields
of meteorological elements and optical parameters of the atmos-
phere and the underlying surface, which form the optical-
meteorological model. To discover these laws, one must use the
radiative transfer equation for the actual atmosphere whose
parameters vary randomly.

In the present chapter, we consider the case of a horizon-
tally homogeneous plane-parallel atmosphere for which we consider
as known the statistical characteristics described in Chapter 3
for the vertical structure of the optical and meteorological
parameters determining the random fluctuations of the vertical,
angular, and spectral distributions of the radiation field, which
is also homogeneous in the horizontal direction. In practice,

this means that the random fluctuations in intensity of the Earth's self-radiation or of the scattered radiation, like the random samples of the corresponding atmospheric physical parameters, depend parametrically on time and on the horizontal coordinates.*

The basic attention will be given to determining the statistical characteristics of the vertical structure of the Earth's self-radiation field, which is associated with the following circumstances:

the phenomenological mechanism for the transfer of long-wave emission in the atmosphere is simpler than that for short-wave radiation; the main atmospheric parameters determining the variability of long-wave radiation are the temperature and humidity, whose vertical structure, as was shown in Chapter 3, has been studied rather well; it is also comparatively simple to account for fluctuations in clouds in a given case, since the variation of the outgoing self-radiation at least is affected by variations in the upper boundary of the clouds, the cloud temperature and the humidity, for which we have already noted methods of statistical investigation that are presently available.

Some of the results of investigations of the vertical structure of long-wave radiation have been described in [1] and they are reproduced below with a number of improvements and additions.

---

* In fact, these dependencies of the atmospheric parameters are determined by a complex system of equations for atmospheric thermodynamics, and therefore, by a large number of physical factors.

As regards the vertical structure of the short-wave radiation field, because of the complexity of the mechanism for scattering solar radiation in the actual atmosphere, we shall examine only the case of a spherical scattering index. A further reason is that the angular structure of actual indices, and this is even /129 more true for the vertical structure, has received practically no study. The vertical and angular structure of the scattering field of solar radiation will be determined, thus, only by the characteristics of the vertical structure of the aerosol scattering coefficient, for which, as we saw in Chapter 3, there are available statistical characteristics obtained from three families of independent measurements $b_\lambda(z)$. To describe the radiation model of the atmosphere, we shall use, as before, the first and second moments of the radiation characteristics considered as random functions of height, direction, and frequency. The use of distribution functions for the physical parameters, in terms of which the optical characteristics of the atmosphere can be expressed, as proposed by Ross [2] and Neilson [3], for the study of scattering in vegetation cover, is not feasible under atmospheric conditions. The fact is that for these parameters (e.g., the concentration of aerosols, the vertical profiles of temperature and humdity), the multidimensional distribution functions are practically unknown. However, even if we were to succeed in constructing empirical distributions, the distribution of the correlation moments for these distributions would entail large uncontrolled errors if they were to deviate from the normal law, for which exact mathematical methods of analysis of random quantities have been developed.

§ 2. Vertical Structure of Long-Wave Radiation

2.1. Basic Relations

We assume that in numerous measurements of the intensity of ascending or descending long-wave radiation $I_\nu^\uparrow(\zeta, \theta)$, $I_\nu^\downarrow(\zeta, \theta)$, at the level $\zeta = p/p_0$ and angle θ to the local vertical, above a given point of the globe, these quantities vary randomly, like the vertical profiles of temperature $T(\zeta)$ and humidity $q(\zeta)$. If we take the emittance of the underlying surface to be unity, then from Equations (2.6) and (2.7) we can easily obtain simple relations connecting the realizations of the random function $I_\nu(\zeta, \theta)$ with realizations of the random functions $T(\zeta)$ and $q(\zeta)$ (we consider water vapor to be the only absorbing substance):

$$I_\nu^\uparrow(\zeta, \theta) = B_\nu[T(1)] \exp[-w_0\tau_\nu(\zeta, 1, \theta)] - $$
$$- \int_\zeta^1 B_\nu[T(t)] \frac{\partial}{\partial t} \{\exp[-w_0\tau_\nu(\zeta, t, \theta)]\} dt; \qquad (4.1)$$

$$I_\nu^\downarrow(\zeta, \theta) = \int_0^\zeta B_\nu[T(t)] \frac{\partial}{\partial t} \{\exp[-w_0\tau_\nu(t, \zeta, \theta)]\} dt; $$
$$\tau_\nu(\zeta, t, \theta) = \sec\theta \int_\zeta^t k_\nu(t) q(t) dt \qquad (4.2)$$

For the radiation intensities $\tilde{I}_\nu = \frac{1}{\Delta\nu} \int_{\Delta\nu} I(\nu') \varphi(\nu, \nu') d\nu'$, averaged for quite narrow spectral intervals $\Delta\nu$, and allowing for the instrumental function $\varphi(\nu, \nu')$, Equations (4.1), and (4.2) take the form

$$\tilde{I}_\nu(\zeta, \theta) = B_\nu[T(1)] P_\nu(\zeta, 1, \theta) - \int_\zeta^1 B_\nu[T(t)] \frac{\partial}{\partial t} P_\nu(\zeta, t, \theta) dt; \qquad (4.3)$$

where B_ν is some average value of the Planck function in the interval $\Delta\nu$:

$$\tilde{P}_{\nu}(\zeta, t, \theta) = \frac{1}{\Delta\nu} \int\limits_{\Delta\nu} \exp\left[- w_0 \sec\theta \int\limits_{\zeta}^{t'} k_{\nu'}(t')\, q(t')\, dt'\right] \varphi(\nu, \nu')\, d\nu' \qquad (4.4)$$

is the atmospheric transmssion function (2.9), allowing for the response function of the instrument.

Integrating Equation (4.3) by parts, we obtain another expression for $\tilde{I}_{\nu}^{\uparrow}$:

$$\tilde{I}_{\nu}^{\uparrow}(\zeta, \theta) = \tilde{B}_{\nu}\,[T(\zeta)] + \int\limits_{\zeta}^{1} \tilde{P}_{\nu}(\zeta, t, \theta) \frac{\partial}{\partial t}\, \tilde{B}_{\nu}\,[T(t)]\, dt. \qquad (4.5)$$

Similar expressions can be obtained also for $I_{\nu}^{\downarrow}$:

$$\tilde{I}_{\nu}^{\downarrow}(\zeta, \theta) = \int\limits_{0}^{\zeta} \tilde{B}_{\nu}\,[T(t)] \frac{\partial}{\partial t}\, \tilde{P}_{\nu}(t, \zeta, \theta)\, dt \qquad (4.6)$$

or

$$\tilde{I}_{\nu}^{\downarrow}(\zeta, \theta) = \tilde{B}_{\nu}\,[T(\zeta)] - \tilde{B}_{\nu}\,[T(0)]\, \tilde{P}_{\nu}(\zeta, 0, \theta) - \int\limits_{0}^{\zeta} \tilde{P}_{\nu}(t, \zeta, \theta) \frac{\partial \tilde{B}_{\nu}\,[T(t)]}{\partial t}\, dt. \qquad (4.7)$$

As was already noted in § 2 of Chapter 2, the transmission function $P_{\nu}^{\downarrow}$ can be measured or calculated from the known molecular characteristics of the water vapor absorption band and from the specific humidity given for each specific case.

Since the form of the transmission and equipment functions will not be of major importance in determining the vertical structure of the radiation field, then, in order to simplify the calculations, we assume that $\varphi(\nu, \nu') \equiv 1$ in the interval $\Delta\nu$ and zero outside this interval (here $\tilde{P}_{\nu} = P_{\nu}^{\downarrow}$), and for $P_{\nu}^{\downarrow}$ we shall use Equations (1.16) or (1.20), which in this case can be represented in the form

$$P_{\nu}(\zeta, t, \theta) = 1 - \Phi\left[\sqrt{\frac{l_{\nu}}{2}\, w_0 \tau(\zeta, t, \theta)}\right] \qquad (4.8)$$

and

$$P_i(\zeta, t, \theta) = \exp\{-\alpha[w_0\tau(\zeta, t, \theta)]^{1-\kappa_0}\}$$ (4.9)

respectively.

Here,

$$\tau(\zeta, t, \theta) = \sec\theta[Q(t) - Q(\zeta)]; \qquad Q(\zeta) = \int_0^\zeta t^\kappa q(t)\,dt.$$ (4.10)

2.2. Statistical Characteristics

Expressions (4.1) – (4.7) allow us to find the relation between the characteristics of the vertical structure of the intensity of the field of Earth self-radiation I_1* and the fields $T_i(\zeta)$ and $q_i(\zeta)$ (i is the sample number of the random function). We represent each of these functions in the following form:

$$I_i(\zeta, \theta) = \bar{I}(\zeta, \theta) + I_i'(\zeta, \theta), \qquad \overline{I_i'(\zeta, \theta)} = 0;$$ (4.11)

$$T_i(\zeta) = \bar{T}(\zeta) + T'(\zeta), \qquad \overline{T'(\zeta)} = 0;$$ (4.12)

$$q_i(\zeta) = \bar{q}(\zeta) + q_i'(\zeta), \qquad \overline{q_i'(\zeta)} = 0,$$ (4.13)

where the bar above a symbol denotes averaging over the whole set /131 of realizations of the given random function (i.e., the norm), and the primes denote deviations from the norms. Then, at fixed angles θ and frequency ν, from Equation (4.3) or (4.5), we can obtain a system of equations for determining $I(\zeta, \theta)$ for the auto-correlation function

$$K_{II}(\zeta, \zeta'; \theta) = \overline{I_i'(\zeta, \theta)I_i'(\zeta', \theta)}$$ (4.14)

---

* We omit the subscript ν and the sign $\sim$ below; the derivation of the formulas and all the calculations will be given for I↑.

222

and for the joint correlation functions

$$K_{IT}(\zeta, \zeta'; \theta) = \overline{I_i'(\zeta, \theta)\, T_i'(\zeta');}$$
$$K_{Iq}(\zeta, \zeta'; \theta) = \overline{I_i'(\zeta, \theta)\, q_i'(\zeta'),}$$

(4.15)

which describe the vertical structure of the radiation field in terms of the set of statistical characteristics of the vertical structure of the temperature and humidity fields: $\overline{T}(\zeta), \overline{q}(\zeta),$ $K_{TT}(\zeta, \zeta'), K_{qq}(\zeta\zeta')$ and $K_{qT}(\zeta, \zeta').$

We assume that $T'(\zeta)$ and $q'(\zeta)$ are small and that we can confine ourselves to linear terms in the expansions

$$B_\nu\,[\overline{T}(\zeta) + T_i'(\zeta)] = B_\nu\,[\overline{T}(\zeta)] + \frac{\partial B_\nu\,[\overline{T}(\zeta)]}{\partial T}\, T_i'(\zeta) + \ldots$$

(4.16)

$$P_\nu\,[\overline{q}(\zeta) + q_i'(\zeta)] = P_\nu\,[\overline{q}(\zeta)] + \frac{\partial P_\nu\,[\overline{q}(\zeta)]}{\partial \tau}\,[Q_i'(t) - Q_i'(\zeta)] + \ldots$$

(4.17)

The average of the transmission function $\overline{P}_\nu$ and its derivative $\partial\overline{P}_\nu/\partial\tau$ in Equation (4.17) are determined by means of Equations (4.8) - (4.10). For example, for the case (4.8)

$$\overline{P}_\nu(\zeta, t, \theta) = 1 - \Phi\left\{\sqrt{\frac{l_\nu}{2}\, w_0 \sec\theta\, [\overline{Q}(t) - \overline{Q}(\zeta)]}\right\};$$

(4.18)

$$\frac{\partial\overline{P}_\nu}{\partial\tau} = -\frac{1}{\sqrt{\pi}}\left[\frac{\frac{1}{2}\, l_\nu w_0 \sec\theta}{\overline{Q}(t) - \overline{Q}(\zeta)}\right]^{1/2} \exp\left\{-\frac{l_\nu}{2}\, w_0 \sec\theta\, [\overline{Q}(t) - \overline{Q}(\zeta)]\right\};$$
$$\overline{Q}(\zeta) = \int_0^\zeta t^n \overline{q}(t)\, dt; \qquad Q_i'(\zeta) = \int_0^\zeta t^n q_i'(t)\, dt.$$

(4.19)

We note that, in a small enough neighborbood of the straight line $t = \zeta$, where the derivatives of the transmission functions (4.8) and (4.9) have integrable singularities, there must be a transition with the asymptote of P_ν at small values of the argument (see

[I.2]). If we substitute Equations (4.11) - (4.13) into
Equations (4.3) or (4.5) then, taking account of Equations (4.16)
and (4.17), we can obtain a system of equations for determining
the characteristics of the vertical structure of the field of
ascending radiation. If the main fluctuations $I'(\zeta, \theta)$ are deter-
mined by the fluctuations T' or q' at the underlying surface or
in the lower layers of the atmosphere (this situation can arise
in regions of slight atmospheric absorption), it is more conven-
ient to use Equation (4.3). But if the fluctuations $I'(\zeta, \theta)$ are due
to higher atmospheric layers (e.g., in regions of strong atmos-
pheric absorption), then it is desirable to replace Equation (4.5)
by Equations (4.11) - (4.13). Performing this substitution and
taking into account Equations (4.16) and (4.17), we obtain

$$I(\zeta, \theta) + I_i'(\zeta, \theta) = B[\bar{T}(\zeta)] + \frac{\partial B[\bar{T}(\zeta)]}{\partial T} T_i'(\zeta) + \int_\zeta^1 \left\{ \bar{P}(\zeta, t, \theta) + \right.$$
$$\left. + \frac{\partial \bar{P}(\zeta, t, \theta)}{\partial \tau} [Q_i'(t) - Q_i'(\zeta)] \right\} \frac{\partial}{\partial t} \left\{ B[\bar{T}(t)] + \frac{\partial B[\bar{T}(t)]}{\partial T} T_i'(t) \right\} dt. \quad (4.20)$$

Averaging Equation (4.20) for all the samples and using Equation /132
(4.19), we obtain an equation for $\bar{I}^i(\zeta, \theta)$

$$\bar{I}^i(\zeta, \theta) = B[\bar{T}(\zeta)] + \int_\zeta^1 \bar{P}(\zeta, t, \theta) \frac{\partial B[\bar{T}(t)]}{\partial T} dt +$$
$$+ \int_\zeta^1 \frac{\partial \bar{P}(\zeta, t, \theta)}{\partial \tau} \int_\zeta^t u^n du \frac{\partial}{\partial t} \left\{ K_{qT}(u, t) \frac{\partial B[\bar{T}(t)]}{\partial T} \right\} dt. \quad (4.21)$$

Multiplying the left and right sides of Equation (4.20) by $I'(\zeta', \theta)$,
averaging over all samples, and neglecting moments of third order,
we obtain an equation for the autocorrelation function K_{II}:

$$K_{II}(\zeta, \zeta', \theta) = \frac{\partial B[\bar{T}(\zeta)]}{\partial T} K_{TI}(\zeta, \zeta', \theta) + \int_\zeta^1 \bar{P}(\zeta, t, \theta) \frac{\partial}{\partial t} \left\{ \frac{\partial B[\bar{T}(t)]}{\partial T} \times \right.$$
$$\left. \times K_{TI}(t, \zeta', \theta) \right\} dt + \int_\zeta^1 \frac{\partial \bar{P}(\zeta, t, \theta)}{\partial \tau} \int_\zeta^1 u^n K_{qI}(u, \zeta', \theta) \frac{\partial B[\bar{T}(t)]}{\partial T} du \, dt. \quad (4.22)$$

224

Thus, if I' is expressed only in terms of the structure functions of the field of T and q, to determine K_{II} we need to have the joint correlation functions K_{II} and K_{qI}. It is not difficult to obtain the latter by multiplying the left and right sides of Equation (4.20) by $T_i'(\zeta)$ or $q_i'(\zeta)$ and subsequently averaging over all the samples:

$$
K_{IT}(\zeta, \zeta', \theta) = \frac{\partial B\,[\bar{T}(\zeta)]}{\partial I'}\, K_{TT}(\zeta, \zeta') + \int_{\zeta}^{t} \bar{P}(\zeta, t, \theta)\, \frac{\partial}{\partial t}\Big\{ K_{TT}(t, \zeta') \times
$$
$$
\times \frac{\partial B\,[\bar{T}(t)]}{\partial I'} \Big\}\, dt + \int_{\zeta}^{t} \frac{\partial \bar{P}(\zeta, t, \theta)}{\partial \tau} \int_{\zeta}^{t} u K_{qT}(u, \zeta')\, \frac{\partial B\,[\bar{T}(t)]}{\partial I'}\, du\, dt;
$$

(4.23)

$$
K_{Iq}(\zeta, \zeta', \theta) = \frac{\partial B\,[\bar{T}(\zeta)]}{\partial I'}\, K_{Tq}(\zeta, \zeta') + \int_{\zeta}^{1} \bar{P}(\zeta, t, \theta)\, \frac{\partial}{\partial t}\Big\{ K_{Tq}(t, \zeta')\, \frac{\partial B\,[\bar{T}(t)]}{\partial I'} \Big\}\, dt +
$$
$$
+ \int_{\zeta}^{1} \frac{\partial \bar{P}(\zeta, t, \theta)}{\partial \tau} \int_{\zeta}^{t} u K_{qq}(u, \zeta')\, \frac{\partial B\,[\bar{T}(t)]}{\partial I'}\, du\, dt.
$$

(4.24)

The system of equations (4.21) – (4.24) enables us to express I', K_{II}, K_{IT}, K_{Iq} in terms of the statistical characteristics of the temperature and humidity fields $\bar{T}$, $\bar{q}$, K_{TT}, K_{Tq}, K_{qq}. The equations to determine the latter can be obtained from the equations for the flux of heat and moisture. This implies a need to examine the equations of atmospheric dynamics. It is known (see, e.g., [4]) that this system of equations can be closed only with very rigorous assumptions about the nature of the fluctuations of the thermodynamic parameters of the atmosphere.

One can close the system of equations (4.21) – (4.24) by using empirical data on the structural characteristics of the T and q fields, obtained by statistical reduction of the results of aerological soundings (these characteristics were presented in Chapter 3). Here one should bear in mind that reliable data on some of the characteristics, e.g., K_{qq} or K_{Tq}, can be obtained

only up to comparatively low altitudes (not more than 8 - 10 km); while in very strong water vapor absorption regions, the radiation intensity I and its structural characteristics are determined by the variations of temperature and humidity in higher layers of the atmosphere. To increase the reliability of determining the statistical characteristics of the vertical structure of the radiation field in these spectral regions one must have improve- /133 ment in methods of measurement of humidity at high |altitudes.

In regions of weak water vapor absorption, the main effect on variations of I↑ comes from variations of temperature of the underlying surface. Therefore, it is more convenient to use Equation (4.3) to obtain the structural characteristics. Substituting expressions (4.11) - (4.13) into Equation (4.3) and performing the required averaging, we can express $I^\dagger$, K_{II}, K_{IT}, K_{Iq}| directly in terms of the structural characteristics of the temperature and humidity of the underlying surface. This can also be done by integrating Equations (4.21) - (4.24) by parts.

For regions with not very strong absorption, we consider another method of determining the statistical characteristics of the vertical structure of the field of long-wave radiation, which enables us to avoid the above peculiarities in the deriva- tive of the transmission function and the need to go to the asymptote of P_ν for $t = \zeta$ in carrying out the calculations. By substituting the expressions| (4.11) - (4.13) and (4.16), written for a single absorber q(p) and for $\delta = 1$, into Equation (4.1) and the boundary condition (2.3), we obtain

$$\cos\theta \, \frac{\partial \bar{I}_\nu}{\partial \zeta} + \cos\theta \, \frac{\partial I'_\nu}{\partial \zeta} = w_\nu k_\nu(\zeta) \, [\bar{q}(\zeta) + q'(\zeta)] \times$$
$$\times \left\{ \bar{I}_\nu(\zeta, \theta) + I'_\nu(\zeta, \theta) - B_\nu [\bar{T}(\zeta)] - \frac{\partial B_\nu [\bar{T}(\zeta)]}{\partial T} \, T'(\zeta) \right\}; \tag{4.25}$$

$$\bar{I}_\nu(1, \theta) + I'_\nu(1, \theta) = B_\nu [\bar{T}(1)] + \frac{\partial B_\nu [\bar{T}(1)]}{\partial T} \, T'(1). \tag{4.26}$$

226

Averaging Equations (4.25) and (4.26), we obtain equations for determining $I_\nu(\zeta, \theta)$:

$$\cos\theta \, \frac{\partial \bar{I}_\nu}{\partial \zeta} = \bar{w} \, k_\nu(\zeta) \, \bar{q}(\zeta) \{ \bar{I}_\nu(\zeta, \theta) - B_\nu[\bar{T}(\zeta)]\} +$$
$$+ w_0 k_\nu(\zeta) \left\{ k_{qI}(\zeta, \zeta; \theta) - \frac{\partial B_\nu[\bar{T}(\zeta)]}{\partial T} K_{qT}(\zeta, \zeta) \right\};$$

(4.27)

$$\bar{I}_\nu(1, \theta) = B_\nu[\bar{T}(1)].$$

(4.28)

Calculating Equation (4.27) from (4.25), and Equation (4.28) from (4.26), respectively, we obtain an equation for determining $I_\nu'(\zeta, \theta)$:

$$\cos\theta \, \frac{\partial I_\nu'}{\partial \zeta} = w_0 k_\nu(\zeta) \, \bar{q}(\zeta) \left\{ I_\nu'(\zeta, \theta) - \frac{\partial B_\nu[\bar{T}(\zeta)]}{\partial T} T'(\zeta) \right\} +$$
$$+ w_0 k_\nu(\zeta) \, q'(\zeta) \{ \bar{I}_\nu(\zeta, \theta) - B_\nu[\bar{T}(\zeta)]\} + w_0 k_\nu(\zeta) \, \varepsilon(\zeta, \theta);$$

(4.29)

$$I_\nu'(1, \theta) = \frac{\partial B_\nu[\bar{T}(1)]}{\partial T} T'(1).$$

(4.30)

In Equation (4.29), the set of second order moments entering into Equation (4.27) is denoted by $\varepsilon(\zeta, \theta)$.

It can be seen from Equations (4.27) – (4.30) that, to solve Equation (4.29), we need to know the average profile of $I_\nu(\zeta, \theta)$, which it is difficult to determine from Equations (4.27) and (4.28) because there is no solution for the correlation moment $K_{qI}(\zeta, \zeta; \theta)$. Therefore, we solve Equations (4.27) and (4.30) by the method of successive approximations. Discarding the second order moments in the solution of Equation (4.27) (with the boundary condition (4.28)), because these moments are small relative to the mean quantities, we obtain a first approximation for $\bar{I}_\nu(\zeta, \theta)$:

$$\bar{I}_\nu(\zeta, \theta) = B_\nu[\bar{T}(1)] \, P_\nu(\zeta, 1; \theta)] - \int_\zeta^1 \left\{ B_\nu[\bar{T}(t)] - \right.$$
$$\left. - \frac{K_{qI}(t, t; \theta) - \frac{\partial B_\nu[\bar{T}(t)]}{\partial T} K_{qT}(t, t)}{\bar{q}(t)} \right\} \frac{\partial}{\partial t} P_\nu(\zeta, t; \theta) \, dt.$$

(4.31)

Substituting the latter into Equation (4.29) and solving this equation with boundary condition (4.30), we find an expression for $I_\nu'(\zeta, \theta)$:

$$I_\nu'(\zeta, \theta) = B_\nu \frac{\partial B_\nu [\overline{T}(1)]}{\partial T} T'(1) P_\nu(\zeta, 1; \theta) - \int_\zeta^t \left\{ \frac{\partial B_\nu [\overline{T}(t)]}{\partial T} T'(t) - \frac{\overline{I}_\nu(t, \theta) - B_\nu [\overline{T}(t)]}{\overline{q}(t)} q'(t) \right\} \frac{\partial}{\partial t} P_\nu(\zeta, t; \theta) dt. \tag{4.32}$$

In Equations (4.31) and (4.32) the quantity $P_\nu(\zeta, t; \theta)$ denotes either the exponential function $\exp\left[-w_0 \sec \theta \int k_\nu(u) \overline{q}(u) du \right]$, or the average transmission function (4.4) over the spectral interval $\Delta\nu$.

By multiplying Equation (4.32) by $I_\nu'(\zeta', \theta)$, $T'(\zeta')$ or $q'(\zeta')$ and averaging over all the samples, it is not difficult to obtain a system of equations for determining the autocorrelation function $K_{II}(\zeta, \zeta'; \theta)$ and the joint correlation functions $K_{IT}(\zeta, \zeta'; \theta)$, $K_{Iq}(\zeta, \zeta'; \theta)$. For example,

$$K_{II}(\zeta, \zeta'; \theta) = \frac{\partial B_\nu [\overline{T}(1)]}{\partial T} K_{TI}(1, \zeta'; \theta) P_\nu(\zeta, 1; \theta) - \int_\zeta^1 \left\{ \frac{\partial B_\nu [\overline{T}(t)]}{\partial T} K_{TI}(t, \zeta'; \theta) - \frac{\overline{I}_\nu(t, \theta) - B_\nu [\overline{T}(t)]}{\overline{q}(t)} K_{qI}(t, \zeta'; \theta) \right\} \frac{\partial P_\nu(\zeta, t; \theta)}{\partial t} dt. \tag{4.33}$$

The functions K_{IT} and K_{Iq} are obtained from Equation (4.33) by replacing the second index of I by the index T or q, respectively. Substituting the function $K_{Iq}(\zeta, \zeta', \theta)$ into Equation (4.31), we can obtain a second approximation for $I_\nu(\zeta, \theta)$ and then improve K_{II}, K_{IT}, and K_{Iq}.

If we are not interested in the joint correlation functions, we can obtain $K_{II}(\zeta, \zeta'; \theta)$ without an intermediate stage of calculating K_{IT} and K_{Iq}. In fact, by multiplying Equation (4.32) by itself (in accordance with the definition of K_{II}) with ζ and ζ' and averaging over all the samples, we obtain the following formula

for $K_{II}(\zeta, \zeta'; 0)$:

$$K_{II}(\zeta, \zeta'; \theta) = \left\{\frac{\partial B_\nu [\overline{T}(1)]}{\partial T}\right\}^2 K_{TT}(1,1) P_\nu(\zeta, 1; \theta) P_\nu(\zeta', 1; \theta) - \frac{\partial B_\nu [\overline{T}(1)]}{\partial T} \times$$

$$\times P_\nu(\zeta', 1; \theta) \int\limits_\zeta^1 \left\{\frac{\partial B_\nu [\overline{T}(t)]}{\partial T} K_{TT}(1,t) - \frac{\overline{I}_\nu(t, \theta) - B_\nu [\overline{T}(t)]}{\overline{q}(t)} K_{Tq}(1,t)\right\} \times$$

$$\times \frac{\partial P_\nu(\zeta, t; \theta)}{\partial t} dt - \frac{\partial B_\nu [\overline{T}(1)]}{\partial T} P_\nu(\zeta, 1; \theta) \int\limits_{\zeta'}^1 \left\{\frac{\partial B_\nu [\overline{T}(t)]}{\partial T} K_{TT}(1,t) - \right.$$

$$\left. - \frac{\overline{I}_\nu(t, 0) - B_\nu [\overline{T}(t)]}{\overline{q}(t)} K_{Tq}(1,t)\right\} \frac{\partial P_\nu(\zeta, t; \theta)}{\partial t} dt + \int\limits_\zeta^1 \int\limits_{\zeta'}^1 \left\{\frac{\partial B_\nu [\overline{T}(t)]}{\partial T} \times \right.$$

$$\times \frac{\partial B_\nu [\overline{T}(u)]}{\partial T} K_{TT}(t,u) - \frac{\overline{I}_\nu(t, \theta) - B_\nu [\overline{T}(t)]}{\overline{q}(t)} \frac{\partial B_\nu [\overline{T}(u)]}{\partial T} K_{qT}(t,u) -$$

$$- \frac{\overline{I}_\nu(u, \theta) - B_\nu [\overline{T}(u)]}{\overline{q}(u)} \frac{\partial B_\nu [\overline{T}(t)]}{\partial T} K_{qT}(u,t) + \frac{\overline{I}_\nu(t, \theta) - B_\nu [\overline{T}(t)]}{\overline{q}(t)} \times$$

$$\left. \times \frac{\overline{I}_\nu(u, \theta) - B_\nu [\overline{T}(u)]}{\overline{q}(u)} K_{qq}(t,u)\right\} \frac{\partial P_\nu(\zeta, t; \theta)}{\partial t} \frac{\partial P_\nu(\zeta', u; \theta)}{\partial u} dt du. \qquad (4.34)$$

Examples of the vertical behavior of some correlation moments, calculated for the intensity of the ascending radiation in regions of strong absorption ($\nu = 1390$ cm^{-1}) and weak absorption ($\nu =$ 1240 cm^{-1}) by water vapor bands at 6.3 μm, using Equations (4.21) - (4.24) for $\theta = 0$, are given in Figures 4.1 and 4.2. The characteristics of the vertical structure of the fields of temperature and humidity were taken for summer soundings above a continental station (see § 2 and § 3 of Chapter 3).

It follows from Figure 4.1 that, in the weak absorption region (solid lines) the elements of the correlation matrix $K_{IT}(\zeta_h, \zeta_l; 0)$, which gave the dependence of $I_\nu(\zeta_h, 0)$ at a fixed level ζ_h on $T'(\zeta_l)$ at different levels ζ_l, decrease with height, pass through zero near the tropopause and become negative above it, i.e., they have the same vertical behavior as elements of the correlation matrix $K_{TT}(\zeta_h, \zeta_l)$. This analogy is due to the fact that deviations in the radiation intensity I_ν for weak absorption (broken lines) are determined, as one should expect, mainly by deviations of temperature $T'(\zeta)$ for the ground surface and the atmospheric boundary layer, which are anticorrelated with $T'(\zeta)$

229
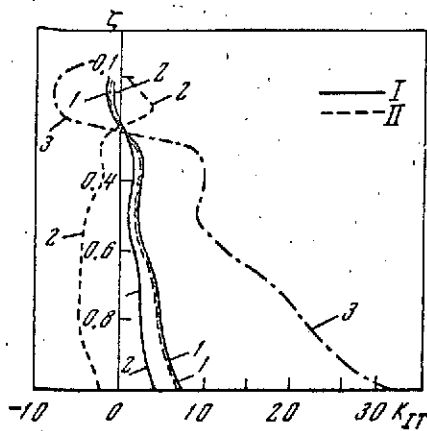
Figure 4.1. Vertical distribution of $K_{IT}(\zeta_k, \zeta_l, \theta)$ (in 10^3 cal/deg/cm^2·min·ster·µm).

1- $K_{IT}(1, \zeta_k)$; 2- $K_{IT}(0,2; \zeta_k)$; 3- $K_{TT}(1, \zeta_k)$ (in deg^2). I- weak absorption; II- strong absorption
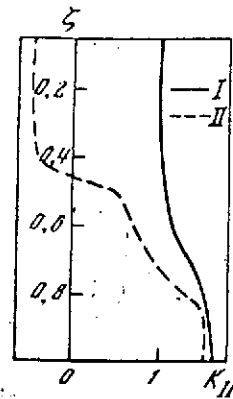
Figure 4.2. Vertical distribution of $K_{II}(1, \zeta_l; 0)$ [in $(10^3$/cal/cm^2·min·ster·µm$)^2$]. The symbols are the same as in Figure 4.1

above the tropopause (see § 2 of Chapter 3). Therefore, the nature of the correlations $K_{IT}(\zeta, \zeta')$ and $K_{TT}(\zeta, \zeta')$ are the same.

Conversely, in the strong absorption region, the variations I_v' at level ζ_k are determined mainly by the variations T' at the same or adjacent levels. Therefore, the correlation between the variations I_v' in the ground layer $(\zeta = 1)$ are proportional to T'(1), and the variations T' at higher levels follow $K_{TT}(1, \zeta)$, while the correlation between I' at level $\zeta = 0.2$ and of T' at the other levels is negative for the lower layers of the atmosphere and positive for the higher layers. Thus, we can explain the vertical distributions of the autocorrelation moments $K_{II}(1, \zeta)$ for regions of weak and strong absorption (Figure 4.2).

Analysis of the equations obtained, Equations (4.21) - (4.24) and (4.31) - (4.34), shows that the vertical structure of the self-radiation field is determined to a considerable extent by the vertical structure of the temperature field,

230

including the variations in the temperature of the underlying surface. As regards the humidity, its variations play a double role in forming the structure of the radiation field. On the one hand, an increase in humidity implies a decrease of intensity because of the increased absorption of radiation in the thermally stratified medium (correspondingly, decrease of $q(\zeta)$ leads to an increase in I_ν). In the second place, variations in humidity /136 lead to variations in I_ν of the same sign, because of the positive joint correlation of q' and T'.

This picture of the effect of variations q' and T' on the variations I' proves in fact to be somewhat more complicated, because of the integration of these effects with height in the different regions of spectral absorption and radiative emission. The total effect, which is a cause of the comparatively weak correlation between the outgoing Earth radiation and the temperature of the underlying surface and the atmosphere at different levels, can be obtained by carrying out appropriate calculations using Equations (4.21) - (4.24) or (4.31) - (4.34). As we shall see below (see § 6 of this chapter), this kind of situation is also observed in statistical reduction of radiation measurements on satellites [3.5]. Equations to determine the structural characteristics of the intensity of incident radiation, including the joint correlations $I^{\downarrow}(\zeta, \theta)$ with meteorological parameters and with the intensity of ascending radiation, can be determined similarly, using Equations (4.6) and (4.7).

2.3. The Structure of Radiative Fluxes

Since now there is a great deal of data on the actinometric sounding of the atmosphere up to great heights (see, e.g., [5, 6]), accompanied by measurements of vertical profiles of temperature and humidity, it is directly possible to compare the statistical

characteristics of the vertical structure of integrated fluxes of ascending and incident radiation, which are determined both theoretically and experimentally. For this purpose, we need to derive equations relating the structural characteristics of the radiative fluxes

$$F(\zeta) = \pi \int\limits_{0}^{\infty} dv \int\limits_{0}^{\pi/2} I_v(\zeta, \theta) \sin 2\theta \, d\theta$$

and the profiles of temperature and humidity. The derivation of these equations is entirely similar to that of the corresponding relations for the radiative intensity. In fact, we integrate Equations (4.1) and (4.2) over all directions within the upper hemisphere for $I_v^\uparrow$ and over the lower atmosphere for $I_v^\downarrow$, and then for all v from 0 to ∞, and introduce the integral transmission function*

$$P(\zeta, t) = \frac{1}{B(T)} \int\limits_{0}^{\infty} B_v(T) \, dv \int\limits_{0}^{\pi/2} \exp\left[- w_0 \sec\theta \int\limits_{\zeta}^{t} k_v(u) \, q(u) \, du \right] \sin 2\theta d\theta, \qquad (4.35)$$

where

$$B(T) = \sigma T^4 \qquad (\sigma = 0.814 \cdot 10^{-10} \text{ cal/cm}^2 \cdot \text{min} \cdot \text{deg}^4). \qquad (4.36)$$

Then, for the fluxes (e.g., for the flux of ascending radiation) Equation (4.1) takes the form:

$$F^\uparrow(\zeta) = B[T(1)] \, P(\zeta, 1) - \int\limits_{\zeta}^{1} B[T(t)] \frac{\partial P(\zeta, t)}{\partial t} \, dt. \qquad (4.37)$$

---

* We note that the integral transmission function depends on T much more strongly that P_v, which is averaged over a narrow spectral range. However, we neglect this dependence, as before.

By repeating for Equation (4.37) all the operations carried out in § 2.2, we can obtain relations of the type (4.21) - (4.24), for $\bar{F}^1, F', K_{FF}, K_{FT}, K_{Fq}$, in which the transmission function and B(T) /137 are replaced by Equations (4.35) and (4.36). For example,

$$K_{FF}(\zeta, \zeta') = \frac{\partial B\,[\bar{T}(\zeta)]}{\partial T}\,K_{TF}(\zeta, \zeta') + \int\limits_{\zeta}^{1} \bar{P}(\zeta, t)\,\frac{\partial}{\partial t}\left\{\frac{\partial B\,[\bar{T}(t)]}{\partial T}\,K_{TF}(t, \zeta')\right\} dt +$$
$$+ \int\limits_{\zeta}^{1} \frac{\partial \bar{P}(\zeta, t)}{\partial \tau} \int\limits_{\zeta}^{1} u K_{qF}(u, \zeta')\,\frac{\partial B\,[\bar{T}(t)]}{\partial t}\,dt\,du. \tag{4.38}$$

Formulas for determining the functions K_{FT} and K_{Fq}, obtained from Equation (4.38) by cyclic substitution of the second subscript F by T or q, will be integral analogs of Equations (4.23) and (4.24).

Examples of normalized correlation moments for the ascending flux of integrated radiation, calculated in [1] by these formulas, are shown in Figures 4.3 - 4.5. The calculations used typical statistical characteristics of the fields $T(\zeta)$ and $q(\zeta)$, obtained in [3.6] (see § 2 and § 3 of Chapter 3) and the integral transmission function of the type (1.20) with parameters $\alpha_0 = 1.3$, $k_0 = 0.8$. The same figures show the corresponding correlation coefficients obtained by Kurilova [7, 8] from statistical reduction of experimental data of actinometric sounding [6], and also including data regarding $T(\zeta)$ and $q(\zeta)$.

Since the correlation functions K_{qq} and K_{qT} calculated in [8] from these data have the same structure as the analogous characteristics of [3.6], a comparison of the theoretical [1] and experimental [7, 8] correlation coefficients can be regarded as quite valid.

This comparison shows that the basic features of the vertical structure of the variations of flux of ascending radiation and the correlation relations for $F'(\zeta)$ and $T'(\zeta)$ are described very
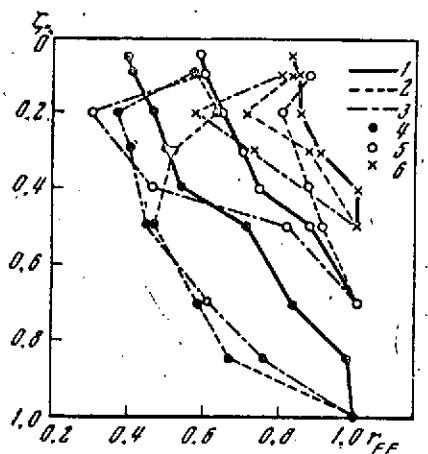
Figure 4.3. Comparison of the vertical behavior of $r_{FF}(\zeta_k, \zeta_l)$ 1- calculation in [1] from Equation (4.38); 2, 3- calculation of [7, 8] for summer and winter, respectively; 4 – 6- $\zeta_k = 1$, 0.7, and 0.5, respectively

satisfactorily by the above relations. It is true (Figure 4.3) that the experimental autocorrelation coefficients $r_{FF}(1, \zeta_k)$ turn out to be somewhat low in comparison with the calculations in the lower layers of the troposphere, especially during summer. One reason for this may be the incorrect normalization of the autocorrelation matrix $K_{FF}(\zeta_k, \zeta_l)$ in [7, 8], relative to the dispersions of $K_{FF}(\zeta_k, \zeta_k)$, only at the points ζ_k (compare this with Equation (3.7)), which appreciably decreases $r_{FF}(\zeta_k, \zeta_l)$ in all cases where $K_{FF}(\zeta_k, \zeta_k)$ is substantially greater than $K_{FF}(\zeta_l, \zeta_l)$.*

The correlation coefficients r_{FF} decrease with height, but in all the situations considered, apart from summer cloud Ac conditions (according to the data of [7]), remain positive. This result can be regarded as evidence that in cloudless conditions, the variations of the ascending flux at large heights are determined mainly by the temperature variations in the lower troposphere. Evidence for this conclusion is the vertical distributions of the joint correlation coefficient $r_{FT}(\zeta_k, \zeta_l)$. As can be seen from Figure 4.4, the rather high correlation of F' and T' in the atmospheric boundary layer decreases with height, passes through zero at the tropopause, and becomes negative in the lower layers

* The fact that $r_{FT}(1, \zeta_k)$ does not pass through zero for winter conditions, according to the data of [8] (Figure 4.4 b), corresponds to the correlation $r_{TT}(1, \zeta_k)$, obtained from the data from simultaneous measurements of $T(\zeta)$ and F (see [8]), being everywhere positive.

234
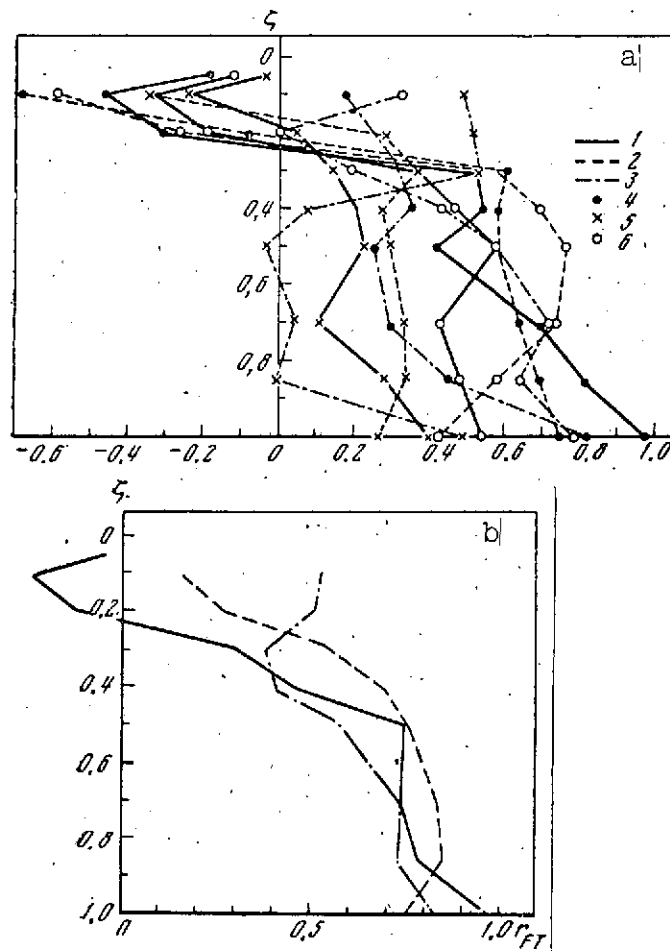
Figure 4.4. Comparison of the vertical behavior of r_{FT} (ζ_k, ζ_l) (a) and r_{FT} (ζ_k, ζ_k) (b)

a: 1- calculation of [1] using the transfer equations; 2, 3- calculation of [7, 8] from experimental data of [6] for summer and winter; 4 - 6- ζ_k = 1, 0.2, and 0.4, respectively

of the stratosphere. This kind of behavior of r_{FT} is fully in agreement with the vertical distribution of r_{TT} (see § 2 of Chapter 3), and in fact it means that the variations F' at all heights are determined by the troposphere variations of T', which are anticorrelated with T' above the tropopause.* With increase

---

* It is probably for the same reason that the correlation coefficients at the levels ζ = 0.2 and 0.1 prove to be overestimated in [7], conversely.

235
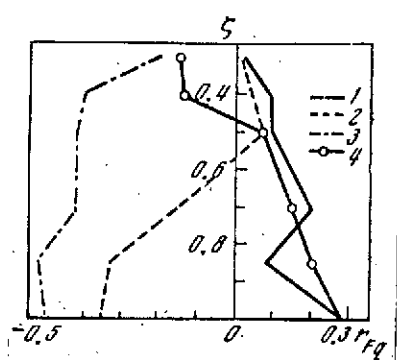
Figure 4.5. Vertical distribution of $r_{Fq}(\zeta_k, \zeta_l)$, according to [1]

1 - 3- ζ_k = 1, 0.5, and 0.2, respectively; 4- $r_{Fq}(\zeta_k, \zeta_k)$

of level ζ_k, the correlation coefficients $r_{FT}(\zeta_l, \zeta_l)$ decrease, and for the top boundary of the troposphere (ζ_k = 0.2), there is generally a weak correlation of F' with T' (0.2) at all levels ζ_l for ζ_l = 0.2 $r_{FT} \approx 0$, and for ζ_l = 0.1 $r_{FT} < 0$).

This decrease in correla- /138 tion results from superposition of the correlation moments $r_{TT}(\zeta_k, \zeta_l)$ of opposite sign, taken in the integrals (4.38) and in the analogous formulas for r_{FT} and r_{Fq} with different weights, which depend, in particular, on the moisture concentration. On the other hand, the joint correlation coefficients r_{Fq} are closely connected with variations T' and with the nature of the joint correlation of T' and q'. The theoretical correlation of F' and q' is rather low. Values of r_{FT} do not exceed 0.3 for a single /139 level ζ_k (Figure 4.5), while the variations of flux at the top boundary of the troposphere are noticeably anticorrelated with q' at all the lower-lying levels. The fact is, probably, that the effect of reduction of radiative flux with increase of moisture concentration has more effect than the opposing effect of increase of F' with increase of q'.

The conclusion that the variations of the meteorological parameters can have a counter influence on the variations of characteristics of the radiation field, the result being that the correlation between these variations is weak, is important we think for investigations of many atmospheric processes, since a

236

similar situation is met with in the interaction of a number of
other parameters (e.g., the connection between the variations
T' and q', considered in § 3 of Chapter 3). In practice, this
means that we are concerned with conditions for these processes
where the useful information is comparable with the noise.

The vertical structure of the radiation fields is appreci-
ably affected by clouds. This is illustrated, for example, in
[7] by the different behavior, depending on height, of the auto-
correlation coefficients $r_{FF}(\zeta_h, \zeta_l)$ for altocumulus cloud (Ac) in
summer conditions (solid lines) and in winter conditions (broken
lines) (Figure 4.6). The negative correlation of flux fluctu-
ations at levels $\zeta_h \geqslant 0.5$ with fluctuations F' at lower-lying
levels for summer, and the positive correlations for winter (or
for stratified clouds) is probably due to differences in the
vertical structure of the upper boundary of the cloud, and also
to the profiles of temperature and humidity. In order to obtain
quantitative evaluations of the effect of clouds and of the
vertical structure of the fields of Earth self-radiation, one must
introduce the statistical characteristics of the meteorological
parameters under cloud conditions into the radiative transfer
equation.

Before going on to this matter, we note that formulas
similar to (4.38) can also be obtained for the statistical char-
acteristics of the vertical structure of fluctuations of the
incident radiative flux, as well as the flux of self-radiation,
which is directly associated with radiation-induced changes of
temperature.

§ 3. Calculations of Cloud Variations

The basic difficulty in establishing the relations between
variations of the characteristics of radiation and cloud fields
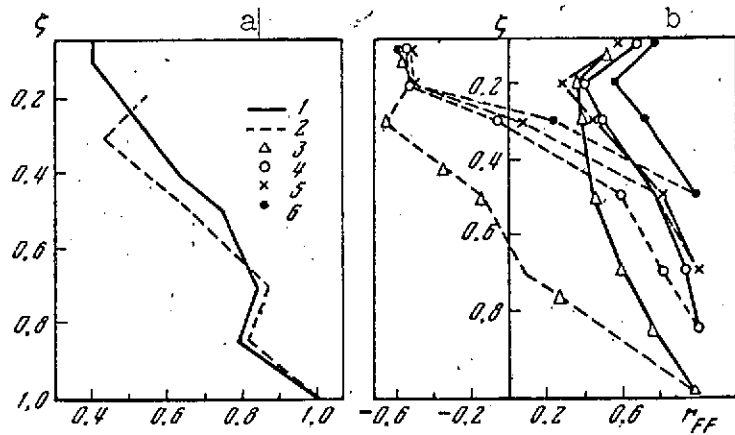
Figure 4.6. Vertical distribution

a- $r_{Fq}(\zeta_k, \zeta_k)$; 1- calculation according to [48]; 2- experiment according to [7]; b- empirical values of $r_{FF}(\zeta_k, \zeta_l)$; 1, 2- for winter and summer, respectively; 3 - 6- ζ_k = 1, 0.85, 0.7, and 0.5, respectively

arises from the lack of reliable data on the structure of the latter for different types of cloud (for stratified clouds with sharp enough boundaries, for which data were presented in § 4 of Chapter 3). Therefore, we consider the statistical character-istics of the vertical structure of the radiation field only for stratified clouds.

We assume, as before, that

$$p_0 = \bar{p}_0 + p_0'; \qquad q_0 = \bar{q}_0 + q_0'; \qquad T(\zeta) = \bar{T}(\zeta) + T'(\zeta) \qquad (4.39)$$

and that the variations of the normalized humidity profile $q(\zeta)$ above the clouds can be neglected, for simplicity (to introduce these variations complicates the relations presented below only a little). It is not difficult to see that

$$w_0 = \bar{w}_0 + w_0'; \qquad \bar{w}_0 = \frac{\bar{p}_0 \bar{q}_0}{g} ; \qquad w_0' = \frac{1}{g} (\bar{p}_0 q_0' + \bar{q}_0 p_0' + p_0' q_0'). \qquad (4.40)$$

Then the equation for transfer of ascending long-wave radiation can be written in the following form, analogous to (4.25):

$$\cos\theta\,\frac{\partial\bar{I}_\nu}{\partial\zeta} + \cos\theta\,\frac{\partial I'_\nu}{\partial\zeta} = (\bar{w}_0 + w'_0)\,q(\zeta)\,k_\nu(\zeta)\left\{I_\nu(\zeta,\theta) + \right.$$
$$\left. + I'_\nu(\zeta,\theta) - B_\nu[\bar{T}(\zeta)] - \frac{\partial B_\nu[\bar{T}(\zeta)]}{\partial T}\,T'(\zeta)\right\}. \tag{4.41}$$

We express the boundary condition at the top edge of the clouds, whose height varies randomly, in terms of the variations of its temperature T_0:

$$\bar{I}_\nu(1,\theta) + I'_\nu(1,\theta) = B_\nu(\bar{T}_0) + \frac{\partial B_\nu(\bar{T}_0)}{\partial T}\,T'_0. \tag{4.42}$$

The equations for $\bar{I}_\nu$ and I'_ν will take the form:

$$\cos\theta\,\frac{\partial\bar{I}_\nu}{\partial\zeta} = \left(\bar{w}_0 + \frac{K_{p_0 q_0}}{g}\right)\,q(\zeta)\,k_\nu(\zeta)\,\{\bar{I}_\nu(\zeta,\theta) - B_\nu[\bar{T}(\zeta)]\} +$$
$$+ \frac{q(\zeta)\,k_\nu(\zeta)}{g}\left\{\bar{p}_0 K_{q_0 I}(\zeta,\theta) - \bar{q}_0 K_{p_0 I}(\zeta,\theta) - \frac{\partial B_\nu[\bar{T}(\zeta)]}{\partial T}\times\right. \tag{4.43}$$
$$\left. \times\,[\bar{p}_0 K_{q_0 T}(\zeta) + \bar{q}_0 K_{p_0 T}(\zeta)]\right\};$$

$$\cos\theta\,\frac{\partial I'_\nu}{\partial\zeta} = \bar{w}_0 q(\zeta)\,k_\nu(\zeta)\left\{I'_\nu(\zeta,\theta) - \frac{\partial B_\nu[\bar{T}(\zeta)]}{\partial T}\,T'(\zeta)\right\} + w'_0 q(\zeta)\,k_\nu(\zeta)\,\times \tag{4.44}$$
$$\times\,\{\bar{I}_\nu(\zeta,\theta) - B_\nu[\bar{T}(\zeta)]\}.$$

Neglecting the second moments (apart from $K_{p_0 q_0}$) in Equation (4.43), we can obtain expressions for the mean intensity profile:

$$\bar{I}_\nu(\zeta,\theta) = B_\nu(\bar{T}_0)\exp\left[-\left(\bar{w}_0 + \frac{K_{p_0 q_0}}{g}\right)\sec\theta\int_\zeta^1 k_\nu(t)\,q(t)\,dt\right] -$$
$$- \int_\zeta^1 B_\nu[\bar{T}(t)]\,\frac{\partial}{\partial t}\left\{\exp\left[-\left(\bar{w}_0 + \frac{K_{p_0 q_0}}{g}\right)\sec\theta\int_\zeta^1 k_\nu(u)\,q(u)\,du\right]\right\}\,dt \tag{4.45}$$

and for the intensity fluctuations:

$$I'_\nu(\zeta, \theta) = \frac{\partial B_\nu(\overline{T}_0)}{\partial T} T'_0 \exp\left[-\overline{w}_0 \sec\theta \int_\zeta^1 k_\nu(t)\, q(t)\, dt\right] -$$

$$- \int_\zeta^1 \left\{\frac{\partial B_\nu[\overline{T}(t)]}{\partial T} T'(t) - \frac{\overline{I}_\nu(t, \theta) - B_\nu[\overline{T}(t)]}{\overline{w}_0} w'_0\right\} \frac{\partial}{\partial t} \times \qquad (4.46)$$

$$\times \left\{\exp\left[-\overline{w}_0 \sec\theta \int_\zeta^t k_\nu(u)\, q(u)\, du\right]\right\} dt.$$

Hence, it is not difficult to obtain expressions for the auto-correlation function

$$K_{II}(\zeta, \zeta'; \theta) = \left[\frac{\partial B_\nu(\overline{T}_0)}{\partial T}\right]^2 K_{T_0 T_0} P_\nu(\zeta, 1; \theta)\, P_\nu(\zeta', 1; \theta) - \frac{\partial B_\nu(\overline{T}_0)}{\partial T} P_\nu(\zeta', 1; \theta) \times$$

$$\times \int_\zeta^1 \left\{\frac{\partial B_\nu[\overline{T}(t)]}{\partial T} K_{T_0 T}(t) - \frac{\overline{I}_\nu(t, \theta) - B_\nu[\overline{T}(t)]}{g\overline{w}_0} (\overline{p}_0 K_{p_0 T_0} + \overline{q}_0 K_{P_0 T_0})\right\} \times$$

$$\times \frac{\partial P_\nu(\zeta, t; \theta)}{\partial t} dt - \frac{\partial B_\nu(\overline{T})}{\partial T} P_\nu(\zeta, 1; \theta) \int_{\zeta'}^1 \left\{\frac{\partial B_\nu[\overline{T}(t)]}{\partial T} K_{T_0 T}(t) -\right.$$

$$\left.- \frac{I_\nu(t, \theta) - B_\nu[\overline{T}(t)]}{g\overline{w}_0} (\overline{p}_0 K_{q_0 T_0} + \overline{q}_0 K_{p_0 T_0})\right\} \frac{\partial P_\nu(\zeta', t, \theta)}{\partial t} dt +$$

$$+ \int_\zeta^1 \int_{\zeta'}^1 \left\{\frac{\partial B_\nu[\overline{T}(t)]}{\partial T} \frac{\partial B_\nu[\overline{T}(u)]}{\partial T} K_{TT}(t, u) - \frac{\partial B_\nu[\overline{T}(t)]}{\partial T} \times\right. \qquad (4.47)$$

$$\times \frac{\overline{I}_\nu(u, \theta) - B_\nu[\overline{T}(u)]}{g\overline{w}_0} [\overline{p}_0 K_{q_0 T}(t) + \overline{q}_0 K_{p_0 T}(t)] - \frac{\partial B_\nu[\overline{T}(u)]}{\partial T} \times$$

$$\times \frac{I_\nu(t, \theta) - B_\nu[\overline{T}(t)]}{g\overline{w}_0} [\overline{p}_0 K_{q_0 T}(u) + \overline{q}_0 K_{p_0 T}(u)] +$$

$$\left.+ \frac{\overline{I}_\nu(t, \theta) - B_\nu[\overline{T}(t)]}{g\overline{w}_0} \frac{\overline{I}_\nu(u, \theta) - B_\nu[\overline{T}(u)]}{g w_0} (\overline{p}_0 K_{q_0 q_0} + \overline{q}_0 K_{p_0 p_0})\right\} \times$$

$$\times \frac{\partial P_\nu(\zeta, t; \theta)}{\partial t} \frac{\partial P_\nu(\zeta', u; \theta)}{\partial u} dt\, du.$$

For the joint correlation functions, we obtain:

$$K_{IT}(\zeta, \zeta'; \theta) = \frac{\partial B_\nu(\overline{T}_0)}{\partial T} K_{T_0 T}(\zeta')\, P_\nu(\zeta, 1; \theta) -$$

$$- \int_\zeta^1 \left\{\frac{\partial B_\nu I[(t)]}{\partial T} K_{TT}(t, \zeta') - \frac{\overline{I}_\nu(t, \theta) - B_\nu[I(t)]}{g\overline{w}_0} [\overline{p}_0 K_{q_0 T}(\zeta') + \overline{q}_0 K_{p_0 T}(\zeta')]\right\} \times \qquad (4.48)$$

$$\times \frac{\partial P_\nu(\zeta, t; \theta)}{\partial t} dt;$$

240

$$K_{Iq_o}(\zeta, \theta) = \frac{\partial B_\nu(\bar{I}_0)}{\partial T} K_{T_0 q_0} P_\nu(\zeta, 1; \theta) -$$

$$- \int_\zeta^1 \left\{ \frac{\partial B_\nu[\bar{T}(t)]}{\partial T} K_{Tq_0}(t) - \frac{\bar{I}_\nu(t, \theta) - B_\nu[\bar{T}(t)]}{g\bar{w}_0} (\bar{p}_0 K_{q_0 q_0} + \bar{q}_0 K_{p_0 q_0}) \right\} \times \qquad (4.49)$$

$$\times \frac{\partial P_\nu(\zeta, t; \theta)}{\partial t} dt;$$

$$K_{Ip_o}(\zeta, \theta) = \frac{\partial B_\nu(\bar{T}_0)}{\partial T} K_{T_0 p_0} P_\nu(\zeta, 1; \theta) -$$

$$- \int_\zeta^1 \left\{ \frac{\partial B_\nu[\bar{T}(t)]}{\partial T} K_{Tp_0}(t) - \frac{\bar{I}_\nu(t, \theta) - B_\nu[\bar{T}(t)]}{g\bar{w}_0} [(\bar{p}_0 K_{q_0 p_0} + \bar{q}_0 K_{p_0 p_0})] \right\} \times \qquad (4.50)$$

$$\times \frac{\partial P_\nu(\zeta, t; \theta)}{\partial t} dt.$$

By analyzing Equations (4.47) - (4.50), and allowing for the statistical characteristics of the structure of stratified clouds and of the meteorological elements above it (see § 4 of Chapter 3), we can observe that the basic parameters which will allow us to best take into account the effect of variation of stratified clouds on the fluctuations of the radiation field are the dispersion of the height of the top boundary of the cloud $K_{p_0 p_0}$, its temperature $K_{T_0 T_0}$, and its humidity $K_{q_0 q_0}$; the autocorrelation moments $K_{T_0 T}$ and K_{TT}, which relate the temperature of the top boundary to that of other underlying atmospheric levels; the joint correlation moments $K_{q_0 T}$ between the humidity and the top boundary of the cloud and the temperature of the underlying levels (we note that excluding fluctuations of the relative profile $q(\zeta)$ from consideration is justified, to some extent, by the smallness of the absolute values of dispersion of the specific humidity above the clouds).

As regards quantities such as the joint correlation moments between fluctuations at the level of the top cloud boundary and the temperature or humidity at this boundary ($K_{p_0 T}$, $K_{p_0 q_0}$), judging from the results of [3.15], they are quite small and can be omitted in Equations (4.47) - (4.50). From the physical viewpoint, this means that random variations in the cloud boundaries are relatively weakly correlated with the corresponding variations in the meteorological elements (e.g., an increase in height of the cloud boundary does not always entail a decrease of temperature or of humidity at this boundary). Therefore, by itself, a change in height of a stratified cloud does not always statistically cause corresponding changes in long-wave Earth radiation.

Having determined the correlation moments from Equations (4.47) - (4.50), one can easily improve the expression for the mean intensity profile I_ν, by substituting the required quantites into Equation (4.43).

To compare the correlations obtained in [7] for stratified clouds with experimental coefficients, we calculated the statistical characteristics of ascending fluxes of integrated radiation (formulas for these characteristics were obtained from Equations (4.47) - (4.50) by replacing the monochromatic intensities and transmission functions by quantities integrated with respect to θ and ν). The statistical characteristics of the vertical structure of stratified cloud and meteorological elements in the calculations were taken from the data of § 4 of Chapter 3. As can be seen from Figure 4.6 a, the empirical and calculated correlation coefficients $r_{FF}(1, \zeta_h)$ are in satisfactory inter-agreement. The positive correlation for F' obtained in [7] for the Sc case at all levels means (as it did in the cloud-free case) that the fluctuations F' at great heights are determined by the fluctuations T' in the lower layers of the troposphere,
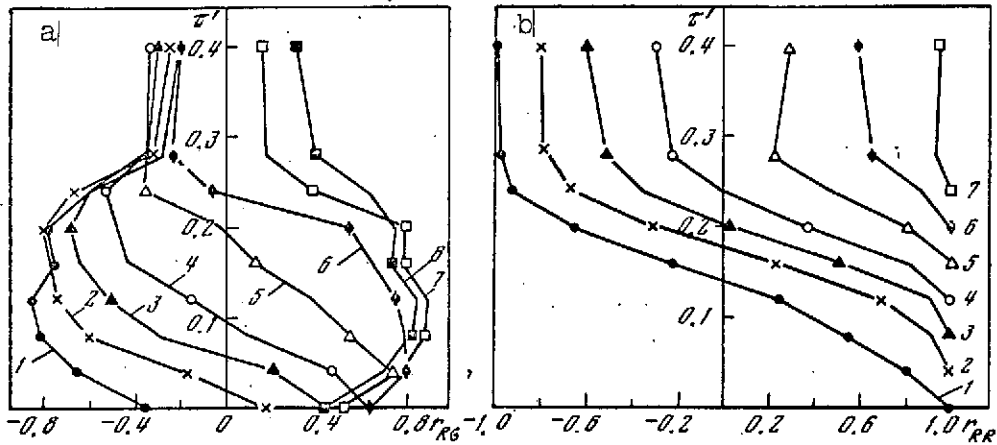
Figure 4.7. Vertical distribution of $r_{R\sigma}(\tau,\tau')$ and $r_{RR}(\tau,\tau')$, according to [9]

a- $r_{R\sigma}(\tau,\tau')$; b- $r_{RR}(\tau,\tau')$; 1- $\tau = 0$; 2- 0.04; 3- 0.08; 4- 0.12; 5- 0.16; 6- 0.20; 7- 0.24; 8- 0.28

especially by variations of T' and the top boundary of the cloud. Also, the latter are positively correlated with T' at all the other levels, at least up to a height of 5 km (see Figure 3.6). As regards other kinds of clouds, the example of calculations of r_{FF} in [7] from measurements of fluxes of self-radiation under conditions of altocumulus cloud (Figure 4.7 b) indicates the possibility of negative correlation of F' in the sub-cloud and above-cloud atmospheric layers. One of the probable causes for this may be the anticorrelation of temperature variations in the corresponding layers. However, this assumption, like a number of other results presented above, should be checked by performing various measurements and calculations of the statistical charac- /143 teristics of the vertical structure of radiative fluxes and meteorological parameters.

§ 4. Angular and Spectral Structure

It was shown in Chapter 2 that the vertical stratification of the atmosphere, particularly the variation of temperature and moisture concentration with height, determines the angular dependence of the intensity of Earth self-radiation, described, for example, by Equation (4.31). Naturally, random variations of vertical profiles of temperature and humidity imply random variations of the angular distribution of long-wave radiation, as follows immediately from Equation (4.32). Therefore, the statistical characteristics of the angular structure of the radiation field can be expressed in terms of the appropriate characteristics of the vertical structure of the fields of temperature, humidity, and cloud.

Within the framework of the horizontally homogeneous atmospheric model, one must expect a very close correlation between the variations of the intensity of the radiation emitted by the Earth at different angles, since in this case a change in the angle θ means, in essence, a change in the weight with which the emission of different atmospheric layers of the atmosphere contributes to the Earth emission for different directions. Therefore, for a weak correlation between the values of temperature or humidity at different levels in the atmosphere, the variations in intensity of radiation $I_\nu'(\zeta, \theta)$ and $I_\nu'(\zeta, \xi)$ at a fixed level ζ, but at different angles θ and ξ, will be noticeably intercorrelated, as follows from immediate examination of Equation (4.32). In fact, by multiplying $I_\nu'(\zeta, \theta)$ by $I_\nu'(\zeta, \xi)$ and averaging over all samples, we obtain an expression for the autocorrelation function

$$K_{II}(\zeta; \theta, \xi) = \overline{I'_\nu(\zeta, \theta)\, I'_\nu(\zeta, \xi)} = \left\{\frac{\partial B_\nu[\overline{T}(t)]}{\partial T}\right\}^2 K_{TT}(1,1)\, P_\nu(\zeta, 1; \theta)\, P_\nu(\zeta, 1; \xi) -$$

$$- \frac{\partial B_\nu[\overline{T}(1)]}{\partial T}\, P_\nu(\zeta, 1; \xi) \times$$

$$\times \int\limits_\zeta^1 \left\{\frac{\partial B_\nu[\overline{T}(t)]}{\partial T}\, K_{TT}(1,t) - \frac{\overline{I}_\nu(t, \theta) - B_\nu[\overline{T}(t)]}{\overline{q}(t)}\, K_{Tq}(1,t)\right\} \times$$

$$\times \frac{\partial P_\nu(\zeta, t; \theta)}{\partial t}\, dt - \frac{\partial B_\nu[\overline{T}(1)]}{\partial T}\, P_\nu(\zeta, 1; \theta) \times$$

$$\times \int\limits_\zeta^1 \left\{\frac{\partial B_\nu[\overline{T}(t)]}{\partial T}\, K_{TT}(1, t) - \frac{I_\nu(t, \xi) - B_\nu[\overline{T}(t)]}{\overline{q}(t)}\, K_{Tq}(1, t)\right\} \times$$

$$\times \frac{\partial P_\nu(\zeta, t; \xi)}{\partial t}\, dt + \int\limits_\zeta^1\int\limits_\zeta^1 \left\{\frac{\partial B_\nu[\overline{T}(t)]}{\partial T}\frac{\partial B_\nu[\overline{T}(u)]}{\partial T}\, K_{TT}(t, u) - \right.$$

$$- \frac{\partial B_\nu[\overline{T}(t)]}{\partial T}\frac{I_\nu(u, \xi) - B_\nu[\overline{T}(u)]}{\overline{q}(u)}\, K_{Tq}(t, u) - \frac{\partial B_\nu[\overline{T}(u)]}{\partial T} \times$$

$$\times \frac{\overline{I}_\nu(t, \theta) - B_\nu[\overline{T}(t)]}{\overline{q}(t)}\, K_{Tq}(u, t) + \frac{\overline{I}_\nu(t, \theta) - B_\nu[\overline{T}(t)]}{-\overline{q}(t)} \times$$

$$\left.\times \frac{\overline{I}_\nu(u, \xi) - B_\nu[\overline{T}(u)]}{\overline{q}(u)}\, K_{qq}(t, u)\right\} \frac{\partial P_\nu(\zeta, t; \theta)}{\partial t}\frac{\partial P_\nu(\zeta, u; \xi)}{\partial u}\, du\, dt. \qquad (4.51)$$

In Equation (4.51) we did not take into account variations in clouds, although it is very clear that they could be allowed for without great difficulty, by means of Equation (4.46).

Calculations performed using Equation (4.51) for the inten- /144 sity of integrated radiation indicate that variations in the long-wave Earth radiation at different directions are strongly intercorrelated. It seems that in actual conditions the angular structure of the field of self-radiation of the atmosphere will be distorted by horizontal nonuniformities of the atmosphere, and in particular by clouds (the horizontal structure of these nonuniformities and the angular structure associated with them will be examined specially in Chapter 5).

Similarly, one can establish the relation between the statistical characteristics of the spectral structure of the field of long-wave radiation and the corresponding characteristics of the fields of temperature, humidity, and cloud. In this case, the weights with which the radiation of different layers of the atmosphere contribute to the emission integrated with height for fixed values of ζ and θ are transmission functions at different frequencies ν and μ. Then

$$
\begin{aligned}
K_{II}(\zeta, \theta; \nu, \mu) &= \overline{I'_\nu(\zeta, \theta) I'_\mu(\zeta, \theta)} = \frac{\partial B_\nu[\overline{T}(1)]}{\partial T} \frac{\partial B_\mu[\overline{T}(1)]}{\partial T} K_{TT}(1,1) P_\nu(\zeta, 1; \theta) \times \\
&\times P_\mu(\zeta, 1; \theta) - \frac{\partial B_\mu[\overline{T}(1)]}{\partial T} P_\mu(\zeta, 1; \theta) \times \\
&\times \int_\zeta^1 \left\{ \frac{\partial B_\nu[\overline{T}(t)]}{\partial T} K_{TT}(1, t) - \frac{\overline{I}_\nu(t, \theta) - B_\nu[\overline{T}(t)]}{\overline{q}(t)} K_{Tq}(1, t) \right\} \times \\
&\times \frac{\partial P_\nu(\zeta, t; \theta)}{\partial t} dt - \frac{\partial B_\nu[\overline{T}(1)]}{\partial T} P_\nu(\zeta, 1; \theta) \times \\
&\times \int_\zeta^1 \left\{ \frac{\partial B_\mu[\overline{T}(t)]}{\partial T} K_{TT}(1, t) - \frac{\overline{I}_\mu(t, \theta) - B_\mu[\overline{T}(t)]}{\overline{q}(t)} K_{Tq}(1, t) \right\} \times \\
&\times \frac{\partial P_\mu(\zeta, t; \theta)}{\partial t} dt + \int_\zeta^1 \int_\zeta^1 \left\{ \frac{\partial B_\nu[\overline{T}(t)]}{\partial T} \frac{\partial B_\mu[\overline{T}(u)]}{\partial T} K_{TT}(t, u) - \right. \\
&- \frac{\partial B_\nu[\overline{T}(t)]}{\partial T} \frac{\overline{I}_\mu(u, \theta) - B_\mu[\overline{T}(u)]}{\overline{q}(u)} K_{Tq}(t, u) - \\
&- \frac{\partial B_\mu[\overline{T}(u)]}{\partial T} \frac{\overline{I}_\nu(t, \theta) - B_\nu[\overline{T}(t)]}{\overline{q}(t)} + \frac{\overline{I}_\nu(t, \theta) - B_\nu[\overline{T}(t)]}{\overline{q}(t)} \times \\
&\left. \times \frac{\overline{I}_\mu(u, \theta) - B_\mu[\overline{T}(u)]}{\overline{q}(u)} K_{qq}(t, u) \right\} \frac{\partial P_\nu(\zeta, t; \theta)}{\partial t} \frac{\partial P_\mu(\zeta, u; \theta)}{\partial t} du dt.
\end{aligned} \tag{4.52}
$$

However, in contrast with the angular structure, the spectral correlation will follow, to a large extent, the correlative relationships between the variations of temperature and humidity at different levels. This conclusion follows immediately from general physical reasoning: the variations in the intensity of radiation in the relatively transparent region of the atmosphere will be determined by variations of temperature and humidity in the atmospheric boundary layer, while the variations in intensity

and radiation in the strong absorption region are related to the variations of $T(\zeta)$ and $q(\zeta)$ in the free atmosphere. We restrict ourselves simply to these comments, since statistical characteristics of the spectral structure will not be used directly in the rest of the book.

§ 5. Vertical and Angular Structure of the Short-Wave Radiation Field

The results described in Chapter 1 show that the vertical, angular, and spectral structure of the field of solar radiation reflected by the Earth are determined mainly by the vertical   /145 structure of aerosols and cloud, and in the absorption bands by the structure of the concentration of atmospheric gases.

Using the equation for transfer of solar radiation in a plane-parallel atmosphere for which the vertical distributions of the optical and meteorological parameters are random functions of height, we can find relations between statistical characteristics of the vertical, angular, and spectral structure of the field of short-wave radiation, and the statistical characteristics of the vertical structure of these atmospheric parameters [9].

For simplicity, we consider the case where the variations of intensity of short-wave radiation are determined only by random variations in the vertical profile of the aerosol scattering coefficient, whose structural characteristics were given in § 5 of Chapter 3. We will consider the aerosol scattering coefficient $\sigma_\nu(z)$ for fixed ν as a random function of height z, and represented in the form

$$\sigma_\nu(z) = \bar{\sigma}_\nu(z) + \sigma'_\nu(z),$$ (4.53)

where the mean profile $\bar{\sigma}_\nu(z)$ includes the molecular scattering coefficient and $\sigma'_\nu(z) = b'_\nu(z)$ is a random deviation which we ascribe only to aerosol scattering $b_\nu(z)$. We could represent the scattering index similarly. However, in the interest of further simplification of the problem, and to explain the role of variations of the scattering coefficient, we shall consider the scattering index to be spherical $(\gamma_\nu \equiv 1)$. This simplification is also desirable for the reason that there are presently no reliable ideas on the vertical structure of the scattering index in the atmosphere.

Putting $\gamma_\nu \equiv 1$, $a_\nu \equiv 0$, $f^{(1)}_\nu \equiv 0$ in the radiative transfer equations (1.1) and (1.2), and representing the radiative intensity in the form

$$I_\nu(z, \theta) = \bar{I}_\nu(z, \theta) + I'_\nu(z, \theta); \qquad R_\nu(z) = \bar{R}_\nu(z) + R'_\nu(z), \qquad (4.54)$$

we obtain equations for the mean profile of the radiative intensity $\bar{I}$ and its deviations from the mean profile I' (ν is omitted):

$$\cos\theta \frac{\partial \bar{I}^\uparrow}{\partial z} = -\bar{\sigma}(z)[\bar{I}^\uparrow(z, \theta) - \bar{R}(z)] - K^\uparrow_{\sigma I}(z, z, \theta) - K_{\sigma R}(z, z); \qquad (4.55)$$

$$-\cos\theta \frac{\partial I^\downarrow}{\partial z} = -\bar{\sigma}(z)[\bar{I}^\downarrow(z, \theta) - \bar{R}(z)] - K^\downarrow_{\sigma I}(z, z, \theta) + K_{\sigma R}(z, z); \qquad (4.56)$$

$$\bar{R}(z) = \frac{1}{2} \int_0^{\frac{\pi}{2}} [\bar{I}^\uparrow(z, \Theta) + \bar{I}^\downarrow(z, \theta)] \sin\theta d\theta; \qquad (4.57)$$

$$\bar{I}^\uparrow(0) = 2A \int_0^{\frac{\pi}{2}} \bar{I}^\downarrow(0, \theta)\cos\theta \sin\theta d\theta; \qquad (4.58)$$

$$K_{\sigma I}(z, z, \theta) = \overline{\sigma'(z)I'(z, \theta)}, \qquad K_{\sigma R}(z, z) = \overline{\sigma'(z)R'(z)}; \\ \bar{I}^\downarrow(\infty, \theta) = \pi S \delta(\theta - \zeta_0); \qquad (4.59)$$

$$\cos\theta \frac{\partial I'^\uparrow}{\partial z} = -\bar{\sigma}(z)\left[I'^\uparrow(z,\theta) - R'(z)\right] - \sigma'(z)\left[I^\uparrow(z,\theta) - \bar{R}(z)\right]; \qquad (4.60)$$

$$-\cos\theta \frac{\partial I'^\downarrow}{\partial z} = -\bar{\sigma}(z)\left[I'^\downarrow(z,\theta) - \bar{R}'(z)\right] - \sigma'(z)\left[I^\downarrow(z,\theta) - \bar{R}(z)\right]; \qquad (4.61)$$

$$I'^\uparrow(0,\theta) = 2A \int_0^{\frac{\pi}{2}} I'^\downarrow(0,\theta)\cos\theta\sin\theta \, d\theta; \qquad (4.62)$$

$$I'^\downarrow(\infty,\theta) = 0. \qquad (4.63)$$

If we omit the second order moments in Equations (4.55) and /146
(4.56) and transfer to the optical depth

$$\bar{\tau}(z) = \int_0^z \bar{\sigma}(t) \, dt; \qquad \bar{\tau}^* = \int_0^\infty \bar{\sigma}(t) \, dt; $$

it is not difficult to obtain the well-known integral equations
for a spherical index, investigated in detail by Kuznetsov and
Ovchinskiy [1.82]. The function $\bar{R}(\zeta)$, represented in the form
of the sum

$$\bar{R}(\tau) = \varphi(\tau) + H\omega(\tau)$$

is calculated by solving the integral equations

$$\varphi(\tau) = \frac{S}{4}\exp\left[-(\tau^* - \tau)\sec\zeta_0\right] + \frac{1}{2}\int_0^{\tau^*} \varphi(t) E_1(|\tau - t|) \, dt; \qquad (4.64)$$

$$\omega(\tau) = E_2(\tau) + \frac{1}{2}\int_0^{\tau^*} \omega(t) E_1(|\tau - t|) \, dt, \qquad (4.65)$$

where

$$H = A \frac{\frac{1}{2} S \exp(-\tau^* \sec\zeta_0)\cos\zeta_0 + \int_0^{\tau^*} \varphi(t) E_1(t) \, dt}{1 - A \int_0^{\tau^*} \omega(t) E_2(t) \, dt}.$$

The mean intensities of scattered radiation are expressed in terms of $\bar{R}(\tau)$ as follows:

$$I^{\uparrow}(\tau, \theta) = He^{-\tau \sec \theta} + \sec \theta \int_0^{\tau} \bar{R}(\tau) e^{-(\tau-t) \sec \theta} dt; \qquad (4.66)$$

$$I^{\downarrow}(\tau, \theta) = \sec \theta \int_{\tau}^{\tau^*} \bar{R}(t) e^{-(t-\tau) \sec \theta} dt. \qquad (4.67)$$

We have calculated these expressions in detail, since they will enter into the corresponding formulas for the deviations I'.

By solving the system of equations (4.60) - (4.61) in these variables with boundary conditions (4.62) and (4.63), we obtain

$$I'^{\uparrow}(\tau, \theta) = 2Ae^{-\tau \sec \theta} \int_0^{\tau^*} \left\{ R'(t) E_2(t) + \frac{\sigma'(t)}{\sigma(t)} \left[\bar{R}(t) E_2(t) - \int_t^{\tau^*} \bar{R}(u) E_1(u) du \right] \right\} dt +$$

$$+ \sec \theta \int_0^{\tau} \left\{ R'(t) + \frac{\sigma'(t)}{\sigma(t)} [\bar{R}(t) - I^{\uparrow}(t, \theta)] \right\} \exp[-(\tau - t) \sec \theta] dt; \qquad (4.68)$$

$$I'^{\downarrow}(\tau, \theta) = \sec \theta \int_{\tau}^{\tau^*} \left\{ R'(\tau) + \frac{\sigma'(t)}{\sigma(t)} [\bar{R}(t) - I^{\downarrow}(t, \theta)] \right\} \exp[-(t - \tau) \sec \theta] dt. \qquad (4.69)$$

Here we obtain an equation similar to (4.64) and (4.65) for the deviation of the function R'(τ). Putting $R'(\tau) = \varphi'(\tau) + H'\omega'(\tau)$, we obtain an equation for determining $\varphi'(\tau)$:

$$\varphi'(\tau) = F(\tau) + \frac{1}{2} \int_0^{\tau^*} \varphi'(t) E_1(|\tau - t|) dt. \qquad (4.70)$$

Here

$$F(\tau) = \frac{1}{2} \int_0^{\tau^*} \frac{\sigma'(t)}{\sigma(t)} \bar{R}(t) E_1(|\tau - t|) dt - \frac{H'}{2} \int_0^{\tau} \frac{\sigma'(t)}{\sigma(t)} E_1(t) dt - \frac{S}{4} \sec \zeta_0 \exp[-$$

$$- (\tau^* - \tau) \times \sec \zeta_0] \int_{\tau}^{\tau^*} \frac{\sigma'(t)}{\sigma(t)} dt - \frac{1}{2} \int_0^{\tau} \frac{\sigma'(t)}{\sigma(t)} dt \int_0^t \bar{R}(u) \frac{e^{-(\tau-u)}}{\tau - u} du - \qquad (4.71)$$

$$- \frac{1}{2} \int_{\tau}^{\tau^*} \frac{\sigma'(t)}{\sigma(t)} dt \int_t^{\tau} \bar{R}(u) \frac{e^{-(u-\tau)}}{u - \tau} du.$$

250

The function $\omega'(\tau)$ has the same accuracy as $\omega(\tau)$, and the constant H' has the form

$$H' = A \frac{\int_0^{\tau^*} \frac{\sigma'(t)}{\sigma(t)} \left[\overline{R}(t) E_2(t) - \int_t^{\tau^*} \overline{R}(u) E_1(u) \, du \right] dt + \int_0^{\tau^*} \varphi'(t) E_2(t) \, dt}{1 - A \int_0^{\tau^*} \omega(t) E_2(t) \, dt}.$$

From Equations (4.68) – (4.70), we could obtain relations for the correlation functions K_{II}, K_{RR}, $K_{R\sigma}$, but these would be rather laborious, mainly because of the calculation of the albedo A. However, to clarify the relation between characteristics of the vertical structure of the radiation field and the scattering coefficient, it is enough to examine the case A = 0.[*] Then, for $R'(\tau) = \varphi'(\tau)$, and from Equations (4.70) and (4.71), we obtain a comparatively simple equation which we write in more compact form

$$R'(\tau) = \frac{1}{2} \int_0^{\tau^*} R'(t) E_1(|\tau - t|) \, dt + \frac{1}{2} \int_0^{\tau^*} \frac{\sigma'(t)}{\sigma(t)} P_0(\tau, t) \, dt -$$
$$- \frac{S}{4} \exp\left[-(\tau^* - \tau) \sec \zeta_0\right] \sec \zeta_0 \int_\tau^{\tau^*} \frac{\sigma'(t)}{\sigma(t)} \, dt, \quad (4.72)$$

where

$$P_0(\tau, t) = \begin{cases} \overline{R}(t) E_1(\tau - t) - \int_0^t \overline{R}(u) \frac{e^{-(\tau - u)}}{\tau - u} \, du, & 0 \leqslant t \leqslant \tau, \\ \overline{R}(t) E_1(t - \tau) - \int_t^{\tau^*} \overline{R}(u) \frac{e^{-(u-\tau)}}{u - \tau} \, du, & \tau \leqslant t \leqslant \tau^*. \end{cases}$$

From Equation (4.72), we obtain the following equations for the correlation functions

$$K_{RR}(\tau, \tau') = \frac{1}{2} \int_0^{\tau^*} K_{RR}(t, \tau') E_1(|\tau - t|) \, dt + \frac{1}{2} \int_0^{\tau^*} K_{R\sigma}(\tau', t) H_0(\tau, t) \, dt -$$
$$- \frac{S}{4} \exp\left[-(\tau^* - \tau) \sec \zeta_0\right] \sec \zeta_0 \int_\tau^{\tau^*} \frac{K_{R\sigma}(\tau', t)}{\sigma(t)} \, dt; \quad (4.73)$$

---

[*] The case with A $\neq$ 0 was considered in [10].

$$K_{R\sigma}(\tau, \tau') = \frac{1}{2} \int_0^{\tau^*} K_{R\sigma}(t, \tau') E_1(|\tau - t|) + \frac{1}{2} \int_0^{\tau^*} K_{\sigma\sigma}(t, \tau') H_0(\tau, t) dt -$$
$$- \frac{S}{4} \exp[-(\tau^* - \tau) \sec \zeta_0] \sec \zeta_0 \int_\tau^{\tau^*} \frac{K_{\sigma\sigma}(t, \tau')}{\bar{\sigma}(t)} dt. \tag{4.74}$$

Here

$$H_0(\tau, t) = \frac{P_0(\tau, t)}{\bar{\sigma}(t)} \tag{4.75}$$

is a negative function. Thus, the autocorrelation between R' at different levels or the joint correlation between R' and σ' is determined by the autocorrelation function $K_{\sigma\sigma}(\tau, \tau')$. It follows from Equation (4.74) that $K_{R\sigma}$ is a superposition of the positive and negative correlations between R' and σ', described, respectively, by the second and third terms of Equation (4.74). This result reflects the fact that the variations of σ' imply, on the one hand, variations of R' of opposite signs, because of the effect of attenuation of the radiation (the third term of Equation (4.74)), and, on the other hand, variations, of R' of the same sign, arising from multiple scattering. Therefore, the vertical structure of the variations R' will undergo deformation, depending on the weight of these two factors. This conclusion is confirmed by calculations of $K_{RR}(\tau, \tau')$ and $K_{R\sigma}(\tau, \tau')$ made in [9] for a model atmsophere, using empirical profiles of $\bar{\sigma}(z)$ and correlation matrices $K_{\sigma\sigma}(z_k, z_l)$ [1.10]. The total optical depth of the atmosphere here was 0.4 and $\zeta = 60°$, $A = 0$. Figure 4.7, which illustrates the results of these calculations, enables us to determine the transformation of the vertical behavior of the correlation coefficients $r_{R\sigma}(\tau_k, \tau_l)$ and $r_{RR}(\tau_k, \tau_l)$.

In fact, at the ground surface level $(\tau = 0)$, the quantity R'(0), which, for a zero albedo, is completely determined by the variations of the descending radiation, $I'^\downarrow(0, \theta)$, is anticorrelated

252

with $\sigma'(\tau)|$ at all levels τ. This means that attentuation plays the main role in the variations of the descending radiation. With increase of τ, the function $R'(\tau)|$ includes variations of the ascending radiation which are mainly determined by variations in the scattering, which quickly leads| to an increase in the negative correlation with $\sigma'(\tau)$ at the higher levels of τ, and to a positive correlation with $\sigma'(\tau)|$ at lower-lying levels. The levels for transition from negative to positive correlation depend, as can be seen from Equation (4.74), on τ^* and ζ, as well as on the vertical behavior of the correlation coefficient $r_{\sigma\sigma}(\tau, \tau')|$. In particular, the presence of a maximum in the ratio $K_{\sigma\sigma}(\tau, \tau')/\bar{\sigma}(\tau)\bar{\sigma}(\tau')|$ at the layer $\tau = 0.16$ to 0.28 ($z = 1.5$ to 4 km) is a cause of corresponding extreme values in the correlation matrix $r_{R\sigma}(\tau, \tau')$.|

This behavior of the joint correlation $K_{R\sigma}(\tau, \tau')|$ also appears in the vertical structure of the fluctuations $R'(\tau)|$ (Figure 4.7 b). However, the region of negative correlation coefficients $r_{RR}(\tau, \tau')|$ /149 is considerably narrowed. As one must expect, because of the contribution of attenuation and scattering in forming the fluctuations $R'(\tau)|$, the coefficient of correlation between $R'(0)|$ and $R'(\tau^*)|$ is of order -1. The levels at which $r_{RR}(\tau, \tau')|$ passes through zero lie above $\tau' = 0.12$ ($z = 1$ km) for $\tau \leq 0.12$. For $\tau > 0.12$, the correlation coefficient $r_{RR}(\tau, \tau')|$ remains positive for all τ and τ'.

A transformation leading to an increase in the scattering component of the brightness field is also observed when one looks at the vertical or angular structure of the intensity of scattered solar radiation.

In fact, for $K_{II}(\tau, \tau'; \theta) = \overline{I'(\tau, \theta)\,I'(\tau', \theta)};$ $K_{I\sigma}(\tau, \tau', \theta) = |\overline{I'(\tau, \theta)\,\sigma'(\tau')};|$ $K_{II}(\tau; \theta, \theta') = \overline{I'(\tau, \theta)\,I(\tau, \theta')}$ for| the ascending radiation, from Equation| (4.68), we obtain the equations|

$$K'_{II}(\tau, \tau'; \theta) = \sec^2 \theta \int_0^\tau \int_0^{\tau'} \{[K_{RR}(t, u) + K_{R\sigma}(t, u) G(u, \theta) + K_{R\sigma}(u, t) G(t, \theta) +$$
$$+ K_{\sigma\sigma}(t, u) G(t, \theta) G(u, \theta)] \exp\{-[(\tau - t) + (\tau' - u)] \sec \theta\} \, du \, dt; \qquad (4.76)$$

$$K'_{I\sigma}(\tau, \tau'; \theta) = \sec \theta \int_0^\tau [K_{R\sigma}(t, \tau') + K_{\sigma\sigma}(t, \tau') G(t, \theta)] \exp[-(\tau - t) \sec \theta] \, dt; \qquad (4.77)$$

$$K'_{II}(\tau; \theta, \theta') = \sec \theta \sec \theta' \int_0^\tau \int_0^\tau [K_{RR}(t, u) + K_{R\sigma}(t, u) G(u, \theta') + K_{R\sigma}(u, t) G(t, \theta) +$$
$$+ K_{\sigma\sigma}(t, u) G(t, \theta) G(u, \theta')] \exp[-(\tau - t) \sec \theta - (\tau - u) \sec \theta'] \, dt \, du. \qquad (4.78)$$

Here

$$G(t, \theta) = \frac{\bar{R}(t) - \bar{I}(t, \theta)}{\bar{\sigma}(t)}.$$

Similar equations for the descending radiation are obtained from Equation (4.69). Examples of correlation coefficients $r'_{I\sigma}(\tau^*, \theta; \tau)$, $r'_{I\sigma}(0, \theta; \tau)$, obtained in [9], for fluctuations of the intensity of ascending radiation $I'^\dagger(\tau^*, \theta)$ and descending radiation $I'^\downarrow(0, \theta)$ are shown in Figure 4.8. It is not difficult to see that not only $I'^\dagger(\tau^*, \theta)$, but also $I'^\downarrow(0, \theta)$ are positively correlated with the fluctuations $\sigma'(\tau)$ at all levels τ, for not very large θ. The correlation coefficients $r'_{I\sigma}(\tau^*, \theta; \tau)$ (solid lines) depend weakly on θ, although the absolute correlation moments of $K'_{I\sigma}(\tau^*, \theta; \tau)$ matrix have a noticeable angular dependence, with a maximum at $\theta = 70°$ (Table 4.1). As regards the correlation coefficient $r'_{I\sigma}(0, \theta; \tau)$ (broken lines), they practically coincide with $r'_{I\sigma}(\tau^*, \theta; \tau)$ over the entire range of angles $0 \leqslant \theta \leqslant 70°$, but differ appreciably for larger θ, taking negative values for $\theta > 80$ degrees.
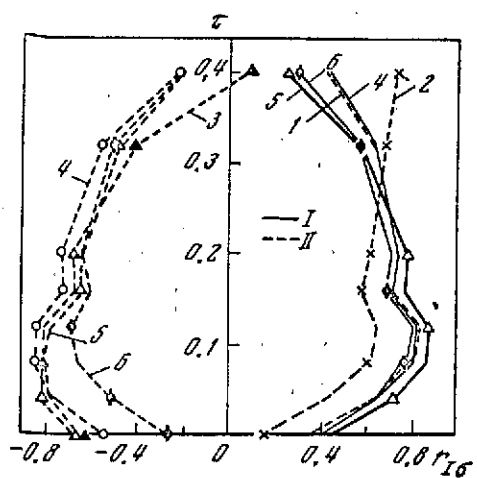
Figure 4.8. Vertical distribution of $r_{I\sigma}^{\dagger}$ $(\tau^*, \theta; \tau)$ (I) and $r_{I\sigma}^{\dagger}$ $(0, \theta; \tau)$ (II)

1- $\theta = 0 - 80°$; 2- $80°$; 3- $82.5°$; 4- $85°$; 5- $87.5°$; 6- $90°$

We still see a large positive correlation in the variations of the angular behavior of the brightness, as follows from consideration of the autocorrelation matrices $K_{II}^{\dagger}$ $(\tau^*, \theta, \theta')$ and $K_{II}^{\dagger}$ $(0; \theta, \theta')$ (below and above the main diagonal of Table 4.2, respectively). It is easy to verify that the correlation coefficients $r_{II}^{\dagger}$ $(\tau^*, \theta, \theta')$ and $r_{II}^{\dagger}(0; \theta, \theta')$ are close to unity for the whole range of angles θ and θ', apart from $\theta > 80°$, where $r_{II}^{\dagger}$ passes through zero and takes negative values.

In order to map out these peculiarities in the angular structure, including the very sharp transition through zero of $K_{II}^{\dagger}$ $(0; \theta, \theta')$, it is desirable to examine the joint correlation /150 matrices $K_{IR}^{\dagger}$ $(\tau^*, \theta; \tau)$ and $K_{IR}^{\dagger}$ $(0, \theta; \tau)$ between the fluctuations of the directional and mean brightnesses, which also describe the interaction of the variations of attenuation and scattering. Table 4.3 shows that the fluctuations $I'^{\dagger}$ (τ^*, θ) are anticorrelated with R' (τ) in the layer $0 \leqslant \tau \leqslant 0.12$ at all θ, and positively correlated for $\tau > 0.12$. The same is true also of $I'^{\dagger}$ $(0, \theta)$, apart from angles $\theta > 80°$, for which $K_{IR}^{\dagger}$ $(0, \theta; \tau) > 0$ for $\tau < 0.12$, and, conversely, $K_{IR}^{\dagger}$ $(0, \theta; \tau) < 0$ for $\tau > 0.12$ (Table 4.4). The region where the correlation moments pass through zero, which corresponds to an equal contribution from the fluctuations in attenuation and scattering, will depend, of course, on the optical parameters of the atmosphere and the position of the Sun. In fact, from the asymptote of Equation (4.68) for $A = 0$ and of Equation (4.69) as $\theta \to \infty$, it follows that

$$\lim_{\theta' \to \frac{\pi}{2}} K_{II}^{\dagger}(\tau^*, \theta; \theta') = K_{IR}^{\dagger}(\tau^*, \theta; \tau^*);$$

$$\lim_{\theta' \to \frac{\pi}{2}} K_{II}^{\dagger}(0, \theta; \theta') = K_{IR}^{\dagger}(0, \theta; 0), \tag{4.79}$$

and therefore, the last and first lines of Tables 4.3 and 4.4 are, respectively, limits for the last column and last line of Table 4.2.

Thus, for the case of a spherical scattering index, we have /151 "determination" of the angular structure of the field of brightness $I^{\dagger}(\tau^*, 0)$, determined by the vertical structure of random fluctuations of the aerosol scattering coefficient $\sigma'(z)$. From the physical viewpoint, this means that the effect of scattering, which is positively correlated with $\sigma'(z)$, plays a dominant role in fluctuations of brightness above the cloud-free ocean (A = 0).

The formulas given above enable us to calculate the statis- /152 tical characteristics of the brightness field even for A ≠ 0. Since this entails an increase in the contribution of reflected direct solar radiation, the role of the attenuation fluctuations must increase, which leads to reduced correlation between the brightness fluctuations at different angles θ. Here one must bear in mind that under actual conditions the albedo A will be a random quantity, uncorrelated with $\sigma(z)$, which also entails reduced correlation of brightness with θ. These assumptions are confirmed by the empirical correlation relations obtained from measured Earth brightness data on the satellite Kosmos 149.

TABLE 4.1.*   JOINT CORRELATION MATRICES $K^{\uparrow}_{IS}$ (τ*, θ; τ) ($\delta = \sigma'/\bar{\sigma}$)**

τ	0°								
	0	30	60	70	80	82,5	85	87,5	90
0	0,69	0,76	1,00	1,09	0,96	0,82	0,64	0,53	0,41
0,04	0,85	0,93	1,22	1,33	1,17	1,00	0,77	0,64	0,53
0,08	0,73	0,80	1,04	1,14	1,00	0,84	0,65	0,53	0,45
0,12	0,82	0,90	1,18	1,29	1,12	0,96	0,73	0,60	0,51
0,16	0,96	1,05	1,38	1,50	1,32	1,11	0,85	0,71	0,60
0,20	0,94	1,03	1,35	1,47	1,29	1,09	0,83	0,69	0,58
0,32	1,02	1,11	1,46	1,59	1,38	1,16	0,85	0,65	0,58
0,40	0,72	0,79	1,04	1,13	0,97	0,79	0,53	0,30	0,30

* Commas in the numbers indicate decimal points.

** To obtain absolute energy units, we must multiply all the numbers by $10^{-2}S^2$.

TABLE 4.2.*   AUTOCORRELATION MATRICES $K^{\uparrow}_{II}$ (τ*; θ, θ') AND $K^{\downarrow}_{II}$ (0; θ, θ')**

θ°	0	30	50	60	70	80	82,5	85	87,5	90
0	0,52 / 0,41	0,57 / 0,62	0,67	0,75	0,81	0,71	0,60	0,45	0,36	0,31
30	0,44	0,48	0,74 / 0,87	0,82	0,89	0,78	0,66	0,49	0,39	0,34
50	0,49	0,53	0,59	0,96 / 1,07	1,05	0,92	0,77	0,58	0,46	0,40
60	0,51	0,55	0,61	0,63	1,17 / 1,27	1,02	0,86	0,65	0,52	0,44
70	0,46	0,50	0,56	0,58	0,52	1,11 / 0,97	0,94	0,71	0,56	0,48
80	0,11	0,12	0,13	0,14	0,12	0,03	0,82 / 0,69	0,62	0,49	0,42
82,5	−0,09	−0,10	−0,11	−0,12	−0,10	−0,02	0,03	0,52 / 0,39	0,41	0,35
85	−0,32	−0,34	−0,38	−0,39	−0,36	−0,07	0,09	0,27	0,31 / 0,25	0,27
87,5	−0,50	−0,54	−0,60	−0,61	−0,55	−0,11	0,14	0,42	0,70	0,21
90	−0,32	−0,34	−0,38	−0,39	−0,35	−0,08	0,08	0,25	0,38	

* Commas in the numbers indicate decimal points.

** To obtain absolute units, we must multiply all the numbers by $10^{-3}S^2$.

TABLE 4.3.* JOINT CORRELATION MATRIX $K^1_{IR}(\tau^*, \theta; \tau)$**

τ	$\theta°$							
	0	30	60	70	80	82,5	85	87,5
0	—0,35	—0,39	—0,51	—0,55	—0,48	—0,41	—0,31	—0,25
0,04	—0,25	—0,28	—0,37	—0,40	—0,35	—0,29	—0,22	—0,17
0,08	—0,15	—0,17	—0,22	—0,24	—0,20	—0,17	—0,12	—0,09
0,12	—0,05	—0,06	—0,07	—0,08	—0,07	—0,05	—0,03	—0,02
0,16	0,07	0,07	0,10	0,11	0,10	0,08	0,07	0,07
0,20	0,19	0,21	0,28	0,30	0,27	0,29	0,18	0,16
0,24	0,32	0,35	0,46	0,50	0,44	0,37	0,29	0,24
0,28	0,42	0,46	0,60	0,66	0,57	0,48	0,37	0,29
0,32	0,38	0,42	0,55	0,60	0,53	0,44	0,34	0,27
0,36	0,35	0,38	0,50	0,55	0,48	0,40	0,31	0,24
0,40	0,31	0,34	0,44	0,48	0,42	0,35	0,27	0,21

* Commas in the numbers indicate decimal points.

**To obtain absolute units, we must multiply all the numbers by $10^{-3}S^2$.

TABLE 4.4.* JOINT CORRELATION MATRIX $K^1_{IR}(0, 0; \tau)$**

τ	$\theta°$							
	0	30	60	70	80	82,5	85	87,5
0	—0,32	—0,34	—0,39	—0,35	—0,08	0,08	0,25	0,38
0,04	—0,29	—0,25	—0,28	—0,26	—0,07	0,04	0,15	0,20
0,08	—0,14	—0,15	—0,17	—0,16	—0,05	0,01	0,07	0,06
0,12	—0,05	—0,05	—0,06	—0,06	—0,03	—0,01	—0,00	—0,05
0,16	0,06	0,06	0,07	0,06	0,01	—0,04	—0,09	—0,18
0,20	0,17	0,18	0,21	0,18	0,02	—0,07	—0,18	—0,30
0,24	0,28	0,30	0,35	0,31	0,05	—0,09	—0,26	—0,41
0,28	0,37	0,40	0,46	0,42	0,09	—0,09	—0,30	—0,47
0,32	0,34	0,37	0,42	0,38	0,08	—0,09	—0,27	—0,43
0,36	0,31	0,33	0,38	0,35	0,08	—0,08	—0,28	—0,39
0,40	0,27	0,29	0,34	0,30	0,08	—0,08	—0,22	—0,34

* Commas in the numbers indicate decimal points.

** To obtain absolute units, we must multiply all the numbers by $10^{-3}S^2$.

§ 6. Angular and Spectral Structure of the Earth's Brightness Field, from Measurements on Kosmos 149

A unique possibility for investigating the angular structure of brightness of various Earth features is the measurement of absolute intensity of reflected solar radiation performed on Kosmos 149 in the spectral region 0.74 μm [11]. This stems from the fact that the TF-3B telephotometer mounted on this satellite surveyed the Earth along the flight trajectory. Therefore, during successive scans, the telephotometer measured the brightness of a single terrestrial object passing in the field of view of the instrument, at different angles to the local vertical, which enabled one to construct the angular distributions of solar radiation reflected by the object. Reduction of the information obtained was performed in [12]. All the angular profiles obtained from Kosmos 149 (Figure 4.9) were divided into three families as regards the brightness coefficient $R_0(\theta, \zeta)$ of the reflecting objects at the nadir direction $\theta = 0$ (the zenith distances of the Sun ζ varied here in the range 50 - 70 degrees). The first family (M_1) included angular profiles of $I(\theta)$, which increased with increase of $\theta (R_0 < 0.6)$. The second family (M_2) included curves of $I(\theta)$ decreasing with increase of R_0 ($R_0 > 0.6$); and finally, in the family of I we distinguish the sub-family M_3 of angular profiles ($0 \leq R \leq 0.4$) which refers to weakly reflecting surfaces $I(\theta)$. For each of these families, composed of N = 20 to 30 curves of $I(\theta_k)$, which are considered to be random vectors, [12] constructed mean profiles $\bar{I}(\theta_k)$, mean square deviations $\sigma_I(\theta_k)$, autocorrelation matrices $K_{II}(\theta_k, \theta_l)$, and correlation coefficients $r_{II}(\theta_k, \theta_l)$. /153 Examples of these characteristics for the above families of angular profiles are given in Figure 4.10.
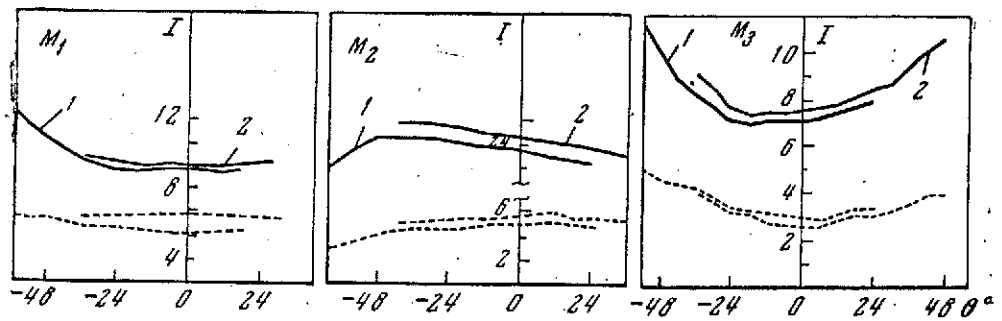
Figure 4.9. Mean profiles of brightness $\bar{I}(\theta)$ (solid lines) and mean square deviations $\sigma_I(\theta)$ (broken lines 1, 2- N $\approx$ 20 and N = 25 - 30, mW/cm^2·ster·μm, respectively

The average profiles of $I(\theta_h)$ describe typical angular distributions of reflected solar radiation above various underlying surfaces: one obtains a concave profile for a low value R_0 of the reflecting surface, and a convex profile for strong reflection (see § 3 of Chapter 1). We note that amongst the family of curves of $I(\theta)$ obtained from Kosmos 149, there is a neutral type of angular profile describing the behavior of the atmosphere brightness above an underlying surface with the mean value of the brightness coefficient (R_0 = 0.5 to 0.8). Here one does not see a single-valued dependence of the type of angular profile on the reflection characteristics or illumination or observation conditions. In addition, for the same average values and closely adjacent values of ζ, and of the azimuth ψ of the scan plane, three types of curves of $I(\theta)$ can be encountered, as is illustrated in Figure 4.11. This means that even finer characteristics of the reflecting surface play a part in forming the distribution of angular brightness, in some cases the microstructure of cloud formations, for which angular profiles of Figure 4.11 were obtained.
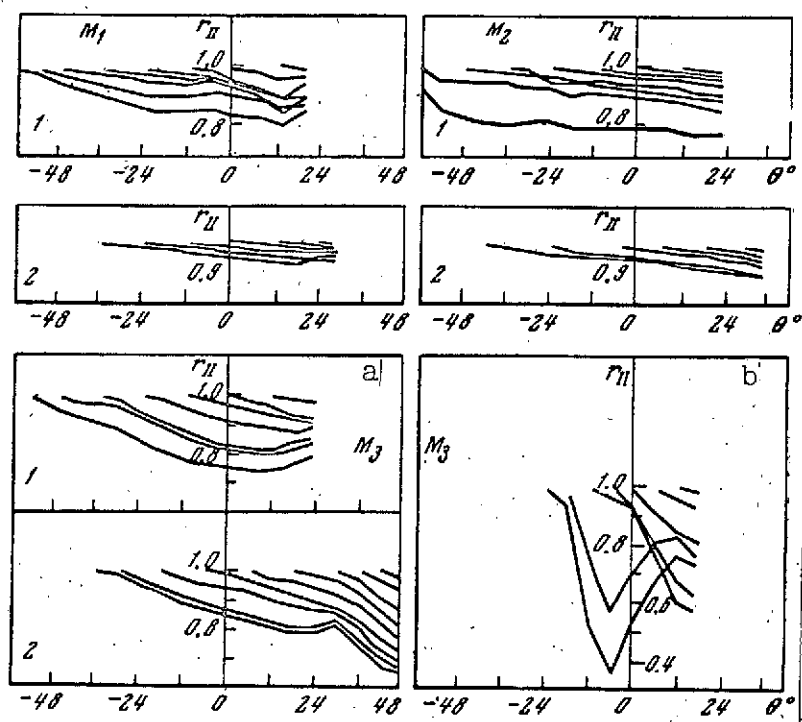
Figure 4.10. Normalized correlation matrices r_{II} $(\theta_k, \theta_l)|$
a- $R_0 \le 0.35$;   b- $R_0 \le 0.2$;   1- $N \approx 20$;   2- $N = 25 - 30$

The mean square deviations $\sigma_I(\theta_k)|$ prove to be weakly dependent on $\theta_k|$ (see Figure 4.9) in almost all cases, which gives reason to hope that the random fluctuations of the angular profiles are homogeneous. A finer structure in the fluctuations of angular brightness profiles can be obtained by examining the autocorrelation matrices $K_{II}(\theta_k, \theta_l)|$ and their eigenvectors. The normalized correlation matrices $r_{II}(\theta_k, \theta_l)|$ presented in Figure 4.10 are evidence as to the rather high degree of correlation of the fluctuations in the angular distributions of brightness in the case of R_0 (see Figure 4.10, M_1 and M_2), which is a consequence of the vertical homogeneity of the cloud formations for which the basic volume of angular profiles of type of M_1 and M_2 was| obtained. However, in the case of small R_0, which characterizes the atmospheric brightness above a water surface, above a comparatively

261
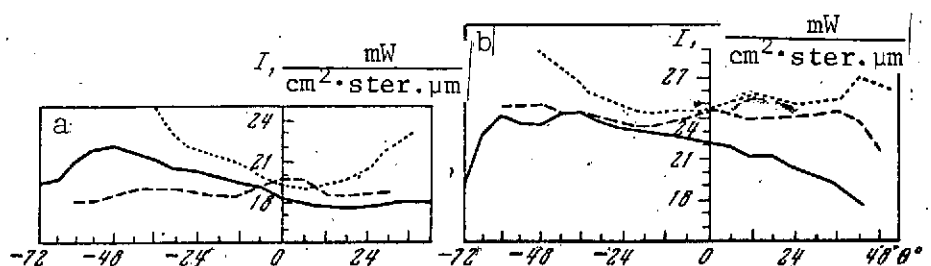
Figure 4.11. Angular profiles of various types

a- R_0 = 0.68, ζ = 48 - 50°, ψ = 100 - 102°; b- R_0 = 0.84 - 0.87, ζ = 48 - 53, ψ = 74 - 96

weakly reflecting land surface, or above a semi-transparent cloud, there is a tendency for a decrease in the coefficient of correlation between the brightness fluctuations in the region of minimum intensity of reflected radiation (near the nadir) and at large θ (see Figure 4.10, M_3). Here the minimum correlation in this region becomes more pronounced when the range of small values of R_0 is narrowed, and it is smoothed out when one combines the corresponding family of curves $I(\theta)$ of angular profiles with higher values of R_0. The correlation between the brightness fluctuations at large θ in the two half-planes of the sky remains high, as before.

This effect can be explained by considering the correlation dependence of the brightness, arising both from fluctuations in the aerosol scattering coefficient, and on the variability of the reflection characteristics of natural surfaces. In fact, for zero reflection, the correlation of the brightness for all angles θ is determined completely by the fluctuations in the scattering coefficient. In the case of weak reflection, the fluctuations of brightness $I'(\theta)$ in the region of the nadir will be determined mainly by fluctuations in the brightness coefficient R_0 of the

reflecting surface, while for large θ the fluctuations of $I'(\theta)$ arise mainly from fluctuations in the atmospheric scattering coefficient, which are not correlated with R_0, of course. This is probably also the cause of the minimum of correlation shown on Figure 4.10 (M_3).

On the other hand, in cases with strong reflection, the fluctuations $I'(\theta)$ are determined for all θ mainly by the variation in the brightness coefficient, which implies a high correlation, as illustrated by the curves r_{II} in Figure 4.10 (M_1 and M_2). The filling in of the correlation minimum near the nadir as the family of angular profiles M_3 expands because of values of $I(\theta)$ corresponding to larger R_0 is exactly linked to the increase in the effect of fluctuations of R_0 on the increase of the correlation coefficient r_{II} at all θ. It should be noted /155 that there is a decrease of r_{II} for families M_1 and M_2 also, even for an enlarged range of angles θ; the fluctuations of brightness for very large θ are weakly correlated with $I'(\theta)$ at small θ. The reason is that there is equalization at large θ of the contribution of the above factors, which are responsible for the correlation of the angular brightness profiles, and also for the effect of the horizontal nonuniformities of reflecting objects in the spatial averaging near the Earth's horizon. The nature of the correlative dependence and the degree of uniformity of the angular brightness profiles is rather clearly described by a system of eigenvectors $\varphi_m(\theta_h)$ of the matrix $K_{II}(\theta_h, \theta_l)$. The examples of the vectors $\varphi_m(\theta_h)$ for the matrices given in Table 4.5 (these correspond to the normalized matrices of Figure 4.10) are shown in Figure 4.12. Interesting features are the convergence and certain differences in the first three eigenvectors for both kinds of angular profile. In some cases, these vectors are reminiscent of the first three functions of an even trigonometric

TABLE 4.5.* AUTOCORRELATION MATRICES $K_{II}^{j}(\theta_k, \theta_l)$ [IN $(mW/cm^2 \cdot ster \cdot \mu m)^2$] FOR ANGULAR PROFILES OF TYPE M_1 AND M_2

θ_k^0	θ_l^0															
	−66	−60	−54	−48	−36	−30	−24	−18	−12	−6	0	6	12	18	24	30
−66	32,3 / 9,2	31,2	30,1	27,2	25,0	24,1	23,1	22,1	21,3	20,8	20,2	20,7	20,4	21,6	—	—
−60	9,7	31,0 / 11,8	30,4	27,9	25,8	24,9	23,9	23,1	22,2	21,7	21,2	21,6	21,0	22,2	—	—
−54	9,9	12,6	31,2 / 14,6	28,9	26,8	26,3	25,2	24,5	23,1	22,6	22,1	22,6	22,0	23,2	—	—
−48	10,2	13,5	15,4	27,1 / 16,8	22,5	24,8	23,8	23,2	21,8	21,2	20,7	21,0	20,4	21,6	—	—
−36	10,6	14,2	16,2	17,7	23,8 / 18,8	23,3	22,6	21,9	20,6	20,0	19,6	19,8	19,2	20,3	—	—
−30	11,1	14,9	16,9	18,6	19,7	23,1 / 20,9	22,4	21,8	20,4	19,7	19,2	19,3	18,8	19,7	—	—
−24	10,9	14,5	16,7	18,2	19,3	20,5	22,4 / 20,4	21,7	20,5	19,5	18,8	18,8	18,2	18,8	—	—
−18	11,2	14,2	16,4	17,7	18,8	19,8	19,8	21,2 / 19,9	20,1	19,2	18,7	18,7	18,2	18,8	—	—
−12	11,2	14,5	16,7	18,2	19,2	20,4	20,3	20,6	19,4 / 21,8	18,5	17,9	17,8	17,5	17,9	—	—
−6	11,7	15,2	17,4	18,8	20,0	21,2	21,2	21,3	22,6	18,5 / 23,6	17,7	17,8	17,5	18,0	—	—
0	11,8	15,2	17,4	18,7	19,9	21,0	20,9	21,3	22,4	23,5	18,8 / 23,7	18,3	18,1	18,5	—	—
6	11,9	15,2	17,4	18,7	19,9	21,0	20,9	21,3	22,3	23,4	23,7	18,0 / 24,0	19,1	19,5	—	—
12	12,0	15,4	17,7	19,0	20,3	21,5	21,4	21,8	22,8	24,0	24,2	24,6	19,9 / 25,3	20,1	—	—
18	11,7	15,1	17,4	18,7	20,6	21,2	21,2	21,5	22,7	23,8	24,0	24,2	24,8	20,7 / 24,8	—	—
24	11,2	14,2	16,4	17,4	18,7	19,9	19,9	20,2	21,4	22,6	22,8	23,1	23,7	23,8	23,0	—
30	11,0	13,9	16,3	17,2	18,4	19,4	19,5	19,9	21,1	22,3	22,4	22,7	23,3	23,4	22,8	22,6

* Commas in the numbers indicate decimal points.

system: $\varphi_1(\theta_h) \sim \text{const}$, $\varphi_2(\theta_h) \sim \cos \alpha\theta_h$, $\varphi_3(\theta_h) \sim \cos 2\alpha\theta_h$. This convergence is observed to an even greater degree for a narrow range of angles θ_k in the region of the nadir, where the brightness fields are more homogeneous. The close relationship between empirical orthogonal vectors and the trigonometric functions is a criterion of the degree of uniformity of the random fields (for uniform fields the eigenfunctions must coincide exactly with the
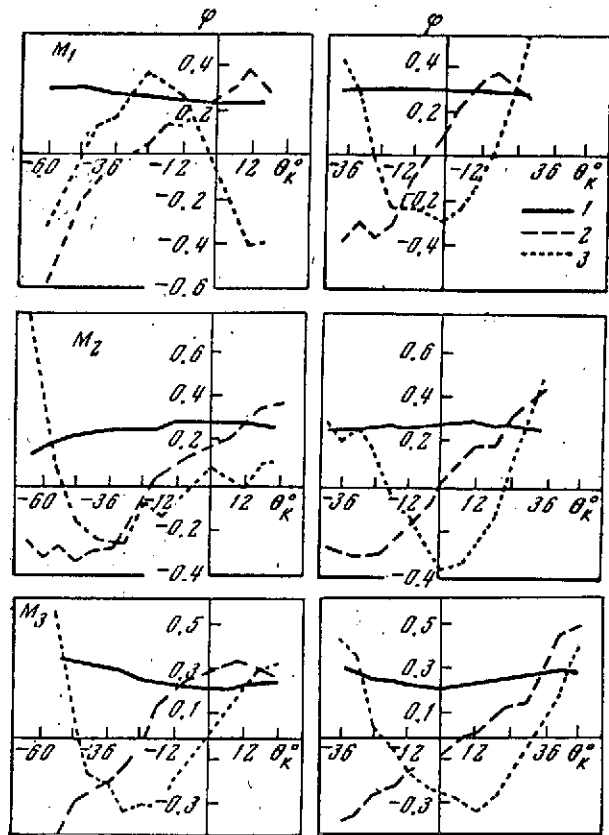
Figure 4.12. Eigenvectors φ_m (θ_k) of the autocorrelation matrices $K_{II}(\theta_k, \theta_l)$, corresponding to Figure 4.10

1- φ_1 ; 2- φ_2 ; 3- φ_3

trigonometric functions).*

§ 7. The Use of Structural Characteristics

The characteristics of the vertical, angular, and spectral structure of radiation fields can be used directly in solving a number of problems associated with the use of satellites for meteorology. An example of this type of problem is the optimal extrapolation of the intensity or flux of outgoing radiation,

---

* This question will be considered in greater detail in § 5 of Chapter 5.

measured for fixed heights or angles, to other levels or direc-
tions. This problem arises during radiation measurements from
satellites, when in fact we know only the intensity of the
ascending radiation at the level of the top boundary of the
atmosphere in a given direction θ, and also the average distri-
bution of the intensity of ascending radiation $I_v(\theta)$ (for self-
radiation, this can be calculated from the statistical character-
istics of the fields $T(\zeta)$ and $q(\zeta)$, and for reflected solar radiation
it can be calculated from the characteristics $\sigma(z)$). Therefore,
at the top boundary of the atmosphere, the deviation $I_v'(\theta)$ from
its mean value will also be known.

By using the correlation matrix $K_{II}(\zeta,\zeta';\theta)$, for example, for
the Earth's self-radiation, we can extrapolate $I_v'(0,\theta)$ in optimum
manner to other fixed levels using the relation

$$I_v'(\zeta, \theta) = c_v(\zeta, \theta)\, I_v'(0, \theta).$$

The coefficient $c_v(\zeta, \theta)$, determined from the condition that the
functional

$$\delta^2\,[c_v(\zeta, \theta)] = \overline{[I_v'(\zeta, \theta) - c_v(\zeta, \theta)\,I_v'(0, \theta)]^2}, \qquad (4.80)$$

should be a minimum has the form

$$c_v(\zeta, \theta) = \frac{K_{II}\,(\zeta, \theta;\, \theta)}{K_{II}\,(0, 0;\, \theta)} \cdot \qquad (4.81)$$

The relative errors in the optimum extrapolation $\varepsilon(\zeta, \theta) = \delta(\zeta, \theta)/$
$[K_{II}(\zeta, \zeta; \theta)]^{1/2}$ can be expressed in terms of the correlation coeffi-
cients $r_{II}(\xi, 0; \theta)$:

$$\varepsilon(\zeta, \theta) = \sqrt{1 - r_{II}^2\,(\zeta, 0;\, \theta)}.$$

The correlation moments required to perform optimum extrapolation
of Equation (4.80), are given in § 2.

Using the joint correlation functions K_{IT}, K_{Iq}, K_{Ip_0}, we can best determine the temperature and humidity profiles, as well as the height of the upper cloud boundary. A statement of the problem of optimal determination of the temperature field from radiation measurements of Earth's self-radiation in the spectral ranges 8 - 30 and 8 - 12 μm, obtained on the Tiros II satellite, was given in [3.5]. However, the joint correlation functions $K_{II}(\rho)$ constructed for this purpose for the horizontal coordinate ρ have shown that, even for the spectral region 8 - 12 μm, the coefficients of correlation between the measured radiative fluxes I and atmospheric temperatures at various levels, but for the same points on the Earth (ρ = 0), do not exceed 0.5 in absolute value. The authors of [3.5] explain this very weak correlation by errors in the taking of the satellite data and the effect of clouds. Without eliminating the possible effect of these factors, we note that the low correlation coefficient $r_{II}(0, \zeta_k)$ obtained in [3.5] is in agreement with the low theoretical values of r_{IT} (see Figure 4.1). An interesting feature is the agreement of the negative correlation between Earth radiation in the transparent window and the temperature of the upper layers of the troposphere.

It is probably because of the weak correlation of r_{II}, which moreover, decreases with ρ, that the authors of [3.5] did not give examples of optimum determination of T from I. In [13] is given a more optimistic assessment of the possible optimum determination of temperature of underlying surface and moisture content from the outgoing Earth radiation. In our view, the solution of this problem should be considered only as an auxiliary means of extrapolating the solution of exact inverse problems in determining the vertical profiles from measurements of emission spectra in the vicinity of the region of measurement.

Another more dependable problem of optimum extrapolation is determination of the intensity of Earth self-radiation for various directions θ' from measurements of $I_\nu(0, \theta)$ in the direction θ. For this purpose, the autocorrelation functions for the angular structure of the radiation field $K_{II}(\zeta, \theta; \theta')$ are used.

In other words, the set of autocorrelation characteristics for the vertical, angular, and spectral structure can be used for best determination of the Earth self-radiation field with height, direction, and wavelength. In particular, the vertical and angular extrapolation of the intensity of integrated radiation, measured, for example, on the satellites Tiros, Meteor, and Nimbus [14 - 16], make possible optimum determination of the flux of ascending radiation $F^\uparrow(\zeta)$. Using the structural charac- /158 teristics of the incident radiative flux $F^\downarrow$ and the joint correlations between $F^\uparrow$ and $F^\downarrow$ (see, e.g., [7, 8]), one can also determine variations in the flux of long-wave radiation.

Similarly, one can perform optimum extrapolation of the intensity of reflected solar radiation, measured on satellites, using the statistical characteristics for the vertical, angular, and spectral structure of the field of short-wave Earth radiation. This procedure allows us, for example, to perform the optimum calculation for the variations of intensity $I'(\theta)$, using the method of deriving fluxes of outgoing short-wave radiation from direct satellite measurements of integrated brightness in direction, as suggested in the work of Shifran and Kolomiytsev, et al. [I.20, 17]. Since the statistical characteristics of the angular structure of the integrated intensity of reflected solar radiation are not available, one can adopt for this purpose the structural characteristics of the spectral brightness obtained from measurements on Kosmos 149 (see § 6). The rather high correlation, suggested in [2.55] for fluctuations in brightness over a wide

range of visible and UV spectral regions for all angles θ,
affords some basis for using these characteristics in the integral
case. Then, using the formula

$$I_\lambda (\theta_0) = I(\theta_0) \frac{S_\lambda}{S} $$ (4.82)

to convert the measured integral brightness $I(\theta_0)$ to the spectral
brightness $I_\lambda(\theta_0)$, at λ = 0.74 μm and thus determining the closest
angular profile $I_\lambda(\theta)$ (e.g., using Figure 4.9), we use the latter
for the inverse calculation of the mean profile of $I(\theta_0)$,
according to Equation (4.82). Then, determining the deviation
of the brightness $I(\theta_0) = I(\theta_0) - I(\theta_0)$, we can apply the method of
optimal extrapolation to find $I(\theta) = I(\theta) + c(\theta) I'(\theta_0)$ for any θ. Here
the coefficient $c(\theta)$ is calculated from the relation

$$c(\theta) = \frac{K_{II}(\tau^*; \theta, \theta_0)}{K_{II}(\tau^*; \theta_0, \theta_0)} , $$ (4.83)

and the correlation moments in Equation (4.83) are taken for
λ = 0.74 μm from Table 4.5 for the respective type of angular
profile determined by the mean profile $I_v(\theta)$. Examples of
optimum extrapolation of $I_\lambda(\theta)$ profiles from $I_\lambda(0)$, given in
Figure 4.13, are evidence that it is possible to determine a
certain sample of the angular distribution of integral brightness
from measurement of I only at a single angle. Here it should be
noted that, because of the single-valued dependence of the type
of angular profile on the brightness coefficient at the nadir
(see Figure 4.12), an error may be made in choosing the type of
mean curve for $I(0)$. However, this error will be small, since
all types of angular profile in these cases differ very little
from the neutral case as can be seen from Figure 4.13. Therefore,
when the measured brightness $I(\theta_0)$ corresponds to a mean value of
the brightness coefficient, it is expedient to use the hypothesis
that the brightness of the object under examination is independent
of θ.

$$I,\ mW/cm^2 \cdot ster \cdot \mu m$$
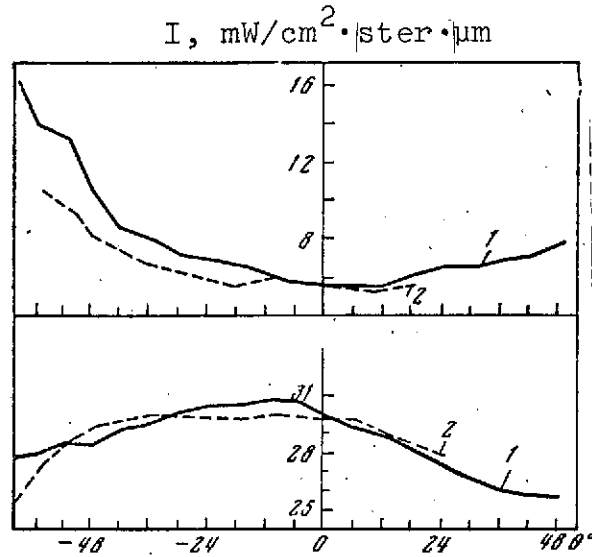
Figure 4.13. Comparison of angular profiles of brightness $I_{0.74}(\theta)$
1- satellite measurements; 2- determined by the method of
optimum extrapolation

The structural characteristics of the radiation field can
be used also in problems of atmospheric thermodynamics, for
which it is important to calculate the heat flux due to radiation.

We first evaluate the order of magnitude of random fluctu-
ations of the flux of long-wave radiation in the special cases
$\theta = \pi/2$ and $\zeta = 1$. For $\theta = \pi/2$ the structural characteristics
of the radiation field take a very simple form, since all the
integral terms in Equations (4.21) - (4.24) go to zero, and

$$P(1.1) = 1. \text{ then} | \ I'(\zeta, \pi/2) = B[\bar{T}(\zeta)];$$

$$K_{IT}\left(\zeta, \zeta'; \frac{\pi}{2}\right) = \frac{\partial B[\bar{T}(\zeta)]}{\partial T} K_{TT}(\zeta, \zeta');$$

$$K_{II}\left(\zeta, \zeta'; \frac{\pi}{2}\right) = \left\{\frac{\partial B[\bar{T}(\zeta)]}{\partial T}\right\}^2 K_{TT}(\zeta, \zeta').$$

Similar expressions are obtained for $\zeta = 1$. In other words, I'
and K_{II} are expressed only in terms of the structural charac-
teristics of temperature. This conclusion is not at all surpris-
ing, since for $\theta = \pi/2$ a plane atmospheric layer radiates as a

270

blackbody |at the temperature of the point at which the radiation is being measured, while for $\zeta = 1$, the fluctuations in radiation are determined only by the flutuations of T' of the ground surface. Also, the correlation function K_{FF} at the Earth is proportional to K_{TT}, and the coefficient of proportionality is $[\partial B \, (\bar{T})/\partial T]^2$. Since for ground temperatures $\partial B/\partial T \approx 0.02 \, B$, the ratio of the mean square deviation $\sigma_{FF} = \sqrt{K_{FF}}$ to $\bar{F}$ is $0.02 \, \sigma_{TT}$. This means that, for the usual values $\sigma_{TT} = 5 - 7$, the mean square deviation δ_{FF} is 10 - 15% of the value of $\bar{F}$, i.e., it is of the same order as the components of heat balance determined by fluctuations of the dynamic parameters. Therefore, to determine the relationship between variations of the thermodynamic parameters and the fluxes of radiative heat, one must use the statistical characteristics describing variations in the radiative fluxes. For example, the connection between variations of the vertical and angular profiles of atmospheric self-radiation with variations in the vertical profiles of temperature $T' \, (\zeta)$ and humidity $q' \, (\zeta)$ can be studied by the method of optimum approximation, using expansions of the random functions $T' \, (\zeta)$ and $q' \, (\zeta)$:

$$T' (\zeta) = \sum_{k=1}^{n} t_k \varphi_k (\zeta);$$

(4.84)

$$q' (\zeta) = \sum_{k=1}^{n} q_k \psi_k (\zeta)$$

(4.85)

from the corresponding empirical orthogonal functions $\varphi_k (\zeta)$ and $\psi_k (\zeta)$ of the temperature and humidity fields (see §2 and §3 of Chapter 3).

By substituting Equations (4.84) and (4.85) into the expressions for I' or F', e.g., into Equation (4.32), and carrying out elementary transformations, we obtain

$$I'(\zeta, \theta) = \sum_{k=1}^{n} [t_k \Phi_k(\zeta, \theta) + q_k \Psi_k(\zeta, \theta)].$$

(4.86)

Here

$$\Phi_k(\zeta, \theta) = \frac{\partial B[\bar{T}(1)]}{\partial T} \varphi_k(1) P(\zeta, 1; \theta) - \int_{\zeta}^{1} \frac{\partial B[\bar{T}(t)]}{\partial T} \varphi_k(t) \frac{\partial P(\zeta, t; \theta)}{\partial t} dt;$$

$$\Psi_k(\zeta, \theta) = \int_{\zeta}^{1} \frac{\bar{I}(t, \theta) - B[\bar{T}(t)]}{\bar{q}(t)} \psi_k(t) \frac{\partial P(\zeta, t, \theta)}{\partial t} dt$$

are universal functions depending on the mean temperature and humidity profiles. Expressions of type (4.86), describing fluxes, can be used for simultaneous solution of the transfer equations for fluctuations of heat, moisture, and radiation. Here, we stress the importance of investigating conditions and space characteristics for change in correlations between fluctuations of radiative and atmospheric parameters.

Finally, the relations between the statistical characteristics of the radiative and atmospheric parameters, considered as integral equations for the correlation functions of these parameters, can be used to determine the correlation functions from the statistical characteristics of the angular or spectral structure of the radiation fields. The solution of these problems, which are inverse problems, is the topic of optical probing of the atmosphere in the general sense. We address ourselves to this question in Part 2 of this book.

CHAPTER 5
SPATIAL STRUCTURE OF THE RADIATION FIELD

§ 1. Statement of the Problem

As has been mentioned, the Earth's radiation field is /161
extremely inhomogeneous in the horizontal directions, due to the
spatial and temporal changes in the physical parameters of the
atmosphere, the underlying surface, and the clouds. The radi-
ation characteristics in different regions of the spectrum
reflect both the stable or slowly varying components, and also
the random components of the spatial nonuniformity. The first
of these is due to nonuniformities of a geographic nature
(continents, oceans, mountains, etc.) or those of climatic
origin (snow cover, vegetation, etc.). The second component
originates from the processes of different scales in the atmos-
phere, which determine its state and the variation of the
meteorological parameters. Hence, it follows that it is impor-
tant to study the spatial structure of the radiation fields,
which results from these processes, and to establish the rela-
tionship with the spatial structure of the fields of meteoro-
logical elements and clouds. Taking into account the fact that
these fields are random, in order to find the necessary depen-
dences, one must use statistical methods, both to reduce the
experimental data on radiation and meteorological elements and
also to describe a mechanism for the transformation of radiant
energy in a medium with randomly distributed physical parameters,
responsible for this transformation.

A statement of the problem, as well as the principles for investigating the spatial structure of the radiation fields, including those obtained using artificial Earth satellites, is given in a paper by Malkevich, et al. [1]. The first results of statistical reduction of specific data of radiation measurements on the American satellites Tiros II and Tiros III were presented by Borisenkov, et al. [2, 3], and also by Gandini, et al. [3, 5]. Similar statistical processing was used for data of flight measurements of radiation above a cloud cover [4], and also data from microphotometric aerophotography of clouds, obtained on aircraft [5, 6], space vehicles [7], and satellites [8]. Recently, statistical characteristics were obtained for the spatial structure of the fields of reflected solar radiation and the Earth self-radiation from measurements on the satellites Kosmos 45 [9], Kosmos 122 [10, 11], Kosmos 149 [12], and Kosmos 243 [13]. In most of these papers, the statistical processing of the experimental data was conducted on the basis of an a priori assumption that the radiation fields were homogeneous and isotropic, for which rigorous methods of mathematical statistics have been developed and the structural characteristics listed in § 1 of Chapter 3 are obtained comparatively simply. However, for the actual fields, these assumptions require justification, since the validity of these statistical characteristics must be verified by calculating them for different sections of a given random function.

On the other hand, one important problem is to find a /162 method for statistical processing of experimental radiation fields, which does not require these assumptions. As has been mentioned in § 1 of Chapter 3, this condition is satisfied by the method of constructing correlation matrices for sections of a random two-dimensional field, considered as a set of random vectors, parametrically dependent on direction. This method, used to construct statistical characteristics of the reflected

solar radiation field in [12] from photometric data, obtained
on the satellite Kosmos 149 [2.55], will be examined in the
present chapter.

Along with this empirical approach to this study of spatial
structure of radiation fields, we will investigate the possi-
bility of using the mechanism of radiative transfer and the
corresponding equations to obtain the theoretical relations
between the statistical characteristics of the spatial structure
of radiation fields and the characteristics of an optical-
meteorological atmospheric model, in a manner similar to what
was done in the study of the vertical structure of the radiation
field. We will consider a method of establishing the relation
between these structural characteristics on the basis of the
radiative transfer equations in a horizontally nonuniform atmos-
phere and the random distributions of the physical parameters,
described in [14]. We will also consider the causes for the
transformation of structural characteristics, arising both from
natural averaging due to scattering, absorption, and emission
of radiation in the atmsophere, and also from purely instru-
mental effects, associated with the angular or spectral
sensitivity of the measuring instruments.

Where possible, the theoretical results will be compared
with data of appropriate measurements. Here, attention will be
directed to features of methods of obtaining empirical charac-
teristics of the spatial structure of radiation fields, including
the possibility of using correlation matrices and their eigen-
vectors to determine analogs of the spatial spectra of nonuniform
random fields.

§ 2. Structure of Self-Radiation Fields

2.1. Basic Relations

The spatial variations of the Earth's self-emission are determined mainly by the horizontal nonuniformity of the clouds and the underlying surface, which manifests itself in changes of temperature, as well as horizontal changes of the vertical profiles of temperature and of atmospheric temperature and humidity. In order to establish quantitative relations between the characteristics of the spatial structure of the corresponding fields, we consider the solution of the transfer equation for long-wave radiation in the atmosphere under the condition that the temperature and humidity profiles, as well as the temperature of the underlying surface and of the top boundary of the clouds, are distributed randomly in space.

For the case where the physical parameters of the atmosphere depend only on a single horizontal coordinate, the solution of the transfer equation (2.28), (2.29) was obtained in § 5 of Chapter 2. If we assume that the variations of the profiles of temperature $T'(\zeta, \xi)$ and humidity $q'(\zeta, \xi)$ are random functions, then the intensity of the self-radiation $I'_\nu(\zeta; \xi; \theta, \psi)$, defined by Equation (2.47), and its Fourier transform $J_\nu(\zeta, \omega; \theta, \psi)$ (2.46) are also random functions. Therefore, the second moments $K_{Iq}(\zeta, \zeta; \theta, \psi)$ and $K_{Tq}(\zeta, \zeta)$ enter into Equation (2.40) for the

mean profile of the radiation intensity $\bar{I}_\nu(\xi; \theta, \psi)$, and these require supplementary relations for their determination. In addition, Equations (2.47) or (2.48) can be used to construct relations for determining the autocorrelation and joint correlation functions $K_{II}(\zeta, \xi; \zeta_1, \xi_1; \theta, \varphi)$, $K_{IT}(\zeta, \xi; \zeta_1, \xi_1; \theta, \psi)$ and $K_{Iq}(\zeta, \xi, \zeta_1, \xi_1; \theta, \psi)$ in terms of the corresponding characteristics of the spatial structure of the temperature and humidity fields for fixed values of θ and ψ. Similarly, we can

calculate the random variations in the top boundary of the clouds p_0, the temperature $T(p_0)$, and the humidity $q(p_0)$ at this boundary.

Relations like these were obtained in [14]. We present results of that paper with some improvements and additions. By multiplying $I_\nu'(\zeta, \xi; \theta, \psi)$ by $I_\nu'(\zeta_1, \xi_1; \theta, \psi)$ and averaging for all points of a chosen region of the radiation field, from Equation (2.48) we obtain the following relation between K_{II} and the correlation functions K_{TT}, K_{qT}, and K_{qq}:

$$
\begin{aligned}
K_{II}(\zeta, \xi; \zeta_1, \xi_1; \theta, \psi) &= \left\{\frac{\partial B_\nu[\bar{T}(1)]}{\partial T}\right\}^2 K_{TT}[\mu(\zeta, \xi, 1); \mu(\zeta_1, \xi_1, 1)] P_\nu(\zeta_1, 1; \theta) \times \\
&\times P_\nu(\zeta, 1; \theta) - \frac{\partial B_\nu[\bar{T}(1)]}{\partial T} P_\nu(\zeta, 1; \theta) \int\limits_{\zeta_1}^{1} \left\{\frac{\partial B_\nu[\bar{T}(u)]}{\partial T} \times\right. \\
&\times K_{TT}[\mu(\zeta, \xi, 1); \mu(\zeta_1, \xi_1, u)] - \frac{\bar{I}_\nu(u, \theta) - B_\nu[\bar{T}(u)]}{\bar{q}(u)} \times \\
&\left.\times K_{Tq}[\mu(\zeta, \xi, 1); \mu(\zeta_1, \xi_1, u)]\right\} \frac{\partial P_\nu(\zeta_1, u; \theta)}{\partial u} du - \\
&- \frac{\partial B_\nu[\bar{T}(1)]}{\partial T} P_\nu(\zeta_1, 1; \theta) \int\limits_{\zeta}^{1} \left\{\frac{\partial B_\nu[\bar{T}(t)]}{\partial T} K_{TT}[\mu(\zeta_1, \xi_1, 1);\right. \\
&\mu(\zeta, \xi, t)] - \frac{\bar{I}_\nu(t, \theta) - B_\nu[\bar{T}(t)]}{\bar{q}(t)} K_{Tq}[\mu(\zeta_1, \xi_1, 1); \mu(\zeta, \xi, t)]\right\} \times \\
&\times \frac{\partial P_\nu(\zeta, t; \theta)}{\partial t} dt + \int\limits_{\xi}^{1}\int\limits_{\xi_1}^{1} \frac{\partial B_\nu[\bar{T}(t)]}{\partial T} \frac{\partial B_\nu[\bar{T}(u)]}{\partial T} \times \\
&\times K_{TT}[\mu(\zeta, \xi, t); \mu(\zeta_1, \xi_1, u)] \frac{\partial P_\nu(\zeta, t; \theta)}{\partial t} \frac{\partial P_\nu(\zeta_1, u; \theta)}{\partial u} dtdu - \\
&- \int\limits_{\zeta}^{1}\int\limits_{\zeta_1}^{1} \left[\frac{\bar{I}_\nu(t, \theta) - B_\nu[\bar{T}(t)]}{\bar{q}(t)} \frac{\bar{I}_\nu(u, \theta) - B_\nu[\bar{T}(u)]}{\bar{q}(u)} \times\right. \\
&\left.\times K_{qq}[\mu(\zeta, \xi, t); \mu(\zeta_1, \xi_1, u)]\right] \frac{\partial P_\nu(\zeta, t, \theta)}{\partial t} \frac{\partial P_\nu(\zeta_1, u; \theta)}{\partial u} dtdu
\end{aligned}
$$
(5.1)

By multiplying $I_\nu'(\zeta, \xi; \theta, \psi)$ by $T'(\zeta_1, \xi_1)$ or $q(\zeta_1, \xi_1)$, we obtain similar expressions for K_{IT} and K_{Iq}:

$$K_{IT}(\zeta, \xi; \zeta_1, \xi_1; \theta, \psi) = \frac{\partial B_\nu [\bar{T}(1)]}{\partial T} K_{TT}[\mu(\zeta, \xi, 1); \zeta_1, \xi_1] P_\nu(\zeta, 1; \theta) -$$

$$- \int_\zeta^1 \left\{ \frac{\partial B_\nu [\bar{T}(t)]}{\partial T} K_{TT}[\mu(\zeta, \xi, t); \zeta_1 \xi_1] - \frac{\bar{I}_\nu(t, \theta) - B_\nu [\bar{T}(t)]}{\bar{q}(t)} \times \right. \quad (5.2)$$

$$\left. \times K_{qT}[\mu(\zeta, \xi, t); \zeta_1, \xi_1] \right\} \frac{\partial P_\nu(\zeta, t; \theta)}{\partial t} dt;$$

6*

$$K_{Iq}(\zeta, \xi; \zeta_1, \xi_1; \theta, \psi) = \frac{\partial B_\nu [\bar{T}(1)]}{\partial T} K_{Tq}[\mu(\zeta, \xi, 1); \zeta_1, \xi_1] P_\nu(\zeta, 1; \theta) -$$

$$- \int_\zeta^1 \left\{ \frac{\partial B_\nu [\bar{T}(t)]}{\partial T} K_{Tq}[\mu(\zeta, \xi, t); \zeta_1, \xi_1] - \right.$$

$$- \frac{\bar{I}_\nu(t, \theta) - B_\nu [\bar{T}(t)]}{\bar{q}(t)} K_{qq}[\mu(\zeta, \xi, t); \zeta_1, \xi_1] \right\} \times \qquad (5.3)$$

$$\times \frac{\partial P_\nu(\zeta, t, \theta)}{\partial t} dt.$$

The following notation is used in Equations (5.1) - (5.3):

$$\bar{T}(1) = \bar{T}_0; \qquad \mu(\zeta, \xi, t) = \xi - a \, \text{tg} \, \theta \cos \psi \ln \frac{t}{\zeta}, \qquad (5.4)$$

and $P_\nu(t, \zeta, \theta)$ is the transmission function (2.9). The reason for the complicated form of the arguments in Equation (5.4) is the same as for the form of the dependence of the deviations of intensity I_ν' for inclined directions of the observer (see § 5 of Chapter 2).

Thus, if we know the correlation functions K_{TT}, K_{qq}, and K_{qT} describing the spatial structure of the fields of temperature and specific humidity in the atmosphere (see § 7 of Chapter 3), then Equations (5.1) - (5.3) allow us to determine the characteristics of the spatial structure of the radiation field, and also to refine the value of $\bar{I}_\nu$ in Equation (2.40).

278

It is easy to see that the behavior of the correlation functions K_{II}, K_{IT}, and K_{Iq} with change in their arguments and parameters will be the same as that of the random function $I'_{\nu,}$ considered in § 5 of Chapter 2. In particular, for $\theta = 0$, they will be determined completely by the values of the correlation functions of temperature and humidity at the points (t, ξ) and (ζ_1, ξ_1), and also by the nature of the transformation of these functions because of absorption and emission of the atmosphere at frequency ν. However, for $\theta \neq 0$, K_{II}, K_{IT}, and K_{Iq} depend also on the values of the correlation functions K_{TT}, K_{qq}, and K_{qT} at all points lying on the straight lines $\xi - a\,\mathrm{tg}\,\theta\,\cos\psi\,\ln(t/\xi)$. For some of these points close to (ζ, ξ), the values of T' and q' will be closely correlated, at least within the field of given meteorological elements. Hence, it follows that even if T' and q' are not correlated at the points (ζ, ξ) and (ζ_1, ξ_1), the correlation between the values of I'_{ν} at these points will be appreciable (in contrast with the local parameters T' and q', the intensity of radiation I'_{ν} is an integral characteristic).

This derivation is important when we investigate the spatial structure of the radiation field and its dependence on the structure of the fields of the meteorological elements, especially because in practice all instruments measuring radiation have a finite aperture and are sensitive to radiation arriving at the instrument from quite a large solid angle.

By way of illustration, we consider the statistical characteristics of radiative fluxes at frequency ν (we drop the subscript ν):

$$F'_n (\zeta, \xi) = \int_0^{2\pi} \int_0^{\frac{\pi}{2}} I'_\nu (\zeta, \xi; \theta, \psi)\, \varkappa_n (\theta) \sin\theta\, d\theta\, d\psi, \qquad (5.5)$$

obtained by means of an instrument pointed to the nadir, with
angular sensitivity $\varkappa_n(\theta)$ given by the formula

$$\varkappa_n(\theta) = \cos^n \vartheta \qquad \left(0 \leqslant \theta \leqslant \frac{\pi}{2}; \quad n = 0, 1, 2, \ldots\right). \qquad (5.6)$$

/165

The special cases n = 0 and n = 1 correspond to instruments
rather frequently used in practice, with spherical and plane
detecting surfaces, with an angle of view of π.

For simplicity, we assume that variations of humidity can
be neglected, i.e., $\sigma(\zeta, \omega) \equiv 0$ in Equation (2.45). Then it is
not difficult to determine the Fourier transform for $F_n'(\zeta, \xi)$:

$$\Phi_n(\zeta, \omega) = \frac{1}{2\pi} \int_{-\infty}^{+\infty} F_n'(\zeta, \xi) e^{i\omega\xi} d\xi. \qquad (5.7)$$

In fact, by substituting Equation (5.5) into Equation (5.7),
changing the order of integration, and taking account of Equation
(2.46), we have the result, for $\sigma(\zeta, \omega) \equiv 0$, that

$$\Phi_n(\zeta, \omega) = \frac{\partial B_\nu[\bar{T}(1)]}{\partial T}\rho(1, \omega)\int_0^{2\pi}\int_0^{\frac{\pi}{2}}\left\{\exp\left[i\omega a \,\mathrm{tg}\,\theta \cos \psi \ln \frac{1}{\zeta}\right]\exp[-\tau(\zeta, 1, \theta] - \right.$$

$$- \int_\zeta^1 \frac{\partial B_\nu[\bar{T}(t)]}{\partial T}\rho(t, \omega)\exp\left[i\omega a\,\mathrm{tg}\,\theta\cos\psi\ln\frac{t}{\zeta}\right]\frac{\partial}{\partial t}\times \qquad (5.8)$$

$$\times \exp\left[-\tau(\zeta, t, \theta]\, dt\right\}\varkappa_n(\theta)\sin\theta d\theta d\psi.$$

Using Equation (2.52) to carry out integration over the hemi-
sphere, we obtain the final expression:

$$\Phi_n(\zeta, \omega) = 2\pi\frac{\partial B_\nu[\bar{T}(1)]}{\partial T}\rho(1, \omega)\,\Psi_{n+2}\left[w_0\int_\zeta^1 k_\nu(t)\,q(t)\,dt, \,\omega a \ln \frac{1}{\zeta}\right] -$$

$$- 2\pi\int_\zeta^1\frac{\partial B_\nu[\bar{T}(t)]}{\partial T}\rho(t, \omega)\frac{\partial}{\partial u}\,\Psi_{n+2}\times \qquad (5.9)$$

$$\times\left[w_0\int_\zeta^t k_\nu(t_1)\,q(t_1)\,dt_1, \,\omega a \ln \frac{t}{\zeta}\right]dt \qquad (\omega \geqslant 0, \quad n = 0, 1, 2, \ldots)$$

280

Here

$$\Psi_m(u, v) = \int\limits_1^\infty e^{-su} J_0\left(v\sqrt{s^2 - 1}\right) \frac{ds}{s^m} \cdot \qquad (m = 1, 2, \ldots) -$$

is the generalized exponential integral function of two variables u and v (see § 7 of Chapter 1); J_0 is a Bessel function; and $\partial/\partial u$ is a partial derivative with respect to u. Expressions of the type (5.9) can also be obtained by not neglecting the function $\sigma(\zeta, \omega)$, in Equation (2.45), but assuming that $I_v(\zeta, \theta)$ depends weakly on θ, and replacing $\bar{I}_v$ by its value averaged for all directions.

2.2. Homogeneous and Isotropic Fields

So far we have made no assumptions as to the nature of the random radiation fields. However, in practice, it is quite laborious to calculate four-dimensional correlation functions (5.1) - (5.3), even for fixed directions of observation, all the more so because at present we have no reliable statistical characteristics for the spatial structure of the temperature and humidity fields under inhomogeneous and nonisotropic conditions. The same thing is true also of the calculation of the spectral density via the Fourier transforms of the random functions $J_v(\zeta, \omega; \theta, \psi)$ or $\Phi_n(\zeta, \omega)$. The relations for the structural characteristics are appreciably simplified if we assume that T' and q' are homogeneous random functions, independent of ζ. Then, as is known (see, e.g., [15]):

$$\overline{|\zeta(\omega)|^2} = S_T(\omega); \qquad \overline{|\sigma(\omega)|^2} = S_q(\omega),$$

where S_T and S_q are the spectral densities of T' and q'.

We note that, because the functions T' and q' are homogeneous, it does not follow, generally speaking, that the random functions $I'_\nu|$ or $F'_n|$ are homogeneous. However, in some cases (these will be discussed below), one can assume that the latter are also homogeneous.

In the light of all these assumptions, from Equation (2.46) for the random function $J'_\nu|$ at fixed $\zeta, \theta|$ and $\psi|$, we obtain relations between the spectral densities of the random functions T' and $I'_\nu|$ (or T' and $F'_n|$):

$$S_I(\zeta, \omega; \theta, \psi) = \overline{|J'_\nu(\zeta, \omega; \theta, \psi)|^2} = S_T(\omega)|A_I(\zeta, \omega; \theta, \psi)|^2. \qquad (5,10)$$

We call the function

$$A_I(\zeta, \omega; \theta, \psi) = \frac{\partial B_\nu[\overline{T}(1)]}{\partial T} \zeta^{-i\omega a\,\mathrm{tg}\,\theta\,\cos\psi} \exp\left[-w_0 \sec\theta \int_\zeta^1 k_\nu(t)\, q(t)\, dt\right] -$$
$$-\int_\zeta^1 \frac{\partial B_\nu[\overline{T}(t)]}{\partial T}\left(\frac{t}{\zeta}\right)^{i\omega a\,\mathrm{tg}\,\theta\,\cos\psi} \frac{\partial}{\partial t}\exp\times \qquad (5.11)$$
$$\times \left[-w_0 \sec\theta \int_\zeta^t k_\nu(t_1)\, q(t_1)\, dt_1\right] dt$$

the frequency characteristic of the atmospheric transfer function. Here the atmosphere is regarded as a dynamic system at whose input there is a random signal T' with spectral density $S_T(\omega)|$, and at whose output there is a transformed signal $I'_\nu|$ with spectral density $S_I(\zeta, \omega; \theta, \psi).|$

In the relation between $S_T(\omega)$ and $S_F^{(n)}(\zeta, \omega) = |\overline{\Phi_n(\zeta, \omega)}|^2|$, obtained from Equation (5.9), the frequency characteristic of the transfer function will have the form

$$A_F^{(n)}(\zeta, \omega) = \frac{\partial B_\nu[\overline{T}(1)]}{\partial T} \Psi_{n+2}\left[w_0 \int_\zeta^1 k_\nu(t)\, q(t)\, dt, \ \omega a \ln\frac{1}{\zeta}\right] -$$
$$-\int_\zeta^1 \frac{\partial B_\nu[\overline{T}(t)]}{\partial T} \frac{\partial}{\partial u} \Psi_{n+2}\left[w_0 \int_\zeta^t k_\nu(t_1)\, q(t_1)\, dt_1, \ \omega a \ln\frac{t}{\zeta}\right] dt. \qquad (5.12)$$

We note that similar expressions can be obtained even in cases where the atmospheric transmission is described by functions other than the exponential (other transcendental functions are then obtained in lieu of Ψ_{nj}).

The exponential functions in Equation (5.11) or the function Ψ_n in Equation (5.12) describe the effect of transformation of temperature variations by the atmosphere (in the case of Equation (5.12) it is by an instrument of finite aperture), including filtering out of small-scale nonuniformities. Using the properties of the functions $\Psi_n(u, v)$ (see § 7 of Chapter 1), it is not difficult to determine the qualitative nature of this transformation and filtering. For example, it follows from Equation (5.12) that, as the first argument of the function $\Psi_n(u, v)$ increases, i.e., with increase in the absorption coefficient k_ν, or of concentration of absorbing material $q(\zeta)$ (other conditions remaining unchanged), the amplitude of the dispersion of the random variations F' will be reduced.

An increase in the index n of the function Ψ_n, associated /167 with a decrease in the field of view of the instrument, leads to an increased effect of filtering of small-scale irregularities. The second argument v of the function $\psi_n(u, v)$ describes the effect of ratios of the geometric scales of irregularities and of the height of the observer ζ on the transformation of the frequency spectrum of the temperature field.

We give some examples to illustrate the effect of different parameters of the atmosphere and the instrument on the frequency characteristic of the transfer function. To this end, we perform the calculation for the limiting simple case where the temperature variations T' at the points ξ separated by a distance r are very weakly correlated, i.e., the correlation function $K_{TT}(r)$ degenerates to the delta function $\delta(r)$, and the spectral density

283
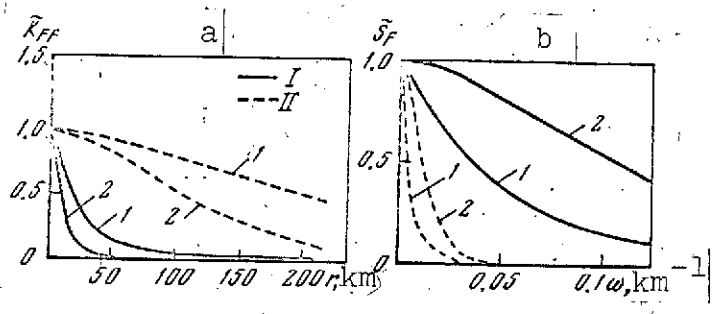
Figure 5.1. Correlation functions $K_{FF}(r)$ and spectral densities $\tilde{S}_F(\omega)$ for wide-angle instruments.
I- $a \ln(1/\zeta) = 10$; II- $a \ln(1/\zeta) = 1$; 1- $m = 0$; 2- $m = 2$

degenerates to the "white noise" $S_T \equiv$ const. Figure 5.1 shows

the transformation of a correlation function of type $K_{TT}(r) = \delta(r)$

(a), and of the corresponding spectral density $S_T(\omega)$ (solid lines)

of the temperature field due to the instrument function of wide-

angle radiometers (b). The calculations of $\tilde{S}_F$ and $\tilde{K}_{FF}$ were made

using Equations (5.16) and (5.17) for m = 0 and m = 2 (curves 1

and 2 respectively) for values of the parameters $a \ln(1/\zeta) = 1$

(broken lines) and $a \ln(1/\zeta) = 10$ (broken lines with points).

We shall also consider the atmosphere to be an absolutely

transparent medium $(k_\nu \equiv 0)$. Then

$$A_\nu(\zeta,\, \omega;\, \theta,\, \psi) = \frac{\partial B_\nu\, [\bar{T}\,(1)]}{\partial T}\, \zeta^{-i\omega a\, \mathrm{tg}\, \theta\, \cos\, \varphi}; \qquad (5.13)$$

$$A_F^{(n)}(\zeta,\, \omega) = 2\pi\, \frac{\partial B_\nu\, [\bar{T}\,(1)]}{\partial T}\, \Psi_{n+2}\left(0,\, \omega a \ln\frac{1}{\zeta}\right). \qquad (5.14)$$

It follows from Equations (5.13) and (5.14) that the variations

in the intensity of radiation I'_ν in a given direction $(\theta,\, \psi)$ remain

"white noise" with a certain changed amplitude, while F'_n will

have an appreciable different nature. In fact, taking into account

284

the property of the functions $\Psi_n(u, v)$ (see § 7 of Chapter 1):

$$\Psi_{n+2}(0, v) = \frac{v^{\frac{n+1}{2}}}{\Gamma\left(\frac{n+3}{2}\right)} K_{\frac{n+1}{2}}(v),$$

where $K_{(n+1)/2}(v)$ is a MacDonald function, we can obtain the rather simple expressions for $A_F^{(2m)}$ even for n = 2m:

$$A_F^{(2m)} = 2\pi \frac{\partial B_\nu [\bar{T}(1)]}{\partial T} \frac{\sqrt{2}}{(2m+1)!!} \zeta^{\omega a} \sum_{k=0}^{m} \frac{(2m+k)!}{k!(m+k)!} \left(2\omega a \ln \frac{1}{\zeta}\right)^{m-k}, \qquad (5.15)$$

which allow us to determine the correlation function in analytical /168 form. In particular, for m = 0, 1, and 2, from Equation (5.15) we obtain:

$$S_F^{(0)}(\zeta, \omega) = 2S_T \left\{\frac{\partial B_\nu [\bar{T}(1)]}{\partial T}\right\}^2 \zeta^{2a|\omega|};$$

$$S_F^{(2)}(\zeta, \omega) = \frac{8}{9} S_T \left\{\frac{\partial B_\nu [\bar{T}(1)]}{\partial T}\right\}^2 \zeta^{2a|\omega|} \left[1 + |\omega| a \ln \frac{1}{\zeta}\right]^2; \qquad (5.16)$$

$$S_F^{(4)}(\zeta, \omega) = \frac{32}{25} S_T \left\{\frac{\partial B_\nu [\bar{T}(1)]}{\partial T}\right\}^2 \zeta^{2a|\omega|} \left[1 + |\omega| a \ln \frac{1}{\zeta} + \frac{1}{3} \left(|\omega| a \ln \frac{1}{\zeta}\right)^2\right]^2.$$

The corresponding correlation functions

$$K_{FF}^{(2m)}(r) = \int_{-\infty}^{+\infty} S_F^{(m)}(\zeta, \omega) e^{-i\omega r} d\omega$$

will have the form

$$K_{FF}^{(2)}(\zeta, r) = 4S_T \left\{\frac{\partial B_\nu [\bar{T}(1)]}{\partial T}\right\}^2 \frac{2a \ln \frac{1}{\zeta}}{\left(2a \ln \frac{1}{\zeta}\right)^2 + r^2};$$

$$K_{FF}^{(0)}(\zeta, r) = \frac{16}{9} S_T \left\{\frac{\partial B_\nu [\bar{T}(1)]}{\partial T}\right\}^2 \frac{\left(a \ln \frac{1}{\zeta}\right)^3 \left[20 \left(a \ln \frac{1}{\zeta}\right)^2 + r^2\right]}{\left[\left(2a \ln \frac{1}{\zeta}\right)^2 + r^2\right]^3}. \qquad (5.17)$$

The normalized functions $\tilde{K}_{FF}(\zeta, r) = K_{FF}(\zeta, r) / K_{FF}(\zeta, 0)$; $\tilde{S}_F(\zeta, \omega) = $
$= S_F(\zeta, \omega) / S_F(\zeta, 0)$ for m = 0 and 1 are shown in Figure 5.1. It is easy to see that, as a result of averaging over directions for a spherical detector (m = 0), the radiation characteristics will be correlated at quite a large distance r, in spite of the absence of temperature correlation. The correlation radius R_0 defined from the condition

$$R_0 = 2 \int_0^\infty \tilde{K}(\zeta, r)\, dr, \qquad (5.18)$$

depends on the parameters a and ζ. For ζ = 1 or a = 0, it follows from Equations (5.17) and (5.18) that R_0 = 0, but the radius of correlation increases with decrease of ζ or increase of a. In fact, for a spherical detector we have $\dot{R}_0 = 2\,\pi a \ln\,(1/\zeta)$. For example, for a = 1 (L = H ≈ 8 km) and $\ln\,(1/\zeta) = 10$ (the height of the top boundaries of the atmosphere is 80 km), R_0 = 63, which corresponds in absolute units to the value ~500 km. Taking into account the fact that the parameter a ln (1/ζ) = z/L, the radius of correlation in this case is proportional to the ratio between the height and the scale of the horizontal nonuniformity.

In the case of odd n, the function $K_{(n+1)/2}(v)$ will not have as simple a form as Equation (5.15). For example, for n = 1, which corresponds to the structure of the radiative fluxes obtained by means of a wide-angle plane detector:

$$A_F^{(1)}(\zeta, \omega) = \frac{\partial B_\nu\,[\bar{T}\,(1)]}{\partial T}\,\omega a \ln \frac{1}{\zeta} K_1\left(\omega a \ln \frac{1}{\zeta}\right).$$

Using tables for the MacDonald function K_1, we can construct the frequency function $A_F^{(1)}$ and the corresponding correlation function $K_{FF}^{(1)}(\zeta, r)$, and distortion in the structure of the radiation fields will be significant as before, although less than in the case of a spherical detector.

286

With further increase in n, i.e., with decrease of the field of view of the instrument, the spectral density will approximate to a constant, the correlation function to a δ-function, while the radius of correlation $R_0 \to 0$.

We note, however, that for the very small angles of view of /169 the measuring instruments frequently used in practice, the approximation for the angular sensitivity $\varkappa_n(\theta)$ by Equation (5.6) is inappropriate, since for large n, expressions of type (5.15) become extremely cumbersome. Examples of specific narrow-angle radiometers, for example the instrument for measuring the Earth's self-radiation in the transparent window, used on the satellite Kosmos 149 [16], show that the angular sensitivity $\varkappa(\theta)$ can be approximated by the exponential function

$$\varkappa(\theta) = e^{-\varkappa_0\theta} \qquad (5.19)$$

with very large values of the exponent $\varkappa_0$ (in the case of the radiometer of [16] $\varkappa_0 = 25 \, \text{rad}^{-1}$).

Substituting Equation (5.19) in place of $\varkappa_n(\theta)$ in Equation (5.8), and integrating with respect to the azimuth ψ, we obtain:*

$$
\begin{aligned}
\Phi_0(\zeta, \omega) = {} & 2\pi \frac{\partial B_\nu[\overline{T}(1)]}{\partial T} \rho(1, \omega) \int_0^{\frac{\pi}{2}} J_0\left(\omega a \, \mathrm{tg}\, \theta \ln \frac{1}{\zeta}\right) \times \\
& \times \exp\left[-w_0 \sec\theta \int_\zeta^1 k_\nu(t)\, q(t)\, dt\right] e^{-\varkappa_0\theta} \cos\theta \sin\theta \, d\theta - \\
& - 2\pi \int_\zeta^1 \frac{\partial B_\nu[\overline{T}(t)]}{\partial T} \rho(t, \omega) \int_0^{\frac{\pi}{2}} J\left(\omega a \, \mathrm{tg}\, \theta \ln \frac{t}{\zeta}\right) e^{-\varkappa_0\theta} \times \\
& \times \cos\theta \sin\theta \, d\left\{\exp\left[-w_0 \sec\theta \int_\zeta^t k_\nu(t_1)\, q(t_1)\, dt_1\right]\right\} d\theta.
\end{aligned}
\qquad (5.20)
$$

* Here we have in mind that the optical axis of the instrument is oriented along the local vertical.

It is easy to see that for large values of $\varkappa_0$ the integrals of the type

$$G(u, v) = \int_0^{\frac{\pi}{2}} J_0(v\,\mathrm{tg}\,\theta)\, e^{-u\sec\theta} e^{-\varkappa_0\theta} \cos\theta \sin\theta\, d\theta \qquad (5.21)$$

practically do not change their values, if we put $\sec\theta \approx \cos\theta \approx 1$; $\mathrm{tg}\,\theta \approx \sin\theta \approx \theta$. In fact, for sufficiently large values of θ like these, for which the last approximation involves large errors, the integrand in Equation (5.21) simply becomes very small because of the rapid decrease in the function $e^{-\varkappa_0\theta}$. In this case we have, to a high degree of accuracy,

$$G(u, v) = e^{-u} \int_0^{\frac{\pi}{2}} J_0(v\theta)\, e^{-\varkappa_0\theta}\theta\, d\theta = \frac{\varkappa_0 e^{-u}}{(\varkappa_0^2 + v^2)^{3/2}} \qquad (\varkappa_0 \gg 1). \qquad (5.22)$$

Therefore,

$$\Phi_0(\zeta, \omega) = 2\pi \frac{\partial B_\nu[\overline{T}(1)]}{\partial T}\, \rho(1, \omega) \frac{\varkappa_0 \exp\left[-w_0 \int_\zeta^1 k_\nu(t)\, q(t)\, dt\right]}{\left[\varkappa_0^2 + \left(\omega a \ln\frac{1}{\zeta}\right)^2\right]^{3/2}} -$$

$$- 2\pi \int_\zeta^1 \frac{\partial B_\nu[\overline{T}(t)]}{\partial T}\, \rho(t, \omega) \frac{\varkappa_0 \frac{\partial}{\partial t} \exp\left[-w_0 \int_\zeta^t k_\nu(t_1)\, q(t_1)\, dt_1\right] dt}{\left[\varkappa_0^2 + \left(\omega a \ln\frac{1}{\zeta}\right)^2\right]^{3/2}}. \qquad (5.23)$$

For a homogeneous random temperature field, the frequency characteristic of the transfer function for the atmosphere plus narrow-angle instrument system, Equation (5.19) will take the following form:

$$A_0(\zeta, \omega) = 2\pi \frac{\partial B_\nu[\overline{T}(1)]}{\partial T} \frac{\varkappa_0 \exp\left[-w_0 \int_\zeta^1 k_\nu(t)\, q(t)\, dt\right]}{\left[\varkappa_0^2 + \left(\omega a \ln\frac{1}{\zeta}\right)^2\right]^{3/2}} -$$

$$- 2\pi \int_\zeta^1 \frac{\partial B_\nu[\overline{T}(t)]}{\partial T} \frac{\varkappa_0 \frac{\partial}{\partial t} \exp\left[-w_0 \int_\zeta^t k_\nu(t_1)\, q(t_1)\, dt_1\right] dt}{\left[\varkappa_0^2 + \left(\omega a \ln\frac{1}{\zeta}\right)^2\right]^{3/2}}. \qquad (5.24)$$
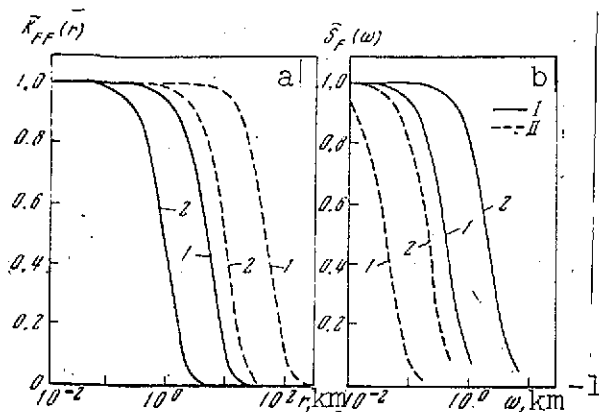
Figure 5.2. Correlation functions $\tilde{K}_{FF}(r)$ and spectral densities $\tilde{S}_F(\omega)$ for narrow-angle instruments:
I-a ln $(1/\zeta)$ = 1; II-a ln $(1/\zeta)$ = 10; 1- κ_0 = 5; 2- κ_0 = 25

If, as before, we consider the atmosphere to be transparent $(k_v \equiv 0)$, then

$$A_0(\zeta, \omega) = 2\pi \frac{\partial B_v[\bar{T}(1)]}{\partial T} \frac{\varkappa_0}{\left[\varkappa_0^2 + \left(\omega a \ln \frac{1}{\zeta}\right)^2\right]^{3/2}} \quad (5.25)$$

describes, to within a constant factor, the transformation of the spectral density of the temperature field due to spatial averaging, caused by the angular sensitivity of the radiometer. It is not difficult to see from Equation (5.25) that a narrow-angle instrument will distort only the high-frequency component of the temperature field. From Equation (5.25), we can obtain an expression for transformation of the correlation function $\delta(r)$, due to the angular sensitivity of the radiometer. In fact, for the transformed correlation function we have

$$K_0(r) = \frac{\pi \varkappa_0}{64 a \ln(1/\zeta)} \exp\left(-\frac{\varkappa_0 r}{a \ln(1/\zeta)}\right)\left[1 + \frac{\varkappa_0 r}{a \ln(1/\zeta)} + \frac{1}{3}\left(\frac{\varkappa_0 r}{a \ln(1/\zeta)}\right)^2\right]. \quad (5.26)$$

Examples of normalized functions $\tilde{S}_0(\omega)$ and $\tilde{K}_0(r)$, calculated from Equations (5.25) and (5.26) for the radiometer used on the Kosmos 149 satellite, are shown in Figure 5.2.* The radius of correlation, calculated from Equation (5.26), is related to the parameters $\varkappa_0$ and $\ln(1/\zeta)$ by the expression

---

* The figure shows a transformation similar to that of Figure 5.1, for a narrow-angle instrument with equipment function (5.19): $\tilde{K}_{FF}(r)(a)$ and $\bar{S}_F(\omega)(b)$. The calculations were made using Equations (5.25) and (5.26) for κ_0 = 5 and 25 rad^{-1} (curves 1 and 2, respectively) for $a \ln(1/\zeta) = 1$(broken line) and $a \ln(1/\zeta) = 10$(broken line with point).

289

$$R_0 = \frac{8a \ln (1/\zeta)}{3\varkappa_0}.$$

Thus, the expressions obtained enable us, comparatively
simply, to evaluate the structural characteristics of the
temperature field, as smoothed due to geometrical averaging.
However, as Equations (5.12) or (5.24) indicate, it is not
difficult to take into account variations in atmospheric emission,
although we will not obtain simple analytical expressions as yet,
apart perhaps, from the atmospheric transparent window. In the
latter case, geometric smoothing will play the main part.
Therefore, we can use equations of type (5.25) in transferring
from the spectral density $S_F(\omega)$, obtained directly from measure-
ments of the radiative flux, to the spectral density $S_F(\omega)$ of the
temperature field, undistorted by the instrument function

$$S_T(\omega) = \frac{S_F(\zeta, \omega)}{A_0(\zeta, \omega)},$$

and thereby improve the $S_T(\omega)$ spectrum in the large ω region.

The distortion of the characteristics of the spatial struc-
ture of radiation fields due to the equipment function of a
narrow-angle instrument will increase if there is deviation of
the optical axis of the instrument from the vertical. A method
of calculating these distortions relative to variations in the
albedo of the underlying surface was considered by Drobyshevich
[17]. Naturally, the problem reduces to solving a two-dimensional
Fredholm equation of the first kind, i.e., it is incorrect.
Using the fact that the kernal of an equation of the type (5.19)
is close to singular, the author of [17] reduced this equation
to a differential equation for a one-dimensional form for which
encouraging numerical experiments were made in [17] to establish
the variations in albedo from smoothed functions with random

290

errors superimposed. This method can also be applied to determine the structural characteristics of the fields of Earth self-radiation and of reflected solar radiation, from the numerous experimental data obtained by means of Kosmos 149 and Kosmos 243 [13].

The above assumption regarding the homogeneity of random fields, which is the basis for relations of type (5.10) – (5.12), is justified best when one considers a region of relative transparency of the atmosphere under stratified cloud conditions. In this case, the variations of the radiation field are determined mainly by the emission of the upper boundary of the clouds whose temperature can be regarded as homogeneous and isotropic random function. Therefore, we must consider the question of the dependence of the structure of the cloud long-wave radiation cloud field.

2.3. Calculation of Cloud Structure

Variations in the Earth's radiation field, associated with changes of clouds, can be expressed, for long-wave radiation, in terms of variations of the upper boundary of the clouds p_0, the temperature $T(p_0)$, and the humidity $q_0 = q(p_0)$ at the level of this boundary.

To obtain relations between variations of these parameters and the radiative intensity, we assume that

$$p_0(\xi) = \bar{p}_0 + p_0'(\xi), \qquad \overline{p_0'(\xi)} = 0;$$
$$q_0(\xi) = \bar{q}_0 + q_0'(\xi), \qquad \overline{q_0'(\xi)} = 0,$$

(5.27)

where the bar indicates averaging throughout the whole range of ξ considered. Hence,

$$w_0(\xi) = \overline{w}_0 + w_0'(\xi);$$

$$\overline{w}_0 = \frac{\overline{p_0 q_0}}{g}; \qquad w_0'(\xi) = \frac{1}{g}[\overline{p}_0 q_0'(\xi) + \overline{q}_0 p_0'(\xi) + p_0'(\xi) q_0'(\xi)].$$

(5.28)

We shall also assume that the vertical profile of the specific humidity $q(\xi, \zeta)/q_0(\xi)$ does not depend on ξ (this assumption has no basis in principle and is only made to simplify the calculations). By substituting Equations (5.27) and (5.28) into (2.28) and the boundary condition (2.30), and separating out the characteristics which describe the average radiation regime and the random variations in the radiative intensity, we obtain, as was done above, relations to determine the statistical characteristics of the horizontal structure of the radiation field in the case of clouds. For example, for ascending radiation of frequency ν, we have the following expressions:

a)   for spatial averaging of the radiative intensity

$$
\begin{aligned}
\overline{I}_\nu(\zeta, \theta, \psi) = {}& B_\nu[\overline{T}(1)]\exp\left[-\sec\theta\left(\overline{w}_0 + \frac{\overline{q_0' p_0'}}{g}\right)\int_\zeta^1 k_\nu(t)\,q(t)\,dt\right] - \\
& - \int_\zeta^1\left\{B_\nu[\overline{T}(t)] - \frac{\overline{p}_0}{g\overline{w}_0 + \overline{q_0 p_0}}\left[\overline{q_0'(\xi)\,I_\nu'(t,\xi;\theta,\psi)} - \right.\right. \\
& - \frac{\partial B_\nu[\overline{T}(t)]}{\partial T}\overline{q_0'(\xi)\,T_0'(t,\xi)} - \frac{\overline{q}_0}{g\overline{w}_0 + \overline{q_0 p_0}}\left[\overline{p_0'(\xi)\,I_\nu'(t,\xi;\theta,\psi)} - \right. \\
& \left.\left.\left. - \frac{\partial B_\nu[\overline{T}(t)]}{\partial T}\overline{p_0'(\xi)\,T'(t,\xi)}\right]\right\}\frac{\partial}{\partial t}\times \right. \\
& \times \exp\left[-\sec\theta\left(\overline{w}_0 + \frac{\overline{q_0' p_0'}}{g}\right)\int_\zeta^t k_\nu(t_1)\,q(t_1)\,dt_1\right]dt;
\end{aligned}
$$

(5.29)

b)   for the Fourier transform

$$J_\nu(\zeta, \omega; \theta, \psi) = \frac{\partial B_\nu[\bar{T}(1)]}{\partial T} \rho(1, \omega) \zeta^{-\varkappa} \exp\left[-\bar{w}_0 \sec\theta \int_\zeta^1 k_\nu(t)\, q(t)\, dt\right] -$$

$$- \int_\zeta^1 \left\{ \frac{\partial B_\nu[\bar{T}(t)]}{\partial T} \rho(t, \omega) - \frac{I_\nu(t, 0) - B_\nu[\bar{T}(t)]}{\bar{w}_0 g} \times \right.$$

$$\times [\bar{p}_0 \sigma(1, \omega) + \bar{q}_0 \rho_0(1, \omega)] \left(\frac{t}{\zeta}\right)^\varkappa \times$$

$$\left. \times \frac{\partial}{\partial t} \exp\left[-\bar{w}_0 \sec\theta \int_\zeta^t k_\nu(t_1)\, q(t_1)\, dt_1 \right\} dt, \right.$$

(5.30)

where

$$\rho_0(1, \omega) = \int_{-\infty}^{+\infty} p_0'(\xi)\, e^{i\omega\xi}\, d\xi;$$

$$\varkappa = i\omega a\, \mathrm{tg}\,\theta \cos\psi;$$

c)   for deviation of the intensity from the mean value

$$I_\nu'(\zeta, \xi; \theta, \psi) = \frac{\partial B_\nu[\bar{T}(1)]}{\partial T} T'[1, \mu(\zeta, \xi, 1)] \exp\left[-\bar{w}_0 \sec\theta \int_\zeta^1 k_\nu(t)\, q(t)\, dt\right] -$$

$$- \int_\zeta^1 \left\{ \frac{\partial B_\nu[\bar{T}(1)]}{\partial T'} T'[t, \mu(\zeta, \xi, t)] - \frac{I_\nu(t, 0) - B_\nu(\bar{T}(t))}{\bar{w}_0 g} \times \right.$$

(5.31)

$$\times [\bar{p}_0 q_0'(1, \mu(\zeta, \xi, t)) + \bar{q}_0 p_0'(1, \mu(\zeta, \xi, t))] \right\} \frac{\partial}{\partial t} \exp\times$$

$$\times \left[-\bar{w}_0 \sec\theta \int_\zeta^t k_\nu(t_1)\, q(t_1)\, dt_1 \right] dt;$$

If these radiation characteristics are averaged over a
certain range, we can use the transmission function (2.9) to
calculate them.

The quantities $\overline{p_0' I_\nu}$; $\overline{q_0' I_\nu}$; $\overline{p_0' T'}$; $\overline{q_0' T'}$ and $\overline{p_0' q_0'}$ appear in Equation
(5.29). The first two are unknowns, but the rest can be obtained
by processing results of measurements of p_0, q_0, $q(\zeta)$, and $T(\zeta)$.
Neglecting these quantities in Equation (5.29), we can obtain a
first approximation for $I_\nu(\zeta, \theta)$ and by using this in conjunction

with Equation (5.31) we can determine I'_1. It is then not diffi-
cult to obtain an expression for $K_{II}(\zeta, \xi; \zeta_1, \xi_1; \theta, \psi)$, similar to Equation
(5.2), the only difference being that now K_{II} is expressed in

terms of the autocorrelation and joint correlation moments between
the level of the top boundary of the cloud and the atmospheric
temperature or humidity $K_{p_0 p_0}$, $K_{p_0 q_0}$, $K_{p_0 T}$, $K_{q_0 q_0}$, $K_{q_0 T}$, K_{TT}. By multiplying
Equation (5.31) by $p'_0(\zeta)$, $q'_0(\zeta)$, $T'(\zeta, \xi)$ and averaging with respect to
ξ, we obtain expressions for the joint correlation functions
$K_{p_0 T}$, $K_{q_0 T}$ and K_{TT}, analogous to Equations (5.2) and (5.3). However,
as was remarked in Chapter 3, there is as yet no information on
the characteristics of the spatial structure of clouds, nor on
the temperature and humidity fields above clouds. Therefore, we
shall not consider in detail here the behavior of the structural
characteristics of the radiation field above clouds, since under
these simplifications, which were made in Section 2.2, the fre-
quency characteristic of the transfer function of the atmosphere-
instrument system in the "cloud" case will take the same form as
in the "cloud-free" case. As regards calculation of correlation
functions for actual fields of cloud and meteorological elements,
during calculation of atmospheric absorption and emission, and
also for arbitrary angular sensitivities of radiometers, these
calculations are as yet cumbersome, although they can certainly
be performed using contemporary computers.

§ 3.   Structure of the Reflected Solar Radiation Field

The spatial structure of the field of reflected solar radi-
ation is determined mainly by the horizontal nonuniformity of
the underlying surface and the cloud cover.

Considering the complexity of the transfer process for solar
radiation in clouds, it is desirable (at least in the first
phase of the solution of this problem) to consider clouds as a

reflecting surface with a given brightness coefficient or albedo. The characteristics of the reflectance of clouds or of the underlying surface, being random functions of the horizontal coordinates, allow us to describe the spatial structure of the cloud fields or of natural surfaces. Therefore, we must consider the problem of the relationship between the structural characteristics of the albedo of reflecting surfaces and the intensity or flux of reflected solar radiation, by assuming that the atmosphere above the surfaces is horizontally uniform.* By using the relations thus established and, having determined the intensities of radiation from measurements, regarded as random functions of the horizontal coordinates, the statistical characteristics of the spatial structure of the radiation field, we can find similar characteristics for the albedo of the underlying surface or the clouds and thus describe the spatial structure of these objects.

For simplicity, we consider the case when the albedo is a random function of only a single horizontal coordinate and that the atmopshere scatters isotropically. Then we can use the /174 results from the solution of the two-dimensional radiative transfer equation, obtained in § 7 of Chapter 1, with some slight transformations.

We base our study on the system of equations in boundary conditions (1.52) - (1.55) for the two-dimensional case $(\partial I/\partial \eta \equiv 0)$, and set

$$I(\tau, \xi; \theta, \psi) = I(\tau; \theta, \psi) + I'(\tau, \xi; \theta, \psi); \qquad (5.32)$$

---

* This assumption was made only to simplify the problem. A calculation of the horizontal nonuniformity of the atmosphere is associated with the three-dimensional variations of the scattering coefficient or index, and also the concentration of moisture, and does not present difficulties in principle, but there are no appropriate empirical data as yet.

$$A(\xi) = \bar{A} + A'(\xi); \qquad (5.33)$$

$$G(\tau, \xi) = \bar{G}(\tau) + G'(\tau, \xi), \qquad (5.34)$$

where the bar denotes averaging over some range of ξ, and the primes denote deviation from the mean intensity. By substituting Equations (5.31) - (5.34) into Equations (1.52) - (1.55) and separating the equations for I and $\bar{I}'$, we obtain

$$- \cos\theta \frac{\partial I^{\uparrow}}{\partial \tau} = \bar{G}(\tau) - \bar{I}^{\uparrow}(\tau; \theta, \psi); \qquad (5.35)$$

$$- \cos\theta \frac{\partial I^{\downarrow}}{\partial \tau} = \bar{G}(\tau) - \bar{I}^{\downarrow}(\tau; \theta, \psi); \qquad (5.36)$$

$$\bar{G}(\tau) = \frac{S}{4} \exp\left[-(\tau^* - \tau)\sec\zeta\right] + \frac{1}{4\pi} \int [\bar{I}^{\uparrow}(\tau; \theta, \psi) + \bar{I}^{\downarrow}(\tau; \theta, \psi)] \, d\omega; \qquad (5.37)$$

$$\bar{I}^{\uparrow}(0; \theta, \psi) = \frac{\bar{A}}{\pi}\left[\pi S e^{-\tau^* \sec\zeta}\cos\zeta\right] +$$

$$+ \int [\bar{I}^{\downarrow}(0, 0, \psi) + \overline{A'(\xi)\,I'^{\downarrow}(0, \xi; 0, \psi)}]\cos\theta \, d\omega; \qquad (5.38)$$

$$\bar{I}^{\downarrow}(\tau^*; \theta, \psi) = 0. \qquad (5.39)$$

If, in Equation (5.38), we neglect the correlation moment $K_{AI} = $ $= \overline{A'(\xi)\,I'^{\downarrow}(0, \xi; \theta, \psi)}$, then, to determine $\bar{I}$ and $\bar{G}$, we obtain relations which coincide completely with Equations (4.64) - (4.67) for the mean albedo $\bar{A}$.

To determine I' and G', we obtain the following system of equations (neglecting second order moments, as before):

$$\cos\theta \frac{\partial I'^{\uparrow}}{\partial\tau} + \frac{\sin\theta\sin\psi}{a(\tau)} \frac{\partial I'^{\uparrow}}{\partial\xi} = G'(\tau, \xi) - I'^{\uparrow}(\tau, \xi; \theta, \psi); \qquad (5.40)$$

$$-\cos\theta \frac{\partial I'^{\downarrow}}{\partial\tau} + \frac{\sin\theta\sin\psi}{a(\tau)} \frac{\partial I'^{\downarrow}}{\partial\xi} = G'(\tau, \xi) - I'^{\downarrow}(\tau, \xi; \theta, \psi); \qquad (5.41)$$

$$G'(\tau, \xi) = \frac{1}{4\pi} \int [I'^{\downarrow}(\tau, \xi; \theta, \psi) + I'^{\uparrow}(\tau, \xi; \theta, \psi)] \, d\omega; \qquad (5.42)$$

$$I'^{\uparrow}_{v}(0, \xi; \theta, \psi) = \frac{A'(\xi)}{\pi} \left[\pi S e^{-\tau^* \sec\zeta} \cos\zeta + \int I'^{\downarrow}(0, \theta) \cos\theta \, d\omega + \right. $$
$$\left. + \frac{A}{\pi} \int I'^{\downarrow}(0, \xi; \theta, \psi) \cos\theta \, d\omega; \right. \qquad (5.43)$$

$$I'^{\downarrow}(\tau^*, \xi; \theta, \psi) = 0. \qquad (5.44)$$

Further, we write the system of equations (5.40) - (5.44) for the Fourier transforms:

$$J(\tau, k; \theta, \psi) = \frac{1}{2\pi} \int_{-\infty}^{+\infty} I'(\tau, \xi; \theta, \psi) e^{ik\xi} \, d\xi; \qquad g(\tau, k) = \int_{-\infty}^{+\infty} G(\tau, \xi) e^{ik\xi} \, d\xi; \qquad (5.45)$$
$$\cos\theta \frac{\partial J^{\uparrow}}{\partial\tau} + J^{\uparrow} \left[1 - ik \frac{\sin\theta\sin\psi}{a(\tau)} \right] = g(\tau, k);$$

$$-\cos\theta \frac{\partial J^{\downarrow}}{\partial\tau} + J^{\downarrow} \left[1 - ik \frac{\sin\theta\sin\psi}{a(\tau)} \right] = g(\tau, k); \qquad (5.46)$$

$$g(\tau, k) = \frac{1}{4\pi} \int [J^{\uparrow}(\tau, k; \theta, \psi) + J^{\downarrow}(\tau, k; \theta, \psi)]\, d\omega; \tag{5.47}$$

$$J^{\uparrow}(0, k; \theta, \psi) = \frac{Q(k)}{\pi}[\pi S e^{-\tau^* \sec \zeta}\cos \zeta + F_0^{\downarrow}] + \frac{\bar{A}}{\pi}\int J^{\downarrow}(0, k; \theta, \psi)\cos\theta\, d\omega; \tag{5.48}$$

$$J^{\downarrow}(\tau^*, k; \theta, \psi) = 0. \tag{5.49}$$

Here, k is the wave number,

$$F_0^{\downarrow} = \int I^{\downarrow}(0, \theta)\cos\theta\, d\omega - \tag{5.50}$$

is the flux of incident radiation (the Earth illumination) corresponding to the mean value of albedo:

$$Q(k) = \int_{-\infty}^{+\infty} A'(\xi)\, e^{ik\xi}\, d\xi.$$

The solution of the system (5.45) - (5.49) has the form:

$$J^{\uparrow}(\tau, k; \theta, \varphi) = J_0(k)\exp\left[-\tau\sec\theta - \frac{ik}{a_0}\ln\left(1 - \frac{\tau}{\tau^*}\right)\operatorname{tg}\theta\sin\psi\right] +$$
$$+ \sec\theta \int_0^{\tau} g(t, k)\exp\left[-(\tau - t)\sec\theta - \frac{ik}{a_0}\operatorname{tg}\theta\sin\psi\ln\frac{\tau^* - \tau}{\tau^* - t}\right]dt; \tag{5.51}$$

$$J^{\downarrow}(\tau, k; \theta, \psi) = \sec\theta \int_{\tau}^{\tau^*} g(t, k)\exp\left[-(t - \tau)\sec\theta - \frac{ik}{a_0}\operatorname{tg}\theta\sin\psi\ln\frac{\tau^* - \tau}{\tau^* - t}\right]dt,$$

where

$$J_0(k) = \frac{F_0^{\downarrow}}{\pi} Q(k) + 2\bar{A}\int_0^{\tau^*}\Psi_2\left(t, \frac{k}{a_0}\ln\frac{\tau^*}{\tau^* - t}\right)g(t, k)\, dt. \tag{5.52}$$

In the derivation of Equations (5.50) - (5.52), it was assumed that $a(\tau) = a_0(\tau^* - \tau)$, i.e., the scattering coefficient decreases exponentially with height.

298

For the transform of the source function, we obtain the
following equation:

$$g(\tau, k) = \frac{J_0(k)}{2} \Psi_2\left[\tau, \frac{k}{a_0} \ln\left(1 - \frac{\tau}{\tau^*}\right)\right] +$$
$$+ \frac{1}{2} \int_0^{\tau^*} \Psi_1\left[|\tau - t|, \frac{k}{a_0} \ln\frac{\tau^* - \tau}{\tau^* - t}\right] g(t, k) dt. \qquad (5.53)$$

The transcendental functions $\Psi_n(u, v)$ were determined in
§ 7 of Chapter 1.

Writing the solution of Equation (5.53) in the form

$$g(\tau, k) = c(k) g_0(\tau, k),$$

we can reduce solution of this problem to determination of the
determinant function $g_0(\tau, k)$ from the equation

$$g_0(\tau, k) = \frac{1}{2} \Psi_2\left[\tau, \frac{k}{a_0} \ln\left(1 - \frac{\tau}{\tau^*}\right)\right] +$$
$$+ \frac{1}{2} \int_0^{\tau^*} \Psi_1\left[|\tau - t|, \frac{k}{a_0} \ln\frac{\tau^* - \tau}{\tau^* - t}\right] g_0(t, k) dt \qquad (5.54)$$

and the random function c(k) from the relation $\underline{/176}$

$$c(k) = \frac{\frac{1}{\pi} F_0^i Q(k)}{1 - 2\bar{A} \int_0^{\tau^*} g_0(t, k) \Psi_2\left(t, \frac{k}{a_0} \ln\frac{\tau^*}{\tau^* - t}\right) dt}. \qquad (5.55)$$

Thus, transofrmation of the random variations of the albedo of
the reflecting surface in a scattering atmosphere is described by
the function $g_0(\tau, k)$ or its integrals. By determining this
function from Equation (5.54), we can find all the remaining
statistical characteristics of the field of reflected solar
radiation, by using the inverse transformation

$$I'(\tau, \xi; \ \theta, \psi) = \frac{1}{2\pi} \int\limits^{+\infty} J(\tau, k; 0, \psi) e^{i\xi k}\, dk.$$

These characteristics take their simplest form when the albedo of the reflecting surface is a homogeneous and isotropic random function. In fact, then we obtain simple relations between the spherical density of the albedo

$$S_A(k) = \overline{|Q(k)|^2}$$

and the spectral density of the intensity of reflected radiation

$$S_I(\tau, k) = \overline{|J(\tau, k)|^2}$$

or the source function

$$S_G(\tau, k) = \overline{|g(\tau, k)|^2}.$$

Since it follows from Equations (5.52) and (5.55) that $J_0(k) = c(k)$, then

$$S_G(\tau, k) = S_A(k)\, A_G^2(\tau, k), \tag{5.56}$$

where A_G is the directionally-averaged frequency characteristic of the atmosphere

$$A_G(\tau, k) = \frac{\frac{1}{\pi} F_0^{\downarrow} g_0(\tau, k)}{1 - 2\bar{A} \int\limits_0^{\tau^*} g_0(t, k) \Psi_2\left(t, \frac{k}{a_0} \ln \frac{\tau^*}{\tau^* - t}\right) dt}. \tag{5.57}$$

A similar relation is obtained for the frequency characteristic of the atmosphere in a given direction (θ, ψ) :

$$A_I(\tau, k; \theta, \psi) = \frac{\frac{F_0^{\downarrow}}{\pi} \left| \exp\left[-\tau \sec\theta - \frac{ik}{a_0} \operatorname{tg}\theta \sin\psi \ln\left(1 - \frac{\tau}{\tau^*}\right)\right]\right|}{1 - 2\bar{A} \int\limits_0^{\tau^*} g_0(t, k) \Psi_2\left(t, \frac{k}{a_0} \ln \frac{\tau^*}{\tau^* - t}\right) dt} + $$
$$+ \sec\theta \int\limits_0^{\tau} g(t, k) \exp\left[-(\tau - t)\sec\theta - \frac{ik}{a_0} \operatorname{tg}\theta \sin\psi \ln \frac{\tau^* - \tau}{\tau^* - t}\right] dt. \tag{5.58}$$

300

Expressions (5.53), (5.57), and (5.58) allow us to calculate
the frequency characteristics comparatively simply, if we know
the optical parameters of the atmosphere and the mean albedo of
the reflecting surface. This, in turn, allows us to determine
the spectral density of the albedo of the reflecting surface,
i.e., the characteristic of the spatial structure of the latter
(in particular, of the cloud), from the spectral densities of the
intensity of reflected radiation $S_I(k)$ or of the mean intensity /177

$S_G(k)$, obtained by statistical reduction of the experimental data.
As can be seen from Equations (5.52), (5.54), (5.57), and (5.58),
for this purpose we need to know the average value of albedo $\bar{A}$
of the section of the Earth in question, the optical thickness of
the atmosphere τ^*, and the incident radiative flux $F_0^\downarrow$ in this
region.

During measurements of $F_0^\downarrow$ from satellites, the albedo $\bar{A}$ can
be found directly from the experiment (we note that the albedo
thus obtained will take into account the reflecting properties of
the Earth atmosphere system and, therefore, will differ somewhat
from the true albedo of the reflecting surface). As regards the
flux $F_0^\downarrow$ and the function $g(\tau, k)$, they must be calculated for
the average optical depths of the atmosphere τ^* in the region of
the spectrum under consideration.*

We have obtained relations which relate the spectral density
of the albedo $S_A(k)$ to the corresponding characteristics of the
intensity of reflected radiation $S_I(k)$ (for an infinitely narrow
field of view) or to the intensity $S_G(k)$ averaged over a hemisphere
(an omni-directional detector). Similar relations are obtained

---

* The value of $F_0^\downarrow$ cannot be determined for the relative charac-
teristics of the structure of the fields.

also for instruments with different angular resolution. If we
assume that the angular sensitivity of the measuring instrument
can be described by the formula

$$\varkappa_n(\theta) = \cos^n \theta, \tag{5.59}$$

then the spectral density for the flux of reflected radiation

$$F_n(\tau, \xi) = \int\limits_0^{2\pi} \int\limits_0^{\frac{\pi}{2}} I(\tau, \xi, \theta, \psi) \cos^n \theta \sin \theta \, d\psi$$

can be represented as follows. Just as for the case of long-wave
radiation (see § 2 of Chapter 5), the Fourier transform Φ_n for F_n
has the form:

$$\Phi_n(\tau, k) = \int\limits_0^{2\pi} \int\limits_0^{\frac{\pi}{2}} J(\tau, k; \theta, \psi) \cos^n \theta \sin \theta \, d\theta \, d\psi = J_0(k) \Psi_{n+2} \times$$

$$\times \left[\tau, \frac{k}{a_0} \ln\left(1 - \frac{\tau}{\tau^*}\right)\right] + \int\limits_0^{\tau} g(t, k) \Psi_{n+1}\left[\tau - t, \frac{k}{a_0} \ln \frac{\tau^* - \tau}{\tau^* - t}\right] dt. \tag{5.60}$$

Therefore,

$$A_F^{(n)}(\tau, k) = \frac{|\Phi_n(\tau, k)|^2}{S_A(k)} =$$

$$= \frac{\frac{F_0^{\downarrow}}{\pi} \Psi_{n+2}\left[\tau, \frac{k}{a_0} \ln\left(1 - \frac{\tau}{\tau^*}\right)\right] + \int\limits_0^{\tau} g(t, k) \Psi_{n+1}\left[\tau - t, \frac{k}{a_0} \ln \frac{\tau^* - \tau}{\tau^* - t}\right] dt}{1 - 2\bar{A} \int\limits_0^{\tau^*} g_0(t, k) \Psi_2\left[t, \frac{k}{a_0} \ln \frac{\tau^*}{\tau^* - t}\right] dt} . \tag{5.61}$$

For n = 1, from Equation (5.61), we find the frequency character-
istic of the atmosphere where the reflected radiation is measured
by a plane detector with an angular field of 2π. Thus, formulas
of type (5.57) or (5.61) describe the distortion in the structure
of the albedo of the reflecting surface arising not only from
the atmosphere, but also from the aperture of the measuring
instrument, oriented in the direction of the local vertical. If
the atmosphere is perfectly transparent $(\sigma \equiv 0)$, the frequency
characteristic describes averaging of the structure of the /178
brightness field due only to the instrument. It is not difficult

302

to show that, in this case, Equations (5.16) – (5.18), (5.25)
and (5.26) are applicable, to within a constant factor. In
particular, for angular sensitivity (5.19), from Equation
(5.61) we obtain:

$$A_F^{(0)}(k) = F_0^1 \frac{\varkappa_0}{\left[\varkappa_0^2 + \left(k\frac{z}{L}\right)^2\right]^{3/2}}$$ (5.62)

and corresponding formulas for the spectral density $S_F(k)$ and
the correlation function $K(r)$.

All the relations obtained above can be generalized compar-
atively simply to two-dimensional random fields, as follows from
Equation (1.93), with the previous assumption that the scattering
index is spherical. For an arbitrary index, the relations
between the statistical characteristics of the spatial structure
of the field of reflected solar radiation and the albedo of the
cloud become considerably complicated. A solution to this
problem was obtained by Drobyshevich [18], who assumed that all
the random fields considered were homogeneous. The basic result
of [18] is that, for a given isotropic field for the cloud
albedo, the calculated brightness field becomes nonisotropic.
The occurrence of local maxima of spectral density for $\theta \neq 0$
is attributed by the author of [18] to superposition of the plane
waves which depend on azimuth.

The determination of the statistical characteristics of the
spatial structure of the fields of reflected solar radiation
and of the Earth self-radiation from the structural characteristics
of the albedo or the cloud temperature (using the formulas given
in § 2 and §|3) can be performed perfectly using contemporary
computers, even in the most general case. However, the charac-
teristics of the spatial structure of the fields of meteorological
elements required for these calculations are very little documented,

while the characteristics of the field of the optical parameters of the atmosphere are practically unknown, mainly because of difficulty in the corresponding measurements. Therefore, the inverse problem is important, that of determining the characteristics of the spatial structure of atmospheric parameters, particularly cloud, from measurements of the radiation characteristics in selected regions of the spectrum. In particular, for study of the structure of the underlying surface or of cloud, it is natural to carry out measurements of radiation in the regions of maximum atmospheric transparency. This allows one to neglect atmospheric scattering and, in the case of investigation, of fine-scale structures, to take into account only the effects of equipmental averaging.

We can also neglect the dependence of the brightness of test objects on the angle of scattering in this case also, and can take it into account parametrically. However, when examining large-scale structure, this factor will play the main role, since for statistical analysis we must extend brightness fields (of the order of several thousands of kilometers), along which the position of the Sun and the direction of the optical axis both vary markedly. For Lambert-type surfaces, this effect is accounted for by the factor $F_0^{\downarrow}$ in Equations (5.50) or (5.62) which describe the flux of direct and scattered solar radiation which irradiates the reflecting surface. For clouds, the dependence of brightness on the scattering angle can be calculated using model calculations of the angular distribution of brightness for various positions of the Sun (see, e.g., [I.7]). However, a more reliable method for calculating this dependence is to use contemporary direct measurements of the angular behavior of the brightness of all the objects whose structure is being investigated. A calculation of this kind, for example, was performed using measurements of Earth brightness by means of scanning telephotometers (see § 5).

§ 4. Fine-Scale Structure of the Brightness of Cloud Fields

The structure of cloud fields can be studied by the methods /179
described above, by using both photometric data on the brightness
of clouds or on aerophotography of clouds, and also radiometric
data on the self-radiation of the cloud cover. A set of these
data, which permit quantitative methods of analysis, allow us to
obtain information not only on the spatial structure, but also
on such characteristics as the micro-structure and the temperature
of the clouds. A set of such measurements of radiation, obtained
using aircraft and satellites, allows us to determine the struc-
tural characteristics of irregularities of different scales.

We consider some results of determining the statistical
characteristics of the spatial structure of cloud from photo-
metric and photographic data on the brightness of the Earth and
of cloud formations.

4.1. Analysis of Airborne Photometric Data

Examples of statistical reduction of data from aircraft
measurements of reflected solar radiation, obtained for two types
of cloud (CU5 and Sci0), by means of a nonscanning radiometer P
in the wide spectral range 0.3 - 3 μm (angle of view, 5 degrees)
and a scanning photometer F in the narrow range around 0.5 μm
(angle of view, 3 degrees) have been considered in [4]. The
basic statistical characteristics of the random fields of reflected
radiation, investigated by means of these instruments, are presented
in Table 5.1. The average brightness $\bar{I}$ for both types of cloud
proves to be close, from the data of P and F instruments. This
is evidence, first that the mean values cannot be used for iden-
tifying clouds. The dispersion $D_{\bar{I}}$ or the mean square deviations
σ_I for Cu and Sc were found in [4] to differ appreciably, which

305

TABLE 5.1.   STATISTICAL CHARACTERISTICS OF RANDOM FIELDS

Type of cloud	Type of instrument	$\bar{I}$, cal/cm^{-2} min^{-1}	D_I, [cal/cm^{-2} min^{-1}]^2
Cu 5	radiometer	0.11	$0.33 \cdot 10^{-2}$
	photometer*	33	256
Sc 10	radiometer	0.12	$0.02 \cdot 10^{-2}$
	photometer*	34	38

* The values of $\bar{I}$ and D_I for the photometer were obtained in [4] in relative units.

we attribute to the presence of a large number of gaps in the cumulus cloud field. However, in averaging the radiation over the surfaces, which was performed, for example, for the measurements from a satellite by radiometers of not very high spatial resolution, there is a smoothing out of fine-scale variations of radiation characteristics. Therefore, the dispersion of brightness for corresponding scales can be close for both types of cloud, which has been observed, in particular, in processing airborne measurements of the flux of reflected solar radiation from wide-angle radiometers [4]. Therefore, we must examine the dependence of dispersion on the sizes of nonuniformities of the cloud field. This information is contained in the autocorrelation functions $K_{II}(r)$ or in the spectra $S_I(\omega)$, of which examples for both types of cloud are given in Figures 5.3 and 5.4 from radiometer data, assuming homogeneous cloud fields.

It can be seen from Figure 5.3 that $K_{II}(r)$ differs as
regards the radius of correlation R_0, determined from the condition $K_{II}(R_0)$ (R_0 = 2.5 km for Cu and 6 km for Sc). Differences also appear when we compare the functions $S(\omega)$, which are obtained in [4] by integration of Equation (3.15) of the approximation to $K_{II}(r)$ by a combination of exponential and trigonometric functions.

306
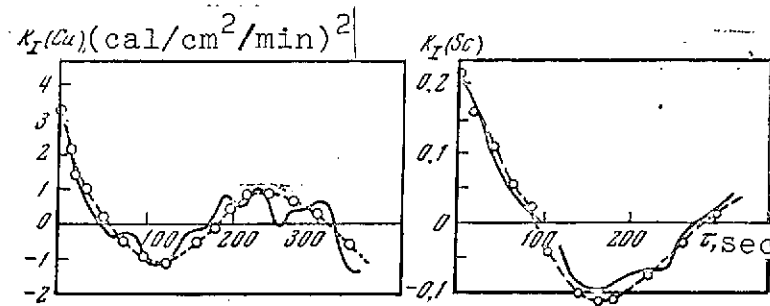
Figure 5.3. Correlation functions for brightness variations of Cu 5 and SC 10 clouds.

The broken line shows the approximation for K_I by a combination of exponential and trigonometric functions

It is easy to see from Figure 5.4 that the spatial brightness spectrum for cumulus and stratocumulus clouds contains frequencies corresponding to the periodic components of the random functions (the period in a linear scale is ~10 km for Cu and ~20 km for Sc). At these frequencies, we find the maximum values of $S_I(\omega)$, and for cumulus cloud S_I is an order of magnitude greater than the corresponding value for stratocumulus cloud.* In the low frequency region, the approximation given in [4] does not provide reliable determination of $S_I(\omega)$. In the higher frequency region, $S_I(\omega)$ has straight-line sections (on a logarithmic scale), which can be approximated by the relations

$$S_I(\omega) \sim \omega^{-k_0} \qquad (5.63)$$

(for Cu $k_0 = 1.95$, and for Sc $k_0 = 2.5$). We note that the parameter k_0 is close to the analogous values obtained in [19] for the brightness of the sky (for a blue sky $k_0 = 3$, for a turbid, cloud-free sky $k_0 = 2$, and in the case of continuous cloud, $k_0 = 1.88$).

---

* There is a misprint in [4]: all the values of $S(\omega)$ should be doubled.

307
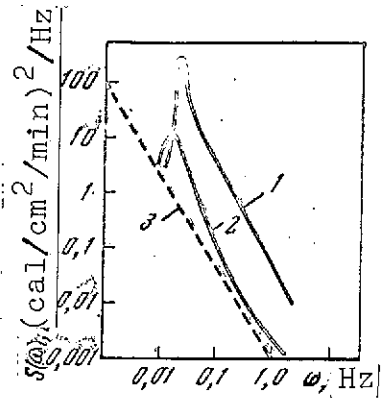
Figure 5.4. Spectral densities $S_I(\omega)$.

1- Cu 5; 2- Sc 10; the broken line shows $S(\omega) \sim \omega^{-5/3}$

Thus, the less homogeneous is the reflecting or scattering medium, the smaller is k_0, i.e., the greater is the weight of the high frequency variations in the spectral density. It is desirable to note that the frequency region for which $S_I(\omega)$ has linear portions is somewhat shifted towards low frequencies, in comparison with the similar region for the spectrum of wind-speed fluctuations [20], fluctuations of temperature [21], and of humidity [22] in the ground layer of air. As regards the frequency regions, there is nothing remarkable, since the nonuniformities of cloud fields are associated with turbulent processes of larger scale. Similar results of investigations of the structure of clouds, based on aircraft measurements of brightness, were obtained in [23].

By using a spectrum analyzer, the authors of [23] obtained empirical spectral densities for several types of cloud (Figure 5.5). Although the reliability of $S(\omega)$ is low in the high frequency region $\omega > 1$ Hz, and in the very low region $\omega \approx 0.01$ Hz (it is improbable that the instrument described in [23] could measure brightness variations over a range of four orders of magnitude with sufficient accuracy), nevertheless the maximum near $\omega = 0.1$ Hz, repeated on all the curves of $S(\omega)$ for Cu, can be considered as quite reliable. This maximum corresponds to the harmonic component of the spatial spectrum with a period of ~ 4 km. Sometimes this period also shows up in the spectrum of Sc clouds.
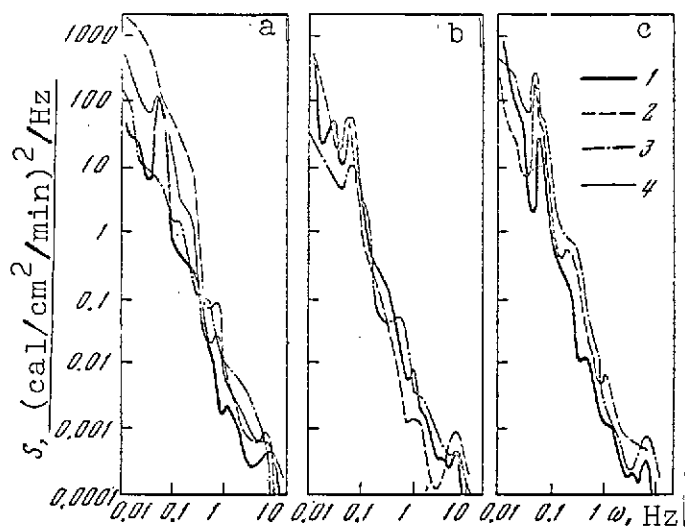
Figure 5.5. Spectral densities for variations of cloud brightness, after [23].
a: 1- Cu 4; 2- Sc 10; 3- Cu 6; 4- Sc 9; b: 1- Cu 7; 2- Sc 9; 3- Cu 7; c: 1- Cufr 4; 2- Cu 4; 3- Sc 7

The notable differences in the values of the periods obtained in [4, 23] can arise both from differences in the original measured data, due, for example, to the measurement technique, the position of the Sun, etc., and also from errors in the statistical reduction itself. No estimates were made in [4, 23] of the errors associated with the use of the theory of stationary random functions to such objects as radiometric sections of cloud brightness of comparatively short extent. The effect of the equipment function of the instrument is also not excluded.

In order to estimate in some way the reliability of the results obtained, we compare them with the results of statistical analysis of the spatial structure of the fields of cloud brightness, obtained by mircophotometry of cloud aerophotographs. The photometric sections of the photographs provide quite a high spatial resolution while allowing investigation of the homogeneous and isotropic features of the corresponding brightness fields.

4.2. Analysis of Cloud Aerophotographs

We now give some results of determination of characteristics of spatial structure obtained by Istomina [5, 6] from aircraft photographs, and by Sonechkin [7], from photographs of clouds from the space vehicles Voskhod and Voskhod 2.

Photometric data from photographs of clouds of types Cu, Sc, Sc-Ac, and Ac, giving the relative brightness $I(r)$, considered as a random function of the coordinate r, were used in [5] to determine the distribution functions for $f(I)$ and the variations $I(r)$, together with the basic moments: the mean value $\bar{I}$, the dispersion $D_I = \overline{[I(r) - \bar{I}]^2}$, and also the asymmetry $a_I = \mu_3 / \sigma_I^3$ and the excess $\varepsilon_I = \mu_4 / \sigma_I^4 - 3$, which describes the deviation from the normal distribution law (μ_3 and μ_4 are the third and fourth moments, and σ_I is the mean square deviation). Examples of the distribution functions are shown in Figure 5.6, and the parameters are given in Table 5.2. It is not difficult to see that $f(I)$ depends strongly on the cloud type. For Cu and Sc, the distribution functions (curves 1 - 3 on Figure 5.6), we have typically a wide range of brightness variations with maxima in the large brightness region, although for one type of Cu (curve 1), a bimodal distribution was obtained. For Ac and Sc-Ac (curves 4 - 6), the brightness variations are concentrated in a narrower range with maxima in the region of small I values. The increase in dispersion for Cu and Sc is explained quite simply by the presence of a large number of gaps, for which we have typically low brightness. The brightness field of Ac and Sc are more homogeneous.

As regards the ratio of the modal values of brightness of different types of cloud, it corresponds completely to the theory of solar radiative transfer in clouds, which can be considered in the visible part of the spectrum as purely scattering media. In

310
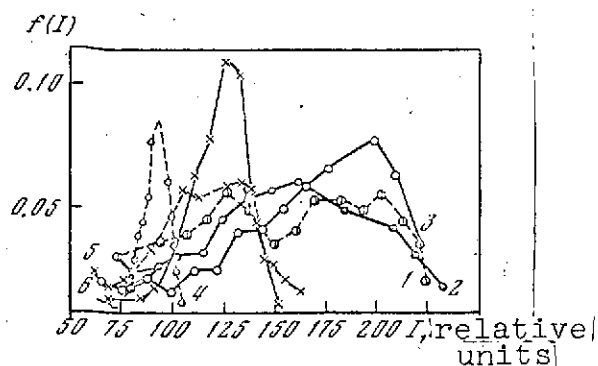
Figure 5.6. Distribution
functions f(I) for some
types of clouds.

For symbols 1 - 6, see
Table 5.2

this case, an increase in cloud thickness (e.g., cumulus) leads to an increase of I.

The figure shows that the distribution functions for I deviate from the normal law, and the asymmetry a_I is negative, i.e., the maximum in the brightness variations is always displaced towards the region of I. However, the reliability of the values of a_I, as was true for ε_I, is small, since they were calculated in [5] by integrating the empirical distribution functions f(I), and therefore, were subject to large errors,

TABLE 5.2.   STATISTICAL CHARACTERISTICS OF RANDOM FIELDS*

Type of cloud	Curve number on Figure 5.6	$\overline{I}$, relative units	D_I, relative units	% $\cdot \frac{I}{I_0}$	a_I	ε_I	R_0, km
Cu	1	87,2	2000	51	—0,14	—1,1	0,8
	2	94,6	1882	46	—0,26	—0,7	1,2
Sc	3	109,6	1510	35	—0,62	—0,6	0,5
Ac	4	46,3	134	25	—0,67	0,2	0,2
	5	60,2	591	40	—0,36	—0,5	0,48
Sc — Ac	6	66,6	252	24	—0,66	2,4	0,25

* Translator's note: Commas in numbers indicate decimal points.

The relations for brightness variations of cloud formations of different scales were described in [5, 6] by the one-dimensional correlation functions $K_{II}(r)$, constructed from photometric profiles of I(r) in different directions, assuming that the cloud brightness fields were homogeneous. Figures 5.7 and 5.8 illustrate the nonisotropic nature of the cloud fields examined in
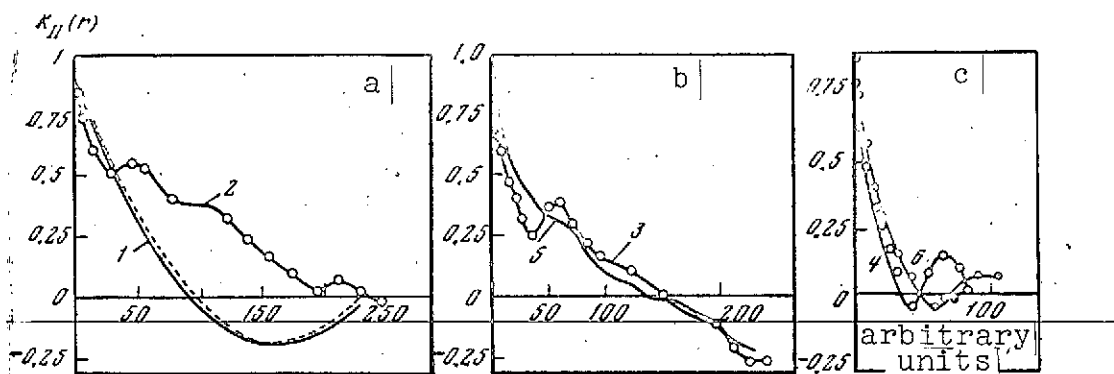
Figure 5.7. Normalized correlation functions.

1, 3, 4- sections in an arbitrary direction; 2, 5, 6- sections along the cloud bank; a- Cu; b- Sc and Sc-Ac; c- Ac and Sc-Ac; the broken line shows the approximation using Equation (5.64)

[5, 6] although in some cases of cumulus and stratified clouds /183 close correlation functions were obtained for the photometric profiles in two mutually perpendicular directions (solid lines and broken lines in Figure 5.8). An analysis of these functions confirms the conclusion drawn above as to the difference in the characteristics of the irregularities for different types of cloud in the small-scale region. For example, the radius of correlation for Cu clouds is 1.2 - 1.7 km, while for Sc and Ac it is 2.5 - 4 km. Here the periodic component appears reliably only in the structure of individual profiles of cumulus cloud brightness. References [5, 6] give examples of correlation functions which were evidence of the substantial nonuniformity of the brightness fields of certain types of cloud. Certainly there are clouds whose brightness can be considered to be a homogeneous random field.

To estimate the applicability of the hypothesis that brightness fields are homogeneous, [6] constructed autocorrelation matrices for the photometric sections considered as random vectors of the horizontal coordinate r. The components of the

312
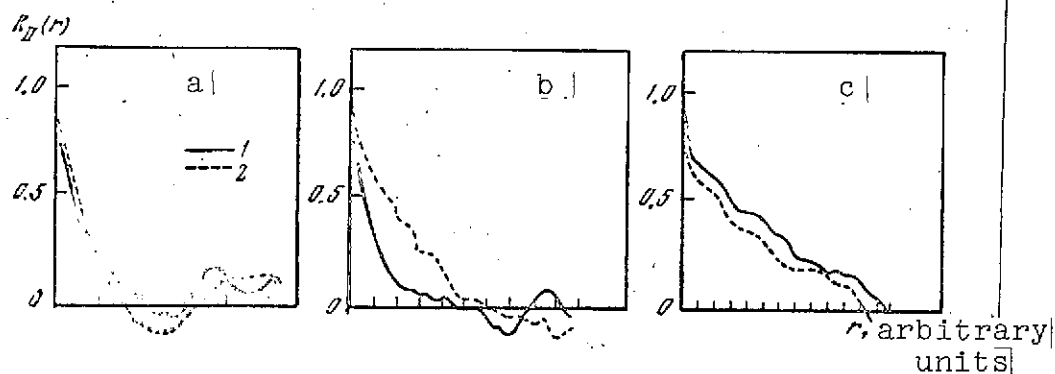
Figure 5.8. Normalized correlation functions $K_{II}(r)$ according to Equation (5.6).

a- Cu, pitch $\Delta r_1 = 0.86$ km; b- Sc, $\Delta r_2 = 0.43$ km; c- Ac, $\Delta r_3 = 0.3$ km; 1, 2- sections in two mutually perpendicular directions

vectors are the brightness values at fixed points of the photograph, at which the photometric sections were taken, and the brightness values along a given photometric profile are realizations of these components. The correlation matrices $K_{II}(r_i, r_j)$ were determined for two families of these random vectors, corresponding to sections in two mutually perpendicular directions for each type of cloud.

It is natural to take, as a criterion of homogeneity of   /184
random brightness fields, the fact that the correlation moments K_{ij} should satisfy the condition $|i - j|$ = const, i.e., the terms on the main diagonal and on diagonals parallel to the main diagonal in the correlation matrix. The results of [6] have shown that only the brightness fields of the alto-cumulus Ac clouds are closest to homogeneous in this sense. For this quasi-homogeneous cloud we find quite high coefficients of correlation between variations of brightness corresponding to different points of the photometric sections. For other types of cloud, particularly for Cu, the conclusions have been confirmed as to the appreciable inhomogeneity, and the correlation connection between

313

variations of brightness proved to be far weaker. However, the scatter in the correlation moments of empirical functions, arising from errors of measurement and the finiteness of selection of random vectors, does not make it possible to make a reliable judgment as to the nature of the random fields being investigated.

A criterion of homogeneity capable of some qualitative evaluation can be associated with the eigenvectors of the correlation matrices, which form natural canonical systems, which are used to expand random vectors of a given ensemble (for stationary or homogeneous fields, this will be systems of trigonometric functions). Examples of sets of the first three eigenvectors obtained in [6] for different types of cloud are shown in Figure 5.9. An interesting feature is the appreciable difference in the eigenvectors for cloud designated inhomogeneous above (Cu) and quasi-homogeneous (Ac). In the latter case, the eigenvectors are reminiscent of trigonometric functions (Figure 5.9, a) in terms of which the even functions are expanded:

$\varphi_0(r) \approx const, \quad \varphi_1(r) \approx c_1 \cos \omega_0 r, \quad \varphi_2(r) \approx | c_2 \cos 2 w_0 r |$, etc. Here ω_0 is the frequency corresponding to the natural period of the harmonic component $T_0 = 2\pi / \omega_0,$ which in the case considered is of the order of 3 - 4 km. We recall that a similar value of the period was obtained in [23] from one-dimensional analysis of the photometric data. This constitutes some evidence for the existence of periodic variations of brightness of clouds at this frequency.

For Sc clouds, the eigenvectors begin to differ from trigonometric functions, although in individual cases (see Figure 5.9, b), we can still speak of a periodic brightness component with approximately the same period (~ 3 - 4 km) as for the Ac. But even for the Cu clouds, the eigenvectors are extremely arbitrary and depend noticeably on the direction of the photometric sections (Figure 5.9, c).

314
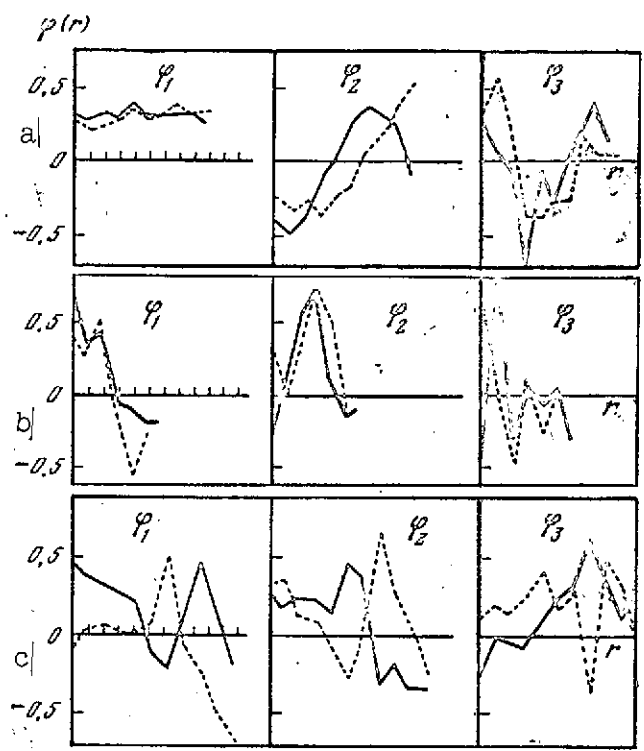
Figure 5.9. Eigenvectors $\varphi_k(r_i)$ of the correlation matrices for mutually perpendicular sections in different types of cloud [6] (see Figure 5.8).

a- Ac, $\Delta r_3 = 0.3$ km; b- Sc, $\Delta r_2 = 0.43$ km; c- Cu, $\Delta r_1 = 0.86$ km.

We note that the fine-scale periodic structure of the brightness field with $T_0 \sim 1.5$ km was observed in [7] from photometry of cloud Ac cloud photographs, obtained on the Voskhod spacecraft. However, [7] did not estimate the value of the corresponding maximum of the spectral density of the cloud brightness variations.

The results of [6] described above allow us not only to determine the parameters of the fine-scale structure of the brightness fields of different cloud formations, but also to evaluate quantitatively the quasi-isotropic and the quasi-homogeneous nature of the random fields investigated using systems of eigenvectors of correlation matrices. These estimates will be given below for large-scale brightness fields, obtained from satellites.

315

§ 5. Large-Scale Structure of the Earth's Brightness from Kosmos 149 Data

A detailed analysis of the operation of the photometric equipment mounted on Kosmos 149 allows a quite reliable statistical reduction (from the viewpoint of technique and measurement errors) of the experimental data obtained from the narrow-angle scanning TF-3A and TF-3B telephotometers. We recall (see [2.55, 4.11]), that the TF-3A scanned perpendicular to the trajectory, while the TF-3B scanned along it. Taking into account the satellite motion, this gave a scan of the brightness field in two mutually perpendicular directions relative to the satellite trajectory, with a spatial resolution at the nadir of the order of 18 - 20 km.

For analysis of the spatial structure of the brightness field, data were used from measurements in the 0.74 μm region, where the atmosphere is rather transparent (the optical thickness is of the order of 0.1 - 0.2). The initial information was the photometric profiles of the brightness field directly obtained from the scans. By examining each such section as a random function of the brightness $I(r)$, we can formally construct the correlation function $K_I(\rho)$ by applying to these sections the methods of the theory of homogeneous random fields. However, because of the angular dependence of $I(r)$ in the scanned plane, this approach leads to substantial distortions of the statistical characteristics of the spatial structure. This is illustrated in Figure 5.10 by comparing the normalized correlation functions $R_I(\rho)$ for two arbitrarily chosen photometric sections, obtained by the TF-3A and TF-3B instruments on Kosmos 149 in the spectral region 0.74 μm [24]. The distortions are particularly large for the TF-3A, whose scan plane was close to the plane of the solar vertical.

316
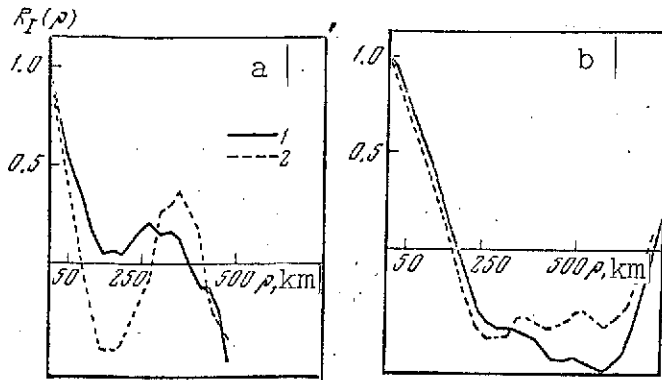
Figure 5.10. Examples of the effect of the angular dependence of brightness on the correlation functions $R_I(\rho)$ from the data of TF - 3A (a) and TF-3B (b).

1- angular behavior not eliminated;
2- eliminated
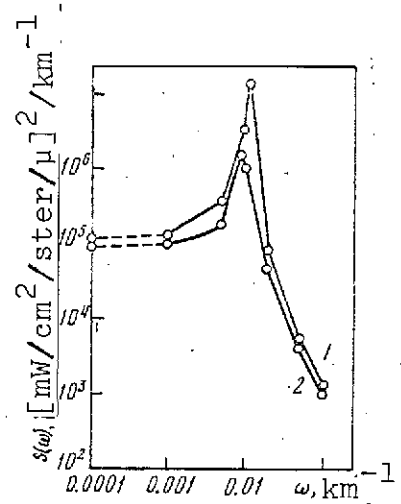
Figure 5.11. One-dimensional correlation functions $R_I(\rho)$, from the data of TF-3A (a) and TF-3B (b).

1- $\theta = 0$; 2- $\theta = -20°$;
3- $\theta = -45°$; 41 $\theta = 45°$;
5- $\theta = 20°$

The inhomogeneity of the random function, associated with the angular dependence of the brightness variations, is due to scattering of solar radiation in the atmosphere, which causes an increase in the correlation radii R_0, and also a displacement and smoothing out of the minimum of the correlation function.

The increase in R_0 is due not only to the contribution of scattered radiation, but also to the increase because of averaging over the field of view of the instrument with increase in the angle θ. In order to eliminate the equipment function of the instrument and the frequency characteristic of the atmosphere, we must apply the formulas of § 3 to determine the empirical spectral density $S_I(\omega)$, using, for example, Equation (3.15) and approximating to $K_I(\rho)$ as follows:

$$K_I(p, \theta) = \sum_{k=1}^{N} c_k e^{-\alpha_k \rho} \cos \beta_k \rho. \qquad (5.64)$$

317

The parameters of Equation (5.64) for the correlation functions depicted in Figure 5.11, depend on θ. We give below these parameters for the case $\theta = 20°$ ($N = 2$; C_1 and C_2 in $(mW/cm^2/ster/\mu m)^2$; α_k, β_k, in km^{-1}; R_0, $T_0 = 2\pi \cdot \beta_2$ in km):

Instrument	c_1	c_2	α_1	α_2	β_1	β_2	R_0	T_0
TF-3A	4.8	18.8	0.015	0.0006	0	0.011	160	600
TF-3B	2.1	15.4	0.032	0.0018	0	0.009	180	700

The corresponding spectral densities

$$S_I(\omega) = \frac{1}{\pi} \sum_{k=1}^{N} c_k \alpha_k \{[(\omega - \beta_k)^2 + \alpha_k^2]^{-1} + [(\omega + \beta_k)^2 + \alpha_k^2]^{-1}\} \qquad (5.65)$$

for $\theta = 20°$ are shown in Figure 5.12. As regards other values of θ, Equations (5.64) and (5.65) become unmanageable, and therefore it is desirable, in order to eliminate atmospheric and equipment effects, to proceed with the help of empirical characteristics of the brightness field, obtained from the same ensemble functions.

This approach was used, for example, in [9], where sliding averages of the photometric sections of extent about 5,000 km were used to eliminate the dependence $I(r)$ on the solar zenith distance ζ_0; the sections were obtained on Kosmos 45 using a photometer directed to the nadir and measuring the brightness of the Sun in the spectral region 0.6 - 0.8 μm [1.58]. However, even for radiation reflected in the vertical direction, the changes in the angular dependence of $I(r)$ on ζ_0 were determined

not only by the dependence of the incident flux on ζ_0, but also by the nature of the reflecting object. It seemed to us that, as a result of these averages, the errors in determining the statistical characteristics of the spatial structure of the brightness field, associated with the angular nonuniformity of the latter, can only be increased, since here the determinant dependence on ζ_0 has a random nature,

which is devoid, however, of physical meaning. Therefore, the scatter obtained in [9] for the correlation functions need not result only from actual inhomogeneity of the random fields.

Figure 5.12. Spectral densities obtained for the correlation functions of Figure 5.11 ($\theta = 20°$), approximated to by Equation (5.64).

1- TF-3A;   2- TF-3B

We can eliminate the effects /187 of radiation scattering and can estimate the degree of inhomogeneity of the random brightness fields by constructing correlation matrices for the photometric sections, considered as random vectors, whose components as before are values of the brightness $I(r_k)$ of areas on the Earth, intersected by the field of view of the telephotometers at distances r_k from the nadir. Examples of such correlation matrices were obtained in [12] from photometric data on Kosmos 149 for 15 and 40-dimensional vectors, corresponding to the brightness of stratified cloud in the 250 km band in the nadir region, and to 1000 km band in the entire region of the

TABLE 5.3. MEAN INTENSITIES AND MEAN SQUARE DEVIATIONS $(\text{IN mW/cm}^2/\text{ster}/\mu\text{m})$*

Instrument	Parameter	Component number														
		1	2	3	4	5	6	7	8	9	10	11	12	13	14	15
TF-3A	$\bar{I}$	12,3	12,4	12,6	12,5	12,2	12,0	12,4	11,3	9,6	10,6	12,3	13,0	14,0	16,1	17,3
	σ_I	4,6	4,9	4,7	4,8	4,6	4,9	5,2	4,8	4,2	4,5	5,5	5,8	5,9	5,6	6,4
TF-3B	$\bar{I}$	12,2	12,2	11,9	11,8	11,4	11,1	10,7	10,4	10,6	10,3	10,2	10,6	10,0	9,5	10,0
	σ_I	4,6	4,5	4,3	4,4	4,3	4,4	3,9	4,5	4,9	5,0	4,9	4,8	4,6	3,8	3,9

* Translator's Note: Commas indicate decimal points.

survey, apart from the Earth's horizon (in the latter case, one must not have overlap of the fields of view with large deviations of the optical axis from the vertical, since this is associated, additionally, with perspective distortion of the scales).

The average brightness vectors $\bar{I}(r_k)$ and the mean square deviations $\sigma_I(r_k)$ are given in Table 5.3 for the 15-dimensional vectors of TF-3A and TF-3B. An interesting feature is the increase in $\bar{I}(r_k)$ for the TF-3A instrument, whose scan plane was close to the solar vertical plane.

For the reading of the TF-3B instrument, which scanned in the perpendicular plane, there is no clear dependence of $\bar{I}(r_k)$ on r_k. This behavior of $\bar{I}(r_k)$ is typical of the angular distribution of reflected solar radiation at different solar azimuth values. We note that $\sigma_I(r_k)$ for TF-3A has also a slight angular dependence, while σ_I remains constant for TF-3B within the limits of measurement error (the sharp minima of $\bar{I}$ and σ_I for the mean components of the vectors are associated with shading

of the field of view by structural members of the instrument when viewing in the region of the nadir). The average $\bar{I}(r_k)$ profiles /188 can be used to eliminate the angular dependence of brightness, which distorts the correlation functions $R_I(\rho)$ constructed from the above-mentioned photometric sections during each scan (see Figure 5.10). This is done by dividing the brightness values $I_i(r_k)$ at the point r_k of a given i^{th} section by the mean brightness value $\bar{I}(r_k)$ at the same point, and by multiplying by $\bar{I}(r_0)$ in the region of the nadir. As the broken lines on Figure 5.10 indicate, this kind of normalization scarcely changes the behavior of the correlation function $R_I(\rho)$ for a section obtained by the TF-3B instrument (here there is a weak angular dependence of the brightness), but substantially corrects the $R_I(\rho)$ function in the case of TF-3A, bringing it closer to the usual form.

In a similar way, we can allow for effects of scattering even in the case of photometric sections used with fixed positions of the photometer axes at different values of θ (see Figure 5.11). For this we must determine, from each value of $I_i(r_k)$ of the ith section, determined by the angle θ, the average value of brightness $\bar{I}(r_k)$, and then carry out the same normalization as above.

All of these effects are automatically eliminated when we construct the correlation matrices $K_{II}(r_k, r_l)$. The normalized correlation matrices $R_{II}(r_k, r_l)$, shown in Figure 5.13, illustrate the rather close correlations between fluctuations of brightness of different sections of cloud fields, and these relations have roughly the same nature in the two mutually perpendicular directions. Within the limits of natural scatter of the empirical values, these fields can be considered to be isotropic.

321
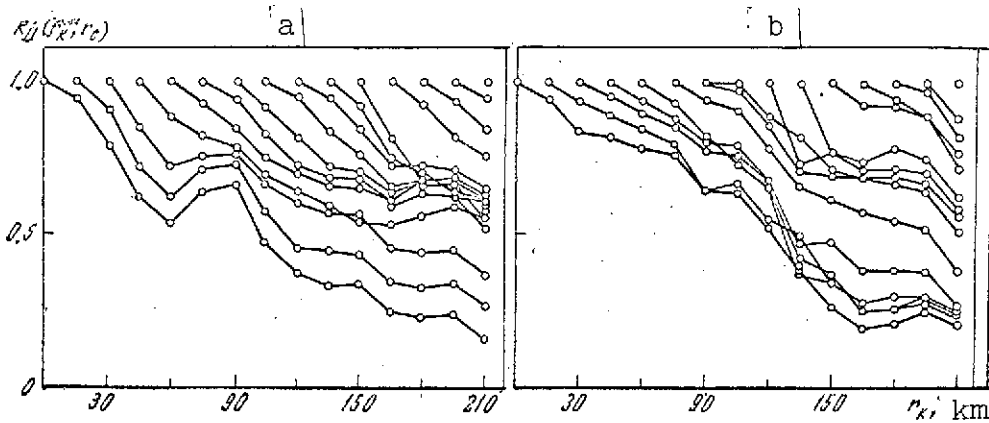
Figure 5.13. Normalized correlation matrices $R_{II}(r_k, r_l)$ for an ensemble of 15-dimensional random brightness vectors.
a- TF-3A; b- TF-3B

More obvious characteristics of the degree of homogeneity and isotropy of fields of brightness fluctuations $I_i'(r_k) = I_i(r_k) - I(r_k)$, capable of numerical evaluation, are the eigenvectors $\varphi_m(r_k)$ of the correlation matrices $K_{II}(r_k, r_l)$, as was demonstrated above when we investigated the fine-scale structure of clouds (see [6]).

Taking into account the small differences between dispersion and correlation moments, located parallel to the main diagonal of the K_{II} matrices, we can expect that at least the first eigenvectors in each case will be congruent with functions of the trigonometric system. In fact, it follows from Figure 5.14, that the components of the first eigenvector oscillate around the constant level $\widetilde{\varphi}_1 = 1 / \sqrt{n}$ (n = 15 is the dimension of the random vectors); the second and third vectors, which have respectively one and two zeros, can be approximated by the expressions $\widetilde{\varphi}_m(r_k) = A_m \cos(m-1)\omega_0 r_k$, where $A_m = \left[\sum_{k=1}^{15} \cos^2(m-1)\omega_0 r_k\right]^{1/2}$ (broken line on the figure). The frequency ω_0 and the natural /189 wavelength $L_0 = 2\pi / \omega_0$ associated with ω_0 can be determined along

322
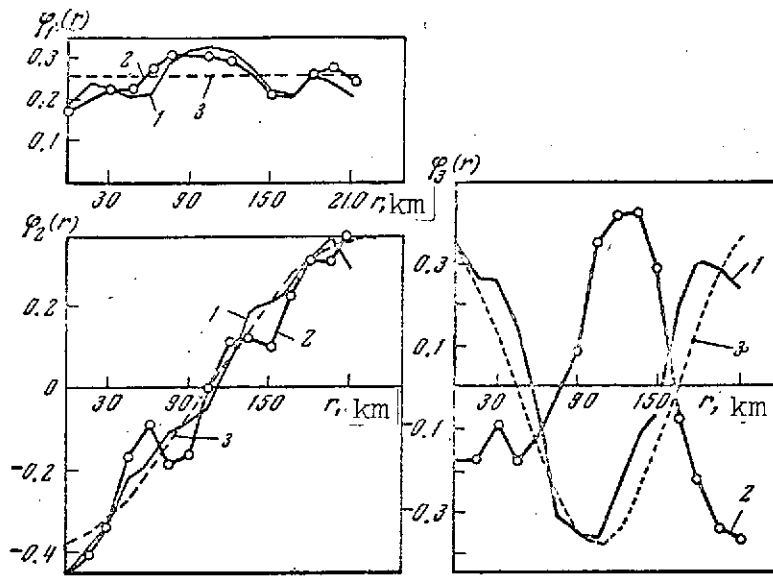
Figure 5.14. Eigenvectors $\varphi_1, \varphi_2, \varphi_3$ of the correlation matrices $K_{II}(r_k, r_l)$.

1- TF-3B;   2- TF-3B;   3- $\varphi_m = A_m \cos(m-1)\omega_0 r_k$

the section in which the "cosine" $\tilde{\varphi}_2(r_k)$ takes maximum values, opposite in sign (this wavelength corresponds to the semi-period of a trigonometric function). It is not difficult to determine from the figure that $L_0 \approx 400 - 500$ km and that $\omega_0 \approx$ 0.013 - 0.016 km^{-1}. By increasing the dimension of the vectors or the interval in which they are defined, we can obtain the full harmonic of $\varphi_2(r_k)$ (see Figure 5.15), whence, allowing for the parallax distortions, we find the same value L_0, close to the value of the period determined above from the one-dimensional correlation functions (see page 317). The closeness of the eigenvectors to the trigonometric functions with empirically determined period can be regarded as a criterion of the quasi-homogeneity of the random fields. As a quantitative character- istic of the degree of homogeneity we can take the matrix D whose elements are determined by the relations

$$d_{ml} = \sum_{k=1}^{n} \varphi_m(r_k) \, \tilde{\varphi}_l(r_k), \quad (m, l = 1, 2, \ldots, n; \quad n = 15). \tag{5.66}$$

323
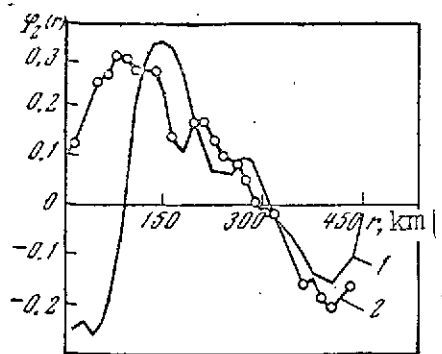
Figure 5.15. Eigenvectors $\varphi_2(r_k)$ for ensembles of 30-dimensional brightness vectors.

1- TF-3A;   2- TF-3B
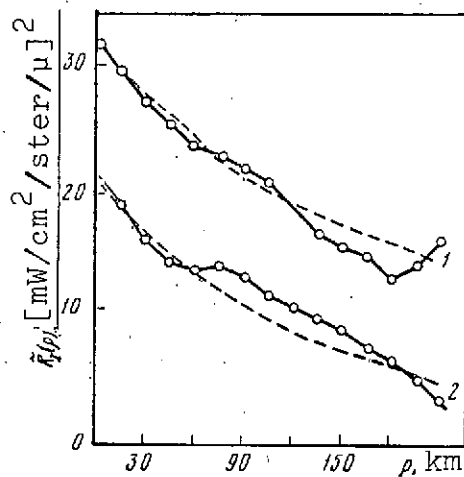
Figure 5.16. Correlation function $R_I(\rho)$ obtained by averaging the diagonal terms of the $K_{II}(r_k, r_l)$ matrices.

1- TF-3A;   2- TF-3B;   the broken lines show an approximation using an exponential function

It is easy to see that, in the case of complete homogeneity, $d_{ml} = 1$ for $m = l$, and $d_{ml} = 0$ for $m \neq l$. An example was given in [5.12] of the matrix D_3, made up of the first three eigenvectors of the Earth's brightness field:

$$|D_3| = \begin{Vmatrix} 0.984 & -0.02 & -0.225 \\ 0.006 & 0.991 & -0.041 \\ 0.140 & -0.063 & 0.895 \end{Vmatrix}$$

As an average characteristic of quasi-homogeneity, we can take the determinants $|D_n|$ or the quantities

$$|\tilde{D}_n| = \left[\frac{1}{n} \sum_{m=1}^{n} \sum_{l=1}^{n} d_{ml}^2 \right]^{1/2},$$

324
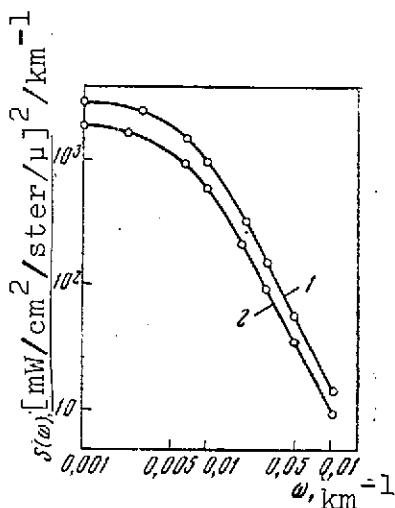
Figure 5.17. Spectral density according to Equation (5.67).

1- TF-3A; 2- TF-3B

which, in the case of complete homogeneity, must be close to unity (for $n=3$, $|D_3|= 0.90$, and $|D_3| = 0.89$).

Because of inhomogeneity of radiation fields, appearing, for example, in the scatter of the one-dimensional correlation functions $K_I(\rho)$, constructed from n sections,* some references (see, e.g., [9]) carry out averaging of the type $\bar{K}_I(\rho) = \frac{1}{n} \sum_{j=1}^{n} K_{II}^{(j)}(\rho)$. For the correlation matrices $K_{II}(r_k, r_l)$, determined above from TF-3A data, this procedure reduces to averaging of all the elements of the matrix $K_{II}(r_k, r_l)$, which satisfy the conditions $|k - l| = \text{const}$. If the brightness field was homogeneous and isotropic, the one-dimensional correlation function $\bar{K}_I(\rho)$ thus obtained would coincide with $\bar{K}_I(\rho)$. In fact, $\bar{K}_I(\rho)$ differs markedly from $\bar{K}_I(\rho)$, as can easily be seen by comparing Figures 5.11 and 5.16, especially at large ρ. For example, because of the dis- /191 placement of the correlation radius for different photometric sections, the transition through zero of the correlation function $\bar{K}_I(\rho)$ shows up weakly, or more generally vanishes. Similar differences will occur also in the corresponding spectral densities. Figure 5.17 shows an example of the spectral density

$$\widetilde{S}_I(\omega) = \frac{2\widetilde{K}_I(0)}{\pi} \frac{\alpha}{\alpha^2 + \omega^2},$$ (5.67)

($\alpha = 0.011$ km^{-1} for TF-3A and $\alpha = 0.009$ km^{-1} for TF-3B, obtained from the approximations for $\bar{K}_I(\rho)$ in Figure 5.16.

---

* This scatter also means that $K_I(\rho)$ and the other statistical characteristics obtained from the limited nonuniform fields should not be considered as completely determined functions.

The question naturally arises as to what empirical charac-teristics or what parameter reflects the actual structure of the random fields being investigated. In choosing such parameters, one must use the correlation matrices and the systems of their eigenvectors and eigenvalues as characteristics, obtained for a minimum number of assumptions concerning the random field. It was already shown above that the eigenvectors can describe the degree of homogeneity of random fields and allow us to establish a natural frequency of the periodic component of random brightness variations. This same frequency can be obtained also using the eigenvalues λ_k of the correlation matrix $K_{II}(r_k, r_l)$, which prove to be closely associated with the average spectral characteristics $\widetilde{S}_I(\omega)$.

Indeed, since the dispersion of the brightness variations is expressed in terms of the sum of the eigenvalues

$$\delta_m = \sum_{k=1}^{m} \lambda_k,$$

these parameters are a generalization of the spectral charac-teristics to the case of arbitrary inhomogeneous fields, and can be used to describe the natural spectrum of random variations, represented in the form of expansions in terms of empirical orthogonal vectors $\varphi_m(r_k)$. (Figure 5.14). If we regard the sums δ_m as discrete values of the integral of the spectral densities

$$\delta(\omega) = n \int_0^\omega S(\omega') \, d\omega', \qquad (5.68)$$

obtained for individual sections of the brightness field or from average correlation functions, then we can expect that the frequencies determined from the equation

$$\delta_m = \delta(\omega_m), \qquad (5.69)$$
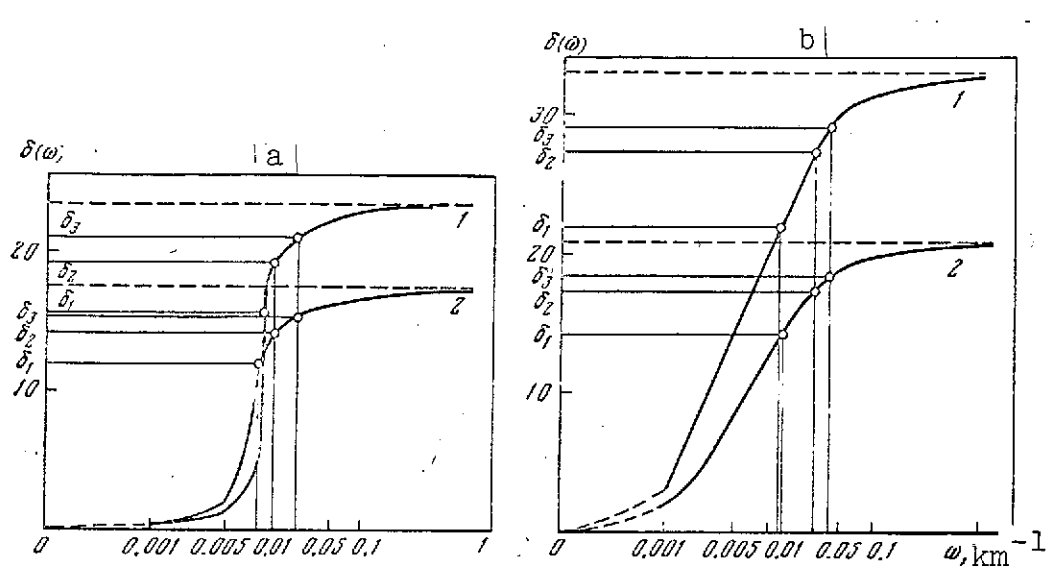
Figure 5.18. Integral of the spectral density $\delta(\omega)$

a- according to Equation (5.70); b- according to Equation (5.71);
 1- TF-3A; 2- TF-3B

should turn out to be multiples of the frequency ω_{0} defined
above as the natural frequency, where $\omega_1 = \omega_0$ (in Equation (5.68)
n is the order of the matrix, and $n\bar{K}_i(0)$ is equal to the trace
of the matrix with appropriate normalization). In fact, by using
expressions for $S(\omega)$ from Equations (5.65) and (5.67), we
obtain, for an individual section (N = 2):

$$\delta(\omega) = \frac{2c_1 n}{\pi} \text{arctg} \frac{\omega}{\alpha_1} + \frac{c_2 n}{\pi} \left[\text{arctg} \frac{\omega - \beta_2}{\alpha_2} + \text{arctg} \frac{\omega + \beta_2}{\alpha_2} \right], \qquad (5.70)$$

and for an averaged correlation function

$$\tilde{\delta}(\omega) = \frac{2\bar{K}(0)\,n}{\pi} \text{arctg} \frac{\omega}{\alpha}. \qquad (5.71)$$

It can be seen immediately from Figure 5.18 that, independently $\underline{/192}$
of the nature of the one-dimensional correlation functions, the
frequencies ω_m , determined using Equations (5.68) - (5.71),
prove to be multiples of $\omega_1 = \omega_0 \approx 0.012 - 0.013$ km^{-1}, at least for
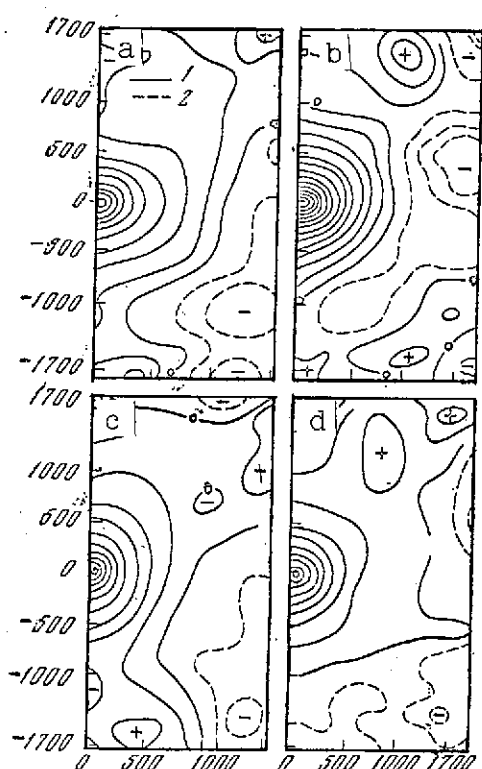
Figure 5.19. Two-dimensional correlation functions according to [25].

a- January; b- April; c- July; d- October; 1- $R(\rho) > 0$; 2- $R(\rho) < 0$

$m = 3$. Below we give these values, calculated in [24], from Equation (5.71) (δ_{m} is in $(mW/cm^{2} \cdot ster \cdot \mu m)^{2}$), $\omega_{m} = m\omega_{0}$ is in $10^{2} km^{-1}$; $\delta_{n} = \sum_{k=1}^{n} \lambda_{k}$ is the trace of the matrix $K_{II}(r_{h}, r_{l})$;

Instrument	$\delta_1 = \lambda_1$	ω_1	δ_2	ω_2	δ_3	ω_3	δ_4	ω_4	δ_5	ω_5	δ_n
TF-3A	396	1,2	532	2,6	554	4,0	568	6,4	580	6,7	602
TF-3B	212	1,3	253	2,6	278	4,0	289	5,7	296	8,0	312

Thus, we can state that systems /19‾ of empirical orthogonal vectors and eigenvalues of the correlation matrices are quite representative characteristics of the spatial structure of the brightness fields, and a parameter of these systems such as the natural period of the brightness variations remains an invariant of the random field (within the limits of natural scatter of the empirical data). It is important to note that a certain effective value ω_0 can be defined in this way for any field without going to the eigenvectors of the corresponding correlation matrix.

The above conclusions require to be checked against diverse experimental data including reliable observations of the spatial distribution of the general number of clouds and measurements of the Earth's self-radiation from satellites. As regards the first of the fields mentioned, investigations of its structure

328

carried out by Sonechkin, et al. [25] confirm the existence of a 500 - 700 km zone of homogeneous and isotropic cloud (Figure 5.19). And the results of statistical analysis of the spatial variations of the Earth's self-radiation, from measurements from satellites of the Tiros and Kosmos series, will be examined in the next paragraph.

§ 6. Structure of the Earth's Self-Radiation Field

The spatial variations of the Earth's self-radiation in the region of the relatively high atmospheric transparency depends on the contrast between the temperatures of the underlying surface and the clouds, and in strong absorption regions, they depend on the contrast between the atmospheric temperature and humidity. Therefore, the application of statistical analysis to measurements of self-radiation in different spectral regions allows us to obtain the thermal structure of the cloud cover or other atmospheric layers. However, as in the case of the reflected solar radiation fields, here as before the major question is the application of the theory of stationary random functions to the field of self-radiation. The first attempts to determine the correlation and structural functions [2.3] and [2.5] from measurements of Earth self-radiation in the spectral regions 8 - 12 and 8 - 30 μm from the Tiros satellites revealed both appreciable differences between these characteristics within one reduction technique [2, 3], and also lack of agreement between the results obtained in [2] and [3.5] as regards the data from the single satellite Tiros II.

For example, the correlation radii R_0, according to calculations of the autocorrelation functions $K_I(\rho)]$ for the above two spectral regions, reach values of approximately 3000 km in [3.5],

but in [2], they do not exceed 700 km.* It is entirely possible that these differences arise from large measurement errors, comparable, as was noted in [2], with the variations of the measured radiation, or with errors in fixing the geographic coordinates. As was shown in [3.5], the position errors entail appreciable changes in the spatial correlations. However, it is more likely that the scatter obtained in the characteristics arises from inhomogeneity and anisotropy of the random fields under study, although the presently available data do not allow a final conclusion on this matter to be made. For example, considering the correlation functions built up in [2] for the joint perpendicular radiometric sections, which were obtained using the Tiros satellite, the radiation fields in the regions 8 - 12 and 3 - 30 μm turned out to be rather isotropic.

The calculations made in [10] of the correlation functions

$$K_{II}(\rho, \varphi) = \overline{I'(r, \varphi) I'(r + \rho, \varphi)},$$

depend parametrically on the polar angle φ between the radiometric /19 section and the coordinate axis (the calculations used measured data for radiation in the spectral regions 8 - 12 and 3 - 30 μm, obtained using the satellites Kosmos 122); the calculations show the existence of a quasi-isotropy only in a circle of radius of approximately 300 km. Outside this circle, the radiation field under examination proved to be appreciably anisotropic (the same thing is true of the reflected solar radiation field in the spectral range 0.3 - 3 μm), and the correlation radii from the data of [10] varied in the range 500 - 2000 km for different directions.

---

* Estimates of R_0 are given from the mean correlation functions presented in [2].
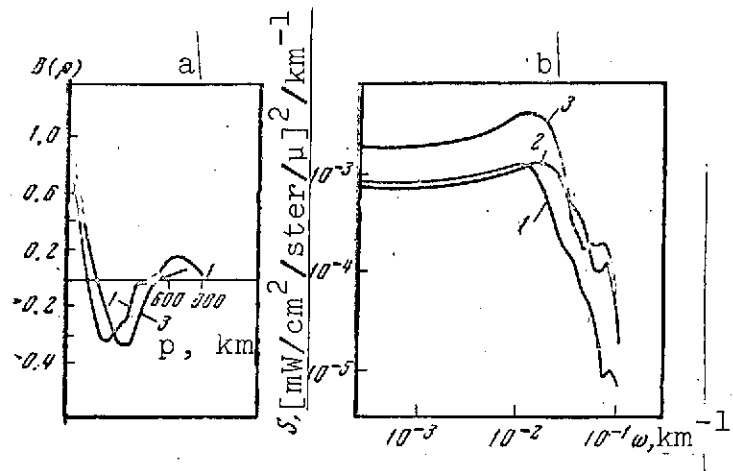
Figure 5.20. Correlation functions $B(\rho)$ (a), and spectral
densities $S(\omega)$ (b), according to [13].
1- first loop; 2- second loop; 3- third loop

At present, we cannot check the applicability of the
homogeneous hypothesis to the fields of Earth's self-radiation
because of the lack of reliable experimental data on two-
dimensional fields.

We shall try to do this by comparing the one-dimensional
correlation functions $K_I(\rho)$ and the spectral density $S_I(\omega)$,
constructed from radiometric data in the transparent window at
10 - 12 μm, which were obtained by means of the narrow-angle
radiometer (approximately 2 degrees) on Kosmos 243, with appro-
priate characteristics, determined in § 4 and §5 from photometric
data. Some possibilities of evaluating the validity of the
statistical characteristics of these fields of self-radiation
can be obtained by a comparison with results of statistical
processing of aerophotographs of the Earth, which were obtained
two days earlier from the space vehicle Zond 5, and which were
analyzed from a synoptic viewpoint in [26].

Examples of the correlation functions $K_I(\rho)$ and the spectral
densities $S_I(\omega)$, presented in Figure 5.20, show that the self-
radiation has periodic components in its three-dimensional

spectrum, corresponding to wave lengths $L_1 \approx 10$ km, and $L_2 \approx$ 500 km. The first of these components is typical of the short-wave region of medium-scale cloud formation, obtained in [6] (see § 4) from aerophotographs of clouds, but smoothed out because of spatial and temporal averaging. A wavelength of 500 km was observed above in the statistical analysis of fields of reflected solar radiation, for which objective criteria of homogeneity (see § 5) were obtained.

The observation of medium-scale peculiarities of the three-dimensional spectrum of radiation confirm the well-known hypothesis that the synoptic and micrometeorological sections of the low-frequency range of temporal spectra are divided by a minimum of the spectral density in the frequency region 1 Hz/hour [1]. The same minimum, obtained by Kolesnikov, et al. [27] from statistical reduction of the fields of meteorological elements, is evidence that the statistical characteristics of the spatial structure of the fields of Earth self-radiation can find immediate application in the investigation of thermodynamic processes in the atmosphere with which the radiation fields are connected.

INVERSE OPTICAL SOUNDING PROBLEMS

CHAPTER 6
DETERMINATION OF VERTICAL ATMOSPHERIC TEMPERATURE PROFILE

§ 1. Problem Formulation and Basic Relations

The idea of determining the vertical atmospheric temperature profile from measurements of the Earth's self-radiation in quite narrow spectral intevals of the CL_2 15 μ absorption band from satellites was proposed by Kaplan in [1]. The basis of this idea is the physical fact that the radiation in different segments of the selected band is generated in different layers of the atmosphere and consequently is determined by the temperature of these layers. This correspondence is quite unique, since the relative CO_2 concentration is constant and well known up to very high altitudes, and absorption by water vapor and other atmospheric substances can be neglected.*

The relationship between the radiation spectral intensity I_ν measured from a satellite and atmospheric temperature is described by the solution of the radiation transport Equation (2.11). For the simplest case of absolutely black surface of the Earth ($\delta_\nu = 1$) and measurement of I_ν at the nadir ($\theta = 0$) this relation will have the form

$$I_\nu = B_\nu[T(1)] P_\nu(1, 0, 0) - \int_0^1 B_\nu[T(\zeta)] \frac{\partial P_\nu(0, \zeta; 0)}{\partial \zeta} d\zeta.$$ (6.1)

---

* In reality water vapor and aerosol absorption may introduce a noticeable contribution to the radiation in the wings of the CO_2 band. Moreover, CO_2 concentration variations existing in the atmosphere may play a definite role. These questions will be examined in § 7.

Here the transmission function P_ν is taken with account for the spectral sensitivity of the equipment and the frequency ν corresponds, for example, to the midpoint of the spectral resolution interval (sometimes we shall take the subscript ν to mean simply the number of the spectrum segment for which the I_ν measurement was made). We note that account for δ_ν and the use of other angles θ do not cause any fundamental difficulties in solving the subject problem.

Relation (6.1), considered as a Fredholm integral equation of the first kind in $T(\zeta)$, permits determining the vertical temperature profile if we know the radiation intensity I_ν as a function of ν and the transmission function P_ν, which is the kernel of the equation.* The seeming simplicity of (6.1) was the reason Wark and Yamamoto [2, 3], in the first attempts to solve it, used formal reduction of (6.1) to systems of algebraic equations, obtained either /196 by approximating the integral by a finite sum [2] or by expanding the unknown function into polynomial series [3].

It was found that as a result of solving such systems without taking definite precautionary measures, quantities may be obtained which are arbitrarily far from the true solution and even physically meaningless (see, for example, [4]) and refinement of the approximations, yielding increase of the order of the algebraic systems, leads to increasing solution instability. To illustrate this instability we present the solution of the equation obtained in [5] by the Yamamoto method [3], who suggested linearizing (6.1) the relation

$$\varepsilon_\nu(T) = \frac{B_\nu(T)}{B_0(T)},$$
(6.2)

* The analogous problem can, in principle, also be solved with respect to the angular distribution $I_\nu(\theta)$. However, in the real atmosphere this involves large errors because of the horizontal nonhomogeneity of the $T(\zeta)$ fields and the presence of cloud cover.

where B_0 (T) is the Planck function for one of the N CO_2 band segments used. If we neglect the dependence of ε_ν (T) on T, which is admissible only for a very narrow spectral interval of the band, then (6.1) will be linear in the function B_0 (T)

$$F_\nu = B_0 [T(1)] P_\nu(1, 1) - \int_0^1 B_0 [T(\zeta)] \frac{\partial P_\nu(1, \zeta)}{\partial \zeta} d\zeta.$$ (6.3)

Here $F_\nu = I_\nu/\varepsilon_\nu$ (we note that the linearization relation $B_\nu [T(\zeta)] = \alpha_\nu B_0 [T(\zeta)] + \beta_\nu$ suggested in [6] has the same drawback as (6.2)). The function $B_0 [T(\zeta)]$ is defined in [3] by expansion into a power-law series

$$B_0 [T(\zeta)] = \sum_{k=1}^n b_k \zeta^k$$ (6.4)

or analogous series in Legendre and Chebyshev polynomials. Substituting (6.4) into the linearized Equation (6.3) and performing elementary transformations, it is not difficult to obtain the system of algebraic equations for determining the coefficients b_k

$$\sum_{k=1}^n D_{\nu k} b_k = F_\nu, \qquad (\nu = 1, 2, \ldots, N),$$ (6.5)

where

$$D_{\nu k} = 1 + k \int_0^1 \zeta^{k-1} P_\nu(1, \zeta) d\zeta \qquad (k = 0, 1, \ldots, n).$$ (6.6)

A check of the effectiveness of this solution method, and incidentally of the other methods examined below, is made by means of numerical experiments. For the given initial profile $T(\zeta)$ and for the known transmission function we calculate with the aid of (6.1) the quantities I_ν for several frequencies. Then the $T(\zeta)$ profile is reconstructed using these I_ν by the proposed method and compared with the initial profile. Solution of (6.3) using (6.4) — (6.6) for n = 3, carried out by Yamamoto [3] to determine the stratosphere vertical temperature profile from I_ν in four segments

of the band CO_2 15 μ (665-670; 675.5-680; 686-691; 692-697 cm^{-1}),
showed that the deviation of the calculated $T(\zeta)$ profile from the
initial profile reached 15°. Particularly large errors are obtained
in the regions of strong temperature gradient variations, including
at the tropopause. It would seem that this discrepancy could be
reduced by increasing the number of terms in the expansion (6.4).

In fact, solutions of (6.5) successively for n = 1, 2, and 3
yield ever better approximations $T_n(\zeta)$ to the initial profile
(Figure 6.1). However, beginning with n = 4 we observe departure /197
of $T_4(\zeta)$ from the preceding approximations and for n = 5 the
solution of (6.3) loses physical meaning. It is interesting to
note on all the curves in the figure the stability of the recon-
structed value of the Earth's surface temperature T(1), which is
associated with the presence in (6.1) of the term B_ν [T (1)]
outside the integral. This stability will also show up in other
examples until the transmission function P_ν (1, 1), characterizing
attenuation of the Earth's surface self-radiation in the atmos-
phere, becomes quite small.

The reason for the instability of these solutions is the mathe-
matical incorrectness of the inverse problems, meaning that arbi-
trarily small measurement or approximation errors may lead to
arbitrarily large errors of the sought solution of the corresponding
equations.

The incorrectness of the inverse problems is a direct conse-
quence of the physical mechanism which determines self-radiation
transport in a stratified atmosphere. As a result of this
mechanism there is smoothing of the radiation variations in the
individual layers of the atmosphere, and the degree of smoothing
is characterized by the kernel of (6.1). For this reason certain
details of the sought functions (like the marked temperature
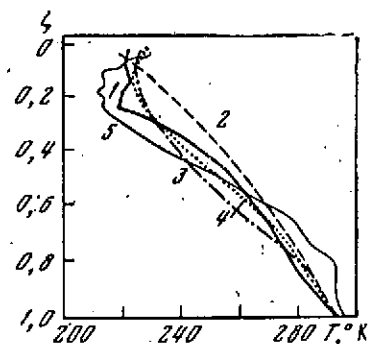
Figure 6.1. Approximations T_n (ζ) of vertical profile $T(\zeta)$

1- initial profile; 2- n = 1; 3- n = 2; 4- n = 3; 5- n = 4

gradient variations mentioned above) either are completely smoothed out and do not appear in the measured intensity I_ν at all, or they yield a contribution at the level of the random I_ν measurement errors or computational errors. During inversion of equations of the form (6.1) these errors are amplified, which then leads to instability of the inverse problem solutions.

Since the incorrectness question is one of the most important for the entire problem of optical sounding of the atmosphere, we shall examine it in more detail.

§ 2. Incorrectness of Inverse Problems

We shall illustrate the concept of incorrectness by the example of Fredholm integral equations of the first kind

$$f(x) = \int_a^b K(x, y)\,\varphi(y)\,dy \qquad (c \leqslant x \leqslant d), \qquad (6.7)$$

to which in the final analysis all the optical atmospheric sounding problems solved in the following reduce. The function f(x), defined on the segment [c, d], is the result of experiment and is practically always known with the random error $\varepsilon(x)$, generally speaking uncorrelated with respect to x, i.e.,

$$f(x) = \bar{f}(x) + \varepsilon(x), \qquad (6.8)$$

337

where $\tilde{f}(x)$ is the exact value of the measured parameter. We include in $\varepsilon(x)$ also the possible errors associated with inaccuracy <u>/198</u> of the kernel $K(x, y)$ and the integration limits, and also the errors of the mathematical transformations in solving (6.7).

It is clear from the preceding that the possibilities of obtaining information on the function $\varphi(y)$ with any particular degree of detail are determined by the information contained in the function $f(x)$, and this is in turn associated with the smoothness of the kernel $K(x, y)$. For example, if

$$K(x, y) = \delta(x - y),$$ (6.9)

where $\delta(x-y)$ satisfies the condition $\delta(x-y) = 0$ for $x \neq y$ and $\int_a^b \delta(x - y)\,dy = 1$ (δ-function), then $\varphi(x) = f(x)$, i.e., the function $f(x)$ contains all the information on the function $\varphi(y)$. In the other extreme case, when

$$K(x, y) \equiv c_1,$$ (6.10)

the function $f(x) = c_2 + \varepsilon(x)$ does not contain any information on $\varphi(y)$ (c_1 and c_2 are constants)*. All the equation kernels which are realized in practice occupy a position intermediate between these extreme cases.

To obtain a clear picture of the physical meaning of inverse problem incorrectness let us examine the case of (6.7) with a difference kernel $K(x, y) = K(x-y)$ and infinite integration limits $a = -\infty$, $b = +\infty$, and let us assume that the functions $f(x)$, $\varphi(y)$, $K(t)$ admit Fourier transformation

---

* An analogous conclusion and all the further corollaries will also hold for the kernel $K(x, y) = K_1(y)$.

$$F(\omega) = \frac{1}{2\pi} \int\limits_{-\infty}^{+\infty} f(x)\, e^{i\omega x}\, dx;$$

$$\Phi(\omega) = \frac{1}{2\pi} \int\limits_{-\infty}^{+\infty} \varphi(y)\, e^{i\omega y}\, dy; \tag{6.11}$$

$$\varkappa(\omega) = \frac{1}{2\pi} \int\limits_{-\infty}^{+\infty} K(t)\, e^{i\omega t}\, dt.$$

Then, converting from (6.7) to the relations between the spectra of the corresponding functions (6.11) under the condition that $K(\omega) \neq 0$, we obtain

$$\Phi(\omega) = \frac{F(\omega)}{2\pi\varkappa(\omega)}. \tag{6.12}$$

Since the spectra $F(\omega)$ and $\varkappa(\omega)$ are known functions of ω, after obtaining the spectrum $\Phi(\omega)$ from (6.12) we can, at first glance, determine $\varphi(y)$ without any difficulty by means of the inverse transformation

$$\varphi(y) = \int\limits_{-\infty}^{+\infty} \Phi(\omega)\, e^{-i\omega y}\, dv. \tag{6.13}$$

In reality, however, the spectrum $F(\omega)$ consists of two parts: the exact function spectrum $\tilde{F}(\omega)$ and the uncorrelated error spectrum, which is "white noise" or at least contains a "white noise" component, i.e.

$$\frac{1}{2\pi} \int\limits_{-\infty}^{+\infty} \varepsilon(x)\, e^{i\omega x}\, dx = \varepsilon_0 = \text{const.} \tag{6.14}$$

Consequently

$$\Phi(\omega) = \frac{\tilde{F}(\omega) + \varepsilon_1}{2\pi\varkappa(\omega)}. \tag{6.15}$$

Applying the Fourier transformation apparatus to the case of the kernel (6.9), we obtain $\varkappa(\omega) \equiv 1$, i.e., the solution spectrum coincides with the spectrum of a known function and the solution of (6.7) is determined with the same error. However, in the case of the kernel (6.10) $\varkappa(\omega) = \delta(\omega)$, i.e., the kernel spectrum is

a δ-function, and we do not obtain the solution of (6.7) even with absolutely exact specification of f (x). In all intermediate cases the possibility of inverse problem solution depends on the relationship between $F(\omega)$, $\varkappa(\omega)$, and the spectrum of the noise ε_0. Since for bounded functions $\bar{f}$ (x) and K (t) their spectra $\tilde{F}$ (ω) and $\varkappa$ (ω) tend to zero as $\omega \to \infty$, the high frequencies in the Φ (ω) spectrum cannot be reconstructed reliably from (6.15). In fact, for large ω the $\tilde{F}$ (ω) spectrum is comparable with the spectrum of the noise ε_0, arbitrarily amplified because of decay of the kernel spectrum. Moreover, for quite large measurement errors (variance of the errors ε_0 is large) or for a quite smooth kernel ($\varkappa$ (ω) decays quite rapidly as $\omega \to \infty$) even the low-frequency component of the Φ (ω) spectrum cannot be reconstructed from (6.15). This is then the physical manifestation of the incorrectness of inverting operators of the form (6.7). For comparison we present the relation analogous to (6.15) for the spectra of the Fredholm integral equation of the second kind, in which the unknown function φ (x) is a term outside the integral (6.7)

$$\Phi(\omega) = \frac{\tilde{F}(\omega) + \varepsilon_0}{1 + \varkappa(\omega)} \cdot$$

It is easy to see that in this case Φ (ω) exists for all ω except for a finite number of roots of the equation $1 + \varkappa(\omega) = 0$. Therefore problems which lead to an equation of the second kind in accordance with the well-known Fredholm theorems are always correct.

Using the Fourier transformation in the general case of the kernel

$$\varkappa(x, \omega) = \frac{1}{2\pi} \int_{-\infty}^{+\infty} K(x, y)\, e^{i\omega y}\, dy; \qquad K(x, y) = \int_{-\infty}^{+\infty} \varkappa(x, \omega)\, e^{-i\omega y}\, d\omega, \qquad (6.16)$$

substituting (6.16) into (6.7) and considering (6.12) and (6.13), Twomey [7] obtained in a similar fashion the following analog of (6.7)

340

$$f(x) = \int_{-\infty}^{+\infty} \varkappa(x, \omega)\,\Phi(\omega)\,d\omega. \qquad (6.17)$$

If K (x, y) and the partial derivative K'$_y$ (x, y) are bounded, then $\varkappa(x, \omega) \to 0$ for $|\omega| \to \infty$ as $|\omega|^{-1}$. Therefore representation of f (x) in the form (6.17) permits treating the Fourier transform of the kernel of (6.7) as a filter which cuts off the quite high frequencies of the transform of the function φ (y) or smooths them to the noise level. Consequently, when inverting (6.7) and (6.17) the information on $\Phi(\omega)$ in the region of these frequencies is determined only by the errors of the function f (x). But since these errors are random and may amplify arbitrarily, as a result we may obtain a set of functions which will satisfy (6.7) in the limits of the errors ε (x) but will not have anything in common with the physically meaningful solution of this equation. Therefore, no matter what the details of the sought function φ (y) corresponding to these frequencies, the information on them contained in f (x) for a sufficiently smooth kernel is located at the level of the random errors ε (x). Consequently, there may exist an infinite number of functions (for example, strongly oscillating) which will satisfy (6.7) with accuracy to ε (x) but are /200 arbitrarily far from the physical solution of the problem.

Thus to obtain the solution of (6.7), an additional operation is required which permits reliable filtering out of those frequencies in the $\Phi(\omega)$ spectrum which for integral transformations of the form (6.7) or (6.17) yield a contribution at the level of the errors ε (x). This operation is termed incorrect problem regularization. For its realization we require some a priori information on the solution which also permits retention of the frequencies carrying useful information on the sought function. A rigorous justification of one method for regularizing incorrect problems and proof of the possibility of constructing their approximate solution was given by Tikhonov in [8, 9]. In this connection we shall describe briefly the problem formulation and basic idea of the method.

§ 3. Tikhonov Regularization Method

To obtain the approximate solution of Equation (6.7) with given accuracy, Tikhonov suggested the following regularization method. Let the function f (x) be such that the solution of the integral Equation (6.7), which we write in operator form

$$A\ [x,\ \varphi\ (y)] = f\ (x)\ (a \leqslant y \leqslant b;\ c \leqslant x \leqslant d),$$

exists and moreover is unique. Assuming that φ belongs to the class of piecewise-continuous functions C and f (x) to the class of square-integrable functions L_2, we introduce a metric: the norm in C

$$\|\varphi\ (y)\| = \max_{a \leqslant y \leqslant b} |\varphi\ (y)|$$

and the norm in L_2

$$\|f\ (x)\| = \left[\int_c^d f^2\ (x)\ dx\right]^{1/2}.$$

Further, let the class of admissible solutions M be compact (the limits of all sequences of functions φ belong to M). Then for any $\varepsilon > 0$ there exists $\delta\ (\varepsilon,\ \varphi)$ such that from the condition $\|f_1 - f_2\| < \delta\ (\varepsilon, \varphi)$ follows $\|\varphi_1 - \varphi_2\| < \varepsilon$, i.e., for sufficiently close functions f the solutions of (6.7) differ little from one another.

For proof of this statement a regularized family of approximate solutions $\varphi_\alpha\ (y)$ of (6.7), satisfying the following conditions, is constructed in [8]:

1) $f_\alpha\ (x) \equiv A\ [x, \varphi_\alpha\ (y)] \to f\ (x)$ as $\alpha \to 0$, i.e., the operator A maps functions from class C into class L_2 continuously;

2) $\varphi_\alpha\ (y) \in M$ for any α, i.e., M is a compact containing the solution $\varphi\ (y)$.

It was shown in [8] that for any function f (x) from the class L_2 there exists a differentiable function $\varphi_\alpha(y)$ which minimizes the smoothing functional

$$M^\alpha[\varphi(y), f(x)] = \int_c^d \{A'[x, \varphi(y)] - f(x)\}^2\, dx + \alpha \int_a^b \sum_{k=0}^n h_k(y) \left[\frac{d^k \varphi(y)}{dy^k}\right]^2 dy. \qquad (6.18)$$

Here $h_k(y)$ are positive functions; the second integral in (6.18) is termed the n-th order regularizing functional, α is the regularization parameter.

The function $\varphi_\alpha(y)$ is determined from the Euler equation for the subject variational problem. In the case n = 1 this equation has the form

$$\int_a^b \overline{K}(x, y)\,\varphi_\alpha(y)\, dy - \overline{f}(x) + \alpha \left\{h_0(y)\,\varphi_\alpha(y) + \frac{d}{dy}\left[h_1(y)\frac{d\varphi_\alpha(y)}{dy}\right]\right\} = 0, \qquad (6.19)$$

where

/201

$$\overline{K}(x, y) = \int_c^d K(s, x)\, K(s, y)\, ds; \qquad \overline{f}(x) = \int_0^d K(s, x)\, f(s)\, ds.$$

Equation (6.19) has a unique solution, determined by the boundary conditions for the sought function $\varphi_\alpha(y)$ and its derivative $\varphi'_\alpha(y)$, and depending on the parameter α. Tikhonov [8] showed that the sequence of solutions $\varphi_\alpha(y)$ converges as $\alpha \to 0$ to the limit function $\varphi(y)$, belonging to the class C_1 (functions having continuous derivative). Consequently, solving (6.19) for various diminishing $\alpha \neq 0$ we will obtain approximations arbitrarily close to the solution until for excessively small α the computational or experimental errors begin to have an influence and the error of the approximations φ_α begins to increase. A finite difference algorithm for determining φ_α was also proposed in [8].

Examples illustrating the Tikhonov method were constructed in [10, 11] and in several other studies for certain particular

343

cases of the kernel of Equations (6.7) having an a priori known exact solution. The authors of [10] also developed a universal program for approximate computer solution of (6.7).

The most important questions in practical use of the Tikhonov method are determination of the regularization parameter in the absence of the required a priori information about the solution and establishment of the connection between the selected α and the problem solution error. In [12, 13] a technique was proposed for selecting the optimum value of α on the basis of a minimum of the norm of the difference of the regularized solutions

$\min\limits_{i} \max\limits_{a \leqslant y \leqslant b} \| \varphi_{\alpha_{i+1}}(y) - \varphi_{\alpha_i}(y) \|$ for two successive regularization parameter

values α_i and α_{i+1}.

The Tikhonov method and the indicated α selection criterion were used in [14, 15] for an idealized case of thermal atmosphere sounding. The authors of [14, 15] made numerical experiments in reconstructing the function B (ζ), given in the form of a parabola reminiscent of the vertical variation of B_0 [T (ζ)] and having a minimum at the level ζ_0. The kernel of (6.3) served as the transmission function for the isolated Lorenz line. The influence of errors in the known function and the kernel and also the selection of the integral equation approximation and the radiation measurement range on the temperature reconstruction accuracy was studied in [14, 15]. The authors of [14, 15] show that the results of these numerical experiments indicate the possibility of applying the regularization method of [8] to the subject problem*.

However, we should note that determination of the variations of the temperature or other atmospheric parameter profiles which,

---

* The results of Tikhonov method application were presented in detail in a monograph by Kondratev and Timofeyev [16].

as was shown in Chapter 3, are random functions of altitude, leads us to incorrect problems of reconstructing functions of complex structure whose description requires the use of statistical methods. In this connection we shall examine the statistical regularization methods in application to the problem of determining the variations of the vertical atmospheric temperature profiles.

In conclusion we note that the regularization methods, which in contrast with the statistical methods we arbitrarily term deterministic methods, were also developed in studies by Phillips [17] and Twomey [18] (a brief survey of these methods is presented in [6]).

§ 4. Optimum Parametrization Method

The use of (6.1) to determine the variations of the vertical temperature profiles permits, first of all, reliable linearization of this equation. In fact, we represent T (ζ) in sum form

$$T(\zeta) = \bar{T}(\zeta) + T'(\zeta), \qquad (6.20)$$

where $\bar{T}$ (ζ) is the mean vertical temperature distribution for the given region and season in the sense of (3.1); T' (ζ) is the deviation from $\bar{T}$ (ζ), small in comparison with $\bar{T}$ (ζ). Substituting (6.20) into (6.1) and considering the high accuracy of (4.16), we obtain a linear equation in T' (ζ)

$$f_v = \frac{\partial B_v[\bar{T}(1)]}{\partial T} P_v(1,1) T'(1) - \int_0^1 \frac{\partial B_v[\bar{T}(\zeta)]}{\partial T} T'(\zeta) \frac{\partial P_v(1,\zeta)}{\partial \zeta} d\zeta \qquad (6.21)$$

Here $f_\nu = I_\nu - \bar{I}_\nu$ and $\bar{I}_\nu$ is obtained from (6.1) by substituting therein $\bar{T}$ (ζ).

Since in this problem formulation T' (ζ) is a random function of ζ, whose structure was investigated in great detail in § 2 of Chapter 3, it is advisable to accomplish optimum approximation of

T' (ζ_i) defined at discrete points ζ_i, by the eigenvectors $\varphi_k(\zeta_i)$ of the correlation matrix B_{TT} (ζ_i, ζ_j)

$$T'_n(\zeta_i) = \sum_{k=1}^{n} c_k \varphi_k(\zeta_i).$$

(6.22)

The expansion (6.22) provides high approximation accuracy by a small number of first vectors $\varphi_k(\zeta_i)$ and consequently avoids the necessity for using high-order harmonics.

Substituting (6.22) into (6.21) and performing elementary transformations, it is not difficult to obtain the system of algebraic equations for determining c_k

$$\sum_{k=1}^{n} D_{vk} c_k = f_v \qquad (v = 1, 2, \ldots, N),$$

(6.23)

where

$$D_{vk} = \frac{\partial B_v [\overline{T}(1)]}{\partial T} P_v(1, 1) \varphi_k(1) - \int_0^1 \frac{\partial B_v [\overline{T}(\zeta)]}{\partial T} \varphi_k(\zeta) \frac{\partial P_v(1, \zeta)}{\partial \zeta} d\zeta.$$

Since when using optimum parametrization systems of the form (6.23) will, as a rule, be overdefined or underdefined $(N \gtrless n)$, we can carry out smoothing by the least squares method. As a result we obtain a new system of equations for c_k

$$\sum_{l=1}^{n} \Gamma_{kl} c_l = F_k \qquad (k = 1, 2, \ldots, n),$$

(6.24)

where

$$\Gamma_{kl} = \sum_{v=1}^{N} D_{vk} D_{vl}; \qquad F_k = \sum_{v=1}^{N} D_{vk} f_v.$$

Examples of the numerical experiments made in [5] to reconstruct T' (ζ_i) by the optimum parametrization method are shown in Figure 6.2. In the calculations the three eigenvectors represented in Figure 3.15 were used. We see from Figure 6.2 that quite good approximation of T'_1 (ζ) (Curve 3) to the initial profile (Curve 1) was obtained, only slightly inferior to direct approximation of /202

346

T' (ζ_i) by the first three eigenvectors (Curve 2), with mean square error about 2°. It is interesting to note that determination of T' (ζ) with the aid of the expansion (6.4) (Figure 6.2a, Curve 4) led to considerably larger discrepancies (mean square error reaches 5°). The most significant errors in reconstructing T' (ζ_i) are obtained at the tropopause level where, as noted in § 2 of Chapter 3, the correlation coefficient r_{TT} (ζ_i, ζ_j) vanishes.
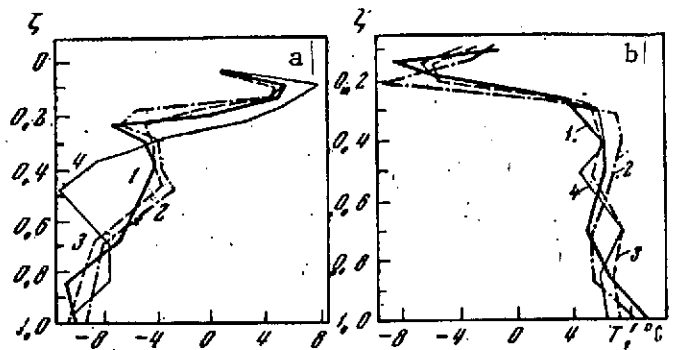
Figure 6.2. Reconstruction of vertical temperature profiles T' (ξ_i) a- for continental station; b- for oceanic station; 1- initial profile; 2- approximation (6.22) with n = 3; 3- solution of (6.21) with n = 3; 4a- solution of (6.21) with aid of (6.4); 4b- solution of (6.21) with aid of φ_k for continental station

Worthy of attention is the well-known universality of the empirical orthogonal vectors used. This follows from Figure 6.2b, illustrating the results of reconstructing T' (ζ_i) for the oceanic case using the eigenvectors of the same random profile sample from which the realization T' (ζ) was taken and using the eigenvectors obtained for the continental case (Figure 6.2b, Curve 4), also used for reconstructing T' (ζ) (Figure 6.2a). We see from Figure 6.2b that the "foreign" system of empirical vectors provided an approximation which is not much rougher than the "proper" system. The optimum parametrization method was tested on empirical data from balloon self-radiation measurements at the 30 km level [19] in the CO_2 band intervals 677.5; 691; 697; 703, 709 cm^{-1} and in the 899 cm^{-1} "window" with resolution 5-7 cm^{-1}. According to the

authors of [19] the measurement error did not exceed 1%. Examples of vertical temperature profile reconstruction using empirical orthogonal vectors are shown in Figure 6.3 [20]. Also shown here are the results of $T(\zeta)$ reconstruction by the authors of [19]. Comparison of the reconstructed profiles for these two cases permits stating that the optimum parameterization method accuracy is somewhat higher in spite of the complex $T'(\zeta)$ structure. However the errors are still significant and are probably associated with initial data errors. In fact, calculations of I_ν using the initial $T(\zeta)$ profile and the transmission functions utilized in the problem differ from the experimental I_ν values by 4-6% in the 677-691 cm^{-1} intervals and by only 1% for 703 and 709 cm^{-1} [20].

We note that the empirical orthogonal vectors have also recently been used to solve incorrect problems in several studies by American investigators [21, 22]. The reason for the effectiveness of the optimum parametrization method is the fact that the very first eigenvector captures the most characteristic features of the vertical temperature variation distribution. As for the succeeding eigenvectors, they permit taking into account certain details of the random vector $T'(\zeta_i)$ being determined. However, We must remember that the vectors $\varphi_k(\zeta_i)|$ were obtained as a result of processing limited $T'(\zeta_i)$ samples and, consequently, include random errors reflecting only the errors of these samples. With increase of k the φ_k errors become dominant in comparison with the real information on the details of the vectors $T'(\zeta_i)$ and upon /204 inversion of (6.2) may be amplified together with the other problem errors. Therefore we cannot guarantee that uncontrolled account for eigenvectors of even low order will not lead, generally speaking, to deterioration of the solution approximation by formulas (6.22) — (6.24).

348
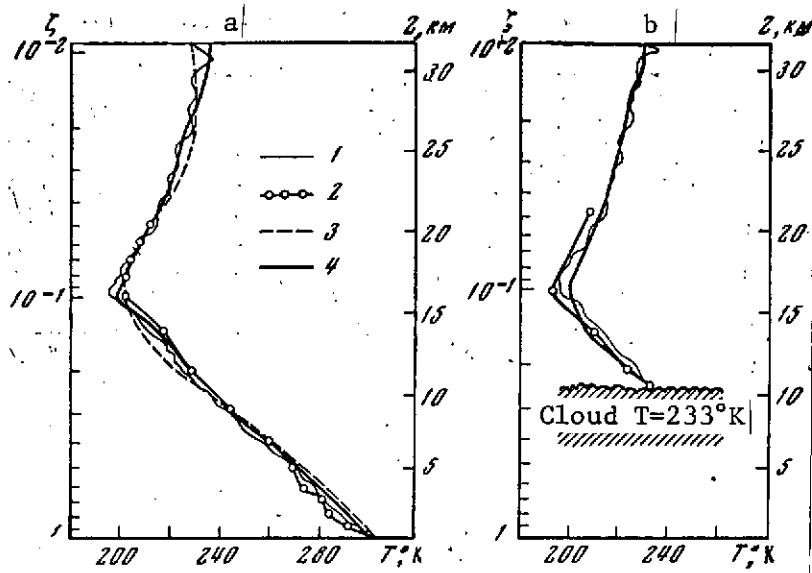
Figure 6.3. Reconstructing vertical temperature profiles from measurements [19]

a- clear; b- cloudy; 1- initial profile; 2- optimum parametrization method [20]; 3- trigonometric function method; 4- method of broken lines [19]

In [5] calculations were made of the amplification coefficients of the errors of the function f_ν when reconstructing T' (ζ_i) by the optimum parametrization method

$$k_n^2(\zeta_i) = \frac{\sigma_T^2(\zeta_i)}{\sigma_f^2}.$$

Here σ_T^2 and σ_f^2 are the variances of the T' (ζ_i) and f_ν errors. For the system of Equation (6.23) k_n (ζ_i) is given by the expression

$$k_n^2(\zeta_i) = \sum_{k=1}^{n} \sum_{l=1}^{n} \sum_{\nu=1}^{N} \left\{ \frac{\partial B_\nu[\bar{T}(\zeta_i)]}{\partial T} \right\}^2 D_{\nu l}^{-1} D_{\nu k}^{-1} \varphi_k(\zeta_i) \varphi_l(\zeta_i), \tag{6.25}$$

and for the system (6.24) by

$$k_n^2(\zeta_i) = \sum_{k=1}^{n} \sum_{l=1}^{n} \sum_{p=1}^{n} \sum_{q=1}^{n} \sum_{\nu=1}^{N} \left\{ \frac{\partial B_\nu[\bar{T}(\zeta_i)]}{\partial T} \right\}^2 \Gamma_{kl}^{-1} \Gamma_{pq}^{-1} D_{\nu k} D_{\nu l} \varphi_k(\zeta_i) \varphi_l(\zeta_i) \tag{6.26}$$

349

$(D_{vk}^{-1}$ and Γ_{kl}^{-1} are elements of the inverse matrices of the systems (6.23) and (6.24)).

The k_n (ζ_i) calculation results presented below show that even when using the first two eigenvectors the error amplification is quite large, particularly near the tropopause level.

Thus, in (6.23) with n = 2, N = 2

ζ_i	1	0.85	0.7	0.5	0.4	0.3	0.25	0.2	0.15	0.1
k_2	3.1	1.1	5.3	2.0	4.7	7.1	17.2	21.3	8.2	8.8

In (6.24) with n = 2; N = 13

k_2	1.8	1.0	1.4	0.5	1.3	2.3	6.0	8.0	2.6	2.5

Since for many atmospheric physics and meteorology problems in- formation on the atmospheric parameters with quite high accuracy is required (for example, for the weather prediction problem the temperature profiles must be known to within 0.5 - 1° [23]), the question of the feasibility of satisfying these requirements on the basis of experimental Earth radiation spectra obtained from satellites is of great importance. This question is obviously associated with the empirical data information content. This question was examined in a rigorous formulation by Marchuk in [24], where he gave a general solution of the problem of validity of the information used for inverse optical sounding problems. The basic idea of [24] lies in establishing the connection between the variations of the functionals describing the input information in the sought function variation and some specially obtained functions characterizing the information validity in relation to these functionals. This idea was used in some degree of concreteness in examining the radiation spectra information content in the statistical inverse problem solution methods.

§ 5. Initial Data Information Content

In application to (6.7) it is natural to formulate the information content question as follows: what useful information on the physical parameter φ_i (y), subject to determination from (6.7), can be extracted from the experimental data f (x), whose error structure ε (x) is known, with account for the given physical mechanism of φ_i (y) transformation into f (x), described by the equation kernel. In this formulation, with the additional assumptions that the structure ε (x) is completely defined by the variance σ_f^2* and that the solution structure as a random function is given by the empirical orthogonal basis φ_{ik}, this question was examined thoroughly by Kozlov in [25, 27]. The results of these studies were verified in the solutions of (6.21) presented in § 4 and are of direct interest for the problem of determining T' (ζ_i). Therefore we shall discuss briefly the basic ideas of [26, 27].

Reconciliation of the inverse problem regularization with the initial information errors was carried out in [26, 27] using the geometric properties of the Fisher information metric [26] corresponding to the given experiment and defined by the kernel of (6.21) and the measurement error structure. Since to each random vector T' (ζ_i) there corresponds a system of n coefficients c_k of the expansion (6.22) in the empirical orthogonal vectors φ_{ik}, the c_k form an n-dimensional space R_n. In the solution space parametrized in this fashion the author of [20] introduces a metric, i.e., the distance between the two random functions T'$_1$ and T'$_2$

$$\rho^2 (T_1', T_2') = \sum_{k,l=1}^{n} g_{kl} \, [c_k^{(1)} - c_k^{(2)}] \, [c_l^{(1)} - c_l^{(2)}], \qquad (6.27)$$

---

* For this it is sufficient to assume that the initial data errors are distributed normally with zero mathematical expectation. We note that this assumption, and use of the empirical orthogonal basis as well, is not fundamental for the following estimates.

where g_{kl} are components of the Fisher information matrix [24], which in the case of (6.21) concides to within the constant factor $1/\sigma_f^2$ with the positive definite matrix of (6.24)

$$g_{kl} = \frac{\Gamma_{kl}}{\sigma_f^2}.$$
(6.28)

In connection with the inverse problem incorrectness there may exist in R_n sets c_k to which there correspond vectors $T'(\zeta_i)$ which do not have the real physical meaning which follows from the a priori information on the solution. Therefore it is necessary to examine only that region D of this space which contains admissible problem solutions. With the aid of the metric (6.27) we can evaluate in this region the possibility of solving (6.24). It is quite clear that if for two vectors T'_1 and T'_2 the distance $\rho(T'_1, T'_2) \leq 1$ these functions are not distinguishable from one another in the limits of the given error of. The instability of the inverse problem solution is associated with the existence of directions in the space R_n along which the region D has dimensions less than unity.

If we take as the region D that set of parameters c_k and corresponding random vectors $T'(\zeta_i)$ from which the autocorrelation function $B_{TT}(\zeta_i, \zeta_j)$ was determined, on the basis of the definition of $B_{TT}(\zeta_i, \zeta_j)$ and the representation (6.22) we obtain

$$B_{TT}(\zeta_i, \zeta_j) = \sum_{k,l} \overline{c_k c_l} \varphi_k(\zeta_i) \varphi_l(\zeta_j).$$

Here the quantities $d_{kl} = \overline{c_k c_l}$ form a matrix specifying the region D.

It $\varphi_k(\zeta_i)$ are eigenvectors of $B_{TT}(\zeta_i, \zeta_j)$ the matrix d_{kl} is diagonal and consists of the eigenvalues of $B_{TT}(\zeta_i, \zeta_j)$ arranged in decreasing order. Applying the matrix (6.27) as before, the author of [25] determines the principal axes $(u_1, \ldots, u_m)$ of region D from the following eigenvalue problem

$$\sum_{k=1}^{n} \sum_{l=1}^{m} g_{kl} d_{km} u_l - \lambda u_m = 0. \tag{6.29}$$

By definition of the metric in D the quantities $\sqrt{\bar{\lambda_1}}, \ldots, \sqrt{\bar{\lambda_n}}$ determine the lengths of the principal axes of region D, normed by the mean-square measurement errors in the corresponding directions. Selecting eigenvalue sequences $\lambda_1, \ldots, \lambda_r$ satisfying the condition $\lambda_i > 1$ $(i = 1, 2, \ldots, r \leqslant n)$ and the corresponding eigenvectors $u_1, \ldots, u_r$, we can sort out those directions in region D for which $\lambda_i < 1$ (i = r + 1, $\ldots$, n), i.e., the initial data do not carry useful information on the solution. This regularization process corresponds to identification of all the independent solution parameters whose definition error is obviously beyond the threshold characterized by the measurement error variance. With account for the expansion (6.22) in the subspace R_r, in which the vector sequence $u_1, \ldots, u_r$ forms an orthogonal (by construction) basis, we can introduce the new system of vectors

$$\psi_m(\zeta_i) = \sum_{k=1}^{n} u_m^k \varphi_k(\zeta_i) \qquad (m = 1, 2, \ldots, r), \tag{6.30}$$

which provide optimum representation of any random vector T (ζ_i) reconciled with the solution structure, equation kernel, and initial data error. If we represent the solution of (6.21) in expansion form

$$T'(\zeta_i) = \sum_{m=1}^{r} \tilde{c}_m \psi_m(\zeta_i), \tag{6.31}$$

substitute (6.31) into (6.21) and apply the least squares method we obtain the diagonal equation system for determining $\tilde{c}_m$

$$\tilde{c}_m = \frac{\tilde{F}_m}{\sqrt{\tilde{\Gamma}_{mm}}} \qquad (m = 1, 2, \ldots, r), \tag{6.32}$$

where

$$F_m = \sum_{v=1}^{N} \tilde{D}_{vm} f_v; \qquad \tilde{\Gamma}_{mm} = \sum_{v=1}^{N} (\tilde{D}_{vm})^2;$$

$$\tilde{D}_{vm} = \frac{\partial B_v\,[\bar{T}\,(1)]}{\partial T'}\,P_v(1,1)\,\psi_m\,(1) - \int_0^1 \frac{\partial B_v\,[\bar{T}\,(\zeta)]}{\partial T'}\,\psi_m\,(\zeta)\,\frac{\partial P_v(1,\zeta)}{\partial \zeta}\,d\zeta.$$

Here the mean square error of $\tilde{c}_m$ determination is $\sigma_f / \sqrt{\tilde{\Gamma}_{mm}}$, and of the solution of (6.31) it self is

$$\sigma_T(\zeta_i) = \sigma_f \left[\frac{\psi_m^2(\zeta_i)}{\tilde{\Gamma}_{mm}}\right]^{1/2}. \tag{6.33}$$

The effectiveness of the described method is illustrated by the example considered in [26, 27] of determining the required problem optimization parameters with the aid of which the profile $T'(\zeta_i)$ used in the numerical experiment of [5] was reconstructed (see Figure 6.2a). The calculations [26] show that the reconciled orthogonal basis consists of three vectors $\psi_m(\zeta_i)$, to which there correspond three eigenvalues exceeding unity: $\lambda_1 = 488.4$; $\lambda_2 = 8.1$; $\lambda_3 = 2.5$. The results of $T'(\zeta_i)$ reconstruction using (6.30) — (6.32) and calculations of the mean square error of the reconstructed profile are shown in Figure 6.4. As we would expect, the largest errors σ_T of $T'(\zeta_i)$ determination, reaching $2°$, are observed near the tropopause. An analogous method using the Shannon information metric for selecting optimum radiation measurement conditions with a broader range of a priori assumptions on the solution was examined by Pokrovskii in [28].

Numerical characteristics of the initial data information content were also obtained in [26, 27]. As mentioned previously, the quantity $\sqrt{\lambda_m}$ represents the number of mutually distinguishable values of the coefficients $\tilde{c}_m$ in the expansion (6.31). Since the reconciled basis (6.30) is orthogonal the $\tilde{c}_m$ are determined independently. Therefore the number of combinations of these coefficients and, consequently, the number of profiles $T'(\zeta_i)$ which

differ from one another in the limits determined by the measurement error σ_f is

$$V = V \overline{\lambda_1 \lambda_2 \ldots \lambda_r.}$$ (6.34)

The quantity V, meaning the volume of an ellipsoid in the space R_r with principal axes $\sqrt{\lambda_1}$, ..., $\sqrt{\lambda_r}$, thus characterizes the volume of information on T' (ζ_i) which can be obtained by the given f_ν measurement method. For the considered spectrum segments with $\sigma_f = 0.4°$ this constitutes several percent of the maximum value of f_ν, V = 95, i.e., the measurement method used makes it possible to obtain on the order of 100 different temperature profiles. This is not too many if we consider that by conventional sounding at ten levels ζ_i with 1° error we can distinguish about 1800 T' (ζ_i) profiles.

In order to increase the information content Kozlov [27] suggested "combining" the spectral intervals in which the I_ν are measured (in [27] this operation is termed "patching" of the corresponding channels, Figure 6.5).

If we assume that the random error variance does not change in this operation the information volume V increases (for example, combining the eight ν intervals used in [27, 29] into three intervals leads to V = 226 in place of 95). The author of [27] explains this effect by the existence of "internal correlation" between intervals of a single group, showing up in consistent f_ν variations when varying $\tilde{c}_m$ for different T' (ζ_i). Therefore suitable spectral resolution reduction does not reduce the information but does reduce the overall measurement error. This conclusion is of paramount importance in developing instrumentation to provide effective solution of optical sounding problems. In fact, as Figure 6.6 shows, reconstruction of T' (ζ_i) (Curve 1) on the basis of I_ν specified in 48 narrow spectral segments of

the CO_2 15 μ ($\Delta\nu = 2cm^{-1}$) band (Curve 2) and in two broad intervals obtained by "patching" (Curve 3) leads to practically the same result. In this case, however, "patching" does not yield any additional information on the given specific profile. The reason is probably that the Kozlov optimization method provides exhaustive use of the initial information obtained by the given measurement method*. This property is also illustrated in the figure.
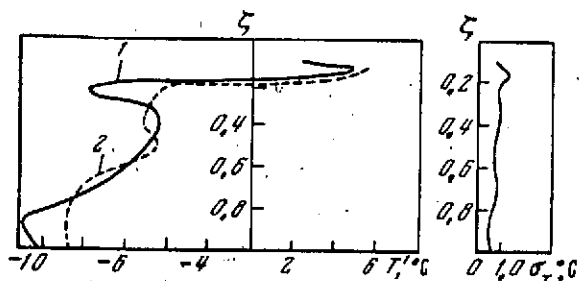
Figure 6.4. Reconstruction of T' (ζ) vertical profile after [27] (a) and the mean-square error profile σ_T (ζ) (b)

1- initial profile; 2- reconstructed
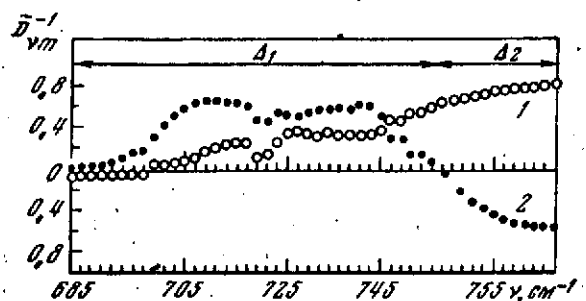
Figure 6.5. Inverse matrix $\tilde{D}^{-1}_{\nu_m}$ (6.32) calculated in [2.40] and spectrum intervals (Δ_1 and Δ_2) which are optimum for noise level 1% (10^{-8} w)

1- $\tilde{D}^{-1}_{\nu_1}$; 2- $\tilde{D}^{-1}_{\nu_2}$
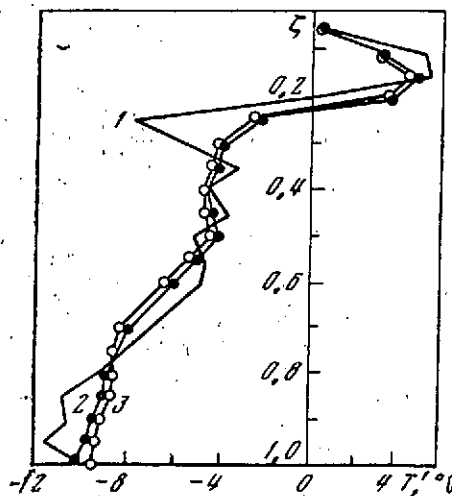
Figure 6.6. Reconstruction of T' (ζ) from I_ν

1- initial profile; 2- using 48 intervals; 3- using two intervals

* In the numerical experiment case the "measurement method" concept also includes the kernel properties and the computational error.

Concrete estimates of the initial data information content for given measurement error and kernel structure but without account for the solution structure were obtained by Twomey in [30]. It was shown in [30] that if there are N f_i measurements with error variance σ_f^2 and if there exist $n \leqslant N$ eigenvalues of the matrix $K = \| k_{ij} \|$

$$k_{ij} = \int_a^b K(x_i, y) K(x_j, y) \, dy \qquad (i, j = 1, 2, \ldots, N),$$

satisfying the inequality

$$\lambda_i \leqslant \frac{\sigma_f^2}{(b-a) \varphi_m^2} \qquad (i = 1, 2, \ldots, N)$$

$(\varphi_m = \max_{a \leqslant y \leqslant b} |\varphi(y)|)$, then among the N components of the vector f_i there are only N - n independent information components.

It is not difficult to see that this information content estimate is less exact and less definite in comparison with the Kozlov estimates [26], since [30] uses a priori information on the solution in the form of the maximum value of the sought function.

The estimates of initial data information content presented in [26, 27] are accompanied by construction of the corresponding incorrect problem regularization method, involving determination of the reconciled basis ψ_m (ζ_i) which cuts off obviously unreliable information. However, as before we cannot guarantee that the harmonics considered in this method, which carry useful information in the average effectiveness estimate case, will provide an acceptable approximation for determining concrete vertical profile realizations. In this connection we shall examine the statistical regularization method, which permits constructing regularized solutions with guaranteed closeness to the true solution.

§ 6. Statistical Regularization Method

It follows from the very nature of incorrect problems that
in the presence of random experimental and computational errors
ε (x) there exists an infinite set of random functions $\widetilde{\varphi}(y)$ which
satisfy (6.1), i.e., the condition

$$\left| f(x) - \int_a^b K(x, y) \widetilde{\varphi}(y) \, dy \right| \leqslant \varepsilon(x),$$
(6.35)

but are not the physical colution of the φ (y) problem. In con-
nection with error amplification these may include functions which
are arbitrarily far from φ (y). Therefore it is natural that the
apparatus of mathematical statistics be used to construct the reg-
ularized solution. This is even more necessary for optical atmos-
pheric sounding problems, since the variations of the atmospheric
parameters being determined are random functions about which the
a priori information is given by statistical characteristics (see
Chapter 3).

The statistical method of regularizing incorrect problems,
developed by Turchin in [31-34], was tested in the problem of
determining vertical temperature profiles [35]. Therefore we
shall discuss the basic idea of the method using this problem
as an example.

We replace (6.7) by a system of algebraic equations

$$\sum_{j=1}^n K_{ij}\varphi_j = f_i + \varepsilon_i \qquad (i = 1, 2, \ldots, N),$$
(6.36)

assuming that ε_i also includes the algebraization errors. The
problem reduces to determining an n-dimensional vector $\varphi = \{\varphi_j\}$
on the basis of the given N-dimensional vector $f = \{f_i\}$, each
component of which includes the error $\varepsilon = \{\varepsilon_i\}$. We shall assume

that the ε_i are statistically independent and are distributed normally with known variance σ_i and zero mathematical expectation. Then the distribution function of the random vectors $\varphi = \{\varphi_j\}$ satisfying (6.36) with accuracy to ε_i (set of unregularized solutions) has the form

$$P\left(\frac{f}{\varphi}\right) = \frac{(\sigma_1 \sigma_2 \ldots \sigma_n)^{-1/2}}{(2\pi)^{n/2}} \exp\left\{-\frac{1}{2}\sum_{i=1}^{N} \sigma_i^{-2}\left[\sum_{j=1}^{n} K_{ij}\varphi_j - f_i\right]^2\right\}. \tag{6.37}$$

Expression (6.37) indicates the conditional probability that for a given state of the sought parameter φ the vector f will be obtained with error $\varepsilon (\sigma_i^2 = \bar{\varepsilon}_i^2)$ as a result of measurements. In order to find among the vectors φ the inverse problem solutions having physical meaning it is necessary to impose on this set limiting conditions characterizing the real state of the quantities being determined, i.e., introduce apriori information on the solution. For atmospheric parameters such information is contained in the statistical characteristics of their vertical structure, specifically, in the correlation matrices $B_{\varphi\varphi}(b_{hj} = \overline{\varphi_h\varphi_j})$. Therefore it is natural to take as the apriori information a normal distribution of the vectors φ such that the correlation matrix for it coincides with $B_{\varphi\varphi}$

$$P(\varphi) = \frac{1}{(2\pi)^{n/2}|B|^{1/2}}\exp\left[-\frac{1}{2}\sum_{k=1}^{n}\sum_{j=1}^{n} c_{kj}\varphi_k\varphi_j\right]. \tag{6.38}$$

Here $C = B^{-1}$ (B^{-1} is the inverse of B, $|B|$ is the determinant of the latter).

Solutions of (6.36) satisfying the problem physical formulation must at the same time be among the distributions (6.37) and (6.38) and, consequently, must form a set of random vectors, characterized in accordance with the Bayes formula by the distribution function

$$P\left(\frac{\varphi}{f}\right) = \frac{P(f/\varphi)\,P(\varphi)}{\int P(f/\varphi)\,P(\varphi)\,d\varphi}. \tag{6.39}$$

Formula (6.39) defines the conditional probability that for the given vector f the physical state of the sought parameter is described by the vector φ (a posteriori regularized solution distribution).

In our case (6.39) will have the form (to within a constant factor, not essential for the further operations)

$$P\left(\frac{\varphi}{f}\right) = \text{const} \exp\left\{-\frac{1}{2}\sum_{i=1}^{N}\sigma_i^{-2}\left[\sum_{j=1}^{n}K_{ij}\varphi_j - f_i\right]^2 - \frac{1}{2}\sum_{k=1}^{n}\sum_{j=1}^{n}c_{kj}\varphi_k\varphi_j\right\}. \qquad (6.40)$$

After elementary transformations and norming (6.40) may be re-written in the form

$$P\left(\frac{\varphi}{f}\right) = \text{const} \exp\left[-\frac{1}{2}\sum_{k=1}^{n}\sum_{j=1}^{n}D_{kj}\varphi_k\varphi_j + \sum_{j=1}^{n}F_j\varphi_j\right], \qquad (6.41)$$

where

$$D_{kj} = \sum_{i=1}^{N}\frac{K_{ik}K_{ij}}{\sigma_i^2} + c_{kj}; \qquad F_j = \sum_{i=1}^{N}\frac{K_{ij}f_i}{\sigma_i^2}. \qquad (6.42)$$

Among the set of regularized solutions satisfying the conditions (6.39) or (6.41) the most probable, naturally, will be the vector $\langle\varphi\rangle$, obtained as the mathematical expectation of φ from the distribution $P(\varphi/f)$

$$\langle\varphi\rangle = \int\varphi R(\varphi/f)\,d\varphi.$$

In the case (6.41) we obtain the system of equations for determining the vector $\langle\varphi\rangle$

$$\sum_{k=1}^{n}D_{kj}\langle\varphi_k\rangle = F_j \qquad (j = 1, 2, \ldots, n), \qquad (6.43)$$

which then yields the unique statistically regularized solution of (6.36) and, consequently, of the inverse optical sounding problems supported by statistical a priori information[*].

[*] We note that the Turchin method can also be used to regularize the problem in the absence of such information, using a priori information on smoothness of the sought solutions (see [31-33].

Since the distrubution function (6.41) yields all the regu-
larized problem solutions it is of interest to estimate the de-
viation of these solutions from $\langle\varphi\rangle$, which is characterized by
the variance

$$\sigma_\varphi^2 = \langle[\varphi - \langle\varphi\rangle]^2\rangle = \int(\varphi - \langle\varphi\rangle)^2 P(\varphi/f)\,d\varphi.$$

In the case of distribution (6.41) the mean-square error of φ
reconstruction is expressed in terms of diagonal elements of the
matrix D^{-1}, i.e.,

$$\sigma_j = \sqrt{(D^{-1})_{jj}} \qquad (j = 1, 2, \ldots, n). \tag{6.44}$$

These results are used below to determine the vertical atmos-
pheric temperature and moisture profiles*. Here it should be
emphasized that the statistical regularization relations presented
above were based on the assumption of normal distributions of the
errors ε (x) and the sought parameters φ. However, these assump-
tions, which may not be satisfied under actual conditions, are
not fundamental. If the empirical multivariate distributions
deviate from the normal distributions, then, approximating these
distributions by suitable functions and using the distributions
for φ as a priori information we can obtain by the Turchin method
the regularization relations for specific physical conditions.

§ 7. Results of Temperature Determination

Reconstruction of the atmospheric vertical temperature profiles
using the statistical regularization method was carried out in [35]
on the basis of balloon measurements of the self-radiation I_ν.

---

* An analogous algorithm for regularizing incorrect problems with
use of apriori information in the form of the correlation matrixes
B_{TT} was obtained in [36, 37] under different initial assumptions.

For this purpose use was made of I_ν measurement data obtained with the aid of a multichannel spectrometer [38] in the six segments of the band CO_2 15 μ mentioned in § 4 and in the 899 cm^{-1} [21] window, and also the radiation spectra measured using a Fourier spectrometer with resolution on the order of 2 cm^{-1} [2.35]. The measurements of [2.35, 21] were made above the same points (Palestine, Texas and Sioux Falls, South Dakota) in the summer season. According to the authors of [2.35, 21] the measurement errors did not exceed 1%.

The vertical temperature and humidity profiles were measured directly simultaneously with I_ν, which made it possible, on the one hand, to check the methods for reconstructing T (ζ) and, on the other hand, to take into account water vapor transmission in the kernel of (6.1). Since in [21] empirical orthogonal functions obtained by statistical processing of the measurement region /212 temperature profiles were used to reconstruct T (ζ), we had the possibility of using the corresponding mean profiles $\bar{T}$ (ζ). Unfortunately the correlation matrices were not presented in [21], therefore we took the matrices obtained from the data of aerological soundings up to 10 mbar [3.26] (see § 3 of Chapter 3).

As for the kernel of (6.1), the authors of [21] calculated the transmission functions for cases of measurements above both points (for Palestine the kernels are presented in Figure 6.7). For our calculations [35] we used the transmission functions obtained during analogous measurements above Palestine in 1964 [21] (see Figure 2.10). These functions were close to the kernels of Figure 6.7.

In [35] the vertical profile variations T' (ζ_i) were determined using closed and unclosed schemes. In the closed scheme (we denote it by A_1) I_ν and $\bar{I}_\nu$ were calculated using (6.1) from the
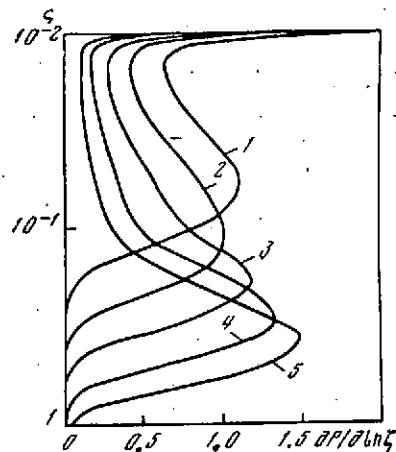
Figure 6.7. Kernel of (6.1) from [21] and [35] for different spectrum segments ($\Delta\nu = 5$ cm^{-1})

1- $\nu = 667.5$ cm^{-1}; 2- 691 cm^{-1}; 3- 697 cm^{-1}; 4- 703 cm^{-1}; 5- 709 cm^{-1}
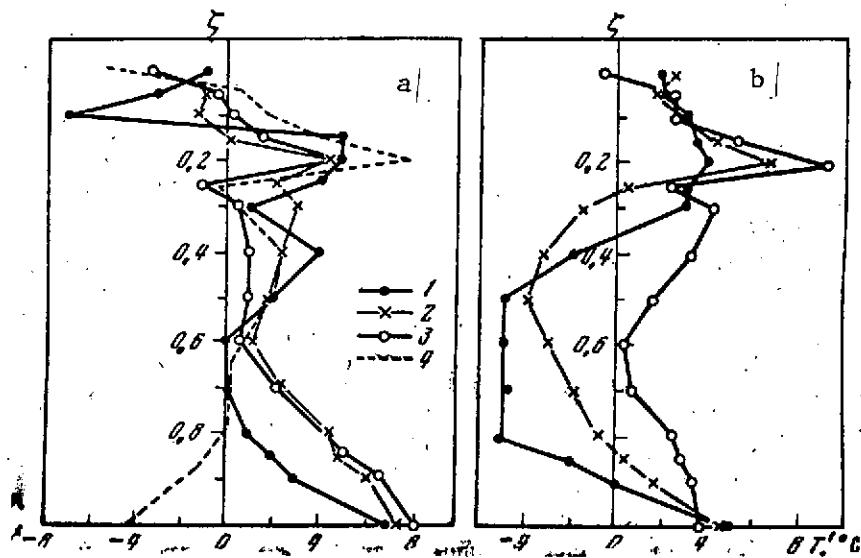
Figure 6.8. Determination of T' (ζ) in [35] from balloon measurement data [6.21]

a- Palestine 15.02 CST; b- Sioux Falls 12.22 CST; 1- initial profile; 2, 3- profiles reconstructed using schemes A_1 and A_2, respectively; 4- calculation using A_2 for morning measurements
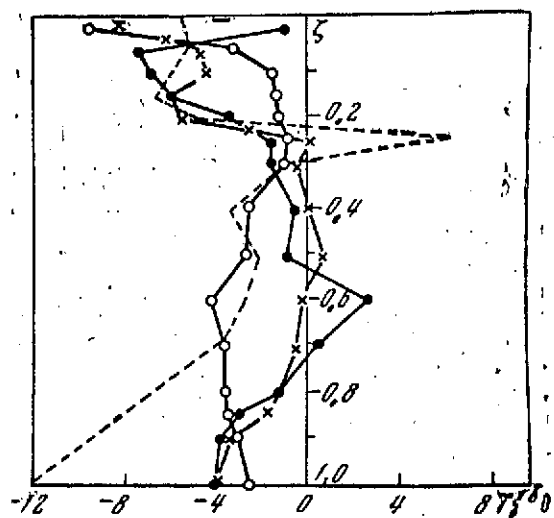
Figure 6.9. Determination of T' (ζ) from interferometric data [23]
Palestine, 8 May 13.30

Notations same as in Figure 6.8
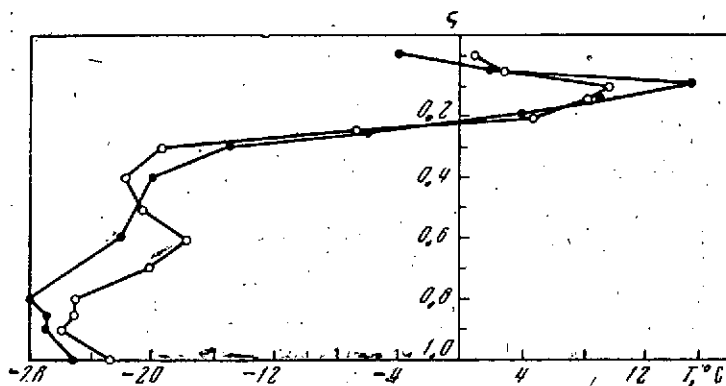
Figure 6.10. Determination of T' (ζ) using closed scheme for
Sioux Falls with mean T̄ (ζ) profile for Palestine

Notations same as in Figure 6.8
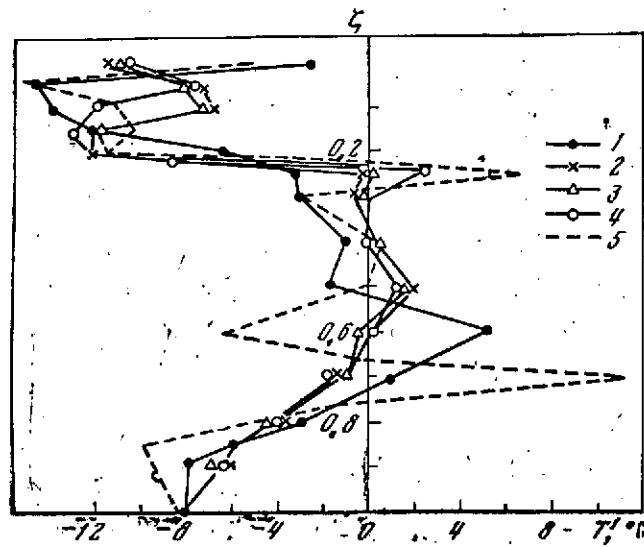
Figure 6.11. Determination of T' (ζ) with different errors and number N of initial I_ν information spectral intervals

1- initial profile; 2, 3- reconstructed profiles for $(\sigma_i/I_i)' = 1\%$ and N = 9 and N = 45, respectively; 4, 5- for $(\sigma_i/I_i) = 0,1\%$ and N = 9 and N = 45, respectively

known realization of the T (ζ_i) profile and the mean $\bar{T}$ (ζ_i) profile. Then a random error with mean-square deviation 1% was added to I_ν and the variation T' (ζ_i) was reconstructed with application of (6.42) — (6.44) to (6.21). Comparisons of the T' (ζ_i) profiles reconstructed using scheme A_1 with the initial profiles are shown in Figures 6.8-6.11.

The mean-square error σ_T of T' (ζ_i) reconstruction using scheme A_1 does not exceed 3° at the tropopause level, which is the most unfavorable level for the method (Table 6.2). However the actual errors of reconstruction of given T' (ζ_i) realizations using (6.42) — (6.44) for direct I_ν measurements (unclosed scheme A_2) were somewhat larger, as can be seen from Figures 6.8 and 6.9 and Table 6.1.

TABLE 6.1.   TEMPERATURE DETERMINATION ERRORS $T_{cal} - T_{true}$ (IN °C) ASSOCIATED WITH MEASUREMENT AND COMPUTATIONAL SCHEME ERRORS (σ_T IS THE MEAN-SQUARE ERROR FOR $\sigma_I/I = 0.01$*

ζ	Palestine, 7.57		Palestine, 15.00		Sioux Falls, 12.20		Palestine, 13.80		Palestine, 8.30	
	A_1	A_2	A_1	A_2	A_1	A_2	A_1	A_2	A_1	σ_T
1	0,6	—14,5	0,3	1,3	0,2	—1,3	0	1,3	—8,0	0,1
0,9	5,2	—5,6	3,2	3,7	1,8	3,5	0,7	0,8	—5,9	1,7
0,85	4,8	—4	3	3,2	2,4	4,9	1,1	—0,7	—5,2	1,7
0,8	5,1	—2	3,5	3,4	4,4	7,7	0,2	—2,3	—5,4	1,8
0,7	4,3	0,1	2,4	2,2	3,1	5,7	—0,9	—4,3	—4,5	1,3
0,6	0,5	—1,3	1,0	0,7	2,0	5,4	—2,8	—6,8	—5,5	1,1
0,5	—0,5	—1,9	—0,2	—1,0	1,2	6,7	1,7	—1,9	—1,4	1,0
0,4	—0,7	—2,6	—1,8	—2,9	—1,4	5,3	4,5	—2,3	—2,8	1,0
0,3	—0,3	—5,7	2,0	—0,5	—4,6	1,1	1,1	0,3	0,9	1,1
0,25	—1,6	—6,3	—1,7	—5,4	—2,6	—0,6	1,6	2,6	7,8	2,6
0,2	1,3	2,9	—0,4	—0,2	2,9	5,3	—2,2	4,3	—1,0	1,9
0,15	—4,4	—0,8	—4,2	—3,4	1	1,9	0,1	4,5	0,5	1,3
0,1	4	7,8	5,6	7,2	—0,2	—0,3	2,6	5,4	1	1,1
0,05	2,4	3,1	2	2,6	—0,1	0,5	2,8	4,3	2,1	1,2
0,01	—3	—6,1	—2,4	—2,1	0,3	—2,6	—7,2	—8,6	—4,5	1,7

* Translator's note: Commas in the numbers represent decimal points.

To clarify the possible reasons for these discrepancies it is necessary to compare the experimental radiation values I_e with the values I_c calculated using the initial T (ζ_i) profiles with the aid of (6.1) for the transmission function shown in Figure 6.7. The results of this comparison presented in Table 6.2 show that the actual initial information error for the given equation kernel and the computational method used exceeds 1% in most cases. Here <u>/215</u> we should keep in mind that the error of the function $f_\nu = I_\nu - \bar{I}_\nu$, which is used directly in inverting the problem, is an order of magnitude larger.

In fact, the best agreement of the temperature profiles calculated using schemes A_1 and A_2 with one another and with the

TABLE 6.2. COMPARISON OF RADIATION MEASUREMENTS I_e WITH CALCULATED VALUES I_c (IN 10^3 cal·cm^2·sr^{-1}·μ^{-1});*

$$\varepsilon = \frac{I_c - I_e}{I_c} \cdot 100\%$$

Center of band		Palestine, morning					Palestine, noon				Sioux Falls, noon .12.22				
λ, μ	ν,см$^{-1}$	$\bar{I}_\nu$	I_e|	I_c|	ε	ε*	I_e|	I_c|	ε	ε*	$\bar{I}_\nu$	I_e|	I_c|	ε	ε*
14,74	677,5	2,91	2,72	2,81	3	3	2,79	2,76	—1	0	2,90	2,92	3,04	4	2
14,47	691,0	2,82	2,75	2,76	0	—1	2,75	2,71	—1	—1	2,89	3,02	3,05	1	0
14,35	697	3,01	3,05	3,05	0	—2	3,01	2,99	—1	—1	2,94	3,10	3,11	0	—1
14,22	703	3,64	3,70	3,81	3	—1	3,67	3,71	—1	—0	3,22	3,48	3,34	—6	—4
14,10	703	4,58	4,69	4,82	3	—3	4,64	4,69	—1	—2	3,77	4,00	3,78	—6	—3
11,23	899	13,7	12,8	15,8	20	20	15,3	15,1	—1		8,43	8,99	9,20	3	0

* Translator's note: Commas in numbers represent decimal points.

initial profile T' (ζ_1) is obtained for the case of I_ν measurements at Palestine at 15.00 (Figure 6.8a), for which the difference $I_e - I_c$ is 1% (see Table 6.2). However, even in this case the reconstructed profiles do not capture the details of the vertical variation T' (ζ_1) in regions of marked temperature gradient change.

Worthy of attention are the large discrepancies between the reconstructed and initial profiles at the Earth's surface and in the boundary layer for the morning hours (dashed curves in Figures 6.8a and 6.9), although as noted above the incorrect problem solution is always stable at the point ζ = 1 thanks to the presence in (6.1) of the term B_ν [T (1)] outside the integral, which describes the Earth's surface radiation attenuation in the atmosphere. This discrepancy is associated with the fact that the initial T (ζ_1) profiles taken for comparison are known only for midday. The lower temperatures recorded by the instrumentation in the morning hours reflect the daily temperature variation, which is marked in the atmosphere layer near the Earth and decreases with altitude (at the 700 mbar level the morning and midday profiles,

shown in Figures 6.8a and 6.9, already approach one another and the initial profile).

Thus the statistical method of temperature reconstruction permits obtaining the temporal variation of T (ζ_i), at least in the atmospheric boundary layer and perhaps also at the tropopause level. The latter possibility is indicated by the opposite-in-sign temporal variations of the temperature in the near-Earth layer and in the tropopause region shown in Figures 6.8a and 6.9, confirming the assumption stated in [3.6] (see § 2 of Chapter 3) concerning the reasons for the negative T' (ζ_i) at these levels.

It should be noted that in all the cases cited the T' (ζ) profiles which were to be reconstructed had quite complex "non-standard" structure (variations of T' of the same sign at all levels in the troposphere were not accompanied by variations of opposite sign in the stratosphere). Particularly complex is the profile in Figure 6.8b, and it is probable that the marked reconstruction errors even when using scheme A_1 are partly associated with this factor. We see from Table 6.2 (Sioux Falls, 12.22) that the reason for the high reconstruction errors when using scheme A_2 are the discrepancies between I_e and I_c, which are the most significant among all the examples considered and are partially due to application to this case of the transmission functions for Palestine (see Figure 6.7). These relationships between I_e and I_c are basically confirmed by the analogous calculations of I_e in [21] (see ε^* in Table 6.2).

The results presented of trials of the statistical regularization method for profiles of complex structure with use of the correlation matrices calculated for a completely different region as a priori information are promising from the viewpoint of the possibilities of actual solution of the posed problem. The method

368

is stable even if the mean profiles $\bar{T}$ (ζ_i) are taken for another region, which is illustrated by the example shown in Figure 6.10. Here the T' (ζ_i) profile for Palestine was reconstructed with use of $\bar{T}$ (ζ_i) for Sioux Falls, which explains the very large temperature variations, which however have a standard structure.

Since in [35] the T' (ζ) profiles were reconstructed using the optimum parametrization method for the same I_ν data for which the inverse problem was solved by the authors who made the measurements [21], it would appear to be well to compare the results obtained in [21] and [35]. However this comparison, shown in Table 6.1 and incidentally indicating approximately the same error of both methods, is not informative. The reason is that based on our extensive experience in using empirical orthogonal /216 functions for incorrect problem solution* reliable determination of the sought parameter even with the accuracy which was obtained, for example, in [5, 21] requires knowledge of the specific values of this parameter (see § 4). However, the statistical regulariza-tion method [31-33, 35] is characterized by quite reliable auto-matic incorrect problem solution based on the principle of determin-ing the most probable solution satisfying for the given measure-ment method the a priori known solution set structure.

An important advantage of the statistical method [31], and of the [25] method as well, is exhaustive utilization of the given information. As mentioned previously, for those averaged spectral transmission functions which are used in our calculations there is no need to measure I_ν in many spectral intervals. For fixed measurement error all the useful information on the solution

---

* The results of optimum parametrization method application for determining T (ζ) were first reported in papers of the author at the All-Union Conference on General Circulation [39] and the 15-th International Astronautic Congress in Warsaw [40].

is contained in a small number of I_ν values and this information is completely extracted with the aid of statistical regularization. In fact, as the example of reconstructing T' (ζ_i) for different numbers of I_ν values (see Figure 6.11) shows, increasing the number of ν intervals from 9 to 45 for fixed measurement error yields practically no additional information on the T' (ζ_i) profile. In other words, for given measurement errors, smoothness of the equation kernel, and nature of the a priori information it is not possible in principle to obtain a "finer" structure of the incorrect problem solution, no matter how much we increase the initial information volume. This conclusion is important in developing measurement techniques and interpreting experimental data intended for determining any atmospheric parameter with guaranteed accuracy. Specifically, the determination of the "fine" vertical temperature profile structure is controlled, first, by the structure of the atmosphere, i.e., by the vertical CO_2 concentration distribution p_0 (ζ) and the absorption band or line structure, i.e., by the behavior of k_ν as a function of ν. Thanks to the decrease of ρ_0 (ζ) with altitude the nature of the transmission function smoothness would not change in comparison with the curves of Figure 6.7 even if it were possible to resolve an individual line. Second, the a priori information taken in the form of the correlation matrices B_{TT}, which describe the most significant features of the T' (ζ_i) structure, imposes definite limitations. It is probable that use of higher order moments is necessary to reconstruct the fine details.

In this connection we cannot expect that simple measurement error reduction which is not coordinated with the other factors will permit obtaining a more refined solution of the incorrect problem. As the example of T' (ζ_i) reconstruction (see Figure 6.11) shows, error reduction with simultaneous increase of the number of ν intervals leads to a result which is at first glance

paradoxical — manifestation of solution instability. The obvious reason for this effect is the marked increase in (6.40), (6.42) of the weight of the first term, which is associated with the equation kernel and the error variance σ_i^2, in comparison with the regularization term. Therefore steps in the same direction such as increasing the number of spectral intervals (from 9 to 45 in Figure 6.11) and reducing σ_1 may lead to weakening of the regularization if we do not coordinate these actions with a priori information selection. This important and delicate question of statistical regularization, and also the question of representativity of a priori information obtained from limited samples of random T' (ζ_1) profiles for individual regions and time intervals, requires special study.

However, we can state that the statistical regularization /217 method with use of the correlation matrices or their eigenvectors as a priori information makes it possible to determine the vertical atmospheric temperature profile with mean-square error of order 2-3°, provided the radiation I_ν is measured to within 1-2% and the equation kernel errors, i.e., the deviations of P_ν (ζ) from the real transmission function, are included in this error.

Examples of Earth's self-radiation intensity measurements using interferometers and multichannel radiometers installed aboard balloons [2, 35, 21] and the Nimbus 3 satellite [41, 42] show that the modern spectral and radiometric apparatus makes it possible to obtain the basic experimental data with the required accuracy. As for taking into account the real IR radiation absorption in the atmosphere, associated with variations of the water vapor, aerosols, temperature, CO_2 concentration, and possibly other atmospheric parameters, this task seems to us to be the most complex in the entire inversion problem even under visually cloudless atmosphere conditions. It becomes still more complex

with the presence of semitransparent cloud cover of the cirrus type. We shall devote a special section to this question.

§ 8. Account for Actual Absorption Variations in the Atmosphere

A study was made in [43] of the influence of the variations of certain physical parameters of the atmosphere which determine the variations of real IR radiation absorption, and we shall discuss certain results of this study here (these questions were also examined in [15]). Using various models of the transmission function in the CO_2 15 μ band (see § 2 of Chapter 2), it is not difficult to obtain a general idea of the I_ν variations associated with the possible variations of the kernel of (6.1). The results of the corresponding calculations are illustrated in Figure 6.12 (the standard T (ζ) distribution and constant relative CO_2 concentration $c_0 = 0.03\%$ were used for the calculations). The figure shows that the I_ν differences reach 20% in this case, i.e., they are commensurate with the I_ν variations due to temperature changes in the given region and even in similar climatic zones. In order to evaluate the temperature profile reconstruction errors when using any particular transmission function [2.21, 2.23] numerical /218 experiments were made for (6.21) using the closed (A_1) and unclosed (A_2) schemes. In scheme A_1 the T' (ζ_i) profiles were reconstructed using I_ν calculated with the aid of the given transmission function which was also used in problem inversion. In scheme A_2 the T' (ζ_i) profiles were reconstructed using the same I_ν but we took as the kernel of (6.21) a different transmission function. The results of these calculations, shown in Table 6.3 for two T' (ζ_i) profiles, indicate significant deviations of the profiles reconstructed using the A_2 scheme from the initial profiles.

Considering that the transmission function depends on the absorbing substance mass, we should also estimate the effects of

372

TABLE 6.3. RECONSTRUCTION OF T' (ζ_i) PROFILES (IN °C) WITH ACCOUNT FOR DIFFERENT TRANSMISSION FUNCTIONS ($T'_{A_i} - I_v$ [2.23], P_v [2.21]) *

T	ζ_i												
	1	0,9	0,18	0,7	0,6	0,5	0,4	0,3	0,25	0,2	0,15	0,1	0,05
T'_{in}	—10,2	—10,5	—9,0	—7,0	—4,7	—5,0	—4,3	—5,5	—7,9	0,3	5,1	5,7	0,6
T'_{A_1} [2.23]	—8,9	—8,5	—8,2	—7,9	—6,2	—4,5	—5,0	—4,5	—2,9	3,8	5,2	3,4	0,6
T'_{A_1} [2.21]	—7,9	—7,6	—7,3	—7,0	—5,5	—4,0	—4,5	—4,0	—2,5	3,3	4,6	3,0	0,6
T'_{A_2}	—17,2	—16	—16	—15	—12	—8,7	—9,8	—8,8	—5,5	7,3	10,1	6,6	1,2
T'_{in}	7,1	4,5	5,5	5,2	4,8	1,8	2,8	1,6	6,9	5,0	—1,7	—6,3	—0,2
T'_{A_1} [2.23]	7,8	7,5	8,2	7,0	5,5	4,0	4,5	4,0	2,5	—3,3	—4,6	—3,0	—0,6
T'_{A_1} [2.21]	7,6	7,3	7,0	6,8	5,3	3,8	4,3	3,9	2,5	—3,2	—4,5	—3,0	—0,5
T'_{A_2}	13,0	12,5	12,0	11,5	9,0	6,5	7,4	6,6	4,2	—5,5	—7,6	—5,0	—0,9

* Translator's note: Commas in numbers represent decimal points.
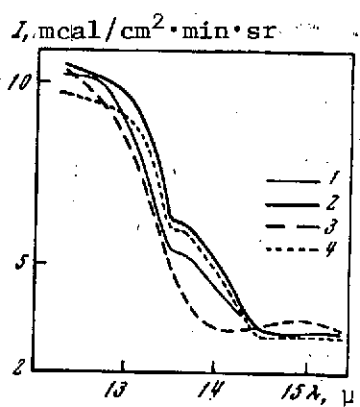
Figure 6.12. Self-radiation intensity I_v

1- calculated using transmission function from [2.21]; 2- from [5.23]; 3- using formula (1.16); 4- using formula (1.16) with account for H_2O vapor absorption
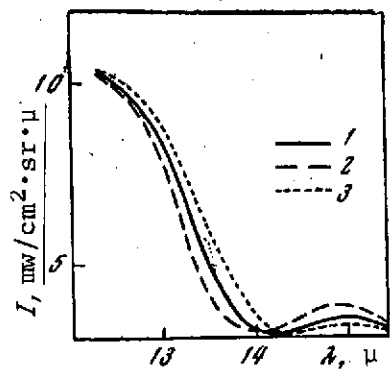
Figure 6.13. Self-radiation intensity I_v for different CO_2 concentrations

1- 0.03%; 2- 0.06%; 3- 0.015%

variations of the concentration c_0 and particularly of water vapor, whose bands overlap the 15 μ CO_2 band. The contribution to I_ν of overlap of the H_2O vapor bands in various segments of the CO_2 band is shown in Figure 6.12. As we would expect, the influence of H_2O vapor is most significant in the band wings. It would seem that the primary distortions of the reconstructed profiles should therefore be found in the lower troposphere. However, examples of comparison of the results of T' (ζ_1) profile reconstruction using scheme A_1 (i.e., with account for H_2O absorption both in I_ν and in the kernel of (6.21)) and using scheme A_2 (i.e., calculation of I_ν with account for H_2O absorption and reconstruction of T' (ζ_1) without account for the H_2O transmission function in the kernel of (6.21)), show (Table 6.4) that the temperature near the tropopause is most sensitive to these kernel variations and this is the region of maximum solution instability. We can also conclude from Table 6.4 that if we reduce the contribution of the band transparent region II to the initial information, then neglect of H_2O absorption does not lead to marked reconstruction errors. It is true that in this case we may not obtain reliable information on the lower troposphere temperature. Therefore a better approach is to develop methods for simultaneous determination of the vertical temperature and humidity profiles (see Chapter 7).

It is interesting to note the significant errors of T' reconstruction at the tropopause level for region II even in the closed scheme A_1. These errors are a direct consequence of the smoothness of the kernel of (6.1), characteristic of weak absorption regions.

As for the CO_2 concentration variations, as shown in [43] (Figure 6.13) the corresponding I_ν variations are relatively small /219 even for extreme c_0 values equal to 0.015 and 0.06% at all altitudes

(the latter condition is naturally unlikely under sea-level conditions). This gives a basis to expect that the real c_0 variations will have negligible influence on the temperature profile determination error.

TABLE 6.4. RECONSTRUCTION OF T' (ζ_i) (IN °C) BY THE OPTIMUM APPROXIMATION METHOD WITH AND WITHOUT ACCOUNT FOR WATER VAPOR ABSORPTION*

T'		ζ_i												
		1	0,9	0,8	0,7	0,6	0,5	0,4	0,3	0,25	0,2	0,15	0,1	0,05
I	T'_{A_1}	—8,3	—7,5	—7,0	—6,8	—5,0	—3,1	—3,8	—4,1	—5	—3,8	5,2	6,4	2,0
	T'_{A_2}	—7,3	—6,6	—6,3	—6,4	—4,8	—3,1	—3,9	—4,1	—6,0	—3,7	5,3	6,3	2,0
II	T'_{A_1}	—8,2	—7,6	—7,1	—6,6	—6,5	—6,01	—6,3	—4,1	5,8	21,2	5,4	—1,0	—1,0
	T'_{A_2}	—7,4	—6,4	—6,5	—6,1	—6,9	—7,8	—7,4	—4,4	—9,9	30,5	6,2	—3,1	—1,7
I	T'_{A_1}	6,0	6,0	6,1	6,2	4,2	2,2	3,1	3,6	6,5	7,9	—3,6	—4,2	—1,0
	T'_{A_2}	3,1	4,2	5,4	6,7	5,0	3,4	4,6	4,9	5,8	1,8	—4,5	—1,3	—0,1
II	T'_{A_1}	6,8	6,6	6,4	6,3	4,9	3,5	4,1	3,8	2,8	—3,2	—4,3	—2,9	—0,6
	T'_{A_2}	5,5	7,3	10,8	16,9	9,9	7,8	12,2	15,1	27,9	26,3	—17,5	—16,4	—5,5

* Translator's note: Commas in numbers represent decimal points.
Note. The initial T'_{in} and $\tilde{T}'_{in}$ profiles are presented in Table 6.3; I and II mean that in reconstructing T' we took, respectively, the regions of strong and weak absorption in the CO_2 band.

We did not evaluate the effect of transmission function variations due to changes of the air temperature itself in determining T (ζ) by the methods described above, since the complex nonlinear dependence of P_ν on T has not yet been studied sufficiently for real atmospheric conditions. Judging by calculations of the intensities of the CO_2 15 μ band lines for different temperatures [2.21, 2.22], this dependence will be quite weak and accounting for| it does not cause any fundamental difficulties (some proposals in this direction were described in [2.29]).

It seems to us that there is no need to evaluate the effect of each of the listed atmospheric parameters, since variations of IR radiation absorption by the aerosol layers and semitransparent cloud cover (particularly the high-altitude cirrus clouds) have the most significant and difficult-to-account-for influence. The random and unpredictable appearance of these objects in the measuring instrument field of view may cause far larger errors in $T(\zeta)$ determination in comparison with the errors due to the other factors listed above.

To illustrate this statement[*] we shall consider examples of $T(\zeta)$ profile determination from I_ν measurements aboard the Nimbus 3 satellite using the SIRS multichannel spectrometer in three cloudless cases [41, 42] (Kingston, Jamaica; Green Bay, Wisconsin; and Resolute Bay, Canada). The $T(\zeta)$ profiles were determined in [44] by the statistical regularization method with use of the same transmission function in all three cases. We see from Figure 6.14 that the closed scheme (A_1) makes it possible to reconstruct $T(\zeta)$ /220 with approximately identical errors, which are the errors of the computational scheme. However, reconstruction of $T(\zeta)$ using the unclosed scheme (A_2) leads to markedly different errors, which in the Kingston case reach 17° (in the tropopause region). However, if we introduce corrections to the transmission function which account for the additional contribution to atmospheric radiation (scheme $\tilde{A}_2$), the $T(\zeta)$ determination errors decrease to a few degrees.

In light of the foregoing the development of a technique for taking into account the corrections to the transmission function

---

[*] We note that this statement differs from the more optimistic conclusion of the authors of [41], according to which cirrus clouds do not represent a serious obstacle in the problem of determining vertical temperature profiles from the Earth's radiation.
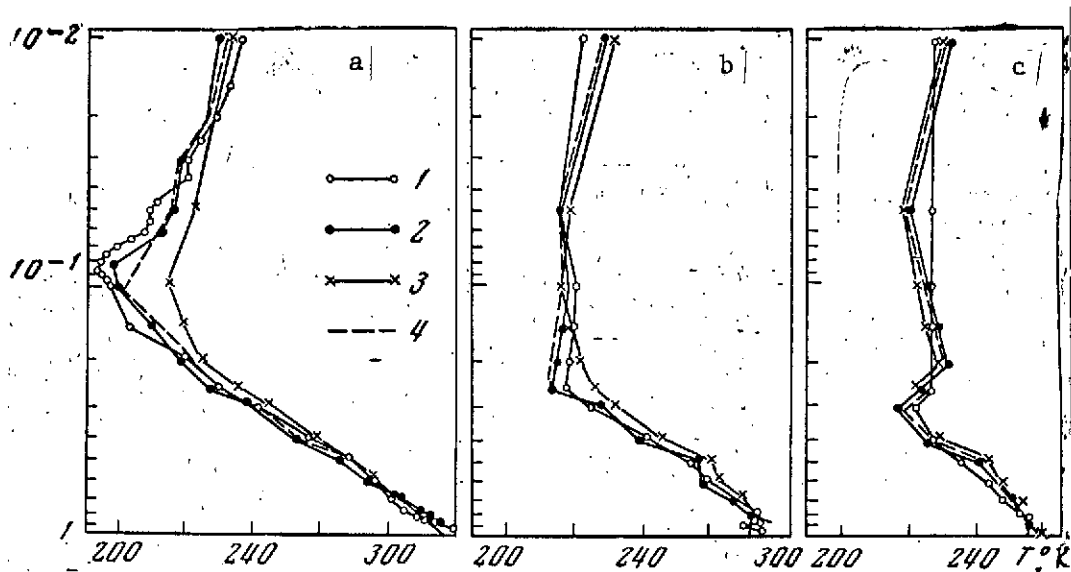
Figure 6.14. Examples of temperature profile T (ζ) determination from I_ν measurements obtained aboard the Nimbus 3 satellite [6.42]

1- initial profiles; 2, 3- profiles reconstructed using schemes A_1 and A_2, respectively; 4- profiles reconstructed with refined transmission function; a- Kingston; | b- Green Bay; c- Resolute Bay

in each specific I_ν measurement case, regardless of the origin of these corrections, takes on great importance. One possible approach to the solution of this problem is joint determination of the temperature profile T (ζ) and transmission function variation profile P_ν (ζ) from the same set of initial data. We propose for this purpose the following iteration process, based on the fact that limited information on the radiation I_ν is required for determining both parameters. After determining the first approximation T_1 (ζ) from I_ν measurements in a small number of spectral intervals and for some model (but sufficiently representative) transmission function P_ν (ζ), we can then use B_ν [T_1 (ζ)] and P_ν (ζ) to introduce an additive correction $\tilde{P}_\nu$ (ζ) to the real transmission function from the equation

$$\bar{f}_\nu = B_\nu [T_1(\zeta)] \, \tilde{P}_\nu(1) - \int_0^1 B_\nu [T_1(\zeta)] \frac{-\partial P_\nu(\zeta)}{\partial \zeta} d\zeta.$$

(6.45)

377

Here $\tilde{I}_\nu = \tilde{I}_\nu - \tilde{I}_\nu^{(1)}$; $\tilde{I}_{\nu}$, are the radiation values measured in the intermediate spectral intervals of the CO_2 band; CO_2; $I_\nu^{(1)} = I\,[B_\nu\,(T_1),\,P_\nu]_1$ is the functional (6.1) of $B_\nu\,[T_1\,(\zeta)]$ and $P_\nu\,(\zeta)$.

The solution of (6.45) for $\partial \tilde{P}_\nu\,(\zeta)/\partial\zeta$ can be carried out by one of the methods described above (an example of transmission function determination from an equation of the form (6.45) is presented in [45]).

The correction can also be introduced by the method proposed in Chapter 3 of optimum account for the real variations of the atmospheric parameters on the basis of the optical-meteorological /221 model of the atmosphere. This was done in the previously mentioned examples of $T\,(\zeta)$ determination from I_ν measurements made using the Nimbus 3 satellite. Assuming that the corrections $\tilde{P}_\nu\,(\zeta)$ are due to aerosol absorption which is independent of ν, we can evaluate the aerosol contribution at different ζ levels, using the statistical characteristics of the vertical structure of the aerosol attentuation coefficient and correcting in suitable fashion the absolute magnitudes of the IR radiation attentuation in the CO_2 15 μ band. We see from Figure 6.14 that these corrections made it possible to refine the vertical $T\,(\zeta)$ profiles.

The actual atmospheric transmission question is also important in connection with the method proposed by Chachine in [46] for determining $T\,(\zeta)$, which according to the author of [46] does not require any a priori information while at the same time providing very high accuracy of the inverse problem solution. The method is based on the possibility of selecting levels ζ_i and corresponding number of frequencies ν_i for which the approximate relation is satisfied

$$\frac{I_{\nu i}^{(1)}}{I_{\nu i}^{(2)}} \approx \frac{B_\nu\,[T_1\,(\zeta_i)]}{B_\nu\,[T_2\,(\zeta_i)]} \qquad (i = 1,\,2,\,\ldots,\,k), \tag{6.46}$$

378

where $I_\nu^{(1)}$ and $I_\nu^{(2)}$ are the radiation intensities (6.1) for two temperature profiles — $T_1(\zeta)$ and $T_2(\zeta)$. It is easy to see that (6.46) is satisfied most precisely for those ζ_i at which the kernel of (6.1) for the given ν_i has a maximum (see, for example, Figure 6.7). If $\partial P_\nu / \partial \ln \zeta$ were a delta function (6.46) would be satisfied absolutely exactly.

With the aid of (6.46) the author of [46] constructs the process for determining $T(\zeta)$, taking as the first approximation an arbitrary profile (for example, the climatological mean profile or even a constant value $T_0(\zeta_i) \equiv T_0$) and determining the succeeding approximation from the recurrence relation

$$B_i[T_n(\zeta_i)] = B_i[T_{n-1}(\zeta_i)] \frac{I_i}{I_i^{(n-1)}} \qquad (n = 1, 2, \ldots).$$

(6.47)

Here I_i is the radiation intensity measured at the frequency ν*. The process is continued until the differences $R_i^{(n)} = (I_i - I_i^{(n)}/I_i$ or their mean value $\langle R^{(n)} \rangle = \frac{1}{k} \sum_{i=1}^{k} R_i^{(n)}$ become less than the I_ν measurement error.

The described method was applied in [46] to determine $T(\zeta)$ at ten levels ζ_i for ten values of ν_i in the CO_2 4.3 μ band (Figure 6.15). The results of $T(\zeta_i)$ determination using various first approximations of $T_0(\zeta_i)$ are shown in Figure 6.16. The mean error of the method, amounting to $1°$, is due to the computational error (~0.4%). The convergence of the iteration method is illustrated by Table 6.5.

At first glance the Chachine method may suggest the possibility of solving incorrect problems without any regularization or a priori information on the solution. In reality, however, it is necessary to know the form of the vertical profiles in order to select the

---

* We note that in [46] a technique for separating the variables ν and ζ in $B^\nu[T(\zeta)]$ is proposed, which is not of fundamental importance to this method.

corresponding frequencies ν_i and the levels ζ_i at which (6.46) is satisfied most exactly. It is by no means obvious that the successive approximations will converge to the true solution if the equation kernels do not have maximum values for the selected ζ_i and ν_i. However, the deviation of real atmospheric transmission from the adopted model does not guarantee that these maxima will be reached. Finally, the fact that obtaining the sought function at a discrete number of specially selected values of the argument in the Chachine method requires an empirical relation of the form (6.46), which in the case of another integral equation will have a different specific form, is essentially a regularization of the incorrect problem based on intuitive and a priori assumptions on the nature of the solution.
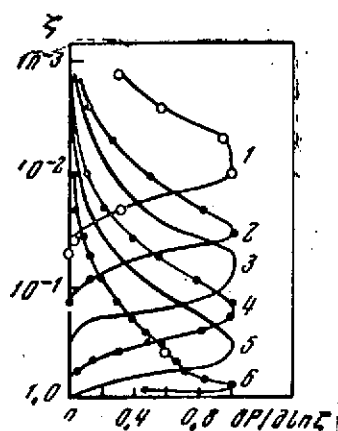
Figure 6.15. Weighting functions $\partial P_\nu / \partial \ln \zeta$ for the CO_2 4.3 μ band 1-6- ν = 2360, 2340, 2315, 2275, 2255, 2215 cm^{-1}, respectively

It is also important to emphasize that the method does not ensure determining the sought function at the intermediate ζ_i levels without increasing the number of $I_{\nu i}$ measurements.

In conclusion we note that use of the CO_2 4.3 μ band for determining T (ζ) involves large errors associated with solar radiation reflection, which in this spectral region is comparable with the Earth's self-radiation. Account for reflection may also
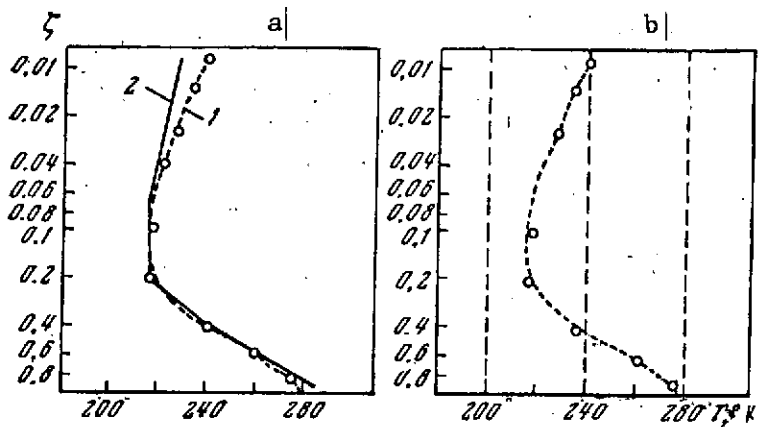
Figure 6.16. Examples of T (ζ) determination by the Chachine iteration method [46] for different zero approximations

a- T_0 (ζ) is the standard profile; 1- zero approximation; 2- reconstructed profile; b- T_0 (ζ) = 200, 240, 280° K

TABLE 6.5. AVERAGE ERRORS $\langle R^{(n)} \rangle$ (IN %) FOR n SUCCESSIVE APPROXIMATIONS*

Zero approximation	n									
	0	1	2	3	4	5	6	7	8	9
Std. profile	26,3	7,0	2,25	1,52	1,02	0,73	0,54	0,40	—	—
T_0 (z) = 280° K	920,1	21,7	10,1	5,49	2,88	1,35	0,81	0,54	0,42	—
T_0 (z) = 240 °K	80,2	21,9	10,3	5,49	2,85	1,33	0,79	0,54	0,43	—
T_0 (z) = 200° K	90,9	22,4	10,8	5,53	2,84	1,31	0,79	0,55	0,46	0,41

* Translator's note: Commas in numbers represent decimal points.

be important for the wings of the CO_2 15 μ band. Since this question is also common to the problem of determining the underlying surface temperature from radiation measurements in the 10-12 μ window, we shall examine it in more detail in Chapter 8.

381

CHAPTER 7
DETERMINATION OF VERTICAL HUMIDITY PROFILE

§ 1. Problem Formulation and Basic Relations

In § 8 of Chapter 6, we noted the need for taking account of
humidity when introducing corrections to the transmission function
in determining the vertical atmospheric temperature profiles from
measurements of the self-radiation spectrum I_ν in the CO_2 15 μ
band. However, since the humidity in the region of I_ν measurements
in the CO_2 band is unknown, it is natural to pose the problem of
determining the vertical gaseous moisture concentration profiles
q (ζ) from simultaneous measurements of the self-radiation I_ν in
several water vapor absorption band segments.

The advisability of making simultaneous measurements of I_ν
in different bands is obviously based on more than just introducing
the mentioned corrections. The vertical humidity profiles are
important to no less a degree than the temperature profiles for
many problems of atmospheric physics and meteorology. However,
in determining q (ζ) from self-radiation measurements it is
necessary to know the vertical temperature distribution. The
reason is that the measured I_ν spectra are a superposition of
the radiation of various layers of the atmosphere which depends
on both the moisture concentration and temperature of each given
layer. The corresponding dependences are described by relations
of the form (6.1), which for the problem of determining q (ζ) are
conveniently written in the form

$$I_\nu = B_\nu \left[T\left(1\right)\right] P_\nu \left[w\left(1\right)\right] - \int_0^1 B_\nu \left[T\left(\zeta\right)\right] \frac{\partial P_\nu \left[w\left(\zeta\right)\right]}{\partial \zeta} d\zeta,$$

$$(7.1)$$

where w (ζ) is the effective water vapor mass in the atmospheric column (0, ζ)

$$w(\zeta) = w_0 \int_0^\zeta t^\varkappa q(t)\,dt, \; w_0 = \frac{p_i q_0}{g} \qquad (0 < \varkappa \leqslant 1).$$ (7.2)

Examining (7.1) as an integral equation in q (ζ) or w (ζ), we can solve the subject problem using the I_ν variations in the water vapor absorption band if we know the Planck function B_ν [T (ζ)], which is the kernel of (7.1). Therefore, it is necessary to first determine the T (ζ) profile from I_ν measurements in the CO_2 15 μ band by the methods described in Chapter 6 without account for overlap of the CO_2 and water vapor bands. Then, using B_ν [T (ζ)] as the kernel of (7.1), taken for the 6.3 μ water vapor band, we can pose the inverse problem of determining q (ζ). Using the q (ζ) profile thus obtained we can, if necessary, refine T (ζ), considering water vapor absorption in the CO_2 15 μ band region and then repeat the iteration relative to q (ζ).

The physical principle on which the possibility of determining the moisture profile is based, is analogous to the principle used in determining the temperature profile (see [1]). The atmospheric radiation I_ν in the central part of the band carries information on the small water vapor concentrations in the upper troposphere or stratosphere. In regions of lower absorption and on the wing /224 of the band, I_ν yields information on the moisture content in the lower layers of the atmosphere. The weights with which this information enters into I_ν are determined by the vertical temperature profiles and the nature of the transmission function humidity dependence.

The problem of determining q (ζ) is an incorrect problem, somewhat more complex than that of determining T (ζ). The complication is associated, first of all, with the essentially nonlinear

transmission function dependence on q (ζ), given, as noted in Chapter 2, either by approximate formulas of the form (1.14) or (1.16) or by empirical relations of the form (1.20). Moreover, P_ν depends directly on the effective mass (7.2) and therefore there is double altitude smoothing relative to q (ζ) expressed by (7.1) and (7.2). This increases the sensitivity of q (ζ) to random measurement and computational errors.

These circumstances probably explain the small number of studies devoted to solution of the problem of determining the q (ζ) profile, although there is no fundamental difficulty in applying to this problem the regularization methods examined in Chapter 6. In the present chapter we shall present some results of q (ζ) determination given in [2-5], and we shall also examine several proposals for determining other humidity characteristics from self-radiation measurements from satellites.

§ 2. Iteration Method

The possibility of simultaneous determination of the vertical temperature and humidity profiles from measurements of the Earth's self-radiation in the CO_2 and water vapor bands is examined by Smith in [4, 5]. For this purpose, Smith uses the so-called iteration method of solving inverse problems. In accordance with this method the T (ζ) and q (ζ) profiles are specified by analytic expressions

$$T(\zeta) = T_0 \zeta^{\varkappa_1} \qquad (0.95 \leqslant \zeta \leqslant 1); \qquad (7.3)$$

$$T(\zeta) = T(0.95) \zeta^{\varkappa_2} \qquad (\zeta_t \leqslant \zeta \leqslant 0.95); \qquad (7.4)$$

$$q(\zeta) = q_0 \zeta^{\varkappa_3} \qquad (\zeta_t \leqslant \zeta \leqslant 1), \qquad (7.5)$$

where $T_0, q_0, \varkappa_1 = Rg/\gamma_1, \varkappa_2 = Rg/\gamma_2, \varkappa_3$ are unknown parameters of the approximations (7.3) — (7.5); R is the gas constant for dry air; g is the gravity acceleration; $\gamma = -\partial T/\partial z$; ζ_t is the pressure at the

tropopause level. For temperature inversions in the atmospheric boundary layer of thickness 50 mbar, the approximation for q (ζ) is given in [3] by the expressions

$$q(\zeta) = \frac{q_0}{u_s(T_0)} u_s[T(\zeta)] \qquad (0.95 \leqslant \zeta \leqslant 1); \qquad (7.6)$$

$$q(\zeta) = q'(0.95)\left(\frac{\zeta}{0.95}\right)^{x_s} \qquad (\zeta_l \leqslant \zeta \leqslant 0.95); \qquad (7.7)$$

here u_s is the relative humidity as a function T (ζ).

Thus, the problem of reconstructing T (ζ) and q (ζ) is reduced in [4] to determining five unknown parameters from the system of transcendental equations obtained upon substituting (7.3) — (7.7) into (6.1), (7.1), (7.2) for the five spectral intervals in which the values of I_ν are measured (in [4] it is proposed that the 1190-1250; 930-970; 750-810; 730-750; 510-550 cm^{-1} spectral intervals be used, centered respectively at 8.2; 10.5; 12.8; 13.5, 18.9 μ). By varying each of the unknown parameters of (7.3) — (7.7) the author of [4] obtains best agreement of the radiation intensities I_e and I_c, measured and calculated from (7.1), (7.2), /225 respectively, for each iteration step.
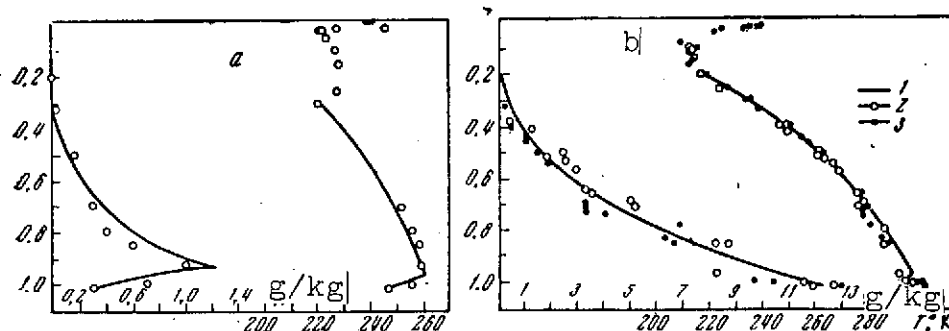
Figure 7.1. Reconstruction of T (ζ) and q (ζ) profiles in [4] by iteration method

a- using closed scheme; b- using balloon measurements; 1- reconstructed profiles; 2, 3- profiles measured at 12.00 and 18.00 hours, respectively

In [4] the following iteration process is realized; first the underlying surface temperature T_0 is selected so that the value of I_c in the 10.5 μ "window" coincides with I_e to within measurement errors. Taking this value of T_0 as the first approximation, the author of [4] varies the parameter $\varkappa_1$, characterizing the temperature gradient in the free atmosphere, until I_c is close to I_e in the 10.5 and 13.5 μ spectral intervals. The parameters $\varkappa_2$, q_0, and $\varkappa_3$ are selected similarly on the basis of I_ν measurements in the 12.8, 8.2, and 18.9 μ spectral regions, respectively.

As an illustration of the proposed method, the author of [4] presents examples of reconstruction of inversion-type T (ζ) and q (ζ) profiles using the closed scheme (Figure 7.1 a) and using I_ν spectrum measurements obtained with the aid of a balloon interferometer [6] (see also [2.35]) with spectral resolution 5 cm^{-1} (Figure 7.1 b). We see from the figure that the error of T (ζ) and q (ζ) reconstruction by the iteration method using the closed scheme does not exceed 2° for T and 0.2 g/kg for q even for such a complex profile structure. However, we must bear in mind in this reconstruction the author of [4] was forced to specify the boundaries of the layers in which the corresponding approximations (7.3) — (7.7) are acceptable. Since this information is lacking under actual conditions of I_ν, measurements from satellites or balloons, the use of these approximations does not ensure very reliable reconstruction of the T (ζ) and q (ζ) profiles. This shows up clearly in Figure 7.1 b, which indicates that the empirical profiles cannot be approximated by (7.3) — (7.7) with adequate accuracy. Therefore the reconstructed profiles (particularly in the lower layer of the troposphere) differ markedly from the initial profiles.

In this connection [5] suggests an improved scheme for determining the profile approximation parameters when using the described method. This improvement includes determination of an

optimum level ζ_0, separating regions of use of $T(\zeta)$ with two different temperature gradients, whose profiles are represented in [5] as follows

$$T(\zeta) = c_1 + c_2 \ln \zeta \qquad (\zeta_0 \leqslant \zeta \leqslant 1); \qquad (7.8)$$

$$T(\zeta) = c_1 + c_2 \ln \zeta_0 + c_3 \ln \frac{\zeta}{\zeta_0} \qquad (\zeta_t \leqslant \zeta \leqslant \zeta_0), \qquad (7.9)$$

where $c_1 = T(1)$, c_2, c_3 are constants subject to determination. In [5] an algorithm is also proposed for the iteration method of determining these constants, which reduces to solving systems of algebraic equations

$$\sum_{j=1}^{3} c_j^{(k)} D_{vj}^{(k-1)} = F_v^{(k-1)} \qquad (v = 1, 2, 3, 4) \qquad (7.10)$$

for successive k-th parameter iterations $c_j^{(k)}$. The coefficients /226 and right side of (7.10) are found by substituting (7.8), (7.9) into an equation of the form (6.1) and (7.1) and making some elementary transformations. Here

$$F_v^{(k-1)} = I_v + \int_0^{\zeta_t} B_v[T(\zeta)] \frac{\partial P_v(\zeta)}{\partial \zeta} d\zeta + \frac{\partial B_v^{(k-1)}[T(1)]}{\partial T} P_v(\zeta_t) T^{(k-1)}(1) -$$

$$- B_v^{(k-1)}[T(1)] P_v(\zeta_t); \qquad (7.11)$$

$$D_{v1}^{(k-1)} = \frac{\partial B_v^{(k-1)}[T(1)]}{\partial T} P_v(\zeta_t), \qquad (7.12)$$

$$D_{v2}^{(k-1)} = \int_{\zeta_0}^{1} d_v^{(k-1)}(\zeta) d\zeta, \qquad D_{v3}^{(k-1)} = \int_{\zeta_t}^{\zeta_0} d_v^{(k-1)}(\zeta) d\zeta,$$

where

$$d_v^{(k-1)}(\zeta) = \frac{P_v(\zeta) - P_v(\zeta_t)}{\zeta} \frac{\partial B_v^{(k-1)}[T(\zeta)]}{\partial T}; \qquad B_v^{(k)} = B_v(T_k).$$

We see from (7.10) — (7.11) that $c_j^{(k)}$ will be functions of the quantity ζ_0, which in [5] is determined from the condition of a minimum of the functional

$$\sum_{v=1}^{4} [I_v - \tilde{I}_v]^2, \qquad (7.13)$$

where $\tilde{I}_\nu$ is the Earth radiation, calculated at each step from the reconstructed temperature profile $\tilde{T}(\zeta)$. For determining the constants C_1, C_2, C_3, ζ_0 [5] proposes using measurements in the spectral intervals $825-975$; $740-780$; $730-770$; $717.5-757.5$; $500-570\ см^{-1}$, centered at 11.1; 13.1; 13.3, 13.6, 18.7 μ.

It should be noted here that the condition (7.13) as a criterion of incorrect problem solution convergence to the initial profile does not in itself ensure obtaining a physically meaningful solution. As was shown in Chapter 6, additional information is necessary to permit obtaining regularized solutions for which closeness of $T_k(\zeta)$ to $T(\zeta)$ follows from statisfaction of the criterion (7.13). In fact, in solving the system of Equation (7.10) the author of [5] encounters incorrectness of the subject problem, which shows up in poor conditioning of the system (7.10).

The Phillips-Twomey method [6.17, 6.18] is used in [5] to regularize the solution of (7.10).

For determining the constant $н_3$, describing the humidity profile (7.4), [5] uses I_ν in the 18.7 μ spectral interval. Representing the k-th approximation of the transmission function

$$P_\nu^{(k)}(\zeta) = P_\nu^{(k-1)}(\zeta) + \frac{\partial P_\nu\,[w\,(\zeta)]}{\partial \ln w} \ln \frac{w_k\,(\zeta)}{w_{k-1}\,(\zeta)}, \tag{7.14}$$

where $w_k(\zeta)$ is the effective water vapor mass for the k-th approximation $q_k(\zeta)$, and substituting (7.14) into (7.1), the author of [5] obtains the following expression for determining $q_k(\zeta)$

$$q_k(\zeta) = q_{k-1}(\zeta)\exp\left\{\frac{(n+\varkappa_3+1)\,[I_\nu - \tilde{T}^{(k-1)}]}{c_2^{(k-1)}\beta_\nu^{(k-1)}(\zeta_0,\,1)+c_3^{(k-1)}\beta_\nu^{(k-1)}(\zeta_l,\,\zeta_0)}\right\}, \tag{7.15}$$

388

$$\beta_\nu^{(k-1)}(\zeta_i, \zeta_j) = \int\limits_{\zeta_i}^{\zeta_j} \frac{\partial B_\nu^{(k-1)}[T(\zeta)]}{\partial T} \frac{\partial P_\nu^{(k-1)}(\zeta)}{\partial \zeta} d\zeta. \qquad (7.16)$$

The iteration process for q_k (ζ) using (7.15) is continued in [5] until the conditions (7.13) and

$$\frac{1}{1-\zeta_t} \int\limits_{\zeta_t}^{1} |T_k(\zeta) - T_{k-1}(\zeta)| d\zeta \leqslant 0.25°.$$

are satisfied simultaneously for the T_k (ζ) approximations. In this case the regularization parameter is selected so that the sum (7.13) does not exceed the variance of the I_ν measurement errors.
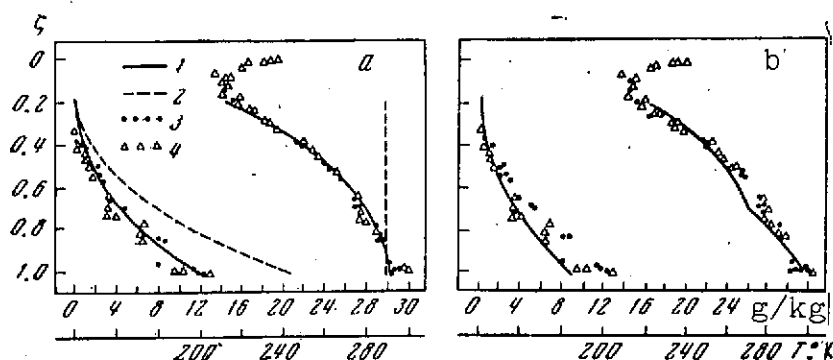
Figure 7.2. Examples of vertical temperature and humidity profile reconstruction by the iteration method of [5] from I_ν measurements [6] at 07.30 (a) and 10.09 (b) hours

1- reconstructed profiles; 2- initial approximations of T_0 (ζ) and q_0 (ζ) profiles; 3, 4- measurements of T (ζ) and q (ζ) at 06.00 and 12.00 CST, respectively

The successive approximation method was tested in [5] using data of balloon radiation spectra measurements [2.35, 6]. The results of T (ζ) and q (ζ) profile reconstruction using these data are presented in Figure 7.2. The choice of regularization parameter by the author of [5] was made using the Twomey method [6.18] on the basis of the I_ν errors. The zero approximation was taken as: temperature T_0 (1) constant with height and equal to the radiation temperature measured in the 11.1 μ window, total water

389

TABLE 7.1.   RELATIVE DIFFERENCES OF THE RADIATION INTENSITIES,
MEASURED (I_e) AND CALCULATED (I_c) FROM THE
RECONSTRUCTED T (ζ) AND q (ζ) PROFILES*

λ, μ	ε_I (5)	ε_I (8)	ε_I (8)	ε_I (3)
11,1	—0,3	—0,1	0,0	0,6
13,1	0,5	0,5	0,5	—0,4
13,3	0,1	—0,5	—1,0	—1
13,5	—0,5	0,2	0,5	1,2
18,7	0,5	0,5	0,4	—0,1
ε_w	—1,5	—27	—5,7	—27

* Translator's note: Commas in numbers represent decimal points.

Note. ($\varepsilon_I = (I_e - I_c)/I_e) \cdot 100\%$; $[\varepsilon_w = (w_e - e_c/w_e)] \cdot 100\%$; w_e, w_c are the experimental and calculated water vapor masses. Numerals in parentheses are number of iterations.

vapor mass w_0 = 6 cm, parameter $\varkappa|_3$ = 2.6. We see from the figure that quite satisfactory T (ζ) and q (ζ) distributions were obtained. Most significant were the errors in the atmospheric boundary layer (deviation of the reconstructed humidity from the initial value reaches 30% at the ground level). The large errors in Figure 7.2 b are explained in [5] by the initial data errors. However we see from Table 7.1, which presents a comparison of the radiation values measured (I_e) and calculated (I_c),|from the reconstructed T and q profiles, that the difference between I_c and I_e does not exceed 1%. Therefore it is still not clear why,| for approximately the same differences $I_e - I_c$ quite large differences of the reconstructed profiles and even differences of the total water vapor mass w (1) were obtained in [5] (according to the author of [5] the accuracy of w determination is intimately connected with temperature profile reconstruction accuracy).

This high sensitivity of the iteration method to initial data errors is probably a consequence of inadequate solution regulari-

zation. However the most significant drawback of the method is
the fundamental impossibility of determining the real vertical
profile variations, which are not described by fixed functions
of the form (7.3) — (7.7). Since these q (ζ) variations are
actually random functions of altitude, to determine the solution
it is necessary to apply statistical regularization methods with
use of a priori information on the vertical structure of the
specific humidity variations.

§ 3. Application of Optimum Parametrization Method

In order to apply the statistical parametrization method
(see Chapter 6) to the integral Equation (7.1) it is necessary to
linearize this equation relative to the function w (ζ), connected
with the sought function q (ζ) by the relation (7.2). Since the
humidity profile variations q' (ζ) are of interest for problems of
terrestrial atmospheric physics, it is natural to represent the
sought function in sum form

$$q(\zeta) = \bar{q}(\zeta) + q'(\zeta), \qquad w(\zeta) = \bar{w}(\zeta) + w'(\zeta); \qquad (7.17)$$

$$\bar{w}(\zeta) = w_0 \int_0^\zeta t^x \bar{q}(t)\, dt, \qquad w'(\zeta) = w_0 \int_0^\zeta t^x q'(t)\, dt. \qquad (7.18)$$

Here $\bar{q}$ (ζ) is the mean profile, determined for the given region
of the terrestrial sphere by statistical processing of aerological
sounding data (see § 3 of Chapter 3).

Substituting (7.17) into (7.1) and considering only the
first two terms of the expansion

$$P_v[\bar{w}(\zeta) + w'(\zeta)] = P_v[\bar{w}(\zeta)] + \frac{\partial P_v[\bar{w}(\zeta)]}{\partial w} w'(\zeta) + \ldots, \qquad (7.19)$$

we obtain the following integral equation, linear in w' (ζ)

$$f_v = B_v[T(1)] \frac{\partial P_v[\bar{w}(1)]}{\partial w} w'(1) - \int_0^1 B_v[T(\zeta)] \frac{\partial}{\partial \zeta} \left\{ \frac{\partial P_v[\bar{w}(\zeta)]}{\partial w} w'(\zeta) \right\} d\zeta, \qquad (7.20)$$

391

where $f_\nu = I_\nu - \bar{I}_\nu$; $\bar{I}_\nu$ is the radiation intensity for the mean profile $\bar{q}(\zeta)$ ($\bar{I}_\nu$ is obtained by substituting into (7.1) $\bar{w}(\zeta)$ in place of $w(\zeta)$).

It should be noted that the derivatives of the transmission function with respect to w in (7.20) have singularities for w = 0 which are integrable with account for the decrease of $w'(\zeta)$ as $\zeta' \to 0$. For example, if the transmission function is given by (1.16) or (1.20), respectively,

$$\frac{\partial P_\nu[\bar{w}(\zeta)]}{\partial w} = -\frac{l_\nu \exp\left[-\frac{l_\nu}{2}\bar{w}(\zeta)\right]}{[2\pi l_\nu \bar{w}(\zeta)]^{1/2}};$$

(7.21)

$$\frac{\partial P_\nu[\bar{w}(\zeta)]}{\partial w} = -\alpha\beta[\bar{w}(\zeta)]^{\beta-1}\exp\{-\alpha[\bar{w}(\zeta)]^\beta\}.$$

(7.22)

Since choice of transmission function form is not of fundamental importance for clarification of the methodological questions of solution of the integral Equation (7.20), in the closed inverse problem solution schemes we can use the quite simple formula (1.16) with the well-known generalized absorption coefficients l_ν (see Table 2.1). This expression for P_ν was actually used in [2, 3] in examining the capabilities of the optimum parametrization method in the problem of determining the vertical atmospheric humidity profiles. For determining $q(\zeta)$ from the experimental I_ν data it is advisable to use the transmission function in the form (1.20) with the empirical coefficients α and β presented in Table 1.3.

Since $q'(\zeta)$ is a random function of ζ, the systems of empirical orthogonal vectors $\psi_k(\zeta_i)$ presented in § 6 of Chapter 3 were taken in [2] as the a priori information for its determination from (7.20) by the optimum parametrization method with account for the equalities (7.18). We recall that these systems were obtained by statistical processing of aerological humidity sounding data at six standard levels ζ_i above continental and oceanic stations (see § 3 of Chapter 3).

392

Examples of the first three empirical vectors for these stations are shown in Figure 3.16. Analogous systems of vectors for a large number of levels ζ_i were obtained from high-altitude aerosounding data [3.9, 3.26]. These systems were used in reconstructing the q' (ζ) profiles in [2, 3, 7].

We see from Table 3.5 that the first three eigenvectors provide approximation of any realization with an error not exceeding 5%, regardless of which station data were used to obtain the empirical orthogonal vectors. Setting

$$q'(\zeta_i) = \sum_{k=1}^{n} c_k \psi_k(\zeta_i)$$
(7.23)

and substituting (7.23) into (7.18) and (7.20), we obtain the algebraic system of equations for determining the coefficients c_k

$$\sum_{k=1}^{n} D_{vk} c_k = f_v \qquad (v = 1, 2, \ldots, N),$$
(7.24)

where

$$D_{vk} = B_v[T(1)] \frac{\partial P_v[\overline{w}(1)]}{\partial w} \Psi_k(1) - \int_0^1 B_v[T(\zeta)] \frac{\partial}{\partial \zeta} \left\{ \frac{\partial P_v[\overline{w}(\zeta)]}{\partial w} \Psi_k(\zeta) \right\} d\zeta;$$
(7.25)

$$\Psi_k(\zeta) = \int_0^\zeta t^x \psi_k(t) \, dt.$$
(7.26)

If the number of v intervals does not coincide with the number of basis vectors, the system of equations (7.24) can be reduced by the least squares method to the system

$$\sum_{k=1}^{n} \Gamma_{jk} c_k = F_j \qquad (j = 1, 2, \ldots, n),$$
(7.27)

where

$$\Gamma_{jk} = \sum_{v=1}^{N} D_{vj} D_{vk}; \qquad F_j = \sum_{v=1}^{N} f_v D_{vj}.$$
(7.28)

The solution of (7.20) was obtained using the following closed scheme. For given T (ζ) and q (ζ) realizations and for

393

the mean profile $\bar{q}$ (ζ), using formula (7.1) with the transmission function (1.16) we calculated I_ν and $\bar{I}_\nu$ in different spectral intervals 25 cm^{-1} wide of the 6.3 µ band.

Examples of the spectral variation of I_ν and $\bar{I}_\nu$ (in 10^3 cal/cm^2·min·sr) for two q (ζ) realizations from aerological soundings at the Bismarck station (7 and 11 July), used in [3.34] to obtain the empirical orthogonal vectors, are presented in Table 7.2.

TABLE 7.2*

		ν, см⁻¹									
		1241	1262	1287	1312	1337	1362	1387	1412	1437	1462	1487
7.VII	$\bar{I}_\nu$	9,14	8,42	7,47	6,31	4,96	3,80	3,35	1,91	1,38	0,91	0,40
	I_ν	8,77	7,98	6,98	5,79	4,52	3,45	3,04	1,75	1,29	0,88	0,43
11.VII	$\bar{I}_\nu$	12,08	10,96	9,52	7,75	5,84	4,34	3,82	2,30	1,77	1,27	0,69
	I_ν	12,13	11,03	9,60	7,85	5,97	4,45	3,91	2,21	1,63	1,12	0,56

* Translator's note: Commas in numbers represent decimal points.

These data, together with the vertical variation of the functions $\Delta P_\nu = (\partial P_\nu/\partial\zeta)\,\Delta\zeta$ for several regions of strong, moderate, and weak radiation absorption in the 6.3 µ water vapor band (Figure 7.3), illustrate clearly the connection between the radiation in the various spectral intervals and the humidity and temperature at the corresponding levels.

Considering I_ν and $\bar{I}_\nu$ as known functions of ν and assuming that the T (ζ) and $\bar{q}$ (ζ) profiles are also known, it is not difficult to obtain with the aid of (7.24) or (7.27) the coefficients c_k of the expansion (7.23)

$$c_k = \sum_{\nu=1}^{n} D_{\nu k}^{-1} f_\nu \qquad (k = 1, 2, \ldots, n)$$

(7.29)

or

$$c_k = \sum_{j=1}^{n} \Gamma_{jk}^{-1} F_j \qquad (k = 1, 2, \ldots, n).$$ (7.30)

Here D_{vk}^{-1} and Γ_{jk}^{-1} are elements of the corresponding inverse matrices.

Examples obtained in [2] of q (ζ) profile reconstruction using the indicated scheme by the optimum approximation method are shown in Figure 7.4. Of interest is the large difference between the initial and reconstructed q (ζ) profiles in the lower layer of the atmosphere. This is associated primarily with double smoothing of the function q (ζ) when integrating (7.2) and (7.1), as a result of which the strong q (ζ) profile variations which occur in these layers do not show up properly in the variations of the spectral distribution of the radiation I_ν. Moreover, the variations q' (ζ) are comparable with the mean profiles $\bar{q}$ (ζ), which does not permit retaining in (7.20) only the linear terms of the expansion (7.19). /231 Therefore refinement of the solution of the linearized Equation (7.20) is required.
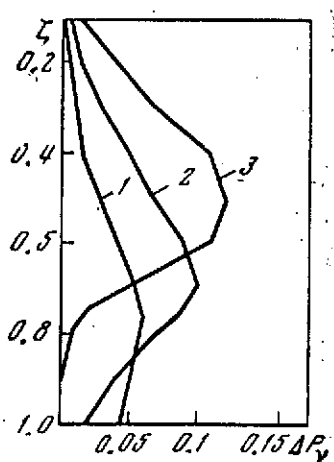
Figure 7.3. Examples of vertical variation of weighting functions in (7.1)

1-3- λ = 8.06; 7.48, 7.21 μ, respectively
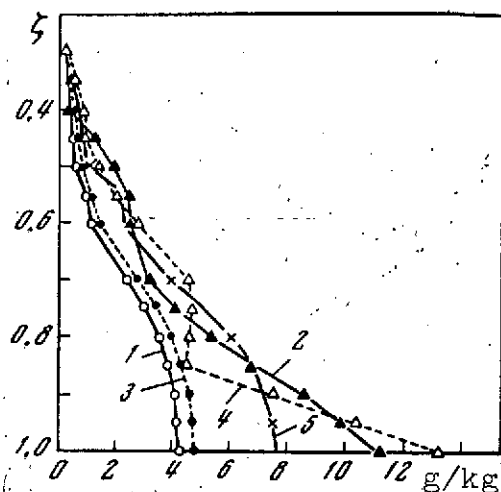
Figure 7.4. Examples of specific humidity profile reconstruction q (ζ_i) using three eigenvectors ψ_k (ζ_i)

1, 2- initial profiles of 7 and 11 July, respectively; 3, 4- reconstructed profiles; 5- mean profile

395

Examining the resulting $q_1(\zeta)$ and $w_1'(\zeta)$ as the first approximations of the solution of the nonlinear Equation (7.1), we apply to (7.1) the Newton method as extended by Kantorovich [8] to nonlinear operators and find the next approximations $q_j'(\zeta)$ and $w_j'(\zeta)$. In [2, 3] this procedure was carried out for (7.1) with the transmission function (1.16). Successive approximations of the coefficients c_k of the expansion (7.23) were determined directly; this expansion is conveniently written for $w'(\zeta)$ as:

$$w'(\zeta) = \sum_{k=1}^{n} c_k \Psi_k(\zeta).$$

We rewrite (7.1) in the form

$$G_\nu(c_k) \equiv B_\nu[T(1)]\, P_\nu\Big[\overline{w}(1) + \sum_{k=1}^{n} c_k \Psi_k(1)\Big] - $$
$$- \int_0^1 B_\nu[T(\zeta)]\frac{\partial}{\partial \zeta}\Big\{P_\nu\Big[\overline{w}(\zeta) + \sum_{k=1}^{n} c_k \Psi_k(\zeta)\Big]\Big\} d\zeta - I_\nu = 0. \qquad (7.31)$$

We consider (7.31) to be a nonlinear equation in the coefficients c_k, as the first approximation $c_k^{(1)}$ for which we take the solution of the linearized Equation (7.20).

The following approximations $c_k^{(j)}$ can be found from the equation

$$\sum_{k=1}^{n} \frac{\partial G_\nu[c_k^{(j)}]}{\partial c_k}[c_k^{(j+1)} - c_k^{(j)}] + G_\nu[c_k^{(j)}] = 0 \qquad (j = 1, 2, \ldots), \qquad (7.32)$$

where

$$\frac{\partial G_\nu[c_k^{(j)}]}{\partial c_k} = B_\nu[T(1)]\frac{\partial}{\partial w}\Big\{P_\nu\Big[\overline{w}(1) + \sum_{k=1}^{n} c_k^{(j)}\Psi_k(1)\Big]\Big\}\Psi_k(1) - $$
$$- \int_0^1 B_\nu[T(\zeta)]\frac{\partial}{\partial \zeta}\Big\{\frac{\partial}{\partial w}P_\nu\Big[\overline{w}(\zeta) + \sum_{k=1}^{n} c_k^{(j)}\Psi_k(\zeta)\Big]\Psi_k(\zeta)\Big\} d\zeta, \qquad (7.33)$$
$$\Big(\frac{\partial P_\nu[\widetilde{X}(\zeta)]}{\partial X} = \frac{\partial P_\nu(X)}{\partial X}\Big|_{X=\widetilde{X}(\zeta)}\Big) - $$

are derivatives of the operator G in the Frechet sense. It is

396

not difficult to note that the coefficients (7.33) are equal to the coefficients (7.25) of (7.24), if in (7.33) we set $c_k^{(j)} = 0$. For simplicity of the calculations in obtaining the successive approximations $c_k^{(j)}$ we can take in (7.32) the same coefficients $\partial G_\nu \left[c_k^{(j)}\right]/\partial c_k$, altering only the free terms $G_\nu\left[c_k^{(j)}\right]$, which for $j = 0$ coincide with f_ν of (7.24).
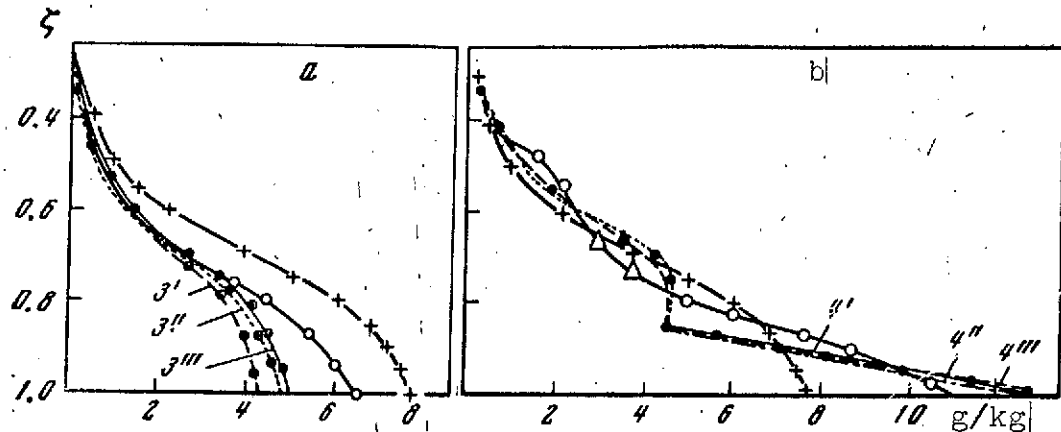
Figure 7.5. Examples of determining q (ζ_i) by the Newton-Kantorovich method for the q (ζ_i) realizations shown in Figure 7.4 a- 7 July; b- 11 July. Notations same as in Figure 7.4. 3'-3" and 4'-4" are successive approximations using (7.32)

The second and third approximations of q (ζ), obtained as a result of solving (7.32) with j = 1 and 2, are shown in Figure 7.5. They improve somewhat the vertical distributions q (ζ) in the lower layers of the atmosphere, however the errors of q (ζ) profile reconstruction in the boundary layer still remain significant. These errors are associated with the errors of the direct calculations of I_ν and $\bar{I}_\nu$ using (7.1) and inversion of the problem by solving (7.32). However, they may be considered random errors of the known function f_ν. Assuming that these errors are uncorrelated with respect to ν and are given by the variance σ_f^2 which is independent of ν, it is not difficult to obtain the error amplification coefficient

$$K_q(\zeta_i) = \frac{\sigma_q(\zeta_i)}{\sigma_f},$$
(7.34)

where $\sigma_q (\zeta_i)$ is the mean square error of $q' (\zeta_i)$ determination by the optimum parametrization method.

The error amplification coefficient can be obtained by representing $q' (\zeta_i)$ directly in terms of elements of the inverse matrices of (7.24), (7.27), or (7.32). For example, for (7.24)

$$q' (\zeta_i) = \sum_{k=1}^{n} \psi_k (\zeta_i) \sum_{v=1}^{N} f_v D_{vk}^{-1}.$$

(7.35)

Assuming that $f_v = \langle f_v \rangle + \varepsilon_v$ and $q' (\zeta_i) = \langle q' (\zeta_i) \rangle + \delta (\zeta_i)$, where $\langle \ \rangle$ denotes averaging over all realizations of f_v measurements and solutions $q' (\zeta_i)$ of the (7.20) and ε_v and $\delta (\zeta_i)$ are random errors with variances indicated above, we obtain from (7.35) the relation (7.34), where

$$K_q (\zeta_i) = \left[\sum_{v=1}^{N} \sum_{k=1}^{n} \sum_{l=1}^{n} D_{vk}^{-1} D_{vl}^{-1} \psi_k (\zeta_i) \psi_l (\zeta_i) \right]^{1/2}.$$

(7.36)

The error amplification coefficient $K_q (\zeta_i)$, calculated from (7.36) at each level ζ_i, is presented in Table 7.3.

TABLE 7.3. ERROR AMPLIFICATION COEFFICIENT*

ζ_i	$n = N = 3$	$n = 3, \ N = 8$	$n = N = 4$	$n = 4, \ N = 8$
1	6,2	5,4	26,5	8,5
0,25	7,6	2,5	29,3	2,5
0,7	5,0	1,8	21,0	2,0
0,5	0,61	0,32	6,3	0,32
0,4	0,40	0,08	2,9	0,10
0,3	0,13	0,05	0,76	0,00

* Translator's note: Commas in numbers represent decimal points.

We see from the table that the K_q are largest for the atmospheric layer near the Earth ($K_q \approx 6$). Above the 500 mbar level

$K_q (\zeta_i)$ diminishes sharply, which is explained by decrease of the eigenvector components. If the number n of basis vectors ψ_k increases (n = 4) K_q increases sharply, reflecting solution instability.

Increase of the number N of intervals in which f_ν is known and application of the least squares method for solution of the corresponding equations lead to some reduction of the coefficient K_q (see Table 7.3 for N = 8) thanks to the smoothing effect, although the solution itself is not always refined in this case. The latter circumstance is associated with the fact that use of different segments of the water vapor absorption band does not bring any additional information on the distribution of q in the troposphere. In fact, for the strong absorption region the transmission function of (7.1) becomes disappearingly small in the lower layers of the atmosphere (see Figure 7.3). However, in the weaker absorption region the quantities f_ν for different ν carry practically the same information on q' (ζ_i) at the corresponding levels.

The humidity reconstruction errors will be significantly smaller if we determine the vertical distributions of the effective mass w (ζ) or its variations w' (ζ) directly from the integral Equations (7.1) or (7.20). In fact we see from Figure 7.6, which shows the results of w (ζ) profile reconstruction using the closed scheme for the q (ζ) realizations shown in Figure 7.4, that even in the second approximation the reconstructed $\tilde{w}$ (ζ) practically coincide with the initial w (ζ). It would appear that by differentiating $\tilde{w}$ (ζ) with respect to ζ in accordance with (7.2) we could obtain a more exact $\tilde{q}$ (ζ) profile. In reality even small differences between $\tilde{w}$ (ζ) and w (ζ) lead to marked errors $\tilde{q}$ (ζ), particularly in the atmospheric boundary layer.

Analogous results are obtained if we apply the optimum parametrization method to q (ζ) determination using direct balloon measurements of the radiation I_ν [2. 35, 6] in the water vapor band. The q (ζ) vertical profiles were also measured by radiosondes during the balloon ascents. Examples of these profiles taken from [5] and also the results of q (ζ) reconstruction by the iteration [5] and optimum parametrization methods are shown in Figure 7.7.

/234
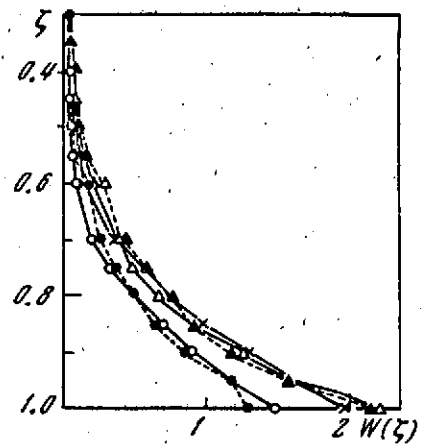
Figure 7.6. Reconstruction of w (ζ) profiles for the vertical distributions shown in Figure 7.4   Notations same as in Figure 7.4
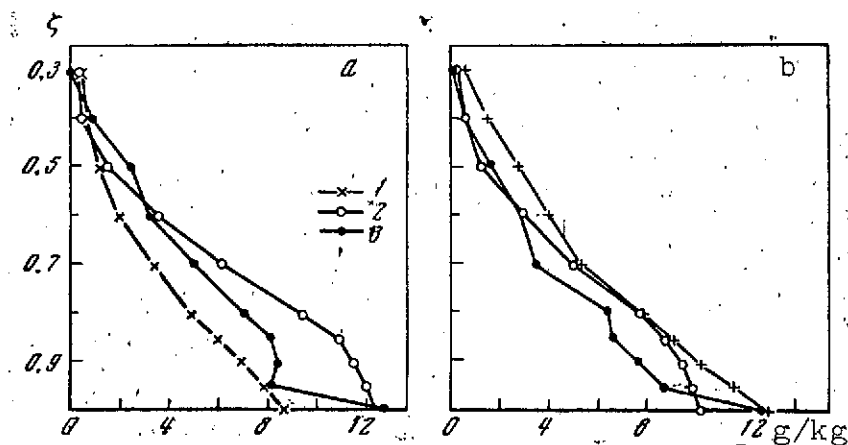
Figure 7.7. Examples of q (ζ) profile reconstruction from measurements above Palestine on 8 May 1966 [2.35]

1- iteration method [5]; 2- optimum parametrization method [3]; 3- radiosonde measurements of q (ζ); a- at 8.10 CST; b- at 13.12 CST

The quite complex structure of the initial q (ζ) profiles, particularly in the atmospheric boundary layer, leads to large errors in reconstructing the humidity profile by [5] method. We see from Figure 7.7 that the optimum parametrization method provides better approximation, however the errors in the atmospheric boundary layer are still significant. These examples illustrate once again the limited capabilities of the subject methods for the problem of determining q (ζ) with the required accuracy.

One possible reason for the indicated drawback of the optimum approximation method is the very high information content of the first and second eigenvectors for the humidity field (see Table 3.5), as a result of which quite good reconstruction of the q' (ζ) profile can be achieved with the aid of 2-3 vectors, except for the atmospheric boundary layer. However addition of the subsequent eigenvectors, describing the fine-scale structure of the q' (ζ) profiles, not only does not improve the approximation in the boundary layer, it actually leads to considerable instability of the inverse problem solution. In other words, the optimum parametrization method, just as in the thermal sounding case, does not yield an objective criterion for selecting the required number of empirical functions for an individual realization of the q (ζ) profile. Therefore for the unclosed problem solution schemes we apply the statistical regularization method [6.35] together with a priori information on the vertical structure of the atmospheric humidity field, represented in the form of correlation matrices for q' (ζ).

§ 4.   Application of Statistical Regularization Method

In direct application of the statistical regularization method to the linearized Equation (7.20) we run into the difficulty

that the finite-difference analog of (7.20) is a system of alge-
braic equations in the effective water vapor mass variation
vector $\{w'_i = w'(\zeta_i)\}$

$$\sum_{i=1}^{n} K_{\nu i} w'_i = f_\nu + \varepsilon_\nu \qquad (\nu = 1, 2, \ldots, N).$$ (7.37)

Here

$$K_{\nu i} = B_\nu [T(\zeta_i)] \frac{\partial P_\nu [\overline{w}(\zeta_i)]}{\partial w},$$ (7.38)

and ε_ν is the overall measurement and the mathematical trans-
formation error characterized by the variance σ_ν^2. Therefore only
$w'(\zeta_i)$ is determined directly from (7.37). The a priori information
required for determining $w'(\zeta_i)$ can be obtained either by statisti-
cal processing of integrals of the form (7.2) of random profiles
$q(\zeta_i)$ or by integrating the correlation matrices K_{qq}

$$K_{ww}(\zeta_i, \zeta_j) = \int_0^{\zeta_i} \int_0^{\zeta_j} K_{qq}(t, u) \, dt \, du.$$ (7.39)

In both cases interpolation between the standard levels ζ_i, ζ_j
at which the q profiles are measured is unavoidable. An example
of autocorrelation matrix K_{ww} calculation using (7.39) and
directly from the random $w(\zeta)$ profiles showed that the matrix
elements obtained by the two techniques coincide at all levels
except for $\zeta_k \leq 0.4$. The quite close correlation between the
variations $w'(\zeta_i)$ up to high altitudes (Figure 7.8) gives a basis
to expect that the reconstructed $w(\zeta_i)$ profiles will be close to
the initial profiles. Using the matrix K_{ww} for statistical reg-
ularization of the system of Equations (7.37) and constructing
the system of regularized equations of form (6.42) — (6.43),
it is not difficult to determine the vertical profiles $w'(\zeta_i)$
and their reconstruction error $\sigma_w(\zeta_i)$.

The profiles $w_1(\zeta_1) = \bar{w}(\zeta_1) + w_1'(\zeta_1)$ obtained in this way, considered as the first approximation of the nonlinear problem, can be refined with the aid of the Newton method [8] applied to (7.1). In fact, representing (7.1) in functional form for the $(j + 1)$-th approximation $w_{j+1}(\zeta)$

$$G_\nu(w_{j+1}) \equiv B_\nu[T(1)]\, P_\nu\{w_j(1) + [w_{j+1}(1) - w_j(1)]\} -$$
$$- \int_0^1 B_\nu[T(\zeta)]\frac{\partial}{\partial\zeta}\, P_\nu\{w_j(\zeta) + [w_{j+1}(\zeta) - w_j(\zeta)]\}\, d\zeta - I_\nu = 0 \qquad (7.40)$$

and assuming that $w_{j+1} - w_j = w_{j+1}' - w_j'$ are sufficiently small quantities for all ζ, we obtain the system of equations for determining $w_{j+1}'(\zeta_1)$ from the previously found approximation $w_j'(\zeta_1)$

$$B_\nu[T(1)]\frac{\partial P_\nu[w_j(1)]}{\partial w}[w_{j+1}'(1) - w_j'(1)] -$$
$$- \int_0^1 B_\nu[T(\zeta)]\frac{\partial}{\partial\zeta}\left\{\frac{\partial P_\nu[w_j(\zeta)]}{\partial w}[w_{j+1}'(\zeta) - w_j'(\zeta)]\right\}d\zeta = I_\nu - I_\nu^{(j)}, \qquad (7.41)$$

where $I_\nu^{(j)}$ is obtained by substituting in (7.1) $w_j(\zeta)$ in place of $w(\zeta)$. It is easy to see that for $j = 0$ (7.41) coincides with (7.20) if we set $w_0(\zeta) = \bar{w}(\zeta)$ and $w_0'(\zeta) \equiv 0$.

The algebraic system for (7.41) will be analogous to (7.37) /236 except that the corresponding matrix elements and free terms will have the form

$$K_{\nu i}^{(j)} = B_\nu[T(\zeta_i)]\frac{\partial P_\nu[w_j(\zeta_i)]}{\partial w}; \quad f_\nu^{(j+1)} = I_\nu - I_\nu^{(j)} + f_\nu^{(j)};$$
$$f_\nu^{(j)} = B_\nu[T(1)]\frac{\partial P_\nu[w_j(1)]}{\partial w}\, w_j'(1) - \int_0^1 B_\nu[T(\zeta)]\frac{\partial}{\partial\zeta}\left\{\frac{\partial P_\nu[w_j(\zeta)]}{\partial w}\, w_j'(\zeta)\right\}d\zeta. \qquad (7.42)$$

The convergence of the iterations with respect to j follows from the general requirements on the operator G_ν, which are satisfied in the subject case. Examples of $w(\zeta)$ and $q(\zeta)$ determination by statistical regularization of (7.37) — (7.41) using the closed

scheme A_1 and using I_ν [2.35] measurements (unclosed scheme A_2) are shown in Table 7.5 and Figure 7.9.
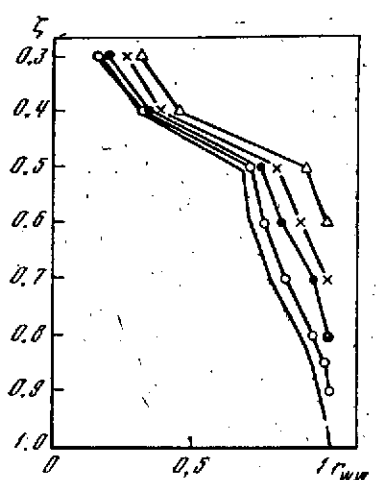
Figure 7.8. Correlation coefficient r_{ww} (ζ_k, ζ_i) calculated from effective water vapor mass realizations (7.2)
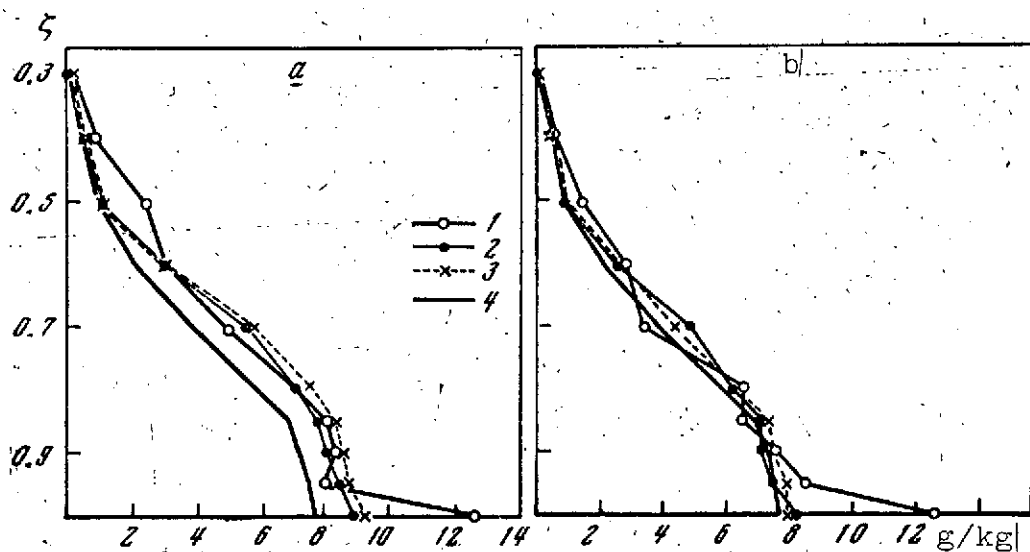
Figure 7.9. Examples of vertical profile q (ζ) reconstruction from I_ν measurements above Palestine on 8 May 1966 [2.35] by statistical regularization [3]

a- at 8.]30; b- at 13.12|; 1- initial profile; 2- profile reconstructed using closed scheme A_1; 3- using unclosed scheme A_2; 4- mean profile

It is not difficult to see that the w (ζ) profile reconstructed using the closed scheme practically coincides with the initial profile. In the unclosed scheme the agreement of w_{in} and w_{rec} is also quite satisfactory, although the error of w (ζ) reconstruction in the surface layer may reach 10%. However, even these errors are significant when we turn to determinations of the profiles q (ζ) or their variations q' (ζ), obtained from w (ζ) by differen- /237 tiating with respect to ζ in accordance with (7.2). In fact, we see from Figure 7.9 that in the surface layer it is not possible to approach an initial distribution q (ζ) having a large gradient, regardless of whether the closed or unclosed scheme is used. However, in all cases the statistical regularization method provides more exact and reliable reconstruction than the iteration [5] and optimum parameterization [3] methods.

Increased accuracy of the local concentration q (ζ) determination, including the atmospheric boundary layer, can be achieved by combining the optimum parametrization and statistical regularization methods. If we represent the q' (ζ) profile in expansion form (7.23) and apply the statistical regularization method to the system of Equations (7.24) relative to the coefficients c_k, which are random numbers, then the probability density (6.38) characterizing the a priori c_k distribution will have a very simple form. In fact, the corresponding correlation matrix $\overline{c_k c_1}$ will be diagonal, since ψ_k (ζ_i) in (7.23) are eigenvectors of the auto-correlation matrix B_{qq} (ζ_i, ζ_j) and

$$\overline{c_k c_k} = \lambda_{k'},$$

where λ_k are the eigenvalues of the matrix B_{qq}. In this case the distribution (6.38) is written in the form

$$P(c_k) = \frac{1}{(2\pi)^{n/2}} \prod_{k=1}^{n} \lambda_k^{-\frac{1}{2}} \exp\left(-\frac{1}{2} \frac{c_k^2}{\lambda_k}\right). \tag{7.43}$$

The system of equations of the type (6.43) for determining the mathematical expectation $<c_k>$ from the distribution (7.43)

EXAMPLES OF RECONSTRUCTING THE PROFILES OF $w|(\zeta)$
(w IN cm OF CONDENSED WATER) BY STATISTICAL REGULARIZATION
BASED ON MEASUREMENTS OF $I_\nu \pm 2.35$

ζ	Time of measurement						
	8.30				13.12		
	$\bar{w}$	$w_{in|}$	w_{A_1}	w_{A_2}	$w_{in|}$	w_{A_1}	w_{A_2}
1	1,99	2,47	2,39	2,59	2,16	2,11	2,09
0,95	1,62	1,98	1,97	2,14	1,71	1,72	1,71
0,9	1,28	1,61	1,59	1,73	1,33	1,38	1,36
0,85	0,97	1,24	1,24	1,34	1,02	1,06	1,03
0,8	0,71	0,93	0,93	1,0	0,75	0,80	0,75
0,7	0,33	0,48	0,45	0,46	0,39	0,38	0,33
0,6	0,13	0,23	0,16	0,16	0,17	0,13	0,12
0,5	0,05	0,088	0,05	0,05	0,055	0,042	0,045
0,4	0,02	0,014	0,016	0,016	0,009	0,015	0,018
0,3	0,004	0,001	0,002	0,002	0,001	0,002	0,004

* Translator's note: Commas in numbers represent decimal points.

$$\sum_{k=1}^{n} \tilde{\Gamma}_{jk} \langle c_k \rangle = F_j \qquad (j = 1, 2, \ldots, n), \qquad (7.44)$$

where

$$\tilde{\Gamma}_{jk} = \sum_{v=1}^{N} \frac{D_{vj} D_{vk}}{\sigma_v^2} + \frac{\delta_{jk}}{\lambda_k}; \qquad F_j = \sum_{v=1}^{n} \frac{I_v D_{vj}}{\sigma_v^2}; \qquad \delta_{jk} = \begin{cases} 0, & j \neq k, \\ 1, & j = k, \end{cases} \qquad (7.45)$$

makes it possible to obtain the sought solution $\qquad$

$$q'(\zeta_i) = \sum_{k=1}^{n} \langle c_k \rangle \psi_k(\zeta_i). \qquad (7.46)$$

The system (7.44), (7.45) gives a very clear picture of the
filtering of the high-frequency ψ_k (ζ_i) harmonics, to which there
correspond coefficients c_k of sufficiently large numbers k. In
reality, since the λ_k decrease very sharply with increase of k
the corresponding terms in the coefficients $\tilde{\Gamma}_{jk}$ (7.45) will increase
strongly. This actually means that the coefficients $\langle c_k \rangle$ of the
high-order eigenvectors in the expansion (7.46) are of order λ_k

$$\langle c_k \rangle \approx \lambda_k F_k. \qquad (7.47)$$

This permits filtering out the strongly oscillating harmonics, which is precisely the objective of incorrect problem regularization.
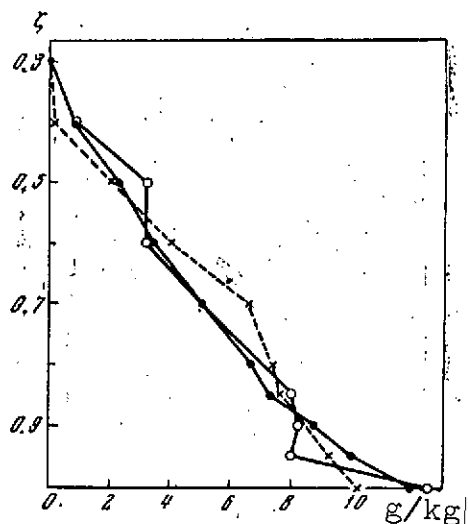
Figure 7.10. Reconstruction of q (ζ) profile by combining the parametrization and statistical regularization methods

Notations same as in Figure 7.9
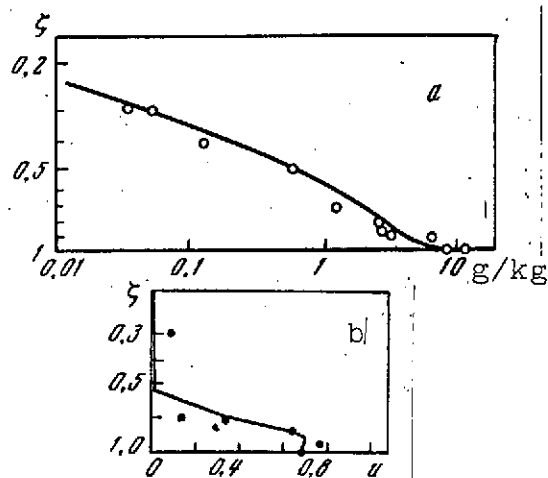
Figure 7.11. Examples of determining profiles of specific (a) and relative (b) humidity after [6.42, 9]

Points are radiosonde data

An example presented in Figure 7.10 of q (ζ) profile reconstruction by the described method on the basis of the previous

six-variate vectors ψ_k (ζ_i) shows, however, that significant refinement of the q (ζ) profile in the atmospheric boundary layer can be obtained with more detailed a priori information on the vertical structure of the q (ζ) profiles at these levels, differentiated with respect to geographical zone and season.

Some idea of the real accuracy is given by the first results of joint q (ζ) and T (ζ) determination from radiation spectrum measurements in the 5-20 micron region with resolution of 5 cm^{-1} aboard the Nimbus 3 satellite using the IRIS interferometer [6.42, 9]. Two methods of q (ζ) reconstruction proposed by Conrath [10] were used in these studies: the iteration method of determining the parameters for approximating q (ζ) by polynomials (Figure 7.11 a), close in concept to the Smith method (see § 2), and the statistical regularization method using the correlation matrix for the relative humidity u (ζ) (Figure 7.11 b). Examples of q (ζ) and u (ζ) determination using these measurements, shown /239 in the figure, illustrate the errors of local humidity reconstruction by the indicated methods with initial data error of about 1%.

On the basis of this analysis we can conclude that the statistical regularization method with use of the statistical characteristics of the humidity field vertical structure makes it possible to determine quite satisfactory integral humidity profiles w (ζ). However, the local humidity is obtained with noticeable error even for small discrepancies which do not cause the radiation $I_{\nu r}$ error to exceed 1-2%. In the subject problem the question of errors (particularly in the transmission function) is very important for its actual solution. Therefore we shall give some estimates of the humidity determination errors for the problem solution cases described above.

§ 5. Analysis of Humidity Determination Errors

The mean square error σ_w (ζ) of vertical profile w (ζ) reconstruction is connected with the mean square error σ_I (ν), the equation kernel, and the correlation matrix K_{ww} by a relation of the form (6.44). As is shown by examination of the errors for the w (ζ) profiles, presented in Table 7.4, reduction of σ_I (ν) leads to reduction of σ_w (ζ), however the error ε_w (ζ) of a specific w (ζ) profile reconstruction may even increase in this case (a similar result was obtained in Chapter 6 in reconstructing the temperature profile).

The reason for this seemingly paradoxical result is that although reduction of the error σ_I permits in principle profile reconstruction with increasing accuracy, actual refinement of the solution requires corresponding accuracy of the equation kernel and computational scheme, and also a finer characteristic of the sought function structure in comparison with the autocorrelation matrix K_{ww} (ζ_i, ζ_j). If the error σ_I is not reconciled with the indicated factors, the profile reconstruction error ε_w (ζ) = $w_{rec} - w_{in}$ will be determined by the actual error ε_I (ν), associated with error of the kernel and computational scheme. This is important in estimating the errors of temperature and humidity profile reconstruction from experimental I_ν data with known measurement error σ_I. Small quantities σ_I do not guarantee obtaining a solution close to the true solution if we do not ensure equally small calculation errors and errors of the kernel of (7.1). The latter factor is particularly important for the problem of determining the humidity q (ζ) or other absorbing substance from the radiation I_ν because of the absence of reliable data on the real radiation absorption in the atmosphere. This situation is illustrated by the data of Table 7.5, in which for several relative errors σ_I/I there are presented the relative errors σ_w/w, ε_w/w at

different levels ζ_i. These data show that the minimum $\varepsilon_w (\zeta_i)$ are achieved with the following optimum values of σ_I/I: 2% for the 8.30 case and 5% for the 13.12 case (although σ_w in these cases are far from minimal). We see from Table 7.6 that for the computational method used above the differences between the experimental values I_ν^e, from which the profiles were reconstructed, and the values I_ν^c, which were calculated from the true humidity profiles with use of the given kernel, were somewhat higher in comparison with the measurement errors indicated in [2.35]. In the 8.30 case the difference $I_\nu^e - I_\nu^c$ varies in the range from 1 to 5% and in the 13.12 case from 3 to 10%. From the viewpoint of the inversion method used these differences are the actual errors ε_I of the right side of (7.1).

If we now take an error σ_I which is low in comparison with the actual error ε_I the weight of the unregularized term associated with the equation kernel in the system coefficients increases. For large σ_I, conversely, the weight of the regularizer K_{ww}^{-1}, which /240 reflects only the general structure of the solution increases. In both cases the reconstruction error will not be optimal. However if the assumed error σ_I is commensurate with the actual method errors, which are characterized by the differences $I_\nu^e - I_\nu^c$, the optimum regularization condition is met and the error ε_w becomes minimal.

As in the problem of determining the temperature profiles, the most critical aspect of all the $q (\zeta)$ reconstruction methods is accounting for the real IR radiation transmission by the atmosphere. At the present time several techniques are being proposed for taking into account broken cloud cover, based on the /241 assumption that clouds radiate like black bodies and on using additional information on the distribution of cloudy and clear regions which fall in the measuring instrument viewing field (see, for example, [4, 5, 9, 11]). The examples presented here of

TABLE 7.5. CONNECTION BETWEEN σ_I/I, σ_w/w, AND ε_w/w (IN %) WHEN USING THE STATISTICAL REGULARIZATION METHOD*

ζ	$\sigma_I/I = 1\%$				$\sigma_I/I = 2\%$				$\sigma_I/I = 5\%$			
	σ_w/w		ε_w/w		σ_w/w		ε_w/w		σ_w/w		ε_w/w	
	8.30	13.12	8.30	13.12	8.30	13.12	8.30	13.12	8.30	13.12	8.30	13.12
1,0	6,4	7,4	4,8	20,9	8,1	9,3	0,4	11,5	10,1	11,6	8,1	3,3
0,95	6,1	7,0	8,0	26,4	7,6	8,8	3,7	15,8	10,8	11,7	5,6	0
0,9	5,0	6,0	7,4	30,8	6,8	8,3	1,9	19,6	11,9	12,0	7,5	2,3
0,85	4,8	5,8	8,1	34,4	7,5	7,9	2,4	18,9	10,7	11,9	8,0	1,0
0,8	4,3	5,3	7,5	30,6	6,5	8,0	2,1	4,0	9,8	12,0	8,6	0
0,7	4,2	5,1	4,2	2,7	6,3	7,7	8,4	5,2	10,7	12,8	16,5	15,5
0,6	6,3	5,9	30,4	35,3	6,2	7,1	30,4	29,4	9,0	11,8	30,2	29,4
0,5	5,0	7,3	37,6	41,9	6,3	9,1	37,6	30,9	9,5	10,9	32,6	18,2
0,4	7,1	11,1	43,0	0	10,7	16,7	43,0	22,2	14,2	22,2	43,0	55,2

* Translator's note: Commas in numbers represent decimal points.

TABLE 7.6. RADIATION MEASURED BY RADIOSONDE (I_ν^e) (8.30 | AND 13.12 ON 8 MAY 1966 [2.35]) AND CALCULATED (I_ν^c)*

ν, см$^{-1}$	8.30		13.12	
	I_ν^e	I_ν^c	I_ν^e	I_ν^c
1241	8,87	8,95	9,58	9,57
1262,5	6,21	6,49	6,33	6,91
1287,5	6,00	6,05	6,19	6,43
1312,5	5,67	5,71	5,91	6,08
1337,5	4,63	4,70	4,77	5,00
1362,5	4,37	4,41	4,86	4,70
1387,5	4,01	4,03	4,59	4,30
1412,5	4,00	4,03	4,57	4,30
1437,5	2,98	2,92	3,41	3,17
1462,5	2,33	2,28	2,80	2,50
1487,5	1,65	1,72	2,16	1,90
1512,5	1,41	1,38	1,35	1,53

*Translator's note: Commas in numbers represent decimal points.

successful q (ζ) profile reconstruction under cloudy conditions are promising. However, as noted in [9], application of these techniques to q (ζ) determination from I_ν measurements aboard the Nimbus 3 satellite does not yield satisfactory results in most cases.

It appears to us that the resolution of this extremely complex question lies in using the data on the three-dimensional structure of aerosol radiation attenuation in the iterational process in § 9 of Chapter 6.

CHAPTER 8
DETERMINATION OF UNDERLYING SURFACE AND CLOUD TEMPERATURES

§ 1. Problem Formulation and Basic Relations

One of the important and most urgent problems of optical sounding from satellites is that of determining the underlying surface and cloud top temperatures from Earth's self-radiation intensity measurements in the 3-4 and 8-12 (or 10-12) micron atmospheric windows.

The formulation of this problem was based on the assumption that the self-radiation of the underlying surface in the indicated spectral regions is distroted relatively weakly during propagation in the cloudless atmosphere. Therefore, if the radiance of the natural surface is close to that of a blackbody the radiation temperature determined directly from Earth's radiation measurement in the window will be close to the true surface temperature. The same applies to the radiation of the top of solid cloud cover, which can be considered a radiating surface with cloudless overlying atmosphere.

In reality, as we have seen in § 2 of Chapter 2, the Earth's atmosphere is far from transparent in these "windows". As a result of the wings of the neighboring strong H_2O and CO_2 absorption bands, the presence of individual lines of these gases, and the strong 9.6 μ ozone band the atmosphere absorbs some fraction of the underlying surface radiation and radiates at all levels with the temperatures of the corresponding layers. As a result the Earth's radiation measured aboard a satellite represents superpositioning of the Earth's surface or cloud radiation

attenuated by the atmosphere and the self-radiation of the atmosphere itself. For this reason the radiation temperature of the Earth measured aboard a satellite differs from the radiation temperature of the Earth's surface region being studied. These differences are determined basically by the vertical atmospheric temperature and humidity distributions and also by the distributions of the absorbing substances which are optically active in the given spectral interval (for example, ozone in the 9.6 μ band or aerosols in the "windows"). Since these parameters are not known at the moment of radiation measurement from the satellite, exact solution of the subject problem is impossible even in a cloudless atmosphere*.

However, even if we were able to determine with sufficient accuracy the radiation temperature of the underlying surface, to determine the true temperature we need information on the surface radiance. As was shown in Chapter 2, the radiance of several natural surfaces differs markedly from one and depends on many uncontrollable factors.

In this connection there is a clear requirement for realisitc estimates of the accuracy of underlying surface and cloud temperature determination when using the existing methods for measuring the Earth's self-radiation in the IR spectrum windows. In the present chapter we examine this question in application /243 to the 8-12 and 10-12 μ windows, in which the Earth's radiation was measured aboard satellites of the Tiros, Kosmos, and Nimbus series [I.13, I.20, I.21, 5.13, 5.16] and extensive data were obtained on the radiation temperature of various terrestrial formations. This examination is also of interest in connection

---

* We must bear in mind that the "cloudless atmosphere" concept for IR radiation in 8-12 μ window region differs from the analogous concept in the visible spectrum region.

with the fact that the 8-12 μ spectral region was used aboard the meteorological satellites Kosmos 122, Kosmos 144, and others [I.20] to obtain television images of the thermal contrasts between the Earth's surface and cloud cover.

As for the 3-4 μ window, in which television images and absolute magnitudes of the Earth's radiation were obtained from satellites of the Nimbus series [I.21], the atmosphere is more transparent in this window than in the 8-12 μ window. Moreover, the radiation in this window is more sensitive to radiator temperature variations. However, along with these advantages the 3-4 μ interval has a significant drawback — the Earth's self-radiation here is comparable with the reflected solar radiation (see § 5 of Chapter 1). Consequently, under daytime conditions (and particularly above clouds) the sum of the self and reflected radiations will be measured, which leads to inacceptably large errors in determining the temperature of the Earth's surface. Therefore measurements in the 3-4 μ interval, which provide thermovision on the nighttime side of the Earth, are valuable in combination with television images in the visible part of the spectrum or with measurements in the 8-12 μ interval window in which we can neglect reflected solar radiation.

With account for the latter factor, the intensity I measured aboard a satellite of the radiation leaving the upper edge of the atmosphere $\zeta = 0$ in the direction $\theta = 0$ is connected with the underlying surface temperature T (1) by the relation (see also (2.10)

$$I\,[T\,(\zeta),\,w\,(\zeta)] = \delta B\,[T\,(1)]\,P\,[w\,(1),\,m\,(1)] - \int_0^1 B\,[T\,(\zeta)]\,\frac{\partial P\,[w\,(\zeta),\,m\,(\zeta)]}{\partial \zeta}\,d\zeta -$$
$$- 2(1 - \delta)\,P\,[w\,(1),\,m\,(1)] \int_0^1 B\,[T\,(\zeta)]\,\frac{\partial}{\partial \zeta}\,\tilde{P}\,[w\,(1) - w\,(\zeta),\,m\,(1) - m\,(\zeta)]\,d\zeta. \tag{8.1}$$

The radiation intensity in this expression, which can be considered an equation in the underlying surface temperature T (1), also depends functionally on the vertical distributions of the temperature T (ζ), humidity w (ζ), and other absorbing substances (for example, ozone m (ζ) or aerosol). For most underlying surfaces we can drop in (8.1) the third term, describing incident radiation reflection from the Earth's surface, however for δ differing strongly from I this term must be considered*.

Relation (8.1) shows that to obtain the underlying surface radiation temperature T_r (1), determined from the condition B [T_r (1)] = δB [T (1)], we need, besides the I measurements, additional information on the vertical profiles of the atmospheric parameters responsible for transformation of the Earth's surface self-radiation. This additional information permits account for the transformation of the underlying surface radiation in the atmosphere with some degree of confidence and introduction of the corresponding corrections. At the present time two techniques for introducing the corrections have been proposed, based on modeling the variations of the temperature and humidity (considered to be the basic factors of this transformation) vertical profiles.

1. The method proposed by Wark et al. [2.1] consists in determining the relationships between the outgoing radiation /244 intensity I, calculated for some sufficiently broad set of vertical temperature, humidity, and ozone concentration profiles, and the underlying surface self-radiation B [T (1)].

2. Use of the statistical characteristics of the temperature and humidity field vertical structure to determine the atmospheric

---

* We note that the spectral sensitivity of the measuring instrument is taken into account in (8.1) with the aid of a transmission function of the form (4.4).

transfer function, which describes transformation δ B [T (1)] of the underlying surface or cloud cover radiation in the overlying atmosphere [6.40, 1, 2].

Before examining these methods we note that they take into account only the meteorological atmosphere model characteristics. However, the reliabiltiy of the account for underlying surface radiation transformation is associated with the validity of the optical atmosphere model characteristics. In this sense the most critical aspect is accounting for aerosol absorption, which may play a significant role in radiation transformation in the 8-12 μ spectral interval (see § 2, 3 of Chapter 2). Aerosol existence and variations, particularly at high altitudes in the temperature minima regions (10, 20, and 80 km), may become the source of significant errors in determining underlying surface radiation temperature.

Another error source in converting from radiation temperature to true temperature is the radiance variations of natural surfaces and clouds. For this reason the most reliable temperatures can be obtained above water surfaces or wooded massifs, whose radiance is close to one. These surfaces will be used primarily to check the methods for determining T (1) from radiation measurements in the 8-12 μ spectral interval window.

§ 2. Yamamoto-Wark Method

On the basis of calculations of the Earth's self-radiation spectral intensity I_ν for more than 100 different realizations of vertical temperature, humidity, and ozone concentration profiles (see § 4 of Chapter 2), Wark, Yamamoto, and Lienesch [2.1] constructed empirical relationships between outgoing radiation intensity and underlying surface radiation. The calculations

were made for the 8-12 μ window with account for the spectral sensitivity of the radiometer installed aboard satellites of the Tiros series.

Since the gases which absorb and emit radiation in the considered part of the spectrum (water vapor and ozone) are basically concentrated in different layers of the atmosphere (water vapor in the troposphere up to 10 km, ozone in the stratosphere above 10 km), the authors of [2.1] calculated the corrections which must be introduced into the measured radiation I in order to obtain B [T (1)] spearately for each gas*. These corrections are shown in Figures 8.1 a and 8.2 b. Since the variations of the ozone concentration vertical distribution in the atmosphere and also the ozonosphere temperature variations are relatively small, the resulting corrections are weakly dependent on these variations. We see from Figure 8.1 a that the relationship between the intensity measured in the window and the correction for ozone absorption and radiation has a linear nature (which is a consequence of the correlation between underlying surface temperature and temperature at other levels) with small scatter of the points.

In contrast with ozone, the amount of water vapor varies strongly in the atmosphere, particularly in the lower troposphere, and in combination with the strong variations and anomalies of the temperature in this layer complicates the determination of the corresponding corrections. Figure 8.2, which presents the corrections as functions of outgoing radiation intensity, shows that although there is a tendency toward correction increase with growth of the outgoing radiation intensity (this increase has a nonlinear nature) the considerable point scatter introduces indeterminacy in selection of the correction factor. This scatter

---

* In [2.1] it is assumed that the underlying surfaces radiate as a blackbody ($\delta_\nu = 1$).

indicates weak correlation of temperature and humidity at the different levels.
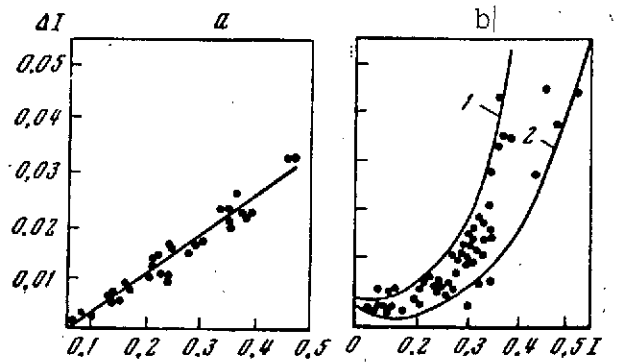
Figure 8.1. Additive corrections ΔI [2.1] (I in 10^5 erg/cm^2·sec·sr) a- correction for ozone absorption; b- correction for water vapor absorption; 1- high humidity; 2- low humidity
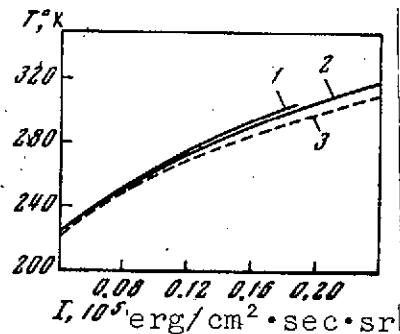
Figure 8.2. Relationship between radiation I and radiation temperature of underlying surface for $\theta = 0$ with account for overall correction

1- high humidity; 2- low humidity; 3- relationship between T and I without account for the corrections

We see from Figure 8.1 b that the two curves suggested by the authors of [2.1] for taking account of the corrections in the high and low humidity cases are not provided with any indication of applicability limits and, what is most important, there is no criterion for selecting a particular curve under the specific conditions of measurements from a satellite. The measure of indeterminacy of water vapor correction introduction is characterized by the entire band of values between the two curves, and

419

in several cases the correction even changes sign (the negative corrections correspond to temperature inversions in the atmospheric boundary layer).

The overall correction plotted with account for the characteristics of the Tiros 2 satellite radiometer (see Figure 8.2) indicates that this indeterminacy may lead to errors in determining the temperature on the order of 10°.

The examples presented in [2.1] of use of the porposed method for converting from the radiation temperature T_r measured aboard the Tiros 2 satellite to the true underlying surface temperature T_s show that the difference between the surface temperature T_{rs} reconstructed in this way and the air temperature T_a at the shelter level varies in the range from -5 to +3.5° (Table 8.1). In the table we note relatively small differences between T_r and T_a, not exceeding 5-6° (larger differences $T_a - T_r$, reaching 10°, relate to measurement cases in which the presence of a thin overcast, which was not recorded at the weather stations is suspected, since the corrections in [2.1] are calculated for cloudless conditions). This circumstance is important in explaining the actual radiation transformation in the atmosphere and the /246 meaningfulness of the T_{rs} and T_a comparison. The reason is that the land surface temperature (see note that all stations in the table are continental stations) may differ markedly from the temperature at the slelter level, and in the daytime hours $T_s > T_a$ nearly always. Therefore, if there is additional radiation absorption in the atmosphere which is not taken into account by the corrections of [2.1] (for example, aerosol absorption) the corresponding radiation temperature measured aboard the satellite will differ quite strongly from T_s (the differences may reach 15-20°). However, if the temperature decreases markedly in the air layer (1-2 m) next to the ground the radiation temperature

TABLE 8.1. COMPARISON OF EARTH'S RADIATION TEMPERATURES T_r MEASURED ABOARD THE TIROS 2 SATELLITE, TEMPERATURES T_{rs} CORRECTED USING THE METHOD OF [2.1], AND THE AIR TEMPERATURES T_a AT SEVERAL USA STATIONS (18.00 GMT, 25 NOV. 1960)*

Station	T_r	T_{rs}	T_a	$T_{rs} - T_a$	$T_a - T_r$	$T_{rs} - T_r$	
Flint	275,3	279,5	279,9	—0,4	4,6	4,2	
Detroit	271,6	276,5	279,9	—3,4	7,3	3,9	
Evansville	275,9	280,3	283,2	—2,9	7,3	4,4	
Springfield	277,1	282,1	282,6	—0,5	5,5	5,0	
St. Louis	278,3	283,2	279,9	3,3	1,6	4,9	
Muskegon	277,8	282,4	279,9	2,5	1,1	4,6	
Akron	277,1	281,6	281,0	0,6	3,9	4,5	
Fort Smith	275,3	280,4	285,4	—5,0	10,1	5,1	
Tulsa	277,1	282,6	282,6	0,0	5,5	5,5	
Cinncinnati	277,1	281,6	281,0	0,6	3,9	4,5	
Mansfield	276,5	280,9	279,9	1,0	3,4	4,4	
Oklahoma City	277,1	282,7	283,2	—0,5	6,1	5,6	
Dayton	277,1	281,6	278,8	2,8	1,7	4,5	
Peoria	275,9	280,2	280,4	—0,2	4,5	4,3	
Columbia	274,0	278,2	280,4	—2,2	6,4	4,2	
Green Bay	273,3	277,3	278,8	—1,5	5,5	4,0	
Sault Ste. Marie	272,6	276,6	277,6	—1,0	5,0	4,0	
Amarillo	277,1	284,5	281,0	3,5	3,9	7,4	
Little Rock	277,1	282,6	286,0	—3,4	8,9	5,5	
Pittsburgh	275,9	280,2	279,9	0,3	4,0	4,3	

* Translator's note: Commas in numbers represent decimal points.

is quite close to the air temperature at the shelter level. Moreover, for sufficiently large gradients we would expect that the measured radiation temperature T_r may even exceed T_a. Such situations are encountered during daytime in cloudless weather, when the Earth's surface is overheated in comparison with the air, or are created by cold air mass intrusion. Therefore comparison of the radiation temperatures with the air temperature cannot be considered legitimate in such cases, and in estimates of the effectiveness of any method of correcting for radiation transformation in the atmosphere we must take into account the actual

temperature gradients in the surface air layer.

Comparison of T_r and T_a above the ocean will be more legitimate, since in this case large temperature gradients in the layer next to the water are unlikely. However, such comparisons made in [3] from Earth radiation measurements in the 8-12 μ window aboard the Tiros 3 satellite showed that the differences between T_r and T_a reach 20°. This difference cannot be explained solely by radiation absorption by water vapor and ozone, which can be seen by examining the results of analogous measurements made in [3] for cloudless North Africa.
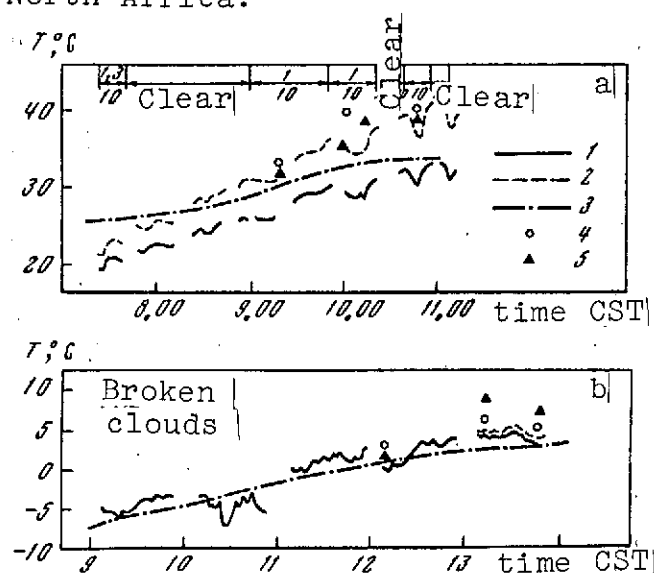
Figure 8.3. Comparison of radiation temperatures T_r and T_{rs} with air temperature T_a [5].
a- Palestine 11 Sept. 1964; b- Sioux Falls 10 Mar. 1965; 1- T_r; 2- T_{rs}; 3- T_a; 4- thermistor measurements; 5- radiometer measurements

In spite of the fact /247 that the radiance of desert sand may differ markedly from one (see Figure 2.15), the radiation temperatures here reach 312° K. Study of this measurement case in [4] showed that during the period of I measurements above North Africa the humidity was quite high (the total water vapor mass reached 2-3 cm), the air temperature was T_a = 315° K, and the surface temperature T_s reached 330° K. But even under these conditions there was some "compensation" for Earth's surface IR radiation attenuation by the large temperature gradients, and this led to the values of T_r and T_a being close to one another.

422

Another confirmation of the assumption made above on the relationship between T_r, T_{rs} and T_a above land areas are the results of underlying surface temperature determination obtained by Saiedy and and Hilleary [5] using balloon measurements of the Earth's radiation spectra in the 11.1 µ window above Palestine (11 Sept. 1964) with very high humidity and above Sioux Falls (10 Mar. 1965) with very low humidity. These results are illustrated in Figure 8.3, which compares the daily variation of the radiation temperatures T_r and T_{rs}, measured aboard balloons and reconstructed, with T_a and the surface temperatures T_s measured by radiation and contact methods right at the surface*.

The introduction of the correction for transformation in the atmosphere was made directly with the aid of (8.1), since T (ζ) and q (ζ) were known for the flight conditions. We see from the figure that in the morning hours, when according to the data of [5] there was a surface temperature inversion above Palestine, the difference $T_a - T_r$ reached 8°. The reconstructed temperature T_{rs} with account for the correction differed from T_r by only 2° and as before was lower than T_a. With approach to midday the difference $T_a - T_r$ approached zero in spite of the fact that the humidity was very high (the total water vapor mass was 5.4 cm precipitable water). The reconstructed temperature T_{rs} exceeded T_a and the difference $T_{rs} - T_a$ reached 8°. Similar relationships between T_r, T_a and T_s, although not so clearly defined, were also obtained for the Sioux Falls region, where the situation was characterized by intrusion /248 of cold arctic air above the comparatively warm soil surface (total water vapor mass did not exceed 0.5 cm precipitable water). We

---

* It should be noted that this comparison is not entirely representative because of the large angular resolution of the spectrometer, which averaged measurements over a 10·10 km² area. Moreover, because of balloon displacement, space-time variation of the measurement data was actually obtained.

note that for this case there is practically no temporal variation of the difference $T_r - T_a$, since in this situation the temperature decrease in the near-surface layer will be independent of the time of day.

The results of [5] are also of interest from the viewpoint of estimating underlying surface radiance. Comparison of the radiation temperature measured near the surface with the soil temperature, obtained with the aid of a thermistor at a distance of 1-2 mm above the surface, shows that these surfaces radiate as blackbodies to within 1-2°.

Thus, the very first attempts to determine underlying surface temperature from self-radiation in the 8-12 μ spectral interval window showed that in order to achieve the required T (1) determination precision of order 1-2° we cannot restrict ourselves to model representations of the temperature and humidity vertical profiles. More representative data on these parameters are required, corresponding to the real situation existing at the time and place of the radiation measurements. We could pose the question of simultaneous determination of the T (ζ) and q (ζ) profiles, necessary for introducing the corrections for radiation transformation in the atmosphere. However, first, as we have seen in Chapters 6 and 7 these problems are an order of magnitude more complex from the experimental viewpoint and also from the viewpoint of interpreting the measurement results. Second, the solution of these problems automatically yields the magnitude of the underlying surface temperature as $\lim_{\zeta \to 1} T(\zeta)$. Therefore it was proposed in [2] that the a priori information in the form of statistical characteristics of the vertical structure of the temperature and humidity fields presented in § 2 and § 3 of Chapter 3 be used for optimum reconstruction of the specific stratification of the atmosphere.

On the other hand, representative account for the optical parameters of the atmosphere, particularly the contribution of aerosol absorption, is very important. For this purpose we shall use the concept introduced in [1] of the transfer function, which makes possible regular account for the optimally reconstructed T (ζ) and q (ζ) profiles and the empirical correction for additional atmospheric absorption.

§ 3. Use of Statistical Temperature and Humidity Characteristics

3.1. Transfer Function of the Atmosphere

As mentioned previously, the radiometers used at the present time measure directly the quantity

$$\tilde{I} = \int_{\nu_1}^{\nu_2} I_\nu \varphi_\nu \, d\nu, \tag{8.2}$$

where I_ν is the Earth's monochromatic radiation intensity, determined for each frequency ν by (8.1); φ_ν is the radiometer spectral sensitivity, which vanished outside the spectral interval $[\nu_1, \nu_2]$. The underlying surface temperature T (1) which is to be determined is connected with the underlying surface radiation by the relation

$$\tilde{B}[T(1)] = \int_{\nu_1}^{\nu_2} \delta_\nu \varphi_\nu B_\nu [T(1)] \, d\nu. \tag{8.3}$$

We introduce the so-called transfer function /249

$$\mathscr{P} = \frac{\tilde{I}}{\tilde{B}[T(1)]}, \tag{8.4}$$

which characterizes, as we see from (8.2) and (8.3), transformation of the Earth's surface self-radiation not only by the atmosphere but also by the instrument itself. The transfer function is a functional of the vertical temperature, humidity, and other absorbing substance profiles, and also of the parameters φ_ν and δ_ν.
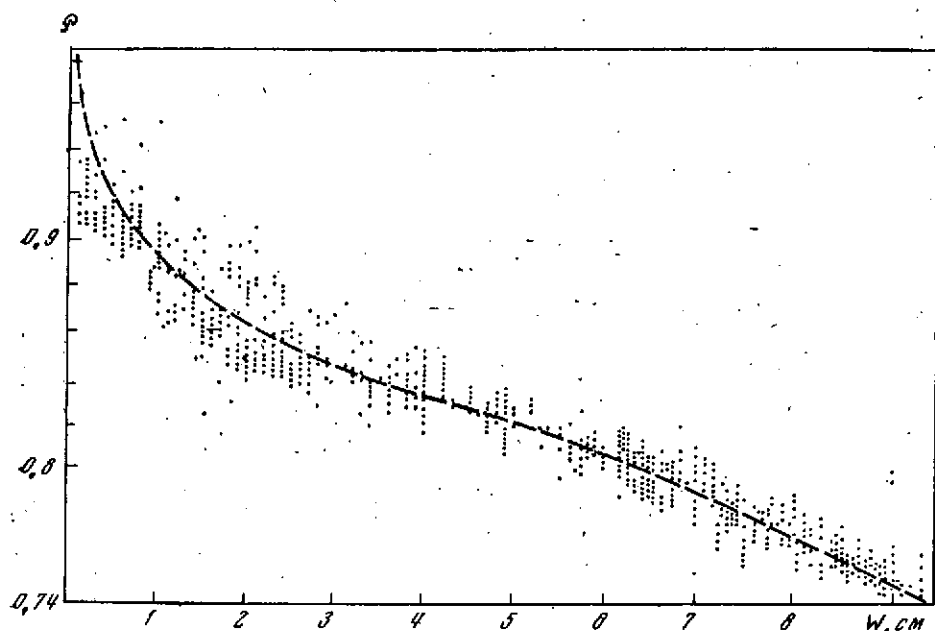
Figure 8.4. Atmospheric transfer function versus total water vapor mass from [2.54]

In the case of weak dependence of δ_ν on ν, which is observed in actuality for narrow spectral intervals (or must be assumed because of inadequate information on δ_ν), the transfer function is practically independent of underlying surface radiance. The transfer function depends just as weakly on the radiometer spectral sensitivity if φ_ν has the usual variation with ν: small deviations from a constant value in the primary part of the spectral interval and marked decrease at the ends of the interval (this variation actually occurs for the radiometers which were installed aboard the Kosmos 149, Kosmos 243, Kosmos 320, and Nimbus 2 satellites).

Thus, if the transfer function $\mathscr{P}$ is known and δ_ν is independent of ν, it is easy to determine $B[T(1)] = \left| \delta \int_{\nu_1}^{\nu_2} \varphi_\nu B_\nu [T(1)]\, d\nu = \delta B [T(1)] \right|$ from (8.4) for the measured $\tilde{I}$. For the known value of the parameter δ and the calibration curve of blackbody radiation versus temperature we determine T (1) (in the following we examine the procedure for determining T (1) for the radiometer installed aboard the Kosmos

426

149 satellite). If δ is not known we obtain the surface radiation temperature $T_{rs} = T_r$ (1). The central problem at this stage is therefore to determine the transfer function which best reflects the specific measurement conditions.

Curves of the transfer function versus total water vapor mass w (1) varying in the 0.1-9 g/cm² range (Figure 8.4) and near-Earth atmosphere layer temperature have been plotted from numerous calculations of I for average climatic temperature and humidity distributions in July and January in all zones of the terrestrial sphere [2.54]. Isolines of the transfer function for the indicated seasons (Figure 8.5) were also plotted in [2.54, 6]. We see from the curves obtained in [2.54, 6] that the results indicate large space and time $\mathscr{P}$ variations which agree with the total water vapor mass variations. At the same time, for fixed values of w (1) marked transfer function variations were obtained (see Figure 8.4), reflecting the vertical temperature and humidity profile variations and to some degree the weak correlation between T (ζ) and q (ζ) for summertime conditions and southern stations (see § 3 of Chapter 3). Therefore direct use of the curve in the figure or the isolines essentially retains the indeterminacies which were examined above in § 2, i.e., in this formulation use of the transfer function does not provide any particular advantages in comparison with the Yamamoto-Wark method. In order to refine the transfer function it is necessary to find a technique to account for these variations, which have a random nature and therefore obviously cannot be obtained by any deterministic technique if we do not know the real T (ζ) and q (ζ) profiles. It is precisely for this purpose that we utilize the ensembles of vertical temperature and humidity field structure statistical characteristics described in § 2 and § 3 of Chapter 3: mean profiles $\bar{T}$ (ζ), $\bar{q}$ (ζ), autocorrelation matrices B_{TT} (ζ_k, ζ_i), B_{qq} (ζ_k, ζ_i), and cross-correlation matrices B_{Tq} (ζ_k, ζ_i).

3.2. Use of Statistical Characteristics

The idea of using the mentioned statistical characteristics for a cloudless atmosphere amounts to the following. Using the mean climatic profiles $\bar{T}(\zeta)$ and $\bar{q}(\zeta)$ for the given region and season (or month), from (8.1) we determine the transfer function $\bar{\mathscr{P}} = \mathscr{P}[\bar{T}(\zeta), \bar{q}(\zeta)]$ corresponding to this average regime (or we use the $\mathscr{P}$ values plotted in [2.54, 6]). With the aid of these functions and direct measurements of the Earth's self-radiation intensity I from the satellite we can find the underlying surface self-radiation

$$\delta B[T(1)] = \frac{I}{\bar{\mathscr{P}}}, \qquad (8.5)$$

and therefore (for known δ) the first approximation of the underlying surface temperature T_1 (1). Thereby we find the first approximation of the underlying surface temperature deviation from the mean

$$T_1'(1) = T_1(1) - \bar{T}(1).$$

The difference between the approximation obtained in this way and the true temperature T_s depends on how much $\bar{\mathscr{P}}$ differs from the specific transfer function realization.

The next temperature approximation may be found with the aid of the correlation matrices B_{TT}, B_{qq}, T_{qT}. Actually, as soon as the temperature deviation T_1' (1) at the underlying surface level is known it is not difficult to obtain $T_1'(\zeta_k)$ at other levels ζ_k, using for this purpose optimum extrapolation of the surface temperature to the other levels (see § 1 of Chapter 3). Representing $T_1'(\zeta_k)$ in linear form

$$T_1'(\zeta_k) = c_k T_1'(1) \qquad (8.6)$$

and determining c_k from the condition of minimum approximation error averaged over all temperature realizations /252

$$\delta_T^2(\zeta_k) = \overline{[T_1'(\zeta_k) - c_k T_1'(1)]^2}, \qquad (8.7)$$

428

Figure 8.5. Isolines of transfer function in 8-12 µ region from [8.6]

a- January; b- July

we obtain the expressions for the coefficients

$$c_k = \frac{B_{TT}(\zeta_k, 1)}{B_{TT}(1, 1)},$$

(8.8)

where B_{TT} are the corresponding moments of the autocorrelation matrix.

Expressions (8.6) — (8.8) make it possible to reconstruct in optimum fashion the first approximation of the vertical temperature profile on the basis of only a single surface value $T_1'(1)$ of the temperature deviation from the mean. The error of this reconstruction for the deviation $T_1'(\zeta_k)$ is expressed through the correlation coefficient $r_{TT}(\zeta_k, 1)$. Actually, substituting (8.8) into (8.7) we find that the mean-square error $\delta_T^2(\zeta_k)$ is expressed as follows

$$\delta_T^2(\zeta_k) = B_{TT}(\zeta_k, \zeta_k) - \frac{B_{TT}^2(\zeta_k, 1)}{B_{TT}(1, 1)},$$

(8.9)

and the relative error $\varepsilon_T(\zeta_k) = \delta_T(\zeta_k)/\sigma_T(\zeta_k)$ has the form

$$\varepsilon_T(\zeta_k) = \sqrt{1 - r_{TT}^2(\zeta_k, 1)}.$$

(8.10)

The data presented in Chapter 3 on correlation coefficients for real vertical temperature profiles in several regions of the terrestrial sphere show that the statistical characteristics provide optimum reconstruction of the variations $T'(\zeta_k)$ with mean-square error on the order of 50% in the lower troposphere (up to the 500 mbar level). The absolute temperature $T_1(\zeta_k) = \bar{T}(\zeta_k) + T_1'(\zeta_k)$, which is necessary in calculating the first approximation of the transfer function, is reconstructed with 1-2% error. In the higher layers of the atmosphere the optimum extrapolation error increases (Table 8.2). However for the subject problem it is important that a sufficiently reliable $T(\zeta)$ profile be determined precisely for the lower troposphere, which makes the primary contribution to transformation of the underlying surface self-radiation in the transparency window, since practically the entire water vapor mass is concentrated in this layer.

TABLE 8.2.   ERRORS OF OPTIMUM T' (ζ)
AND q' (ζ) EXTRAPOLATION*

	ζ_k									
	1	0,5	0,7	0,6	0,4	0,3	0,5	0,2	0,15	0,1
σ_T, °C	5,3	4,7	4,6	2,7	3,1	2,9	3,1	4,2	3,5	2,9
δ_T, °C	0	1,5	3,0	2,0	2,3	2,3	2,9	3,8	2,9	2,4
ε_T, %	0	32	65	74	74	79	94	91	83	83
σ_q, g/kg	2,01	1,72	1,56	0,66	0,30	0,10	—	—	—	—
δ_q, g/kg	0	0,30	1,48	0,66	0,30	0,10	—	—	—	—
ε_q, %	0	17	95	100	100	100	—	—	—	—

* Translator's note: Commas in numbers represent decimal points.

It is quite clear that it is also necessary to reconstruct the first approximation of q' (ζ) in order to find the transfer function which describes more exactly the specific radiation transformation conditions and permits obtaining the succeeding approxi- /253 mations of T' (1). For this purpose we can utilize optimum extrapolation of the specific humidity q' (ζ_k) to the level ζ_k using the already obtained T'_1 (ζ_k) profile

$$q'_1(\zeta_k) = \sum_{i=1}^{n} d_i^{(k)} T'_1(\zeta_i),$$

(8.11)

so that the mean-square extrapolation error

$$\delta_{qT}^2(\zeta_k) = \overline{\left[q'_1(\zeta_k) - \sum_{i=1}^{n} d_i^{(k)} T'_i(\zeta_i) \right]^2}$$

(8.12)

will be minimal.

From the (8.12) minimum condition and averaging over all realizations, we obtain the system of equations for determining the coefficients $d_i^{(k)}$

$$\sum_{j=1}^{n} B_{TT}(\zeta_i, \zeta_j) d_j^{(k)} = B_{qT}(\zeta_k, \zeta_i) \qquad (i = 1, 2, \ldots, n),$$

(8.13)

in the right side of which there appear the elements of the cross-correlation matrix B_{qT}.

The mean-square error of this extrapolation is obtained from the relation

$$\delta_{qT}^2(\zeta_k) = B_{qq}(\zeta_k, \zeta_k) - \sum_{i=1}^{n} B_{qT}(\zeta_k, \zeta_i)\, d_i^{(k)}, \qquad (8.14)$$

and the relative error is

$$\varepsilon_{qT}^2 = \frac{\delta_{qT}^2(\zeta_k)}{\sigma_q(\zeta_k)\,\sigma_T(\zeta_k)} = \sqrt{1 - \sum_{i=1}^{n} r_{qT}^2(\zeta_k, \zeta_i)\, d_i^{(k)}}. \qquad (8.15)$$

The system (8.13) is poorly conditioned and in addition the correlation coefficients r_{qT} in many cases, for example, for cases of flights above land, are small (on the order of 0.5). However, since r_{qT} reach the maximum value for variations q' (ζ_k) and T' (ζ_k) at the same level, we took only one term of T' (ζ_k) in (8.11). The quantities $\sigma_{qT}(1.1)$, $\delta_{qT}(1.1)$, $\varepsilon_{qT}(1.1)$ for the statistical characteristics taken from [3.8] are shown in Table 8.3.

TABLE 8.3. ERRORS OF OPTIMUM q' (1) APPROXIMATION USING T' (1)*

	Bismarck July	Bismarck Jan.	Ship C July	Ship C Jan.
σ_{qT} (1,1), g/kg	2,01	1,05	1,25	1,19
δ_{qT}, g/kg	1,93	0,47	0,79	0,50
ε_{qT}, %	96	45	63	42

* Translator's note: Commas in numbers represent decimal points.

The most reliable optimum reconstruction of the q_1' (ζ_k) profile variations can be accomplished using as the reference level that at which the correlation coefficient r_{qT} (ζ_k, ζ_i) is maximum and

432

using as a priori information the autocorrelation matrix B_{qq} $(\zeta_k,$ $\zeta_i)$. Then, setting

$$q_i'(\zeta_k) = d_i^{(k)} q_i'(\zeta_i),$$ (8.16)

we obtain, just as above, the relations for determining the /254 coefficients

$$d_i^{(k)} = \frac{B_{qq}(\zeta_i, \zeta_k)}{B_{qq}(\zeta_i, \zeta_i)}.$$ (8.17)

The extrapolation error is calculated from the formulas

$$\delta_q^2(\zeta_k) = B_{qq}(\zeta_k, \zeta_k) - \frac{B_{qq}^2(\zeta_i, \zeta_k)}{B_{qq}(\zeta_i, \zeta_i)}$$ (8.18)

and

$$\varepsilon_q^2(\zeta_k) = 1 - r_{qq}^2(\zeta_i, \zeta_k).$$ (8.19)

After reconstructing in this way the profiles T_1' (ζ_k) and q_1' (ζ_k) in the first approximation, we can refine the transfer function and approach its true value, as suggested in [3.8]. This permits determining the second approximation of T_1' (1) with the aid of (8.5), in which we take in place of $\tilde{\mathscr{P}}$ the refined transfer function, and after repeating the described procedure permits finding in the second approximation the temperature T_2 (ζ_k) and humidity q_2 (ζ_k) profiles.

Before turning to use of the proposed technique for determining T (1) from existing self-radiation measurements in the 8-12 μ window from satellites, we shall examine the question of using the statistical characteristics of the temperature and humidity field vertical structure with account for radiation transformation in the atmosphere with the aid of additive corrections, as is done, for example, in the Yamamoto-Wark method [2.1] (in these terms the transfer function determines a multiplicative correction).

3.3. Successive Additive Correction Approximations

The primary advantage of the method described in section 3.2 is the existence of a definite algorithm accounting for the meteorological parameters for the specific situation, at least in the statistically optimum sense. However the structural characteristics of the temperature and humidity profiles can also be used to determine additive corrections. We shall illustrate this for the modification of the Yamamoto-Wark method which was adopted in [5]. We represent (8.1) for the n-th approximation of the Earth's surface self-radiation in the form

$$\delta B\left[T_n(1)\right] = \frac{I - \Delta I\left[T_{n-1}(\zeta),\, q_{n-1}(\zeta)\right]}{P\left[w_{n-1}(1),\, m_{0_3}(1)\right]}. \tag{8.20}$$

Here I is the directly measured self-radiation intensity; $\Delta I\left[T_{n-1},\, q_{n-1}\right] = \int_0^1 B\left[T_{n-1}(\zeta)\right]\frac{\partial P\left[w_{n-1}(\zeta)\right]}{\partial \zeta}\, d\zeta$ is the correction for radiation transformation in the atmosphere, calculated for the (n − 1)-th approximation of the profiles $T_{n-1}(\zeta),\, q_{n-1}(\zeta);\, P\left[w_{n-1}(\zeta)\right]$ is the transmission function, calculated for the (n − 1)-th water vapor mass approximation $w_{n-1}(\zeta) = \int_0^\zeta t^x q_{n-1}(t)\, dt$ with account for measuring instrument spectral sensitivity.

It is not difficult to construct the successive approximation algorithm for determination of the underlying surface radiation temperature $T_n(1)$. Taking as the zero approximation the mean distributions $T_0(\zeta) = \bar{T}(\zeta)$ and $q_0(\zeta) = \bar{q}(\zeta)$, we calculate $\Delta I_0 = \Delta I\left[\bar{T}(\zeta),\, \bar{q}(\zeta)\right]$ and then use (8.20) to determine $B_1 = \delta B\left[T_1(1)\right]$. From the calibration curve of radiation intensity versus tempera- ture (see, for example, Figure 8.2) we find the first approximation of the radiation temperature $T_r^{(1)}(1)$ or for a known quantity δ the temperature $T_1(1)$. The further procedure for optimum recon-struction of $T_1(\zeta)$ and $q_1(\zeta)$ on the basis of $T_r^{(1)}(1)$ and the correlation matrices B_{TT}, B_{qT}, B_{qq} as before (see section 3.2).

434

Using the resulting $T_1(\zeta)$ and $q_1(\zeta)$ we can calculate the
first approximation of the correction $\Delta I_1 = \Delta I\,[T_1(\zeta),\, q_1(\zeta)]$ and using
(8.20) we can find the second approximation $B_2 = \delta B\,[T_2(1)]$ and $T_2(1)$.
It is not difficult to show that the successive approximation
process converges. In fact, in (8.20) we can fix the denominator
$P_0 = P(\bar{w}, \bar{m})$. Then the behavior of the differences

$$\delta(B_n - B_{n-1}) = \frac{1}{P_0}[\Delta I_n - \Delta I_{n-1}] = \frac{1}{P_0}\left\{\frac{\partial \Delta I_n}{\partial T}[T_n(\zeta) - T_{n-1}(\zeta)] + \right.$$
$$\left. + \frac{\partial \Delta I_n}{\partial q}[q_n(\zeta) - q_{n-1}(\zeta)]\right\}$$

will be determined by the behavior of the differences $T_n - T_{n-1}$
and $q_n - q_{n-1}$. The difference $B_n - B_{n-1}$ may be arbitrarily small
if the successive approximation differences $|T_n(\zeta) - T_{n-1}(\zeta)|$
and $|q_n(\zeta) - q_{n-1}(\zeta)|$ are sufficiently small. This follows
from the fact that the derivatives (in the Frechet sense [7.8]) of
the functional ΔI with respect to T and q are bounded (see § 3 of
Chapter 7). If the optimum extrapolation method ensured approach
to the true $T(\zeta)$ and $q(\zeta)$ profiles and, in addition, the optical
parameters of the atmosphere and underlying surface used in the
calculations coincided with the real parameters the suggested
successive approximation method would converge to the true under-
lying surface temperature $T(1)$. However, becasue of the definite
optimum extrapolation error and the unknown error introduced
by the optical parameters used in the calculation the process
will converge to some temperature $\tilde{T}(1)$, generally speaking dif-
ferent from $T(1)$.

Expression (8.20) permits determining the overall $T(1)$
determination error, associated with the indicated errors and with
the radiation intensity measurement error σ_I

$$\sigma_T(1) = \frac{1}{\partial B/\partial T}\max_{\zeta}\left|\frac{\sigma_I - \left[\frac{\partial \Delta I}{\partial T}\sigma_T(\zeta) + \frac{\partial \Delta I}{\partial q}\sigma_q(\zeta)\right]}{P[\bar{w}(1),\,\bar{m}(1)]} + \frac{I - \Delta I}{P^2[\bar{w}(1),\,\bar{m}(1)]}\sigma_p\right|. \tag{8.21}$$

Thus the error σ_T (1) obtained as a result of optimum extrapolation is determined by the nature of the correlation relations B_{TT}, B_{Tq} and B_{qq}. As for the influence of errors associated with the existence of other absorbing substances which are not considered in the calculations, for this purpose we need empirical data on the possible calculated transmission function deviations from the true values (the same applies to accounting for the errors of natural surface radiance deviations from unity in determining T (1)). It is clear that the most significant errors will occur in the case when there is semitransparent cloud cover, which leads to strong uncontrollable variations of the transmission function. However, even in the visually cloudless atmosphere case we can assume the existence of marked aerosol absorption of IR radiation, since the aerosol is basically a water substance and, as is well known [2.13], the IR radiation absorption coefficients of liquid water are higher by several orders in comparison with the visible and near-IR spectral regions. Account for this factor is also important because of the fact that calculation of atmospheric radiation corrections depends considerably on successful selection of the transfer function zero approximation. Therefore determination of the real Earth's surface self-radiation attenuation in the atmosphere is the most important step at this stage in solving the subject problem. With the existing knowledge of IR radiation absorption /256 at different levels in the atmosphere, this question can be resolved at present on the basis of purely empirical relationships between the radiation measured aboard the satellite and the self-radiation of underlying surfaces whose radiance is quite well known. In other words, it is necessary to find the empirical transfer functions of the atmosphere using the existing data of self-radiation measurements in the transparency windows.

§ 4. Empirical Transfer Function

A large number of airplane, balloon, and satellite measurements have now been made of the Earth's self-radiation I, which permit determining the empirical transfer function

$$\mathscr{P}_e(\zeta) = \frac{I(\zeta)}{\delta B\left[T(1)\right]}$$

above underlying surfaces for which $\delta \approx 1$ and their temperature T (1) is close to that of the surface air layer. For those cases which we term cloudless $\mathscr{P}_e$ should be quite close to the theoretical transfer function (8.4), in which only water vapor, and when necessary ozone or carbon dioxide, absorption is taken into account.

Determination of $\mathscr{P}_e$ was carried out in [5.13, 5.16, 7] from I measurements aboard the Kosmos 149 satellite in the 8-12 μ window and aboard Kosmos 243 in the 10-12 μ window (the characteristics of the corresponding radiometers are presented in [5.13, 5.16, 7]). Comparison of the empirical and theoretical transfer functions determined for guaranteed cloudless oceanic cases is shown in Figure 8.6. The calculations of $\mathscr{P}_e$ were made using (8.1) and (8.4) with account for the temperature and humidity profiles obtained during aerological sounding aboard satellites close to the I measurement region and at quite close time intervals. Radiation absorption by atmospheric gases was taken into account using the optical characteristics presented in Chapter 2.

In the figure $\mathscr{P}_e$ and $\mathscr{P}_c$ are represented as functions of the near-water (or near-land) air layer temperature T_a, which can be measured at the weather station network more reliably in comparison with the other meteorological parameters on which the transfer function depends. Of interest, first, is the fact that $\mathscr{P}_e$ is markedly smaller than $\mathscr{P}_c$ and, second, that the two functions have opposite behavior, approaching one another at high temperatures T_a. We

437

emphasize that $\mathcal{P}_{e|}$ not only does not decrease with increase of T_a (and also, probably, with increase of the total water vapor mass w (l), with which T_a correlates strongly, particularly above the ocean) but, conversely, probably even increases slightly with T_a and w (l). Here the indicated behavior of the transfer function $\mathcal{P}_{e|}$ is independent, within the limits of empirical quantity scatter, of which transparency window was used in the experiments.

One explanation for the very significant differences (quantitative and qualitative) between $\mathcal{P}_{e|}$ and $\mathcal{P}_{c|}$ may be the previously mentioned IR radiation absorption by the water aerosol, which either is not taken into account at all in the calculations or is taken into account by effective increase of the coefficient of radiation absorption by water vapor (in the latter case it is actually assumed that the aerosol is distributed in altitude just as the water vapor is).

The presence of the water aerosol reduces the absolute magnitude of the transfer function. This reduction is particularly marked at low temperatures T_a, when the probability of moisture condensation increases. In connection with the quite high coefficient of temperature correlation at different levels in the troposphere and at altitudes of 20-30 km (see § 2 of Chapter 3), the aerosol concentration increase expected in this case may take place simultaneously in several layers of the atmosphere.

We further note that $\mathcal{P}_{e|}$ reduction is observed even wtih simultaneous reduction of the gaseous moisture, which should lead to increase of the transfer function.

Conversely, with temperature increase the aerosol concentration decreases, which leads to increase of $\mathcal{P}_{e|}$, again in spite of simultaneous increase of the gaseous moisture (correlating with the temperature), which should lead to reduction of the transfer
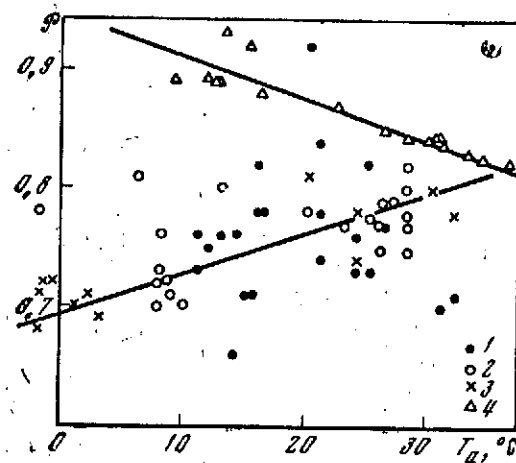
Figure 8.6. Empirical transfer functions $\mathscr{P}_e$ versus temperature of air layer near the water surface and water vapor mass

1, 2- from Kosmos 149 and Kosmos 243 measurements, respectively; 3- values of $\mathscr{P}_e$ above land; 4- transfer function calculation

function. In other words, the contribution of aerosol IR radiation absorption may be so large that it more than compensates for the opposite effect of radiation absorption by water vapor. Carlon [8, 9] came to analogous conclusions, showing that the mixture of water vapor and water aerosol which exists over a wide range of relative humidities can weaken markedly the radiation in the 8-12 μ window.

We consider this explanation only a hypothesis, which requires thorough verification using radiation measurement data which must obviously be obtained with quite high accuracy. An attempt was made to obtain such data in experiments aboard the Kosmos 149 and Kosmos 243 satellites with the aid of radiometers providing (judging by the results of laboratory studies) radiation temperature measurement accuracy of 1° for $T \approx 300°$ K. However, the absence of any sensitivity check of the entire measurement circuit on board the satellites did not completely guarantee constancy of the equipment characteristics during the time of flight. For the measurements obtained aboard the Kosmos 149 satellite, check of the radiometer sensitivity was accomplished by constructing the regression relation between the measured radiation temperature T_r and

the air temperature T_a near the water for the cloudless atmosphere (Figure 8.7). It was found that the instrument sensitivity increased with time [10]. This deficiency was eliminated in the radiometer installed aboard the Kosmos 243 satellite by checking the electronic circuit in flight [7], however no check was made of the entire optical system.

The results obtained in [7] from analysis of radiation temperature measurements in the 10-12 μ window showed that the average difference between the radiation temperature and the temperature of the air layer near the water above cloudless ocean, just as in the case of the 8-12 μ window, amounts to 15 ± 5° (Figure 8.7), although the scatter of the difference $T_a - T_r$ for the 10-12 μ interval was somewhat less than for the 8-12 μ interval (we note that the short-wave wing of the 10-12 μ filter, which had comparatively weak transmission in the 11 μ window, extended to the 9.6 μ ozone band [5.13]). Naturally, we cannot exclude the possibility that the large $T_a - T_r$ correction in the Kosmos 243 satellite /258 measurements is associated with uncontrolled systematic equipment error.
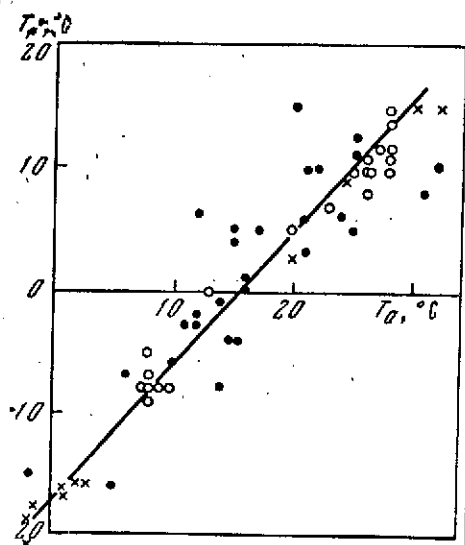
Figure 8.7. Regression relation between T_r and T_a from measurements in the 8-12 μ (Kosmos 149) and 10-12 μ (Kosmos 243) windows. Notations same as in Figure 8.6.
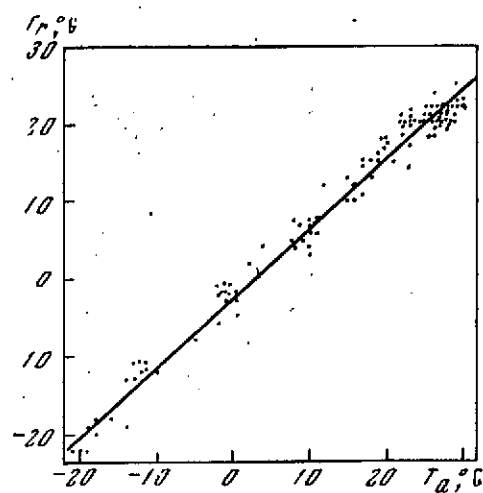
Figure 8.8. Regression relation between T_r and T_a from measurements in the 10.5 - 11.5 μ window (Kosmos 320)

440

More refined self-radiation measurements in the quite narrow 10.5 - 11.5 μ window were made aboard the Kosmos 320 satellite [5.13, 11]. The radiometer installed aboard this satellite was calibrated periodically in flight relative to a blackbody whose temperature was measured with high degree of precision. Moreover, the instrument null was checked at intervals in flight. Figure 8.8 shows that in this case the average correction $T_a - T_r$ was considerably smaller (3 ± 4°), which can be explained by the practically complete absence of absorption bands in the spectral sensitivity region of the radiometer used aboard the Kosmos 320 satellite.

Judging by the literature [6.40], a radiometer which was quite advanced from the sensitivity checking viewpoint was installed aboard the Nimbus 2 satellite to measure the Earth's radiation in five spectral intervals (including the 10-11 μ region). Unfortunately, in the report [12] on the results of radiation measurements aboard this satellite no data are presented for the 10-11 μ channel. Only in a single publication [13] with which we are acquainted, in which some results of measurements aboard the Nimbus 2 satellite are analyzed, are the radiation temperature pattern above the USA for the 10-11 μ channel and a cloud map given. From examination of these data we can conclude that the radiation temperatures do not exceed 290° K above coastal cloudless regions, although the water temperature in this period reached about 300° K here. Above cloudless land, however, T_r is estimated to be 300° K or more.

Thus, measurements of the Earth's self-radiation from satellites show that the actual transfer function of the atmosphere in the 8-12 μ window may depend significantly on aerosol absorption of the radiation. Since this question is of paramount importance for the problem of determining underlying surface temperature, corresponding airplane and balloon measurements of the radiation temperature were undertaken along with simultaneous measurements

of the vertical atmospheric temperature and humidity profiles
[5, 14-16]. Of greatest interest, naturally, are the airplane
measurements, since they permit tracing the vertical variation of
the transfer function, at least in the limits of the troposphere.
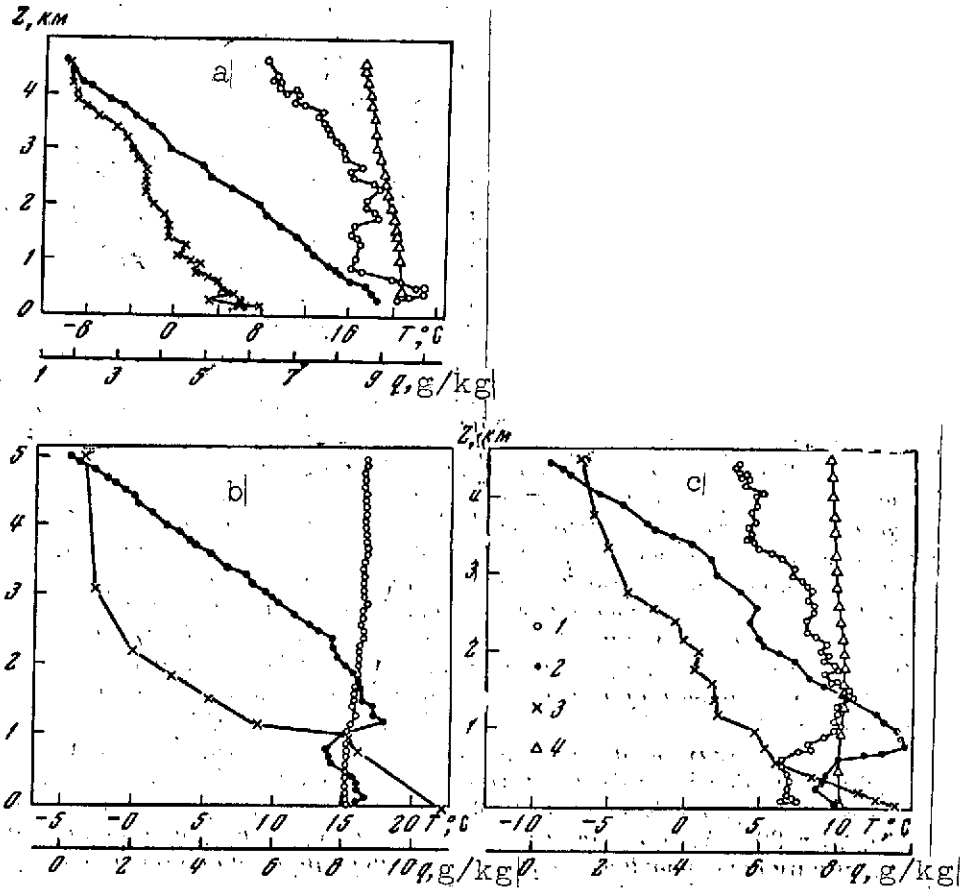
Figure 8.9. Vertical profiles of T from airplane measurements of
IR radiation in the 8-12 μ (a) and 10-12 μ (b, c) windows

1- T_r; 2- T_a; 3- q; 4- calculation of T_r from empirical T_a and q

The results of such vertical soundings made using an airplane
radiometer version [17] installed aboard the Kosmos 149 and Kosmos
243 satellites were obtained in [14]. Typical examples of the
vertical profiles of the measured and calculated radiation tempera-
tures for the 8-12 μ and 10-12 μ windows are shows in Figure 8.9
(in the calculations only radiation absorption by water vapor was
considered; the vertical water vapor concentration and air tempera-

442

ture profiles are shown in the figure). The figure and Table 8.4 show, first, significant difference between the empirical and theoretical transfer functions and, as we would expect, $\mathscr{P}_e < \mathscr{P}_c$, which indicates the presence of absorbing substances which are not considered in the calculations. Second, it was found in [15] that for the 10-12 μ window transformation of underlying surface radiation in the atmosphere is practically absent, and the transfer function even increases slightly and exceeds unity because of the small temperature inversion.

The seeming contradiction between the airplane measurements and the T_r measurements presented above made aboard the Kosmos 149 and Kosmos 243 satellites is a consequence of the fact that these data are not comparable if, naturally, we do not assume that the overlying atmosphere does not absorb IR radiation. On the other hand, thanks to the large variations of the temperature, humidity, and aerosol concentration profiles in the lower troposphere it is not impossible that during the measurements [15] in the atmosphere there existed distributions of these parameters which compensated for absorption of underlying surface radiation and lower-lying atmospheric layer radiation by the radiation of these same layers. The T_a and q (ζ) profiles shown in Figure 8.9 b, c correspond to the following conditions: inversion and weak decrease of the temperature in the 0-1 km layer, and also the quite deep inversion in the 1-1.5 km layer is accompanied by marked decrease of the moisture above these layers. It appears that the main mass of troposphere absorbing substances is concentrated in this boundary layer. Then the previously mentioned compensation will take place here with practically constant temperature T_a. Judging by the humidity variation, the atmosphere above the boundary layer is quite transparent and has practically no effect on the outgoing radiation.

TABLE 8.4. COMPARISON OF EXPERIMENTAL AND CALCULATED
TRANSFER FUNCTIONS FROM AIRPLANE MEASUREMENT DATA [14]**

Flight No.	Altitude, km	$T_r (0,95) - T_r (t)$	$\mathscr{P}_e$	$\mathscr{P}_c$
1	3	4	0,915	1,00
2	4,5	3,5	0,927	0,983
3	4,5	9	0,832	0,976
4	4,5	9	0,837	0,942
5	4,5	12	0,792	0,959

* 1-4- above Caspian Sea; 5- above desert
** Translator's note: Commas in numbers represent decimal points.

We note that similar situations were observed during airplane
measurements of the radiation spectrum in the 8.5-16 µ region
obtained in [16] above the Mojave Desert (California). Examples
of these spectra, measured on 10 May 1967 at three altitudes
(0.7-0.9, 3.2, and 10 km) above certain underlying surface types,
are presented in Figure 8.10 (instrument spectral resolution
$\lambda/\Delta\lambda$ = 50, viewing angle 2 x 2°). At the same time the surface
radiance and the aerosol concentration profiles were measured at
these altitudes.

The results obtained in [16] show that conditions existed in
the atmosphere for which the radiation temperature of the underlying
surface and of the atmospheric boundary layer in the 10-12 µ
window was either practically not transformed up to the 3-km level
(Figure 8.10 a) or decreased by 10° (Figure 8.10 b). However, the
conclusion from [16] which is most important for the subject
problem is that in all cases the radiation temperature T_{rs}
decreased by 10-20° at the 10-km level. Unfortunately the authors
of [16] do not present the corresponding temperature, humidity,
and aerosol concentration distributions. It is simply noted that the
opacity of the atmosphere above the dry lakes (Figure 8.10 a) was

greater than above the lava and desert (Figure 8.10 b). This is
probably associated with the aerosol particle nature. The aerosol
will be dry above the desert, while above the dry lake salt particles
may be carried into the atmosphere and because of the hygroscopicity
of these particles the aerosol will actually be a water aerosol
(we emphasize that similar but still more highly concentrated
aerosol layers may develop above the ocean in the form of water
solutions of salts).

On the basis of this discussion we can assume that the aerosol
layers located in the troposphere and stratosphere in the minimum
temperature regions (10, 20, and 80 km) make a considerable con-
tribution to self-radiation attentuation. As a result of this the /261
attenuation of the Earth's surface and low-lying atmosphere radiation
is not compensated by the comparatively weak radiation of these
layers, as is the case for comparatively smooth aerosol and tem-
perature distributions in the lower troposphere. Measurements of
the vertical solar radiation spectrum distribution up to high
altitudes are necessary for a more categorical statement. We note
that airplane measurements of the spectra to 12 km, similar to
those made in [18], do not give a reliable answer to this question,
since these measurements were made for large air masses.
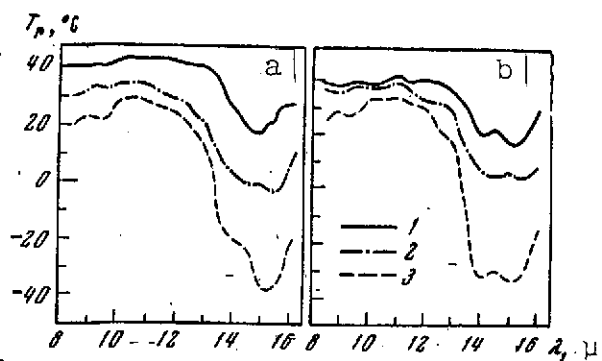
Figure 8.10. IR radiation spectra
 obtained during airplane sounding
 of the atmosphere [16] at levels
 0.7-0.9 km (1), 3.2 km (2),
 and 10 km (3)

a- above dry lake; b- above lava
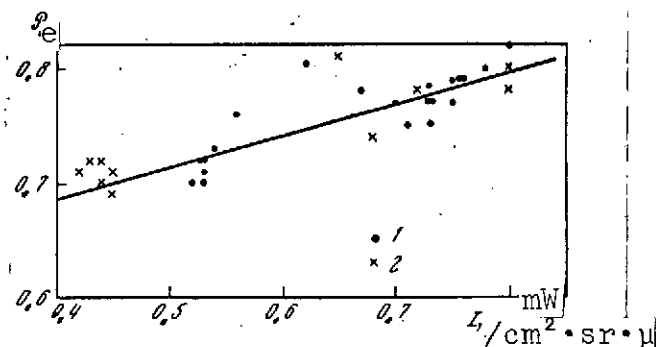
Figure 8.11. Dependence of
 empirical transfer function
 on radiation intensity mea-
 sured aboard Kosmos 243 satel-
 lite above ocean (1) and
 land (2)
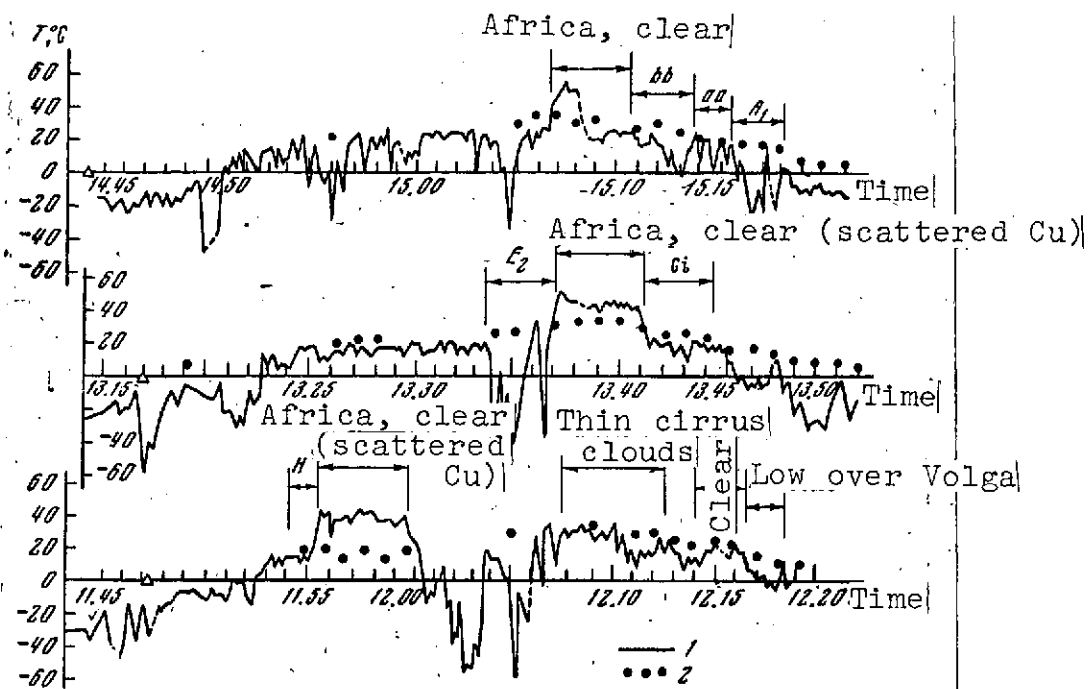
Figure 8.12. Comparison of T_{rs} from measurements aboard Kosmos 243 satellite (1) with T_a (2)
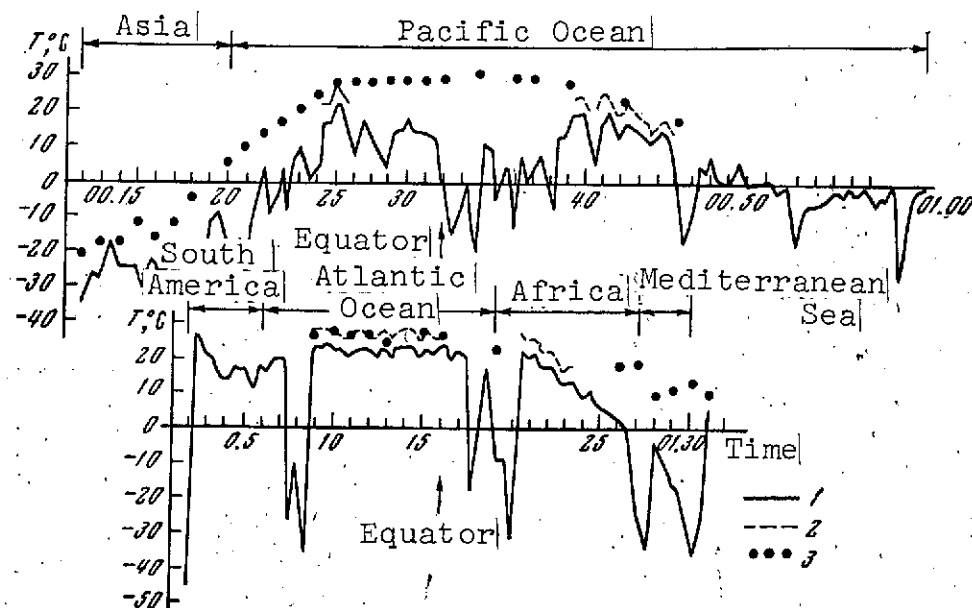
Figure 8.13. Comparison of T_r (1), T_{rs} (2), T_a (3) from measurements aboard Kosmos 320 satellite

On the basis of the results obtained above, we can suggest the following method for taking into account transformation of underlying surface IR radiation in the cloudless atmosphere. As the first approximation of the transfer function for use in (8.22) it is necessary to take the function $\mathscr{P}_{e|}$, shown in Figure 8.11 as a function of the radiation intensity I measured by the given radiometer above typical underlying surfaces. The transfer function variations associated with T (ζ) and q (ζ) variations, which are necessary for further refinement of the underlying surface temperature, can be taken into account by the optimum extrapolation method with use of the statistical characteristics of the vertical structure of T (ζ) and q (ζ), as was described in § 3.

Determination of the underlying surface temperature T_s with the aid of the empirical transfer function was carried out in [5.13] using radiation measurements aboard the Kosmos 149, Kosmos 243, and Kosmos 320 satellites. The comparison of T_{rs} and T_a presented in Figure 8.12 shows that on the basis of the Kosmos 243 data we can speak of T_{rs} reconstruction with an error of 3-4° only above cloudless ocean. It is important to note that the author of [5.13] had the possibility of comparing the radiometric data and the global cloud cover distribution obtained from Earth photographs taken from Zond 5 [5.26].

These comparisons permitted, specifically, supplementing the synoptic cloud cover analysis with a quantitative characteristic (cloud top temperature) and also noting a case of marked attenuation of the ocean IR radiation by substances which could not be detected in the photographs. In Figure 8.12 we see clearly regions where the radiation temperature is higher than the surface air temperature in Africa (by up to 10-15°), associated with significant superheating of the land under daytime cloudless conditions. /263

The possibilities of reliable underlying surface temperature determination are illustrated in Figure 8.13 by Kosmos 320 satellite radiometric data. The comparatively small error (1-2°) of T_{rs} determination above the ocean gives a basis to recommend the radiation measurement technique used aboard the Kosmos 320 satellite for use in operational practice. Considering that the predominant mass of the radiometric information relates to cloudy conditions, we should concentrate our main attention on cloud cover radiation measurement interpretation.

§ 5. Cloud Temperature Determination

In examining the problem of determining underlying surface temperature in the cloudy case, three situations are clearly identified in which the technique for solving this problem is entirely different: 1) the case of optically dense, continuous, and single-layer cloud cover; 2) the case of continuous semitransparent cloud cover above homogeneous underlying surface; 3) the case of discontinuous multilayer cloud cover, when radiation of objects with different temperature falls in the instrument viewing field.

In connection with the strong IR radiation absorption by liquid droplet moisture, in the case of continuous and sufficiently dense cloud cover we can ignore the radiation of the atmosphere layer below the clouds and of the lower cloud layers and examine, at least in the first approximation, the cloud cover top as the radiating surface. In this case the interpretation can be accomplished by the method described above and the corrections for cloud top radiation transformation in the overlying atmosphere layer, in which the water vapor and near-surface aerosol concentrations decrease markedly, will be significantly smaller in comparison with the cloudless case. The transformation will take place primarily in in the upper aerosol layers, however as a result of the low cloud top temperatures this effect will be quite weak.

The central question for this situation is account for cloud radiance. The reason is that the overlying atmosphere layer IR radiation incident on the cloud is partly back-scattered. Moreover, part of the IR radiation which is generated within the cloud layer reaches the cloud top. As a result the cloud top radiation differs from blackbody radiation at the cloud top temperature. Calculations show (see, for example, I. 7) that cloud radiance in the 8-12 μ window may differ from unity by 15-20% (i.e., the albedo A = 1 - δ may reach 0.2), and according to the data of I.7 this quantity is independent of cloud water content and thickness. Radiance calculations made for λ = 10 μ in [2.53] show that cloud albedo varies from 1 to 10% as a function of droplet concentration, optical thickness, and ratio of the cloud and atmospheric layer temperatures. An albdeo value of 10% was obtained in [19] for lower clouds from airplane measurements of the cloud cover radiation spectrum I_ν. However, we must bear in mind that to determine cloud albedo from I_ν measurements it is necessary to measure at the same time the cloud "top" temperature, and this concept is somewhat arbitrary even in the case of stratus clouds. Under actual conditions the cloud cover top is diffuse and may vary considerably in altitude (up to 200 m in stratus clouds), and along with this there will be temperature variation, particularly since an inversion layer is usually located near the cloud tops. Analysis of airplane measurements of the temperature profile in stratus clouds [3.16] shows that the inversion layer constitutes on the average /264 200-300 m and the temperature may increase by 5-10° in this layer. The radiance determination error due to the indefinite nature of the cloud top level to which the temperature measured aboard the airplane should be assigned will lie in the range of the assumed radiance variations (δ = 0.8-1 with average value 0.9). Therefore we can recommend the value δ = 0.9 as the first approximation in determining cloud top temperature from cloud-top self-radiation measurements.
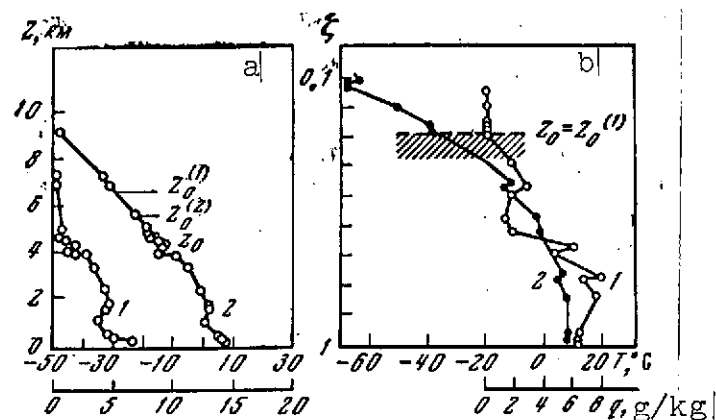
Figure 8.14. Determination of cloud top height from self-radiation measurements aboard Kosmos 149 (a) and Kosmos 243 (b) satellites in the 8-12 μ and 10-12 μ windows. Initial altitude is determined from aerological sections — humidity (1) and temperature (2)

Examples of cloud top temperature determination from radiation measurements aboard the Kosmos 149 [5.16] and Kosmos 243 satellites are shown in Figure 8.14. The true temperature was estimated from the aerological data with use of singular points in the form of temperature inversions and marked humidity decrease. We see from the figure that it is possible to determine solid cloud-cover top temperature to within 3-5°. From this temperature we can determine the cloud top height z_0, using the T (ζ) profile if it is known (in the figure the height is determined with an error of about ~ 1 km).

If the T (ζ) profile in the measurement region is not known, we can use the climatic average profiles $\bar{T}$ (z) for approximate determination of cloud top height $z_0^{(1)}$

$$\bar{T}\,[\zeta\,(z_0')] = T_r.$$

(8.22)

Determination of solid cloud-cover top temperature and height is the most important problem of optical sounding in the IR spectral region windows from satellites, since this is practically the only way to obtain information on these parameters on a global scale.

We note that cloud top height may be determined independently, for example, with the aid of simultaneous measurements of reflected solar radiation in the oxygen band, as was done aboard the Kosmos 320 satellite (see Chapter 9).

In the semitransparent cloud case we cannot determine reliably either underlying surface temperature or cloud cover temperature. The reason is that even small variations in cloud optical thickness lead to marked attenuation of the Earth's surface radiation. On the other hand, these clouds radiate very little, since as a rule they are located at high altitudes and have low temperatures. As a result cirrus cloud radiance from the data of [12] varies in the range from 0.05 to 0.95. Therefore the radiation recorded by a radiometer in the "windows" is strongly variable in space. Account for such large variations under actual conditions can not yet be accomplished. The same applies to the case of an optically dense but discontinuous or multilayer cloud cover, for which the measuring instrument as result of its finite aperture may sum the radiation /265 of the underlying surface and clouds with undetermined weights.

From this statement follows, specifically, the inadequacy of the method proposed by Smith (6.4, 6.5) for determining the temperature profile from the Earth's radiation in the CO_2 band under conditions of broken or semitransparent cloud cover (see § 5 of [7]), since the method requires determination of cloud top temperature from radiation measurements in the atmospheric windows.

The way out of these difficulties must be sought in use of a priori information on the vertical and spatial structure of the cloud cover, temperature, and humidity, which can be used as the first approximation in interpreting measurements under discontinuous cloud cover conditions.

CHAPTER 9
CLOUD TOP HEIGHT DETERMINATION .

As indicated above, measurements of solar radiation reflected
by the Earth and self-radiation of the planet can be used to inves-
tigate the vertical structure of cloud fields. One of the important
characteristics of cloud cover boundary structure is cloud top
height. In Chapter 8 we examined the possibilities of obtaining
information on this parameter on the basis of cloud self-radiation
measurements in the 8-12 μ atmospheric window or in narrower
spectral intervals of the window. These measurements make it possible
to determine cloud top height on both the illuminated and unillumi-
nated (by the sun) sides of the Earth. However, their use involves
the need for data on the vertical temperature profiles in the
measurement region.

On the illuminated side of the Earth we can use other methods
for determining cloud top height, based on measurements of the
reflected solar radiation in various parts of the spectrum, including
the absorption bands of atmospheric gases whose concentration varies
weakly in time and space (such gases are, for example, oxygen and
carbon dioxide).

The method amounts to the following. If we measure the intensity
I_1 of the solar radiation reflected from a cloud for given sun
position ζ_0 and viewing direction θ in the absorption band and the
intensity I_2 in a neighboring spectral interval outside the band,
then the ratio

$$P[u(h), m] = \frac{I_1}{I_2}$$
(9.1)

depends on the absorbing substance mass u in the atmospheric column between the cloud and observer, and also on the air mass $m = \sec \zeta_0 + \sec \theta$ along the incident and reflected ray path. Since the absorbing substance concentration is constant, the mass u will be a function of the reflecting surface boundary height h.

Hanel [1] suggested using reflected solar radiation measurements in the 2 μ CO_2 absorption band for determining cloud height. However this band overlaps the 1.87 μ water vapor absorption band, which makes interpretation of the measurements much more difficult and may introduce uncontrollable errors in cloud height determination.

Yamamoto and Wark [2], and also independently Chapman [3] and Rozenberg (see [2.37]), proposed using measurements of reflected solar radiation in the 0.76 μ (A) molecular oxygen absorption band for determining cloud height. This spectral region has several advantages in comparison with the 2 μ CO_2 band region: 1) the 0.76 μ O_2 band does not overlap the water vapor bands and alongside it there is located the 0.74 μ spectral comparison interval, within which there are segments of very weak liquid water absorption; 2) the solar energy magnitudes in this spectral region are much higher than the corresponding quantities in the 2 μ region; 3) for this spectral region there are high-sensitivity stable radiation receivers (PEA) [Photoelectric Amplifier] which permit /267 making measurements with high spectral resolution.

However there are several difficulties which complicate the solution of the posed problem under actual conditions even if the required initial quantities (I_1 and I_2) are measured with sufficient accuracy. These difficulties are associated with the quite complex process of solar radiation transformation in the atmosphere and in clouds. In fact, reflected solar radiation is a superpositioning of several components and these components have a different

nature for the absorption band and for the comparison interval, even if we take the radiation scattering coefficient and indicatrix to be the same in these segments of the spectrum. The solar radiation reaching the cloud in the absorption band region will be practically completely absorbed in the central parts of the lines (some fraction of this radiation will be back-scattered by the atmosphere layer lying above the cloud). Radiation corresponding to the line wings, somewhat attenuated as a result of absorption and back-scattering, reaches the cloud. Moreover, on the cloud there falls the radiation which has been multiply scattered by the overlying atmospheric layer and also that radiation which was reflected from the cloud and has again been scattered by the atmosphere to the cloud. As all this radiation penetrates into the cloud it will be scattered by water droplets or ice particles and absorbed along the scattering path by oxygen and liquid water.

The solar radiation reflected by the cloud into outer space is absorbed and scattered by the atmospheric layer above the cloud as it travels to the upper edge of the atmosphere. This radiation together with the part of the radiation scattered by the atmospheric layer above the cloud will be measured aboard the satellite. To this we must add also that part of the solar radiation which passes through the cloud to the Earth's surface, is reflected from the latter, and again returns to the upper edge of the atmosphere (in the case of strong reflection from the Earth's surface this part may be significant). Thus the ratio (9.1), measured at the upper edge of the atmosphere, depends not only on the oxygen mass in the air column but also on the mass of oxygen and liquid water along the photon trajectory in the cloud, which in turn depends on cloud cover microstructure and thickness*.

---

* The ratio (9.1) may depend also on the cloud layer temperature, since the liquid water absorption band center and coefficient depend on this temperature.

The layer above the clouds or multilayer cloud cover may make a definite contribution.

It is quite clear that a definite complex of radiation measurements and also the use of additional information on cloud cover properties are necessary in order to take into account some of these factors in each specific case. In the following we shall examine one version of such a measurement complex carried out aboard the Kosmos 320 satellite.

In accordance with the described process of reflected solar radiation field formation, the problem of determining cloud top height from measurements in the O_2 0.76 µ band can be broken down into the following basic parts:

1. Determination of the atmospheric transmission function for different sun and observer positions with the aid of calculations based on the absorption band fine structure parameters (line position, intensity, halfwidth, and form) and measurements under actual conditions which are suitable for the computation conditions. These data are required to establish the relationship between atmospheric transmittance and the oxygen mass along the ray path (or the pressure at the reflecting surface level).

2. Development of a technique for taking into account the additional absorption of solar radiation by the oxygen and water along the photon trajectory during their scattering in the cloud layer. Since the geometric, optical, and microstructural charac-   /268 teristics of the clouds under the specific measurement conditions are not known, the methods of introducing to the ratio (9.1) the corrections associated with the additional absorption will be statistically optimal.

3. Estimation of the h determination errors due to solar radiation scattering in the atmospheric layers above and below the clouds, which are associated primarily with variations of the aerosol component.

These three problems do not by any means exhaust the entire complex of particular problems of the overall task of determining cloud height in the real atmosphere, for example, such as account for multilayerness and nonhomogeneity of the cloud cover. However, these three problems are basic and development of methods for solving them constitutes the subject matter of the present chapter.

§ 2. Parameters of Oxygen A Band Structure

The molecular oxygen absorption band centered at 7620 $\overset{\text{o}}{\text{A}}$ has been used very little to date in problems of atmospheric physics, primarily because of its small role in solar radiation absorption in comparison with the water vapor bands. However, the fine structure of this band has been studied quite carefully in connection with problems of spectroscopy and astrophysics. A detailed presentation of band structure study results was provided in [4, 5], but the contradictory nature of these results led to the recent appearance of new studies [6-9] in which attempts were made to obtain refined molecular parameters of the A band on the basis of more complete measurements of its spectra. The data obtained in [6-9] make it possible to establish the most reliable magnitudes of the parameters, which are used in the following for calculations of the atmosphere transmission functions in the A band.

The 0.7620 μ molecular oxygen band consists of the R branch, located in the interval 7593-7616 $\overset{\text{o}}{\text{A}}$, and the P branch in the 7620-7700 $\overset{\text{o}}{\text{A}}$ wavelength region. Each branch consists of line pairs P_P, P_Q, P_R, R_Q of different intensity and with different relative

positioning. The exact line position values v_{0i} obtained in [10] are shown in Table 9.1.

The following procedure is used in [5-8] with some variations for determining the individual line intensity

$$S_i = \int_0^\infty k_i(v)\,dv \qquad (9.2)$$

From absorption spectra measurements for different pressures of pure oxygen or mixtures of oxygen and nitrogen the total band intensity is determined

$$S = \int_0^\infty k(v)\,dv, \qquad (9.3)$$

which, following [6], we characterize by the oscillator force magnitude

$$f_0 = \frac{m_e c^2 T}{\pi e^2 T_0}\,\frac{S}{c_0 N_L u}, \qquad (9.4)$$

where m_e, e^2 are the electron mass and charge; c is the speed of light; c_0 is the oxygen concentration; u is the equivalent absorbing layer thickness at standard pressure and temperature T_0; N_L is the Losschmidt number; T is the temperature of the medium.

The relative contribution of each line to the overall intensity is described by the relation

$$S_J = S F(J) Q^{-1}(T) \exp\left(-\frac{hcE''}{kT}\right), \qquad (9.5)$$

where h and k are the Planck and Boltzmann constants; E" is the lower energetic level; $Q(T) = \sum_J F(J) \exp(-hcE''/kT)$; F(J) is a weighing function which depends on the line rotational quantum number J.

TABLE 9.1.   CENTER LOCATION, INTENSITY S_J, AND HALFWIDTH γ_0
(S_J IN $10^5 \cdot cm^{-2} \cdot atm^{-1}$) FROM DATA OF [6-8]*/

ν_{0i}, cm^{-1}	λ_{0i}, Å	S_J [6]	S_J [7]	S_J [8]	γ [7], $cm^{-1}atm^{-1}$	γ [8], $cm^{-1}atm^{-1}$
13118,04	7620,29	8,52	8,05	6,47	0,079	0,050
13114,09	7623,29	10,9	9,50	9,94	0,074	0,092
13112,01	7624,50	15,7	15,1	13,1	0,069	0,050
13107,62	7627,05	16,5	15,1	13,0	0,066	0,048
13105,60	7628,22	20,7	19,8	16,8	0,064	0,049
13100,81	7631,02	19,5	18,1	15,3	0,062	0,048
13098,84	7632,16	22,9	22,1	18,4	0,061	0,048
13093,64	7635,19	19,3	18,7	15,8	0,060	0,047
13091,70	7636,33	22,5	21,8	18,3	0,060	0,046
13086,11	7639,59	18,1	17,2	14,4	0,060	0,046
13084,19	7640,11	20,0	19,5	16,3	0,059	0,048
13078,22	7644,20	15,0	14,5	12,4	0,059	0,045
13076,32	7645,31	16,3	16,1	13,8	0,058	0,046
13069,95	7649,03	11,5	11,2	9,63	0,057	0,042
13068,07	7650,13	12,1	12,2	10,8	0,055	0,044
13061,31	7654,09	8,10	8,05	7,15	0,054	0,043
13059,45	7655,18	8,65	8,77	7,67	0,052	0,042
13052,31	7659,37	5,40	5,46	4,91	0,051	0,039
13050,47	7660,45	5,67	5,75	4,98	0,050	0,040
13042,93	7664,88	3,30	3,45	3,15	0,049	—
13041,11	7665,95	3,50	3,60	3,44	0,048	—
13033,19	7670,61	1,90	1,97	2,08	0,047	—
13031,38	7671,67	2,00	2,08	2,17	—	0,045
13023,07	7676,57	1,03	1,09	—	—	0,044
13021,28	7677,62	1,07	1,15	—	—	0,043
13012,58	7682,76	0,52	0,56	0,42	—	—
13010,81	7683,80	0,37	0,59	0,43	—	—
13162,49	7595,26	3,54	3,73	—	—	—
13161,61	7595,76	1,92	2,00	—	—	—
13160,80	7596,23	5,80	6,03	—	—	—
13160,34	7596,50	3,30	4,02	—	—	—
13158,73	7597,42	8,85	9,05	—	—	—
13158,67	7597,46	5,40	5,05	—	—	—
13156,61	7598,65	8,15	8,2	—	—	—
13156,27	7598,85	12,7	12,8	—	—	—
13154,17	7600,06	11,6	11,5	—	—	—
13153,42	7600,49	16,8	16,8	—	—	—
13151,34	7601,70	15,1	14,9	12,0	—	—
13150,19	7602,36	20,6	20,7	16,5	—	—
13148,13	7603,55	18,3	17,8	14,6	—	—
13146,57	7604,45	23,3	22,0	18,6	—	—
13144,53	7605,63	20,2	19,7	16,1	—	—
13142,57	7606,76	23,9	23,7	18,6	—	—
13140,56	7607,93	20,0	19,2	16,1	—	—
13138,19	7609,30	21,8	21,7	17,1	—	—
13136,20	7610,45	17,2	16,5	13,8	—	—
13133,43	7612,06	16,8	17,1	13,4	—	—
13131,48	7613,19	11,8	11,2	9,54	—	—
13128,26	7615,06	9,53	10,2	8,18	—	—
13126,38	7616,15	4,20	4,03	3,47	—	—

* Translator's note: Commas in numbers represent decimal points.

We see from (9.5) that in order to determine the absolute line
intensities for known value of S (or f_0) it is necessary to find
the function F (J). The latter is determined in [6-8] from
absorption spectra measurements with quite high resolution:
0.15 - 0.3 cm^{-1} in [6], 0.6 - 1.2 cm^{-1} in [7] and 0.053 cm^{-1} in
[8]. The function F (J) was also calculated previously by Shlapp
[11] on the basis of quantum theory and obtained experimentally by
Childs and Mecke in [12]. The comparisons of the relative (or
normed in various ways) S_J distributions made in each of the studies
[6-8] show satisfactory agreement with the distributions of [11]
and [12]*. However the absolute values of S_J, which practically
coincide in the studies [6, 7], differ by 15-20% from the S_J values
obtained in [8] (see Table 9.1), although the oscillator force
magnitudes were similar in these studies.

To explain the possible reasons for these discrepancies it is
necessary to examine the methods and results of line halfwidth
determination γ_0 at standard pressure, obtained in [6-7] from the
same high-vacuum spectra. The method used to determine γ_0 in [7-8]
was based on using the known expression for the integral absorption
(or equivalent width) of an isolated line with Lorentz contour

$$w = \int_0^\infty A(v)\,dv = 2\pi\gamma x e^{-x}[I_0(ix) - iI_1(ix)],$$
(9.6)

where

$$x = \frac{Su}{2\pi\gamma} \qquad \left(\gamma = \gamma_0\frac{p}{p_0}\right),$$
(9.7)

---

* The relatively large discrepancy between the S_J values measured
in [7] and those calculated from the Shlapp data is explained by
the author of [8] by the use in [7] of the original Shlapp calcu-
lations, which were later refined in [11].

and I_0, I_1 are Bessel functions of imaginary argument. For small x (weak lines or small u) w is independent of γ; for $x \gg 1$

$$w = 2(\gamma S u)^{1/2}. \quad |$$

(9.8)

Thus, if the S_J are known and w are measured for sufficiently large x the expressions (9.6) and (9.7) permit determining the line half-widths. However, we should note that the γ values obtained by this method will include errors associated with the following factors: influence of the spectral instrument apparatus function, overlap of neighboring lines for large x, assumption on the dispersion contour of the line wings, which yield the primary absorption contribution for large x. It is probable that the various methods for taking these errors into account explain the comparatively large discrepancies between the γ_0 values obtained in [7, 8] when using the described procedure (see Table 9.1). In turn, these values differ from the γ_0 values obtained in [6] by extrapolation of the experimental relations γ (p) to small p.

The large differences in the S_J and γ_0 values make it difficult to select the most reliable band parameters for use in calculations of the transmittances P_v, particularly since the examples presented in [5-7] of comparison of P_v measured and calculated from the corresponding S_J and γ_0 show quite satisfactory agreement in all cases. Therefore we must first of all analyze the reasons for this P_v agreement in [5-8] for such different initial parameters, <u>/271</u> examining for this purpose the most significant characteristics of the technique of each of these studies.

In [5] the oscillator force and S_J distribution were determined on the basis of sea-level solar spectra measurements in the A band, which complicated the problem somewhat because of nonhomogeneity of the atmosphere and variation of its temperature with altitude, and also because of the possibility of additional solar radiation

attenuation by other absorbing substances present in the atmosphere
(the latter factor may play a strong role, since in [5] the
measurements were made for very low sun positions, requiring account
for layer curvature and ray refraction). The expression obtained
in [5] for determining the total band intensity S included in
explicit form the line halfwidth γ_0, which the authors of [5],
referring to several previous studies, took equal to 0.048 cm^{-1}.
However the value of S calculated in this case, corresponding to
the oscillator force $f_0 = 2.4 \cdot 10^{-10}$, was increased by the authors
of [5] to the value $f_0 = 3.2 \cdot 10^{-10}$ in order to provide best agree-
ment of the measured and calculated transmittance (the degree of
closeness of the P_ν curves is illustrated in Figure 9.1 a).

The S_J distribution is not presented in [5]. However,
judging by the value of f_0 and the weighting function F (J) used
in the calculations (based on [11] and [12]) the line intensities
must have been high by 20-30% in comparison with the analogous
parameters in [6-8] (see Table 9.1). Considering that the deter-
mination of these parameters in [5] was based on absorption spectra
measurements in an unadequately controlled medium, and also taking
into consideration the arbitrariness of γ_0 selection and absence
of estimates of the influence of the line dispersion contour wings,
the parameters S_J and γ_0 proposed in [5] cannot be recommended
for reliable calculations of the tranmittances P_ν under different
atmospheric conditions or sun and observer positions. More
reliable from a methodological viewpoint are the spectra measure-
ments in a homogeneous controlled medium made in [6-8]. These
measurements permitted determining S_J and γ_0 from a closed system
of experimental data and computational formulas, and also permitted
evaluation of the influence of line form.

Because of the relatively low resolution in [7] the spectral
measurements were made in the range of pure O_2 (or $O_2 + N_2$ mixture)
pressures from 7 to 13.6 atm, for which the total intensity was
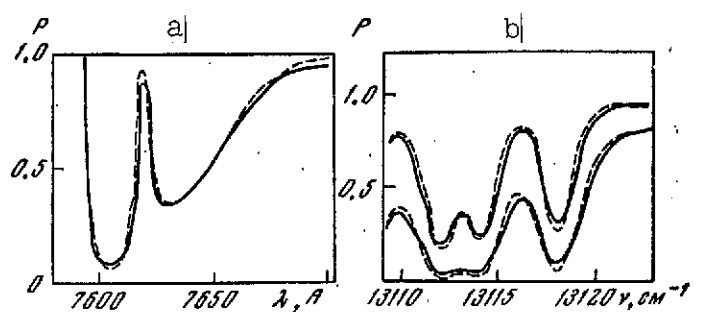
Figure 9.1. Comparison of measured (solid curves) and calculated (dashed) transmittances in the 0.76 μ O_2 band

a- at sea level for m = 2 [5]; b- using pure oxygen with
 ζ = 2 atm, u = 311 g/cm² [7]

independent of pressure and the line halfwidth was comparable with the spectral instrument slot width. The line overlap obtained in this case required, according to the authors of [7], the introduction of small corrections. In any case the total band intensity determined in [7] was close to the analogous values of [6, 8] (f_0 = 2.4·10^{-10}) and the individual line intensities practically coincided with the S_J of [6] (see Table 9.1). As for the line halfwidths, they were quite large in comparison with the analogous values of other studies (for pure O_2 the average value γ_0 = 0.060 cm^{-1}) and according to the authors of [7] this value should be increased by 5% for the O_2 + N_2 mixture. Moreover, in [7] a conclusion was drawn on the weak influence of line wing deviations /272 from the dispersion contour on the transmittance in the O_2 band under atmospheric conditions.

Using the parameters obtained, the authors of [7] calculated the transmittances P_ν for the same conditions for which the initial spectra measurements were made. Figure 9.1 b shows that just as in [5] the measured and computed P_ν agree quite well with one another (the authors of [7] associate the small discrepancies with differences between the actual apparatus functions and those used in the calculations). However the average γ_0 value exceeds that

used in [5] by 25%, i.e., by approximately the magnitude of the oscillator strength increase in [5]. This gave a basis for the authors of [7] to state that the increase of f_0 and S_J in [5] is a sort of compensation for the low value of $\gamma_0 = 0.048$ cm^{-1}, since for the measurement conditions in [5] the absorption function is proportional to the product $(\gamma S_J)^{1/2}$. It is probable that this is the reason why the transmittances calculated in [5, 7] for markedly different S_J and γ_0 were close to the measured P_ν. Analysis of the [7] results is difficult because of confusion in the methods for introducing the estimates of the errors associated with line overlap, apparatus function exclusion, and line wing influence. Moreover, these factors may become a source of seriuos errors, particularly in γ_0 calculations. This confirmed to some degree by comparison of the parameters obtained in [7] with the results of [6, 8], based on more complete experiments and an adequately closed interpretation technique.

In [8] the same relations were used for determining S_J and γ_0 as in [7], however in this case the corrections for line wing shape (using the Benedict formula [13]) and the apparatus function were taken into consideration. Thanks to the high spectral resolution in [8] the apparatus function correction was estimated as a few percent. The absolute S_J values, obtained both directly from individual line spectra measurements and from the band intensity ($f_0 = 2.3 \cdot 10^{-10}$) with a priori given distribution of the type [11], were identical within the measurement error limits. We see from Table 9.1 that the S_J values were lower by 15-20% than the analogous values obtained in [6, 7]. In [8] the line halfwidths were determined directly from the line profile measurement with elimination of the apparatus function and with account for the Doppler halfwidth ($\gamma_D = 0.014$ cm^{-1} atm^{-1}), which is significant at low pressures. The authors of [8] indicate that the γ_0 differences for pure oxygen and air are within the measurement error limits.

This conclusion contradicts the results of [6], in which S_J and γ_0 were also determined from absorption spectra measurements in the A band with resolution 0.2 - 0.3 cm^{-1} in pure oxygen and in mixtures with nitrogen at pressures from 1 to 20 atm. The relative intensities S_J measured directly and calculated in [6] from the oscillator strength and the F (J) distribution of [11] were close to one another and to the distribution of [12]. We see from Table 9.1 that the absolute S_J values are about 15-20% higher than S_J values from [8] but close to the values of [7]. As for the line halfwidths, which in contrast with [7, 8] were determined not with the aid of (9.6) and (9.7) but rather by extrapolation of the experimental γ (p) relations to small p, the smallest γ_0 values of all the studies examined (mean $\gamma_0 \approx 0.042$ cm^{-1} atm^{-1} for pure O_2 and 0.038 cm^{-1} atm^{-1} for air with mean-square error of order $\pm$ 0.03 cm^{-1} atm $^{-1}$ and tendency toward decrease with increase of J, which agrees well with the data of [7, 8]) were obtained in [6]. When using the parameters S_J and γ_0 to calculate the transmittances, the authors of [6] came to the conclusion that it is necessary to alter the line contour wing form, specifying the latter by the formula

$$k_q(\nu) = k_{max} \left[\left(\frac{\nu - \nu_0}{\gamma_0 (p/p_0)} \right)^q + 1 \right]^{-1}.$$

(9.9)

Formula (9.9) for q < 2 yields high absorption coefficients k_q (ν) in the line wings in comparison with the Lorentz contour (q = 2).

The examples presented in [6] of comparison of the transmittances measured in the surface air layer [1.8] and calculated for various q showed that the best agreement is obtained with q = 1.9 (Figure 9.2). As noted in [6], this contour form selection is in agreement with the conclusion of Mizushima [14] and other investigators that the wings of the real line contours should be 20-30% more intense that the dispersion contours. Without delving into
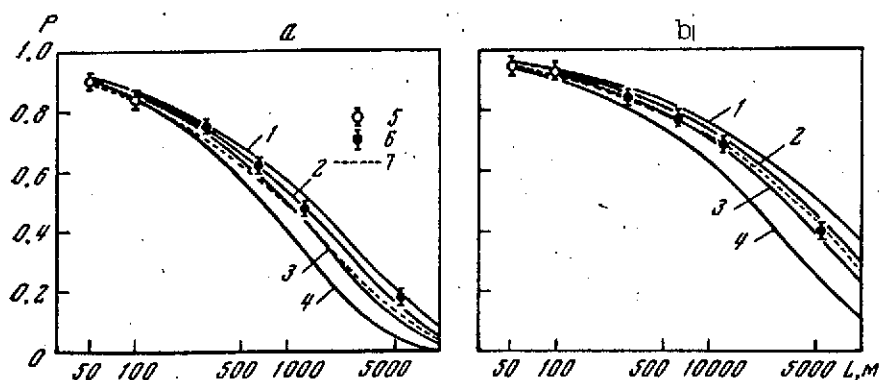
Figure 9.2. Comparison of experimental and theoretical O_2 transmittances [6]

a- $\gamma = 7604$ Å; b- $\lambda = 7630$ Å; 1-4- calculations using (9.9) for q = 2, 1.9, 1.8, 1.6, respectively; 5- measurements in cuvette [6]; 6- in surface air layer [1.8]; 7- calculation after [5]

the physical bases of this question, we note that an analogous relation is obtained with a high halfwidth value; for sufficiently distant line wings $k^{(1)}(\nu) < k^{(2)}(\nu)$ for $\gamma_0^{(1)} < \gamma_0^{(2)}$.

Evaluating the results of [5-8] from the viewpoint of their use for transmittance calculations in the real atmosphere, we can conclude:

1. The differences in the ensemble of parameters S_J and γ_0 are associated with the inadequacy of the measurement and interpretation methods in these studies. Leaving aside the measurement method differences, we simply note one specific interpretation difference — the absence of integrated account for the basic factors (total band intensity, individual line intensity distribution, connection between halfwidth and the measured quantities, line wing shape, line overlap elimination, and apparatus function) in determining S_J and γ_0 in all the studies except [8].

2. It would appear that the interpretation scheme closure and quite high measurement level in [8] would yield a basis to assume that the parameters S_J and γ_0 obtained in [8] are the most reliable. However the use in [8] of the distant line wing contour following Benedi t [13], described by (9.9) with unknown value of the parameter q, does not permit analysis of the reason for the discrepancy between the results of [6] and [8]. It is also not clear how valid the statement of the authors of [8] is, which contra- dicts [6], concerning the small differences in pure oxygen and in mixtures of oxygen and nitrogen.

3. The ensemble of parameters S_J and γ_0 obtained in [6] on the basis of independent measurements should be quite reliable. Here the required closure is achieved by selecting a suitable line wing contour to provide the best agreement with experiemnt for the given ensemble of parameters S_J and γ_0.

4. The line contour is obviuosly that factor, common to all the subject studies, which makes it possible to use any of the S_J and γ_0 ensembles obtained for transmittance calculation, provided /274 the line contour is compatible with the method used to extract these parameters from the experimental data. For example, after fixing the value $\gamma_0 = 0.048$ cm^{-1} and the line dispersion contour the authors of [5] were forced to increase the parameters S_J in order to correlate the calculations with the stronger actual absorption, associated to a certain degree with the more intense wings of the actual line contours.

An analogous result was also obtained in a natural fashion in [7], in which the dispersion contour was also used and the parameters S_J were essentially fixed. Therefore, in accordance with the experimental data reduction technique the adjusting parameter was the halfwidth, elevated values of which were used to provide the increased absorption in the line wings which was necessary for

agreement with the measurements. To confirm these conclusions it is necessary to compare the results of calculations of the transmittances P_ν from various ensembles of parameters S_J and γ_0, both with one another and with the available results of P_ν measurements.

§ 3. Transmission Function

The parameters of the oxygen A band presented above permit calculating the transmittance in various parts of the band in an atmosphere which is uniform or nonuniform as a function of altitude with the aid of (1.12) and (1.13), respectively. Such calculations were made in [5-7] to check the band parameters obtained therein, and also in [15] on the basis of the computational method developed in [16]. In all these studies examples are presented which indicate quite satisfactory agreement of the calculated and experimental transmittances (see Figures 9.1 and 9.2), in spite of the difference in the initial band parameters.

We mentioned previously the possible factors which may lead to this agreement. In the following we shall present results of calculations of the transmission functions P_ν, made in [30] for various combinations of parameters S_J and γ_0 [5-8] using the same technique with account for the corresponding line contours. Since comparisons of these calculations with the data of P_ν measurements in the surface layer and along paths inclined toward the sun are required, in computational formulas of the type (1.12) and (1.13), we can also take into account the instrument apparatus function $\varphi\,(\bar{v} - v)$:

$$P\,(\bar{v},\,u) = \frac{1}{\Delta v} \int_{v_1}^{v_2} \varphi\,(\bar{v} - v)\exp\,(-\,k_v u)\,dv; \qquad (9.10)$$

$$P\,(\bar{v},\,\zeta) = \frac{1}{\Delta v} \int_{v_1}^{v_2} \varphi\,(\bar{v} - v)\exp\left[-\,mu_0 \int_0^\zeta k_v\,(t,\,T)\,dt\right]dv. \qquad (9.11)$$

In these formulas $u_0 = c_0 bL$ is the oxygen mass along a uniform and isothermal path of length L, reduced to standard pressure (p_0) and temperature (T_0) (c_0 is the O_2 concentration; b is the pressure in atm); $u_0 = c_0 p_0/g\rho_0$ is the uniform oxygen atmosphere height; $\zeta = p/p_0$ is the observer's leight; $m = \sec \zeta_0 + \sec \theta$ is the air mass (ρ_0 is the O_2 density for $p = p_0$, ζ_0, θ are the zenith distances of the sun and observer, respectively).

Since the theoretical transmission functions can be used with different spectral resolution the question of the averaging interval width $\Delta\nu$ is important. The computational program permitted averaging over any $\Delta\nu$. However, considering the tremendous volume of information obtained in the P_ν calculations for small $\Delta\nu$ (on the order of the line halfwidth) and also bearing in mind the compara- tively coarse resolution of the spectral apparatus used at the present time in full-scale measurements (including aboard satellites), we performed the averaging in (9.10) and (9.11) in the limits of each line. In this case the integrands in (9.10) and (9.11) were calculated at 40 points on both sides of the line centers with s spacing 0.005 cm^{-1}. The remaining ν segments on the neighboring line wings were divided in half and in each half the integrands of (9.10) and (9.11) were calculated at 20 additional points. Consequently, within the limits of each line we calculated 80 values of the monochromatic transmittance with account for neighboring line overlap. In these calculations we took $\varphi(\bar{\nu} - \nu) \equiv 1$ within the interval (ν_1, ν_2) and $\varphi(\bar{\nu} - \nu) \equiv 0$ outside the latter. The transmittances obtained in this way for each set of parameters S_J and γ_0 were compared with one another and with the P_ν measured with the aid of instruments whose resolution was much less than Δ^ν.

In transmittance calculations for the nonuniform atmosphere significant difficulties are associated with accounting for the dependences of S_J and γ_0 on the temperatures profile T (ζ). It

was shown in [5] that the transmittances for the standard, arctic, and tropic $T(\zeta)$ profiles differ from one another by 1% (Table 9.2). This permits taking atmospheric stratification into account by the effective temperature $T_e = \int_0^1 T(\zeta)\,d\zeta$ (in the standard atmosphere case $T_e \approx 250^\circ$ K). The comparison examples presented in Table 9.2 of $P(\bar{\nu}, T_e)$ calculations for $T_e = 250 - 290^\circ$ K and the transmittances for the three-layer atmosphere (each layer is isothermal and the S_J are taken for $T = 200, 250, 290^\circ$ K) show that the error arising in this case does not exceed 5%. The introduction of T_e simplifies /276 the calculations, since the integration in (9.11) over ζ for the dispersion contour $k(\nu, T_e)$ is performed in closed form. We must bear in mind here that it is necessary to integrate with respect to ζ from some $\zeta_{min} > 0$, since for $\zeta = 0\,k_{\nu}$ in the Lorentz contour becomes infinite*.

Integrating in (9.11) with respect to t in the limits from $\zeta_{min} = 0.01$ to an arbitrary level ζ with account for the Lorentz line shape (1.15) in the dependence of γ on ζ and T, we obtain

$$P(\bar{\nu}, \zeta, m) = \frac{1}{\Delta\nu}\int_{\nu_1}^{\nu_2} \varphi(\nu - \bar{\nu})\left[\frac{\left(\frac{\nu - \nu_0}{\gamma_0}\right)^2 + \zeta_{min}^2}{\left(\frac{\nu - \nu_0}{\gamma_0}\right)^2 + \zeta^2}\right]^x dv, \qquad (9.12)$$

where

$$x = \frac{S(T_e)\,mu}{2\pi\tilde{\gamma_0}}; \qquad \tilde{\gamma_0} = \gamma_0\sqrt{\frac{T_e}{T}}.$$

The transmission function calculation examples shown in Figures 9.3 and 9.4 confirm the necessity for matching the parameters S_J /277

---

* In reality for low pressures we must use the combined and Doppler contours (see [15]); the contribution to P_ν of these factors and variations of $\zeta_{min} > 0.01$ is within the limits of the initial band parameter errors.

TABLE 9.2.   COMPARISON OF TRANSMISSION FUNCTIONS CALCULATED IN [5] FOR STANDARD (P_s), TROPIC (P_t), AND ARCTIC (P_a) TEMPERATURE PROFILES WITH P_ν FOR THREE-LAYER ($\tilde{P}$) AND ISOTHERMAL ($\hat{P}$) ATMOSPHERES*

ζ	P_s	P_a	P_t	$\tilde{P}$	$\hat{P}$ (290)	$\hat{P}$ (250)
			$m = 2$			
1	0,34	0,32	0,35	0,36	0,36	0,35
0,9	0,38	0,37	0,39	0,41	0,42	0,40
0,8	0,43	0,42	0,44	0,46	0,46	0,45
0,7	0,48	0,46	0,49	0,51	0,52	0,50
0,6	0,53	0,52	0,54	0,56	0,57	0,54
0,5	0,59	0,58	0,60	0,63	0,64	0,62
0,4	0,66	0,64	0,66	0,69	0,69	0,68
0,3	0,73	0,73	0,73	0,74	0,74	0,73
0,2	0,82	0,82	0,81	0,82	0,82	0,82
0,1	0,91	0,91	0,91	0,91	0,92	0,91
			$m = 6$			
1	0,12	0,11	0,14	0,14	0,14	0,12
0,9	0,16	0,15	0,17	0,18	0,19	0,17
0,8	0,20	0,20	0,21	0,23	0,23	0,21
0,7	0,25	0,24	0,26	0,28	0,29	0,27
0,6	0,30	0,29	0,32	0,34	0,35	0,33
0,5	0,37	0,36	0,38	0,41	0,41	0,39
0,4	0,46	0,44	0,46	0,46	0,47	0,45
0,3	0,56	0,56	0,56	0,57	0,58	0,57
0,2	0,69	0,69	0,68	0,70	0,70	0,70
0,1	0,84	0,84	0,84	0,85	0,85	0,85

* Translator's note: Commas in numbers represent decimal points.

and γ_0 with the line shape.   Actually, the values of P ($\bar{\nu}$, L) calculated using the parameters of [6] and [8] practically coincide (Figure 9.3)** while the calculations using S_J and γ_0 from [7], where such agreement does not exist, yield low values of P ($\bar{\nu}$, L) (however the latter are close to the experimental values of [1.8] and [17]).   This is also seen from the examples of P ($\bar{\nu}$, ζ, m) calculations for the nonuniform atmosphere (Figures 9.4 and 9.5),

** Since the value of the parameter q in (9.9) was not indicated in [8], we used in the calculations the value q = 1.9, recommended in [6].
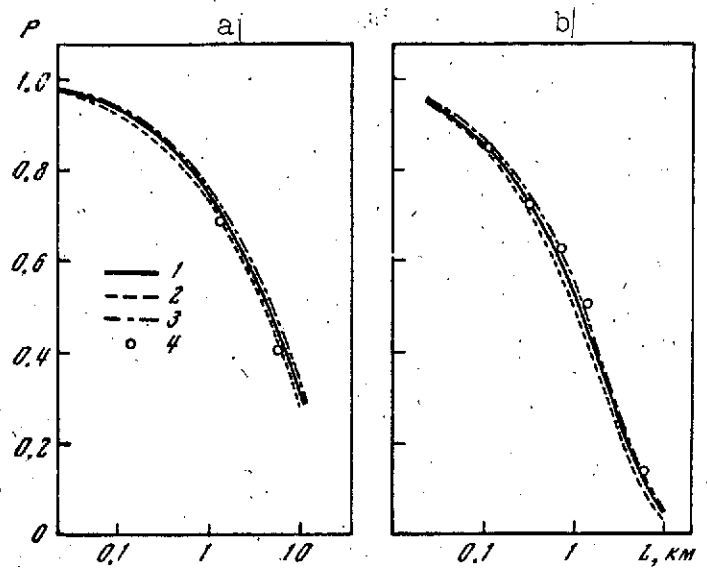
Figure 9.3. Comparison of transmission functions P (ν, L) calculated for uniform atmosphere with measurements [1.8]

a- $\bar{\lambda}$ = 7605 Å; b- λ = 7630 Å; 1- from [6]; 2- from [7]; 3- from [8]; 4- measurements
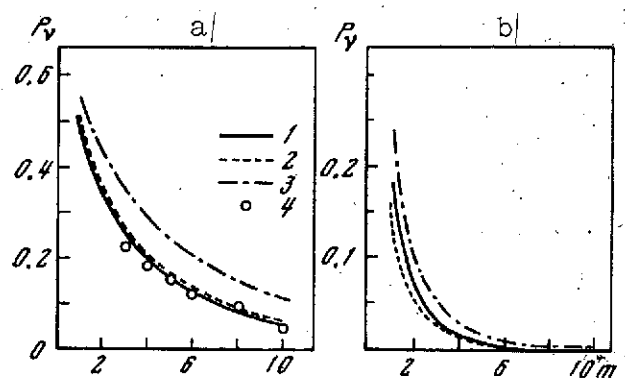
Figure 9.4. Comparison of P ($\bar{\nu}$, m) for nonuniform atmosphere

1- calculation from [5]; 2, 3- calculation from [7] and [8], respectively; 4- measurements [1.8]

in which the dispersion contour and elevated values of the parameters S_J [5] or γ_0 [7] were used. Thus, the transmission functions calculated using either matched S_J, γ_0, and line contour ensembles or corrected parameters which provide description of the absorption under actual conditions can be used to determine the cloud top height h. Here we must bear in mind that in the cloud height range

471

(h ≤ 12 km) the dependence of the absorption function (A = 1 - p) on the absorbing substance mass is close to the square-root law (9.8). Therefore we can expect increase of the relative errors in determining h for low clouds.

It would seem that the h determination errors could be reduced if we use transmission functions in band regions with different absorption. For example, it was noted in [5] that P_ν in the 7607 Å region is more sensitive to high clouds and in the 7632 Å region is more sensitive to low clouds. But we see from Figure 9.6 that in the limits of realistic transmission function measurement errors the sensitivity, described by the derivative $\partial P_\nu/\partial z$, was practically the same for these two spectral intervals. If the transmission function is measured with absolute error 0.04 in the range of P_ν variation from 0.1 to 0.7, then cloud height can be determined with an error less than 1 km. The conclusion on identical sensitivity of P_ν in different segments of the A band is important in selecting the optimum method for transmission function measurement from satellites. However, in selecting the measurement method it is also necessary to have estimates of the other cloud height determination errors, the most important of which are the errors in accounting for additional solar radiation absorption in clouds with unknown optical characteristics.
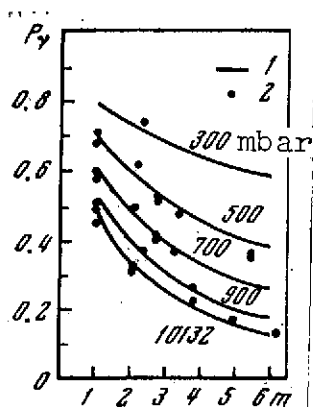
Figure 9.5. Comparison of P ($\bar{\nu}$, m) calculated for nonuniform atmosphere in [5.9] with measurements of [17]
  mosphere in [5.9] with measurements of [17]
1- calculation; 2- measurements. λ = 7630 Å

472
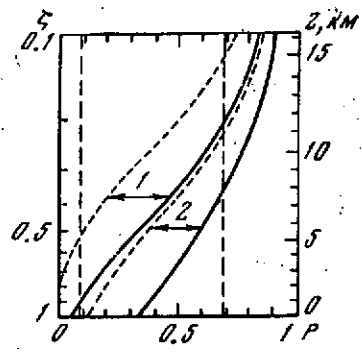
Figure 9.6. Dependence of P on ζ from calculations of [5], illustrating sensitivity of P_ν to reflecting surface height h

Solid curves are for m = 2, dashed are for m = 6. The dashed straight lines bound the range of P_ν values in which the error $\delta P_\nu \approx 0.04$ leads to an error $\delta h \approx 1\, км$. 1- $\lambda = 7607\, Å$; 2- λ = 7632 Å

§ 4. Account for Radiation Absorption in Clouds and in the Atmos-
phere

Solar radiation absorption along the scattering path in a cloud depends significantly on the microstructure, water content, and geometric parameters of the cloud, and also on the relationship between the absorption and scattering coefficients. Since there is generally no information on these parameters for the clouds above which reflected solar radiation is measured from satellites, in developing a technique for taking into account the corresponding correction in determining cloud cover height it is necessary to use additional information on cloud cover characteristics, obtained independently on the basis of calculations and statistical analysis of experimental data. The calculations required for this purpose of the reflected solar radiation intensity dependences on the cloud parameters and also on the sun and observer positions are based on solving the transport equation in a flat layer of an optically dense medium (the optical thicknesses τ^* reach magnitudes of 30-50) having very elongated scattering indicatrix (the forward radiation scattering exceeds the scattering in the back direction by 3-4 orders of magnitude). The relationship between the absorption and

473

scattering coefficients is taken into account in this cloud model using the quantum survival probability $\Lambda = \sigma/(\sigma + \alpha)$, which varies from unity (for pure scattering) to small values close to zero (for very strong absorption). The technique and results of such calculations for some models of optically dense layers are presented in several studies [I. 7; 18-24]. Direct application of the method of [21] to the oxygen A band was carried out in [25].

The Monte Carlo method [1.94, 1.95] has recently been used for analogous calculations; it permits taking into account selective absorption in a scattering medium using a transmission function of the form (1.20). Experimental studies of transformation of the 0.76 μ band in clouds were made in [26, 27].

We shall present some results obtained in [25] of calculations of the corrections for absorption in clouds, since these data were used by the authors of [25] to determine cloud heights from observations aboard the Gemini 5 spacecraft. To simplify the calculations the authors of [25] divided clouds into three types on the basis of altitude ζ_h — low (St, $\zeta_h = 0.7 - 1$), middle ($Ac, As, \zeta_h =$ 0.5 — 0.7) , and high ($Ce, \zeta_h, <0.5$) — with the same normal drop size distribution laws (mean particle size $\bar{r}_0 = 10$ μ, variance $\sigma_r = 4$ μ^2), water content (0.2 g/cm^3 for St and As and 0.3 g/cm^3 for Cb), and water vapor content. The authors of [25] take into account selective atmospheric absorption in the 7607 and 7632 $\overset{o}{A}$ intervals, for which the transmission functions were calculated in [5] in the layer up to 100 mbar using the equivalent absorption coefficient k_q, determined from the relation

$$P_v(\zeta, m) = \frac{1}{\Delta v} \int_{v_1}^{v_2} \exp\left[-mu_0 \int_0^\zeta k_v(t)\,dt\right] = \exp\left[-mu_3 \int_0^\zeta k_a(t, \zeta_0, \theta)\right]dt. \quad (9.13)$$

The coefficients k_q averaged for the low, middle, and high clouds over the layers $\zeta = 0.7$-1, 0.5-0.7, and 0.3-0.5, respectively, were

used in the calculations of radiation scattering in the clouds. It
is easy to see that the method used in [25] to account for selective
absorption in a scattering medium cannot be considered sufficiently
correct, since the coefficient k_a will depend not only on the ζ
level and angles of incidence ζ_0 and reflection θ, but also on the
absorbing substance mass along the path traveled by a photon in
the cloud. For optically very dense clouds with large angles ζ_0
and θ this method will probably lead to excessive corrections for
radiation absorption in the cloud. This shows up to some degree
in comparing the corrections obtained in [25] and in the earlier
study [27] by the two-stream method (in the latter case the
correction factors were significantly smaller). Examples of cor-
rection factor dependences on cloud thickness Δh and angle ζ_0 for
fixed angle $\theta = 18°$ are shown in Figure 9.7. On the basis of the
reciprocity principle these corrections can be used by exchanging
places of ζ_0 and θ. According to the data of [25], the correction
azimuthal dependence was negligibly small. When using these cor-
rection factors to interpret observations from the Gemini 5 space-
craft, the authors of [25] were forced to make additional assumptions
on the observed cloud geometric thickness on which these corrections
depend. This reduces correction introduction reliability, moreover
the corrections are obtained on the basis of only a single cloud
model, whose applicability limits are not known.
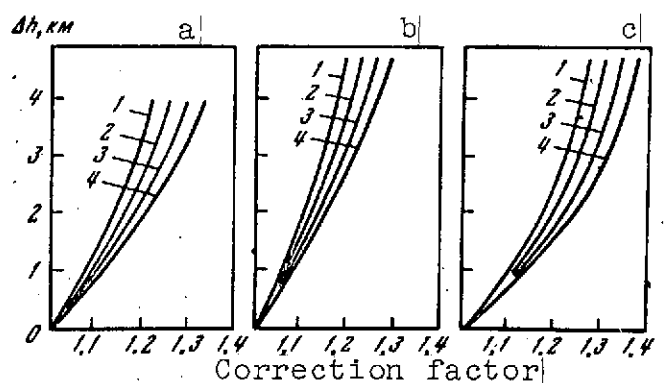
Figure 9.7. Correction factor as function of Δh and ζ_0 according to
[25]

a- low clouds; b- middle; c- high; 1-4- ζ_0 = 18.2; 41.4; 63.3,
75.5°, respectively

The difficulties of cloud geometric thickness selection may be reduced somewhat if we use the statistical characteristics of cloud boundary vertical structure, an example of which was presented in § 4 of Chapter 3 for stratus clouds. As was shown in § 4 of Chapter 3, stratus cloud base and top heights correlate closely with one another (see Table 3.3). This circumstance makes it possible to determine for this type of cloud cover the cloud base height h_1 if the cloud top height h_2 is known (or vice versa) by using the optimum extrapolation method.

In fact, if we represent the cloud base (top) height deviations $h_1' (h_2')$ from the norm $\bar{h}_1 (\bar{h}_2)$ in the form of a linear dependence on the corresponding cloud top (base) height deviations $h_2' (h_1')$:

$$h_{1i}' = a_1 h_{2i}', \; h_{2i}' = a_2 h_{1i}' \qquad (i = 1, 2, \ldots, N),$$

(9.14)

the unknown coefficients $a_m \; (m = 1.2)$ can be determined from the condition of minimum of the functional

$$\delta_h^2 (a_m) = \overline{[h_{mi}' - a_m h_{ki}']^2} \qquad (m, k = 1, 2).$$

(9.14)

Here the overbar denotes averaging over all realizations $i = 1, 2, \ldots, N$ occurring in the experiment.

Performing the requires operations in (9.15) and applying the condition for minimum of the functional

$$\frac{\partial \delta_h^2 (a_m)}{\partial a_m} = 0,$$

we obtain the relation

$$a_m = \frac{B_{hh} (h_m, h_k)}{B_{hh} (h_k, h_k)} \qquad (m, k = 1, 2).$$

(9.16)

The correlation moments $B_{hh} (h_m, h_k), B_{hh} (h_k, h_k)$ are presented in Table /280 3.3. The total height h_m is obtained by adding h_m to the corresponding norm shown in Table 3.2.

476
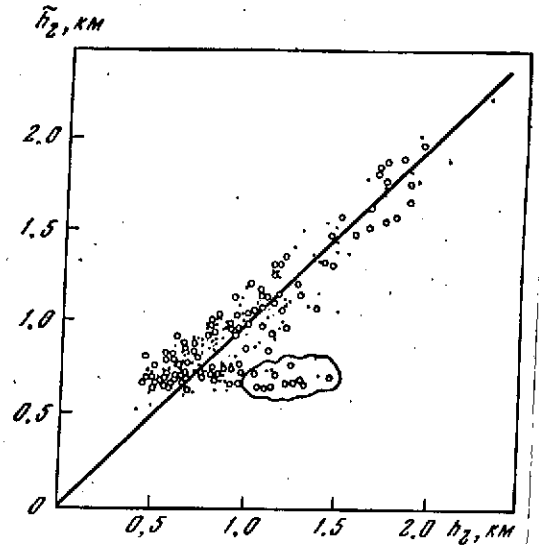
Figure 9.8. Regression relation between h_2 and $\tilde{h}_2$ from [3.15] for cold (circles) and warm (points) half of the year

We should keep in mind that the cloud top heights are determined by the optimum method with the absolute error δ_h, which also may be expressed in terms of the correlation matrix elements (see Table 3.3)

$$\delta_h^2 = B_{hh}(h_m, h_m) - \frac{B_{hh}^2(h_m, h_k)}{B_{hh}(h_k, h_k)}.$$ (9.17)

The relative error $\varepsilon_h = \delta_h/\sigma_h$ is expressed in terms of the correlation coefficient $r_{hh}(h_m, h_k)$:

$$\varepsilon_h = \sqrt{1 - r_{hh}^2(h_m, h_k)}.$$ (9.18)

Therefore, in spite of the quite high correlation coefficient $r_{hh}(h_2, h_1)$ = 0.88 for the warm half of the year and 0.89 for the cold half, we find that $\delta_h = 0.18$ км and $\varepsilon_h = 47\%$. Consequently, on the average the stratus cloud top height may be determined by the described method with mean-square error $\sim 30\%$, which for lack of other possibilities can be considered acceptable for the subject problem. To illustrate the method the quantities $\tilde{h}_2$ were calculated

477

in [3.15] under the assumption that the quantities h_1 are known from measurements and the norms $\bar{h}_1$ and $\bar{h}_2$ are known from the statistical analysis presented above. Figure 9.8 shows the regression relation between the heights h_2 measured during airplane sounding [3.27] and $\tilde{h}_2$ determined by the optimum extrapolation method. Although in individual cases the errors of this determination are quite large and reach 0.75 km* (these cases are circled in Figure 9.8), most of the h_2 values are obtained with quite satisfactory accuracy.

Similarly and with the same accuracy, from the cloud top height h_2 we can determine the cloud base height h_1 and, consequently, the thickness Δh, which is necessary for introduction of the corrections in determining h_2 from reflected Earth radiation measurements /281 from satellites in the 0.76 μ absorption band, for example, with the aid of the curves in Figure 9.7. To obtain these corrections in the stratus cloud case we suggest the following algorithm, which permits estimation in addition to Δh of certain optical parameters of these clouds. From directly measured ratios I_1/I_2 of the intensities in the band (I_1) and outside the band (I_2) and from the known transmission function of the form (9.11), for given m we determine the first height approximation $h_2^{(1)}$ without account for additional absorption in the cloud. Then, using optimum extrapolation and formulas (9.14), (9.16) we calculate the first approximation $h_1^{(1)}$ and the cloud thickness $\Delta h^{(1)} = h_2^{(1)} - h_1^{(1)}$. On the other hand, from measurements of I_2 and from $h_2^{(1)}$ we can estimate the cloud optical thickness $\tau_2^{(1)}$ outside the band, using the calculations mentioned above of solar radiation reflected from optically dense media for different τ_2 (see, for example, [21]). Then it

---

* Careful synpotic-aerological analysis of the experimental data [3.27] showed that the scatter in Figure 9.8 is associated with the fact that the stratus clouds in these cases are not the air mass type, i.e., they should be excluded from consideration.

478

is easy to determine the average coefficient of scattering in the cloud $\sigma^{(1)} = \tau_2^{(1)}/\Delta h^{(1)}$ and, consequently, the quantum survival probability $\Lambda^{(1)} = \sigma^{(1)}/(\sigma^{(1)} + \alpha)$ (α is the coefficient of oxygen absorption in the selected band segment for the given cloud level). The quantities $\sigma^{(1)}$, $\tau_2^{(1)}$, $\Lambda^{(1)}$ can be considered the input parameters in calculating the corrections for additional radiation absorption in the cloud by any of the existing computational methods, the Galin method [24] for example, and we can obtain the refined cloud top height $h_2^{(2)}$.

The corrections for absorption in stratus clouds were obtained in [17] experimentally with the aid of an airplane-borne spectrograph which permitted measuring the reflection and transmission spectra in the O_2 0.76 μ band with resolution 2.5-5 Å. The interval near 7630 Å was studied in [17], for which the transmission functions of the atmospheric layer above the clouds were measured at various altitudes with and without account for reflection from the clouds and for different air masses (for this purpose the spectra of solar radiation reflected from the cloud and from a diffusion screen were measured at various levels). A comparison of the experimental and calculated transmission functions is shown in Figure 9.5. The cloud top heights were determined from the optical measurements and were measured directly using an altimeter. As we would expect, the true cloud top heights were systematically greater than the heights obtained optically (the mean value of this difference was 1.4 km, the mean-square deviation was 0.3 km for cloud thicknesses 1-1.3 km). The correction factors calculated in [17] on the basis of solution of the transport equation by the two-stream method were close to the measured values (0.8-1.3 km). In the techniques proposed above for taking account of solar radiation absorption in clouds we neglected scattering in the atmospheric layer above the clouds, as a result of which the effective radiation

absorption may also increase. Estimates of this effect obtained in [28] for a very opaque atmosphere (the optical thickness of the entire atmospheric layer for λ = 0.76 μ was taken to be 0.45) showed that when neglecting multiple scattering the transmission function error reaches 10% of the absolute value of P_ν, i.e., it is within the limits of P_ν measurement error. This correction depends only weakly on cloud height variation, cloud albedo, and the angles ζ_0 and θ (ζ_0 and θ < 70°).

Thus, at the present time some information is available on the structure of the 0.76 μ oxygen band and the atmospheric transmission function in this band, and also on the corrections for solar radiation absorption in the cloud layer, which makes it possible to determine cloud top height to within 0.5-1 km if the corresponding reflected solar radiation measurements from satellites make it possible to obtain the transmission function with absolute error of order 0.02-0.04 (relative error 5-10%).

§ 5. Cloud Height Determination From Satellites /282

Measurements of reflected solar radiation in the 0.76 μ oxygen band in order to determine cloud top height were undertaken aboard the Gemini 5 spacecraft [25] and aboard the Kosmos 320 satellite [29]. A hand-held spectrograph was used aboard Gemini 5, which permitted obtaining spectrograms in the 7500-7800 Å spectral interval with resolution 5 Å and simultaneous photography of the clouds. Examples of the spectrograms for three cloud cover types with tops located at low, middle, and high altitudes are shown in Figure 9.9. In the individual cases the cloud height was measured directly during simultaneous airplane flights, which made it possible to evaluate the accuracy of the measurement and interpretation methods. The transmission functions calculated in [5] for the 7607 and 7632 Å regions

480

and the corrections for absorption in the cloud calculated in [25] as a function of sun zenith distance (see Figure 9.7) and cloud thickness were used for the interpretation. The cloud thickness is introduced in [25] as the most probable value for the given cloud type. We see in one of the four examples in Table 9.4 that when using this parameter the cloud height determination error was significant. In the other cases quite good agreement between the actual height and the height measured aboard Gemini 5 was obtained, although we cannot judge the effectiveness of the method proposed in [25] for introducing the correction for absorption in the cloud on the basis of a small number of examples. This is also recognized in [25], whose authors consider the question of accounting for the correction for radiation absorption in each specific case to be one of the most important questions in the problem of determining cloud height by reflection.

TABLE 9.3

Cloud type	m	Thickness, km	Correction	Measured height, mbar		Actual height, mbar
				Uncorrected	Corrected	
Hurricane Doreen	2.03	5	1.33	323	195	350-320
Alto- cumulus	2.12	0.8	1.11	370	330	320
Same	2.12	5	.38	460	340	320
Stratus	2.40	0.5	1.06	980	950	960

The use for this purpose not only of the average heights of clouds of various types but also the second moments, which characterize the connection between the tops and bases of clouds of different types, as was proposed previously for stratus cloud cover, makes it possible to reconstruct the actual situation in an optimum fashion and obtain a more reliable absorption correction.
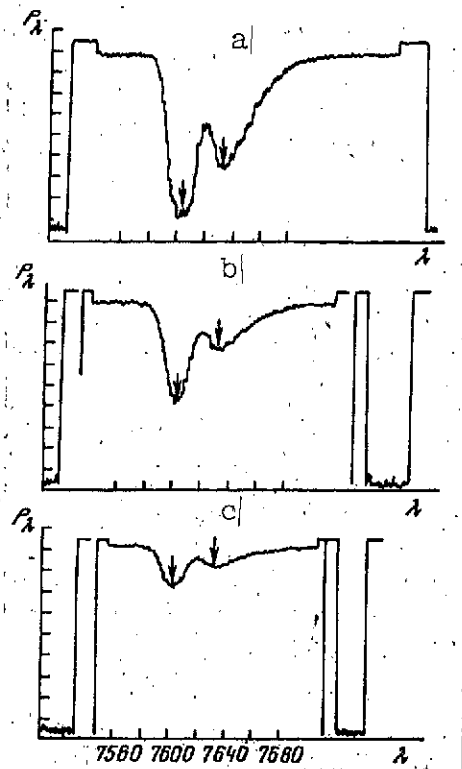
Figure 9.9. Spectrograms for clouds of different levels from [25]
a- low stratus clouds; b- middle clouds of the intratropical
center; c- clouds of hurricane Doreen. Arrows denote λ = 7607
and 7631 Å
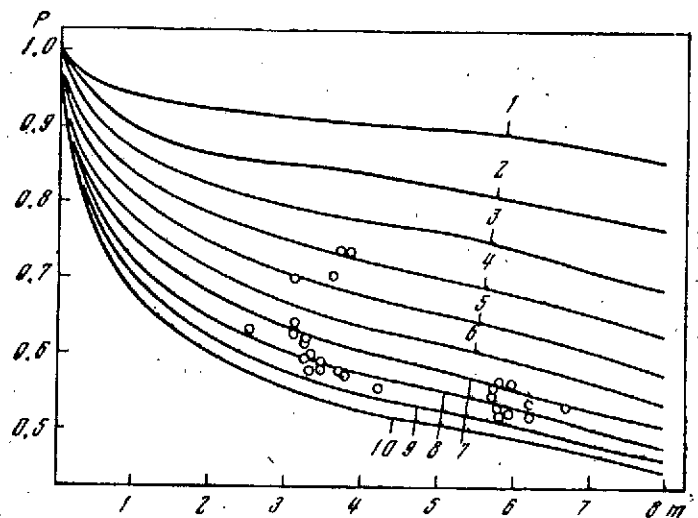
Figure 9.10. Atmospheric transmission function versus m and ζ
1-10- ζ = 0.1; 0.2; 0.3; 0.4; 0.5; 0.6; 0.7; 0.8; 0.9 and 1,
respectively. Circles denote experiment

482

The method for determining cloud top height h was checked on the basis of reflected solar radiation intensity measurements in the band O_2 0.76 μ (I_2) and in the comparison interval 0.738 μ (I_2) made aboard Kosmos 320 using scanning telephotometers. These measurements were part of a complex of optical studies of the atmosphere from satellites [I.30], including measurements of cloud self-radiation in the 10.5-11.5 μ [5.13] window, which permitted determining h by two independent methods and thereby improved considerably the photometric and radiometric data interpretation reliability.

Quite high measurement accuracy was provided by periodic calibrations of the equipment aboard the satellite. Calibration of the telephotometers was accomplished by measuring the extra-atmospheric solar radiation S_ν and the dark current during each scan*. Therefore the errors in determination of the ratios I_1/I_2, connected with the transmission function P_ν (ζ, m) and cloud height ζ_h by the relation

$$\frac{I_1}{I_2} \doteq c \frac{\int_{\nu_1}^{\nu_2} S_\nu P_\nu(\zeta, m) \cdot \varphi_\nu^{(1)} d\nu}{\int_{\nu_3}^{\nu_4} S_\nu \varphi_\nu^{(2)} d\nu} = P(\zeta_h, m), \tag{9.19}$$

amounted essentially to the signal recording errors. In (9.19) $\varphi_\nu^{(1)}$ and $\varphi_\nu^{(2)}$ are the telephotometer spectral sensitivities inside and outside the band, which are determined in the measurement error limits by the transmission of narrow-band filters ($\Delta\nu = 30$ Å) which select the spectral intervals (ν_1, ν_2) and (ν_3, ν_4); c =

$$\int_{\nu_4}^{\nu_4} S_\nu \varphi_\nu^{(2)} d\nu \Big/ \int_{\nu_1}^{\nu_2} S_\nu \varphi_\nu^{(1)} d\nu \Big| .$$

---

* The technique for measuring the Earth's self-radiation aboard Kosmos 320 was described in [5.13] (see also Chapter 8).

Curves of integral transmittance $P(\zeta_h, m)$ as a function of /284
ζ_h and m (Figure 9.10) were plotted to determine cloud height
on the basis of the ratios I_1/I_2 using the transmission funcions
calculated in § 3. Comparison of these curves with experimental
values of the ratio (9.19) shows that the effective cloud height
determination error (without account for absorption in the cloud),
associated with the $p(\zeta_h, m)$ determination error, amounts to 0.5 km
for low clouds and 1 km for high clouds. Naturally, this error
is retained in determining the true height with account for the
correction, however the error due to the latter factor cannot
be estimated because of the absence of direct ζ_h measurements.
Some estimates of these errors (obviously high) are obtained in
comparing the cloud heights determined using the previously
mentioned simultaneous measurements aboard Kosmos 320 of reflected
solar radiation (h_Φ) and self-radiation (h_p). The example of
such a comparison presented in regression form in Figure 9.11
based on more than 250 measurements of h_p and h_Φ shows that in
half the cases the difference $\Delta h = h_p - h_\Phi$ does not exceed ± 0.5 km,
and in 75% of the cases does not exceed ± 1 km. The mean-square
magnitude of this difference, calculated using the entire set of
points shown in Figure 9.11, amounts to about 1 km. However, in
many cases $|\Delta h|$ reaches 2-3 km, which goes far beyond the limits
of possible telephotometer reflected solar radiation and self-
radiation measurement errors.

One possible reason for such large Δh differences may be
associated with the different viewing fields of the instruments
used aboard the Kosmos 320 satellites, which leads to different
spatial averaging of cloud formation and cloudless segment radia-
tion in the case of broken clouds for the telephotometers and
radiometers. Thereby the random element associated with purely
geometric factors (we recall that for solid cloud cover, uniform
in the instrument viewing field limits, h_Φ will always be low in

484
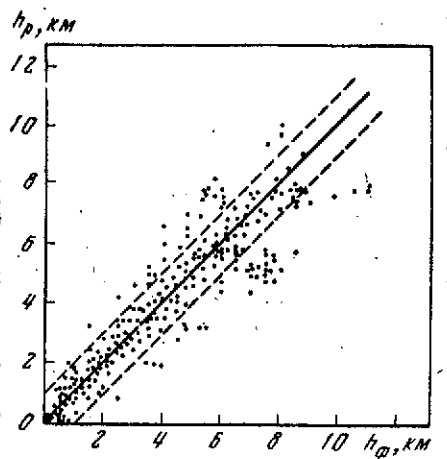
Figure 9.11.   Regression relation between cloud heights h_Φ and h_p from Kosmos 302 data [29]

comparison with the true cloud height h_{tr} while h_p, conversely, will be high, i.e., h_{tr} under these conditions lies between h_p and h_Φ) in the relationship between h_p and h_Φ is intensified. The fact that the large Δh differences are connected not with the physical relationships forming the basis for determining h_p and h_Φ but, rather with random factors is confirmed to some degree by the equiprobable distribution of all the cases, for which $0.5 \leqslant |\Delta h| \leqslant 1$ км; $1 \leqslant \Delta h \leqslant 2$ км; $2 \leqslant |\Delta h| \leqslant 3$ км.

In order to account for (or exclude) large errors it is necessary to use additional information in the form of cloud cover television images obtained from the Meteor satellite system or the American ESSA satellites. At the same time the combination of photometric and radiometric data with these images will enhance the nephanalysis and synoptic interpretation of the cloud cover images.

CONCLUSION

In conclusion we shall list the basic results and conclusions presented in the monograph and shall also give some recommendations on further development of Earth atmosphere studies from satellites using optical sounding methods.

1. Analysis of calculations of the Earth's outgoing radiation field characteristics made by several authors for various spectral regions and comparison of the corresponding results with one another and with experimental data obtained from satellites show that the atmospheric models used in the calculations describe the basic patterns of the vertical, angular, and spectral distributions of the solar radiation reflected by the Earth and the self-radiation of the planet into outer space. However, these models do not provide a reliable description of the variations of the radiation field characterics associated with variations of the physical parameters of the atmosphere, clouds, and Earth's surface responsible for the formation of these fields.

2. The majority of these parameters (aerosol scattering coefficients and indicatrices, brightness coefficients or albedo of the clouds and underlying surface, temperature and humidity of the atmosphere and clouds as radiating objects) are random functions of the spatial coordinates, time, and in the optical parameter case the wavelength or scattering angle. Therefore multivariate random function statistical analysis methods are used to study the spatial, angular, and spectral structures of the radiation fields and also to determine the specific realizations of several parameters of the atmosphere, cloud cover, and the Earth's surface. The basic idea of the monograph, which

permits significant simplification of the solution of the subject problems and permits obtaining easily visualized results, consists in using the statistical characteristics of the spatial and spectral structure of the atmospheric parameters. The complete ensemble of these characteristics obtained by statistical analysis of the data of aerological soundings and measurements of the optical parameters of the atmosphere and the underlying surface forms the optical-meteorological model of the atmosphere.

3. As the first approximation of such a model we propose the ensemble of vertical and spectral distributions of the aerosol attenuation coefficients, scattering indicatrix angular distributions, vertical atmospheric temperature and humidity profiles, and also the corresponding autocorrelation matrices and their eigenvectors and cross-correlation matrices averaged over random ensembles of different completeness. This model can be considered a statistical generalization of the previously proposed Shifrin-Minin closed optical model, applied to the real atmosphere which is a multi-parameter system. The model provides optimum parametrization of any specific realization of the ensemble of selected optical and meteorological characteristics, and also permits reconstruction of such a realization in optimum fashion from a limited number of available measurements.

4. Systems of equations describing the connections between /286 the first and second moments of the vertical, angular, and spectral structures of the radiation fields and the corresponding characteristics of the vertical structure of the optical and meteorological parameters are obtained. Mathematical closure of the system is accomplished by neglecting higher order moments. The statistical characteristics of the optical-meteorological model are introduced as a priori information for physical closure of the problem.

5. The autocorrelation matrices of the spectral intensities
I and integral fluxes F of the Earth's self-radiation field are
obtained: $K_{II}(\zeta_h, \zeta_l; 0)$, $K_{FF}(\zeta_h, \zeta_l)$ at various levels ζ_h, ζ_l for fixed
observation angles θ, describing the vertical structure of the
radiation field; the autocorrelation matrices $K_{II}(\theta_i, \theta_j)$, describing
its angular structure, and also the cross-correlation matrices:
$K_{IT}(\zeta_h, \zeta_l; \theta)$, $K_{Iq}(\zeta_h, \zeta_l; \theta)$, $K_{FT}(\zeta_h, \zeta_l)$, $K_{Fq}(\zeta_h, \zeta_l)$, characterizing the con-
nection between the $I(\zeta_h, \theta)$, and $F(\zeta_h)$ variations and the tempera-
ture $T'(\zeta_l)$, and humidity $q'(\zeta_l)$ variations. The matrices K_{FF}, K_{FT},
K_{Fq} agree satisfactorily with the analogous empirical characteris-
tics obtained by analysis of actinometric sounding data.

6. The analogous equations for the reflected solar radiation
are solved under the assumption of spherical scattering indicatrix
and with account only for the variations of the aerosol attenuation
coefficient $\sigma (\zeta)$ with the aid of the correlation matrix $K_{\sigma\sigma}(\zeta_h, \zeta_l)$.
Comparison of the calculated reflected solar radiation angular
structure characteristics $K_{II}(\theta_i, \theta_j)$ with the results of statistical
analysis of the Earth's brightness measurements obtained with the
aid of the Kosmos 149 satellite makes it possible to evaluate the
influence of variations of σ and natural surface reflective
characteristics on the angular structure in different directions.

7. Analysis of the equations for the radiation field statis-
tical characteristics makes it possible to establish regions of
positive and negative auto- and cross-correlations, reflecting the
physical fact that variations of the optical or meteorological
parameters can lead to radiation variations of opposite signs
which enter with different weight at different levels. As a re-
sult regions of weak correlation of the radiation and atmospheric
parameters are created in which the variations of the latter do
not contain information on the variations of the former, and vice
versa.

8. On the basis of the equation of self-radiation or solar radiation transport in a two-dimensional or three-dimensional medium systems of equations are constructed which describe the connections between the statistical characteristics of the radiation field horizontal structure and the corresponding characteristics of the optical and meteorological parameter fields. For the case of uniform and isotropic fields we determine the atmospheric frequency characteristic, describing the transformation of the spatial spectra of the reflecting or radiating boundaries of the medium as a result of radiation absorption and scattering in the atmosphere (this characteristic also takes into account the influence of measuring instrument angular sensitivity on distortion of the spectra).

9. The application of statistical analysis to the brightness field photometric sections obtained aboard the Kosmos 149 satellite in the visible part of the spectrum, to the self-radiation field radiometric sections obtained aboard the Kosmos 243 satellite in the 10-12 μ atmospheric window, and also to cloud cover aerial photograph microphotometry data makes it possible to determine the basic characteristics of the cloud system spatial structure. Specifically, we find extrema of the spectral densities in the 5-10 and 500-700 km scale region, as should follow from statistical analysis of the other meteorological parameter fields.

10. An objective criterion is proposed for evaluating the quasi-homogeneity and quasi-isotropicity of the empirical two-dimensional cloud cover fields, based on the following property of the autocorrelation matrix eigenvectors constructed for mutually perpendicular sections of brightness fields of different horizontal dimensions: in the homogeneous field case these vectors will be close to segments of trigonometric functions in the same region of definition, in the isotropic case the eigenvectors coincide for

both sets of sections. The eigenvalues of the autocorrelation matrices can be considered in this treatment as a generalization of the spectrum concept to quasi-homogeneous fields. Matrix analysis is also used to exclude the distorting factors associated with reflected solar radiation angular variation and with multiple scattering.

11. The ensemble of radiation field statistical characteristics (first and second moments) is defined as the radiation model of the atmosphere. Establishment of the connections between the radiation characteristics and optical-meteorological model makes it possible to treat the atmosphere as a "dynamic system" which transforms the input signals (direct solar radiation or self-radiation of the Earth's surface) into random signals described by the radiation model characteristics. The problems of finding the laws governing the transformed signal constitute the class of direct problems of atmospheric optics.

12. Determination of the random (or statistical) characteristics of the system itself from the output signals (or from their statistical characteristics) constitutes the class of inverse problems, which reduce in most cases to integral equations of the Fredholm type of the first kind and are incorrect in the mathematical sense. Explanations for the physical sources of inverse problem incorrectness and a brief summary of current methods for their regularization are given. The solution of specific problems of optical atmosphere sounding is carried out by the statistical regularization method using the optical-meteorological model characteristics as a priori information.

13. The problem of determining the vertical atmospheric temperature profiles $T(\zeta)$ from measurements of the Earth's radiation from satellites in the CO_2 15 μ band is solved. Two statistical regularization variants are tested: 1) optimal parametrization,

which permits representing the temperature profiles by a minimum (in comparison with other bases) number of eigenvectors of the correlation matrix $K_{TT}(\zeta_k, \zeta_l)$ with given accuracy (regularization reduces to filtering out the high-frequency harmonics); 2) finding a solution statistically averaged over the set of random vectors which satisfy at the same time both the initial equation with specified accuracy and the regularizing condition of belonging to the a priori ensemble of temperature profiles given by a normal distribution law with the empirical correlation matrix K_{TT}. For a mean-square radiation measurement error of 1-2% the mean-square error of $T(\zeta)$ reconstruction reaches 2-3° in the tropopause region. The statistical regularization method is tested successfully on data of Earth radiation spectra measurements from satellites and balloons.

14. The problem of determining the vertical effective water vapor mass $w_e(\zeta)$ and specific humidity $q(\zeta)$ profiles of the atmosphere from Earth's radiation spectra measurements in the 6.3 μ water vapor band is solved similarly. For the regularization we use the correlation matrix $K_{qq}(\zeta_k, \zeta_l)$ and its eigenvectors, describing the vertical structure of the humidity field. The mass $w_e(\zeta)$ as the integral humidity characteristic on which the measured radiation depends directly is reconstructed with a high degree of accuracy (the mean-square error does not exceed 1-2%). However, /288 the error of $q(\zeta)$ determination as a local characteristic increases markedly (reaching 25% in the atmospheric boundary layer) which is a direct consequence of amplified problem incorrectness. The error can be reduced with the aid of more detailed a priori information on the structure of the $q(\zeta)$ profiles in the boundary layer. The method for determining $q(\zeta)$ is tested on examples of balloon radiation measurements.

15. Examination of the reasons for the possible errors in the vertical temperature and humidity profile determination shows the primary problem is the error of the transmission function, which plays the role of the integral equation kernel. Since under actual conditions these errors may be significant and unknown, in the study we examine the possibilities of constructing an iteration process for simultaneous determination of the $T(\zeta)$, $q(\zeta)$, and transmission function variation profiles. Here we use the fact that the $T(\zeta)$ and $q(\zeta)$ profiles can be determined from very limited information on the radiation spectrum. The introduction of corrections to the transmission function is accomplished during reconstruction of the $T(\zeta)$ profiles from radiation spectrum measurements aboard the Nimbus 3 satellite.

16. Analysis of the existing methods and results of solution of the problem of determining underlying surface and cloud temperature from Earth's radiation measurements in the atmospheric windows 8-12, 10-12, and 10.5-11.5 μ from satellites of the Tiros series show some contradiction of the results, associated with deficiencies of the interpretation methods or with uncontrollable measurement errors. For the solution of this problem using the radiometric data obtained by the Kosmos 149, Kosmos 243, and Kosmos 320 satellites (in the last case instrument calibration using a blackbody was carried out aboard the satellite) we introduce the concept of the transfer function $\mathscr{P}$, characterizing underlying surface radiation transformation in the atmosphere. Comparison of the calculated and experimental values of $\mathscr{P}$ above cloudless ocean shows that the radiation absorption in the 8-12 μ window of the real atmosphere exceeds the water vapor absorption used in the calculations. As a result the difference between the measured radiation temperature and the ocean temperature amounts to 15 ± 5° (we assume that the excess absorption is associated with aerosol layers). According to the data obtained aboard the Kosmos 320 satellite this difference amounts to ± 4° in the 10.5-11.5 μ interval.

17. Radiation measurements in the "windows" above clouds make it possible to determine cloud top height h as the level at which the radiation temperature is equal to the temperature of the climatic or standard $T(\zeta)$ profile. The accuracy of h determination above solid clouds is on the order of 0.5-1 km. Cloud height is also determined with an error of the same order from reflected solar radiation measurements in the 0.76 μ oxygen band, which was part of the optical experiment program aboard the Kosmos 320 satellite. To determine h from these measurements we calculate the transmission function of the atmosphere in the O_2 band using the most reliable band molecular constants. To account for solar radiation absorption in the cloud we propose use of the statistical characteristics of the cloud cover boundary vertical structure for the example of the correlations of these boundaries for stratus clouds. The availability of joint information broadens considerably the interpretation capability, specifically it permits solution of the problem of discriminating between snow cover and cloud cover and identification of cirrus cloud cover.

18. Several results presented in the book were used in developing and carrying out an integrated program of optical studies of the atmosphere with the aid of the Kosmos 149, 243, and 320 satellites, and also for interpretation of the experimental data.

The results listed above do not by any means exhaust the variety of problems of interpretation of large-scale measurements of the Earth's radiation field characteristics. The objective of further studies within the framework of the present volume /289 should include: 1) extension and refinement of the optical-meteorological model of the atmosphere for various seasons and geographical regions; 2) development of the theory of radiation transport in a medium with randomly distributed parameters; 3) determination of the physical basis of cloud system spatial structure obtained from optical measurements; 4) improvement of

the methods for statistical regularization of the inverse problems, including the use of adequate a priori information and determination of the real transmission functions together with the vertical temperature and humidity profiles; 5) improvement of the method for determining the height and other characteristics of clouds from radiometric and photometric data, specifically, obtaining reliable corrections for absorption in the clouds.

INTRODUCTION

1.   Kondrat'yev, K.Ya.   Luchistaya Energiya Solntsa (Solar Radiant
     Energy), Gidrometeoizdat, 1954.

2.   Kondrat'yev, K.Ya.   Luchistyi teploobmen v atmosfere (Radia-
     tive Heat Transfer in the Atmosphere), Gidrometeoizdat,
     Leningrad, 1956.

3.   Kondrat'yev, K.Ya.   Aktinonetriya (Actinometry), Gidrometeo-
     izdat, 1965.

4.   Rozenberg, G.V.   Sumerki (Twilight), Fizmatgiz, 1961.

5.   Shifrin, K.S.   Rasseyaniye sveta v mutnoy srede (Light
     Scattering in a Turbid Medium), Gostekhizdat, 1961.

6.   Sobolev, V.V.   Perenos luchistoy energii v atmosferakh zvezd
     i planet (Radiative Energy Transfer in Stellar and Plane-
     tary Atmospheres), Gostekhizdat, 1956.

7.   Feygel'son, Ye.M.   Radiatsionnyye protsessy v sloistoobraznykh
     oblakakh (Radiative Processes in Stratified Clouds),
     Nauka, 1964.

8.   Goode, R.   Atmospheric Radiation.   Basic Theory.   Mir,
     Moscow, Vol. 1, 1966.

9.   Kuznetsov, Ye.S.   Theory of Slant Path Visibility, Izvestiya
     Akad. Nauk SSSR, Seriya geografika i geofizika, No. 5,
     1943.

10. Kondrat'yev, K.Ya.   Meteorologicheskiye sputniki (Weather
     Satellites), Gidrometeoizdat, 1963.

11. Kondrat'yev, K.Ya., et al.   Prakticheskoye ispol'zovaniye
     dannikh meteorologicheskikh sputnikov (Practical Uses of
     Weather Satellite Data), Gidrometeoizdat, 1966.

12. Kondrat'yev, K.Ya., et al.   Posle izlucheniya Zemli kak
     planety (Radiation of the Earth as a Planet), Gidrometeo-
     izdat, 1967.

13. Rockets and Artificial Satellites in Meteorology, Foreign
     Literature Press (IL), Moscow, 1963.

14. Raketnaya i sputnikovaya meteorologiya. Trudy Pervogo mezh-
     dunarodnogo simposiuma po raketnoy i sputnikovoy meteoro-
     logii.(Rocket and Satellite Meteorology. Proceedings of
     the First International Symposium on Rocket and Satellite
     Meteorology), Gidrometeoizdat, 1964.

15. Voprosy interpretatsii dannikh meteorologicheskikh sputnikov
     (Interpretation of Weather Satellite Data), Trudy GGO,
     No. 166, 1964.

16. Interpretatsiya i ispol'zovaniye sputnikovikh dannykh
     (Interpretation and Use of Satellite Data), Trudy Gidromet.
     N-i Tsentra, No. 20, 1968.

17. Vetlov, I.P. Investigation of Cloud Cover and Outgoing
     Radiation by Means of the Satellite Kosmos 122, Meteoro-
     logiya i gidrologiya, No. 1, 1967.

18. Weinstein, M. and V.E. Suomi. Analysis of Satellite In-
     frared Radiation Measurements on a Synoptic Scale.
     Monthly Weather Rev., Vol. 89, No. 11, 1961.

19. Malkevich, M.S., V.M. Pokras and L.I. Yurkova. Measurements
     of Radiation Balance on the Satellite Explorer VII,
     Iskusstv. sputniki Zemli, No. 14, 1962.

20. Sputnikovaya meteorologiya (Satellite Meteorology), Trudy
     GGO, No. 221, 1968.

21. The Nimbus II Data User's Guide. Nat. Space Sci. Data Center.
     Goddard Space Flight Center, 1966, p. 601.

22. Shifrin, K.S., V.Yu. Kolomiytsev and N.P. Pyatovskaya.
     Opredeleniye potoka ukhodyashchey korotkovolnovoy radiatsii
     s pomoshch'yu iskusstvennogo sputnika Zemli (Determination
     of Outgoing Short-Wave Radiative Flux by Means of an
     Artificial Earth Satellite). Trudy GGO, No. 166, 1964.

23. Jones, L.M., F.F. Fischbach and J.W. Peterson. Satellite
     Measurements of Atmosphere Structure by Refraction.
     Planet. Space Sci., Vol. 9, 1962.

24. Tamarskiy, V.I. Determination of Atmospheric Density from
     Measurements of Phase and Angle of Refraction from a
     Satellite, Izvestiya Akad. Nauk SSSR, Seriya fizika atmos-
     fery i okeana, Vol. 4, No. 7, 1968 (see also Vol. 4, No. 8,
     1968).

25. Rozenberg, G.V. and Yu.-A.R. Mullamaa. Possibilities for
     Determining the Wind Speed above an Ocean Surface from
     Observations from Satellites, Izvestiya Akad. Nauk SSSR,
     Seriya Fizika atmosfery i okeana, Vol. 1, No. 3, 1965.

26. Shifrin, K.S. and V.Yu. Kolomiytsov. Opredeleniye skorosti
     vetra i volneniya morya po izmereniyam s ISZ parametrov
     solnechnoi dorozhki. Sputnikovaya meteorologiya (Determina-
     tion of Wind Speed and Sea Swell from Satellite Measurements
     of Solar Trail Parameters. Satellite Meteorology), Trudy
     GGO, No. 221, 1968.

27. Shvets, M.Ye., B.Ye. Shneyerov and L.F. Koloskova. Ob ispol'-
     zovanii resul'tatov radiatsionnikh izmereniy so sputnikov
     v modeli krupnomasshtabnykh atmosfernykh dvizheniy (Use
     of Satellite Radiation Measurement Results in a Model of
     Large-Scale Atmospheric Motions), Trudy GGO, No. 166, 1964.

28. Musaelyan, Sh.A. and A.Z. Chekirda. O chislennoy interpret-
     atsii informatsii ob oblachnosti, postulayushchey s meteo-
     rologicheskikh sputnikov (Numerical Interpretation of In-
     formation on Clouds from Weather Satellites), Trudy GGO,
     No. 166, 1964.

29. Musaelyan, Sh.A. Nekotorye voprosy chislennoy interpretatsii
     oblachnoy informatsii, postulayushchey s iskusstvennykh
     sputnikov Zemli (Aspects of Quantitative Interpretation
     of Information on Clouds from Satellites), Trudy GGO,
     No. 166, 1964.

30. Ganopol'skiy, V.A., A.K. Gorodetskiy and A.M. Kasatkin.   /291
     Scientific Program and Equipment Complex for the Satellite
     Kosmos 149, Izvestiya Akad. Nauk SSSR, Seriya Fizika At-
     mosfery i okeana, Vol. 5, No. 3, 1969.

31. Faraponova, G.P., Ye.F. Klimchuk and B.P. Kozyrev. Method
     and Some Results of Measurement of Earth Short-Wave and
     Long-Wave Radiative Fluxes on Kosmos 149, Izvestiya Akad.
     Nauk SSSR, Seriya Fizika atmosfery i okeana, Vol. 5, No. 4,
     1969.

CHAPTER 1

1. Penndorf, R. Tables of the Refractive Index for Standard Air
    and the Rayleigh Scattering Coefficient for the Spectral
    Region Between 0.2 and 20 μ and their Application to
    Atmospheric Optics. J. Opt. Soc. America, Vol. 47,
    No. 2, 1957.

2. Van de Hulms, G. Scattering of Light by Small Particles
   IL, 1961.

3. Zel'manovich, I.L. and K.S. Shifrin. Tablitsy po svetroas-
   seyaniyu III. Koeffitsienty oslableniya, rasseyaniya i
   luchevogo davleniya (Light Scattering Tables III. Coef-
   ficients for Attenuation, Scattering, and Radiation
   Pressure), Gidrometeoizdat, 1968.

4. Pyaskovskaya-Fesenkova, Ye.V. Issledovaniye rasseyaniya sveta
   v zemnoy atmosfere (Measurements of Attenuation of Solar
   Light in the Upper Atmosphere), Izdatel'stvo Akademii Nauk
   SSSR (AN SSSR), 1957.

5. Faraponova, G.P. Izmereniya oslableniya solnechnogo sveta
   v svobodnoy atmosfere (Measurements of Solar Light Attenua-
   tion in the Upper Atmosphere), Trudy TsAO, No. 32, 1959.

6. Rabinovich, Yu.I. Spektral'noye oslableniye i kontrast v
   svobodnoy atmosfere (Spectral Attenuation and Contrast in
   the Upper Atmosphere), Dissertation, Leningrad, 1961.

7. Knestrik, G.L., T.H. Cosden and J.A. Curcio. Atmospheric
   Scattering Coefficients in the Visible and Infrared Regions.
   J. Opt. Soc. America, Vol. 52, No. 9, 1962.

8. Georgiyevskiy, Yu.S. Issledovaniye spektral'noy prozrachnosti
   prizemnogo sloya vozdukha (Investigation of Spectral
   Transmission of the Surface Air Layer), Dissertation,
   Moscow, 1966.

9. Malkevich, M.S., L.I. Koprova and V.S. Malkova. Metodika
   issledovaniya uglovogo i spektral'nogo raspredeleniya
   otrazhennoy solnechnoy radiatsii i sobstvennogo izlucheniya
   Zemli, Ch. I (Technique for Investigation of the Angular
   and Spectral Distribution of Reflected Solar Radiation and
   Earth Self-Radiation, Part I), Proceedings of the Institute
   for the Physics of the Atmosphere (IFA), 1967.

10. Koprova, L.I. Statistical Characteristics of the Vertical
    Structure of the Aerosol Scattering Coefficient. Izvestiya
    Akademii Nauk SSSR, Seriya fizika atmosfery i okeana,
    Vol. 4, No. 8, 1968 (see also Vol. 5, No. 2, 1969).

11. Selezneva, Ye.S. Atmosfernye aerozoli (yadra kondensatsii)
    (Atmospheric Aerosols (Condensation Nuclei)), Gidrometeoiz-
    dat, 1966.

498

12. Rozenberg, G.V., A.B. Sandomirskiy and V.K. Pyldmaa. Iz-
    mereniya vysotnogo khoda koeffitsienta rasseyaniya v
    stratosfere. "Serebristye oblaka" (Measurement of the
    Behavior of the Scattering Coefficient with Height in the
    Stratosphere, In the collection: "Noctilucent Clouds"),
    Izdatel'stvo Nauka, 1967.

13. Elterman, L. An Atlas of Aerosol Attenuation and Extinction
    Profiles for Troposphere and Stratosphere. Rept. AFCRL,
    Vol. 66, 1966, p. 822.

14. Handbook of Geophysics, Macmillan Co., No. 4, 1960.

15. Dianov-Klokov, V.I. and O.A. Mameyeva. Effect of $(O_2)_2$ and
    $(O_2-N_2)_2$ Groups on the Transmission of the Surface Air
    Layer in the 2800-2300 A Region, Izvestiya Akademii Nauk
    SSSR, Seriya fizika atmosfery i okeana, Vol. 2, No. 12,
    1966.

16. Wyatt, P.J., V.R. Stull and G.N. Plass. The Infrared Trans-
    mittance of Water Vapor. Appl. Opt., Vol. 3, No. 2, 1964.

17. Stull, V.R., P.J. Wyatt and G.N. Plass. The Infrared Trans-
    mittance of Carbon Dioxide. Appl. Opt., Vol. 3, No. 2, 1964.

18. Burch, D.E., D. Gryvnak, E.B. Singleton et al. Infrared
    Absorption by Carbon Dioxide Water Vapor and Minor Atmos-
    pheric Constituents. Res. Rept. Ohio State Univ., Contract
    AF Vol. 19, No. 604, 1962, p. 2633; Appl. Opt., Vol. 2,
    No. 6, 1963.

19. Andreyev, S.D. and A.G. Pokrovskiy. Comparison of Calculated
    H_2O and CO_2 Spectra with Laboratory Measurements, Izvestiya
    Akademii Nauk SSSR, Seriya fizika atmosfery i okeana, Vol.
    4, No. 11, 1968.

20. Golubitskiy, B.M. and N.I. Moskalenko. Spectral Trans-
    mission Functions in H_2O and CO_2 Bands, Izvestiya Akademii
    Nauk SSSR, Seriya fizika atmosfery i okeana, Vol. 4, No. 3,
    1968 (see also Vol. 4, No. 1, 1968).

21. Howard, J.N., D.E. Burch and D. Williams. Near Infrared
    Transmission Through Synthetic Atmospheres. Geophys. Res.
    Paper No. 40, Air Force Cambridge Res. Center 1955; J.
    Opt. Soc. America, Vol. 46, No. 3, 1956.

22. Koprova, L.I. and M.S. Malkevich. Teplovoye izlucheniye
     sfericheskoy Zemli. Trudy 5-to Vses. coveshch. po aktino-
     metrii i atmosfernoi optike (Thermal Radiation from the
     Spherical Earth. Proc. 5th All-Union Conf. on Actinometry
     and Atmospheric Optics), Izdatel'stvo AN SSSR, 1964.

23. Kiseleva, M.S., B.S. Neporent and Ye.O. Fedorova. Absorp-
     tion of Infrared Radiation with Unresolved spectral Struc-
     ture for Inclined Paths in the Atmosphere, Izvestiya
     Akad. Nauk SSSR, seriya fizika atmosfery i okeana, Vol. 3,
     No. 6, 1967.

24. Taylor, J.N. and H.W. Yates. Atmospheric Transmission in
     the Infrared. J. Opt. Soc. America, Vol. 47, No. 3.
     1957.

25. Barry, P.J., C.B. Farmer and D.B. Lloyd. Atmospheric Trans-
     mission Measurements in the 4.3 μ CO_2 Band at 5200 m Alti-
     tude. Appl. Opt., Vol. 4, No. 9, 1965.

26. Gates, D.M., R.F. Calfee and D.M. Hansen. Computed Trans-
     mission Spectra for 2.7 Micron H_2O Band. Appl. Opt.,
     Vol. 2, No. 11, 1963.

27. Livshits, G.Sh., V.Ye. Pavlov and S.N. Milyutin. O poglosh-
     chenii sveta atmosfernymi aerozolyami (Absorption of
     Light by Atmospheric Aerosols), Trudy Instituta Akad. Nauk
     Kaz. SSR, Vol. 7, 1966.

28. Sekihara, K. On the Absorption Properties of Atmospheric   /292
     Dust Particles as Considered from Various Kinds of Ground
     Level Observations, Report of the International Symposium
     on Radiation, Leningrad, 1964.

29. Zdunkawsi, W., D. Henderson and J.V. Hales. The Influence of
     Haze of Infrared Radiation Measurements Detected by Space
     Vehicles. Tellus, Vol. 17, No. 2, 1965.

30. Foitzik, L. and H. Zschack. Measurement of the Spectral
     Scattering Function of Air Near the Ground with Good Visi-
     bility, Dew, and Fog. Z. Meteorol, Vol. 7, No. 1, 1953.

31. Barteneva, O.D., Ye.N. Dovgyallo and Ye.A. Polyakova. Eks-
     perimental'nye issledovaniya opticheskikh svoystv prizem-
     nogo sloya atmosfery (Experimental Investigations of the
     Optical Properties of the Surface Atmospheric Layer),
     Trudy GGO, No. 220, 1967.

32. Rozenberg, G.V. Properties of Atmospheric Aerosols from Optical Investigations, Izvestiya Akad. Nauk SSSR, seriya fizika atmosfery i okeana, Vol. 3, No. 9, 1967.

33. Gorchakov, G.N. Eksperimental'noye issledovaniye matritsy rasseyaniya sveta prizemnym vozdukhom i nekotopye svoystva atmosfernoy dymki (Experimental Investigation of the Matrix for Light Scattering by Surface Air and Some Properties of Atmospheric Haze), Dissertatatsiya, Moscow, 1966.

34. Lyubovtseva, Yu.S. Issledovaniye oreol'noy chasti indikatrisy rasseyaniya i mikrostruktury aerozolya v prizemnom sloye vozdukha (Investigation of the Halo Part of the Scattering Index in the Surface Air Layer) Dissertatsiya, Moscow, 1966.

35. Lifshits, G.Sh. Rasseyaniye sveta v atmosfere, (Scattering of Light in the Atmosphere) Chapter I Alma-Ata, 1965.

36. Sandomirskiy, A.B., N.P. Al'tovskaya and G.I. Trifonova. Brightness Indices at Heights 8 to 17.5 km, Izvestiya Akad. Nauk SSSR, seriya geofizika, No. 6, 1964.

37. Krinov, Ye.L. Spektral'naya otrazhatel'naya sposobnost pripodnykh obrazovaniy (Spectral Reflectance of Natural Formations), Izdatel'stvo AN SSSR, Moscow-Lenin-grad, 1947.

38. Krasil'shchikov, L.B., O.I. Golikov and Ye.P. Novosel'tsev. Fotoelektricheskiye izmereniya spektral'nykh otnositel'nykh koeffitsiyentov yarkosti (Photoelectric Measurements of Relative Spectral Brightness Coefficients), Trudy GGO, No. 68, 1957 (see also Trudy GGO, No. 203, 1967).

39. Bartman, F.L. The Reflectance and Scattering of Solar Radiation by the Earth. Techn. Rept. Univ. Michigan, 05863-11-T, February, 1967.

40. Middleton, W.E.K. and A.G. Mungal. The Luminous Directional Reflectance of Snow. J. Opt. Soc. America, Vol. 42, No. 8, 1952.

41. Kozlova, V.P. and Ye.O. Fedorova. Spatial Distribution of Lower-Level Cloud Brightness, Izvestiya Akad. Nauk SSSR, seriya geofizika, No. 7, 1962.

42. Zirkind, R. The Near Medium IR Earth Albedo, its Use for Cloud Height Determination. Planet. Space Sci., Vol. 13, No. 4, 1965.

43. Blau, H.H., R.P. Espinola and E.C. Reifenstein. Near Infrared Scattering by Sunlit Terrestrial Clouds. Appl. Opt., Vol. 5, No. 4, 1966.

44. Hovis, W.A. and M. Tobin. Spectral Measurements from 1.6 to 5.4 μ of Natural Surfaces and Clouds. Appl. Opt., Vol. 6, No. 8, 1967; Vol. 5, No. 5, 1966; Vol. 7, No. 6, 1968.

45. Coulson, K.L., J.V. Dave and Z. Sekera. Tables Related to Radiation Emerging from Planetary Atmospheres with Rayleigh Scattering. Univ. California Press, 1960.

46. Chandrasekhar, S. Radiative Transfer IL, 1953.

47. Feygel'son, E.M., M.S. Malkevich and S.Ya. Kogan. Raschet yarkosti sveta v atmosfere pri anizotropnom rasseyanii (Calculation of Atmospheric Brightness with Anisotropic Scattering) Chapter I, Trudy In-ta Fizika Atmosfery, Vol. 1, 1958.

48. Atroshenko, V.S., K.S. Glazova and M.S. Malkevich. Raschet yarkosti sveta v atmosfere pri anizotropnom rasseyanii, (Calculation of Atmospheric Brightness with Anisotropic Scattering) Chapter II, Trudy In-ta fiziki atmosfery, Vol. 2, 1962.

49. Shifrin, K.S. and N.I. Minin. K teorii negorizontal'noy vidimosti (Theory of Non-Horizontal Visibility) Transactions of the Main Geophysical Observatory (Trudy GGO), No. 68, 1957.

50. Shifrin, K.S. and N.P. Pyatovskaya. Tablitsy neploskoy dal'nosti vidimosti i yarkosti bezoblachnogo neba (Tables of Non-Two-Dimensional Visible Range and Brightness of the Cloud-Free Sky), Gidrometeoizdat, 1961.

51. Fraser, R.S. Computed Intensity and Polarization of Light Scattered Outwards from the Earth and on Overlying Aerosols. J. Opt. Soc. America, Vol. 54, No. 2, 1964.

52. Sobolev, V.V. Perenos luchistoy energii v atmosfere zvezd i planet (Radiative Transfer in Stellar and Planetary Atmospheres), Gostekhizdat, 1956.

53. Sekera, Z. Recent Developments in the Study of the Polarization of Sky Light. Advances in Geophysics, N.Y., Acad. Press Inc., Vol. 3, 1956.

54. Malkevich, M.S. Angular and Spectral Distribution of Radiation Reflected to Space by the Earth, Iskusstvennye sputniki Zemli, No. 14, 1962.

55. Arking, A. Angular Distribution of Scattered Radiation as Measured from "Tiros". Papers International Symposium on Radiation, Leningrad, U.G.G.I. Monogr. Paris, 1965, p. 28.

56. Ruff, I., R. Koffler,|S. Fritz et al. Angular Distribution of Solar Radiation Reflected from Clouds as Determined from Tiros IV Radiometer Measurements. ESSA Techn. Rept. NESC-38, Washington, 1967.

57. Chapurskii, L.I., V.V. Klemin and N.I. Andreyeva. Spektral'-naya yarkost' oblakov i ob'yektov landshafta v vidimom i blizhnem infrakrasnom uchastkakh spektra (Spectral Brightness of Clouds and Natural Objects in the Visible and Near IF), Trudy GGO, No. 221, 1968 (see also Trudy GGO, No. 196, 1966).

58. Lebedinskiy, A.I., V.A. Krasnopol'skiy and A.P. Kuznetsov. Investigation of Atmospheric Radiation in the Visible and UV. In the collection: Issledovaniya kosmich.| prostranstva | (Deep Space Investigations), Izdatel'stvo Nauka, 1965.|

59. Krasnopol'skiy, V.A., A.P. Kuznetsov and A.I. Lebedinskiy. UV Spectrum of the Earth from Measurements on Kosmos 65, Geomagnetizm i aeronomiya, Vol. 6, No. 2, 1966.

60. Krasnopol'skiy, V.A. UV Spectrum of Radiation Reflected by the Atmosphere and its Use to Determine the Total Content and Vertical Distribution of Atmospheric Ozone, Geomagnetizm i aeronomiya, Vol. 6, No. 2, 1966.

61. Friedman, R.M., R.O. Rawcliffe and C.E. Meloy. Radiance of the Upper Atmosphere in the Middle Ultraviolet. J. Geophys. Res., Vol. 68, 1963, p. 24.

62. Rawcliffe, R.D.,and D.D. Elliot. Latitude Distribution of Ozone at High Altitudes Deduced from a Satellite Measurement of the Earth's radiance at 2840 Å. J. Geophys. Res., Vol. 71, No. 2, 1966.|

63. Brinkmann, R.T., A.E.S. Green and C.A. Barth. Atmospheric Scattering of the Solar Flux in the Middle Ultraviolet. Appl. Opt. Vol. 6, No. 3, 1962. |

64. Hennes, J.P., W.R. Fowler and L. Dunkelman. Middle Ultra-
    violet Day Radiance of the Atmosphere. Trans. Amer.
    Geophys. Union, Vol. 43, 1962, p. 436.

65. Band, H.E. and L.C. Block. Spectral Radiance Measurements
    of the Earth from High Altitudes. Appl. Opt., Vol. 4,
    No. 3, 1965.

66. Green, A.E.S. Attenuation by Ozone and the Earth Albedo in
    the Middle Ultraviolet. Appl. Opt., Vol. 3, No. 2, 1964.

67. Germogenova, T.A. and M.S. Malkevich. Spectral Distribution
    of Radiation Reflected by the Earth in the 0.20 - 0.34 μ
    Ozone Absorption Band, Izvestiya Akad. Nauk SSSR, seriya
    fizika atmosfery i okeana, Vol. 1, No. 9, 1965.

68. Germogenova, T.A. and L.D. Krasnokutskaya. Angular and
    Vertical Distribution of Radiation Reflected by the
    Earth in the 0.20 - 0.34 μ Ozone Absorption Band, Izvestiya
    Akad. Nauk SSSR, seriya fizika atmosfery i okeana, Vol. 1,
    No. 11, 1965.

69. Tohmatsu, T. The Schuman — Runge Day Airglow. Rept. Iono-
    sphere and Space Res. Japan, Vol. 17, 1963, p. 3.

70. Germogenova, T.A. Nature of the Solution of the Transfer
    Equation for a Two-Dimensional Layer, Zhurnal vych.matem.
    i matem.fiz., Vol. 1, No. 6, 1961.

71. Johnson, F.S. and L.D. Purcell. Direct Measurements of the
    Vertical Distribution of Atmospheric Ozone to 70 km Alti-
    tude. J. Geophys. Res., Vol. 57, No. 2, 1952.

72. Henenway, C.L., R.K. Soberman and G. Witt. Sampling of
    Noctilucent Cloud Particles. Tellus, Vol. 16, No. 1, 1964.

73. Chu, Chao-min, C.C. George and Clark W. Churchill. Tables
    of Angular Distribution Coefficients for Light Scattering
    by Spheres. Engng. Res. Inst. Univ. Michigan, 1957.

74. Zirkind, R. On Infrared Spectral Reflectance of Terrains
    from Airborne Platforms. Planet. Space Sci., Vol. 13,
    No. 10, 1965.

75. Kushpil', V.I. and K.F. Khazak. Measurement of the Planetary
    Brightness of the Earth in the 1.40 μ Water Vapor Absorp-
    tion Band and in the 1.25 μ Transmission Window, Izvestiya
    Akad. Nauk SSSR, seriya fizika atmosfery i okeana, Vol. 2,
    No. 7, 1966.

504

76. Avaste, O., Yu. Mullamaa and K.S. Shifrin. Pole ukhodyashchey korotkovolnovoy radiatsii v vidimoy i blizkoy infrakrasnoy oblastyakh spektra pri neortotropnoy podstilayushchey poverkhnosti (Field of Outgoing Short-Wave Radiation in the Visible and Near IF Spectral Regions with a Non-Orthotropic Underlying Surface), Issl. po fizike atmosfery In-ta fiiziki i astronomii, Akad. Nauk Est. SSR, No. 6, 1964.

77. Shifrin, K.S. and I.P. Pyatovskaya. Pole korotkovolnovoy radiatsii nad tipichnymi podstilayushchimi poverkhnostyami (Short-Wave Radiation Field Above Typical Underlying Surfaces), Trudy GGO, No. 166, 1964.

78. Avaste, O.A. Resul'taty raschetov intensivnostey i potokov ykhodyashchego izlucheniya pri sfericheskoy Zemle v blizkoy infrakrasnoy oblasti spektra (Results of Calculations of Intensities and Fluxes of Outgoing Radiation in the Near IF, for the Spherical Earth Model), Trudy GGO, No. 166, 1964.

79. Germogenova, T.A., L.I. Koprova and T.A. Sushkevich. Investigation of the Angular, Spatial and Spectral Structure of the Earth's Brightness Field for a Typical Model of the Spherical Atmosphere, Izvestiya Akad. Nauk SSSR, seriya fizika atmosfery i okeana, Vol. 5, No. 12, 1969.

80. Malkevich, M.S. Effect of Non-Orthotropy of the Underlying Surface on the Scattered Light in the Atmosphere, Izv. AN SSSR, ser. geofiz., No. 3, 1960.

81. Kuznetsov, Ye.S. Accounting for Diffuse Light Reflection by the Earth's Surface in Atmospheric Scattering, Izv. AN SSSR, ser.geogr. i geofiz., No. 9, 1945.

82. Kuznetsov, Ye.S. and B.V. Ovchinskiy. Resul'taty chislennogo resheniya integral'nogo uravneniya teorii rasseyaniya sveta v atmosfere (Results of Numerical Solution of an Integral Equation in the Theory of Light Scattering by the Atmosphere), Tr. geofiz. in-ta AN SSSR, Vol. 131, No. 4, 1949.

83. Jefferies, J.T. Radiative Transfer with Central Sources of Non-Uniform Directional Intensity. Proc. Phys. Soc. Sect. B, Vol. 69, 1956, p. 437; Optica acta, Vol. 2, No. 3, 1955.

84. Giovanelli, R.G. and J.T. Jefferies. Radiative Transfer with Distributed Sources. Proc. Phys. Soc. Sect. B, Vol. 69, 1956, p. 443, B.

85. Malkevich, M.S. Accounting for Underlying Surface Irregularities in Light Scattering in the Atmosphere, Izv. AN SSSR, ser.geofiz., No. 5, 1957.

86. Malkevich, M.S. Effect of Horizontal Changes of Underlying Surface Albedo on Scattering of Light in a Homogeneous Atmosphere, Izv. AN SSSR, ser. geofiz., No. 8, 1958.

87. Malkevich, M.S. Approximate Method for Calculating Horizontal Changes of Underlying Surface Albedo in Scattering of Light in the Atmosphere, Izv. AN SSSR, ser. geofiz., No. 2, 1960.

88. Gradshteyn, I.S. and I.M. Ryzhik. Tablitsy integralov, summ, ryadov i proizvedeniy (Tables of Integrals, Sums, Series and Products), Gos. Izdatel'stvo fiz.-matem. lit., 1962.

89. Sobolev, V.V. and N.I. Minin. Scattering of Light in the $\underline{/294}$ Spherical Atmosphere, Iskusstvennye sputniki Zemli, No. 14, 1962.

90. Minin, N.I. and V.V. Sobolev. Scattering of Light in the Spherical Atmosphere: II, III, Kosmich.issled., Vol. 1, No. 2, 1963; Vol. 2, No. 4, 1964.

91. Smoktiy, O.I. Multiple Light Scattering in the Homogeneous Spherically Symmetrical Planetary Atmosphere, Izv. AN SSSR, ser. fizika atmosfery i okeana, Vol. 3, No. 3, 1967 (see also Vol. 3, Nos. 3 and 4, 1967).

92. Lenoble, J. and Z. Sekera. Equation of Radiative Transfer in Planetary Spherical Atmosphere. Proc. Nat. Acad. Sci. USA, Vol. 47, No. 3, 1961.

93. Sekera, Z. and W. Viezce. Distribution of the Intensity and Polarization of the Diffusely Reflected Light Over a Planetary Disc. Rept. USAF Project RAND. Contract. N AF49 (368)=700, 1961.

94. Marchuk, G.I. and G.A. Mikhaylova. O reshenii zadach atmosfernoy optiki metodom Monte-Karlo (Solution of Problems in Atmospheric Optics by the Monte-Carlo Method). Report of the Computation Center of the Siberian Dept. of the AN SSSR (VTs SO), 1966.

95. Marchuk, G.I. and G.A. Mikhaylov. Results of Solution of Some Atmospheric Optics Problems by a Monte-Carlo Method, Izv. AN SSSR, ser. fizika atmosfery i okeana, Vol. 3, No. 4, 1967.

96. Rozenberg, G.V. and V.V. Tereshkova-Nikolayeva. Stratospheric Aerosols from Measurements from a Space Vehicle. Izv. AN SSSR, ser. fizika atmosfery i okeana, Vol. 1, No. 4, 1965.

97. Germogenova, T.A. and T.A. Sushkevich. Osesimmetrichnaya zadacha o rasprostranenii izlucheniya v sfericheskoy sisteme (Axisymmetric Problem of Radiation Propagation in a Spherical System), Report of the Institute of the Problems of Mechanics (IPM), Moscow, 1966.

CHAPTER 2

1. Wark, D.Q., G. Yamamoto and J.H. Lienesh. Methods of Estimating Infrared Flux and Surface Temperature from Meteorological Satellites. J. Atmos. Sci., Vol. 19, No. 5, 1962.

2. Kondrat'yev, K.Ya. and Yu.M. Timofeyev. Use of Approximate Methods of Accounting for Atmospheric Nonuniformities in Calculating the Transmission Function for a Water Vapor Rotational Band. Izv. AN SSSR, ser. fizika atmosfery i okeana, Vol. 3, No. 3, 1967.

3. Palmer, C.H. Experimental Transmission Functions for the Pure Rotation Band of Water Vapor. J. Opt. Soc. America, Vol. 50, No. 12, 1960.

4. Murcray, D., F. Murcray and W. Williams. Distribution of Water Vapor in the Stratosphere as Determined from Infrared Absorption Measurements. J. Geophys. Res., Vol. 67, No. 2, 1962; J. Opt. Soc. America, Vol. 51, No. 1, 1961.

5. Kondrat'yev, K.Ya. and Yu.M. Timofeyev. Transmission Function for a Water Vapor Rotational Band. Izv. AN SSSR, ser. fizika atmosfery i okeana, Vol. 2, No. 3, 1966.

6. Yamamoto, G. On a Radiation Chart. Sci. Rept. Tohoku Univ., Geophys., Series 5, 1952, p. 4.

7. Elsasser, W.M. and M.F. Culberston. Atmospheric Radiation Tables. Meteorol. Monthly, Vol. 4, 1960, p. 23.

8. Zhevakin, S.A. and A.P. Naumov. Absorption of Electromagnetic Radiation by Water Vapor at Wavelengths 10 μ – 2 cm in the Upper Atmospheric Layers, Geomagnetism i aeronomiya, Vol. 3, No. 4, 1963.

9. Roach, W.T. and R.M. Goody. Absorption and Emission in the Atmospheric Window from 770 to 1250 cm^{-1}. Quart. J. Roy. Meteorol. Soc., Vol. 84, 1958, p. 362.

10. Saiedy, F. and R.M. Goody. The Solar Intensity at 11 μ. Monthly Notices Roy. Astron. Soc., Vol. 119, No. 3, 1959.

11. Bignell, K., F. Saiedy and P.A. Sheppard. On Atmospheric Infrared Continuum. J. Opt. Soc. America, Vol. 53, 1963, p. 4.

12. Kondrat'yev, K.Ya., I.Ya. Badinov and S.B. Andreyev. Some Results of Ground Investigations of the IR Absorption Spectrum and Thermal Radiation of the Atmosphere. Izv. AN SSSR, ser. fizika atmosfery i okeana, Vol. 1, No. 4, 1965.

13. Badinov, I.Ya. and S.A. Andreyev. Transparency of the Earth's Atmosphere and Division of the Optical Thickness into Components in the 8-13 μ IR Region. Problemy fiziki atmosfery, No. 3, 1965.

14. Yurganov, L.N. and V.I. Dianov-Klokov. Dependence of Diffuse Attenuation on Humidity in the 8-13 μ Window. Izv. AN SSSR, ser. fizika atmosfery i okeana, Vol. 8, No. 3, 1972.

15. Shukurov, A.Kh. Issledovaniye variatsiy propuskaniya atmosfery v spektral'nom diapazone 0.3-14 μ (Investigation of Atmospheric Transmission Variations in the 0.3-14 μ Spectral Range), Dissertatsiya, Moscow, 1972.

16. Girard, A. and M.-P. Lemaitre. Profiles experimentaux de l'horizon infrarouge de la terre (Experimental Profiles at the Infrared Horizon on the Earth), XXII-me Reunion Plen. COSPAR, Prague, 1969.

17. Bignell, K.J. The Water-Vapor Infrared Continuum. Quart. J. Roy. Meteorol. Soc., Vol. 196, 1970, p. 409.

18. Carlon, H.R. Infrared Emission by Fine Water Aerosols and Fogs. Appl. Opt., Vol. 9, No. 9, 1970.

19. Carlon, H.R. Model for Infrared Emission of Water Vapor Aerosol Mixtures. Appl. Opt., Vol. 10, No. 10, 1971.

20. Madden, R.P. A High Resolution Study of CO_2 Absorption /295 Spectra Between 15 and 18 Microns. J. Chem. Phys., Vol. 35, 1961, p. 16.

21. Yamamoto, G. and T. Sasamori. Calculation of the Absorption of the 15 μ Carbon Dioxide Band. Sci. Rept. Tohoku Univ. Geophys. Series 5, Vol. 10, No. 10, 1958; Vol. 13, No. 1, 1961.

508

22. Drayson, S.R. and C. Young. The Frequencies and Intensities of Carbon Dioxide Absorption Lines Between 12 and 18 Microns. Univ. Michigan. Dept. Aerospace Engng. Techn. Rept. 08183-1-T, November 1967.

23. Drayson, S.R. Atmospheric Slant Path Transmission in the 15 μ CO_2 Band. Techn. Rept. 05863-6-T. Univ. Michigan, Dept. Aeronaut. and Astronaut. Engng., November 1964.

24. Shved, G.M. and I.V. Tsaritsyna. Infrared Radiation Absorption Runctions in the Mesosphere and the Upper Stratosphere, Problemy fiziki atmosfery, No. 1, 1963.

25. Drayson, S.R., S.Y. Li and C. Young. Atmospheric Absorption by Carbon Dioxide, Water Vapor and Oxygen. Final Rept. 08183-2-F, Univ. Michigan, Dept. Aerospace Engng., February 1968.

26. Kaplan, L.D. and D.F. Eggers. Intensity and Line Width of the 15-micron CO_2 Band Determined by Curve-of-Growth Method. J. Chem. Phys., Vol. 25, 1956, p. 856.

27. Young, C. Tables for Calculating the Voigt Profiles. Univ. Michigan Dept. Aerospace Engng., Techn. Rept. 05863-7-T, July 1965.

28. Burch, D.E., E.B. Sigleton, W.L. France et al. Absorption Line Broadening in the Infrared. Appl. Opt., Vol. 1, No. 3, 1962.

29. Kondrat'yev, K.Ya. and Yu.M. Timofeyev. Computer Modeling of Transmission Functions for Narrow Spectral Intervals of the 15 μ CO_2 Band. Izv. AN SSSR, ser. fizika atmosfery i okeana, Vol. 5, No. 4, 1969.

30. Wark, D.Q., F. Saiedy and D.G. James. Indirect Measurement of Atmospheric Temperature Profiles from Satellites. VI High-Altitude Balloon Testing. Monthly Weather Rev., Vol. 95, No. 7, 1967.

31. Lebedinskiy, A.I., D.N. Glovatskiy and V.I. Tulupov. Infrared Spectrophotometry of Earth Thermal Radiation. In the collection: Issled. kosmich. prostr. (Investigation of Space), Izdatel'stvo Nauka, 1965.

32. Lebedinskiy, A.I., V.G. Boldyrev and V.I. Tulupov. Meteorological Interpretation of Spectra of Outgoing Radiation, Recorded on the Kosmos Satellites, Geomagnetizm i aeronomiya, Vol. 8, No. 1, 1968.

33. Lebedinskiy, A.I., T.G. Polyakova and V.I. Tulupov. Angular and Spectral Distribution of Earth Infrared Radiation to Space Near the Horizon, from Satellite Observations, Geomagnetizm i aeronomiya, Vol. 8, No. 2, 1968.

34. Block, L.C. and A.S. Zachor. Inflight Satellite Measurements of Infrared Spectral Radiance of the Earth. Appl. Opt., Vol. 3, No. 2, 1964.

35. Chaney, L.W., L.T. Loh and M.T. Surh. Fourier Transform Spectrometer for the Measurement of Atmospheric Thermal Radiation. Univ. Michigan, Dept. Aerospace Engng., Techn. Rept 05863-12-T, May 1967.

36. Kondrat'yev, K.Ya. and K.Ye. Yakushevskaya. Spectral Distribution of Outgoing Thermal Radiation, Problemy fiziki atmosfery, No. 2, 1963.

37. Malkevich, M.S. Nekotorye voprosy interpretatsii polya ukhodyashchey radiatsii Zemli (Some Problems in Interpretation of the Field of Outgoing Earth Radiation), Trudy GGO, No. 166, 1964.

38. McGee, R.A. An Analytical Infrared Radiation Model of the Earth. Appl. Opt., Vol. 1, No. 5, 1962.

39. Lienesch, J.H. and D.Q. Wark. Infrared Limb Darkening of the Earth from Statistical Analysis of Tiros Data. J. Atmos. Sci., Vol. 6, No. 4, 1967.

40. Kuznetsov, Ye.S. Radiative Equilibrium of a Gaseous Envelope Surrounding a Perfectly Black Sphere, Izv. AN SSSR, ser. geofiz., No. 3, 1951.

41. Kondrat'yev, K.Ya. and K.Ye. Yakushevskaya. Angular Distribution of Outgoing Thermal Radiation in Various Spectral Regions, Iskusstvennye sputniki Zemli, No. 14, 1962 (see also Trudy GGO, No. 166, 1964; and Problemy fiziki atmosfery, Collection 2, 1963).

42. Kondrat'yev, K.Ya. and Kh.Yu. Niilisk. Nekotorye resul'taty teoreticheskikh raschetov uglovogo raspredeleniya teplovogo izlucheniya Zemli kak planety v real'nykh usloviyakh (Some Results of Calculations of the Angular Distribution of Earth Planetary Thermal Radiation Under Actual Conditions), Trudy GGO, No. 166, 1964.

43. Hanel, R.A., W.R. Bandeen and B.J. Conrath. The Infrared Horizon of the Planet Earth. J. Atmos. Sci., Vol. 20, No. 2, 1963.

44. Wark, D.Q., J. Alishouse and G. Jamamoto. Variation of the Infrared Spectral Radiance Near the Limb of the Earth. Appl. Opt., Vol. 3, No. 2, 1964.

45. Koprova, L.I. and M.S. Malkevich. Thermal Radiation of the Spherical Atmosphere, Kosmich. issled., Vol. 2, No. 6, 1964.

46. Kolosov, S.G. Dependence of the Field of Outgoing Radiation of the Earth and the Troposphere on the Temperature Field, Iskusstvennye sputniki Zemli, No. 14, 1962.

47. Kostyanoy G.N. Dependence of Outgoing Flux of Long-Wave Radiation of the Earth and the Troposphere on the Temperature of the Mean Energy Level, Izv. AN SSSR, ser. fizika atmosfery i okeana, Vol. 1, No. 7, 1965.

48. Kislovskiy, L.D. Optical Characteristics of Water and Ice, Optika i Spektroskopiya, Vol. 7, No. 3, 1960.

49. Arlt, H. and H.J. Belle. Investigation of the Infrared /296
Emission Spectrum of the Atmosphere and Earth. Part 1. Angle Dependent Reflectivity of Natural Surfaces, 1-12 micron. Fin Sci. Rept. AF 61 (52) - 778. Meteorol Instr., Munich, August, 1968.

50. Gier, I.T., R.V. Dunkle and J.T. Bevans. Measurements of Absolute Spectral Reflectivity from 1.0 - 15 µ. J. Opt. Soc. America, Vol. 44, No. 2, 1964, p. 558.

51. Hovis, W.A. Optimum Wavelength Intervals for Surface Temperature Radiometry. Appl. Opt., Vol. 5, No. 5, 1966.

52. Eisner, L., E.E. Bell, J. Young et al. Spectral Radiance of Sky and Terrain at Wave Lengths Between 1 and 20 microns. III. Terrain Measurements. J. Opt. Soc. America, Vol. 52, No. 2, 1962.

53. Yamamoto, G., M. Tanaka and K. Kamitani. Radiative Transfer in Water Clouds in the 10-micron Window Region. J. Atmos. Sci., Vol. 23, No. 3, 1966.

54. Boldyrev, V.G. Calculation of Atmospheric Transfer Functions in the 8 - 12 µ Range for Land Areas in the Northern Hemisphere, Izv. AN SSSR, ser. fizika atmosfery i okeana, Vol. 1, No. 7, 1965.

55. Malkevich, M.S., V.I. Syachinov and L.G. Ismotina. Some Results of Investigations of Earth Brightness by Means of Kosmos 149, Izv. AN SSSR, ser. fizika atmosfery i okeana, Vol. 5, No. 3, 1969.

56. Yakushevskaya, K.Ya. Effect of Refraction on the Intensity
     of Outgoing Long-Wave Radiation, Izv. AN SSSR, ser.
     fizika atmosfery i okeana, Vol. 3, No. 7, 1967.

57. Markov, M.N., Ya.I. Merson and M.R. Shamilev. Investigation
     of the Thermal Radiation Field of the Stratosphere and
     Troposphere and Troposphere in the IR Spectrum, Using
     Geophysical Balloons, Kosmich, issled., Vol. 1, No. 2,
     1963.

58. Bazhylin, O.A., A.V. Karmashev and M.N. Markov. Investiga-
     tion of Angular and Spectral Distribution of Earth Radia-
     tion in the IR Spectrum by Means of Kosmos 45, Kosmich.
     issled., Vol. 4, No. 4, 1966.

59. Liventsov, A.V., M.N. Markov and Ya.I. Merson. Investigation
     of Angular Distribution of Earth Thermal Radiation to
     Deep Space During the Ascent of the Geophysical Rocket on
     27 August 1958, Kosmich. issled., Vol. 4, No. 4, 1966.

CHAPTER 3

1. Obukhov, A.M. Statistical Orthogonal Expansions of Empirical
    Functions, Izv. AN SSSR, ser. geofiz., No. 3, 1960.

2. Bagrov, N.A. Analiticheskoye predstavleniye posledovatel'-
    nosti meteorologicheskikh poley posredstvom estestvennykh
    ortogonal'nykh predstavleniy (Analytical Representation
    of a Sequence of Meteorological Fields by Means of Natural
    Orthogonal Representations), Tr. TsII, No. 74, 1959.

3. Anderson, T. Vvedeniye v mnogomernyi statisticheskii analiz
    (Introduction to Multi-Dimensional Statistical Analysis),
    Gosizdat, 1963.

4. Gandin, L.S. Ob optimal'noi interpolyatsii i ekstrapolyatsii
    meteorologicheskikh poley (Optimum Interpolation and Extra-
    polation of Meteorological Fields), Trudy GGO, No. 114,
    1963.

5. Gandin. L.S. and V.P. Boltenkov. K metodike obosnovannogo
    analiza aktinometricheskoy informatsii s meteorologicheskikh
    sputnikov Zemli (Method of Basic Analysis of Actinometric
    Information from Meteorological Earth Satellites), Trudy
    GGO, No. 166, 1964.

6. Popov, S.M. Some Statistical Characteristics of the Verti-
    cal Structure of the Temperature and Humidity Fields,
    Izv. AN SSSR, ser. fizika atmosfery i okeana, Vol. 1,
    No. 1, 1965.

7. Boltenkov, V.P. Issledovaniye statisticheskoy makrostruktury temperatury vozdukha (Investigation of the Statistical Micro-Structure of Air Temperature), Trudy GGO, No. 165, 1965.

8. Boldyrev, V.G., L.I. Koprova and M.S. Malkevich. Calculation of Variations of Vertical Temperature and Humidity Profiles During Determination of Underlying Surface Temperature from the Outgoing Radiation, Izv. AN SSSR, ser. fizika atmosfery i okeana, Vol. 1, No. 7, 1965 (see also Trudy GMTs, No. 11, 1966).

9. Scherhag, R. Results of Balloon Ascents of the Radial Probe Station at the Berlin Free University Institute for Meteorology and Geophysics. Abhandl. Inst. Meteorol. and Geophys., Vol. 21, No. 9, 1965.

10. Mertsialova, O.B. Metodika rascheta vertikal'nykh korrelyatsionnykh svyazey temperatury i davleniya v svobadnoy atmosfere i nekotopye vyvody iz polychennykh resul'tatov (Method of Computing Vertical Temperature and Pressure Correlations in the Upper Atmosphere and Some Conclusions from the Results Obtained), Transactions of the Scientific Research Institute of Aeroclimatology (Trudy NIIAK), No. 30, 1965.

11. Stel'makh, F.N. Vertikal'nye korrelyatsionnye svyazy temperatury v svododnoy atmosfere nad severnym polushariem (Vertical Temperature Correlations in the Upper Atmosphere Over the Northern Hemisphere), Trudy NIIAK No. 30, 1965.

12. Komarov, V.S. Statistical Structure of Vertical Humidity Profiles, Izv. AN SSSR, ser. fizika atmosfery i okeana, Vol. 4, No. 11, 1968.

13. Komarov, V.S. Statisticheskaya struktura polya vlazhnosti v svobodnoy atmosfere nad territoriei SSSR (Statistical Structure of the Humidity Field in the Upper Atmosphere Over USSR Territory), Trudy NIIAK, No. 70, 1971.

14. Laktionov, A.G., Yu.S. Lyubovtseva and M.S. Malkevich. Some Statistical Characteristics of the Micro-Structure in the Surface Atmospheric Layer, Izv. AN SSSR, ser. fizika atmosfery i okeana, Vol. 9, No. 2, 1973.

15. Malkevich, M.S. and I.P. Polovina. Statistical Characteristics of the Vertical Structure of Stratified Cloud Boundaries and Meteorological Elements, Izv. AN SSSR, ser. fizika atmosfery i okeana, Vol. 1, No. 10, 1965.

16. Rukhovets, L.V. Statistically Optimal Representations of /297
the Vertical Distributions of Some Meteorological Elements,
Izv. AN SSSR. ser. geofizika, No. 4, 1963 (see also Trudy
GGO, No. 165, 1964).

17. Mertsialova, O.B. and M.V. Sokolova. Statisticheskiye svyazy
mezhdu davleniyem na raznykh urovnyakh v svodobnoi atmos-
fere (Statistical Pressure Correlations at Different Heights
in the Upper Atmosphere), Trudy NIIAK, No. 30, 1965.

18. Cole, A. and A. Court. Density Distribution Interlevel
Correlations and Variation with Wind. Air Force Surveys
in Geophysics, Vol. 151, 1962. Air Force Cambridge Res.
Lab., Res. Rept 64 - 815.

19. Shafrin, Yu.A. Statisticheskiye kharakteristiki ozonosfery
kak istochnik dopolnitel'noy v sputnikovoy i nazemnoy
ozonometrii. Aktinometriya i optika atmosfery (Statisti-
cal Characteristics of the Ozonosphere as an Additional
Source in Ground-Based and Satellite Ozonometry. Actinometry
and Optics of the Atmosphere), Trudy VI Mezhved, soveshch.
po aktin. i atm. optike (Proc. VI Joint Conf. on Actin.
and Atm. Optics), Tartu, 1968.

20. Sandomirskiy, A.B., L.I. Koprova and G.I. Trifonova. Some
statistical Characteristics of Brightness Indices at
Height 17.5 km, Izv. AN SSSR, ser. fizika atmosfery i
okeana, Vol. 6, No. 7, 1970.

21. Wadsworth, F.S. Short Range and Extended Forecasting Statis-
tical Methods. Air Weather Service, TR. 105 - 37, 1948.

22. Myach, L.G. O statisticheskikh kharakteristikakh i ob'yek-
tivnom analize polya vlazhnosti i temperatury u poverk-
hnosti Zemli (Statistical Characteristics and Objective
Analysis of Temperature and Humidity Fields at the Earth's
Surface), Tr. NIIAK, No. 24, 1963.

23. Boldyrev, G.V. and V.I. Khamarin. K voprosu ob odnopodnosti
i izotropnosti polya prizemnoy temperatury. Voprosy sput-
nikovoy meteorologii (Homogeneity and Isotropy of the
Surface Temperature Field. Topics in Satellite Meteorology),
Tr. GMTs, No. 2, 1967.

24. Feoktistov, K.P., G.V. Rozenberg and A.B. Sandomirskiy.
Some Results of Observations During the Flight of the
Voskhod Space Vehicle. In the collection: Fizika kos-
micheskogo prostranstva ("Space Physics"), Izdatel'stvo
Nauka, 1965.

514

25. Sonechkin, D.M. Ob'yektivnye metody diagnoza oblachnosti (Objective Methods of Cloud Forecasting), Trudy GMTs, No. 30, 1968 (see also Trudy MMTs, No. 8, 1965).

26. Koprova, L.T. and V.G. Boldyrev. Statistical Characteristics of the Vertical Structure of Temperature and Humidity Fields to High Altitude, Izv. AN SSSR, ser. fizika atmosfery i okeana, Vol. 6, No. 2, 1970.

27. Polovina, I.P. Raspredeleniye temperatury v oblakakh i blizi ikh granits (Temperature Distribution in Clouds and Near Their Boundaries), Transactions of the Ukrainian Scientific Research Hydrometeorological Institute (Trudy Ukr. NIGMI), No. 42, 1964.

28. Khrgian, A.Kh, editor. Fizika oblakov (Cloud Physics), Gidrometeoizdat, 1961.

29. Sandomirskiy, A.B. and G.V. Rozenberg. Vysotnyy khod koeffisienta rasseyaniya v stratosfere po izmereniyam s kosmicheskogo korablya "Soyuz 3". Dokl. na Mezhdynarodnom simposiume po serebristym oblakam (High-Altitude Behavior of the Scattering Coefficient in the Stratosphere, from Measurements on the Space Vehicle Soyuz 3. Report of the Internat. Symp. on Stratified Clouds), Tbilisi, 1969.

30. Rozenberg, G.V. Optical Investigation of Atmospheric Aerosols, Uspekhi Fiz. Nauk, Vol. 95, No. 1, 1968.

31. Laktionov, A.T. Variation of Drop Size and Concentration During Dissipation of Fog, Izv. AN SSSR, ser. fizika atmosfery i okeana, Vol. 3, No. 5, 1967.

32. Gurvich, A.S. and N.S. Time. Variations of Atmospheric Absorption and Brightness Temperature, Izv. AN SSSR, ser. fizika atmosfery i okeana, Vol. 2, No. 8, 1968.

33. Gal'tsev, A.P. Statistical Characteristics of Atmospheric Transparency Due to Water Vapor, Izv. AN SSSR, ser. fizika atmosfery i okeana, Vol. 5, No. 6, 1969.

34. Koprova, L.I. and M.S. Malkevich. Empirical Orthogonal Functions for Optimal Parametric Representation of Temperature and Humidity Profiles, Izv. AN SSSR, ser. fizika atmosfery i okeana, Vol. 1, No. 1, 1965.

35. Marchuk, G.I. Chislennyye metody v prognoze pogody (Computer Methods in Weather Forecasting), Leningrad, 1967.

36. Marchuk, G.I. Theory of Bi-Orthogonal Expansions of Fields of Meteorological Elements, Dokl. AN SSSR, Vol. 179, No. 4, 1968.

37. Gavrilin, B.L. Parametric Representation of the Vertical Structure of Humidity, Izv. AN SSSR, ser. fizika atmosfery i okeana, Vol. 3, No. 9, 1967.

38. Yudin, M.I. Ob izuchenii faktorov, obuslavlivayushchikh nestatsionarnost' obshchey tsirkulyatsii atmosfery. Dinamika atmosfernykh krupnomasshtabnykh protsessov (Study of Factors Causing Non-Stationary General Circulation of the Atmosphere. Dynamics of Large-Scale Atmospheric Processes), Izdatel'stvo Nauka, 1967.

39. Holmström, I. On a Method for Parametric Representation of the State of the Atmosphere. Tellus, Vol. 15, No. 1, 1963.|

CHAPTER 4

1. Malkevich, M.S. Relationship Between the Characteristics of the Vertical Structure of the Long-Wave Radiation Field and the Fields of Temperature and Humidity, Izv. AN SSSR, ser. fizika atmosfery i okeana, Vol. 1, No. 10, 1965.

2. Ross, Yu.K. Some Aspects of the Mathematical Theory of Photosynthesis of Vegetation Cover. In the collection: Voprosy radiatsionnogo rezhema rastitel'nogo pokrova (Aspects of Radiation Conditions of Vegetation Cover), Tartu, 1965.

3. Nil'son, T.A. Matematicheskoye modelirovaniye radiatsionnogo rezhima rastitel' noog pokrova (Mathematical Modeling of the Radiation Conditions of Vegetation Cover), Dissertatsiya, Tartu, 1968.

4. Monim, A.S. and A.M. Yaglom. Statisticheskaya gidrodinamika, ch. 2. Mekhanika turbulentnosti (Statistical Hydrodynamics, Part 2. Mechanics of Turbulence), Izdatel'stvo Nauka, 1967.

5. Kuhn, P.M., V.E. Suomi and D.L. Darnaw. Soundings of Terrestrial Radiation Flux. Monthly Weather Rev., Vol. 87, No. 4,| 1959;|J. Geophys. Rev., Vol. 65, No. 11, 1960.|

6. Kostyanoy, G.N. An Actinometric Probe, Meteorologiya i gidrologiya, No. 7, 1963.

7. Kurilova, Yu.V. Strukturnye osobennosti dlinnovolnovogo izlucheniya v atmosfere. Sputnikovaya meteorologiya (Structural Peculiarities of Long-Wave Radiation in the Atmosphere. Satellite Meteorology), Trudy MMTs, No. 11, 1966.

8. Kurilova, Yu.V. and Yu.K. Fedorov. O vertikal'noy struk-
    ture poley dlinnovolnovoy radiatsii. Voprosy sputnikovoy
    meteorologii (Vertical Structure of Long-Wave Radiation
    Fields. Topics in Satellite Meteorology), Trudy GMTs,
    No. 11, 1967.

9. Babayev, VV. and M.S. Malkevich. Vertical and Angular
    Structure| of the Field of Scattered Radiation, Izv. AN
    SSSR, ser. fizika atmosfery i okeana, Vol. 7, No. 5, 1971.

10. Babayev, V.V. Statistical Characteristics of the Angular
    Structure of the Field of Scattered Solar Radiation,
    Izv. AN SSSR, ser. fizika atmosfery i okeana, Vol. 7,
    No. 11, 1971.

11. Klimchuk, Ye.F., Ye.M. Kozlov and M.S. Malkevich. Equipment
    for Measurement of Earth Brightness of Kosmos 149, Izv.
    AN SSSR, ser. fizika atmosfery i okeana, Vol. 5, No. 3,
    1969.

12. Malkevich, M.S., V.I. Syachinov and L.U. Chagar. Some Sta-
    tistical Characteristics of the Angular Structure of the
    Field of Earth Brightness, Izv. AN SSSR, ser. fizika
    atmosfery i okeana, Vol. 7, No. 2, 1971.

13. Puchkov, V.V. and S.I. Titov. Use of Outgoing Radiation
    Data to Determine Temperature and Humidity Fields,
    Izv. AN SSSR, ser. fizika atmosfery i okeana, Vol. 2,
    No. 1, 1966 (see also Trudy GGO, No. 221, 1968).

14. Bandeen, W.R., M. Halev and J. Strange. A Radiation Climato-
    logy in the Visible and Infrared from Tiros Meteorological
    Satellites. Godd. Space Flight Center, NASA X-651-64-218,
    1964.

15. Belov, P.I., Yu.V. Kurilova and L.V. Berkovich. Nekotorye
    kharakteristiki poley ukhodyashchei radiatsii (Some
    Characteristics of Emergent Radiation Fields), Trudy GMTs,
    No. 30, 1968.

16. Raschke, E. and M. Pasternak. The Global Radiation Balance
    of the Earth Atmosphere System Obtained from Radiation Data
    of the Meteorological Satellite Nimbus II. Space. Res.,
    Amsterdam, North Holland Publ. Co., Vol. 8, 1967. |

17. Shifrin, K.S. and N.P. Pyatovskaya. Opyt ispol'zovaniya
    dannykh o pole ukhodyashchey korotkovolnovoy radiatsii,
    poluchennykh s ISZ "Kosmos-122" (Experience in Use of
    Data on the Field of Emergent Short-Wave Radiation, Taken
    on Kosmos 122), Trudy GGO, No. 221, 1967.

CHAPTER 5

1. Malkevich, M.S., A.S. Monin and G.V. Rozenberg. Spatial
    Structure of the Radiation Field as a Source of Meteorolo-
    gical Information, Izv. AN SSSR, ser. geofiz., No. 3, 1964.

2. Borisenkov, E.P., Yu.P. Doronin and K.Ya. Kondrat'yev.
    Structural Charachteritics of the Radiation Field of the
    Planetary Earth, Kosmich. issled., Vol. 1, No. 1, 1963.

3. Borisenkov, E.P., Yu.P. Doronin and K.Ya. Kondrat'yev. Struc-
    tural Characteristics of the Emergent Radiation Field
    from Tiros II and Tiros III Data and Their Interpretation,
    Kosmich. issled., Vol. 3, No. 3, 1965.

4. Malkevich, M.S., I.P. Malkov and L.A. Pakhotova. Determina-
    tion of Statistical Characteristics of Radiation Fields
    Above Clouds, Kosmich.| issled., Vol. 2, No. 2, 1964.

5. Istomina, L.G. Determination of Statistical Characteristics
    of Spatial Structure of Clouds Fields from Aero-photographs,
    Izv. AN SSSR, ser. fizika atmosfery o okeana, Vol. 2,
    No. 3, 1966.

6. Istomina, L.G. and Ye.M. Kozlov. Two-Dimensional Spatial
    Structure of Cloud Field Brightness, Izv. AN SSSR, ser.
    fizika atmosfery i okeana, Vol. 2, No. 7, 1968.

7. Solov'yeva, I.S., D.M. Sonechkin and V.F. Kharitonov.
    Obrabotka i analiz televizionnykh izobrazhenii oblachnosti
    na EVM (Computer Processing and Analysis of Television
    Cloud Pictures), Trudy GMTs, No. 73, 1971.

8. Lessc, J.A. and S. Epstein. Application of Two-Dimensional
    Spectral Analysis to the Quantification of Satellite Cloud
    Photographs. J. Appl. Meteorol., Vol. 2, No. 5, 1963.|

9. Boldyrev, V.G.,|D.M. Sonechkin and V.I. Tulupov. Korrelyat-
    sionnye funktsii i spektral'nye plotnosti intensivnosti
    ukhodyashchego izlucheniya v intervale spektra 0.6 - 0.8
    mkm (po izmereniyam so sputnika "Kosmos-45") (Correlation
    Functions and Spectral Densities of Emergent Radiative
    Intensity in the Spectral Range 0.6 - 0.8 μ (from measure-
    ments on Kosmos 45), Trudy GMTs, No. 36, 1968.

10. Boldyrev, V.G., D.M. Sonechkin and V.I. Khamarin. O statis-
    ticheskoy strukture poley ukhodyashchey radiatsii (Sta-
    tistical Structure of Emergent Radiation Fields), Trudy
    GMTs, No. 20, 1968.

11. Vimberg, G.H., Yu.A. Drazhinnikova and V.I. Ivanov. Sta-
     tisticheskiye kharakteristiki signalov skaniruyushchey
     infrakrasnoy apparatury (Statistical Characteristics of
     Signals from IR Scanning Equipment), Trudy GGO, No. 221,
     1968.

12. Malkevich, M.S., L.G. Istomina and V.I. Syachinov. Spatial
     Structure of the Earth's Brightness Field from Kosmos 149
     Measurements, Izv. AN SSSR, ser. fizika atmosfery i okeana,
     Vol. 5, No. 7, 1970.

13. Gorodetskiy, A.K. Eksperimental'noye issledovaniye sobst-
     vennogo izlucheniya Zemli v "oknakh prozrachnosti" atmos-
     fery so sputnikov (Experimental Investigation of Earth
     Self-Radiation in the Atmospheric "Windows", Using Satel-
     lites), Izv. AN SSSR, ser. fizika atmosfery i okeana,
     Vol. 2, No. 4, 1966.

14. Malkevich, M.S. Spatial Structure of the Earth's Long-Wave
     Radiation Field, Izv. AN SSSR, ser. fizika atmosfery i
     okeana, Vol. 2, No. 4, 1966.

15. Pugachev, V.S. Teoriya sluchaynykh funktsii (Theory of   /299
     Random Functions), Fizmatgiz, 1960.

16. Gorodetskiy, A.K., Ye.F. Klimchuk and M.S. Malkevich.
     Technique and Some Results of Determination of Underlying
     Surface Temperature from the Satellite Kosmos 149, Izv.
     AN SSSR, ser. fizika atmosfery i okeana, Vol. 5, No. 4,
     1969.

17. Drobyshevich, V.I. Determination of Albedo Variations from
     a Satellite, Allowing for the Equipment Characteristics,
     Izv. AN SSSR, ser. fizika atmosfery i okeana, Vol. 5,
     No. 1, 1969.

18. Drobyshevich, V.I. Svyaz' statisticheskikh kharakteristik
     poley oblachnosti i ukhodyashchey korotkovolnovoy radiatsii
     (Relationship of the Statistical Characteristics of the
     Cloud Field and that of Outgoing Short-Wave Radiation),
     Trudy VI Vses. soveshch. po aktin. i atm. optike, Tartu,
     1967.

19. Aroych, G.F. The Technique of Spatial Filtering. Proc.
     IRE, Vol. 47, No. 9, 1959.

20. Gurvich, A.S. Spektry pul'satsii vertikal'noy komponenty
     skorosti vetra i ikh svyazi s mikrometeorologicheskimi
     usloviyami (Spectra of Fluctuations of the Vertical Wind
     Velocity Component and Their Relationship with Micro-Me-
     teorological Conditions) Transactions of the Institute of
     Physics of the Atmosphere (Trudy IFA), No. 4, 1962.

21. Tsvang, L.R.   Izmereniya turbulentnykh potokov tepla i spek-
     trov temperaturnykh pul'satsii (Measurement of Turbulent
     Heat Fluxes and Spectra of Temperature Fluctuations),
     Trudy IFA, No. 4, 1962.

22. Yelagina, L.G.   Ob izmerenii chastotnykh spektrov pul'satsii
     absolyutnoy vlazhnosti v prizemnom sloe atmosfery (Measure-
     ment of Frequency Spectra of Absolute Humidity Fluctuations
     in the Surface Atmospheric Layer), Izv. AN SSSR, ser.
     geofiz., No. 12, 1963.

23. Kostyanoy, G.N. and L.A. Pakhomova.   Izmereniye kosffitsienta
     yarkosti podstilyayushchey poverkhnosti i oblakov s camoleta
     (Measurement of Brightness Coefficient of the Underlying
     Surface and Clouds from Aircraft), Trudy Tsentr. aerol.
     obs., No. 66, 1965.

24. Malkevich, M.S. and L.G. Istomina.   Scattering Calculation
     in Determining the Statistical Characteristics of the
     Reflected Solar Radiation Field, Izv. AN SSSR, ser. fizika
     atmosfery i okeana, Vol. 7, No. 2, 1971.

25. Sonechkin, D.M. and I.S. Khandurova.   Resul'taty issledovaniya
     prostranstvennovremmenoy izmenchivosti oblachnosti na
     yevropeyskoy territorii SSSR (Results of Investigation of
     Space and Time Variations of Clouds over the European
     USSR), Trudy GMTs, No. 50, 1969.

26. Bugayev, V.A, T.P. Popova and B.S. Chuchkalov.   Analysis of
     the State of the Atmosphere Above the Globe from a Photo-
     graph Taken from Zond 5 at 90,000 km, Meteorologiya i
     Gigrologiya, No. 7, 1969.

27. Kolesnikova, V.N. and A.G. Monin.   Spectra of Oscillations
     of Meteorological Fields, Izv. AN SSSR, ser. fizika
     atmosfery i okeana, Vol. 1, No. 7, 1965.

CHAPTER 6

1.   Kaplan, L.D.   Inference of Atmosphere Structure from Remote
     Measurements.   J. Opt. Soc. America, Vol. 49, No. 10, 1959.

2.   Wark, D.Q.   On Indirect Temperature Soundings of the Strato-
     sphere from Satellites.   J. Geophys. Res., Vol. 66,
     No. 1, 1961.

3.   Yamamoto, G.   Numerical Method of Estimating the Strato-
     spheric Temperature Distribution from Satellite Measure-
     ments of CO_2 Band.   J. Meteorol., Vol. 18, No. 5, 1961.

4. Malkevich, M.S. Some Aspects of Interpretation of Satellite Radiation Measurements, Kosmich. issled., Vol. 2, No. 2, 1964.

5. Malkevich, M.S. and VI.I Tatarskiy. Determination of the Vertical Profile of Atmospheric Temperature from the Outgoing Radiation in the CO_2 Absorption Band, Kosmich. issled., Vol. 3, No. 3, 1965.

6. Wark, D.Q. and H.E. Fleming. Indirect Measurements of Atmospheric Temperature Profiles from Satellites. I. — Introduction. Monthly Weather Rev., Vol. 94, No. 6, 1966.

7. Twomey, S. The Application of Numerical Filtering to the Solution of Integral Equations Encountered in Indirect Sensing Measurements. J. Franklin Inst., Vol. 279, No. 2, 1965.

8. Tikhonov, A.N. Solution of Incorrectly Posed Problems and a Method of Regularization, Dokl. AN SSSR, Vol. 151, No. 3, 1963.

9. Tikhonov, A.N. Regularization of Incorrectly Posed Problems, Dokl. AN SSSR, Vol. 153, No. 1, 1963.

10. Glasko, V.B. and P.N. Zaikin. Program Algorithm for a Fredholm Equation of the First Kind. In the collection: Vychislitel'nye metody i programmirovaniye (Numerical Methods and Programming, No. 5), Izd. MGTs., 1966.

11. Zaikin, P.N. Numerical Solution of an Inverse Problem of Operational Calculus in the Real Region, Zhurnal vych. matem. i matem. fiz., Vol. 8, No. 2, 1968.

12. Tikhonov, A.N. and B.V. Glasko. Approximate Solution of Fredholm Integral Equations of the First Kind, Zhurnal vych. matem. i matem. fiz., Vol. 4, No. 3, 1964.

13. Tikhonov, A.N. and V.B. Glasko. Use of the Method of Regularization in Nonlinear Problems, Zhurnal vych. matem. i matem. fiz., Vol. 5, No. 3, 1965.

14. Glasko, V.B. and Yu.M. Timofeyev. Use of the Method of Regularization to Solve Problems Relating to Thermal Probing of the Atmosphere, Izv. AN SSSR, ser. fizika atmosfery i okeana, Vol. 4, No. 12, 1968.

15. Glasko, V.B. and Yu.M. Timofeyev. Possible Use of the Method of Regularization in Solution of Thermal Atmospheric Probing Problems, Izv. AN SSSR, ser. fizika atmosfery i okeana, Vol. 4, No. 12, 1968.

16. Kondrat'yev, K.Ya. and Yu.M. Timofeyev. Termicheskoye zondirovaniye atmosfery so sputnikov (Thermal Probing of the Atmosphere from Satellites), Gidrometeoizdat, 1970.

17. Phillips, D.I. A Technique for the Numerical Solution of Certain Integral Equations of the First Kind. J. Assoc. Comput. Mach., Vol. 9, No. 1, 1962.|

18. Twomey, S. On the Numerical Solution of Fredholm Integral /300 Equations of the First Kind by the Inversion of the Linear System Produced by Quadrature. J. Assoc. Comput. Mach., Vol. 10, No. 1, 1963.|

19. Hilleary, D.T., D.Q. Wark and D.G. James. An Experimental Determination of the Atmospheric Temperature Profile by Indirect Means. Nature, Vol. 205, No. 4970, 1965.|

20. Malkevich, M.S., V.P. Kozlov and I.A. Gorshakova. On Application of the Statistical Method for Determination of Atmospheric Temperature Profiles from Satellites. Tellus, Vol. 21, No. 3, 1969.|

21. Wark, D.Q., F. Saiedy and D.G. James. Indirect Measurements of Atmospheric Temperature Profiles from Satellites. VI High-Altitude Balloon Testing. Monthly Weather Rev., Vol. 95, No. 7, 1967.|

22. Alishouse, J.C., L.J. Crone, H.E. Fleming et al. A Discussion of Empirical Orthogonal Functions and Their Application to Vertical Temperature Profiles. Tellus, Vol. 19, No. 3, 1967.|

23. Dobryshman, Ye.M. Accuracy and Frequency Requirements of Hydrometeorological Information, Meteorologiya i gidrologiya, No. 11, 1968.

24. Marchuk, G.I. An Equation for the Value of Information from Weather Satellites and Statement of Inverse Problems, Kosmich.| issled., Vol. 2, No. 3, 1964.

25. Kozlov, V.P. Capacity of a Set in Signal Space and Riemann Metrics, Dokl. AN SSSR, Vol. 116, No. 4, 1966.

26. Kozlov, V.P. Determination of High-Altitude Temperature Profile from the Spectrum of the Outgoing Radiation, Izv. AN SSSR, ser. fizika atmosfery i okeana, Vol. 2, No. 2, 1966.

27. Kozlov, V.P. Numerical Determination of the High-Altitude Temperature Profile from the Spectrum of Outgoing Radiation, and Optimization of the Method of Measurement, Izv. AN SSSR, ser. fizika atmosfery i okeana, Vol. 2, No. 12, 1966.

28. Pokrovskiy, O.M. Optimum Conditions for Indirect Atmospheric Probing. Izv. AN SSSR, ser. fizika atmosfery i okeana, Vol. 5, No. 12, 1969.

29. Gorchakova, I.A. and V.P. Kozlov. Choice of Spectral Region in Temperature Probing of the Atmosphere. In the collection: "Aktinometriya i optika atmosfery" (Actinometry and Atmospheric Optics), Trudy VII Mezhved, soveshch. po aktin. i atm. optike, Gidrometeoizdat, 1968.

30. Twomey, S. Indirect Measurements of Atmospheric Temperature Profiles from Satellites. II. Mathematical Aspects of the Inversion Problem. Monthly Weather Rev., Vol. 94, No. 6, 1966.

31. Turchin, V.F. Solution of a Fredholm Equation of the First Kind in a Statistical Ensemble of Smooth Functions, Zhurnal vych. matem. i matem. fiz., Vol. 7, No. 6, 1967.

32. Turchin, V.F. Choice of Ensemble of Smooth Functions in the Solution of an Inverse Problem, Zhurnal vychisl. matem. i matem. fiz., Vol. 8, No. 1, 1963.

33. Turchin, V.F. and V.Z. Nozik. Statistical Regularization of the Solution of Incorrect Problems, Izv. AN SSSR, ser. fizika atmosfery i okeana, Vol. 5, No. 1, 1969.

34. Turchin, V.F., V.P. Kozlov and M.S. Malkevich. Use of Methods of Mathematical Statistics to Solve Incorrect Problems, Ukr. Fiz. Nauk, Vol. 102, No. 3, 1970.

35. Turchin, V.F., M.S. Malkevich and I.A. Gorchakova. Use of Statistical Regularization to Determine the Vertical Atmospheric Temperature Profile, Izv. AN SSSR, ser. fizika atmosfery i okeana, Vol. 5, No. 5, 1969.

36. Strand, O.N. and E.R. Westwater. The Statistical Estimation of the Numerical Solution of Fredholm Integral Equations of the First Kind. J. Assoc. Comput. Mach, Vol. 15, No. 1, 1968.

37. Westwater, E.R. and O.N. Strand. Statistical Information Content of Radiation Measurements Used in Indirect Sensing. J. Atmos. Sci., Vol. 25, No. 5, 1968.

38. Hilleary, D.T., E.L. Heacock, W.A. Morgan et al. Indirect Measurements of Atmospheric Temperature Profiles from Satellites. III. The Spectrometers and Experiments. Monthly Weather Rev., Vol. 94, No. 6, 1966.

39. Malkevich, M.S. Determination of Meteorological Elements Using Satellites. In the collection: Meteorologicheskie issledovaniya. Obshchaya tsirkulatsiya (Meteorological Investigations. General Circulation). Izdatel'stvo Nauka, 1969.

40. Malkevich, M.S. Some Problems of Interpretation of Radiative Measurements from Satellites. Proc. XV Internat. Astronaut. Congr., Warszawa, Vol. 11, 1964.

41. Wark, D.Q. and D.T. Hilleary. Atmospheric Temperature: A Successful Test of Remote Probing. Science, Vol. 165, No. 3899, 1969.

42. Hanel, R. and B. Conrath. Preliminary Results from the Interferometer Experiment on Nimbus III. Science, Vol. 165, No. 3899, 1969.

43. Malkevich, M.S. and I.A. Gorchakova. Variations of Outgoing Radiation in the 15 µ Carbon Dioxide Absorption Band, Izv. AN SSSR, ser. fizika atmosfery i okeana, Vol. 2, No. 6, 1966.

44. Kozlov, V.P., M.S. Malkevich and V.F. Tourchin. Some Aspects of Sounding the Vertical Temperature and Humidity Profiles. Symposium of Remote Sounding of the Atmosphere. XIII Meeting COSPAR, Leningrad, May 1970.

45. Timofeyev, Yu.M. and O.M. Pokrovskiy. Actual Example of Determination of an Atmospheric Temperature Profile, Izv. AN SSSR, ser. fizika atmosfery i okeana, Vol. 5, No. 10, 1969.

46. Chachine, M.T. Determination of the Temperature Profile in an Atmosphere from its Outgoing Radiation. J. Opt. Soc. America, Vol. 58, No. 12, 1968.

CHAPTER 7   /301

1. Kaplan, L.D. The Spectroscope as a Tool for Atmospheric Sounding by Satellites. J. Quant. Spectros. Radiat. Transfer., Vol. 1, No. 2, 1961.

2. Malkevich, M.S. and V.I. Tamarskiy. Determination of Temperature and Humidity of the Earth's Atmosphere from Satellite Measurements of Earth Radiation. In the collection: Issled. kosmich. prostr. (Investigation of Deep Space), Izdatel'stvo Nauka, 1965.

3. Gorchakova, I.A., M.S. Malkevich and V.F. Turchin. Determination of the Vertical Atmospheric Humidity Profile from Measurements of Earth Self-Radiation, Izv. AN SSSR, ser. fizika atmosfery i okeana, Vol. 6, No. 6, 1970.

4. Smith, W.L. An Interative Method for Deducing Tropospheric Temperature and Moisture Profiles from Satellite Radiation Measurements. Monthly Weather Rev., Vol. 95, No. 6, 1967.

5. Smith, W.L. An Improved Method for Calculating Tropospheric Temperature and Moisture from Satellite Radiometer Measurements. Monthly Weather Rev., Vol. 96, No. 6, 1968.

6. Chaney, L.W., S.R. Drayson and C. Young. Fourier Transform Spectrometer — Radiative Measurements and Temperature Inversion. Appl. Opt., Vol. 6, No. 2, 1967.

7. Gorchakova, I.A., M.S. Malkevich and A.P. Naumov. Examples of Determination of the Vertical Humidity Profile from Ground Measurements of Atmospheric Thermal Radiation of the 1.35 cm H_2O Line Absorption, Izv. AN SSSR, ser. fizika atmosfery i okeana, Vol. 7, No. 7, 1971.

8. Kantorovich, L.V. O metode N'yutona (Newton's Method), Trudy Matem. in-ta im. V.A. Steklova, No. 28, 1949.

9. Conrath, B.J., R.A. Hanel, V.G. Kunde et al. The Infrared Interferometer Experiment Nimbus 3. Goddard Space Flight Center, NASA X-620-70-213, Green Belt, Maryland, June 1970.

10. Conrath, B.J. On Estimation of Relative Humidity Profiles from Medium-Resolution Infrared Spectra Obtained from a Satellite. J. Geophys. Res., Vol. 74, 1969, p. 13.

11. Pokrovskiy, O.M. and Yu.M. Timofeyev. Thermal Sounding of the Atmosphere, Problemy fiz. atm., No. 8, 1969.

CHAPTER 8

1. Malkevich, M.S.   Metody interpretatsii radiatsionnykh izmerenii so sputnikov   (Methods of Interpretation of Satellite Radiation Measurements), Trudy 6-go mezhdedomstvennogo soveshchaniya po aktinometrii i optike atmosfery.(Proc. 6th Interdepartmental Conf. on Actinometry and Atmospheric Optics), Izdatel'stvo Valgus, Tallin, 1968.

2. Boldyrev, V.G., L.I. Kaprova and M.S. Malkevich.   Calculation of Variations of Vertical Profiles of Temperature and Humidity in the Determination of Underlying Surface Temperature from Outgoing Radiation, Izv. AN SSSR, ser. fizika atmosfery i okeana, Vol. 1, No. 7, 1966.

3. Nordberg, W., W.R. Bandeen, B.J. Conrath et al.   Preliminary Results of Radiation Measurements from Tiros III Meteorological Satellite.   J. Atmos. Sci., Vol. 19, No. 1, 1962.|

4. Kern, C.D.   Desert Soil Temperatures and Infrared Radiation Received by Tiros III.   J. Atmos. Sci., Vol. 20, No. 2, 1963.|

5. Saiedy, F. and D.T. Hilleary.   Remote Sensing of Surface and Cloud Temperature Using the $899-cm^{-1}$ Interval.   Appl. Opt., Vol. 6, No. 5, 1966.|

6. Boldyrev, V.G.   K voprosu ob ispol'zovanii izmerenii ukhodyashchey radiatsii dlya rascheta temperatury zemnoi poverkhnosti i vysoty verkhney granitsy oblakov (Use of Emergent Radiation Measurements to Calculate Ground Surface Temperature and Height of Upper Cloud Boundary), Trudy MMTs, No. 8, 1965.

7. Gorodetskiy, A.K., M.S. Malkevich and A.P. Orlov.   Determination of Ocean Temperature from IR Radiation Measurements on Kosmos 243, Izv. AN SSSR, ser. fizika atmosfery i okeana, Vol. 6, No. 5, 1970.

8. Carlon, H.R.   The Apparent Dependence of Terrestrial Scintillation Intensity Upon Atmospheric Humidity.   Appl. Opt., Vol. 4, No. 9, 1965.|

9. Carlon, H.R.   Humidity Effects in the 8 - 13 µ Infrared Window.   Appl. Opt., Vol. 5, No. 5, 1966.|

10. Gorodetsky, A.K. and M.S. Malkevich. Determination of Surface and Top-Cloud Temperature by Measurements of Earth Radiation in Window 8 - 12 microns by Kosmos-149. Sympos. Internat. Com. Radiation, Bergen, August 1969.

11. Malkevich, M.S. Characteristics of Cloudiness and of Infrared Radiation in the Window Obtained from Kosmos-149, Kosmos-243 and Kosmos-320 Measurements. XIII-th Meeting COSPAR, Leningrad, May 1970.

12. Nordberg, W. Summary Report on the Nimbus II Satellite. Space Res., Amsterdam, North Holland Publ. Co., Vol. 8, 1967.

13. Fritz, S. and K.P. Rao. On Infrared Transmission Through Cirrus Clouds and Estimation of Relative Humidity from Satellites. J. Appl. Meteorol., Vol. 6, No. 6, 1967.

14. Gorodetskiy, A.K., A.S. Gurvich and A.V. Migulin. Determination of Underlying Surface Temperature from Aircraft Measurements of Outgoing Radiation in the 8 - 12 μ Range, Izv. AN SSSR, ser. fizika atmosfery i okeana, Vol. 3, No. 6, 1967.

15. Migulin, A.V. Determination of Underlying Surface Tempera- /302 ture from Aircraft Measurement of Outgoing Radiation in the 10 - 12 μ Range, Izv. AN SSSR, ser. fizika atmosfery i okeana, Vol. 4, No. 6, 1968.

16. Hovis, W.A., L.R. Blaine and W.R. Callahan. Infrared Air-Craft Spectra Over Desert Terrain 8.5 μ to 16 μ. Appl. Opt., Vol. 7, No. 6, 1968.

17. Gorodetskiy, A.K. And A.M. Kasatkin. Radiometr dlya opredeleniya temperatury zemnoy poverkhnosti i oblakov (Radiometer for Determining Temperatures of Ground Surface and Clouds). Tr. VI Mezhved. soveshch. po aktin. i optike atm. (Proc. VIth Interdisc. Conf. on Actinometry and Atmospheric Optics) Tartu, 1966, Izdatel'stvo Nauka, 1968.

18. Thekaekara, M.P., R. Kruger and C.H. Duncan. Solar Irradiance Measurements from a Research Aircraft. Appl. Opt., Vol. 8, No. 8, 1969.

19. Reshetnikova, I.S. and O.I. Popov. Emittance of Low-Level Clouds in the 8 - 12 μ Window, Izv. AN SSSR, ser. fizika atmosfery i okeana, Vol. 6, No. 4, 1970.

CHAPTER 9

1. Hanel, R.A. Determination of Cloud Altitude from a Satellite. J. Geophys. Res., Vol. 66, No. 4, 1961.

2. Yamamoto, G. and D.Q. Wark. Discussion on the Letter by R.A. Hanel "Determination of Cloud Altitude from a Satellite". J. Geophys. Res., Vol. 66, No. 10, 1961.

3. Chapman, R.M. Cloud Distributions and Altitude Profiles from Satellite. Planet Space Sci., Vol. 9, 1962, Jan. - Febr.

4. Dianov-Klokov, V.I. Eksperimental'nye issledovaniya spektra pogloshcheniya kondensirovannogo kisloroda v oblasti 12600-3000 A (Experimental Investigation of the Absorption Spectrum of Condensed Oxygen in the 12600-3000 A Range) Dissertatsiya, Moscow, 1964.

5. Wark, D.Q. and D.M. Mercer. Absorption in the Atmosphere by the Oxygen "A" Band. Appl. Opt., Vol. 4, No. 7, 1965.

6. Adiks, T.G. and V.I. Dianov-Klokov. Molecular Parameters of the 0.7620 μ O_2 Absorption Band and Subsequent Calculation of Transmission Function, Izv. AN SSSR, ser. fizika atmosfery i okeana, Vol. 4, No. 10, 1968.

7. Burch, D.E. and D.A. Gryvnak. Strengths, Widths, and Shapes of the Oxygen Lines Near 13,100 cm^{-1} (7260 Å). Appl. Opt., Vol. 8, No. 7, 1969.

8. Miller, J.H., R.W. Boesse and L.P. Giver. Intensity Measurements and Rotational Intensity Distribution for Oxygen A-Band. J. Quant. Spectrosc. Radiat. Transfer, Vol. 9, No. 11, 1969.

9. Wallace, L. and D.M. Hunten. Dayglow of the Oxygen A-Band. J. Geophys. Res., Vol. 73, 1968, p. 15.

10. Babcock, H.D. and L. Herzberg. Fine Structure of the Red System of Atmospheric Oxygen Bands. Astrophys. J., Vol. 108, No. 2, 1948.

11. Shlapp, R. Fine Structure in the $^3\Sigma$ Ground State of the Oxygen Molecule and the Rotational Intensity Distribution in the Atmospheric Band. Phys. Rev., Vol. 51, No. 5, 1937.

12. Childs, W.H. and R. Mecke. Intensity Measurement in the Atmospheric Oxygen Band λ 7600. Z. Phys., Vol. 34, No. 8, 1956.

13. Benedict, W.S., R. Herman, G.E. Moore et al. The Strengths, Widths and Shapes of Infrared Lines. Canad. J. Phys., Vol. 34, No. 8, 1956.

14. Mizushima, M. Velocity Distribution in Spectral Line Shape. J. Quant. Spectrosc. Radiat. Transfer, Vol. 7, 1967, p. 505.

15. Pokrovskiy, A.G. and A.K. Suslov. Experience in Calculating the Absorption Spectrum of Atmospheric O_2 and Constructing a Growth Curve, Problemy fiziki atmosfery, sb. 7. Izd. Len. Gosud. Univ., 1969.

16. Pokrovskiy, A.G. and V.Ya. Galin. Method of Calculating Absorption of IR Solar Radiation Over Oblique Optical Paths in the Atmosphere, Problemy fiziki atmosfery, sb. 7, Izd. LGU, 1969.

17. Saiedy, F., D.T. Hilleary and A. Morgan. Cloud-Top Altitude Measurements from Satellites. Appl. Opt., Vol. 4, No. 4, 1965.

18. Rozenberg, G.V. Optical Properties of Thick Layers of a Homogeneous Scattering Medium. In the collection: Spektroskopiya svetorasseivayushchikh sred (Spectroscopy of Light-Scattering Media), Minsk, 1963.

19. Rozenberg, G.V., G.K. Il'ich and S.A. Makarevich. Brightness of Clouds (Results of a Set of Investigations), Izv. AN SSSR, ser. fizika atmosfery i okeana, Vol. 6, No. 4, 1970.

20. Romanova, L.M. Reflection and Transmission of Radiation by Thick Layers of a Trubid Medium. Determination of Parameters of the Rozenberg Equation, Opt. i spektr., Vol. 17, No. 2, 1964.

21. Twomey, S., H. Jacobowitz and H.B. Howell. Matrix Methods for Multiple-Scattering Problems. J. Atmos. Sci., Vol. 23, No. 3, 1966.

22. Twomey, S., H. Jacobowitz and H.B. Howell. Light Scattering by Cloud Layers. J. Atmos. Sci., Vol. 29, No. 1, 1967.

23. Katawar, G.W. and G.N. Plass. Influence of Particle Size Distribution on Reflected and Transmitted Light from Cloud. Appl. Opt., Vol. 7, No. 5, 1968.

24.   Galin, V.Ya.   Chislennoye modelirovaniye perenosa izlucheniya
       v atmosfere i zadacha opredeleniya vysoty oblakov s ISZ
       (Computer Modeling of Radiative Transfer in the Atmosphere
       and the Problem of Determining Cloud Height from Satel-
       lites), Dissertatsiya, Moscow, 1972.

25.   Saiedy, F., H. Jacobowitz and D.Q. Wark.   On Cloud-Top   /303
       Determination from Gemini-5.   J. Atmos. Sci., Vol. 24,
       No. 1, 1967.

26.   Dianov-Klokov, V.I. and I.P. Malkov.   Intensification of
       Absorption Bands in Passage Through a Cloud Layer,
       Izv. AN SSSR, ser. fizika atmosfery i okeana, Vol. 2,
       No. 5, 1966.

27.   Dianov-Klokov, V.I., Ye.P. Kropotkina and I.P. Malkov.   De-
       formation of Absorption Bands and Effective Light Path
       Length in Clouds,   Izv. AN SSSR, ser. fizika atmosfery i
       okeana, Vol. 6, No. 8, 1970.

28.   Koprova, L.I.   Allowance for Radiation Scattering in Determin-
       ing Cloud Height from Satellites,   Izv. AN SSSR, ser.
       fizika atmosfery i okeana, Vol.,5, No. 10, 1969.

29.   Gorodetskiy, A.K., M.S. Malkevich and V.I. Syachinov.   De-
       termination of Cloud Height from Radiation Measurements
       on Kosmos 320,   Dokl. AN SSSR, Vol. 200, No. 3, 1971.

30.   Adiks, T.G., Yu.S. Georgiyevskiy and M.S. Malkevich.   Atmos-
       pheric Transmission in the 0.76 μ Band,   Izv. AN SSSR,
       ser. fizika atmosfery i okeana, Vol. 7, No. 4, 1972.